Flow (Photo-)Chemistry and Online Spectroscopy for Synthesis and Analysis of Fine Chemicals

Dissertation

zur Erlangung des Grades "Doktor der Naturwissenschaften" (Dr. rer. nat.)

im Promotionsfach Chemie

am Fachbereich Chemie, Pharmazie, Geographie und Geowissenschaften

der Johannes Gutenberg-Universität Mainz

Vorgelegt von M. Sc. Christoph Martin Deckers
geboren in Mannheim

Mainz, 2022

1. Berichterstatter: [redacted]

2. Berichterstatter: [redacted]

Tag der mündlichen Prüfung: 19.12.2022

Eidesstattliche Erklärung

Die vorliegende Dissertation wurde im Zeitraum von September 2018 bis Juli 2022 am Department Chemie der Johannes Gutenberg-Universität Mainz in Kooperation mit Fraunhofer IMM angefertigt. Hiermit versichere ich, Christoph Martin Deckers, dass ich die vorliegende Arbeit selbstständig verfasst und keine anderen Quellen und Hilfsmittel als die angegebenen verwendet habe.

Diese Dissertation ist in gleicher oder ähnlicher Form weder veröffentlicht noch einer anderen Fakultät vorgelegt worden.

Mainz, den 15.11.2022 _____

Christoph Martin Deckers

Für meine Eltern

„Durch Fehler wird man klug, darum ist einer nicht genug“

- Wilhelm Busch -

Zusammenfassung

In dieser Arbeit werden neue Konzepte zur kontinuierlichen Herstellung von Feinchemikalien vorgestellt, die die Vorteile der Flow Chemistry und Mikroverfahrenstechnik nutzen.

Der erste Teil behandelt die **Herstellung von substituierten Biphenylen und die Integrierung einer Online-Analytik** in diesen Prozess. Während klassische Methoden auf übergangsmetallkatalysierte Kreuzkupplungen setzen, wird hier ein **photochemischer Weg** zur direkten C-H-Arylierung von Arenen mittels Diazoniumsalzen gewählt. Für die kontinuierliche Synthese erweisen sich die gebräuchlichen, aber unlöslichen Tetrafluoroborat-Salze jedoch als nicht geeignet, weshalb **Diazoniumtrifluoroacetat-Salze** eingeführt werden müssen. Die neue Syntheseroute, in der *meta*-(Trifluoromethyl)biphenyl als Benchmark-Molekül hergestellt wird, wird optimiert und mit literaturbekannten Konzepten verglichen. Dabei werden Umsatz und Selektivität erfolgreich erhöht, und mildere Bedingungen können angewendet werden.

Zwei verschiedene Reaktorkonzepte, der Fallfilm Mikroreaktor (FFMR) und der Kapillarphotoreaktor werden getestet. Beide Reaktoren eignen sich zur Prozessierung der Reaktion und erlauben die **Integration von heterogenen Photokatalysatoren**, wie zum Beispiel **Titandioxid**. Die photochemische Synthese der Benchmark-Verbindung im FFMR ist zunächst wenig effektiv und die Vorteile der Mikroverfahrenstechnik kommen noch nicht zum Tragen.
Daher wird der Prozess auf den Kapillarphotoreaktor übertragen, was längere Bestrahlungszeiten erlaubt. Mit Hilfe einer Mehrphasen-Pfropfenströmung ist es möglich, den festen Photokatalysator zu verwenden, und eine adäquate Anregung der photokatalytisch aktiven Spezies bei 455 nm ermöglicht die Synthese des Biphenyls.

Stetige Verbesserungen in der Herstellung der verwendeten Diazoniumverbindung und des Gesamtprozesses führen schließlich zu einem signifikanten Anstieg von Umsatz und Selektivität. Bestmögliche Ergebnisse werden erreicht, wenn die Diazoniumtrifluoroacetat-Salze in Gegenwart von **zwei Äquivalenten Trifluoressigsäure** hergestellt werden. Die anschließendene **katalysatorfreie direkte C-H-Photoarylierung** der Benzol-Derivate erfolgt dann auf Grund der Ausbildung von Charge-Transfer-Komplexen. Diese werden mittels UV-A Licht angeregt

und Biphenyle entstehen. Die kontinuierliche Synthese von **13 verschiedenen Derivaten** wird erfolgreich ausgeführt und mittels online ^{19}F-NMR Spektroskopie quantifiziert, da die enthaltenen Fluorsubstituenten als Sonde agieren. Daher ist die eingesetzte NMR-Spektroskopie ein geeignetes Quantifizierungs-Tool, um die Synthese der gewünschten **Feinchemikalien von industrieller Bedeutung im multi-Gramm Maßstab** verlässlich zu überwachen.

Im zweiten Teil dieser Arbeit wird die **Automatisierung und Digitalisierung von kontinuierlichen Prozessen** hin zu selbstlernenden Syntheseapparaturen behandelt. Selbstständige Optimierung lässt sich durch den Einsatz von künstlicher Intelligenz realisieren, wenn diese in eine **offene und flexible Kontroll- und Analyseplattform** integriert wird. Dafür muss die Software in der Lage sein, Daten und Informationen über den aktuellen Zustand des Prozesses von Sensoren und Prozessanalytik zu erhalten. Häufig kann zum Beispiel ein einzelnes Spektrometer einen komplexen Prozess nicht vollständig abdecken. Daher ist es umso wichtiger, das Verhalten des Prozesses genauestens zu verstehen, um dann die verschiedenen online-Spektrometer gezielt zu integrieren.

Daher wird eine **(halb-)automatische Versuchsanlage**, gesteuert durch eine selbstentwickelte Software, für die kontinuierliche zweistufige Herstellung von *Z*-Stilben entwickelt. In diesem Modellprozess entstehen zunächst die beiden Isomere durch eine Wittig-Reaktion. Nach einem Quench-Schritt wird **Online-Spektroskopie** (NMR, UV/VIS und IR) zur Analyse eingesetzt, um Umsatz und Ausbeute zu bestimmen. In der anschließenden Photoisomerisierung wird ein Sensibilisator hinzugefügt und das gewünschte Produkt bei Bestrahlung mit 455 nm hergestellt. Zur Überwachung dieser Isomerisierung wird ein nichtdispersiver IR-Sensor eingesetzt.
Die Software wird im **halb-automatischen Modus** betrieben, um ein **schnelles Parameter-Screening (DoE)** durchzuführen. Die Steuerung ist so entwickelt, dass sich ein vollständig automatisierter Selbstlern-Prozess jederzeit ermöglichen lässt, wenn künstliche Intelligenz mit integriert wird.

Tests der **modularen Spektrometer-Module** zeigen die Hürden bei der Integration von verlässlicher online-Analytik auf. Nicht jedes Modul kann daher im frühen Stadium einer Prozessentwicklung erfolgreich integriert werden. Eine **genaue Bestimmung des Hintergrundsignals** ist von großer Bedeutung, um akkurate Ergebnisse zu erhalten.

Abstract

New concepts are presented in this thesis, which all deal with syntheses of fine chemicals while using the benefits of continuous flow approaches and micro reaction technology.

The first part is about the **synthesis of substituted biphenyls including the integration of an online analysis tool.** While classic methods use transition metal-catalyzed cross coupling reactions, a **photochemical pathway** for a direct C-H arylation of arenes via diazonium salts is chosen in the presented thesis. As common diazonium tetrafluoroborate salts fail, soluble **aryl diazonium trifluoroacetates** must be introduced. The new route, where *meta*-(trifluoromethyl)biphenyl is used as a benchmark molecule, is optimized and compared to literature-known concepts. Better conversion and selectivity towards the favored product are successfully aspired, while mild conditions can be applied.

Two reactor concepts, the falling film micro reactor (FFMR) and the capillary photoreactor are tested. Both are suitable concepts and allow the **handling of solid photocatalysts**, like **titanium(IV) oxide**. The photochemical synthesis of the benchmark molecule is feasible in the FFMR, but the overall performance is low at first. This does not highlight the beneficial effects of the micro reactor technology.

Therefore, the capillary photoreactor is put into focus, allowing a much longer irradiation time of the process medium. With the Serial Micro Batch Reactor (SMBR), concept it is possible to introduce even solid photocatalysts as a multiphase plug flow system. This allows an adequate excitation of the photocatalytic active species at 455 nm and the production of the benchmark molecule.

Permanent improvements in the synthesis of the diazonium compound and the overall process lead to a significant increase in conversion and selectivity. Best results are achieved when diazonium trifluoroacetates are synthesized using **two equivalents of trifluoroacetic acid**. The **catalyst-free direct C-H photoarylations** of benzene-derivatives are performed by the formation of charge-transfer complexes. These are excited with UV-A light and biphenyl formation results. Continuous syntheses of **13 different samples** are successfully carried out and quantified via online ^{19}F-NMR spectroscopy, as the fluorine-containing substituents act as a probe. Therefore, online NMR-spectroscopy is a perfect tool to monitor the continuously operated system, which produces **fine chemicals of industrial relevance in the multigram scale.**

The second topic of this thesis deals with **automation and digitalization of continuous processes** in research and development towards self-learning facilities. Self-optimization can be realized by artificial intelligence which is connected to an **open and flexible control- and analysis platform**. The software has to receive data and information on the condition of the process via sensors and process analytical technology (PAT) systems. Not every online analysis tool is suitable to cover the complete and complex process. Therefore, it is necessary to understand the behavior of the process mixture to realize an appropriate integration of different online spectrometers.

A **(semi-)automated lab reactor system**, controlled by a self-developed software, is designed to control the continuous two-step synthesis of *Z*-stilbene. In this model process, both stilbene-isomers are obtained by the well-known Wittig reaction. After quenching the reaction, **online process analysis** (NMR-, UV/Vis- and IR-spectroscopy) is implemented to analyze the first step with respect to conversion and selectivity.
A photosensitizer is subsequently added to the product-stream and a photoisomerization step towards the favored product is conducted at 455 nm. A nondispersive IR-sensor is used to monitor the isomerization.

The software is designed to be operated in **semi-automated mode**. This mode is used for **quick parameter screening (DoE)**. The program sequence can be easily converted into a fully automated self-learning process by "one click" if artificial intelligence is integrated.

Testing the **modular spectroscopy modules** reveals pitfalls in integration for reliable online quantification. Not every analyzer can be successfully integrated, especially in early stages of process development. A **precise determination of background and reference signal is mandatory** to achieve high accuracy.

Danksagung

Mein größter Dank geht an Herrn [redacted]. Ich finde es beeindruckend und bewundernswert, dass Sie immer wieder Studierende, so auch mich, betreuen, die mit Ihrem Hauptforschungsfeld „organische Synthese und supramolekulare funktionale Systeme“ nur wenige oder vereinzelte Schnittpunkte haben. Dies zeigt mir, dass es immer wichtig ist ein Auge auf das „große Ganze“ zu haben. Es tauchen überall spannende und interessante Neuerungen und Alternativen auf, die man schnell einmal übersehen kann, wenn man sich in Kleinigkeiten verliert.

Hieran anschließen möchte ich meinen Dank an den ganzen AK Besenius. Danke, für die herzliche Aufnahme und Eure stetige Loyalität mir gegenüber, auch wenn ich, bedingt durch räumliche Distanz, nicht so häufig präsent war. Im Besonderen möchte ich [redacted] und [redacted] für das Organisieren der Seminare danken. Die ausdauernde Hilfe bei präparativer HPLC von [redacted], [redacted] und [redacted] ist nicht zu vernachlässigen und hat so einige Probleme bereinigt. Alle namentlich nicht genannten, behalte ich in guter Erinnerung.

Außerdem möchte ich mich bei Herrn [redacted] für die Aufnahme am Institut und die Erstellung des Zweitgutachtens bedanken. Durch Ihr Vertrauen (nicht vergessen ist die gesamte Institutsleitung/Controlling) mir gegenüber durfte ich Wissen in neuen Tätigkeitsfeldern erlernen.

Lieber [redacted], lieber [redacted], für das Schaffen meiner Promotionsstelle und die thematische Initiierung meiner Arbeitsfelder bin ich euch außerordentlich dankbar. Ich hätte niemals erträumt, dass mir solch ein großer Freiraum zum Ausleben eigener Ideen gegeben wird, der zum Glück immer wieder durch Euch neue Akzente bekam. Eure erbrachte Geduld, besonders Deine, [redacted], bewundere ich zutiefst.

[redacted], [redacted], [redacted] [redacted], [redacted], [redacted], [redacted], [redacted] und [redacted] möchte ich für jegliche gegenseitige fachliche, wie seelische Unterstützung und Hilfe danken. Ohne Euch hätte oftmals ein grauer Schatten über allem geschwebt. Danke an die Ingenieure [redacted] und [redacted] Ihr seid mein Ass im Ärmel, wenn die Technik streikt und schnelle, ausgefeilte Lösungen hermüssen.

[redacted] und [redacted] danke ich für Elektronik- und Softwarelösungen. Ihr besitzt Wissen und Fertigkeiten, die ich bewundere.

Durch die Erstellung von Bild- und Videoaufnahmen von [redacted] und [redacted] wird diese Arbeit ebenfalls bereichert. [redacted] danke ich für seine geduldige Unterstützung in der NMR-Spektroskopie.
Bedanken möchte ich mich bei [redacted] und [redacted] für Eure Herzlichkeit. Bei Euch kann man einfach mal abschalten.
Meinen (ehemaligen) Kommilitonen [redacted], [redacted], [redacted], [redacted], [redacted], [redacted], [redacted] und [redacted] möchte ich für die gemeinsame Zeit während des gesamten Studiums danken. Egal ob Praktikum, Vorlesung oder sonstige private Festivitäten - was haben wir miteinander Zeit verbracht?! Daher mein innigster Wunsch: Mögen wir uns nie ganz aus den Augen verlieren.

Auch wenn es mittlerweile schon etwas her ist: Danke, Herr [redacted], für Ihre Unterstützung und Betreuung während Bachelor- und Masterarbeiten. Damit haben Sie den Grundstein für meine Begeisterung an angewandter Forschung und Mikroverfahrenstechnik gelegt.

All meinen Kameraden und Kameradinnen des Technischen Hilfswerk - Ortsverband Worms danke ich für die Schaffung eines Gegenpols. Dank Euch weiß ich, dass man auch in dunklen Zeiten immer Freunde hat, auf die man sich verlassen darf und kann.

Zuletzt möchte ich meinen Eltern den wohl wichtigsten Dank aussprechen. Ihr seid und wart immer mein „Back-Office“ und ich durfte von euch während meines Studiums eine bindungslose Unterstützung erfahren. In so manch einer Situation hatte mich der Mut und die Kraft schon fast verlassen - Ihr wisst, was ich meine.

Abbreviations

Symbol	Explanation	Dimension
A	Reactor surface area	m^2
A_λ	Absorbance	-
A_{sp}	Specific surface area	$m^2 \times m^{-3}$
c	Molar concentration	$mol \times L^{-1}$
D	Molecular diffusivity	$mm^2 \times s^{-1}$
d	Layer thickness cuvette	cm
δ	Film thickness FFMR	mm
E_{photon}	Photon energy	$kg \times m^2 \times s^{-2}$
ε_λ	Molar extinction coefficient	$L \times mol^{-1} \times cm^{-1}$
I_0	Light intensity previous to interaction with matter	$W \times m^{-2}$
I	Light intensity after interaction with matter	$W \times m^{-2}$
l	Length microchannel FFMR	mm
L	Diffusion path length	m
L_{CP}	Specific productivity capillary photoreactor	$mol \times L^{-1} \times h^{-1}$
L_{FFMR}	Specific productivity FFMR	$mol \times L^{-1} \times h^{-1}$
λ	Wavelength	nm
η	Dynamic viscosity	Pa×s
n_{P}	Number of product molecules	-
n_{Photon}	Number of photons	-
Re	Reynold number	-
QE_λ	Quantum efficiency	-
ϕ	Photon flux	$cm^{-2} \times s^{-1}$
r_{m}	Particle radius	m
T	Temperature	K
T_1	Spin-lattice relaxation time	s
τ or TR	Acquisition time	s
τ_{R}	Residence time in the sensitive volume of the flow cell	s
t	Time	s
$t_{\mathrm{irradiation}}$	Irradiation time	min
t_{R}	Residence time	min
t_{m}	Mixing time	s
w	Width microchannel FFMR	µm
v	Frequency	s^{-1}
V	Reactor Volume	mL
V_{p}	Prepolarization volume of the flow cell	mL
V_{s}	Sensitive volume of the flow cell	mL
$\dot{V}$	Flow rate	$mL \times min^{-1}$
Y	Yield	-

Symbol	Explanation
AI	Artificial intelligence
API	Active pharmaceutical ingredient
ATR	Attenuated total reflection
BA	Benzaldehyde
BTTP	Benzyltriphenylphosphonium bromide
c_0	Speed of light (in vacuum)
CB	Conduction band
CH	Cyclohexane
CMB-C_3N_4	Carbon nitride prepared from cyanauric acid, melamine, and barbituric acid
CFL	Compact Fluorescent Light
CT	Charge-transfer
DBU	Diazabicycloundecene
DMSO	Dimethyl sulfoxide
DoE	Design of experiment
DSC	Differential scanning calorimetry
EA	Ethyl acetate
EDA-complex	Electron donor acceptor complex
EDG	Electron donating group
EWG	Electron withdrawing group
FEP	Fluorinated ethylene propylene
FFKM	Perfluoroelastomer
FFMR	Falling film micro reactor
FID	Free induction decay
FTIR	Fourier-transform infrared spectroscopy
g	Gravitational constant
h	Planck constant
HF	High-field
HOMO	Highest occupied molecular orbital
HWHM	Half width at half maximum
ID	Inner diameter
IHM	Indirect Hard Modeling
IR	Infrared
ISC	Intersystem crossing
k_{B}	Boltzmann constant
LED	Light emitting diode
LF	Low-field
LUMO	Lowest unoccupied molecular orbital
ML	Machine learning
MRT	Micro reactor technology
NMR	Nuclear magnetic resonance
NHE	Normal Hydrogen Electrode
OD	Outer diameter
PAT	Process analytical technology
PC	Photocatalyst
PEEK	Polyether ether ketone
PDMS	Polydimethylsiloxane
PCTFE	Polychlorotrifluoroethylene
PFA	Perfluoroalkoxy alkane
PMMA	Poly(methyl methacrylate)

Symbol	Explanation
PTFE	Polytetrafluoroethylene
qNMR	Quantitative NMR
RT	Room temperature
S_0	Singlet ground state
S_1	First excited singlet state
SCE	Saturated calomel electrode
SEM	Scanning electron microscope
SET	Single-electron transfer
SMBR	Serial Micro Batch Reactor
SNR	Signal-to-noise ratio
T_1	First excited triplet state
TBD	Triazabicyclodecene
TEM	Transmission electron microscopy
TFA	Trifluoroacetic acid
TPPO	Triphenylphosphine oxide
UV	Ultraviolet
Vis	Visible
VB	Valence band
XPS	X-ray photoelectron spectroscopy
XRD	X-ray crystallography

Content

Introduction 1
1 Motivation and Outline 5
2 Theoretical considerations 7
2.1 The concept of Flow (Photo-)Chemistry 7
2.1.1 Specific reactor surface area 7
2.1.2 Mixing efficiency and selectivity 7
2.1.3 Mass transfer and multiphase reactions 8
2.1.4 Residence time distribution and upsides of segmented flow 9
2.2 Principles of photochemistry 11
2.2.1 Light induced photochemical reactions without catalysts 15
2.2.2 Photosensitized and photoredox reactions using catalysts 16
2.2.3 Irradiation and radiation transport 18
2.2.3.1 Light sources 19
2.2.3.2 Materials and solvents 20
2.3 Reactor design for continuous photochemical applications 21
2.3.1 The Falling Film Micro Reactor 22
2.3.2 The Capillary Photoreactor 26
2.4 Embedding process analytical technology into Flow Chemistry applications 28
2.5 NMR-Spectroscopy for online quantification 31
2.5.1 Basic concepts of quantitative NMR-spectroscopy 31
2.5.2 Evaluation of online NMR-spectroscopy 36
2.5.3 NMR-spectroscopy in flow 37
3 Results and Discussions 39
3.1 Continuous synthesis of biphenyls by a photochemical arylation of arenes via diazonium trifluoroacetates and its quantification with online ^{19}F-NMR spectroscopy 39
3.1.1 Reactivity of arene diazonium salts 40
3.1.1.1 General reactivity and stability of diazonium salts 40
3.1.1.2 Preparation of diazonium salts 44
3.1.1.3 Possibilities of visible light photoredox arylation reactions 45
3.1.2 Biphenyl synthesis using heterogeneous photocatalysts in versatile reactor concepts 48
3.1.2.1 Catalyst evaluation 48
3.1.2.2 Heterogeneous photocatalytic arylation in a Falling Film Microreactor 50
3.1.2.3 Heterogeneous photocatalytic arylation in a capillary photoreactor 60
3.1.2.4 Conclusions 74

3.1.3 Catalyst-free photochemical direct C-H arylation in a capillary photoreactor using arene diazonium trifluoroacetates and its process optimization 75
3.1.3.1 Influence of temperature 76
3.1.3.2 Influence of light.....77
3.1.3.3 Influence of trifluoroacetic acid 78
3.1.3.4 Influence of pressure and process intensification.....82
3.1.3.5 Classification of the catalyst-free C-H arylation using arene diazonium trifluoroacetates in context to published literature.....84
3.1.3.6 Conclusions.....88
3.1.4 ^{19}F-NMR spectroscopy for online quantification of continuous photo arylation synthesis.....89
3.1.4.1 Spectra evaluation via standard integration methods 93
3.1.4.2 Spectra evaluation via chemometrics software.....94
3.1.5 Scope evaluation of photochemical arylation using arene diazonium trifluoroacetates.....100
3.1.5.1 Long-term continuous synthesis and quantification of selected examples..102
3.1.6 Studies on the mechanism of photochemical arylation using arene diazonium trifluoroacetates.....104
3.1.6.1 Synthesis and stability of 3-CF_3-phenyldiazonium trifluoroacetate 104
3.1.6.2 Charge-transfer photoarylation with arene diazonium trifluoroacetates...105
3.1.7 Conclusions and outlook 108
3.2 Development of a (semi-)automated continuous lab-plant and the integration of online spectroscopy for a two-step synthesis of Z-stilbene 110
3.2.1 Specification and design of a lab-plant considering physicochemical and technical challenges 112
3.2.1.1 Selection of components for a Wittig-olefination reaction 112
3.2.1.2 E-Z-photoisomerization of stilbene 115
3.2.1.3 Lab plant design and construction 117
3.2.2 Development of software and hardware components 119
3.2.3 Implementation of calibration and chemometrics into the software 131
3.2.3.1 Online NMR-spectroscopy 133
3.2.3.2 Online ATR-FTIR-spectroscopy 139
3.2.3.3 Online nondispersive IR-sensor.....145
3.2.4 Verification of the developed process analysis tools at the continuous two-step synthesis of *Z*-stilbene 150
3.2.4.1 Variation of temperature and flowrate as process parameters 152
3.2.4.2 Variation of LED light intensity as process parameter.....156

3.2.5 Conclusions and valuation of PAT in a continuous two-step synthesis of *Z*-stilbene 158
4 Experimental Section 161
4.1 General remarks 161
4.2 Continuous synthesis of biphenyls with a photochemical arylation of arenes via diazonium trifluoroacetates and its quantification with online ^{19}F-NMR spectroscopy 167
4.2.1 Biphenyl synthesis using heterogeneous photocatalysts in versatile reactor concepts 167
4.2.1.1 Synthesis of 3-CF_3-phenyldiazonium tetrafluoroborate 25 167
4.2.1.2 Synthesis of 4-chlorophenyldiazonium tetrafluoroborate 20 169
4.2.2.3 Catalyst investigation in batch for optimal synthesis of 26b 171
4.2.2.4 Explorative experiments with the falling film micro reactor 171
4.2.2.5 Optimization of 26b using heterogeneous photoarylation via different arene diazonium salts and wavelengths 172
4.2.2.6 Influence of anatase and light on a batch synthesis of 26b via in-situ generated arene diazonium trifluoroacetate 176
4.2.2.7 Iterative synthesis of 26b in a falling film micro reactor via a premixed reaction mixture 177
4.2.2.8 Synthesis of 26b in a semi-batch operated falling film micro reactor via an in-situ generated reaction mixture 178
4.2.2 Heterogeneous photocatalytic arylation in a capillary photoreactor 179
4.2.2.1 Batch screening reactions of 3-CF_3-biphenyl via diazo anhydrides 179
4.2.2.2 General procedure for preparation of a catalyst slurry 180
4.2.2.3 Experiments with a gas-liquid(-solid) SMBR concept via diazo anhydrides 180
4.2.2.4 Experiments with a (gas-)liquid-liquid-solid SMBR concept via diazonium trifluoroacetate in a premixed catalyst slurry 181
4.2.2.5 Experiments with a (gas-)liquid-liquid-solid SMBR concept via in-situ generated diazonium trifluoroacetate 183
4.2.3 Catalyst-free photochemical direct C-H arylation in a capillary photoreactor using arene diazonium trifluoroacetates and its process optimization 184
4.2.3.1 Standard working procedure for catalyst-free continuous synthesis of bi-(hetero-)arenes 184
4.2.3.2 Colorization experiments of in-situ diazo compound generation 191
4.2.3.3 Batch-synthesis of 26b via optimized parameters 191
4.2.3.4 Batch-synthesis of 26b using trimethylsilyl trifluoroacetate for diazotation 191
4.2.3.5 Standard procedure for experiments considering ^{19}F-NMR spectroscopy and scope evaluation 192
4.2.3.6 Long-term continuous synthesis and quantification of selected examples 234

4.2.3.7 Synthesis and isolation of 3-CF_3-phenyldiazonium trifluoroacetate 235
4.2.3.8 Studies on the mechanism of photochemical arylation using arene diazonium trifluoroacetates 236
4.2.3.9 Batch-synthesis of 3-CF_3-biphenyl to exclude a cationic mechanism 238
4.2.3.10 Stability and decomposition test of 3-CF_3-phenyldiazonium trifluoroacetate 239
4.3 Development of a (semi-)automatic continuous lab-plant and the integration of online spectroscopy for a two-step synthesis of *Z*-stilbene 239
4.3.1 Online UV/Vis-spectroscopy 239
4.3.2 Online ^{31}P-NMR spectroscopy 239
4.3.3 Online ^{1}H-NMR spectroscopy 240
4.3.3.1 Spectrometer calibration 240
4.3.4 Online IR-spectroscopy and liquid-liquid phase separation 240
4.3.4.1 IR-spectroscopy of toluene/methanol mixtures 241
4.3.4.2 Solvent extraction and phase-separation performance test 241
4.3.4.3 Substrate extraction and phase transfer experiments 242
4.3.4.4 IR-spectrometer calibration 242
4.3.5 Online nondispersive IR-sensor 243
4.3.5.1 Sensor calibration in acetonitrile 243
4.3.5.2 Sensor calibration in toluene/methanol 244
4.3.6 Continuous isomerization of E-stilbene and online analysis in MeCN 244
4.3.7 Stilbene synthesis in batch 244
4.3.8 Continuous stilbene synthesis and variation process parameters 245
4.3.9 Continuous stilbene synthesis and variation of light intensity in the photoisomerization process 246
5 Appendix 247
6 Literature 288

Introduction

Fine chemicals have gained increasing relevance in the academic and industrial community within the last decades. In contrast to basic- or bulk-chemicals, these are manufactured in much smaller scales (<1000 $t \times a^{-1}$). They are highly active materials and therefore being sold at a high price (>10 $\$ \times kg^{-1}$).[1]
In most cases, these chemicals have complex molecular structures including special functional groups and usually demanded a high purity grade. This often leads to extensive multi-step synthesis and cost-intensive purification.
Fine chemicals are divided into sub-groups for special chemicals in industry (e.g. surfactants, polymers, dyes, construction chemicals) and life science (e.g. agrochemicals, biopolymers, food and animal nutrition).[2,3]

In addition, active pharmaceutical ingredients (API) are classified as fine chemicals as well. Especially, those have come to the fore in politics, society and industry recently. The availability of APIs is expected to be ubiquitous, to provide an optimal health care and medical treatment - which in reality is not the case.
Most of the Top Ten manufacturers of fine chemicals like Lonza, Boehringer-Ingelheim, DSM, Merck, Sigma-Aldrich, BASF, Lanxess and Albemarle are located in the "Western world". Hence, it is hardly surprising that the biggest players (on sales) in API syntheses as Pfizer, Merck, GSK, Sanofi or Novartis are located in these regions.[3,4]
In 2020, the German association Pro Generika e.V. published a study about the origin of APIs. Their summary drastically outlines a major problem. 93 necessary APIs are not manufactured in Europe and over 60% of all permissions for API-syntheses are located in Asia and being distributed to a few companies only. In consequence, a supply reliability is not given at all time.[5]
Beside political motivation, economical purposes should be attractive to relocate production plants back to the "Western world". But, 50% of the manufacturing costs are caused by the plant itself and cannot be reduced without innovation in synthesis.[3]
Therefore, it is time to re-think existing knowledge. Applied science plays a key role and this thesis will contribute in improving chemical synthesis. The development of modern, sustainable processes in the sense of "Green Chemistry" does not impede tackling of the major challenges of our time, and safes costs as well.[6]

Flow Chemistry gains more and more relevance in comparison to the common batch chemistry. Flow Chemistry is as versatile as the synthesis of chemical substances itself.

Containers, pumps, mixers and reactors (thermal, photochemical or electrochemical) are connected to an overall system and the synthesis is performed continuously. Flow Chemistry considers both, the industrial/pilot scale (liters and tons per year) as well as the Microreactor Technology (MRT), where devices and components have a lateral dimension of <1 mm.[7] The biggest advantages of this miniaturization is the drastically increased surface-to-volume ratio in comparison to a batch mode synthesis performed in a flask or tank, leading to an optimized and faster mass- and energy transfer.[8]

Process intensification and high reproducibility are guaranteed while key parameters like temperature, residence time, electrical current or irradiation time/electrical current are precisely adjusted. The combination with a suited reactor will increase conversion and selectivity towards the favored product and (toxic) catalysts and other "boosters" are not necessary anymore. Atom efficiency is increased drastically as those additives are not present in the target molecule. This includes purification as well and leads to ecologically friendly processes and - more important - less waste.[9]

Mixing of sensitive reactants by filigree microreactors is possible and slow reactions (>30 min) can be operated safely.[10] This is especially important when using reactive intermediates (for example diazonium salts). Those tend to be explosives, when releasing gaseous nitrogen spontaneously during decomposition.[11,12,13] For safety reasons, it is essential to handle a minimal amount of the reactive material. With Flow Chemistry a low hold-up is feasible as those intermediates are generated *in-situ* and they are directly further processed without any isolation/purification.

Biphenyls are common and frequent motives in API synthesis. They are essential building blocks for pharmaceuticals, for example to treat diabetes type two (e.g. AMG837, see Figure 1) or being used as anticancer drugs. Generally, bio-receptors are stimulated or blocked by those materials.[14,15,16] They are likely modified with fluorine or trifluoromethyl groups, as they drastically increase the polarity of those molecules. A change in the lipophilicity/hydrophilicity balance is caused and an improved bio-availability is the consequence.[17] In 4-nitrobenzylthioinosine NBTI (Figure 1), an API for treatment of ischemic heart diseases and strokes, activity is increased by a factor of 25 when using a 3-CF_3-biphenyl substituent instead of an ethyl phenyl group.[18]
Eventually, this work contributes in the development of a modern biphenyl synthesis via phenyl diazonium salts in a direct photochemical C-C-coupling with arenes.

Stilbenes are another important motive in pharmaceutical applications. One of the most known representatives is Combretastatin A-4 (Figure 1), which is used as an anti-tumor drug. Hereby, studies highlighted the special role of the *Z*-isomers, as they show a higher activity instead of the *E*-isomer. In most stilbene syntheses, both diastereomers are obtained and therefore (photo-)isomerization has to be applied to yield the favored product. Such reactions are excellent processes to be realized in continuous flow.[19–21]

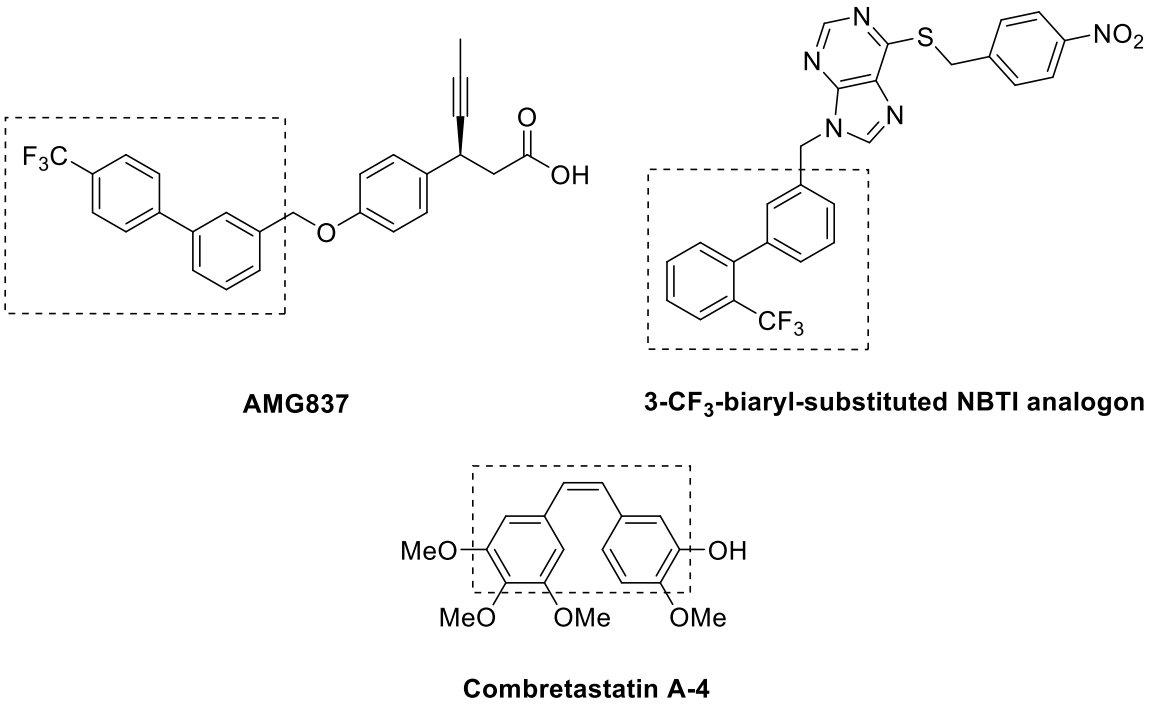

Figure 1: Trifluoromethyl biphenyls and *Z*-stilbenes are common motives in APIs.[14,18,19]

Fast forward optimization of a reaction or retrosynthesis to plan new synthetic routes of fine chemicals is enhanced by online and simultaneously provided information about concentrations and synthesized substance amounts. This requires the development of matching sensors for process analytical technology (e.g. NMR-, IR-, UV/Vis-spectroscopy) in flow. All this is completed by the integration of artificial intelligence and machine learning which easily establish connections and dependencies in data.[22,23–25]

1 Motivation and Outline

This thesis is divided into two parts, which both address continuous synthesis of fine chemicals.

The first topic presents new pathways in the synthesis of biphenyls. Classically, a Suzuki reaction or other transition metal-catalyzed cross coupling reactions are applied, but complex (noble-)metal catalysts, boronic acid precursors or special microwave reactors are required.[16,26,27] A less complex route will be realized by a photochemical approach supported by the amplifying properties of a continuous process.

Here, arene diazonium compounds are irradiated with a suitable wavelength followed by the release of nitrogen. An intermediate (usually a cation or a free radical) is generated, which subsequently undergoes a direct C-H arylation of a second arene forming biphenyls. So far, specific productivities >0.1 $mol \times L^{-1} \times h^{-1}$ of biphenyls are only obtained by high energy irradiation using a wavelength of ~300 nm, but this approach results in low selectivity. Besides, bi(hetero)arene production is significantly easier to realize when using blue light of the visible spectrum.[28–31]

With the development of a new synthetic route for derivatives of *meta*-(trifluoromethyl)biphenyl, the usefulness and effectivity of common photocatalysts such as titanium(IV) oxide or eosin Y are discussed. A continuous catalyst-free direct C-H photoarylation is developed, using *meta*-(trifluoromethyl)biphenyl as a benchmark molecule. After successful optimization, the protocol will be transferred to its derivatives. Long-term online NMR spectroscopy will be used to monitor high reproducibility over several hours.

The second topic is about the design and development of a (semi-)automated computer assisted and continuously operated chemical process. Such a setup, with many different hardware components, is a crucial fundament for automated (self-)optimization procedures. Therefore, the software must be programmed in such way, that optimization, performed by artificial intelligence, can be integrated at any time. Process monitoring requires permanent data collection by various online process analysis technologies (PAT).

A two-step synthesis process for selective production of *Z*-stilbene, including a Wittig reaction[32] and a *E*-*Z*-photoisomerization[21] is a useful model-reaction to improve hardware and software of a computer assisted process. Different PAT-modules as NMR-, IR-, UV-spectroscopy and an IR-sensor are tested. Successful integration of these requires

detailed knowledge and expertise of the chemical process itself and the fundamentals of each analysis tool. This is shown by a systematical series of validating experiments.

2 Theoretical considerations

2.1 The concept of Flow (Photo-)Chemistry

2.1.1 Specific reactor surface area

Research facilities and industry tend to have high (cost) efficient processes, where chemical starting materials are used with the highest outcome. In this context, terms like process intensification and miniaturization have been developed using Flow Chemistry applications and microreactor technology in small dimensions. By miniaturization of all components a drastically increased surface-to-volume ratio is achieved. The specific reactor surface area A_{sp} is calculated by the reactor surface area A (contact area to the respective medium) divided by the volume V of the medium.

$$A_{sp} = \frac{A}{V} \tag{1}$$

A 100 mL round bottom flask, typically used for batch reactions, usually has a specific surface of ~100 $m^2 \times m^{-3}$, whereas specific surface areas of ~20000-50000 $m^2 \times m^{-3}$ are rapidly accessible when using microreactor concepts.[33]

2.1.2 Mixing efficiency and selectivity

In standard batch laboratory glassware setups mixing efficiency depends on many factors as kinematic viscosity η, diffusivity D, reactor volume V, energy dissipation or stirring intensity.[34]

In microstructured reactors, flow patterns are precisely described or manipulated by technical facilities (e.g. mixers, slits, deflectors). In most cases, hydrodynamics appear as a laminar, directed and symmetric flow. Reynold numbers between 1 and 1000 are the consequence and may only vary due to flow velocity and capillary dimensions. In this regime, turbulences are absent and large capillary dimensions or low flowrates will reduce secondary flow (eddy characteristic) further. Therefore, mixing inside a microchannel is only driven by molecular diffusion D described by the Einstein-Smoluchowski equation:[33,35]

$$D = \frac{k_B T}{6\pi \eta r_m} \text{ and } t_m = \frac{L^2}{D} \tag{2}$$

Molecular diffusivity D is usually around 10^{-5}-10^{-6} $cm^2 \times s^{-1}$ in standard solvents. According to equation (2), mixing time t_m is short, due to a small (diffusion) path length L in microreactors. Reactions with a high energy dissipation rate benefit from the mentioned factors, as components are mixed at a macro- and micro-scale. Molecular concentration gradients and temperature hot spots are avoided, side reactions are reduced and selectivity is increased.
Usually, high concentration and temperature gradients can be observed in batch reactions and hence diluted systems, or lowered temperatures T must be applied to overcome those issues. This procedure is contrary to the mentioned Einstein-Smoluchowski equation.[36,37]

In photochemical applications insufficient heat transfer or "high" temperature caused by waste heat of light sources influences selectivity, additionally. High-energetic UV-lamps or UV-LEDs are a source for thermal energy and side-reactions via a thermal route are promoted.[38,39]

2.1.3 Mass transfer and multiphase reactions

A drastically increased surface-to-volume ratio in Flow Chemistry applications is perfect for multiphase reactions. Those are either two-phase (e.g. solid-liquid, liquid-liquid, liquid-gas, solid-gas) or even three-phase systems and mass transfer from one to another phase is usually the rate determining step. With a high specific surface area a large interfacial area is created.[34]
Mass transfer is an essential contribution, which is exemplarily described by a photosensitized multiphase oxygenation reaction. First, oxygen has to perform a transfer from the gaseous phase into the liquid phase. In a subsequent step, singlet oxygen is generated by means of a photosensitizer in the organic liquid phase and finally this singlet oxygen is able to undergo the oxygenation reaction.[40]
In a standard batch reaction, a uniform oxygen distribution can be hardly realized and will lead to a lowered overall kinetic in combination with insufficient irradiation of the liquid phase.

2.1.4 Residence time distribution and upsides of segmented flow

In a standard batch synthesis, the reaction time of a chemical synthesis is defined as the period between the addition of the substrates to the reaction flask and the introduced termination of the chemical reaction. The latter can either be a quenching step, extraction or the removal of heat.

However, in microreactors a designated starting point of the reaction cannot be clearly identified due to the continuous flow conditions and the permanent addition of "fresh" substrates. Therefore, reaction time is replaced by the residence time t_{R}, defined by the volume V in the reactor and the volumetric flow rate of the fluid $\dot{V}$.

$$t_{\mathrm{R}} = \frac{V}{\dot{V}} \tag{3}$$

Modulation of a defined residence time without dispersion is not possible in a homogeneous single-phase fluid, as laminar flow will cause a velocity profile in the channel resulting in a parabolic shape (Hagen-Poiseuille distribution). Moreover, residence time distribution is additionally broadened by axial and radial diffusion of the molecules.[41,42]

Residence time distribution is reduced to a minimum, when a homogeneous flow is compiled into a segmented flow by the introducing a second, immiscible fluid (Figure 2). Examples for this heterogeneous flow pattern are slug- (gas-liquid) or plug-flows (liquid-liquid). Each dispersed phase can be seen as single enclosed reactor when complete encapsulation by the continuous phase occurs. A serial micro batch reactor system (SMBR) is created and shear forces between the phases lead to a circulation inside the droplets. This induced axial diffusion enhances mixing, beside the already present diffusion processes for mass- and heat transfer.[37,42,43]

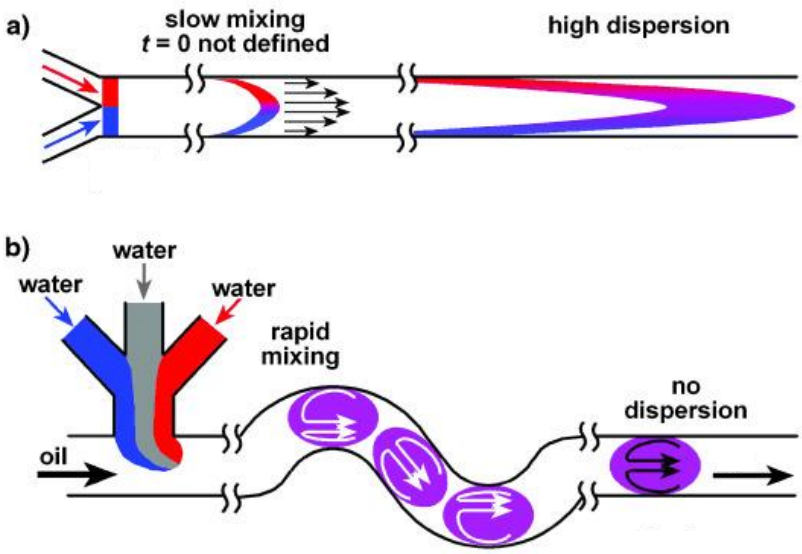

Figure 2: Mixing and residence time distribution of two fluidic media (red and blue) in a capillary tube using different flow pattern: **a)** a homogeneous flow with a parabolic shape leads to a high dispersion of the residence time and slow mixing; **b)** a heterogeneous plug flow pattern using oil as continuous phase leads to a SMBR concept. Shear forces enhance mixing inside the droplets and residence time distribution is minimized by the plug flow. Adapted with permission from Ref. [42] copyright 2003 Wiley-VCH.

The SMBR concept is used for photochemical flow applications, wherever heterogeneous photocatalysts cannot be immobilized onto a capillary wall. The solid catalyst has to be pumped through the small reactor channels, beside a liquid (and a gas) phase. As a consequence, a high risk of catalyst deposition or agglomeration appears, which causes an "inhomogeneous" and unreproducible process stream. Finally, clogging inside the reactor can occur, preventing a reliable technical realization.[9,43–45] Pieber *et al*. elude this problem by setting up a SMBR concept (Figure 3 b) with nitrogen as gaseous continuous phase and a mixture of acetonitrile and water as liquid phase. The high interfacial forces between the two phases lead to a well-defined segmented pattern, being necessary for a stable solid transport inside the capillary. In this approach graphitic carbon nitride (CMB–C_3N_4), as the heterogeneous photocatalyst, is provided by a suspension in a viscous ionic liquid ([Bmim]BF_4). The setup is used for a decarboxylative fluorination of phenoxyacetic acid using SelectFluor. Those substrates are previously added to the liquid phase. The catalyst suspension is added via a T-junction into the liquid phase of the slug flow. The segmented flow is finally irradiated with LED-stripes (420 nm, 12 W). Within 14 minutes the decarboxylative fluorination leads to 94% yield. Generated CO_2 diffuses into the nitrogen slugs and the solid-liquid SMBR remains perfectly stable.[43]

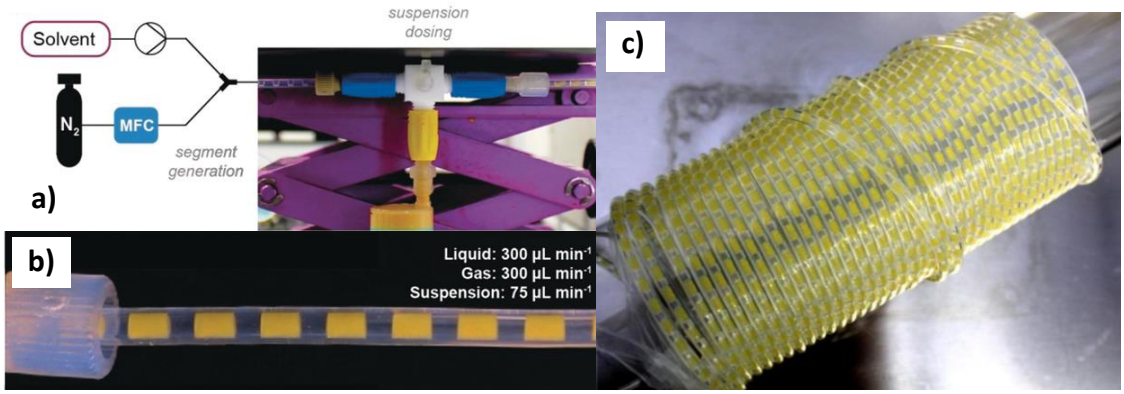

Figure 3: a) Setup used by Pieber *et al.* for elaboration of a three-phase SMBR concept; **b)** Slug flow with nitrogen as gaseous continuous phase and solid CMB-C_3N_4 photocatalyst in the liquid phase; **c)** SMBR concept in the steady state. Every plug acts as a single enclosed reactor. Adapted with permission from Ref. [43] copyright 2018 Wiley-VCH.

The mentioned method is a stable and reliable routine for the application of solid photocatalysts in capillaries and many substrates or catalysts can be used herein.

As an alternative, a heterogeneous photocatalyst can be immobilized onto the transparent capillary wall of the reactor. The reaction requires either irradiation from the front (via the liquid phase) or the back of the photocatalyst (via the capillary wall). Main disadvantages are the realization of a homogeneously immobilized catalyst (can be unique for each single catalyst) and the reduced quantum efficiency, when shining light from the backside onto the catalyst (no direct interaction of light, solid catalyst and liquid phase).[46–48]

2.2 Principles of photochemistry

Every photochemical reaction intrinsically depends on irradiation with light in the UV- (200 - 400 nm) or Vis- (400 - 700 nm) range. Those two regions are only a small part of the available spectrum. Light can be interpreted as an electromagnetic wave (Figure 4) and its frequency v is calculated by its wavelength λ and the velocity of propagation c_0 (~3.00×10^8 m×s^{-1} in the vacuum).[49]

$$v = \frac{c_0}{\lambda} \tag{4}$$

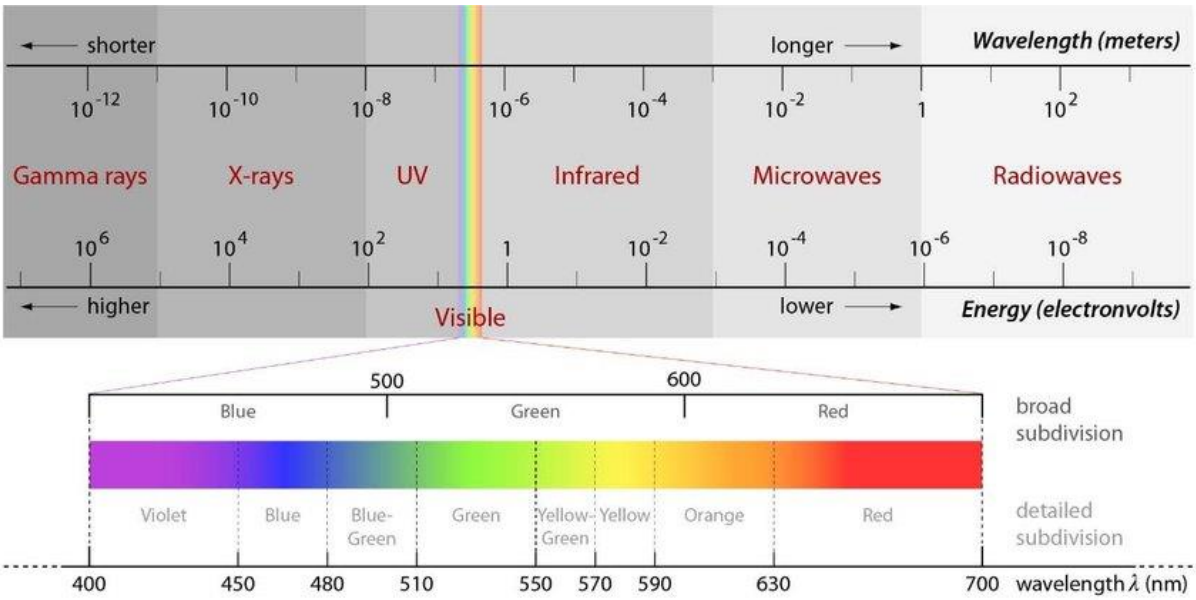

Figure 4: The electromagnetic spectrum with special focus on the UV/Vis-subdivision. Adapted with permission from Ref. [49] 2017; by Geert Julien Verhoeven licensed under CC-BY-4.0.

Energy transfer between radiation and matter precedes quantized and a distinct amount is required for every transition. Eventually, Albert Einstein was able to prove that an energy transfer of electromagnetic radiation on electrons occurs by quantized photons, whose energy E_{Photon} is calculated with the Planck constant h.[50,51]

$$E_{\text{Photon}} = hv = h \times \frac{c_0}{\lambda} \tag{5}$$

Following the first law of Photochemistry (Grotthuss-Draper Law) electromagnetic radiation will result in a photochemical process only, if absorbed by matter. Usually the electric field of the electromagnetic wave is responsible for the energy transfer onto an electron, which is transferred into an excited state at a higher energy level.[52]

A Jablonski diagram visualizes the different (excited) states of an electron and its processes after photon energy absorption. The electronic ground state is called S_0 (singlet state, see Figure 5). Every electronic state has several vibrational states (thin black energy level in Figure 5). The molecule/electron can either loose its additional energy by non-radiative processes - internal conversion - producing (vibrational) heat energy or by emitting a photon via fluorescence or phosphorescence. The latter requires a preliminary change (intersystem crossing) into a triplet state T_1 with a change of multiplicity (spin flip of the electron).[53,54,55]

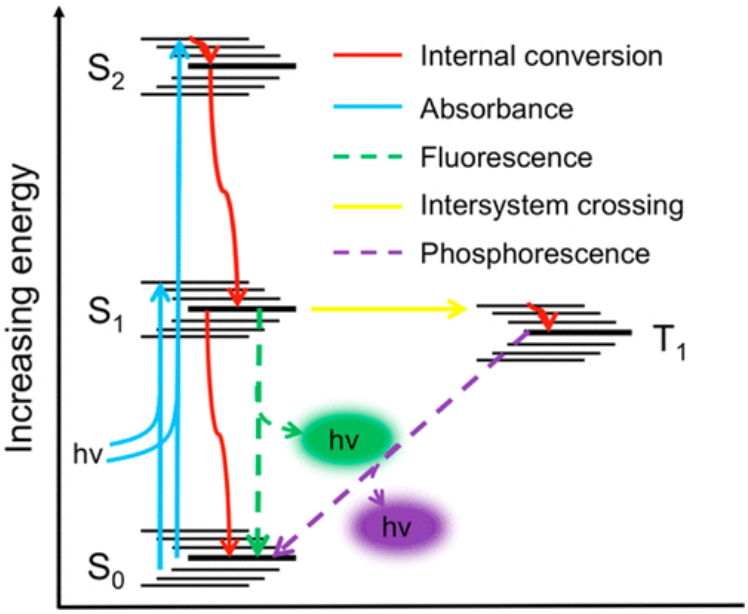

Figure 5: Schematic Jablonski diagram with all important electronic and vibrational states and processes for energy absorption and emission. Adapted with permission from Ref. [55] copyright 2016 American Chemical Society.

A molecule absorption spectrum is recorded by UV/Vis-spectroscopy and the energy, absorbed by that molecule, is visualized. Different electronic transitions (bands) are classified with the help of the participating molecular orbitals. Usually, electrons form occupied σ-, π- or n-orbitals are transferred into the empty σ*- or π*-orbitals (Figure 6a). Hence, the required energy for a transition is proportional to the distance between the different energetic levels. In consequence, this circumstance can be used to address a favored transition by choosing the correct wavelength of a light source, if more than one band is present in the spectrum.[56]

Molecular orbitals are assigned to specific functional groups, called chromophores, within the molecular structure. The actual required energy of an electron-transition is drastically depending on steric, inductive or mesomeric effects, as chromophores may appear in conjugated systems. A selection of chromophores with approximated absorption wavelength and the characteristic electronic transition is listed in Table 1. Not all transitions are allowed and therefore transition probability is expressed by the molar extinction coefficient ε_λ. The extinction coefficients may vary, depending on the solvent and surrounding matrix (Figure 6b).[56]

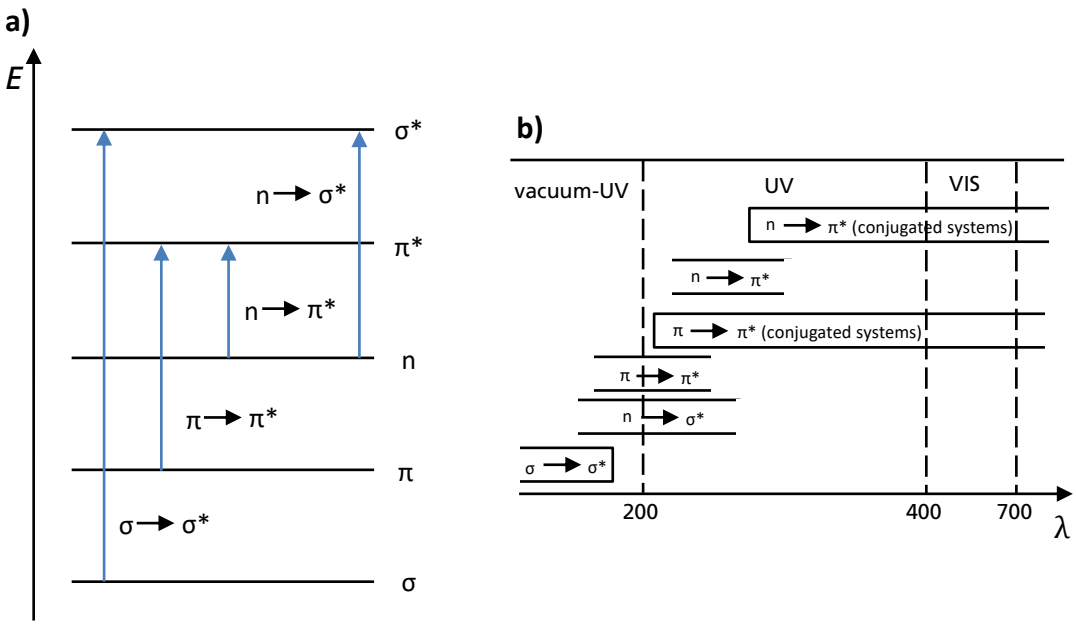

Figure 6: a) Molecular orbitals and electron transitions; **b)** Absorption regions of different electron transitions.[56]

Table 1: Selection of absorption bands from isolated chromophores.[56]

chromophore	transition	example	λ_{max} [nm]ᵃ	ε_{max} [nm]ᵃ
C−H	σ-σ*	CH_4	122	intensive
>O<	n-σ*	CH_3-OH	183	200
—N—	n-σ*	$(H_5C_2)_3N$	213	2170
>C=C<	π-π*	$CH_2=CH_2$	165	16000
—C≡C—	π-π*	H−C≡C−C_2H_5	172	2500
>=O	π-π*	H_3C−C(=O)−CH_3	187	950
	n-π*		273	14
—N=N—	n-π*	H_3C−N=N−CH_3	347	15
—N=O	n-π*	$(CH_3)_3C$−N=O	300	100
			665	20
—NO_2		H_3C−NO_2	210	10000
			278	10

a: λ_{max} and ε_{max} vary depending on the solvent.

2.2.1 Light induced photochemical reactions without catalysts

Direct homolytic cleavage of a covalent bond between two atoms is one method to initiate a photochemical reaction. If no photocatalyst is used, direct irradiation of the sample is inevitable to perform these processes. Common and probably most used reactions are [2+2]-cycloadditions,[57] photocyclizations,[58] photoisomerizations,[21] photochlorinations[59] or photobrominations.[60] Due to the use of the high-energetic light, electrons of other chromophores will undergo unspecific excitation as well, leading to the initialization of other side reactions.

A very common reaction is shown to illustrate the basic concept of a photochemical reaction: Oxetanes are synthesized via a Paternò-Büchi reaction by a carbonyl compound and an alkene. Irradiation ≥280 nm leads to an n-π* transition of the carbonyl-group in the first step. Different mechanisms appear, when either electron-rich or electron-poor alkenes are used (Scheme 1). A triplet electron will interact with the HOMO (highest occupied molecular orbital) of an electron-rich alkene. However, electron-poor alkenes will form a new σ-bond via its LUMO (lowest occupied molecular orbital) using a singlet electron of the carbonyl-compound. A subsequent intersystem crossing is necessary to allow ring-closure in the first case, as a triplet biradical has to be formed at all times.[54,57]

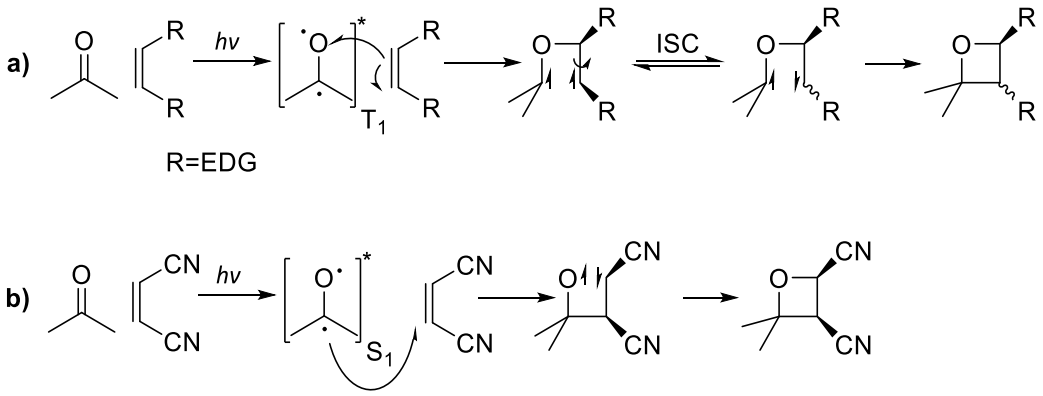

Scheme 1: Mechanism of a Paternò-Büchi reaction using **a)** electron-rich and **b)** electron-poor alkenes.[54]

2.2.2 Photosensitized and photoredox reactions using catalysts

Photocatalysis is a convenient alternative to perform photochemical reactions under mild and much more selective conditions. Less-energetic visible-light is used, which reduces unwanted side-reactions.[61,62] A photocatalyst (PC) can be used to collect and transfer photon energy onto the organic substrates, which is called a photosensitized reaction. Here, the PC is excited from its ground state S_0 into the first excited state S_1. Via a subsequent intersystem crossing, a triplet electron is provided by the PC. The energy transfer E_{T}, which is nearly isoenergetic, leads to the excitation of the acceptor molecule. This process basically happens via a Dexter-type energy transfer.
While the triplet electron loses its energy and relaxes back into the ground state S_0, an electron of the acceptor molecule gains energy at T_1 state (Figure 7b). This process is feasible as long as the triplet energy of the photosensitizer is higher than that of the organic substrate. Furthermore, the sensitizer should have a high intersystem crossing rate, to populate many T_1 states for a high quantum yield.[63]

A lot of photocatalyzed reactions require a single-electron transfer (SET) between the catalyst and the substrate. This process can be either realized via an oxidative (${E_{1/2}}^{M^+/M^*}$) or reductive (${E_{1/2}}^{M^*/M^-}$) quenching of the catalyst. In both cases, the PC is initially exited via visible-light irradiation into the triplet state T_1. Now, the excited catalyst molecule is an even stronger oxidant/reductant in comparison to its ground state and an electron can be added to or removed from the substrate molecule, creating radicals or radical-ion species (Figure 7a).[63]

In photoredox catalysis it is crucial to have knowledge about the properties of the excited PC as well as the organic substrates. For example, different transition-metal complexes (mostly based on ruthenium or iridium),[64] organic dyes (e.g. Rose Bengal or eosin Y)[65] or inorganic semiconductors like TiO_2, ZnO or Bi_2O_3[31,66,67] are used. By choosing the correct photocatalyst, the energy level of the ground and excited state can be precisely adjusted (Figure 8).

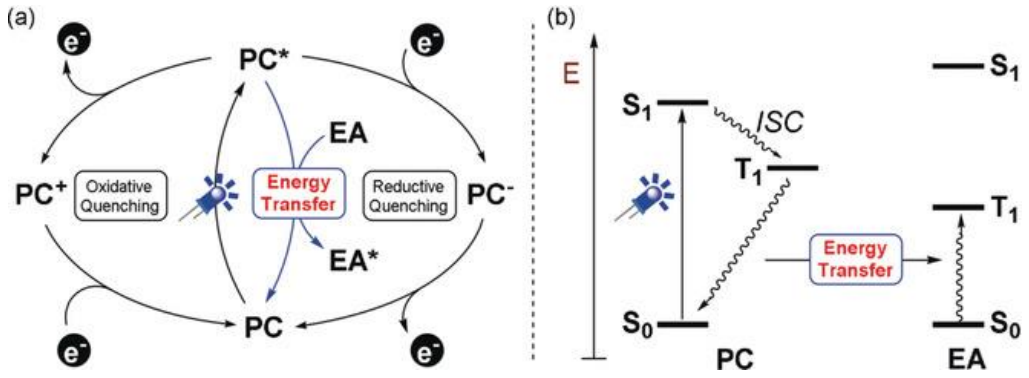

Figure 7: a) Processes of a photocatalyst PC after excitation: reductive quenching, oxidative quenching, energy transfer; **b)** Process during a photosensitized energy transfer. Adapted with permission from Ref. [63] copyright 2019 Wiley-VCH.

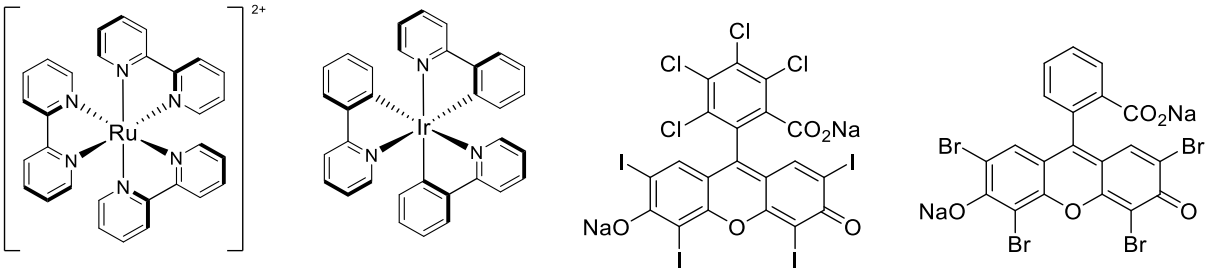

$[Ru(bpy)_3]^{2+}$	*fac*-$Ir(ppy)_3$	Rose Bengal	Eosin Y
$E_{1/2}^{M^+/M^*}$ (vs SCE) = -0.81 V	$E_{1/2}^{M^+/M^*}$ (vs SCE) = -1.73 V	$E_{1/2}^{M^+/M^*}$ (vs SCE) = -1.33 V	$E_{1/2}^{M^+/M^*}$ (vs SCE) = -1.58 V
$E_{1/2}^{M^*/M^-}$ (vs SCE) = +0.77 V	$E_{1/2}^{M^*/M^-}$ (vs SCE) = +0.31 V	$E_{1/2}^{M^*/M^-}$ (vs SCE) = +1.18 V	$E_{1/2}^{M^*/M^-}$ (vs SCE) = +1.23 V
E_T = 46.5 kcal/mol	E_T = 57.8 kcal/mol		
λ_{max} = 452 nm	λ_{max} = 375 nm	λ_{max} = 549 nm	λ_{max} = 520 nm

TiO_2 (anatase)	TiO_2 (rutile)
E_{VB}(vs $NHE_{pH\,0}$) = +2.95 V	E_{VB}(vs $NHE_{pH\,0}$) = +2.92 V
E_{CB}(vs $NHE_{pH\,0}$) = -0.18 V	E_{CB}(vs $NHE_{pH\,0}$) = -0.07 V
ΔE = +3.2 eV	ΔE = +3.0 eV
λ = 385 nm	λ = 413 nm

Figure 8: Prominent metal-complexes, organic dyes and heterogeneous metal oxides and their specific photocatalytic characteristics.[64,65,68]

2.2.3 Irradiation and radiation transport

Photochemical reactions benefit from photoreactors with small dimensions and take advantage from their increased specific reactor surface area, allowing better and precise interactions of photons with the molecules.

Radiation transport in an (optimal) microreactor setup is always accompanied by absorption, out-scattering, in-scattering and emission. Absorption is caused by all molecules being present in a solution. These are either the reactants, the catalyst or the solvent itself. Emission of radiation by the reaction mixture can be neglected at low or mild temperatures, typically used in those photoreactions. Out-scattering and in-scattering of light are absent in a homogeneous solution. The intensity of (monochromatic) light will stay constant, if light propagation will proceed only in one direction.

In (real) microreactor setups light propagation and the photon flux ϕ (number of photons n_{photon} reaching the reactant per unit area A and unit time t) are determined by the reactor geometries and compontents.[34,38,69]

$$\phi = \frac{n_{\text{photon}}}{A \times t} \tag{6}$$

The reactor components can cause additional absorption, scattering, reflection or reflection especially when reactors with non-linear radiation pathways are used (Figure *9*).

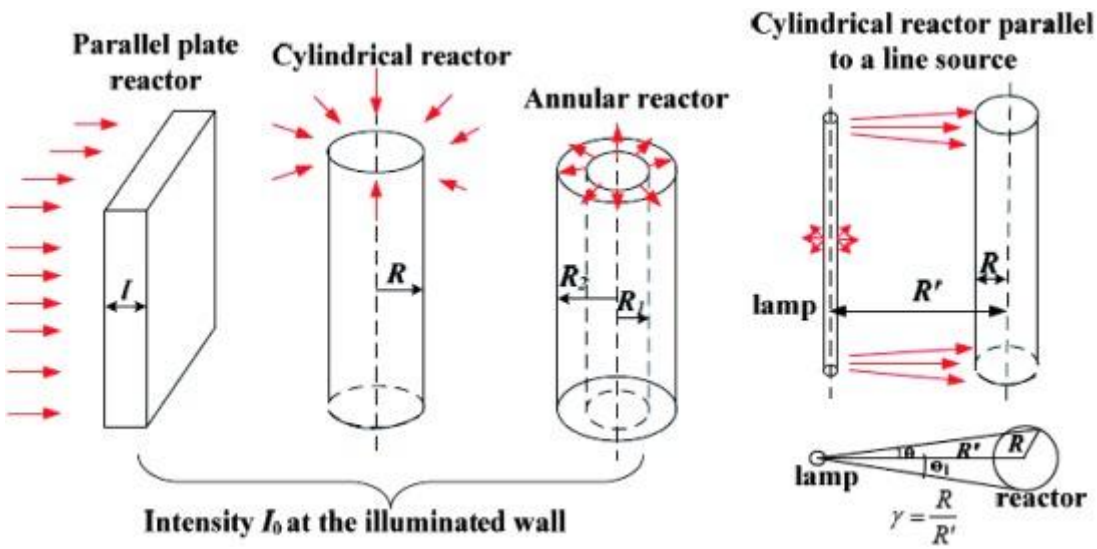

Figure 9: Samples of reactor geometries with simplified treatments of light sources. Adapted with permission from Ref. [34] copyright 2014 Wiley-VCH.

An efficient and homogeneous distribution of the radiation is crucial for an effective application of the photons in a chemical reaction. The quantum yield or quantum efficiency QE_λ (both is often used with identical meaning[70]) is eventually used to describe the number of molecules n_P being converted by the number of absorbed photons:[34,70]

$$QE_\lambda = \frac{n_\mathrm{P}}{n_\mathrm{Ph}} \tag{7}$$

Photon absorption intrinsically depends on the molar excitation coefficient ε_λ (wavelength depended) which exists for all present substances in a system. Together with the molar concentration c of the species and the path length d, the well-known Beer-Lambert-Law is obtained:[71]

$$\mathrm{A}_\lambda = \log_{10}\left(\frac{I_0}{I}\right) = \varepsilon_\lambda \cdot c \cdot d \tag{8}$$

with I_0 and I being the light intensity before and behind the sample. The absorbance A_λ or "optical density" of the species at a given wavelength represents the transmissibility and the ability of radiant propagation in the media along the path length. In consequence, most photons are absorbed by the first few "layers" of the reactant close to the light source and intensity will decrease exponentially. The mentioned photon flux has an additional effect on the photochemical reaction. Photon flux will be large for a small microreactor volume and decreases for bulk- or batch-applications (at constant power/intensity of the light source), simply by changing the dimensions. With respect to the Beer-Lambert-Law this problem can be hardly compensated with a higher photon intensity.[34]

Eventually, the mentioned assumptions are only valid for the physicochemical absorption of photons without any consecutive reaction and have to be applied on diluted, homogeneous (lateral and axial) solutions along the micro reactor.[72]

2.2.3.1 Light sources

Best performance of a photochemical or photocatalyzed reaction is achieved, if the correct wavelength is chosen (Figure 10). It is crucial that the emission spectrum of the radiation source and the absorption spectrum of the substrate or catalyst have a correct overlap. In the past, low or medium pressure lamps were commonly used to introduce UV-light into an application.[51,73] CFL bulbs emit in the region of blue, green and

orange/red light.[28] Those lamps require additional filters, if a single wavelength has to be used.[28,51,74]

Due to the ongoing development of efficient and inexpensive light emitting diodes (LEDs), more and more downsides appeared with the old "light bulb" technique. High cost, low energy efficiency, and mostly improper dimensions cause difficulties when bringing the photons into the medium.[38] Nowadays, LEDs easily emit light in the visible spectrum from 360-700 nm.[75] Latest developments provide light irradiation even in the UV-C regime (e.g. Nichia NCSU434A (280 nm)[76]).

One major advantage is the ability to select a very narrow emission band, which reduces side-reactions immensely. Furthermore, they efficiently convert electrical power into light, while showing long lifetimes. LEDs show further advantages, as they can be easily switched on and off within short intervals. So they can be used for "pulsed" operations or dimming as well. This pulsed mode is rather new, as pressure lamps would easily burn out.[51,77]

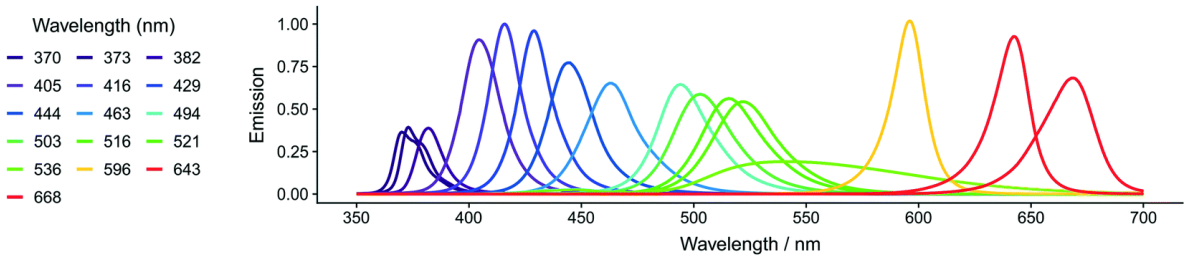

Figure 10: Emission spectra of different LED-arrays (selection). Adapted with permission from Ref. [75] copyright 2019 Royal Society of Chemistry.

2.2.3.2 Materials and solvents

The design and development of a photochemical reactor has to consider an adequate transparency of the materials and solvents being used in a reaction. In comparison to thermal reactions not every material (e.g. stainless steel or PEEK) is suited as those cover the reactor from being irradiated or filter a certain wavelength. Identical behavior is detected for all solvents. When choosing a solvent, the correct polarity for the reaction should be considered and photochemical quenching has to be avoided. A list of materials for photoreactor-manufacturing and the characteristic cut-off wavelength for a selection of common solvents is given in Table 2.[34,78]

Table 2: Cut-off wavelengths of materials and solvents used in photochemical applications.

material	cut-off wavelength [nm]		solvent[34]	cut-off wavelength [nm][e]
optical glass[78]	360[a]		water	185
borosilicate glass[78]	330[a]		acetonitrile	190
special optical glass[78]	320[a]		ethanol	204
quartz glass[78]	260[a]		cyclohexane	215
PMMA[79]	315[b]		acetone	330
PFA[80]	350[c]		benzene	280
FEP[81]	330[d]		toluene	285
			DMSO	268

a: >80% transmission @ 2.5 mm thickness; **b**: >80% transmission @ 3 mm thickness; **c**: ~80% transmission @ 125-200 µm thickness; **d**: 80.4% transmission @ 250 µm thickness; **e**: 10% transmission @ 10 mm path length.

Reactors and capillaries made from special glass are usually individual devices, which make them expensive. High pressure and temperature can be challenging, as this material is too fragile.[44,82]

A very high number of photoreactors is made from polymer-based materials, as those polymers are cheap and easy to handle. Most concepts for continuous (photo-)flow reactions use fluorinated polymer capillaries. They are available in a satisfactory length and various cross sections can be chosen to provide optimal film thickness and residence time for the photochemical reaction. FEP is one of the best materials to build up capillary photoreactors, due to its high transparency, offering a low cut-off wavelength, being resistant against most chemicals and tolerating high pressures and temperatures.[38,83]

2.3 Reactor design for continuous photochemical applications

Nearly every reactor concept and shape can be realized with subtractive and additive manufacturing techniques. Classic subtractive methods like milling, turning or drilling (to give an incomplete list) are used to (mass) produce reactors and parts of it easily and budget-friendly. Additive manufacturing, like 3D-printing of (transparent) polymers, is an alternative to produce very complicated reactors, substructures or inlays even in dimensions of millimeters. Additionally, this process can be used to print holders for LED-arrays or brackets to assist reactor assembly.[84]

Companies like Peschl Ultraviolet GmbH, Creaflow B.V., Syrris Ltd., Vapourtec Ltd., ThalesNano Inc. or Corning S.A.S even offer commercially available photoreactors.

In the following chapters, two reactor concepts are presented, which are developed and manufactured by Fraunhofer IMM (formerly IMM - Institut für Mikrotechnik Mainz GmbH) and used in this thesis.

2.3.1 The Falling Film Micro Reactor

The falling film micro reactor (FFMR) was initially developed for an efficient solvent removal of diluted mixtures or to conduct highly exothermic reactions safely. Whenever a massive heat transfer for thermal physicochemical processes is required, a FFMR is a suitable and perfect device providing a specific interface of 20,000 $m^2 \times m^{-3}$. A falling film is realized by a liquid stream, which vertically spreads over a reaction plate mainly by gravity (Figure 11). By combination of interfacial forces of the reaction plate surface, flow rate and viscosity of the liquid, thin films of a few tens of micrometer can be formed.[85,86]

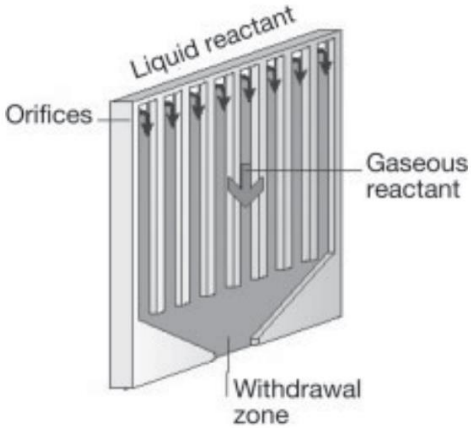

Figure 11: Basic principle of the falling film micro reactor FFMR. Adapted with permission from Ref. [87] copyright 2006 Wiley-VCH.

The liquid enters the FFMR via a lateral bore and contacts the reaction plate at the back. A slit allows crossing of the liquid in order to contact the parallel microchannels at the front. This principle guarantees a homogeneous distribution of the liquid over all microchannels. The liquid leaves the plate via a second slit at the bottom. Additionally, connectors for gases are provided. The large gas chamber can be filled with reactive or inert gases either in co-flow or counter-flow direction. Different reactor plates are offered to adapt the reactor for a specific reaction (see Table 3).[85]

The front of the FFMR is equipped with a multipurpose quartz glass window. It can be either used for inspection a constant distribution of the thin film or used to allow photochemical reactions (Figure 12). So far, photochlorinations of aromatic isocyanates,[88] cycloadditions of singlet oxygen into cyclopentadiene[89] and cycloaddition of singlet oxygen into 1,5-dihydroxynaphthalene for the synthesis of juglone[90] are remarkable examples for continuous flow applications. Either large lamps or a LED-array mounted on aluminum plates for optimal heat dissipation can be used.

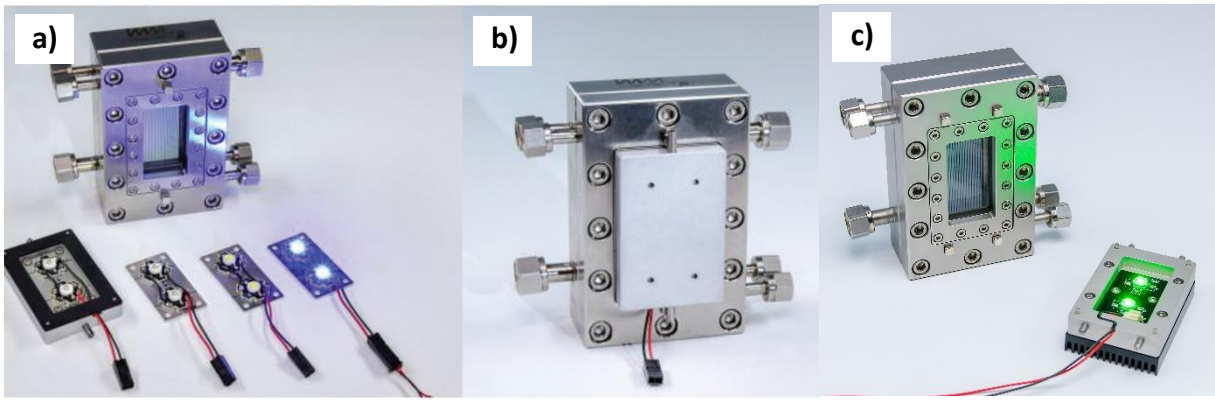

Figure 12: a) FFMR as the key element of the lab plant with a royal blue LED-array in an aluminum heat exchanger **b)** magnetically fixed to the top plate of the microreactor. Adapted with permission from Ref. [31] copyright 2017 Royal Society of Chemistry; **c)** Different LED-arrays are available (©Fraunhofer IMM).

A catalyst immobilization procedure, presented by Zapf *et al.*, allows effective heterogeneous photocatalysis in those microchannels. A wide range of solid metal oxides can be immobilized by preparation of a metal oxide, poly-(vinyl alcohol) wash coat, which is calcinated afterwards. TEM, SEM and XRD measurement showed constant surface quality of the used nanoparticle despite this rough treatment (Figure 13).[31,91]

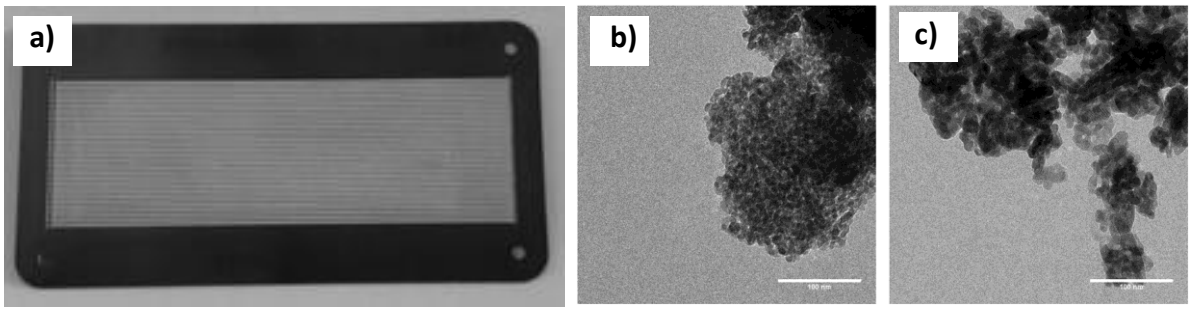

Figure 13: a) FFMR reaction plate with TiO2 immobilized in 32 microchannels; TEM images of TiO_2 particles before **b)** and after **c)** calcination at 450 °C (length scale: 100 nm). Adapted with permission from Ref. [31] copyright 2017 Royal Society of Chemistry.

Falling film micro reactors are scalable in their size. This allows an easy scale-up and numbering-up of the process within a single reactor, as essential characteristics keep constant. For this purpose, the FFMR-LARGE (Figure 14) is introduced having an optimized film distribution. Thin films <100 µm scalability guarantee a constant specific interface, while volumes of up 1.2 $L \times h^{-1}$ can be handled.[86] Even this scaled reactor provides different dimensioned reactor plates, optimal heat dissipation and different LED-arrays can be used.

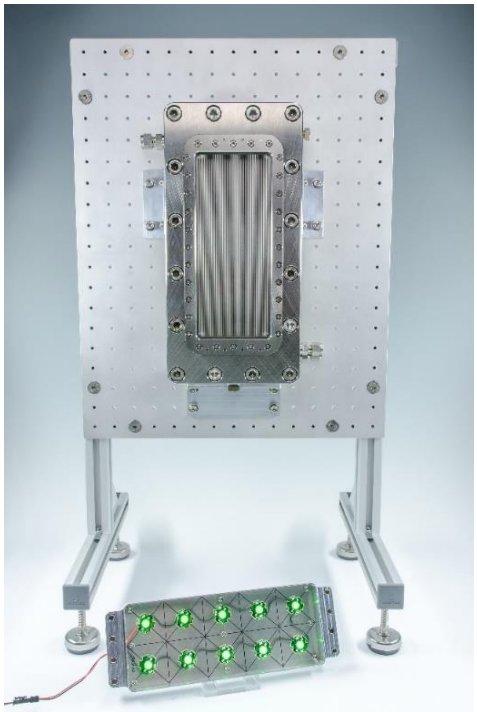

Figure 14: FFMR-LARGE for photochemical applications mounted on a rack (©Fraunhofer IMM).

Table 3: Technical data and operating conditions of the FFMR and FFMR-LARGE.[86]

	FFMR	FFMR-Large
width × depth × height [mm]	120×76×40	320×156×40
Max. pressure [bar]	10	10
Max. temperature [°C]	180	180
ports	1/4"	1/4"
wetted parts	stainless steel 1.4571, FFKM, quartz glass	Stainless steel 1.4571, FFKM, quartz glass
dimensions microchannels: Width depth (number) [µm]	- 300×100 (64) - 600×200 (32) - 1200×400 (16)	- 600×200 (100) - 1200×400 (50)
length microchannels [mm]	76	261
window size for irradiation width × height [mm]	29×54	81×210
Max. flowrate [L×h^{-1}]	300×100 µm dimension: 0.05 600×200 µm dimension: 0.6 1200×400 µm dimension: 1.5	0.24 - 1.2
residence time [s]	0.8 - 20	8 - 23
liquid film thickness [µm]	25-100	60-100
interfacial area [m^2×m^{-3}]	up to 20000	up to 16780

The specific productivity of a falling film micro reactor L_{FFMR} is calculated by:[92,93]

$$L_{\mathrm{FFMR}} = \frac{c_{\text{starting material}} \times Y_{\text{product}}}{t_{\mathrm{R}}} \tag{9}$$

with $c_{\text{starting material}}$ being the concentration of the respective starting material and Y_{product} the obtained yield of the product. t_{R} is the residence time in the reactor. Since falling films are used, t_{R} is calculated by:

$$t_{\mathrm{R}} = \frac{N \times V_{\text{channel}}}{\dot{V}} = \frac{N \times w \times l \times \delta}{\dot{V}} \tag{10}$$

with N being the number of microchannels and V_{channel} being the volume of each channel. This volume is calculated by its widths w, its lengths l and the film thickness δ. The film thickness is calculated by:

$$\delta = \sqrt[3]{\frac{3 \times \dot{V} \times \eta_{\text{liq}}}{N \times \rho_{\text{liq}} \times w \times g}} \tag{11}$$

with η_{liq} as the dynamic viscosity of the liquid, ρ_{liq} as the density of the used liquid and the gravitational constant g. In this thesis, the dynamic viscosity of an acetonitrile/arene/diazonium compound-mixture is estimated as 0.8839 mPa×s and its density is estimated as 0.8910 g×cm^{-3}.[31] Those values are used for all calculations concerning the specific productivity of the FFMR.

2.3.2 The Capillary Photoreactor

The principle of a capillary photoreactor was first introduced by the group of Booker-Milburn. They simply wrapped a FEP capillary around a cylindrical immersion well to build a reactor for Flow Chemistry applications. In their case, they used components from the lab and a medium pressure mercury lamp for reactor construction. With this setup, they were able to adjust residence and irradiation time precisely. The principle of a capillary photoreactor was used and adapted by many groups.[94]

Fraunhofer IMM presented a new interpretation of the capillary photoreactor concept using exchangeable LED-arrays to perform flow (photo-)reactions in a uniform reactor to provide stable reaction conditions over a long period of experiments. A 1/16" FEP capillary photoreactor (Figure 15b) was extensively tested and characterized in the master thesis of Sidonie Durieux.[95]

Main parts of the capillary photoreactor are two 1/16" FEP tubes (800 µm ID), which are wrapped around a borosilicate glass cylinder (100 mm OD, 150 mm height). The first capillary is directly contacting the glass cylinder concentrically and the second tube lays directly on top of the first one. Those two capillaries can either be used to perform separated reactions or be connected to double up residence time. The borosilicate glass transmits 90% of visible light,[96] while the FEP capillaries provide 77-91% transmission.[34] A second borosilicate glass cylinder (130 mm OD, 140 mm height) and the top and bottom plate create the room for the heat exchanger medium (water).

Studies of Babić *et al.* showed, that the number and position of LEDs on an array are important and influence the efficiency of a photoreactor.[97] Therefore, a hexagonal shaped bar is used to mount six LEDs in a row per face. With this 6×6 LED-array, a homogenous irradiation of the FEP capillary is approximated. A cooling finger in the center of the photoreactor is used as a holder for the LED-array, guaranteeing optimal heat dissipation for an optimal performance of the LEDs.

A related 1/8" FEP capillary photoreactor (see Figure 27d) was manufactured additionally. Different homogeneous and heterogeneous photoreactions can be performed with the reactor as various LED-arrays are provided (Table 4).

A former version (V.0) of the 1/16" FEP capillary photoreactor is also available (Figure 15a).[98,99] This reactor uses one 1/16" FEP capillary (800 µm ID), which is concentrically wrapped around borosilicate glass cylinder (100 mm OD, 150 mm height).

Photochemical reactions have to be performed at room temperature with this version. A cylindrical cooling finger is used to connect top and bottom plate of the reactor and 5×2 LEDs (five LED connected in a row, two parallel strands) emitting 455 nm are equally distributed on the cylinder. Additional wavelengths by other LEDs are provided as well.

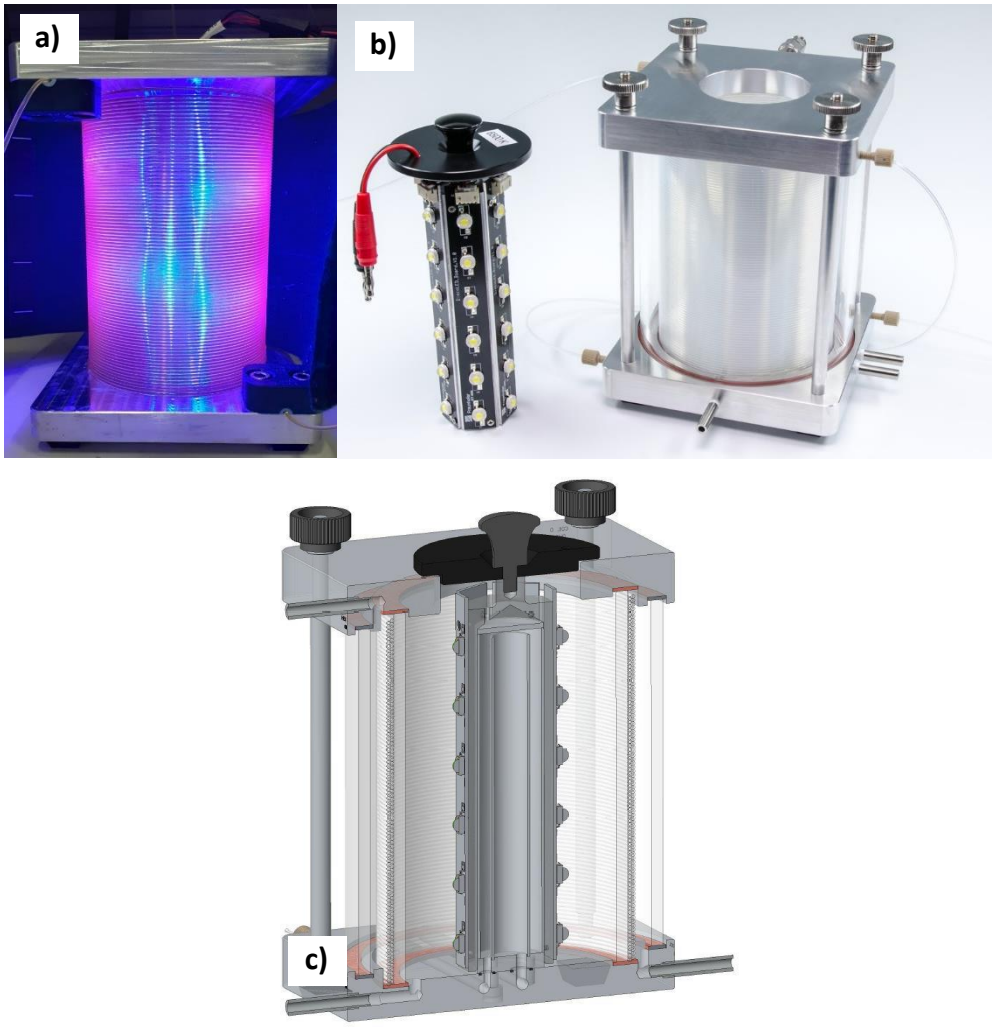

Figure 15: a) 1/16" FEP capillary photoreactor V.0 (800 µm ID, 15 mL, 5×2 455 nm LEDs max. ~11 W_{el}) filled with the reaction mixture for a *E*-*Z*-photoisomerization (in toluene/methanol V/V=84/16, 2mol% $[Ru(bpy)_3]Cl_2$) performed in chapter 3.2.4.2; **b)** 1/16" FEP capillary photoreactor with exchangeable 6×6 LED-arrays; **c)** Cross section of the 1/16" FEP capillary photoreactor; (© Fraunhofer IMM).

Table 4: Technical data of the different capillary photoreactors.

Volume capillary - 1/16" FEP capillary photoreactor V.0	15 mL
Volume of inner capillary - 1/16" FEP photoreactor	15 mL
Volume of outer capillary - 1/16" FEP photoreactor	15.08 mL
Volume of inner capillary - 1/8" FEP photoreactor	28.9 mL
Volume of outer capillary - 1/8" FEP photoreactor	29.9 mL
Available wavelength of 6×6 LED modules for the 1/16" and 1/8" FEP capillary photoreactors	365 nm
	410 nm
	455 nm
	520 nm
	610 nm
	6500 K

The specific productivity of a capillary photoreactor L_{CP} is calculated by:[92]

$$L_{\mathrm{CP}} = \frac{c_{\text{starting material}} \times Y_{\text{product}}}{t_{\mathrm{R}}} \tag{12}$$

with t_{R} being the residence time of the liquid inside the capillary. In this setup the considered capillary gets irradiated completely and t_{R} equals $t_{\text{irradation}}$, if the complete capillary is filled with the liquid (incompressible) phase of the reaction mixture.

2.4 Embedding process analytical technology into Flow Chemistry applications

Process analytical technology (PAT), in general, includes every device that samples, analyzes and monitors an application. Especially in continuous flow synthesis, PAT provides information on physical and chemical conditions inside a reactor or setup. This helps understanding and optimizing a process along its axial dimension.

In consequence, data on yield, conversion, process stability, throughput or space time yield can be provided. For this purpose, spectrometers and sensors have to be applied, which withstand harsh conditions, like aggressive, corrosive, unstable chemicals or viscous, heterogeneous, hot, cold or pressurized media. The installed PAT tool has to provide a stable and constant operability at the mentioned conditions at any time. In addition, the monitoring device has to cope with small changes and instabilities of the process.

A system, which does fulfill the mentioned requirements, is perfectly suited to be used in an automated process development or intensification. When assisted by machine learning and artificial intelligence, inaccuracy of humans can be reduced.[100]

The correct positioning of a PAT tool along the reaction path can be important, as a certain position will give direct information about the progress and the conditions inside the capillary at this particular place. However, not every position for the PAT tool can be realized, as there is a sufficient influence of the chosen sampling technique or measuring principle. Requirements, like precise and homogeneous sample concentrations, adequate flow velocities or appearing backpressure, have to be considered and are only a few examples of factors influencing the position of the PAT.
To prevent mutual disturbance of the flow process with the process analysis tool, different sampling techniques are categorized into four groups (Figure 17): on-line, in-line, at-line and off-line sampling.[100]

On-line PAT (or online PAT) refers (in its originally meaning) to measuring techniques, which are connected to the main flow via a by-pass. The probe of those tools is in direct contact with the reaction mixture. Generally, non-destructive methods as NMR-, IR-, Raman-, UV/Vis-spectroscopy are chosen. A flow-cell (Figure 16) is used to connect and integrate the device into the stream. Depending on the applied sampling technique, the by-pass stream can be additionally manipulated, if flow velocity is too high which eventually can cause unreliable results. Partial separation can lead to a time lag as flow rate is usually choked. A complete exchange of the media inside the by-pass is required before a new measurement can be started.

The term “online” analysis is commonly associated with all sampling procedures which take place directly in the stream of the process. It represents all techniques, which take place on the spot and at real-time without physically removing an aliquot as sample.[100,101]

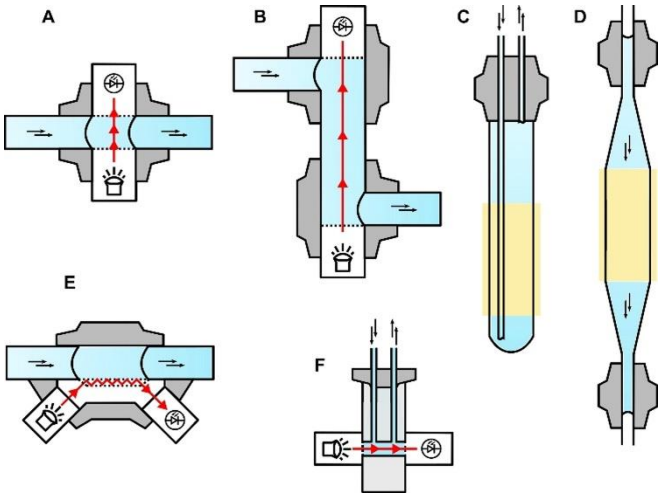

Figure 16: Different flow cells for in-line and on-line analysis in continuous flow: **A** Conventional transmission flow cell; **B** Z-path transmission flow cell; **C** Top-to-top NMR flow cell; **D** Top-to-bottom NMR flow cell; **E** FTIR-ATR flow cell; **F** Flow cuvette; Yellow: NMR detection zone. Adapted with permission from Ref. [100] copyright 2021 Wiley-VCH.

In-line PAT (or inline PAT) is closely associated with online monitoring. All tools, techniques, probes and flow cells, which are used in online PAT can be used here as well. As they are directly integrated into the process stream, they quickly deliver information without any distortion (in comparison to on-line analysis). Analysis, which requires preliminary sample treatment, destructive detection or chromatographic separation techniques, cannot be used in this setup.

At-line PAT is an automated sampling technique. An aliquot of the product stream is collected, treated and processed via chromatography or another method. Since most of those methods require more time as online or inline PAT, the frequency of repetition is less. In most cases the sample will not reenter the reactor after processing.

Off-line PAT describes every sample analysis with any kind of analysis tool. Off-line techniques are usually used, if the method cannot be integrated into the set-up or samples have to be taken manually. Moreover this group is chosen, if (many) time consuming steps as filtration or phase transfer have to be applied in the sample preparation process.[100]

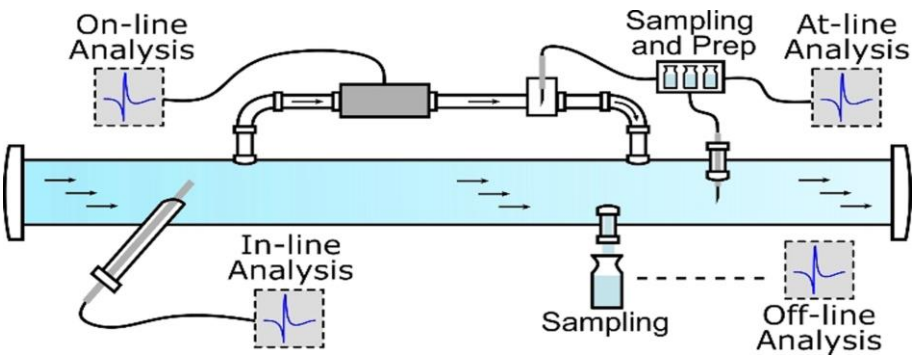

Figure 17: On-line, in-line, at-line and off-line sampling for process analytical technology in continuous flow. Adapted with permission from Ref. [100] copyright 2021 Wiley-VCH.

2.5 NMR-Spectroscopy for online quantification

2.5.1 Basic concepts of quantitative NMR-spectroscopy

Quantitative NMR-spectroscopy (qNMR) with sensitive high-field (HF) or low-field (LF) spectrometers is a common method to analyze and evaluate vaccines, drugs, natural products, peptides, polymers, composite materials, agrochemicals, food and beverages. Those analyses are performed offline mostly. Online qNMR applications gain more and more influence in research. Especially ^{1}H, ^{13}C, ^{19}F and ^{31}P NMR-spectroscopy for common nuclei in organic molecules are frequently used. Those nuclei offer a high relative sensitivity E_r in comparison to the ^{1}H-NMR spectroscopy (E_r=1) and hence show a good detectability.[102]

Main factors are the nuclear spin of I=1/2 and the specific gyromagnetic ratio γ_{i}:[103]

$$E_r = \frac{4}{3}\,\mathrm{I}(\mathrm{I}+1)\left(\frac{\gamma_{\mathrm{i}}}{\gamma_{\mathrm{H}}}\right)^3 \tag{13}$$

Besides coulometry, gravimetry, titration and other methods, NMR relies on the colligative properties of the investigated molecules. This makes NMR spectroscopy a primary method for analysis and implies direct usage in a quantitative manner.[104]
The following considerations (basing on a review of Ulrike Holzgrabe) influence sensitivity and apply to HF and LF spectrometers, as both types are used for quantification:[102]

$$I_{\mathrm{A}} = k_{\mathrm{S}} \cdot N_{\mathrm{nucleus}} \tag{14}$$

The intensity I_A of an NMR-signal is proportional to the number N of nuclei, which create this signal. Only a response factor k_S of the used device does influence this dependency. The response factor should be as high and stable as possible, which is not the case at any time. Therefore, the operator of a spectrometer should stick to the following rules:

The spectrometer has to be shimmed and tuned properly to the best possible homogeneous magnetic field. According to the obtained spectrum, the signals should be clearly separated and not overlapping with other signals. This fact can be influenced only by a solvent/matrix change as shifts depend on the used chemicals, which often can barely be changed. A singlet signal is easier to integrate in comparison to a multiplet.

Especially when using non-deuterated solvents, prominent ^{13}C-satellite signals can overlap with other signals. In case of a constant solvent concentration, subtraction of the satellite is the easiest way to get rid of the additional area. Alternately, the influence of those signals can be reduced by decoupling techniques using the "gated" or, preferred, the "inverse-gated" method for qNMR.

The spectrometer has to run as stable and constant as possible. To achieve constant k_S, pulse excitation has to be uniform and should be as short as possible. The flip time τ_p determines the time to flip the nuclear spin from the z-axis towards the y-axis. Usually, 90° flips are intended as less signal intensity is lost during acquisition. Acquisition time τ should be at least five times T_1. This relaxation time T_1 is slightly different for every considered signal and describes the time until thermal relaxation along the z-axis.

Since this free induction decay (FID) is an exponential function at least 99.3% of magnetization has disappeared:

$$M_z = M_0 \left(1 - exp^{\left(\frac{\tau}{T_1}\right)}\right) \tag{15}$$

with M_z being the magnetization along the z-axis and M_0 the magnetization in the equilibrated state. Theoretically, the signal should completely decay within the first half of acquisition. This guarantees, that enough data points (above the half-height of the signal) are recorded.[102]

The sensitivity of the spectrometer is very important as well, as accuracy of the integration is depending on this factor. It can be increased by appropriate parameters chosen previously to the sample recording. A spectrometer with a high field strength,

will increase the macroscopic magnetization of the sample. Alternatively, the number of molecules which are likely to be addressed can be increased. This is done by working in a higher concentrated medium. A third method is the application of more scans per sample. The signal-to-noise ratio (SNR) correlates with the square root of the number of scans n. In consequence, the number of scans has to be raised by a factor of four to improve the SNR by a factor two:

$$\mathrm{SNR} = \frac{I_{\mathrm{A}}}{\left(\frac{\text{peak to peak noise}}{2.5}\right)} \sim \sqrt{\mathrm{n}} \tag{16}$$

SNR is calculated by the maximum amplitude of the noise (peak to peak) and the intensity of the signal I_{A}.
Alternatively, SNR can be improved by apodization or zero filling. A correct and proper phase and baseline correction will result in a proper line shape of the signal.

Precise quantitative NMR-spectroscopy requires SNR values (deviation < 1%) of >250 for ^{1}H, >300 for ^{19}F, and >600 for ^{31}P nuclei.

LF-benchtop NMR-spectrometers are likely to be used in laboratories, as they are less cost intensive in comparison to high-field spectrometers. The usage of permanent and non-cryogenically cooled magnets allows easy (re-)arranging to different hoods, if necessary.

At the moment, benchtop spectrometers with Larmor frequencies ≤100 MHz are available, but development is ongoing.[105] The physical equipment of a LF-spectrometer will generate a higher signal dispersion and less sensitivity in comparison to HF-device. Those factors can be reduced by the implementation of higher concentrations or pre-magnetization/hyperpolarization techniques. Nevertheless, signal dispersion and signal overlap will remain.[106] Table 5 reviews commercially available benchtop spectrometers. Some companies even offer flow cells to perform measurements in flow or kinetic investigations (of batch reactions) in stopped flow.

Despite the downsides of a benchtop spectrometer, the nature of a primary analysis method still is present and quantitative analysis is still possible. If constant, permanent conditions and settings are existent, the spectrometer constant k_{S} will not change for a single specific nucleus, irrespective of the applied chemical matrix.

Quantitative NMR with LF-spectrometers requires precise data acquisition and subsequent data processing is at least as meaningful. Most important are the phase and

baseline correction as they will influence the quantitative nature of a spectrum. Via phase correction, a symmetrical line shape of the spectrum is created. In most spectra, the real part of the acquired data will be processed after Fourier transformation. If insufficient phase correction is used, a deflected absorption spectrum will be imaged, leading to an imprecise integration of the signal. Baseline correction is usually performed by application of certain polynomic functions. Global baseline correction is useful, if two signals of similar shape and size are compared. Fractional baseline correction is recommended whenever signals have to be integrated which are close to each other and differ in size. A separated baseline correction should be applied, if the signals are apart from each other.[104]

Table 5: Commercially available LF-benchtop NMR spectrometers.

company	type	nuclei	number of nuclei	MHz (^{1}H)	line width 50% [Hz]	sensitivity	lock	flow cell availability	auto-sampler	refer-ence
Bruker	Fourier 80	^{1}H, ^{13}C, ^{31}P, ^{129}Xe	^{1}H only, or 2	80	≤0.4	240 (^{1}H only); 160	external	yes	yes	[107]
Bruker	InsightMR for High Field NMR - Flow Cell	-	-	-	-	-	-	-	-	[108]
Magritek	Spinsolve 60	^{1}H, ^{19}F, ^{7}Li, ^{11}B, ^{13}C, ^{15}N, ^{23}Na, ^{29}Si, ^{31}P	2 or 3	60	≤0.4 (Standard); ≤0.35 (Plus); ≤0.2 (Ultra)	180 (^{1}H and ^{19}F only); 120	external	yes	yes	[109]
Magritek	Spinsolve 80	^{1}H, ^{19}F, ^{7}Li, ^{11}B, ^{13}C, ^{15}N, ^{23}Na, ^{29}Si, ^{31}P	2 or 3	80	≤0.4 (Standard); ≤0.25 (Ultra)	200	external	yes	yes	[110]
Magritek	Spinsolve 90	^{1}H, ^{19}F, ^{7}Li, ^{11}B, ^{13}C, ^{15}N, ^{23}Na, ^{29}Si, ^{31}P	2 or 3	90	≤0.4	>240	external	yes	yes	[111]
Nanalysis	NMReady60e	^{1}H, ^{19}F	2	60	< 1.0	100	internal	yes	yes	[112]
Nanalysis	NMReady60Pro	^{1}H, ^{19}F, ^{7}Li, ^{11}B, ^{13}C, ^{31}P	2 or 3	60	≤1.0	100	internal	yes	yes	[113]
Nanalysis	100PRO	^{1}H, ^{19}F, ^{7}Li, ^{11}B, ^{13}C, ^{31}P	2	100	< 1.0	220	internal	yes	yes	[114]
Oxford Instruments	X-Pulse	^{1}H, ^{19}F, ^{7}Li, ^{11}B, ^{13}C, ^{23}Na, ^{29}Si, ^{31}P	2,3 or 8	60	< 0.35	130	internal	yes	yes	[115]
Thermo Scientific	picoSpin 45 II	^{1}H, ^{19}F	1	45	< 1.8	> 1000	internal	yes	no	[116]
Thermo Scientific	picoSpin 82 II	^{1}H, ^{19}F	1	82	< 1.6	> 4000	internal	yes	no	[116]

2.5.2 Evaluation of online NMR-spectroscopy

Different methods can be applied to evaluate a recorded spectrum. The easiest way is the usage of an external calibration, followed by the application of an internal standard. The latter will reduce inaccuracy slightly, as small non-uniformities are comprised and smoothed. This method requires an additional chemical compound, which is introduced together with the analyte. It is necessary, that this standard will not change its concentration or show reactivity to other compounds. Moreover, this substance should not overlap with other signals or cause solubility issues. In addition to the usage of the signal intensity, electronic referencing methods like Electronic REference To access In vivo Concentrations (ERETIC) or PUlse Length-based CONcentation measurement (PULCON) can be used. But they require additional non-standard hardware, likewise hyperpolarization.[106,117,118]

Beside the mentioned univariate calibration methods, multivariate analysis is an optimal tool, especially, if overlapping signals are present in a spectrum. Those multivariate models are created by a defined training data set. Training data, with known concentrations and compounds, is recorded with identical settings as the subsequent process spectrum.

One method is represented by partial least squares regression (PLSR). According to Wold *et al*. this method is summarized as: "PLSR is a method for relating two data matrices, X and Y, by a linear multivariate model, but goes beyond traditional regression in that it models also the structure of X and Y. PLSR derives its usefulness from its ability to analyze data with many, noisy, collinear, and even incomplete variables in both X and Y. PLSR has the desirable property that the precision of the model parameters improves with the increasing number of relevant variables and observations."[119] Another alternative is the application of Indirect Hard Modelling (IHM) techniques, where every (overlapping) signal is deconvoluted into (sets of) single spectra. Those spectra sets are then assigned to models of a pure components.[118,120] Indirect Hard Modeling is explained in more detail in chapter 3.1.4.2.

2.5.3 NMR-spectroscopy in flow

NMR-experiments in a continuous flow lead to an unneglectable influence on spectrometer sensitivity and resolution. This dependence is mainly caused by the moving liquid stream, effecting the sensitive volume V_s of the flow cell.
First to be mentioned is the "inflow-effect". Unexcited (no experience of a pulse from the transmitter coil), polarized spins constantly refresh the sensitive volume of the flow cell between two acquisitions. Finally, the longitudinal relaxation rate T_1^{static} can be replaced by an effective relaxation rate T_1^{flow}, if fully polarized spins replenish the flow cell. This leads to a drastic enhancement of the signal intensity allowing shorter acquisition times TR:

$$\frac{1}{T_1^{\text{flow}}} = \frac{1}{T_1^{\text{static}}} + \frac{1}{\tau_R} \tag{17}$$

The "inflow-effect" depends on the residence time (sensitive volume) τ_R and the flow rate inside the flow cell. As long as a sufficient time is spent in the pre-polarization volume V_p, all spins can be fully polarized. The maximum flow rate $\dot{V}_{\text{max}}$ is depending on five times the relaxation time T_1 (of a stopped flow measurement):

$$\dot{V}_{\text{max}} = \frac{V_p}{5 \cdot T_1} \tag{18}$$

If the flow rate gets too high, pre-polarization will be ineffective as too many un-polarized spins pass V_p. The "outflow-effect" can amplify this circumstance additionally. At high flow rates many excited spins will leave the sensitive volume even before they are detected by the receiver. In consequence, a maximum flow rate $\dot{V}_{\text{max}}$ results by the TR/T_1 ratio (see Figure 18).[23,121]

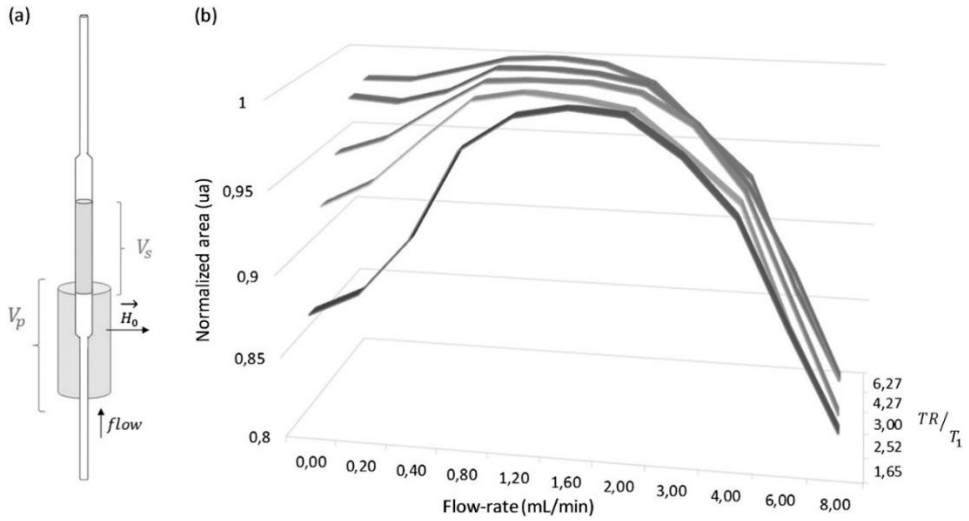

Figure 18: **a)** Bottom-to-top NMR flow-cell implemented inside a benchtop NMR spectrometer. $\overrightarrow{H_0}$ represents the vector of the static magnetic field. V_s and V_p are the sensitive and pre-polarization volumes; **b)** Exemplary curves of intensity as a function of the flowrate displayed for different TR/T_1 ratios. Each intensity matches with the mean value of three successive experiments performed on a sample of ethanol at 40% in H_2O. The intensity is measured by the area of the ethanol triplet located at 1.05 ppm. Adapted with permission from Ref. [121] copyright 2017 Wiley-VCH.

3 Results and Discussions

3.1 Continuous synthesis of biphenyls by a photochemical arylation of arenes via diazonium trifluoroacetates and its quantification with online ^{19}F-NMR spectroscopy

Direct C-H arylation of arenes like benzene and its derivatives is performed via different photochemical pathways (with and without photocatalysts) and different reactor setups, e.g. falling film micro reactor or capillary photoreactor. In the following chapters, results of direct C-H arylation considering physicochemical as well as technical impacts are presented, evaluated and discussed. Comparability is ensured by applying a model reaction to synthesize 3-CF_3-biphenyl as benchmark.

Its synthesis relies on the coupling of benzene by a *meta*-trifluoromethylphenyl group. Benzene is selected for two reasons: First, it will form only one isomer allowing simple qualification and quantification. Second, its reactivity is considered as reference for most aromatic substitution reactions in comparison to other benzene/acene derivatives[122]. As a source for the *meta*-trifluoromethylphenyl group, corresponding aniline is used, because it is easily available and safely manageable. A reactive intermediate is obtained by the generation of diazonium salts. Irradiation of the diazonium compound with different wavelengths (mainly 365 nm or 455 nm) will create an excited state followed by expulsion of nitrogen and introducing C-H arylation of the arene.

This work shows the development of a direct C-H arylation towards the use of arene diazonium trifluoroacetates.

Furthermore, a method for continuous monitoring of the ongoing reactor performance will be integrated into the lab-scale setup. A common and reliable method for quantification and qualification of molecules containing fluorine is provided by ^{19}F-NMR spectroscopy using the fluorine groups as a probe. In this case, a commercially available benchtop NMR-spectrometer, equipped with a well-suited flow-cell, is used.

3.1.1 Reactivity of arene diazonium salts

3.1.1.1 General reactivity and stability of diazonium salts

Arene diazonium compounds, especially arene diazonium salts **1**, are prominent precursors to generate aryl radials or aryl cations.[123] Due to their reactivity, those intermediates are used in lots of thermal and photochemical substitution reactions. Most common and related reactions are the hydroxydediazotation to yield phenols,[124] the Sandmeyer reaction to give aryl chlorides and aryl cyanides,[125] the Balz-Schiemann reaction for the generation of aryl fluorides[126] or the Meerwein-reduction for substitution with a hydrogen atom[127] (Scheme 2). Diazonium salts have the lowest reduction potential (~0 V vs. SCE) in comparison to diaryliodonium salts, aryl sulfonyl chlorides or aryl halides, which all are appropriate precursors for photoredox arylations or the formation of biphenyls, for example.[128]

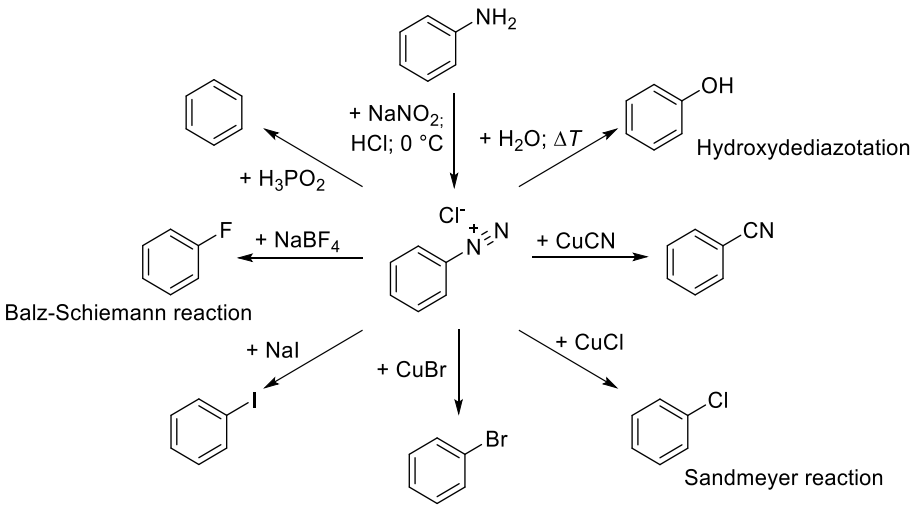

Scheme 2: Prominent reactions using arene diazonium salts as precursor.

The diazonium group is therefore one of the most electron-attracting substituents and one of the best leaving group in organic chemistry. Lots of diazonium coupling reactions and dediazotation precede via an electrophilic aromatic substitution and other homolytic or heterolytic mechanisms.

Experiments of C. Wittwer and H. Zollinger confirmed the dibasic (Lewis) acid character of the diazonium salts. Nucleophiles (e.g. OH^-, OR^-, OAr^-, CN^-, amines or aromatic systems with electron-donating substituents) will easily undergo a reaction with the β-nitrogen of the diazonium group.[123,129]

Secondary amines **2** form very stable aryl alkyl triazenes **3** (Scheme 3). Here, the diazo group appears as an *E*-isomer, which is thermodynamically more stable than the *Z*-isomer. Systematic studies of Schotten *et al*. using DSC were recently conducted to explain the structure–stability relationship.[13]

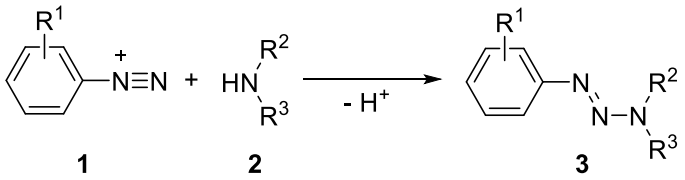

Scheme 3: Formation of a triazene by a diazonium salt and a secondary amine.

Under mild acidic or mild basic conditions electron-rich aromatic systems, like *N*,*N*-dimethylaniline **4**, will result in an azo coupling. A large conjugated π-electron system **5** with a stable and colorful structure is created, which can be used as an organic dye (Scheme 4).[130]

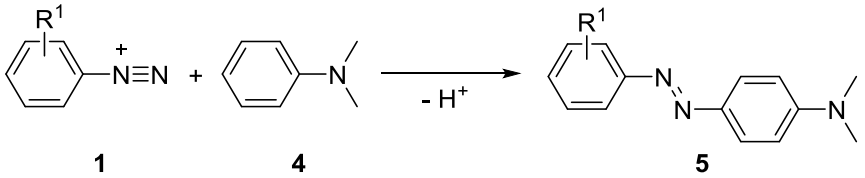

Scheme 4: Synthesis of an azo dye by a diazonium salt and an electron-rich aromatic system. Methyl yellow represents compound **5**, when R^1=H.

Diazohydroxide **6** is formed in an aqueous basic medium as product. A higher pH-value is required for the formation of **6** than for the generation of a diazotate anion **7**. Therefore, the latter is likely to be generated (Scheme 5). Those diazotate-anions will also form diazo anhydride **8** (highly explosive, if isolated) with remaining diazonium cations.[131]

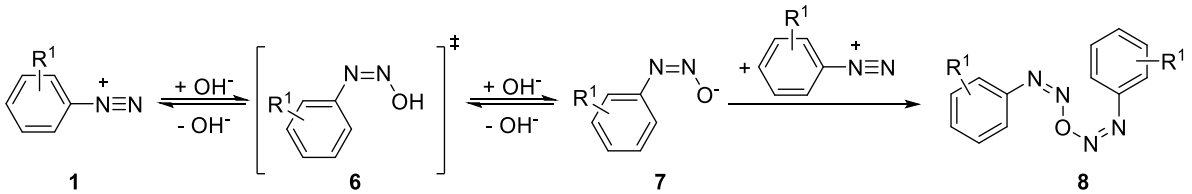

Scheme 5: Formation of unstable arene diazotate anions and diazo anhydrides in an aqueous basic medium.

Diazohydroxides appear as a *Z*-isomer, as the present nucleophile OH^- will interact with the aromatic ring. The distance between the nucleophile and the β-nitrogen will be short and the N_β-lone pair is directed into a *trans*-configuration. One can say, that the configuration of a product, of diazonium cation and nucleophilic anion, is mainly influenced by the stabilization (solvation energy) of the anion and the effective ionic radii determining the Coulomb attraction and repulsion.[132,133]

Furthermore, Zollinger reported on the key role of the nucleophile and the special characteristics of the diazonium salt **1** to give a cleavage of the C(1)-N_α bond. This (thermal) cleavage can be either homolytic or heterolytic and yields aryl cations or radicals **1a**.[123] Exact verification of a mechanism can be challenging as small changes in the reactants, solvents or additives may impact kinetics, atom distances or steric configuration. This behavior was approved by Kaul *et al.*, as a heterolytic mechanism (in DMSO) appears in an arylation of benzenediazonium salt with nitrobenzene. However, biphenyl formation is performed via a homolytic mechanism when *p*-nitrobenzenediazonium ions react with nitrobenzene in DMSO.[134] A homolytic mechanism is generally favored, if additives **9** are present, which are good nucleophiles and have the ability to form radicals **9a** itself (Scheme 6 a). If only one attribute is present, arylation using a radical mechanism can still be catalyzed by solvents (as DMSO), bases (as pyridine)[123] or sodium iodide (Scheme 6 b). Kosynkin *et al*. presented a thermal arylation route using pentafluorophenyl diazonium tetrafluoroborate **10** and an arene **11** (e.g. toluene, *o*-xylene, *p*-xylene, nitrobenzene, chlorobenzene) with a catalytic amount of iodide to gain biphenyls **12** with 24-79% yield. Depending on the catalyst amount, up to 37% iodopentafluorobenzene **10b** is obtained as by-product.[135]

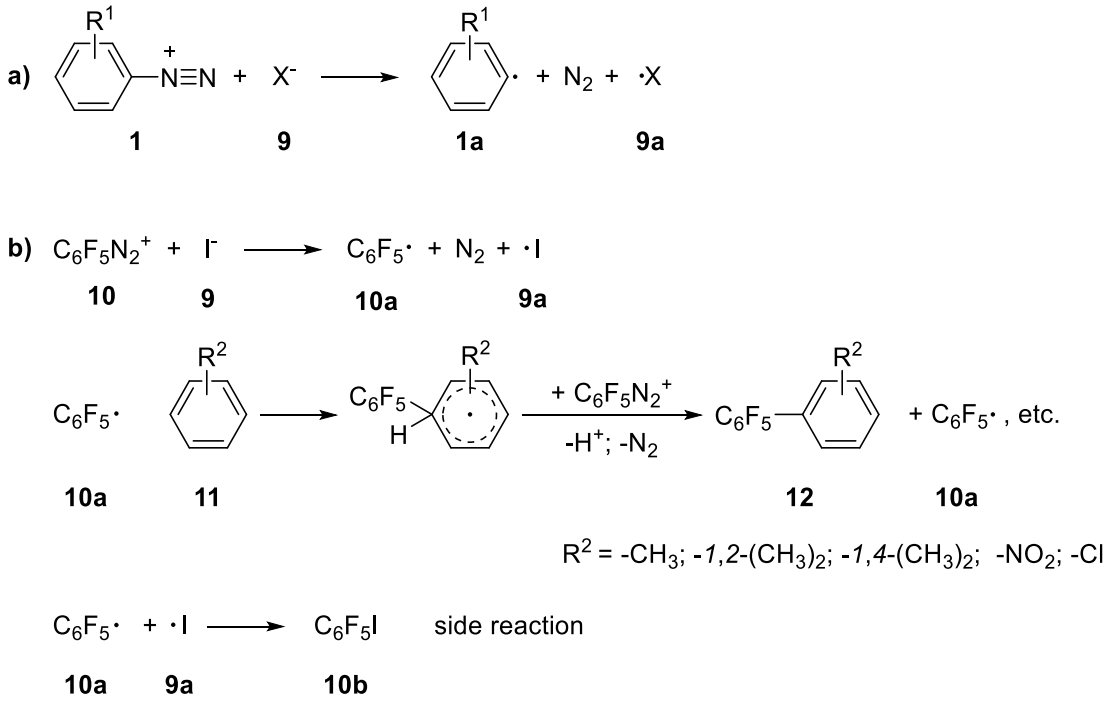

Scheme 6: a) Generation of aryl radicals using nucleophiles **9**; **b)** thermal synthesis of biphenyls **12** using sodium iodide as catalyst.

Moreover, mesomerism has a huge impact on the stability of the arene diazonium cations. Stability is increased, if electron-donating groups are present at the *ortho*- or *para*-position of the aromatic ring. Phenolate or amine groups are prominent examples. As a consequence, electron-density is shifted towards the diazo group, which results in a reduced electrophilicity of the latter (Scheme 7b).

But, stability is reduced, if electron-withdrawing groups such as a nitro or diazonium groups are inserted (Scheme 7c). Less destabilization occurs, if electron-withdrawing groups are present in the *meta*-position. In this case, only the inductive effects will contribute.[131]

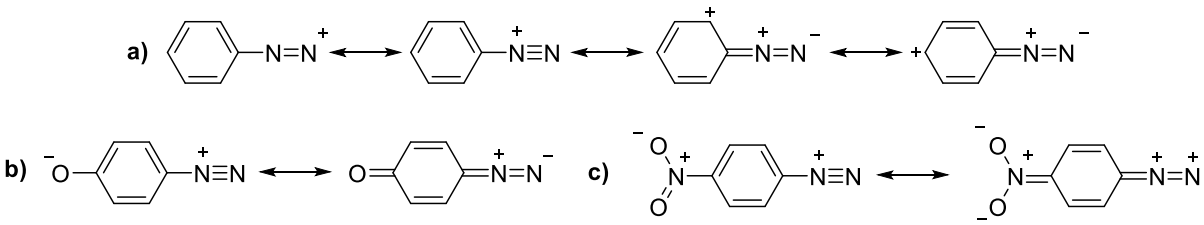

Scheme 7: a) Stabilization of arene diazonium salts by mesomerism enhanced by **b)** an electron-donating group or reduced by **c)** an electron-withdrawing group.

3.1.1.2 Preparation of diazonium salts

From a historically point of view, diazonium salts are produced in aqueous acidic media using an aryl amine, nitrous acid or sodium nitrite. Especially, in the case of nitrous acid dissociation is not strong enough and a (mineral) acid is added additionally (Scheme 8a). Kinetic studies revealed an attack on the nitrosonium ion **13** by the free amine **1b**. Subsequently a nitrosamine is yielded and after the abstraction of water, the diazonium compound is created. Generally, diazotation is a rather quick reaction, with the first step being the slowest (Scheme 8c). In highly concentrated acids the nitrosonium ion will be present, whereas in a diluted acidic medium other thermodynamically stable forms will appear. This can be either a nitrosacidium ion **14** or dinitrogen trioxide **16**. Nitrosyl halides **15**, as an additional alternative, will only be formed in water-free medium. However, the nitrosonium ion shows highest reactivity and electrophilic character (Scheme 8b).[131]

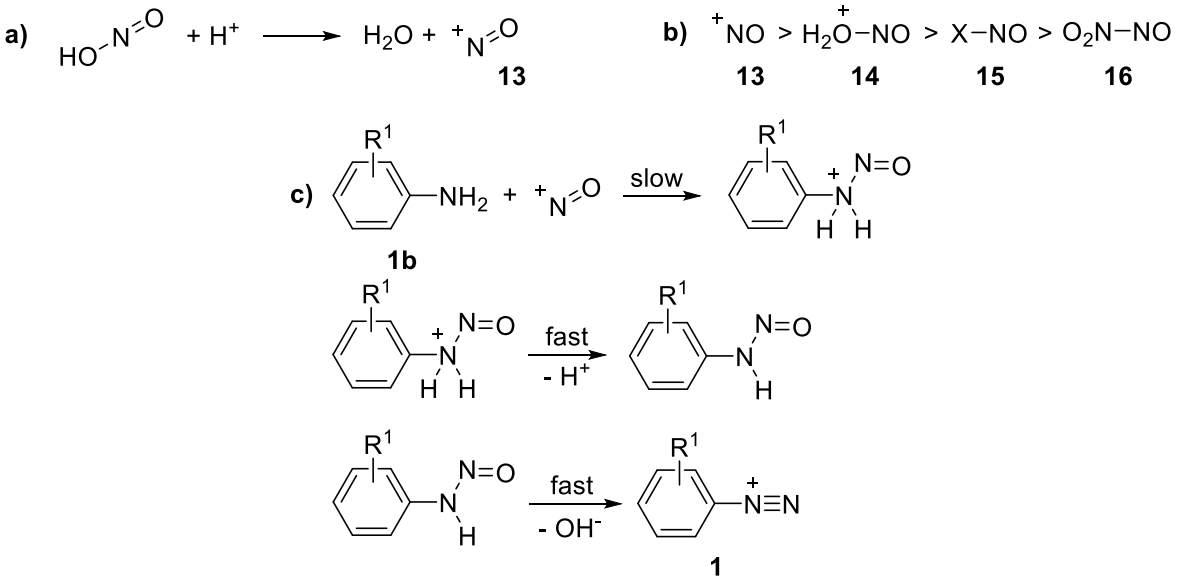

Scheme 8: a) Formation of the nitrosonium ion **13** in an aqueous acid medium; **b)** different diazotation reagents; **c)** diazotation mechanism of aryl amines giving arene diazonium salts.

In order to avoid side reactions, like azo coupling or generation of diazo amino compounds, an excess (high concentration) of the acid is usually used. Early decomposition of the diazonium salt is hindered at lower pH-values, whereas basic media will lead to unstable compounds as already mentioned. Diazotation in cold media (~0-10 °C) will reduce decomposition as well. Water soluble diazonium chlorides are obtained via diazotation in aqueous hydrochloric acid in most cases. Regularly, they

are not isolated and directly used in further applications. Isolated diazonium chlorides are unstable and potentially explosive. This phenomenon can occur, if the salt is extensively dried.[136]

Stable diazonium salts, required for safe handling in the laboratory, are obtained when using the tetrafluoroborate anion instead of chloride. Those diazonium tetrafluoroborates can be prepared in a similar procedure and the salt will precipitate in water.[131] They are insoluble in apolar solvents, like benzene, diethyl ether or alkanes. In acetone, DMSO, hexafluoroisopropanol and other polar solvents they show good solubility. The isolated and dried compounds are storage-stable in a fridge.

To isolate water-soluble diazonium salts, diazotation can be performed in an appropriate organic solvent as well. In this case, the respective aryl ammonium salt and an alkyl nitrite as derivative of nitrous acid are used (Scheme 9). The diazonium salt will now precipitate in apolar solvents. If polar solvents are used, multi-step reactions can be performed directly in non-aqueous media and even under flow conditions.[137]

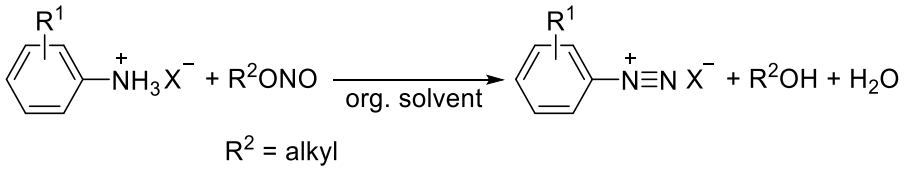

Scheme 9: Preparation of arene diazonium salts in organic solvents using alkyl nitrites as diazotation agent.

3.1.1.3 Possibilities of visible light photoredox arylation reactions

Diazonium salts, as an excellent aryl radical precursor, are used in various direct C-H arylations of (hetero)arenes, alkenes, alkynes, enons or enol acetates. In most cases, different photochemical approaches mediate the reactions towards an easily manageable process, performed under mild conditions. In those cases, the photochemical route is usually enabled or enhanced with the help of homogeneous photocatalysts like $[Ru(bpy)_3]Cl_2$, *fac*-$Ir(ppy)_3$, Rose Bengal or eosin Y.[128]

König *et al*. present a mild route for the generation of bi(hetero)arenes. Key factor is the usage of eosin Y (1mol%) as photocatalyst, which is used for a single-electron transfer after 530 nm excitation (2 h, 20 °C) to give the necessary aryl radicals. The presence of a radical mechanism (Scheme 10) is proven via TEMPO-trapping and the products **17** and **18** are identified. Subsequent to the formation of the radical

intermediate **19**, two different reaction pathways are possible. Intermediate **19** will reduce the photocatalyst eosin Y to give the required cationic intermediate or a radical chain propagation including an electron transfer onto a diazonium compound is initiated. An efficient radical propagation theoretically results in high quantum yields >1. In their studies, the authors do not focus on this topic and no information on the quantum efficiency are provided.[138]

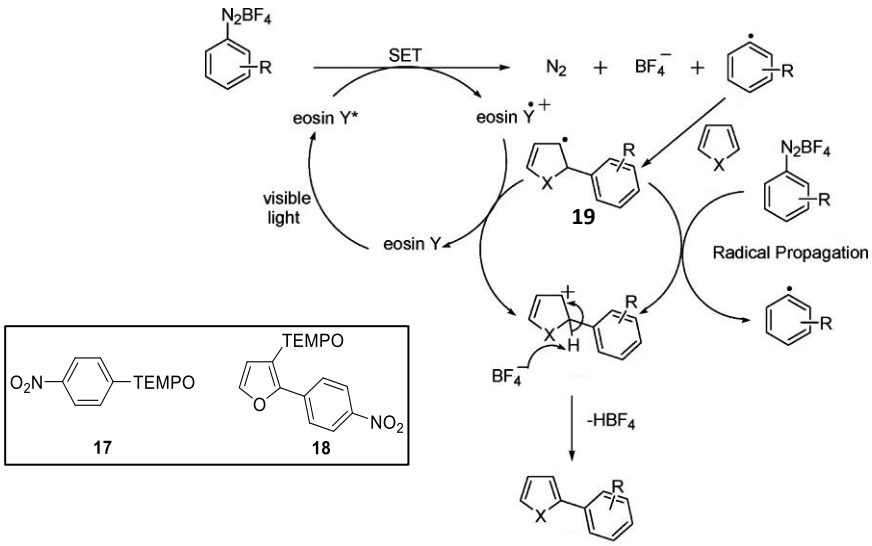

Scheme 10: Radical mechanism for a photocatalytic direct C–H arylation of heteroarenes suggested by König *et al.* and TEMPO-trapped intermediates. Adapted with permission from Ref. [138] copyright 2012 American Chemical Society.

The same group extended this eosin Y photocatalyzed arylation onto substances like styrene, phenyl acetylene, quinone and cumarine. Those substrates are now selectively arylated at the activated unsaturated vinyl- or acetylene group. Similar to a thermal Meerwein arylation the aromatic ring system keeps untouched. The effectivity of these arylations is even enhanced by a catalyst optimization towards $[Ru(bpy)_3]Cl_2$.[139]

Bi(hetero)arenes derived from pyridine are successfully generated in water by a photochemical approach using blue light (450 nm), even without any requirement of a photocatalyst (Figure 19 a). Main reason of this catalyst-free arylation is the formation of an electron donor-acceptor EDA complex[30] (alternative: charge-transfer CT-complex), which is also identified in the photochemical arylation of hydroquinone, 1,4-dimethoxybenzene or furfurylamine via arene diazonium tetrafluoroborates.[29] De Oliveira *et al*. confirm the appearance of a charge-transfer complex in arylation of pyridine motives by UV/Vis-spectroscopy and ^{1}H-NMR spectroscopy (Figure 19c). In comparison to spectra of separated substances, a low-field shift (deprotection) of

pyridine and a high field shift (protection) of the diazonium salt is observed in mixtures of both. This is an obvious argument for the shift of the electron density towards the diazonium salt.[30]

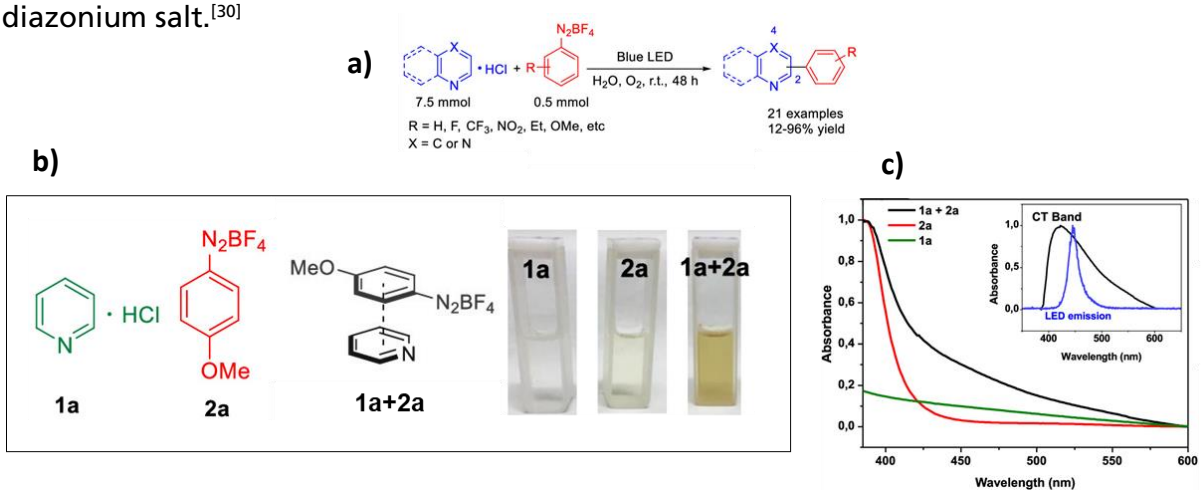

Figure 19: a) Photoarylation of pyridines using aryl diazonium salts and visible light; **b)** images of the solutions 1a, 2a, 1a + 2a in water; **c)** UV/Vis spectra of 1a, 2a and 1a + 2a in water, Inset: CT-band of (1a + 2a) EDA- complex. Adapted with permission from Ref. [30] copyright 2019 American Chemical Society.

The previous synthesis procedure of pyridine or (hetero-)arene arylation can be enhanced to shorter reaction times by heterogeneous photocatalysis using metal oxides. Hereby, Zoller *et al*. focus on different titanium(IV) oxide catalysts in ethanol as solvent. They are able to synthesize 95% 2-(4-chlorophenyl)furan **24a** from furan **23a** and 4-chlorophenyl diazonium tetrafluoroborate **20** within 4 h using 1 equiv. of titanium(IV) oxide and a 11 W CFL bulb. Different modifications and metal oxides are considered, due to small differences in their respective band gap. Process optimization yields the best result, when rutile modification is used. An absorption maximum at 413 nm is observed for neat Rutile. The same maximum also appears (but weaker), if above mentioned furan and diazonium salt are both dissolved in ethanol. No maximum is observed, when pure 4-chlorophenyl diazonium tetrafluoroborate is tested. An ethyl azoether **21** is formed in the presence of furan (weak base), as this compound will act as a promoter. Formation of the ethyl azoether is confirmed by addition of sodium ethylate.

In the presence of titanium(IV) oxide a new absorption maximum at 448 nm appears, as UV/Vis studies reveal. A TiO_2-azoether **22** is formed, if furan, diazonium salt and the heterogeneous photocatalyst are mixed. Both, ethyl- and TiO_2-azoether (being in equilibrium), suffer a single electron transfer (Scheme 11) due to excitation of

titanium(IV) oxide and aryl radicals are obtained as a result. These radicals initiate the arylation of the (hetero-)arenes.[67]

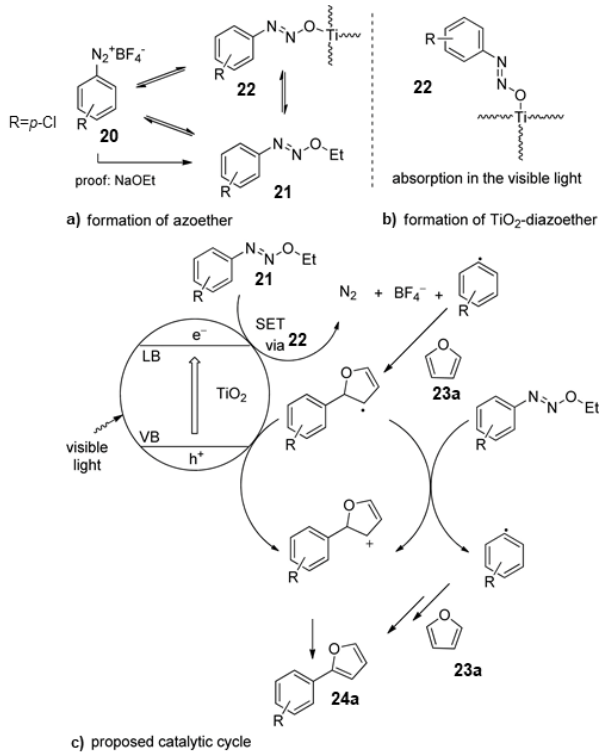

Scheme 11: Radical mechanism for direct C–H arylation of heteroarenes using titanium(IV) oxide as heterogeneous photocatalyst suggested by Fabry *et al*. Adapted with permission from Ref. [67] copyright 2015 American Chemical Society.

3.1.2 Biphenyl synthesis using heterogeneous photocatalysts in versatile reactor concepts

3.1.2.1 Catalyst evaluation

As presented in chapter 3.1.1.3, Fabry *et al.* report the "unexpected dual role of titanium(IV) oxide" for bi(hetero-)arene production.[67] Two years later, this procedure is successfully converted into a continuously operated synthesis. Herein, all microchannels of a falling film micro reactor reaction plate are coated with titanium(IV) oxide and in combination with blue light irradiation, all advantages of a thin film photocatalysis are optimally used. The result is quantitative conversion of 3-CF_3-phenyl diazonium tetrafluoroborate **25** giving 2-(3-CF_3-phenyl)furan **26a** after a single pass (Table 8 entry #1).[31]

Having the excellent performance of the FFMR for bi(hetero-)arene synthesis in mind, an adaption of the literature known procedure with respect to the benchmark molecule is intended. For optimal addressing of the reported azoethers with 455 nm, different metal oxides (TiO_2-anatase modification, TiO_2-rutile modification, $BaTiO_3$, $SrTiO_3$) are tested in batch. Since ethanol is reported as an appropriate solvent for heterogeneous metal oxide photocatalysis, this alcohol is now used as well.

3-CF_3-phenyl diazonium tetrafluoroborate **25** and one equivalent of the catalyst are suspended in equal amounts of ethanol and benzene **23b** (Scheme 12). Irradiation at 455 nm for 17 h gives 30% of 3-CF_3-biphenyl **26b**, if the anatase modification is used (Table 6 entry #1). Likewise to literature,[31] this modification shows best results in comparison to the other tested metal oxides.

In contrast, photocatalytic arylation is not supported by the addition of trifluoroacetic acid, which potentially can trigger an *in-situ* anion exchange.[29] Main reason might be the higher acidic environment, suppressing TiO_2-azoether formation.

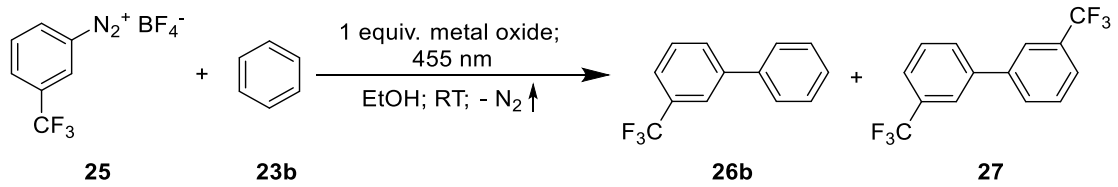

Scheme 12: Photocatalytic C-H arylation of benzene using a diazonium tetrafluoroborate in ethanol.

As expected, arylation yield is far lower for benzene, in comparison to other hetero-arenes like furan or pyridine. This result is caused by the energetically stable HOMO of benzene.[29,31,67,140] As consequence, there is a less strong overlap between the aryl radical and the arene, causing lower selectivity and side-product formation.

In this particular case of using the rutile modification as photocatalyst, a notable formation of the by-product **27** (3,3´-bis(trifluoromethyl)-1,1´-biphenyl) is promoted. This reaction is caused by homocoupling of two 3-CF_3-phenyl radicals. When using column chromatography (eluent: n-heptane) as work-up procedure, ~1.5% of the isolated material consist of this by-product (determined by GC/MS).

Since Fabry *et al.* report poor yields for other metal oxide photocatalysts, like ZnO and Bi_2O_3,[31] these are not investigated.

Table 6: Influence of different heterogeneous metal oxide photocatalysts on the formation of 3-CF_3-biphenyl via a 3-CF_3-phenyl diazonium tetrafluoroborate.[a]

#	catalyst	note	by-product **27**	yield **26b** [%][b]
1	TiO_2 - anatase	-	traces	30
2	TiO_2 - anatase	+ 1 equiv. TFA	traces	22
3	TiO_2 - rutile	-	~ 1.5%	18
4	$BaTiO_3$	-	traces	18
5	$SrTiO_3$	-	traces	15

a: Reaction conditions: 50 mM 3-CF_3-phenyldiazonium tetrafluoroborate, 1 equiv. metal oxide, ethanol/benzene (V/V=1/1), 10 mL, RT, 455 nm 6 W_{el}; **b:** Yield after chromatographic purification.

3.1.2.2 Heterogeneous photocatalytic arylation in a Falling Film Microreactor

Titanium(IV) oxide (anatase modification) shows best performance for the photocatalysis of **26b** (see previous chapter 3.1.2.1). Having evaluated the best heterogeneous catalyst, the literature known procedure[31] is applied to a continuous synthesis of 3-CF_3-biphenyl using the falling film micro reactor (FFMR, from Fraunhofer IMM). Therefore, the FFMR is equipped with a reaction plate having 32 microchannels and 23 mg of anatase are immobilized onto the surface of these channels. A 455 nm 4x1 LED-array (6 W_{el}) is positioned in front of inspection window to irradiate the falling film directly.

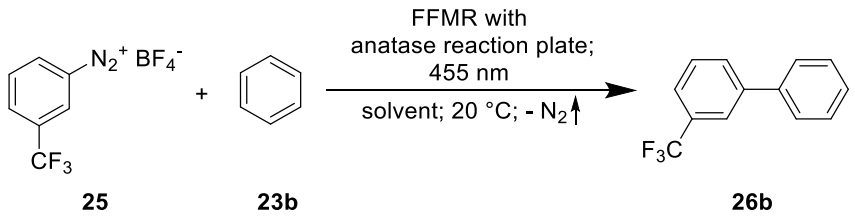

Scheme 13: Continuous photocatalytic C-H arylation of benzene using diazonium tetrafluoroborate in a falling film micro reactor.

Several tests show elementary issues, which avoid a “simple” transfer of the known procedure (Scheme 13). In ethanol/benzene (V/V=1/1) 3-CF_3-phenyldiazonium tetrafluoroborate **25** shows poor solubility. Even the replacement of ethanol by other polar solvents like methanol, isopropyl alcohol, n-butanol, tetrahydrofuran and acetonitrile gives incomplete dissolving. In hexafluoroisopropanol, all diazonium salt dissolves, but subsequent arylation reaction is completely suppressed. Replacing 30% of ethanol by dimethyl sulfoxide gives a clear mixture of

50 mM 3-CF_3-phenyldiazonium tetrafluoroborate in benzene. A single pass in the FFMR results in 10% **26b** with a significant amount of the by-product **27** (~3%). In comparison to this, a single pass of a reaction mixture using only ethanol as solvent (remaining undissolved solid is removed by filtration) gives 5% yield of 3-CF_3-biphenyl, but formation of the by-product is completely avoided.

Beside the tetrafluoroborate anion, causing solubility issues in the benchmark reaction, different other counter ions are tested for (photoredox) arylation of (hetero-)arenes (Figure 20). Arylazo sulfones and sulfonates show eligible photoreactivity and trifluoroacetates, as well as trifluoromethanesulfonates, are already used for thermal biphenyl synthesis in neat benzene.[141,142] Hu *et al*. presented a promising overview for continuous production of diazonium salts in aqueous or organic media. Most of the presented procedures form the corresponding salts *in-situ* using the corresponding acid in slight excess. Diazotation procedures under acid free conditions, using corresponding TMS-protected acids, are reported as well.[137] In most cases, the polar aprotic acetonitrile in combination with *tert*-butyl nitrite show best performance. In another example, an arene diazonium methanesulfonate for Sonogashira cross-coupling is synthetized *in-situ* using *tert*-butyl nitrite (1.2 equiv.) and methanesulfonic acid (1.2 equiv.) in acetonitrile. The ionic character of this arene diazonium methanesulfonate **28** is proven by coupling with diisopropylamine, giving a stable triazene.[12,143,143,144]

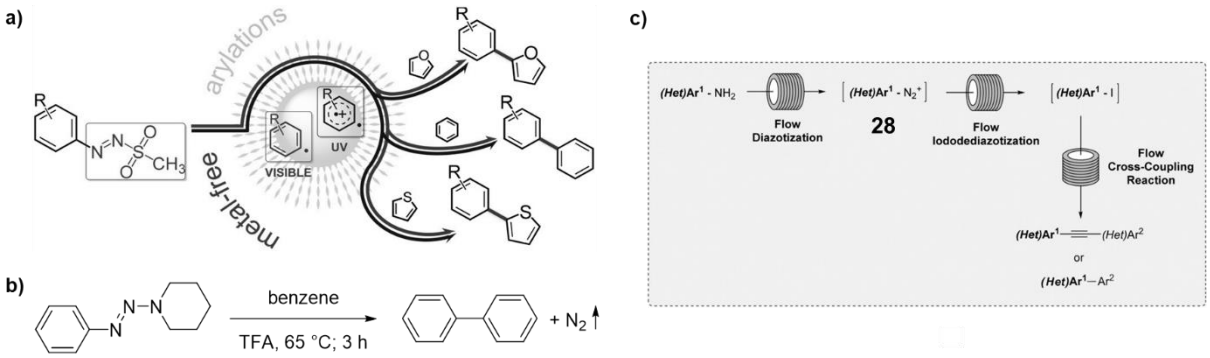

Figure 20: a) Visible light direct C-H arylation using arylazo sulfones as precursor. Adapted with the permission from Ref. [142] copyright 2016 American Chemical Society; **b)** Thermal biphenyl synthesis using triazenes[141]; **c)** Flow diazotation of anilines giving arene diazonium methanesulfonates **28** as precursor for cross-coupling. Adapted with the permission from Ref. [143] copyright 2016 WILEY-VCH.

Since the mentioned results are not satisfactory, the synthetic route has to be reviewed. A new set of conditions for the heterogeneous photocatalyzed direct C-H arylation in the FFMR is defined:

- highly soluble, easily accessible but safe and stable substrates
- organic solvent promoting the reaction
- titanium(IV) oxide - anatase modification will still be used
- avoid additives, promoting side-reactions: e.g. organic bases

A non-complex solvent matrix with only one compound will be used to avoid any unpredictable side-effects.
Moreover, any additives, like inorganic or organic bases, will not be used. Organic bases (e.g. pyridine) show a high possibility to undergo an arylation reaction as well. A competitive reaction is expected, due to the higher electron density, even at low concentrations.[30,145]

With all those information in mind, several alternative counter-ions are tested in screening reactions (for parallel studies, batch experiments are used). Generation of a soluble diazonium salt is realized by diazotation of the corresponding 3-CF_3-aniline **25a** (50 mM) with 1.2 equivalents *tert*-butyl nitrite and one equiv. organic acid. *In-situ* formation of the diazonium salt and photocatalyzed arylation are performed in one pot using one equivalent anatase and benzene to produce 3-CF_3-biphenyl **26b** (Scheme 14). In particular, the influence of different organic acids, solvents and wavelengths is evaluated (Table 7). In the first move, the circumstance of providing one equivalent of TFA is accepted for better comparability with the other organic acids, although corresponding diazonium trifluoroacetates occur as double salts when isolated.[131,146,147]
The influence of different amounts of trifluoroacetic acid is discussed later in chapter 3.1.3.3.

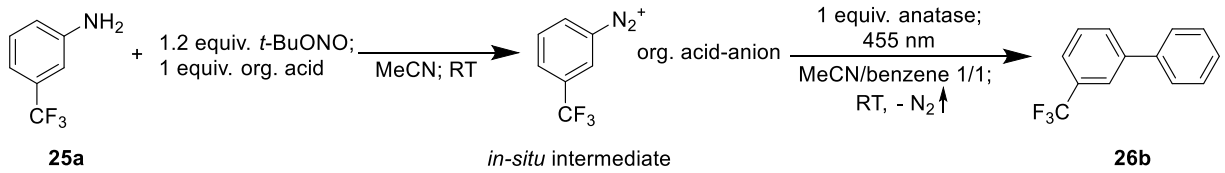

Scheme 14: Photocatalytic C-H arylation of benzene using an *in-situ* generated, highly soluble diazonium salt.

Table 7: Batch screening reactions of 3-CF_3-biphenyl using *in-situ* generated diazonium salts.[a].

#	solvent	organic acid	photocatalyst	λ [nm]	*t* [h]	by-product **27**	yield **26b** [%][b]
1	MeCN	TFA	TiO_2 - anatase	455	17	traces	80 / 58[c]
2	MeCN	CH_3SO_3H	TiO_2 - anatase	455	17	~ 5%	10
3	MeCN	CF_3SO_3H	TiO_2 - anatase	455	17	~ 1%	16
4	MeCN/EtOH 7/3	TFA	TiO_2 - anatase	455	17	~ 1%	58
5	EtOH	TFA	TiO_2 - anatase	455	1	~ 8%	8
6	MeCN	TFA	TiO_2 - anatase	455	1	traces	36
7	MeCN	TFA	-	455	1	traces	18
8	MeCN	TFA	TiO_2 - anatase	365	1	traces	34
9	MeCN	TFA	-	365	1	traces	34

a: Reaction conditions: 50 mM 3-CF_3-aniline, 1.2 equiv. *t*-BuONO, 1 equiv. organic acid, 1 equiv. metal oxide, solvent/benzene (V/V=1/1), 10 mL RT, 6 W_{el}; **b:** Determined by GC/MS; **c:** Yield after chromatographic purification.

80% 3-CF_3-biphenyl, without any by-product **27**, is found by applying one equivalent trifluoroacetic acid in combination with one equivalent anatase (in acetonitrile) and 17 h irradiation time (455 nm, see Table 7 entry #1). Other tested organic acids, like methanesulfonic acid or trifluoromethanesulfonic acid, result in less yield. Reasons are a lowered selectivity for diazonium salt generation or a stabilized diazo functionality with less reactivity in the subsequent photoredox step. Furthermore, the aryl ammonium methanesulfonate is insoluble in acetonitrile, which is inappropriate with respect to a continuous operability. Acetonitrile seems to be an elegant solvent, since mixtures of or neat ethanol decreases yield of the benchmark reaction drastically.

The omission of ethanol leads to no further formation of ethyl azoethers anymore. However, a promoting effect of titanium(IV) oxide as photocatalyst is observed and listed in entry #6 and #7 of Table 7. Titanium(IV) oxide implies a supporting effect on conversion by a single electron transfer. Moreover it is known, that trifluoroacetic acid promotes the photoactivity of titanium(IV) oxide. Trifluoroacetic acid will act an electron scavenger, as photocatalytic experiments of acetone oxidation, as well as UV/Vis spectroscopy or XPS analysis show. This reduces recombination of photogenerated electrons and holes on the metal oxide.[148]

Production rate does not benefit from the high-energy UV-A light (Table 7 entry #8 and #9). It seems, that 365 nm wavelength directly addresses the diazonium compound, because no difference is found with or without the photocatalyst. Still no by-product **27** is formed, which is worth to be mentioned.

Following that, several UV/Vis spectra (Figure 21) are recorded for better understanding of the observed phenomena. Either acetonitrile or acetonitrile/benzene (V/V=1/1) are used as matrix. It is assumed, that a high ratio of benzene can have a significant effect onto the system (appearance of CT-bands).

3-CF_3-aniline **25a** as well as its trifluoroacetate salt **25b** show a n-σ^* transition at 301 nm (Figure 21 — graphs), as expected.[56] The addition of 1.2 equivalents *tert*-butyl nitrite initiates *in-situ* formation of 3-CF_3-phenyldiazonium trifluoroacetate. Formation of the diazonium salt is indicated indirectly by the appearance of a second absorption band at 350 nm (refer Figure 21 c and d — graphs). This absorption band is assigned to different electronic transitions. Side-products or intermediates (including diazo group and nitrosamine/diazo hydroxide, respectively) occur, which show a n-π^* transition in this region.[56,149] Another fact is the occurrence of charge-transfer complexes of the diazonium trifluoroacetate in combination with the starting material 3-CF_3-aniline and its ammonium trifluoroacetate (refer chapter 3.1.6).

A weak absorption maximum at 354 nm is found for the anatase suspension (Figure 21 — graphs) in neat acetonitrile as well as in acetonitrile/benzene (V/V=1/1). The general baseline offset in those spectra is explained by the overall absorption of the solid metal oxide particles.

When mixing anatase particles with the *in-situ* generated diazonium trifluoroacetate, no additional absorption or charge-transfer bands are observed in the range of 455 nm, even when using a high excess of anatase.

Replacing benzene by anisole has no beneficial effect either (Figure 21 d). This means, that no CT-band in the range of 455 nm is formed by this π-electron donor. In this particular case, UV/Vis spectroscopy gives no explanation, why C-H arylation via arene diazonium trifluoroacetates at 455 nm comes along with a high selectivity of 3-CF_3-biphenyl.

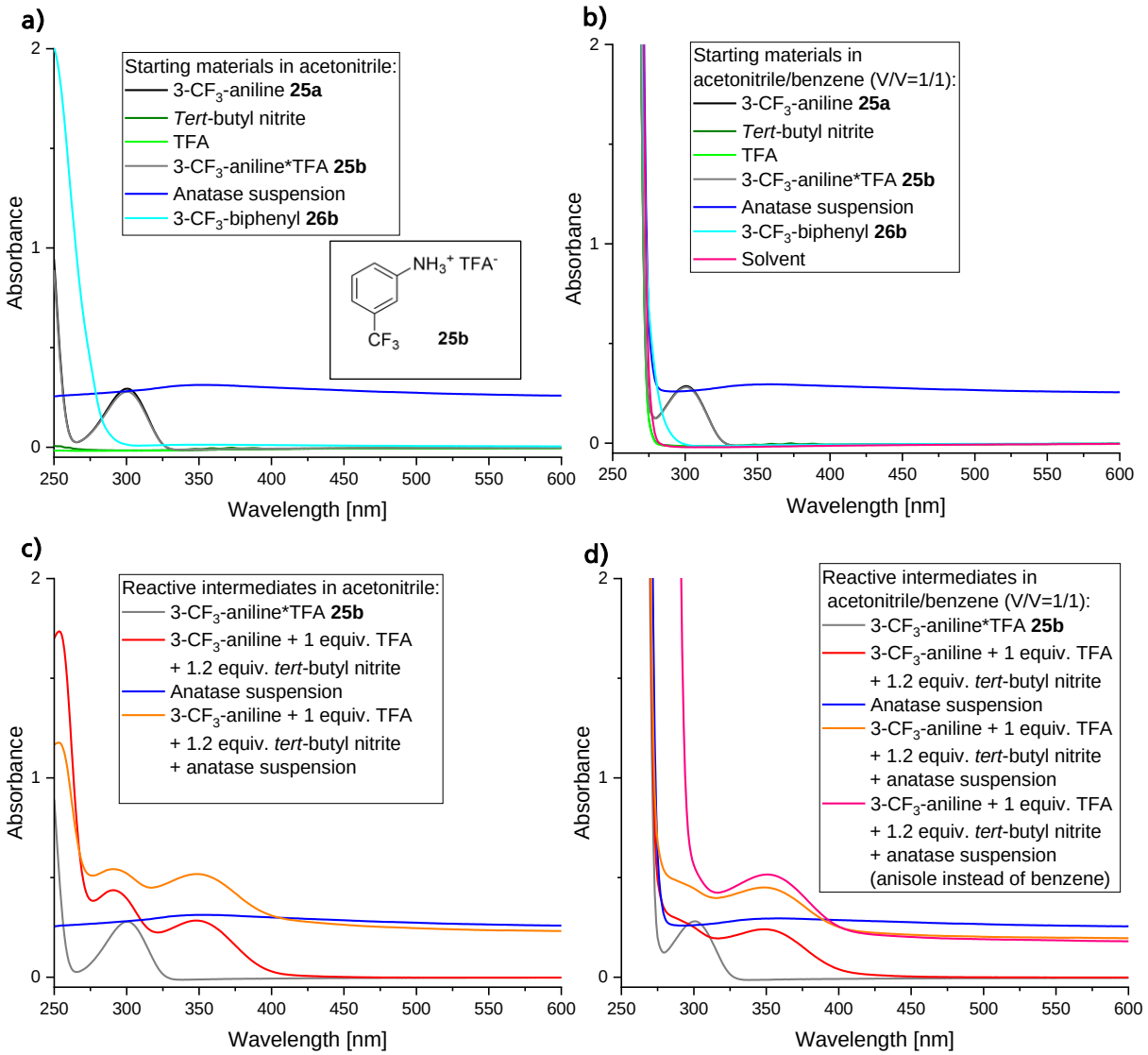

Figure 21: UV/Vis spectra of different components of heterogeneous photoarylation; **a)** in MeCN: — 1.25 mM 3-CF_3-aniline, — 1.5 mM *t*-BuONO, — 1.25 mM TFA, — 1.25 mM 3-CF_3-aniline + 1 equiv. TFA, — ~20 mM anatase suspension, — 1.25 mM 3-CF_3-biphenyl; **b)** in MeCN/benzene (V/V=1/1): — 1.25 mM 3-CF_3-aniline, — 1.5 mM *t*-BuONO, — 1.25 mM TFA, — 1.25 mM 3-CF_3-aniline + 1 equiv. TFA, — ~20 mM anatase suspension, — 1.25 mM 3-CF_3-biphenyl; — solvent; **c)** in MeCN: — 1.25 mM 3-CF_3-aniline + 1 equiv. TFA, — 1.25 mM 3-CF_3-aniline + 1 equiv. TFA + 1.2 equiv. *t*-BuONO, — ~20 mM anatase suspension, — 1.25 mM 3-CF_3-aniline + 1 equiv. TFA + 1.2 equiv. *t*-BuONO + ~20 mM anatase suspension; **d)** in MeCN/benzene (V/V=1/1): —1.25 mM 3-CF_3-aniline + 1 equiv. TFA, — 1.25 mM 3-CF_3-aniline + 1 equiv. TFA + 1.2 equiv. *t*-BuONO, — ~20 mM anatase suspension, — 1.25 mM 3-CF_3-aniline + 1 equiv. TFA + 1.2 equiv. *t*-BuONO + ~20 mM anatase suspension, — 1.25 mM 3-CF_3-aniline + 1 equiv. TFA + 1.2 equiv. *t*-BuONO + ~20 mM anatase suspension (in anisole instead of benzene).

In a next step, more detailed batch experiments (Figure 22) are conducted, giving an impression of the beneficial effect of titanium(IV) oxide in the anatase modification as photocatalyst. Reaction kinetics are distinguishable with respect to the presence of the photocatalyst and irradiation. A linear trend is found when using 455 nm (6 W_{el}) in

combination with one equivalent of anatase, due to a zero-order kinetics of the photocatalytic arylation reaction. Again, 80% of **26b** is achieved after 17 h without any formation of **27**.

For short irradiation time, results of each route do not differ much. Interestingly, a relative high yield of 3-CF_3-biphenyl is obtained after 30 minutes in all experiments. This circumstance is promoted by a parallel thermally induced reaction pathway, having a higher reaction rate in comparison to the favored photochemical route. The thermal reaction is confirmed by a batch experiment without any light and catalyst.

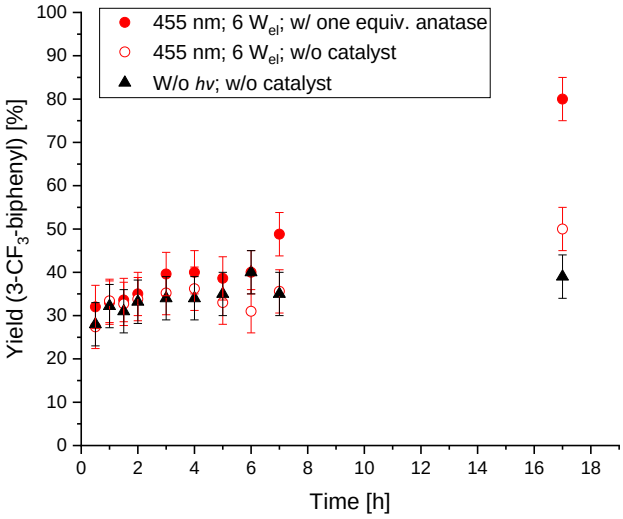

Figure 22: Batch synthesis of 3-CF_3-biphenyl **26b** using *in-situ* generated diazonium trifluoroacetate: ● reaction assisted with 1 equiv. anatase and 455 nm 6 W_{el}, ○ reaction assisted with 455 nm 6 W_{el}, ▲ reaction w/o light and w/o catalyst; General reaction conditions: 50 mM 3-CF_3-aniline, 1.2 equiv. *t*-BuONO, 1 equiv. TFA, MeCN/benzene (V/V =1/1), RT, 10 mL; no occurrence of by-product **27**; determined by GC/MS.

This procedure, using diazonium trifluoroacetates, is transferred into a continuous protocol using the FFMR.

One aim has to be the continuous *in-situ* production of the diazonium trifluoroacetate using one equivalent of TFA before adding benzene (Scheme 15).

As aforementioned results have shown, a relative low conversion rate per FFMR-pass is estimated. In consequence, it is planned to recirculate the reaction mixture more often. In ideal circumstances, thermal side-reactions giving 3-CF_3-biphenyl or the by-product are suppressed effectively.

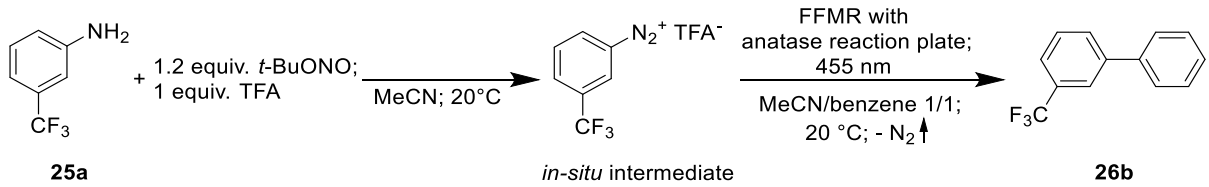

Scheme 15: Continuous photocatalytic C-H arylation of benzene with *in-situ* generated diazonium trifluoroacetate in a falling film micro reactor.

In a first orienting experiment, a premixed solution (all substrates are mixed in a separate vial), containing the diazonium trifluoroacetate and benzene in acetonitrile, passes the reactor 20 times. In each separated cycle (Figure 23, • graph), the complete volume is irradiated. Similar to the mentioned batch experiments, thermal reaction results in 24% **26b** directly after the first cycle. With a (rather) linear trend, yield increases to 56% after 20 cycles, which stands for a productivity rate of ~1.6% per cycle. In comparison to the presented batch reactions, by-product formation returns. It is stated, that direct homocoupling is caused by a thermal effect as well as insufficient mixing, since ~4% of the starting material are initially converted into the by-product **27** (no further by-product formation observed after the first cycle).

Instead of evaluating the maximum yield of this reaction by simply adding more cycles, the setup is adapted towards a full continuous procedure. Therefore, the concept of a continuously operated FFMR including a loop for cyclisation (refer Figure 24) is realized as far as possible with a semi-batch setup.
Here, diazonium trifluoroacetate is generated *in-situ* via a separated element (10 minutes residence time) and benzene is added just before entering the FFMR loop. A Postnova syringe pump is used to circulate the solution with a flow rate of 0.5 mL×min^{-1}. When reaching a steady state configuration (loop filled with medium after a single FFMR pass), the by-pass and the infeed of fresh substrate are closed. The liquid circulates inside the isolated FFMR loop permanently for 120 minutes (FFMR loop volume: 4 mL). Having passed the irradiation zone of the FFMR 15 times (statistically), 52% yield of **26b** is obtained (Figure 23, ▲ graph). This corresponds to an average productivity rate of ~1.5% per cycle, which is comparable to the previously conducted experiment (Figure 23, • graph). Identical amount of by-product **27** is formed once again.

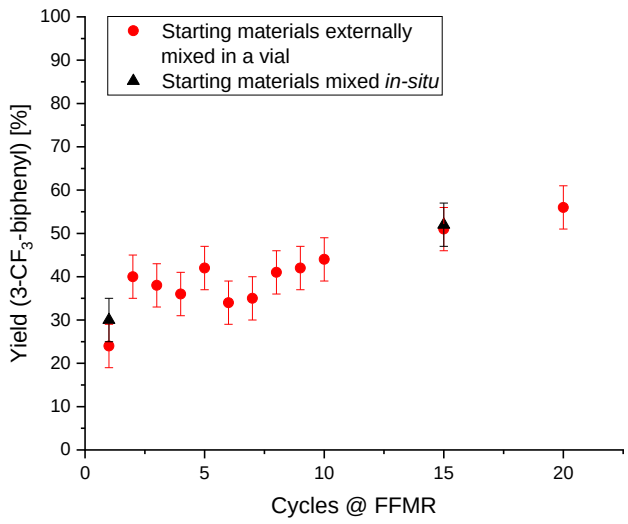

Figure 23: Yield of 3-CF_3-biphenyl synthesis using the FFMR: ● all compounds are combined and mixed separately before use, ▲ *in-situ* generation of diazonium trifluoroacetate and mixing with benzene; General reaction conditions: 50 mM 3-CF_3-aniline, 1.2 equiv. *t*-BuONO, 1 equiv. TFA, MeCN/benzene (V/V =1/1), RT, 455 nm 6 W_{el}, 23 mg anatase immobilized on the reaction plate; determined by GC/MS.

In comparison to the 17 h batch experiment, specific productivity is increased by a factor of 6 to 0.013 mol×(L×h)$^{-1}$ with the here presented FFMR setup (Table 8 entry #4). In this special case, specific productivity considers the residence time inside the whole reactor setup. The residence time is calculated by the inner volumes of the FFMR, capillaries, pump and the required gas/liquid separator.

In contrast to the residence time, irradiation time focuses only on that interval in which reaction mixture is irradiated. Assuming an irradiation time of 2.25 min (15 cycles; 9 s residence time per cycle in the FFMR[31]), specific productivity increases drastically to 0.684 mol×(L×h)$^{-1}$. Complete irradiation of the solid-liquid interfacial area is guaranteed, since light will pass the thin liquid film completely. In contrast, most light is absorbed in a batch process without starting any essential photochemical reaction. This clearly shows the beneficial effect of the photocatalytic thin film irradiation inside the FFMR.

Table 8: Specific productivity of different heterogeneous C-H arylation with respect to process/ irradiation time.

#	synthesis type	starting material	product	process time	irradiation time	yield	specific productivity by process time [mol×(L×h)$^{-1}$]	specific productivity by irradiation time [mol×(L×h)$^{-1}$]
1	flow[a]	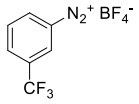	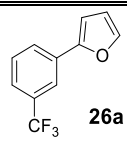 **26a**	9 s	9 s	91% [31]	17.94	17.94
2	batch[b]	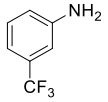	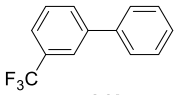 **26b**	17 h	17 h	80%	0.002	0.002
3	batch[c]	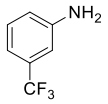	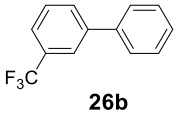 **26b**	17 h	17 h	50%	0.001	0.001
4	flow[d]	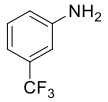	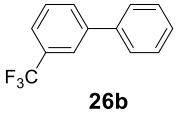 **26b**	2 h	2.25 min	52%	0.013	0.684

a: 50 mM 3-CF_3-phenyldiazonium tetrafluoroborate, ethanol/furan (V/V=1/1), 455 nm, RT, 2.4 W_{el}, FFMR with anatase reaction plate; **b:** 50 mM 3-CF_3-aniline, 1 equiv. TFA, 1.2 equiv. *t*-BuONO, MeCN/benzene (V/V=1/1), 455 nm, RT, 6 W_{el}, 1 equiv. anatase, 10 mL; **c:** 50 mM 3-CF_3-aniline, 1 equiv. TFA, 1.2 equiv. *t*-BuONO, MeCN/benzene (V/V=1/1), 455 nm, RT, 6 W_{el}, 10 mL; **d:** 50 mM 3-CF_3-aniline, 1 equiv. TFA, 1.2 equiv. *t*-BuONO, MeCN/benzene (V/V=1/1), 455 nm, RT, 6 W_{el}, FFMR with anatase reaction plate (23 mg), 4 mL.

Technical realization of a continuously operated process with an in- and out-flow (see Figure 24) is not discussed any further. Since an overall infeed rate of ~0.033 mL×min^{-1} is the consequence, when considering 15 passes in the FFMR loop, even lower flow rates of the aniline, alkyl nitrite and arene feed result. Even in a lab scale setup, these low flow rates are difficult to realize for a continuous application, while a high reliability of the setup is worsened at the same time. Optimization of cyclisation in the FFMR loop is not considered yet, resulting in lower flow rates.

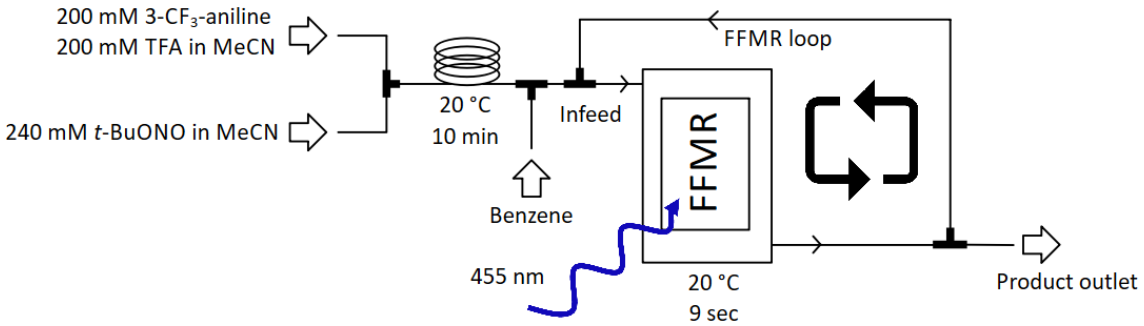

Figure 24: Schematical sketch for continuous production of 3-CF_3-biphenyl with a FFMR. The diazonium salt is generated *in-situ* and benzene is added separately within the infeed of the reactor. After irradiation and recirculation in the FFMR, same volume is removed via the product outlet.

In summary, the FFMR provides the feasibility of enhancing the specific productivity for 3-CF_3-biphenyl synthesis via diazonium trifluoroacetates. Nevertheless, productivity is drastically restrained by technical limits. To overcome these issues, different optimization methods are suggested. A decrease of the loop volume (dead volume) would significantly lower the process time. Modification of the falling film micro reactor (e.g. usage of the FFMR-LARGE) with a longer reaction plate would increase irradiation time and therefore the number of cycles could be decreased.

Another way of achieving much longer irradiation time, while having technical realizable flow rates, is the application of a capillary photoreactor. However, with such a reactor type, continuous transport of a solid (here: heterogeneous photocatalyst) is mandatory and has to be implemented.

3.1.2.3 Heterogeneous photocatalytic arylation in a capillary photoreactor

A heterogeneous photocatalytic arylation reaction is reported as a two-phase system in the previously mentioned chapters of 3.1.2. The solid catalyst is either suspended directly in the liquid organic phase (batch concept) or immobilized onto the reaction plate of the FFMR. Emerging and migrating nitrogen does not play a crucial role as additional third phase, since a gaseous phase “above” the media is permanently present in both cases.

New challenges appear, when applying a capillary or a tube as a (photo-)reactor. Nitrogen, as an additional phase, can´t be neglected in a capillary (photo-)reactor, since its volume will unavoidably consume space. As result, the capillary volume, usually used for the liquid or solid, is replaced by this third phase, if the reaction is conducted at atmospheric pressure. One has to keep in mind that lowered flow rates cause a longer reaction time (and usually higher conversion), which generates more nitrogen gas by arylation. In consequence, this will push the media out of the capillary more quickly.

Furthermore, heterogeneous catalyst slurry has to be "tamed" by an appropriate setup. In this case, a small serial micro reactor (SMBR) concept is used to overcome this issue.[43] To prepare a satisfactory SMBR flow with a stable and continuous transport of a solid catalyst, a model reaction using diazo anhydrides for the generation of 3-CF_3-biphenyl **26b** is chosen (Scheme 16).[28] Irradiation with 455 nm and the presence of anatase have a positive effect on the formation of the benchmark molecule, which is proven by batch screening. In comparison to the previously described process using diazonium trifluoroacetate (chapter 3.1.2.2) yield is lowered to 40% after 17h (Table 10 entry #2). First of all, this circumstance is neglected, because focus is put on the formation of a stable particle transport.

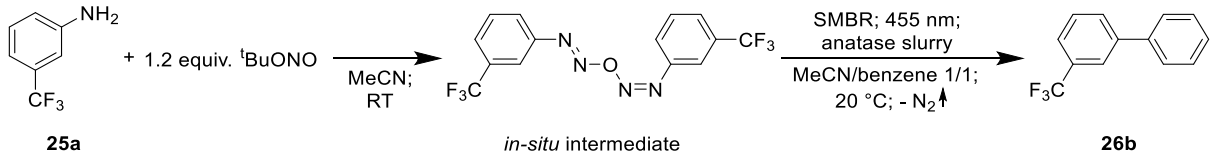

Scheme 16: Continuous photocatalytic C-H arylation of benzene via a diazo anhydride in a SMBR concept.

A solid-liquid-gas SMBR concept, analog to Pieber *et al.*, has one major disadvantage according to the catalyst transport. Pure acetonitrile/benzene (V/V=1/1) as liquid phase is too apolar (beside its low viscosity) and does not stabilize a suspension of anatase nanopowder (surface OH functionalities) efficiently.[150] The catalyst quickly deposits along the first few centimeters of the capillary, causing a complete loss of whole catalyst to the end of the reactor outlet. Interestingly, literature reports the deposition of TiO_2-nanoparticels on fluorinated capillary walls, in order to perform

photocatalysis.[46,151] For this reason, hurdles have to be overcome, with a non-trivial continuous flow setup, to prevent clogging or deposition.

Table 9: Technique and guidelines to overcome clogging in capillaries (table by F. Scheiff, D. W. Agar in *Micro-Segmented Flow: Applications in Chemistry and Biology*. Adapted with the permission from Ref. [152] copyright 2014 Springer-Verlag).

Technique	Guidelines to overcome clogging
Prevent coagulation and cluster formation	- Remove exceptionally large particles from polydisperse samples - Stabilize particles sterically or electrostatically - Avoid curved geometries an inertial deposition
Microchannel design	- Select wall materials that inhibit attraction of particles
Process procedures	- Flush microchannel or dissolve deposits occasionally - Use flow structures that prevent particle-wall contact
External forces	- Apply external forces to maintain uniform dispersions, e.g. ultrasound

By following the guideline of Table 9, an optimized SMBR concept (Figure 25, Figure 27 and Figure 28) is developed for the synthesis of **26b** via diazo anhydrides.
Cluster formation of catalyst particles, which causes clogging, is eluded by the use of the 1/8" FEP capillary photoreactor. Edges or hitches in the SMBR generator (Figure 26) are avoided by using flangeless fittings, Y/T-junctions and connectors with a same bore diameter as the capillary. All capillaries are placed in a wide radius to prevent any kinks. A Y-junction shows best performance to create a segmented nitrogen-liquid flow and the alkyl nitrite is added by a 3-way valve. As shown in Figure 27b, alkyl nitrite enters each liquid plug, as color change due to diazo anhydride formation indicates. Via a second 3-way valve, a reliable and consistent transfer of the solid catalyst into the liquid phase is enabled (Figure 27c). To avoid mass gradients, the anatase slurry feed is permanently mixed by a magnetic stirring bar, being placed inside the syringe.[48] The stirring bar is moved by an external bar magnet, mounted on a small spinning disc. Constant mixing efficiency is realized by attaching the holder of the spinning disc onto the drive slide of the syringe pump, giving a constant distance between the two magnets. This holder is specially designed and build for a Chemyx Nexus 6000 syringe pump. Easy adaption to other syringe pumps is feasible, since most of them have

threads in the plungers drive slide, which usually secure a bracket for withdraw operations (see Figure 225 in the appendix).

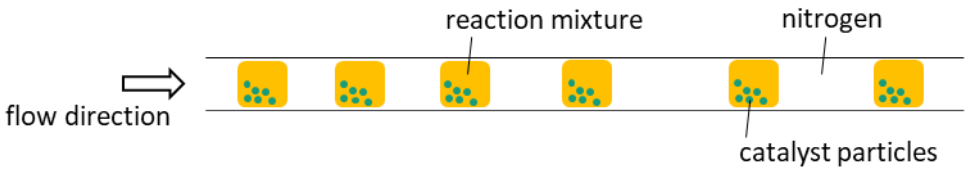

Figure 25: Concept of gas-liquid-solid SMBR flow: nitrogen is used as continuous phase to push the liquid plugs along the capillary (additional gas expulses during the reaction); solid catalyst particles are suspended in the liquid phase.

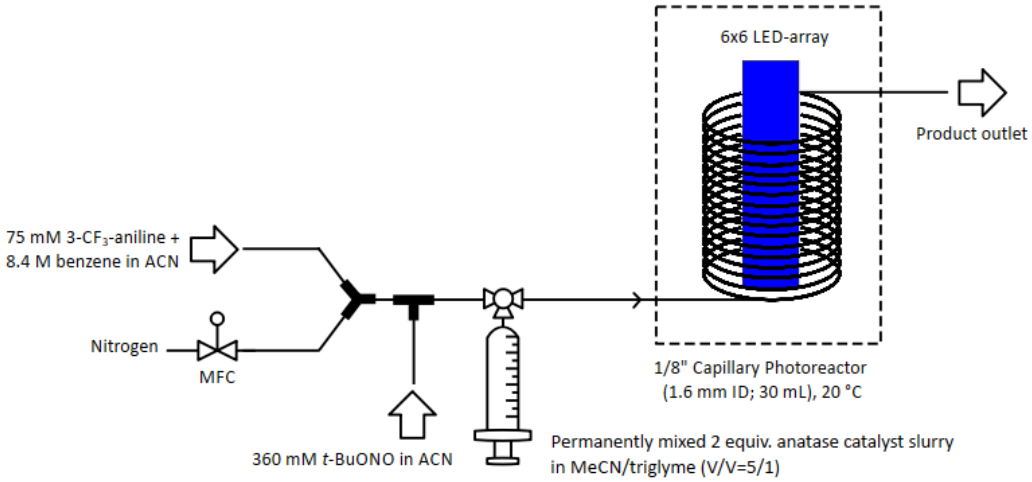

Figure 26: Schema for continuous production of 3-CF_3-biphenyl using a gas-liquid-solid SMBR concept. A Y-junction generates a gas-liquid slug flow. Via a 3-way-valve *tert*-butyl nitrite is added into the slug to start the reaction. A second 3-way valve adds the heterogeneous anatase catalyst slurry into the liquid phase and heterogeneous photocatalysis is conducted in a 1/8" FEP capillary photoreactor.

As mentioned, polarity of the liquid has to be adjusted towards a lowered surface tension between solid and liquid. Therefore, the liquid phase is tuned by replacing acetonitrile step-wise with other solvents. Co-solvents like glycol or DMSO are tested, but the benchmark molecule **26b** is created in traces only.

Finally, a stable SMBR flow is formed by addition of 7% triglyme (triethylene glycol dimethyl ether). Unfortunately, experiments with this co-solvent show a complete deactivation of the catalyst. As listed in Table 10 entry #5, usage of 2 equivalents anatase catalyst gives 25% of 3-CF_3-biphenyl. In comparison, 30% **26b** is obtained with a gas-liquid slug flow without any catalyst (triglyme is not required). Same yield (24%) results, when working in absence of the catalyst and light.

This indicates a completely blocked catalyst. Polarity adaption of the liquid phase with triglyme devastates all reinforcing aspects of a MRT application, including shear force induced mixing and optimal mass transfer inside the small dimensioned slugs.[48,153] With this presented gas-liquid-solid SMBR setup, the advantages of this promising concept cannot be put to full use.

Table 10: Comparison of different setups for 3-CF_3-synthesis using diazo anhydride as intermediate: Batch vs. gas-liquid slug flow vs. SMBR flow with anatase nanopowder in a 1/8" FEP capillary photoreactor.

#	synthesis type	photo catalyst	wavelength [nm]	process time	by-product **27**	yield **26b** [%][a]
1[b]	batch	-	-	17 h	4%	16
2[c]	batch	anatase (1 equiv.)	455	17 h	traces	40
3[d]	two phase slug flow	-	-	1 h	2%	24
4[e]	two phase slug flow	-	455	1 h	1%	30
5[f]	SMBR flow	anatase (2 equiv.)	455	1 h	1%	25

a: Determined by GC/MS; **b:** 50 mM 3-CF_3-aniline, 1.2 equiv. *t*-BuONO, MeCN/benzene (V/V=1/1), RT, 6 W_{el}, 10 mL; **c:** 50 mM 3-CF_3-aniline, 1.2 equiv. *t*-BuONO, MeCN/benzene (V/V=1/1), 1 equiv. anatase, RT, 6 W_{el}, 10 mL; **d:** 50 mM 3-CF_3-aniline, 1.2 equiv. *t*-BuONO, MeCN/benzene (V/V=1/1), 20 °C; **e:** 50 mM 3-CF_3-aniline, 1.2 equiv. *t*-BuONO, MeCN/benzene (V/V=1/1), 20 °C, 50 W_{el}; **f:** 50 mM 3-CF_3-aniline, 1.2 equiv. *t*-BuONO, (MeCN + triglyme)/benzene (V/V=1/1), 2 equiv. anatase; 20 °C, 50 W_{el}.

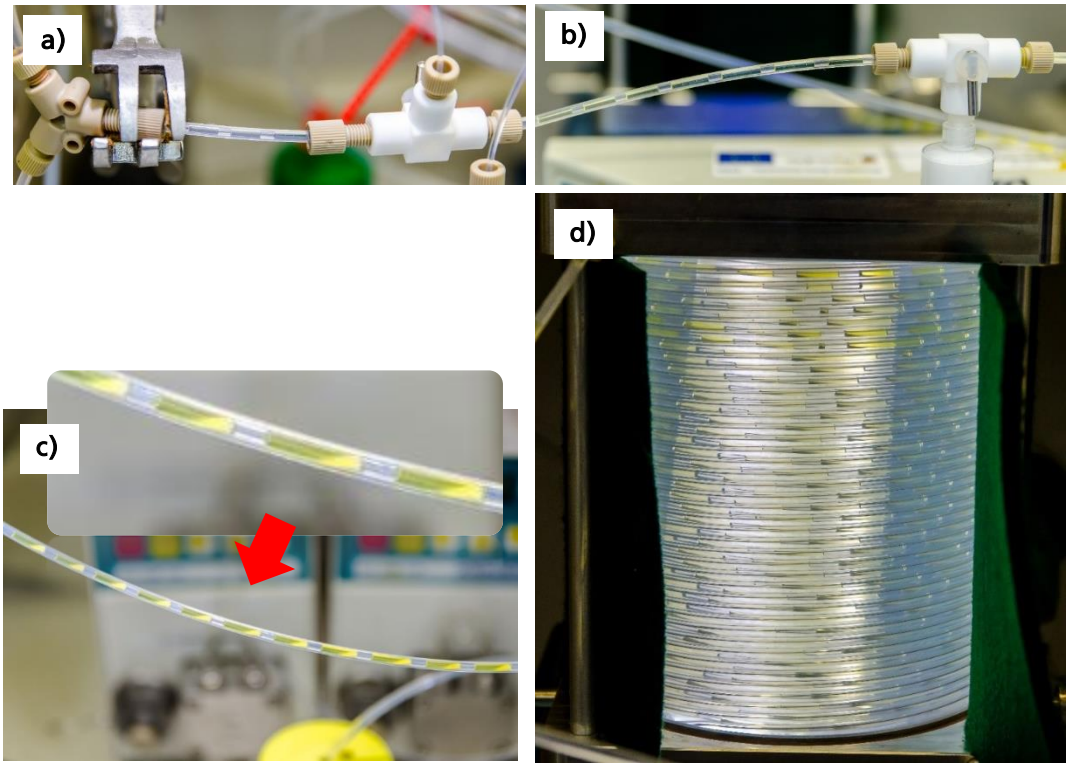

Figure 27: Generation of a stable gas-liquid-solid SMBR concept in 1/8" FEP capillaries; **a)** Via a Y-junction (bore 1.6 mm) a gas-liquid slug flow is generated with nitrogen $\dot{V}_{nitrogen}$=0.2 mL×min^{-1} and a liquid component (75 mM 3-CF_3-aniline + 8.4 M benzene in MeCN) $\dot{V}_{Feed\ A}$=0.2 mL×min^{-1}; **b)** diazo anhydride is generated *in-situ* in the liquid phase by adding 360 mM *t*-BuONO in MeCN $\dot{V}_{Feed\ B}$=0.05 mL×min^{-1}; **c)** via a 3-way valve (right side at b) a stable gas-liquid-solid plug flow is generated (Feed C: anatase 480 mg in 5 mL ACN + 1 mL triglyme, $\dot{V}_{Feed\ C}$=0.05 mL×min^{-1}); **d)** the stable SMBR flow is irradiated in a 1/8" FEP capillary photoreactor - 455 nm (50 W_{el}) - for better contrast white LED is used (© Fraunhofer IMM).

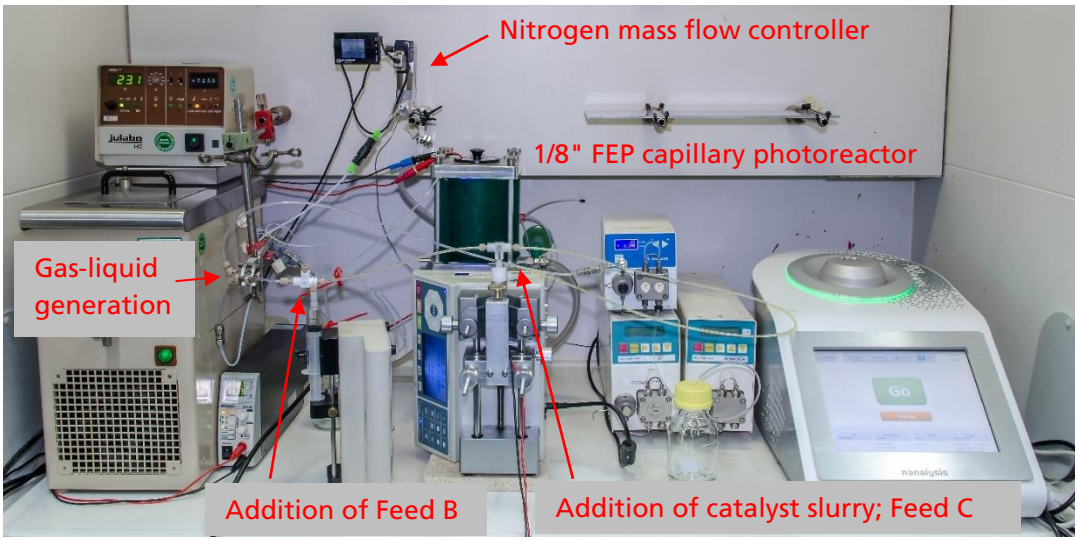

Figure 28: Complete setup for stable generation of a gas-liquid-solid SMBR concept and synthesis of 3-CF_3-biphenyl via diazo anhydride using 2 equiv. of anatase as photocatalyst in a 1/8" FEP capillary photoreactor - 455 nm (50 W_{el}) (© Fraunhofer IMM).

The existing SMBR concept is rethought and optimized (using *in-situ* generated diazonium trifluoroacetate as intermediate, Scheme 17).

A stable (gas-)liquid-liquid-solid SMBR-setup is realized by replacing the initial nitrogen feed with a fluorinated liquid (Fluorinert™ FC-40). The inert and immiscible character of this liquid is often used to create a continuous phase in microfluidic applications for the implementation of plug flows or core-shell droplets.[154] Its high transmittance (refer Figure 223 in the appendix) is another key factor, allowing usage of UV-A light for photochemical applications. In this particular case, FC-40 acts as a smear layer and waveguide.[155] Due to its electrostatic character, it will coat the FEP capillary wall completely. As observed, the solid catalyst will stay inside the organic phase and deposition along the wall is avoided (Figure 29). Ongoing N_2 formation of the C-H arylation via diazonium trifluoroacetate creates an additional fourth phase for further segmentation of the slugs. Due to the positive effect of FC-40, the solid photocatalyst can be used in the even smaller 1/16" FEP capillary photoreactor.

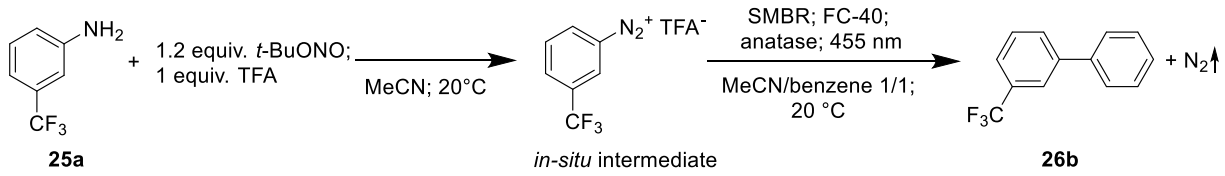

Scheme 17: Continuous photocatalytic C-H arylation of benzene with an *in-situ* generated diazonium trifluoroacetate in a SMBR.

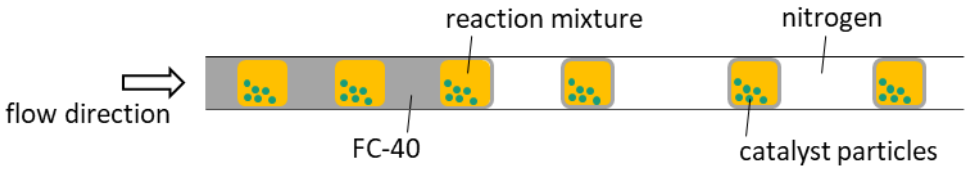

Figure 29: Concept of (gas-)liquid-liquid-solid SMBR flow: immiscible Fluorinert™ FC-40 is used as continuous phase to push the liquid plugs along the capillary, solid catalyst particles are suspended in the liquid phase, additionally nitrogen gas emerges during the reaction.

A segmented flow (Figure 30 and Figure 32 - Figure 39), using FC-40, is created with a slurry containing acetonitrile/benzene and anatase nanopowder (V/V=1/1 and 80 mg anatase nanopowder per 10 mL). The slurry is stabilized in a syringe by permanent mixing with a magnetic stirring bar, as aforementioned. Via a T-junction (bore 1.6 mm) a stable three phase plug flow is realized. Finally, the SMBR flow exits the capillary

photoreactor without any deposition of catalyst material along the FEP capillary walls. The reactor is tilted into a horizontal position allowing additional mixing of the particles inside the liquid phase by gravity due to the vertically oriented capillary windings.[37,41] Despite its high density, no entry of FC-40 into the syringe is observed at the respective 3-way valve (see Figure 227 in the appendix).

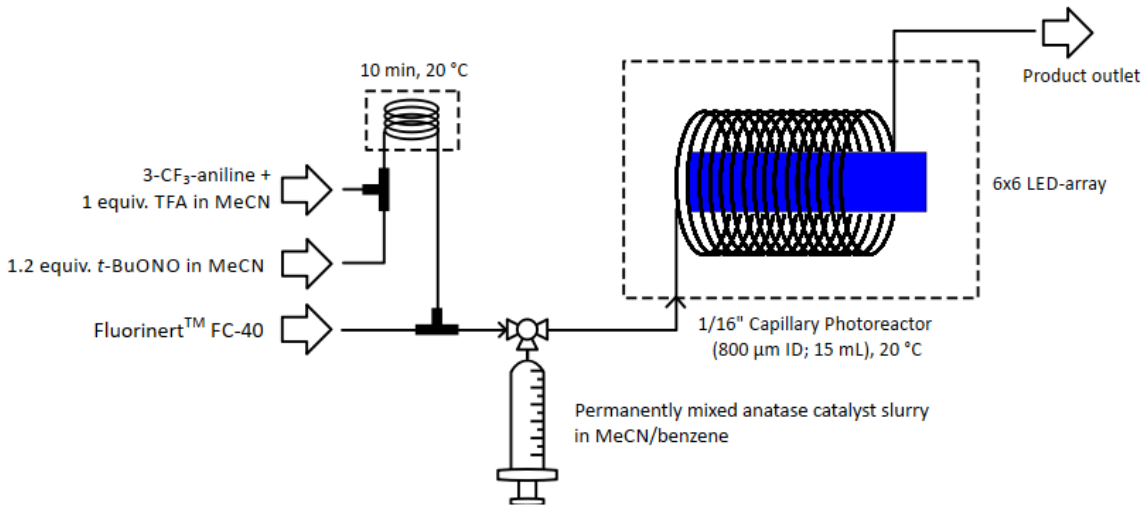

Figure 30: Schema for continuous production of 3-CF_3-biphenyl using a (gas-)liquid-liquid-solid SMBR concept. Via a T-junction liquid-liquid plug flow of Fluorinert™ FC-40 and diazonium trifluoroacetate is generated. A 3-way valve adds the heterogeneous anatase catalyst slurry into the liquid phase containing starting materials and heterogeneous photocatalysis is conducted in a 1/16" FEP capillary photoreactor.

As mentioned in chapter 3.1.2.2, a method for a longer irradiation time inside a photoreactor is required for the conduction of heterogeneous catalysis producing 3-CF_3-biphenyl. With the optimized SMBR concept, a residence time of at least 3 hours (according to the flow rate) is feasible.

First of all, reactor performance is tested with a "premixed" suspension by adding all compounds, required for *in-situ* generation of diazonium trifluoroacetate, into the catalyst slurry (acetonitrile/benzene V/V=1/1 + 80 mg anatase in 10 mL). The generated three phase plug flow is pumped through the 1/16" FEP capillary photoreactor at different residence times. After 3 h an unexpected high yield of 70% **26b** (Figure 31 ■ graph) is obtained using a low power LED-array (455 nm, 6 W_{el}) for irradiation of a (gas-)liquid-liquid-solid SMBR flow. To suppress thermal pathways and for a process development towards a full continuous arylation process, a separately *in-situ* generation for diazonium trifluoroacetate is aspired.

In experiments (Figure 31) with an *in-situ* generation of the diazonium trifluoroacetate intermediate, a lowered productivity of 3-CF_3-biphenyl formation (33% yield after 2 h, 455 nm, 6 W_{el}) is observed, although there are no obvious reasons. However, catalyst activity is not effected by FC-40, since high yield of 3-CF_3-biphenyl is obtained when using a "premixed" suspension. Even an increased photon flux by a boosted LED power (50 W_{el}) has no beneficial effect. Interestingly, yield is increased to 42% (1 h) when using a 365 nm 50 W_{el} LED-array.

Comparison of different flow concepts at 365 nm: solid anatase catalyst + FC-40 (SMBR, Figure 31 ◀ graph), no catalyst + FC-40 (Figure 31 ● graph), no catalyst + no FC-40 (Figure ***31*** ◆ graph) shows identical yield of 3-CF_3-biphenyl for each tested residence time inside the 1/16" capillary photoreactor. Unexpectedly, 70% yield of the benchmark product is also obtained with 365 nm (50 W_{el}) via an *in-situ* generated diazonium trifluoroacetate without any catalyst and FC-40.

At first glance, irradiation with 365 nm minimizes the beneficial effects of a serial micro batch reactor using titanium(IV) oxide - anatase modification as heterogeneous photocatalyst. However, unstable substrates might result in side-product formation by uncontrolled decomposition, if UV-A light is used to activate the photochemical reaction. In this case, it is important to use a photocatalytic reaction (with 455 nm visible light irradiation) for a significant increase of selectivity.

As long as resistant substrates can be irradiated with 365 nm, a promising catalyst-free synthetic route for a direct C-H arylation is found, which definitely deserves further investigations and experiments.

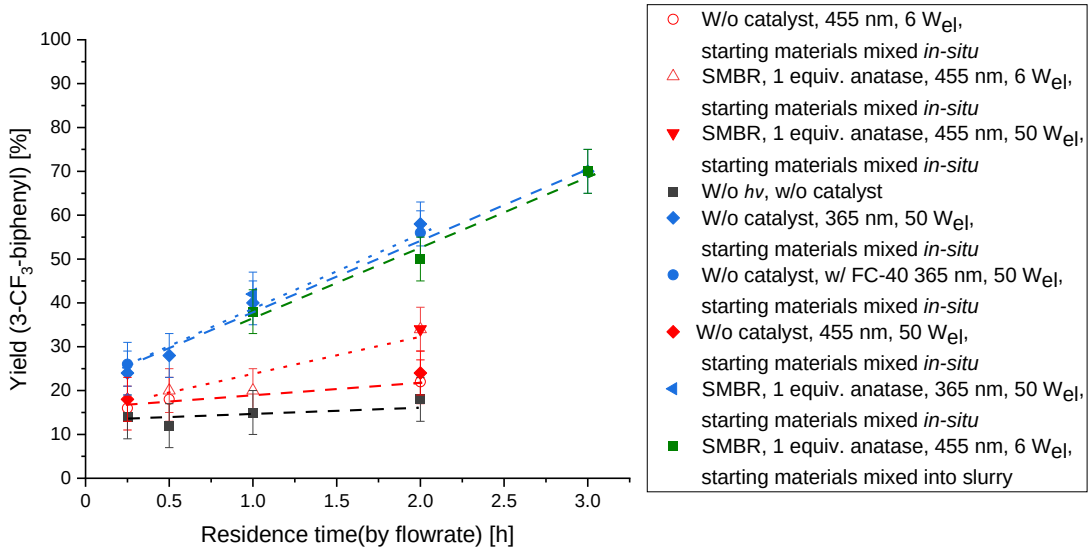

Figure 31: Synthesis of 3-CF_3-biphenyl using a (gas-)liquid-liquid-solid SMBR concept via *in-situ* diazonium trifluoroacetate in a 1/16" capillary photo reactor; General reaction conditions: 50 mM 3-CF_3-aniline, 1.2 equiv. *t*-BuONO, 1 equiv. TFA, MeCN/benzene (V/V =1/1), 20°C and parameters: ■ w/o light, w/o anatase, w/o FC-40, - - - data-trend; 455 nm, 6 W_{el}, 1 equiv. anatase, w/ FC-40, all components mixed into catalyst slurry, - - - data-trend; △ 455 nm, 6 W_{el}, 1 equiv. anatase, w/ FC-40 · · · data-trend; ▼ 455 nm, 50 W_{el}, 1 equiv. anatase, w/ FC-40; ○ 455 nm, 6 W_{el}, w/o anatase, w/o FC-40, - - - data-trend; ◆ 455 nm, 50 W_{el}, w/o anatase, w/o FC-40; ◀ 365 nm, 50 W_{el}, 1 equiv. anatase, w/ FC-40; ◆ 365 nm, 50 W_{el}, w/o anatase, w/o FC-40, - - - data-trend; ● 365 nm, 50 W_{el}, w/o anatase, w/ FC-40, · · · data-trend; by-product formation in all experiments ~1-4%; Determined by GC/MS.

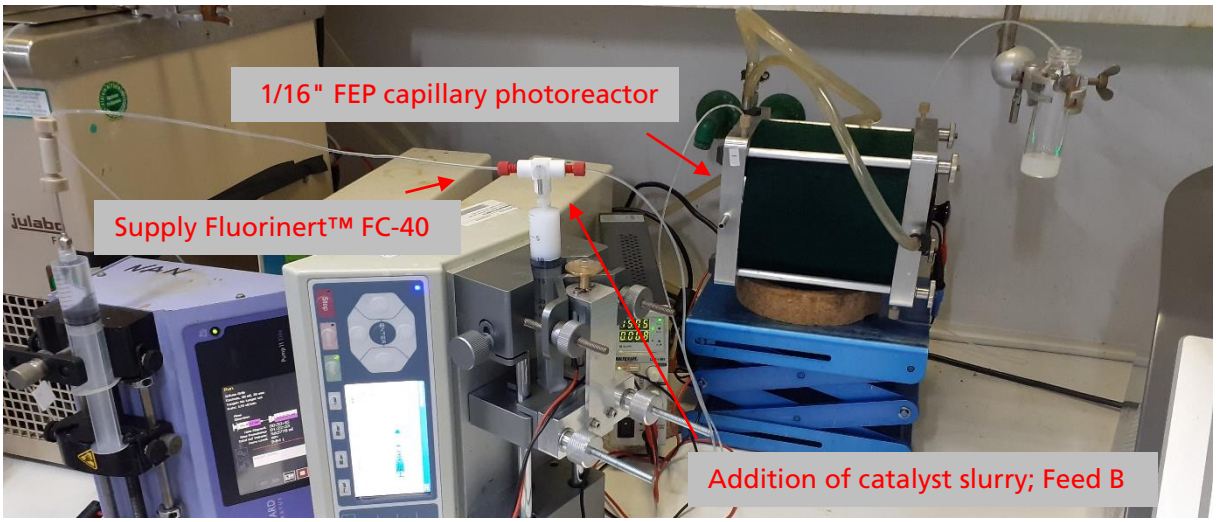

Figure 32: Complete setup for stable generation of a liquid-liquid-solid SMBR concept using anatase as solid catalyst in a horizontal 1/16" FEP capillary photoreactor - Feed A: Fluorinert™ FC-40, Feed B: 80 mg anatase nanopowder in 20 mL MeCN/benzene V/V=1/1).

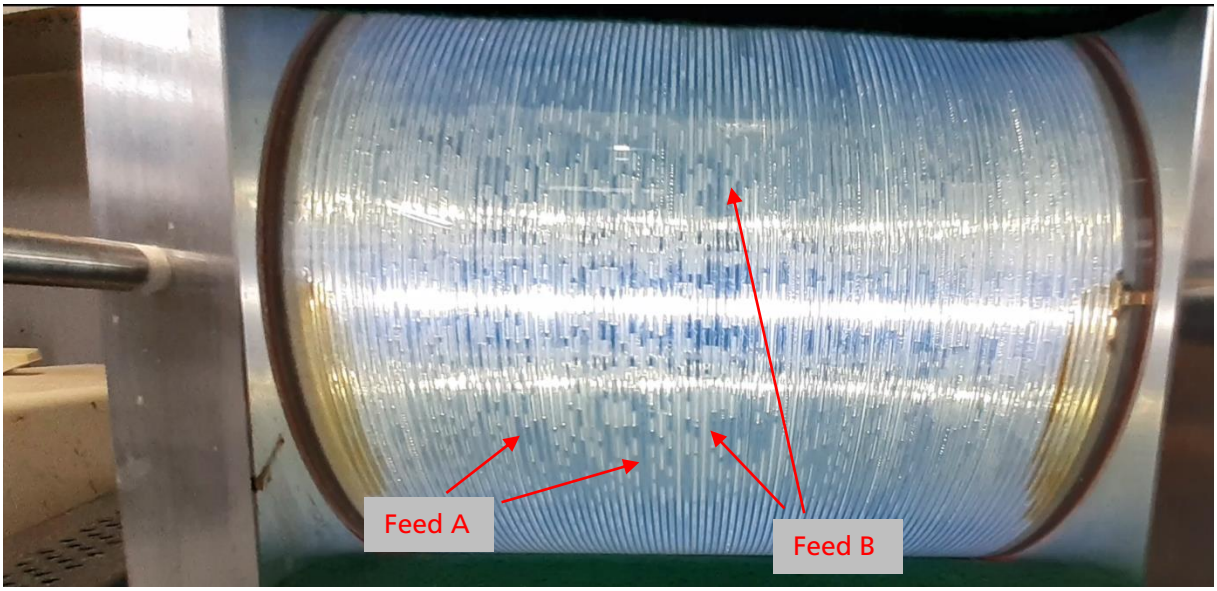

Figure 33: Stable liquid-liquid-solid SMBR flow using anatase as solid catalyst in a horizontal 1/16" FEP capillary photoreactor - Feed A: Fluorinert™ FC-40, Feed B: 80 mg anatase nanopowder in 20 mL MeCN/benzene V/V=1/1) - for better contrast white LEDs are used; brown material at the glass-aluminum transition: 2-component epoxy adhesive as assembly assistance.

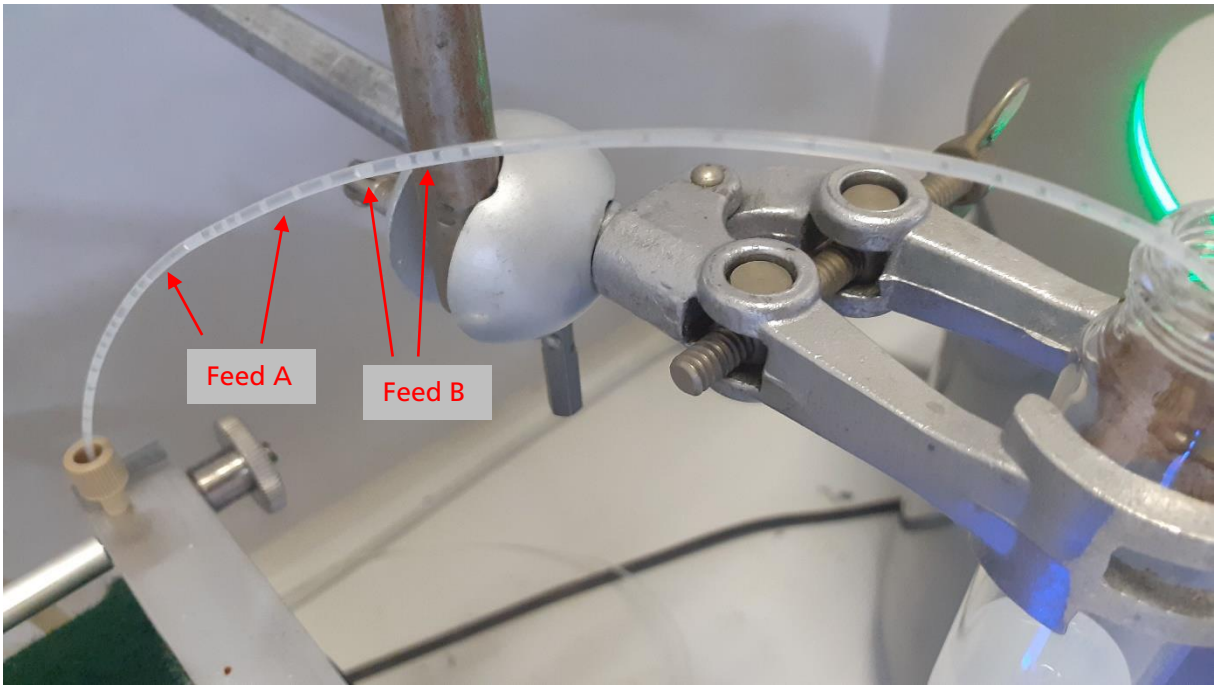

Figure 34: Reactor outlet; Stable liquid-liquid-solid SMBR flow using anatase as solid catalyst in 1/16" FEP capillary; Feed A: Fluorinert™ FC-40, Feed B: 80 mg anatase nanopowder in 20 mL MeCN/benzene V/V=1/1).

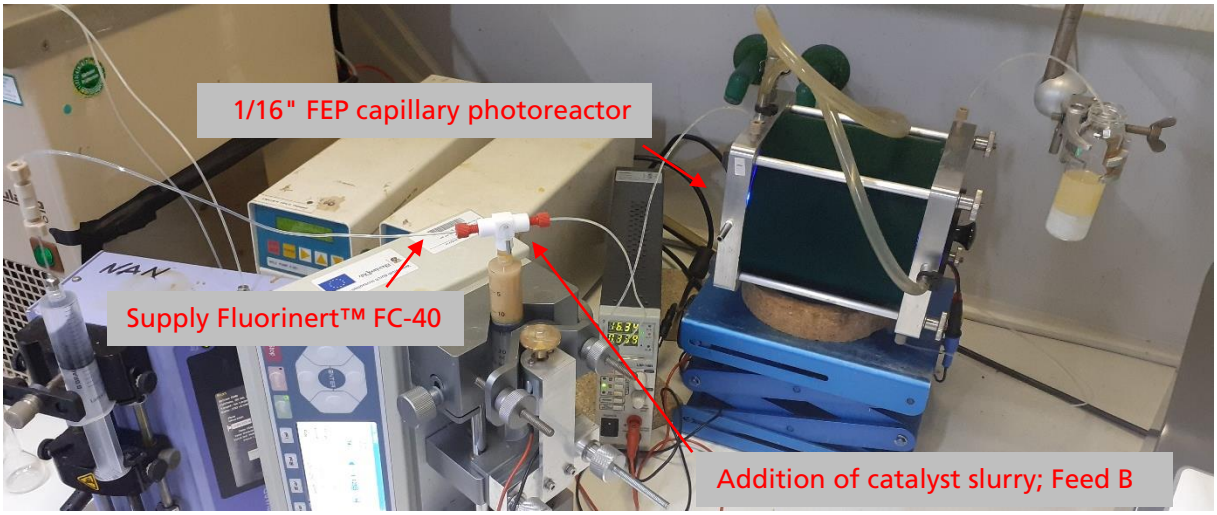

Figure 35: Complete setup for stable generation of a (gas-)liquid-liquid-solid SMBR concept and synthesis of 3-CF_3-biphenyl via *in-situ* generated diazonium trifluoroacetate in a horizontal 1/16" FEP capillary photoreactor - Feed A: Fluorinert™ FC-40, Feed B: 80 mg anatase nanopowder in 20 mL MeCN/benzene V/V=1/1 + 50 mM 3-CF_3-aniline, 1.2 equiv. *t*-BuONO, 1 equiv. TFA).

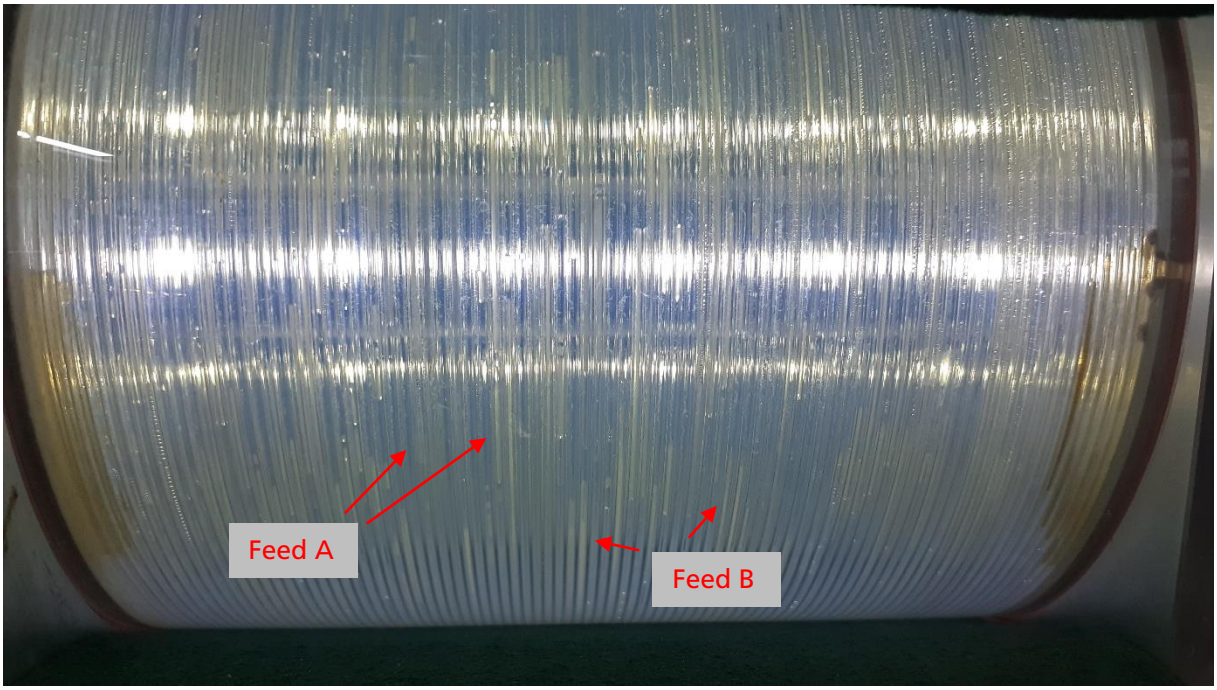

Figure 36: Stable (gas-)liquid-liquid-solid SMBR flow and synthesis of 3-CF_3-biphenyl via *in-situ* generated diazonium trifluoroacetate in a horizontal 1/16" FEP capillary photoreactor - Feed A: Fluorinert™ FC-40, Feed B: 80 mg anatase nanopowder in 20 mL MeCN/benzene V/V=1/1 + 50 mM 3-CF_3-aniline, 1.2 equiv. *t*-BuONO, 1 equiv. TFA); unfortunately nitrogen gas slugs are not visible due to refraction) - for better contrast white LEDs are used; brown material at the glass-aluminum transition: 2-component epoxy adhesive as assembly assistance.

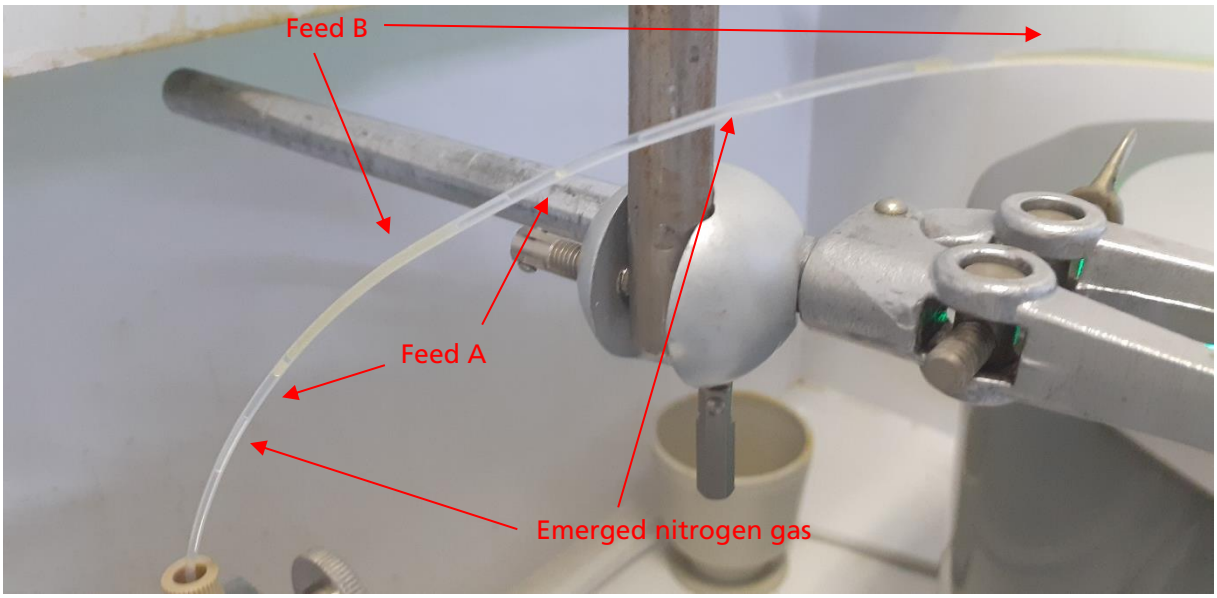

Figure 37: Reactor outlet; Stable (gas-)liquid-liquid-solid SMBR flow and synthesis of 3-CF_3-biphenyl via *in-situ* generated diazonium trifluoroacetate in 1/16" FEP capillary; Feed A: Fluorinert™ FC-40, Feed B: 80 mg anatase nanopowder in 20 mL MeCN/benzene V/V=1/1 + 50 mM 3-CF_3-aniline, 1.2 equiv. *t*-BuONO, 1 equiv. TFA).

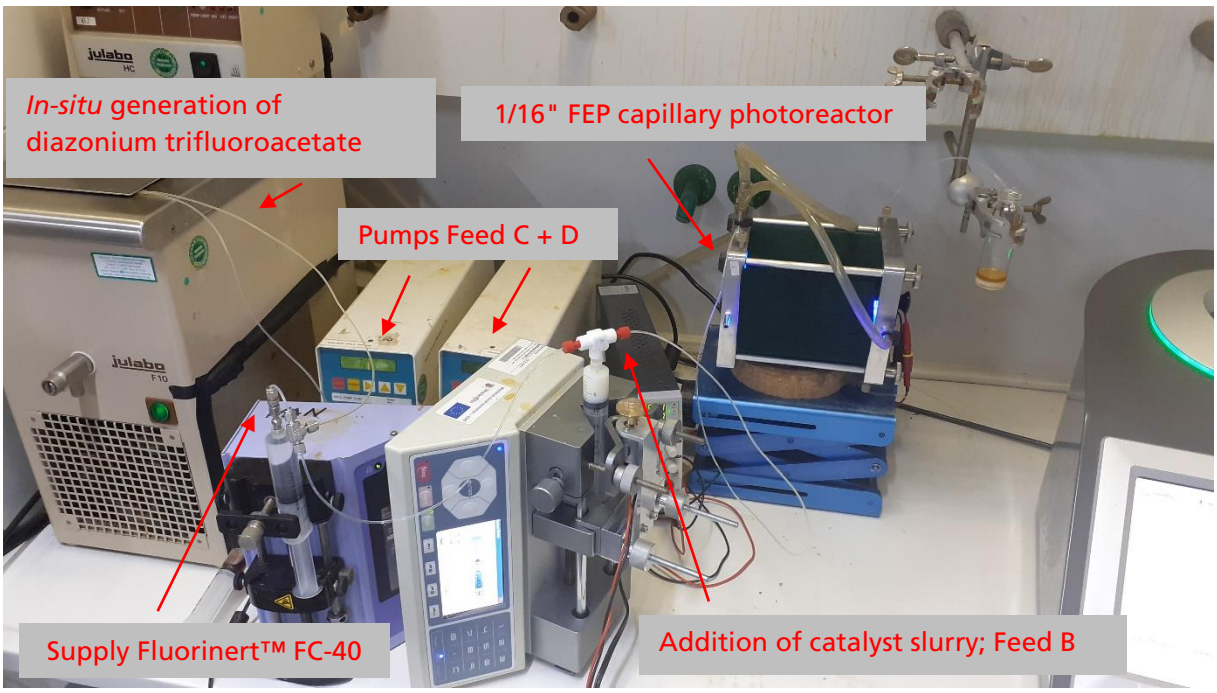

Figure 38: Complete setup for stable generation of a (gas-)liquid-liquid-solid SMBR concept and synthesis of 3-CF_3-biphenyl via separately *in-situ* generated diazonium trifluoroacetate in a horizontal 1/16" FEP capillary photoreactor - Feed A: Fluorinert™ FC-40, Feed B: anatase catalyst in MeCN/benzene; Feed C: 3-CF_3-aniline + 1 equiv. TFA in MeCN; Feed D: 1.2 equiv. *t*-BuONO in MeCN.

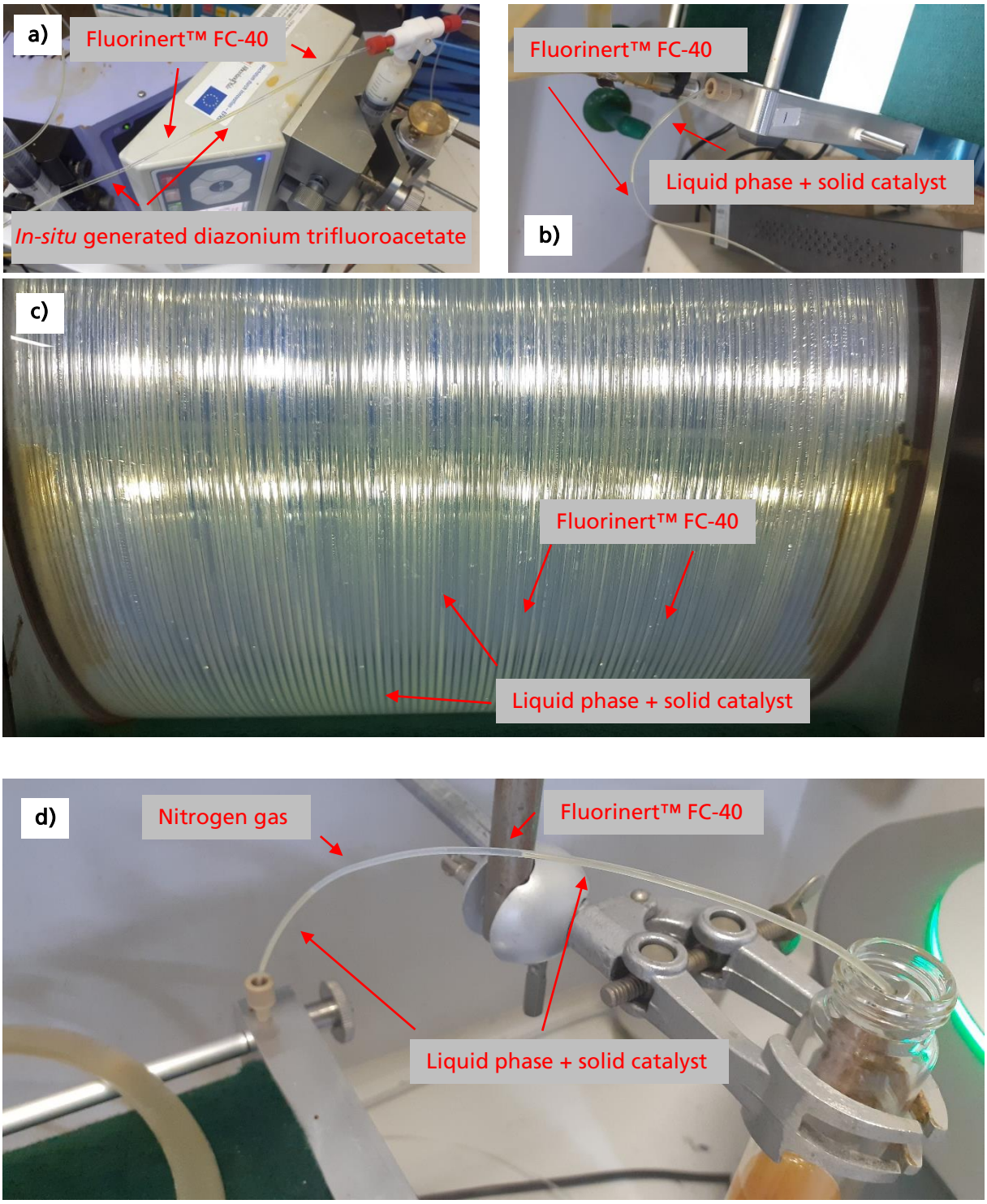

Figure 39: Generation of a stable (gas-)liquid-liquid-solid SMBR concept in 1/16" FEP capillaries; **a)** Via a 1/16" Swagelok T-junction liquid-liquid plug flow is generated using immiscible Fluorinert™ FC-40 and separately *in-situ* generated diazonium trifluoroacetate; **b)** Via a 3-way valve (right side a)) a stable (gas-)liquid-liquid-solid plug flow is generated, solid anatase catalyst particles are suspended in the liquid phase containing the components for 3-CF_3-biphenyl synthesis; **c)** The stable SMBR flow is irradiated in a 1/16" FEP capillary photoreactor - for better contrast white LEDs are used; brown material at the glass-aluminum transition: 2-component epoxy adhesive as assembly assistance; **d)** SMBR flow at the reactor outlet.

3.1.2.4 Conclusions

The design and development of a stable SMBR flow, including heterogeneous photocatalysts, needs a multidisciplinary consideration of technical requirements as well as a suitable catalyst activity. Both domains exhibit a significant mutual influence, as shown by the biphenyl synthesis via diazo anhydrides. Triglyme, which is used as a co-solvent to realize a proper solid transport in the liquid phase, deactivates the catalyst and therefore the reactor concept is disabled.

The SMBR concept is successfully improved by introducing the inert liquid Fluorinert™ FC-40 as continuous phase. The fluorinated liquid acts as a smear layer in FEP capillaries to prevent deposition of the solid catalyst along the capillary wall. With this method, even catalyst materials with bad suspension behavior are stabilized.

Various thermal- or light driven reactions can be accelerated, whenever a heterogeneous (gas-)liquid-liquid-solid SMBR segmented flow is necessary. In contrast to glass capillary reactors, a setup with polymer capillaries can be used to be independent of any surface wetting behavior. Moreover, wavelength cut off is shifted and the residence time can be easily adjusted for each individual reaction.[156]

3.1.3 Catalyst-free photochemical direct C-H arylation in a capillary photoreactor using arene diazonium trifluoroacetates and its process optimization

Up to 70% yield of 3-CF_3-biphenyl is gained, when using the SMBR concept for a photoredox synthesis via 3-CF_3-phenyldiazonium trifluoroacetate (1 equiv. TFA). In this context, irradiation wavelength is varied from 455 nm to 365 nm, resulting in 70% yield as well. Moreover, a satisfactory kinetic behavior is present in this reaction, even if no heterogeneous metal oxide photocatalyst is used. In this case, application of the inert liquid Fluorinert™ FC-40, as technical requirement, can be abolished.

Continuous *in-situ* generation of the reactive diazonium intermediate is realized by using a residence time element, preliminary attached to the capillary photoreactor. The diazonium intermediate is generated continuously at 20 °C within 10 minutes and. benzene is added via a T-junction subsequently. Inside the 1/16" FEP capillary photoreactor (800 µm ID, 15 mL), the reaction mixture is irradiated to initiate the photochemical step forming the benchmark molecule **26b** (Figure 40).

In order to achieve best productivity of the benchmark reaction, different optimization procedures are presented in the subsequent sections of this chapter.

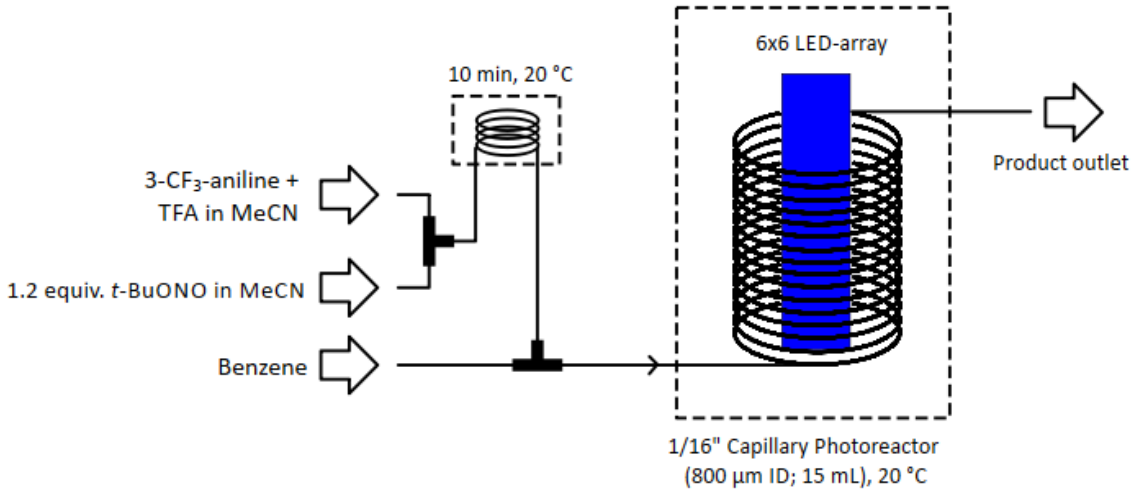

Figure 40: Schema for a catalyst-free continuous production of 3-CF_3-biphenyl with a capillary photoreactor. Diazonium salt is generated *in-situ* (protected from light) and benzene as arene for corresponding C-H arylation is added separately. Irradiation is carried out in a 1/16" FEP capillary photoreactor to give 3-CF_3-biphenyl.

3.1.3.1 Influence of temperature

A thermal reaction pathway always accompanies the photochemical formation of 3-CF_3-biphenyl via direct C-H arylation.[141] Moreover, thermal decomposition of the intermediate can occur as competitive reaction, if diazonium compounds are exposed to high temperature. This means, that a reduced selectivity and low yield of the favored product is the consequence.

Most published studies, on the decomposition of diazonium salts, are conducted in water using stable tetrafluoroborate or hexafluorophosphate salts.[157] For example, 4-NO_2-phenyl-, 4-methoxyphenyl- or phenyl-diazonium chloride in aqueous solution are quiet stable in the range of -10 to 20 °C. Significant decomposition (≥ 5%), forming the corresponding phenolic product, starts at ~33 °C[137] and results in a faster decomposition beyond this limit. In this work, slight hydroxydediazotation is observed in acetonitrile - technical grade - containing traces of water. Small traces of the corresponding 3-CF_3-phenol appear in the presented experiments via an involved aryl cation.[158]

Formation of aryl fluorides, via a "Schiemann fluorination" is not observed in the following experiments, when using trifluoroacetate as anion and avoiding inorganic fluorine anions, like BF_4^-, SiF_6^- or PF_6^-.[126,159]

Decomposing diazonium compounds can undergo reactions with the solvent acetonitrile, forming N-arylnitrilium salts (Scheme 18). In some cases isolation and characterization is feasible, but hydrolysis often occurs and the corresponding amide is formed (Ritter-type reaction).[160]

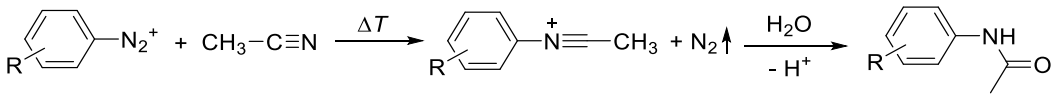

Scheme 18: Formation of acetamides by diazonium salts in acetonitrile.

Focus is put on the noteworthy parallel thermal dediazotation pathway, most likely giving aryl radical intermediates. Biphenyl molecules are then inevitably formed in the presence of arenes.[141]

Therefore, 12% 3-CF_3-biphenyl is detected via a thermal reaction pathway in continuous flow at 20 °C without any light (1h). This amount is doubled at 40 °C (Figure 41). In further investigations, it is necessary to conduct the catalyst-free arylation of benzene at

ambient temperature in order to avoid large interferences. Having the conclusions of Baumann *et al.* in mind, no further studies are conducted at lower temperatures.
A single cryostat, operated at 20 °C, is used in all experiments, to cool the complete experimental setup (residence time element, capillary photoreactor and LED-array).

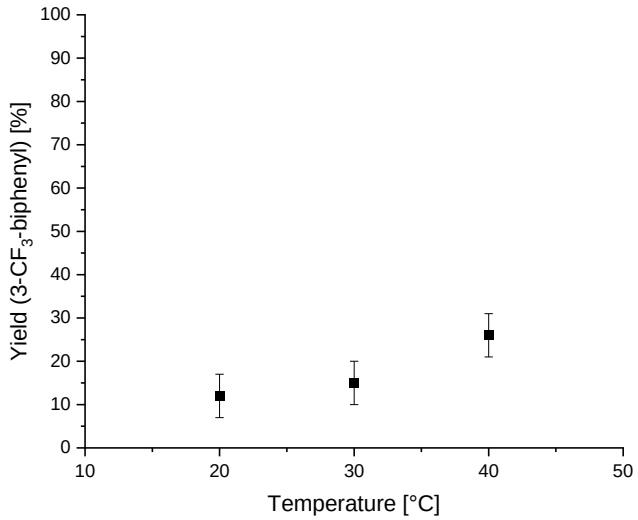

Figure 41: Thermal induced synthesis of 3-CF_3-biphenyl via *in-situ* generated diazonium trifluoroacetate in a 1/16" capillary photoreactor without any irradiation; General reaction conditions: 50 mM 3-CF_3-aniline, 1.2 equiv. *t*-BuONO, 1 equiv. TFA, MeCN/benzene (V/V =1/1), ~1 h residence time (calculated by flow rate); Determined by GC/MS.

3.1.3.2 Influence of light

The influence of different wavelength and intensity (Figure 42) is investigated, using the catalyst-free reaction conditions (50 mM 3-CF_3-aniline, 1 equiv. TFA, 1.2 equiv. *tert*-butyl nitrite in acetonitrile/benzene (V/V=1/1)). Irradiation with 365 nm in combination with a high photon intensity result in best performance. 455 nm irradiation gives only a slightly higher productivity of **26b**, in comparison to a reaction where light is excluded.

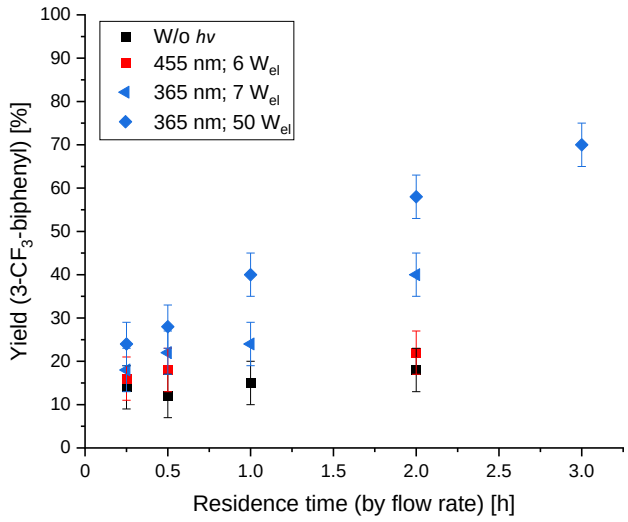

Figure 42: Catalyst-free synthesis of 3-CF_3-biphenyl via *in-situ* generated diazonium trifluoroacetate in a 1/16" capillary photoreactor; General reaction conditions: 50 mM 3-CF_3-aniline, 1.2 equiv. *t*-BuONO, 1 equiv. TFA, MeCN/benzene (V/V =1/1), 20°C and parameters: ■ no light; ■ 455 nm, 6 W_{el}; ◀ 365 nm, 7 W_{el}; ◆ 365 nm, 50 W_{el} ; Determined by GC/MS.

3.1.3.3 Influence of trifluoroacetic acid

Literature reports the appearance of an aryl diazonium trifluoroacetate double salt as isolated solid. One molecule of free trifluoroacetic acid and aryl diazonium trifluoroacetate are found per purified "molecule unit". Pettit *et al.* therefore suggest the general formula R-N_2^+ $^-OOCCF_3 \cdot CF_3COOH$ (R=aryl) and this ratio was confirmed by cryoscopy and molecular weight determinations. This group successfully used diazonium trifluoroacetate double salts, as starting material, for the thermal synthesis of azo-β-naphthols or biphenyl derivatives (Scheme 19).[146,147]

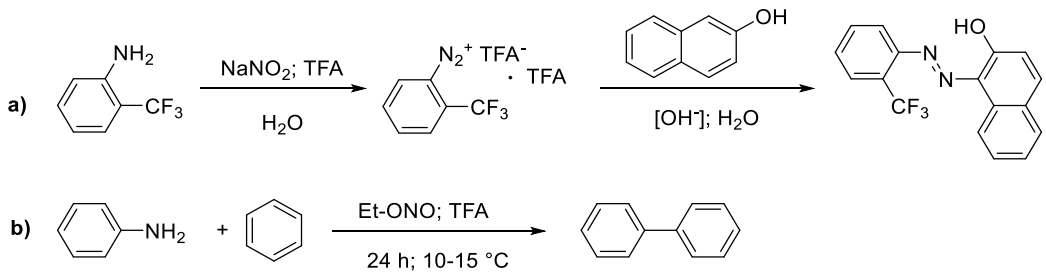

Scheme 19: Synthesis of arene diazonium trifluoroacetates and their use in **a)** azo-β-naphthol and **b)** biphenyl derivatization; Reported by Pettit *et al.*[146,147]

The influence of trifluoroacetic acid on the benchmark system (50 mM 3-CF_3-aniline, 1.2 equivalents *tert*-butyl nitrite in acetonitrile/benzene (V/V=1/1)) has to be investigated. Two equivalents of trifluoroacetic acid represent the literature described case. The absence of TFA should represent in-situ generation of a diazo anhydride as reactive intermediate.[28] Decomposition of diazo anhydrides is stated by Müller et al. giving aryl radicals, which form biphenyl products in presence of aromatic benzene-derivatives.[161]

First of all, the effect of different TFA amount is observed visually. 3-CF_3-aniline/TFA and *tert*-butyl nitrite in acetonitrile appear as colorless solutions (Figure 43a and b). Mixing of those compounds results in an immediate colorization (0-1 equivalents TFA, Figure 43c). It is stated that diazo anhydride is formed, causing a colorization even in little fractions.[132,162] Not until one minute of mixing (Figure 43d), a pale yellow colorization appears in the vials carrying 1.5 to 4 equivalents of TFA. In the meantime, colorization has intensified in vials containing 0 to 1.5 equivalents, but colorization is still very pale after 20 minutes for those with two or more equivalents TFA (Figure 43e).

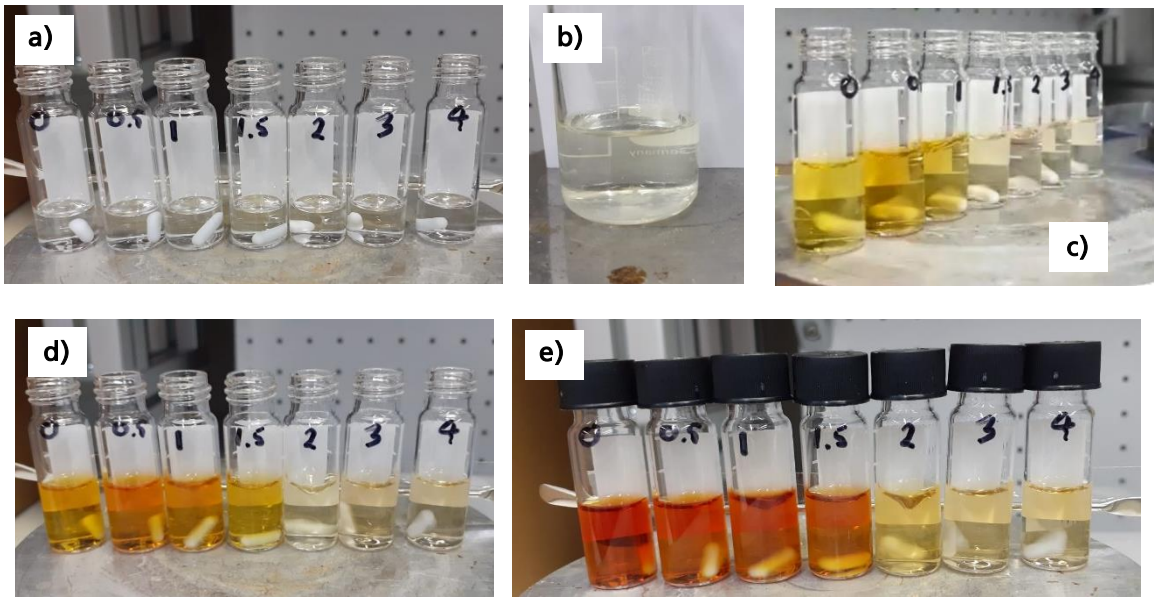

Figure 43: Colorization experiments with different equivalents of TFA for *in-situ* generation of reactive diazo intermediate basically representing experimental conditions; **a)** 200 mM 3-CF_3-aniline **25a** in MeCN containing 0 to 4 equiv. of TFA; **b)** 240 mM *t*-BuONO in MeCN; Colorization of a) and b) mixtures (equal volume) after **c)** 1 min, **d)** 3 min and **e)** 20 minutes.

Same colorization effects are observed, when the experiment is transferred into a continuous synthesis of 3-CF_3-biphenyl in the 1/16" FEP capillary photoreactor. As Figure 44 presents, conversion and selectivity of the benchmark synthesis is depending on the

amount of trifluoroacetic acid being used. Without any carboxylic acid, only 18% of 3-CF_3-biphenyl is obtained. In this case, 3-CF_3-aniline and the alkyl nitrite seem to form the colored diazo anhydride as photochemical active molecule for direct C-H arylation.
Despite reported literature, the corresponding diazo anhydride gives only poor yield for **26b**. In contrast, Cantillo *et al.* present the photochemical decomposition of diazo anhydride (>350 nm) forming reactive aryl radicals, which are able to undergo satisfactory arylation of furan and thiophene.[28]
Highest yield of the favored product **26b** (86±5%) is obtained by adding two equivalents of trifluoroacetic acid. Additional trifluoroacetic acid (three or four equivalents) has no further beneficial effect. In general, an average yield of 78% 3-CF_3-biphenyl is obtained in further repetitive experiments, using two to four equivalents of TFA, which indicates the statistical maximum in conversion and selectivity.
Complete dissociation of diazonium trifluoroacetates is reported, when dissolved in polar solvents.[163] As results of chapter 3.1.6 show, trifluoroacetic free acid coordinates to the dissociated diazonium salt. This implies formation of quasi-homodimers of the trifluoroacetates within the diazonium salt, even when 0 to <2 equivalents of the organic acid are used. The starting material reacts with *tert*-butyl nitrite to give an aryl nitrosamine **29**. Via tautomerization a diazo hydroxide **29a** is formed (Scheme 20). In absence of any mineral or organic acid, these colored tautomers will condensate and yield in the corresponding diazo anhydride **29b**.[28] Although direct evidence of these tautomers could not be established, it is assumed, that they form meta-stable intermediates, producing diazonium trifluoroacetates **25c** whenever free TFA dimers are present. Referring to Figure 42, one equivalent TFA is only able to form ~70% **26b,** if intermediates (nitrosamine/diazo hydroxide) are present, which are able to produce new diazonium salt species even after three hours. The mentioned observations are not possible, if nitrosamine/diazo hydroxide intermediates form diazo anhydrides in favor.

In all experiments, homocoupling of the 3-CF_3-phenyl radial yielding in the by-product **27** is not observed. Since higher amounts of TFA do not enhance the reactivity, two equivalents of this organic acid are used in further studies on the catalyst-free photochemical arylation of benzene.

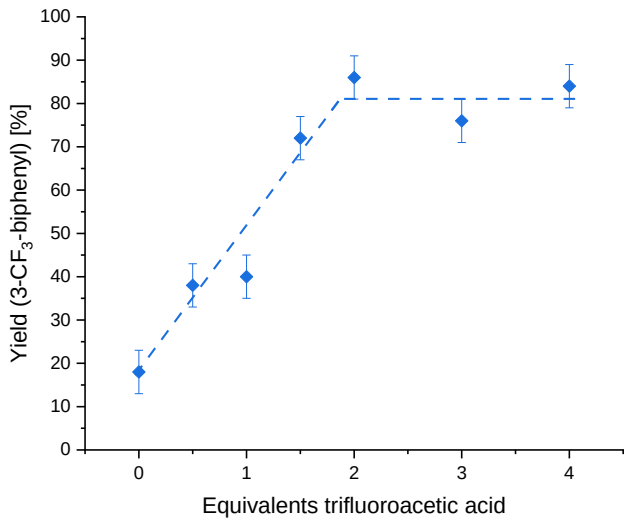

Figure 44: Continuous synthesis of 3-CF_3-biphenyl via *in-situ* generated diazonium intermediates using different equivalents of trifluoroacetic acid in a 1/16" capillary photoreactor; General reaction conditions: 50 mM 3-CF_3-aniline, 1.2 equiv. *t*-BuONO, and MeCN/benzene (V/V =1/1), 365 nm 50 W_{el}, 20 °C, ~1 h residence time; Determined by GC/MS.

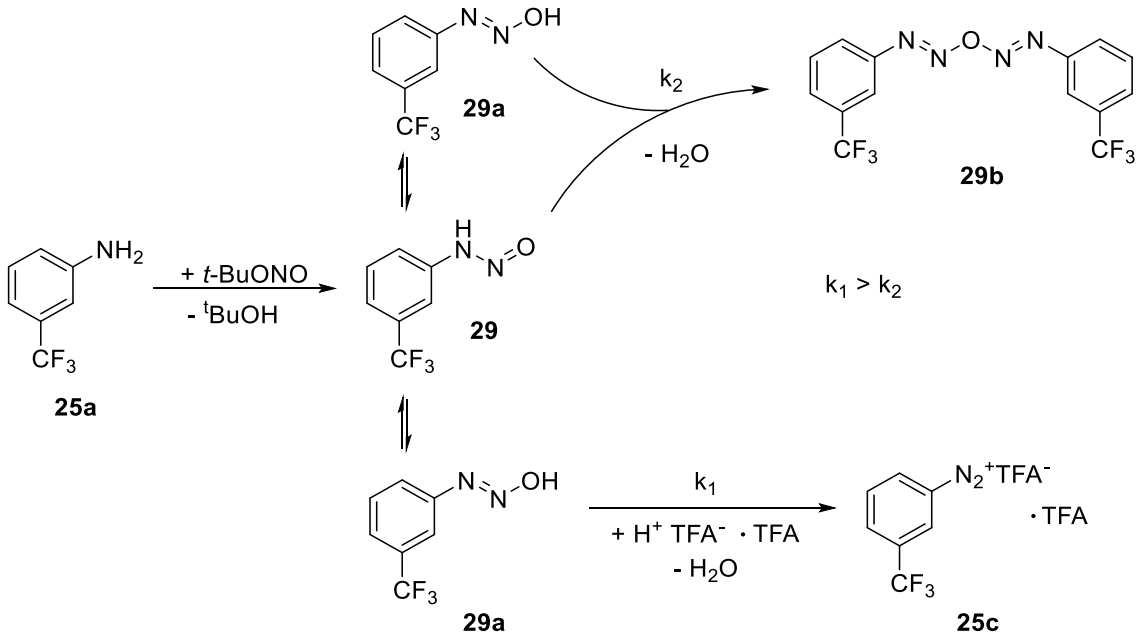

Scheme 20: Different diazotation routes of 3-CF_3-aniline in presence/absence of TFA.

3.1.3.4 Influence of pressure and process intensification

Further investigations on the photochemical arylation are conducted with respect to the residence/irradiation time inside the capillary photoreactor. When using a starting material concentration of 50 mM, a maximum yield is already obtained after 30 minutes (according to flow rate). An unavoidable release of nitrogen gas C-H arylation via the diazonium trifluoroacetate is observed by a formation of a slug flow. This gas inevitable displaces the liquid phase. Irradiation time will be high, only if reaction mixture is pumped through the reactor with low flow rates. In inverse proportion, this displacement effect will be more intense in comparison to a high flow rate and short irradiation time. This effect will be permanently present, when working at standard atmosphere and residence time can be estimated only with low accuracy.

In order to set a precisely adjustable residence/irradiation time, the whole setup is pressurized with an excess pressure of >280 $mbar_{exs}$ (Figure 45). This guarantees complete solvation, of generated nitrogen, into the liquid phase with acetonitrile and benzene as major compounds.[164] For technical reasons, the experiments are operated at ~4 bar_{exs} using a spring-loaded proportional relief valve. This guarantees constant pressurization while testing different flow rates and still 78% of 3-CF_3-biphenyl are obtained after 30 minutes.

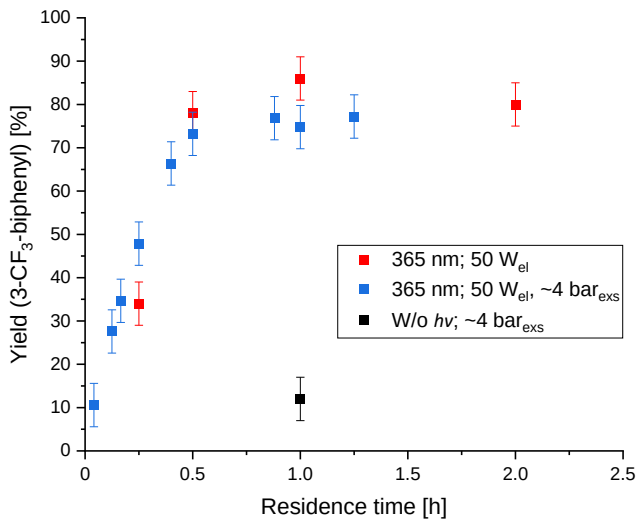

Figure 45: Continuous synthesis of 3-CF_3-biphenyl via *in-situ* generated diazonium trifluoroacetate in a 1/16" capillary photoreactor: ■ 365 nm, 50 W_{el}, at standard atmosphere, residence time calculated by flow rate; ■ 365 nm, 50 W_{el}, at ~4 bar_{exs}, residence time precisely determinable; ■ without light, at ~4 bar_{exs}; General reaction conditions: 50 mM 3-CF_3-aniline, 1.2 equiv. *t*-BuONO, 2 equiv. TFA and MeCN/benzene (V/V =1/1); Determined by GC/MS.

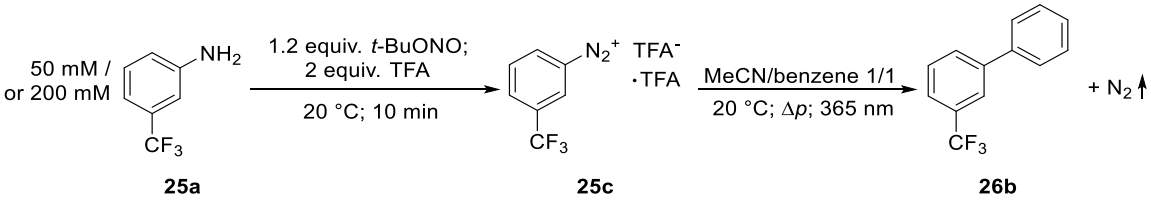

Scheme 21: Continuous catalyst-free C-H arylation of benzene using *in-situ* generated diazonium trifluoroacetate in a pressurized capillary photoreactor.

Experimental results take advantage of the high benzene excess so far (112 equiv. referring to 50 mM 3-CF_3-aniline). This excess is now reduced by increasing the concentration of starting material from 0.05 to 0.2 M **25a**. This option is chosen to increase specific productivity, while reducing the excess of benzene to 28 equivalents at the same time (Scheme 21). Moreover, higher concentration of molecules containing fluorine groups will increase the intended integration of online ^{19}F-NMR spectroscopy. Since more nitrogen is generated now, the excess pressure of the reactor system has to be increased further. A stable continuous flow with a complete solvation of nitrogen in the liquid phase is set at 17 bar_{exs} (Table 11). When pressure is released via the valve, a strong nitrogen gas formation occurs and the reaction mixture, containing the product **26b**, is shot into the reservoir.

Table 11: Process development of 3-CF_3-biphenyl synthesis towards a continuous flow with predictable residence time *in-situ* generated diazonium trifluoroacetate in a 1/16" capillary photoreactor.[a]

#	excess pressure [bar_{exs}]	yield **26b** [%][b]	visible nitrogen formation	note
1	6.4	60	high amount of gas slugs	jerkily flow, lots of stops
2	15.7	60	small amount of gas slugs	less jerkily flow
3	17	60	no gas slugs	continuous flow

a: General reaction conditions: 200 mM 3-CF_3-aniline, 1.2 equiv. *t*-BuONO, 2 equiv. TFA in MeCN/benzene (V/V=1/1), 365 nm 50 W_{el}, residence time ~53 min; **b:** Determined by GC/MS.

By process optimization, the intensified catalyst-free benchmark synthesis reaches 78% 3-CF_3-biphenyl after 1.25 hours (Figure 46 ◆ graph). Reaction kinetics slows down in comparison to the lower concentrated experiments, by two major reasons: According to Beer-Lambert law,[71] the higher concentration of photoactive material leads to a 4-times higher optical density of the liquid. This causes more absorption processes and a reduced transmission. Light is damped and less photons will reach the outward area of

the capillary. Diffusion inside the capillary allows a proper irradiation of the mixture. In the same time, light intensity is not increased and identical photon flux is provided for both implementations.

Finally, excess of benzene is reduced to 10 equivalents (Figure 46 ■ graph) and a maximum yield decreases to 42% 3-CF_3-biphenyl after 1.25 h. A comparable kinetic behavior of the reactive intermediate is observed, since favored photoarylation is interrupted after identical residence time. More side reactions occur and the reactions suffers from a selectivity loss.

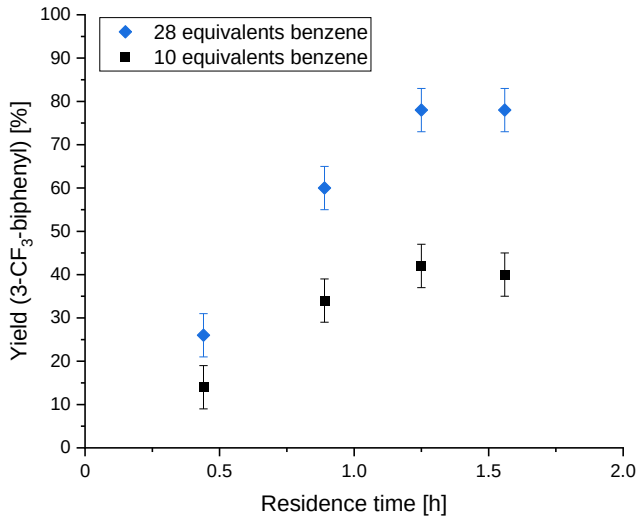

Figure 46: Continuous synthesis of 3-CF_3-biphenyl via *in-situ* generated diazonium trifluoroacetate in a 1/16" capillary photoreactor using different amount of benzene: ■ 10 equiv. benzene (MeCN/benzene V/V=4.63/1); ◆ 28 equiv. benzene (MeCN/benzene V/V=1/1); General reaction conditions: 200 mM 3-CF_3-aniline, 1.2 equiv. *t*-BuONO, 2 equiv. TFA in MeCN, 365 nm 50 W_{el}, 20 °C; Determined by GC/MS.

3.1.3.5 Classification of the catalyst-free C-H arylation using arene diazonium trifluoroacetates in context to published literature

Comparison, with already published photochemical syntheses, is used to put the presented catalyst-free continuous photoarylation into context with the known literature. Beside numerous reported batch reactions, only few are converted into continuous flow.[165]

One of these is a synthesis, presented by Fabry *et al.*, using heterogeneous photocatalysis in the falling film microreactor.[31] The previous chapters established that synthesis of 3-CF_3-biphenyl is not accessible with those process conditions. Most fundamental impact, preventing technical realization, is the poor solubility of the substrate. Nevertheless, the reported 0.684 mol×L^{-1}×h^{-1} specific productivity of the falling film microreactor is very impressing with respect to net irradiation time.

Kappe *et al.* present a continuous synthesis route, using diazo anhydrides as reactive intermediate. They report the synthesis of bi-(hetero)arenes (8 equivalents of heteroarene) within 45 min and apply a Hg-lamp with >350 nm (150 W) or >300 nm (75 Watt) to produce 80% of 2-(4-chlorophenyl)thiophene. Only 45% of 2-phenylthiophene is obtained with >300 nm 150 W and, consequently, selectivity is only at 42%, due to a high amount of side-reactions caused by the intense and high-energy irradiation with UV-B light.[28]
Finally, the authors elaborate the >300 nm (75 Watt) light source to run continuous synthesis for several biphenyls with best possible results. 4-chlorobiphenyl **24b** (68%, Table 12 entry #5) and 4-chloro-4´-methoxybiphenyl (75%) starting with the corresponding aniline and rather low excess of arene (0.2 M 4-chloroaniline and 8 equiv. benzene or anisole) are successfully manufactured in 45 min in a capillary photoreactor.
As already mentioned, a reaction path using diazo anhydride is not beneficial for the benchmark product, due to low reactivity and selectivity of the starting material. Synthesis of 3-CF_3-biphenyl **26b** via diazo anhydrides gives only 16% yield, if a 365 nm light source is used (Table 12 entry #8). Theoretically, usage of a UV-B LED-array could overcome this issue, but studies in the 1/16" FEP capillary photoreactor (365 nm, 50 W_{el}) reveal 55% 2-(4-chlorophenyl)furan **24a** (Table 12 entry #7). The same molecule is synthesized by Kappe *et al.* with 71%, when using >300 nm 75 Watt (Table 12 entry #6). This identifies a lower reactivity of the substrate and no technical hindrance.

Beside the here presented catalyst-free layout, a continuous synthesis route is presented by Ackermann *et al.* using manganese-photocatalysis.[166,167] Production of biphenyls is conducted via $CpMn(CO)_3$ in DMSO within 30 minutes (Table 12 entry #9). Diazonium tetrafluoroborates are used as substrate to generate aryl radicals as reactive intermediates. It is worth mentioning, that this mild route can be conducted in rather concentrated media (0.5 M diazonium salt) using LED irradiation at 450 nm, 24 Watt and 15 equivalents of arene. Hereby, a wide range of phenyl diazonium salts (including functional groups as 4-CF_3-, 4-MeO-, 4-NO_2-, 4-CO_2Et-, 4-Cl-, 3-Me-) are combined with

benzene, 1,4-dimethoxybenzene, *p*-xylene, furan, thiophene or *N*-Boc-pyrrol (15 equivalents each) giving yields of 51 - 85%. In a scaled procedure, 1.42 g (64%) of 4-CF_3-biphenyl **30b** is obtained after 1 h.

The authors confirm the benefit of a continuous synthesis by conduction of a comparative batch-reaction, where yield is halved to 25%.[166] This behavior is also observed in the here presented catalyst-free biphenyl synthesis using diazonium trifluoroacetates. The process solution has to be irradiated in batch-mode for 7 h using 365 nm (6 W_{el}) to gain maximum yield (see Table 12 entry #2 and Figure 228 in the appendix).

In additional experiments, the protic trifluoroacetic acid can be successfully replaced by trimethylsilyl trifluoroacetate to form 46% of **26b** (Scheme 22). The protected trifluoroacetate is a very promising alternative, whenever proton-labil substrates are present. For example, mono-*N*-Boc protected *tert*-butyl 4-aminophenylcarbamate can be used as substrate for amino-biphenyls and double diazotization is suppressed as far as possible.[137]

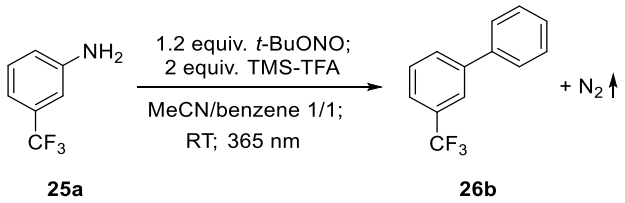

Scheme 22: Catalyst-free photoarylation of benzene using trimethylsilyl trifluoroacetate to produce reactive diazonium intermediate.

A related (catalyst-free) batch synthesis of bi-(hetero-)arenes is presented by Fürst *et al*. They observe formation of a CT complex, when mixing diazonium chlorides or tetrafluoroborates (pure or in aqueous media), respectively, with an arene (e.g. hydroquinone, 1,4-dimethoxybenzene, 3-hydroxypyridine or furfurylamine). This allows irradiation of most complexes with visible light. For example, 80% 4-chlorobiphenyl **24b** (Table 12 entry #3) is synthesized by 4-chlorophenyl diazonium tetrafluoroborate in neat benzene after 120 h irradiation (450 - 470 nm, 20 Watt). Due to very low solubility of the tetrafluoroborates in arenes, 39 equivalents of trifluoroacetic acid have to be added, to form the soluble diazonium trifluoroacetate via an *in-situ* anion-exchange.[29,141,168]

In literature, metal-free organic dyes like eosin Y (1mol%) are used for homogeneous photocatalysis. König *et al.* synthesize bi-(hetero-)arenes by green light irradiation in

batch experiments (1 mL in DMSO), starting with diazonium tetrafluoroborates as well. When using furan for arylation experiments, respectable yields (40 - 86%, Table 12 entry #10) are obtained for prominent diazonium salts. Other heteroarenes require irradiation times up to 24 hours, due to their decreased reactivity.[128,138]

Kappe *et al.* analyze the use of eosin Y as photocatalyst for batch synthesis via diazo anhydrides as well. 50% 2-(4-chlorophenyl)thiophene is obtained after 3 h, requiring two equivalents of $BF_3 \cdot Et_2O$. Interestingly, synthesis is not affected by this catalyst and usage is resigned, when operating a CFL lamp.

Observations of Ackermann *et al.* give similar results, when eosin Y is applied as homogeneous photocatalyst in 4-CF_3-biphenyl synthesis (33%). Even though UV/Vis absorption spectrum implies green light irradiation, 450 nm is used.[169] All this is congruent with own observations and experimental results. In contrast to the work of Rehm *et al.*,[98] where full conversion is reported, continuous synthesis (via the corresponding diazonium tetrafluoroborate) of 2-(3-CF_3-phenyl)furan **26a** gives 16% (Table 12 entry #11) via the eosin Y route and 11% of benchmark biphenyl (Table 12 entry #12), respectively. In both reactions full conversion of the diazonium salt is observed, while 40% of the isolated material is the by-product **27**.

Important samples and their specific productivities of the discussed continuous flow procedures are presented in Table 12. A distinct consideration of optical power is neglected, since presented setups and components are diverse.

Table 12: Comparison of different new and literature known continuous routes for biphenyl (and bi-hetero-aryl) synthesis via diazonium salts.

#	synthesis type	starting material	product	excess (hetero)-arene	note	λ [nm]	P [W_{el}]	t_R [h]	yield [%]	specific productivity [mol× (L×h)$^{-1}$]
1	capillary reactor[a]	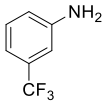	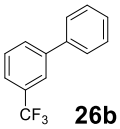 **26b**	28 equiv.	**catalyst -free, 2 equiv. TFA, 17 bar_{exs}**	365	50	1.25	78	**0.125**
2	batch reactor[a]	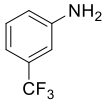	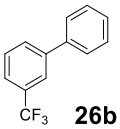 **26b**	28 equiv.	catalyst -free, 2 equiv. TFA	365	6	7	78	0.022
3	batch reactor[b]	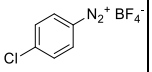	**24b** 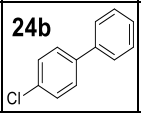	100 equiv.	39 equiv. TFA	450-475	20	120	80 [29]	0.0006

#	synthesis type	starting material	product	excess (hetero)-arene	note	λ [nm]	P [W_{el}]	t_R [h]	yield [%]	specific productivity [mol× (L×h)$^{-1}$]
4	FFMR[a]	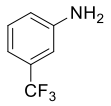	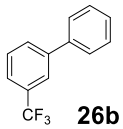 **26b**	112 equiv.	anatase catalyst, 1 equiv. TFA	455	6	2	52	0.013
5	capillary reactor[b]	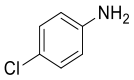	**24b** 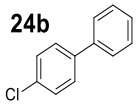	8 equiv.	via diazo anhydride	>300	75	0.75	68 [28]	0.181
6	capillary reactor[b]	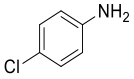	**24a** 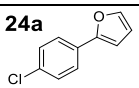	8 equiv.	via diazo anhydride	>300	75	0.75	71 [28]	0.189
7	capillary reactor[a]	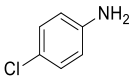	**24a** 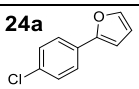	10 equiv.	via diazo anhydride	365	50	1.25[c]	55	0.088
8	capillary reactor[a]	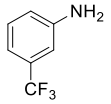	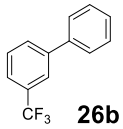 **26b**	10 equiv.	via diazo anhydride	365	50	1.25[c]	16	0.026
9	capillary reactor[b]	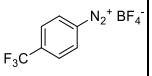	**30b** 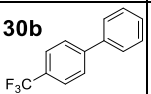	15 equiv.	$CpMn(CO)_3$ 10mol%	455	24	0.5	64 [166]	0.640
10	batch reactor[b]	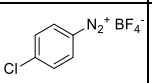	**24a** 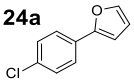	10 equiv.	Eosin Y 1mol%	530	1	2	74 [138]	0.074
11	capillary reactor[a]	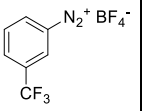	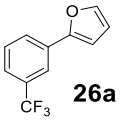 **26a**	10 equiv.	Eosin Y 1mol%	520	32	0.62[c]	16	0.051
12	capillary reactor[a]	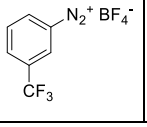	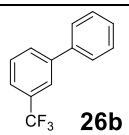 **26b**	10 equiv.	Eosin Y 1mol%	520	32	0.62[c]	11	0.035

a: data from experiments reported in this work; **b:** data reported from literature; **c:** residence time calculated by flow rate.

3.1.3.6 Conclusions

A catalyst-free direct C-H photoarylation of arenes is developed. The synthesis of the benchmark product **26b** is performed via diazonium trifluoroacetates, which represent a highly soluble alternative to the commonly used tetrafluoroborates. The process parameters considering an optimal temperature, the irradiation wavelength/intensity, the amount of trifluoroacetic acid and the excess of arene are elaborated. The whole process is exposed to 17 bar excess pressure for a precise adjustment of the residence time. Even though nitrogen gas is pressed into in the liquid phase, no influence on the chemical equilibrium is observed.

The benchmark reaction is optimized to 78% yield after 1.25 h, while having a high specific productivity (L_{CP} = 0.125 mol×(L×h)$^{-1}$). This result exceeds benchmark syntheses via literature known processes, which are discussed in chapter 3.1.3.5. As shown in Table 12, synthesis routes using organic dye photocatalysts and diazo anhydrides, show far less efficiency. Specific productivity can only be topped by the application of UV-B light (accompanied by low selectivity) or a manganese-photocatalyst.

3.1.4 ^{19}F-NMR spectroscopy for online quantification of continuous photo arylation synthesis

The elaborated continuous catalyst-free synthesis of 3-CF_3-biphenyl is now extended with an online analysis module. A low-field (56.98 MHz) benchtop ^{19}F-NMR spectrometer (Nanalysis NMReady 60-PRO) is used for inline quantification and the ongoing process performance is monitored.

The synthesis setup has to be adapted and extended before ^{19}F-NMR spectroscopy is implemented. One big advantage of the presented route is the absence of any catalyst. Therefore, no catalyst material influences the spectrum acquisition or has to be removed preliminarily. Nevertheless, nitrogen formation of the photo arylation has to be considered.
Passive or active methods for a gas removal from continuous process streams can be used.[170,171] With passive methods, the present excess pressure has to be relieved in order to use bubble traps or unpressurized separators.[172] The gas volume is usually larger than the trap volume and a constant removal is required at a certain time. An unpressurized gas liquid separator requires an additional pump to transport the liquid phase into the spectrometer.[173] Active gas removal is provided by gas permeable membranes (or capillaries) made from PDMS or Teflon AF-2400/ AF-1600. In combination with a vacuum pump, continuous gas separation is guaranteed inside a capillary.[170,174] Anyway, large technical effort is necessary for these kinds of realization.

A much easier and more practicable way to overcome the gas management is the usage of a NMR flow cell, which can handle the process conditions. Pressurization of the setup to 17 bar_{exs} already utilizes nitrogen solvation for a precise irradiation and is now extended for online process monitoring (Figure 47 and Figure 48). A commercial flow cell, for this spectrometer, is glass-made and tolerates only several mbar excess pressure.

For this reason, a PEEK bottom-to-top flow cell (adapted design from a bottom-to-top glass flow cell; Fraunhofer IMM[98]) is manufactured to fit into the spectrometer. This cell has an outer diameter of 4.8 mm and an internal volume of ~330 µL. It represents the glass NMR-tube architecture, known from standard offline NMR-spectroscopy (see Figure 229 and Figure 230 in the appendix). All joints of the flow cell are press fit and stand an excess pressure of 25 bar_{exs} at least.

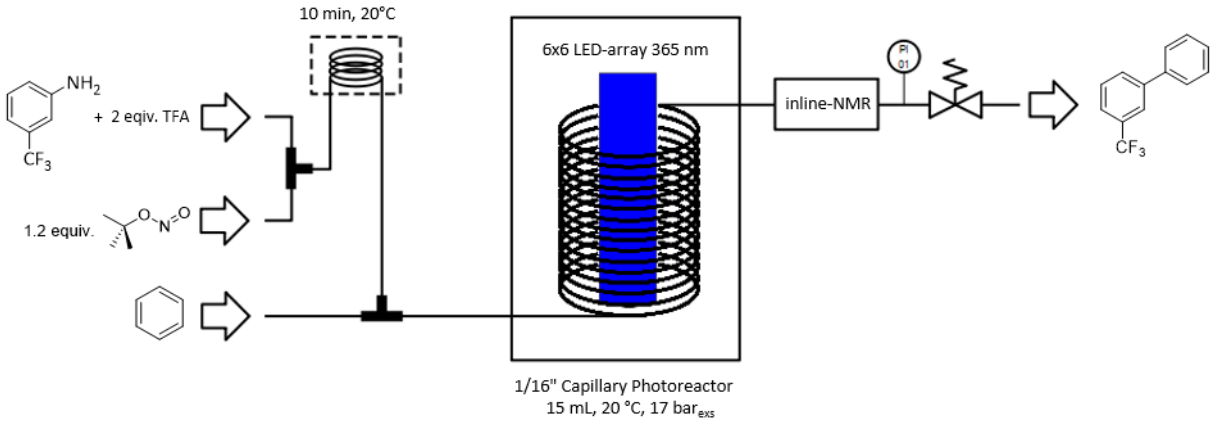

Figure 47: Schema for continuous catalyst-free synthesis of 3-CF_3-biphenyl with a capillary photoreactor including online process analysis by a ^{19}F-NMR benchtop spectrometer.

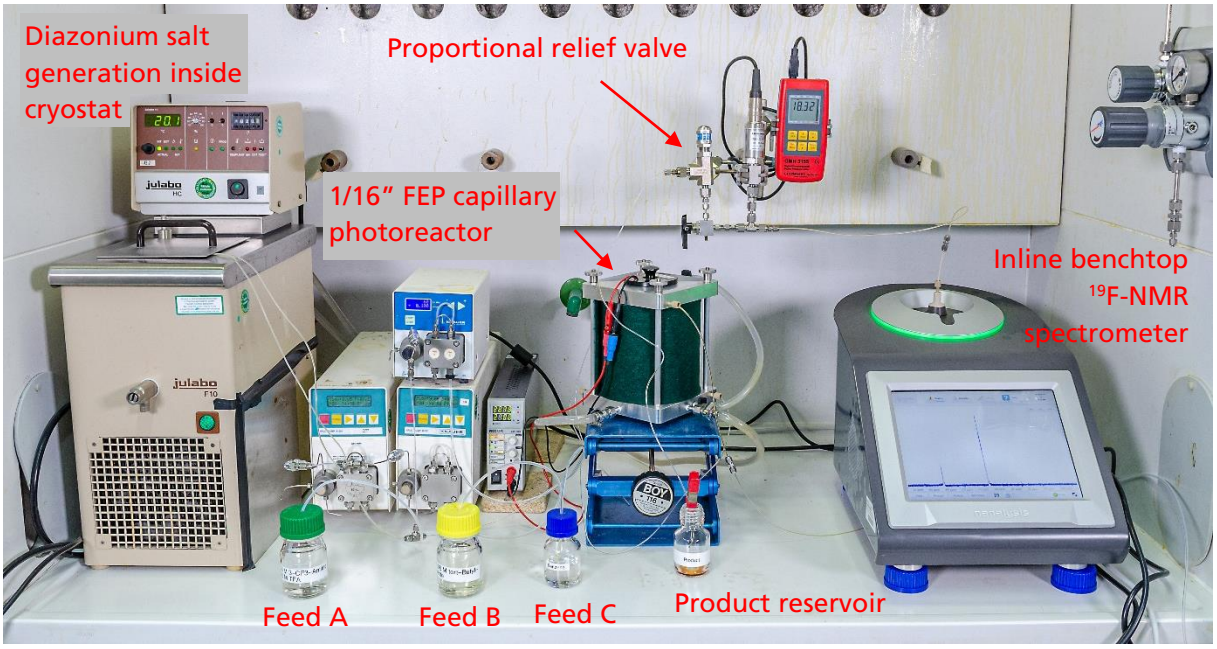

Figure 48: Setup for continuous catalyst-free synthesis of 3-CF_3-biphenyl with a capillary photoreactor including online process monitoring; Feed A: 0.8 M 3-CF_3-aniline, 2 equiv. TFA in MeCN; Feed B: 0.96 M *t*-BuONO in MeCN; Feed C: neat benzene; capillary photoreactor equipped with a 365 nm 50 W_{el} 6×6 LED-array (© Fraunhofer IMM).

The performance of the NMR-spectrometer is tested with the following settings to ensure operability for quantitative analysis: 80.49° pulse, 1.9 s acquisition time and 2.9 s repetition time, recently shimmed spectrometer. 64 scans are used to get a best possible signal-to-noise ratio (SNR). A measuring time of 185 seconds is still acceptable in comparison to 75 min residence time of a photoarylation step inside the capillary photoreactor. No influence of the PEEK material or pressurization (with respect to line shape and peak position) is observed in general. ^{19}F-NMR spectra of all known compounds (starting material, intermediate and product) are recorded (Figure 49) and the δ_F-shifts are assigned to every CF_3-group with reference to trichlorofluoromethane δ_F= 0 ppm (Table 13).

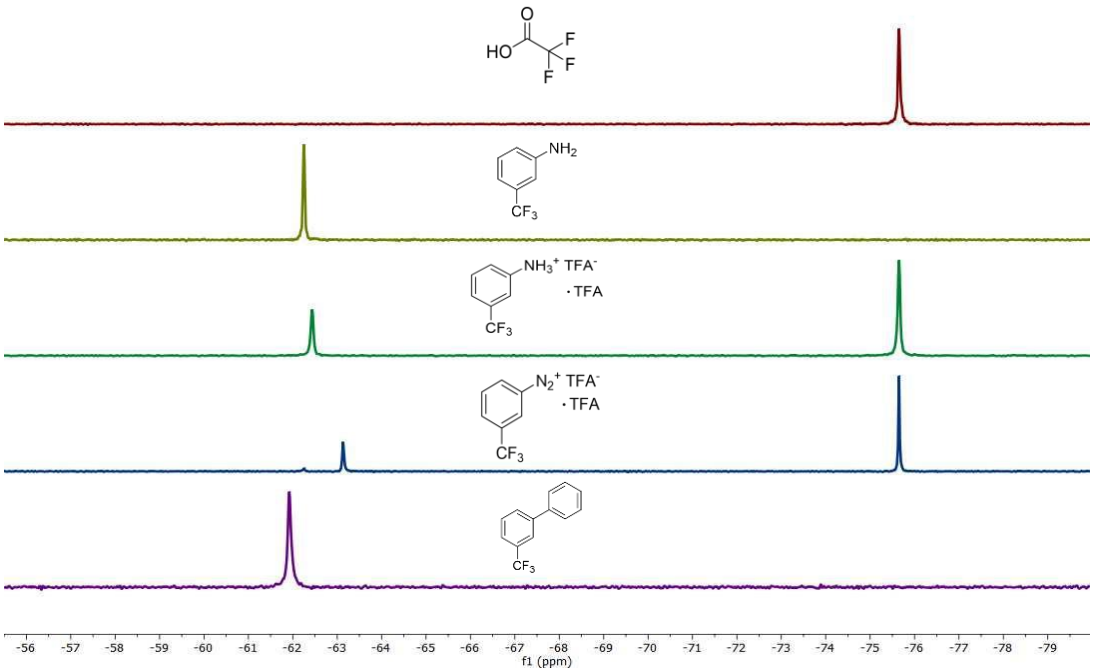

Figure 49: ^{19}F-NMR spectra (56.98 MHz, PEEK flow cell) in MeCN in reference to $CFCl_3$ δ_F= 0 ppm; — TFA; — 3-CF_3-aniline; — 3-CF_3-aniline + TFA (1:2 molar ratio); — 3-CF_3-phenyldiazonium trifluoroacetate by *in-situ* generation; — 3-CF_3-biphenyl.

Table 13: ^{19}F-NMR shifts of identifiable compounds being present at 3-CF_3-biphenyl synthesis in proteo-acetonitrile.

#	substance	δ_F [ppm]	note
1	$CFCL_3$	0.00	NMR-shift reference
2	3-CF_3-aniline	-62.25	starting material
3	Trifluoroacetic acid	-75.65	internal standard
4	3-CF_3-aniline + Trifluoroacetic acid	-62.44	δ of arylic CF_3-group – formation of quaternary ammonium salt
5	3-CF_3-phenyldiazonium trifluoroacetate	-63.13	δ of arylic CF_3-group
6	3-CF_3-biphenyl	-61.92	product

Beside the excellent performance of trifluoroacetic acid in the photochemical synthesis of 3-CF_3-biphenyl as diazonium anion, its chemical shift does not vary in ^{19}F-NMR spectroscopy, despite being present in different states (TFA-anion and TFA). Therefore, trifluoroacetic acid is used as an excellent internal standard for quantification and all integrations can be referenced to this peak. Applying positive exponential function (1 Hz) as apodization, zero filling of 32k data points, phase- and baseline-correction results in best SNR ratio (Table 14 and refer to Figure 231 in the appendix).

Table 14: ^{19}F-NMR (56.98 MHz, PEEK flow cell, stopped flow) integral variance and SNR values of TFA and 3-CF_3-aniline; 64 scans, 1 Hz exponential function as apodization, 32k zero filling, phase- and baseline-correction in stopped flow.

#	TFA (0.4 M) reference integral	3-CF_3-aniline gravimetric concentration	3-CF_3-aniline integral #1	3-CF_3-aniline integral #2	3-CF_3-aniline integral #3	3-CF_3-aniline mean integral	3-CF_3-aniline integral variance	SNR - TFA	SNR - 3-CF_3-aniline
1	3	0.05 M	0.383	0.367	0.358	0.369	0.009		23
2	3	0.1 M	0.712	-0.720	0.750	0.727	0.015		46
3	3	0.15 M	1.068	1.062	1.059	1.063	0.003		68
4	3	0.2 M	1.52	1.500	1.480	1.500	0.013	213	103

Investigations show a linear behavior of all fluorine atoms with a system response factor of ~1. This is evaluated by recording spectra of four different concentrations (0.05 - 0.2 M, three measurements each) of 3-CF_3-aniline in 0.4 M TFA. The mean integrals are plotted against the gravimetric concentrations in reference to the internal standard and 50 mM concentrations are detected reliably as well (Figure 50).

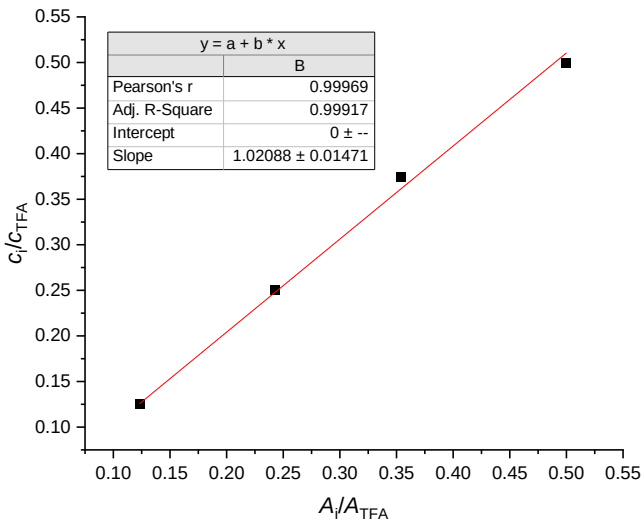

Figure 50: Average response factor of 3-CF_3-aniline in reference to the internal standard in ^{19}F-NMR (56.98 MHz, PEEK flow cell, stopped flow) spectroscopy in stopped flow.

NMR-spectroscopy of 0.2 M 3-CF_3-aniline and 0.4 M TFA (in acetonitrile) at different flow rates (one measurement at 0, 0.2 and 1.0 mL×min^{-1}) has a deviation of ~9% (Figure ***51***). With repetitive experiments, variance is assigned as a statistical instrumental error and no dependency on the flow rate is identified. In further quantitative evaluation, the sum of all (relevant) integrals are weighted with respect to the TFA integral and the difference to the theoretical value is set as measuring error.

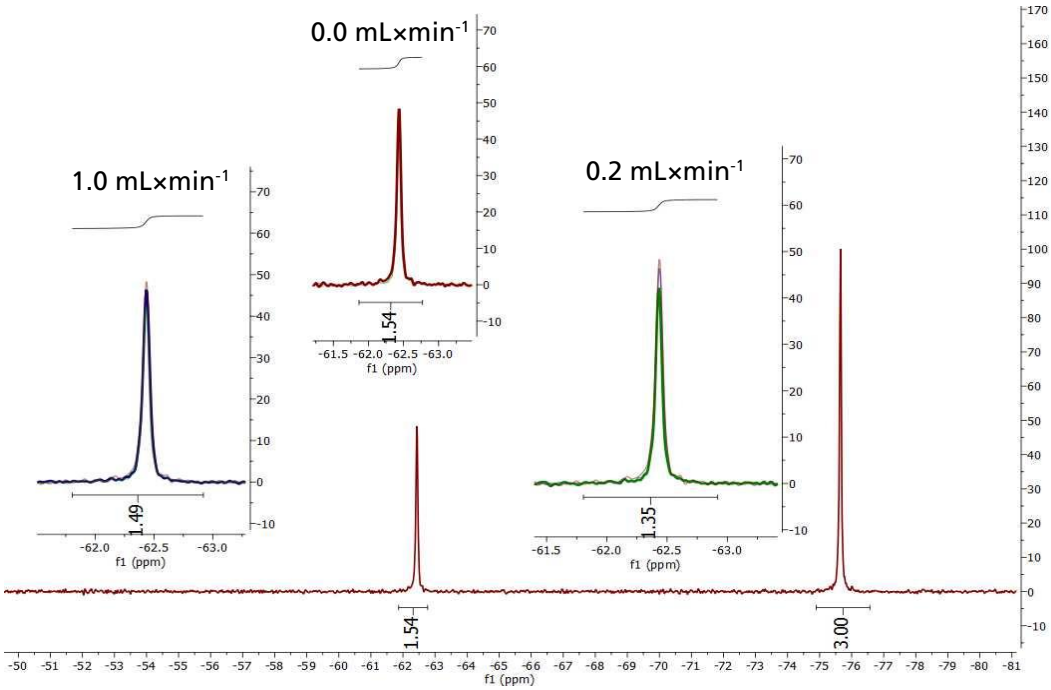

Figure 51: ^{19}F-NMR integrals (56.98 MHz, PEEK flow cell) of 0.2 M 3-CF_3-aniline and 0.4 M TFA in MeCN in reference to TFA δ_F= -75.65 ppm: — stopped flow; — 0.2 mL×min^{-1}; — 1.0 mL×min^{-1}.

3.1.4.1 Spectra evaluation via standard integration methods

Online ^{19}F-NMR spectroscopy is applied as process monitoring of the optimized catalyst-free synthesis of 3-CF_3-biphenyl at 17 bar_{exs}. Evaluation of such spectra shows complete conversion of the diazonium trifluoroacetate intermediate after 1.25 h, as the peak at -61.13 ppm is completely disappeared. A new signal at -61.92 ppm appears, which is assigned to the favored product. This is confirmed by recording a ^{19}F-NMR spectrum of purified 3-CF_3-biphenyl.

Time independent NMR measurements of the process require steady state conditions inside the complete reactor setup. This guarantees data acquisition of an identical substance composition, in the NMR flow cell, in repeating experiments with identical settings (statistical error excluded). As Kern *et al.* report, comparison of a time corrected

spectra with an ongoing continuous process is very challenging and leads to defective validation and quantification.[120]

For evaluation of the NMR-spectra MestReNova 12 (Mestrelab Research S.L) is used and peak areas are integrated manually. This results in 71±7% yield of the benchmark product **26b** (Figure 52). By means of the existing measuring errors in NMR as well as in GC/MS analysis, both results agree with each other. Nevertheless, reliability of the result is reduced due to the occurrence of a second smaller peak (high-field shift), which overlaps with the product signal. This indistinct product signal avoids precise peak integration, since integration borders have to be chosen individually by the operator, which undoubtedly influences evaluation.

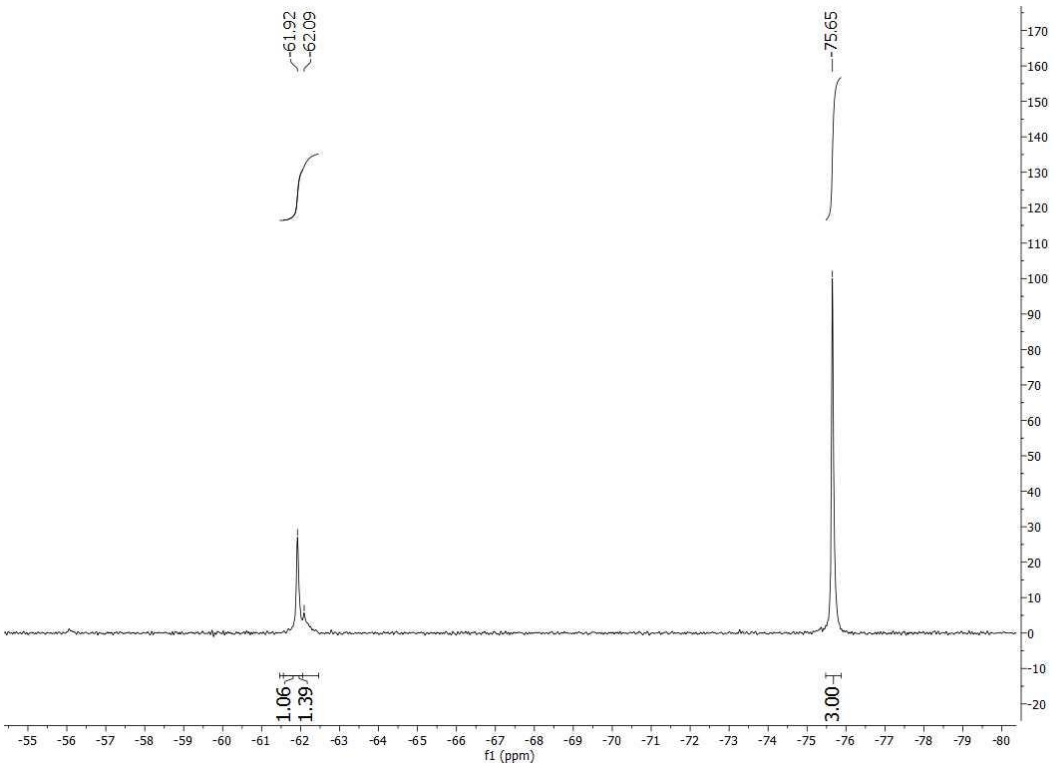

Figure 52: Evaluation of an online ^{19}F-NMR spectrum (56.98 MHz, PEEK flow cell) of continuous 3-CF_3-biphenyl synthesis in a 1/16" FEP capillary photoreactor; General reaction conditions: 200 mM 3-CF_3-aniline, 1.2 equiv. *t*-BuONO, 2 equiv. TFA in MeCN, 365 nm 50 W_{el}, 20 °C, 17 bar_{exs}, 1.25 h residence time; MestReNova 12 used to integrate the peak areas.

3.1.4.2 Spectra evaluation via chemometrics software

Spectra analysis has to be automated and standardized for higher reliability in ^{19}F-NMR spectroscopy. For this reason, PEAXACT 5.3 (S-PACT, Aachen, Germany) as chemometrics software is used. A recorded spectrum is reverse engineered by mathematical functions

with this tool, for a precise determination of compound quantities via their signal area. This procedure is called Indirect Hard Modelling IHM and it makes use of basic information within the NMR spectrum. Each peak signal in a NMR experiment is represented by a Lorentzian line shape, in optimal conditions, due to their physical nature.[175,176] In reality, the signal is always broadened by inhomogeneities of the instruments permanent magnet or the applied electro-magnetic field during acquisition. This is usually represented with a Gaussian function, broadening the Lorentzian function.[120]

$$P = \alpha \cdot \left[\beta \cdot \exp\left(-ln(2)\frac{(x-\delta)^2}{\gamma^2}\right) + (1-\beta)\frac{\gamma^2}{(x-\delta)^2+\gamma^2}\right] \tag{19}$$

With: P = Peak intensity at x

x = independent variable

α = peak maximum at the peak's center position

β = Gaussian-Lorentzian-ratio between 0 and 1

γ = half width at half maximum (HWHM)

δ = center position of the signal

Each NMR-spectrum (mixtures of known substances as well as mixtures containing unknown substances) can be modeled as a weighted sum of peak functions. A parameter set of each peak is individually adjusted, which is called peak fitting. The complete spectrum is deconvoluted into its pure component spectrum. Their parameters (peak position(s), HWHM and Gaussian part) are fixed.

Pure component hard models of 3-CF_3-biphenyl (Figure 53 and Figure 54) and TFA (Figure 55 and Figure 56) are created to evaluate the yield of the benchmark product inside an untreated reaction mixture. Combining those pure component models gives an overall Indirect Hard Model, which is applied onto the recorded spectrum (Figure 57 and Figure 58). Peak fitting allows disaggregation of an unknown NMR-spectrum into concentrations of known components (here TFA and 3-CF_3-biphenyl) and unidentified substances (by-products). With peak fitting (see Figure 232 in the appendix), global residuals between experimental data and the IHM component fits are minimized. In comparison to manual peak integration, the principle of IHM is optimal for overlapping NMR signals. Peak areas are precisely calculated, giving access to a reliable quantitative analysis.[118,120,175,176,177]

In the case of online ^{19}F-NMR spectroscopy in 3-CF_3-biphenyl synthesis, the following steps of Indirect Hard Modelling are performed:

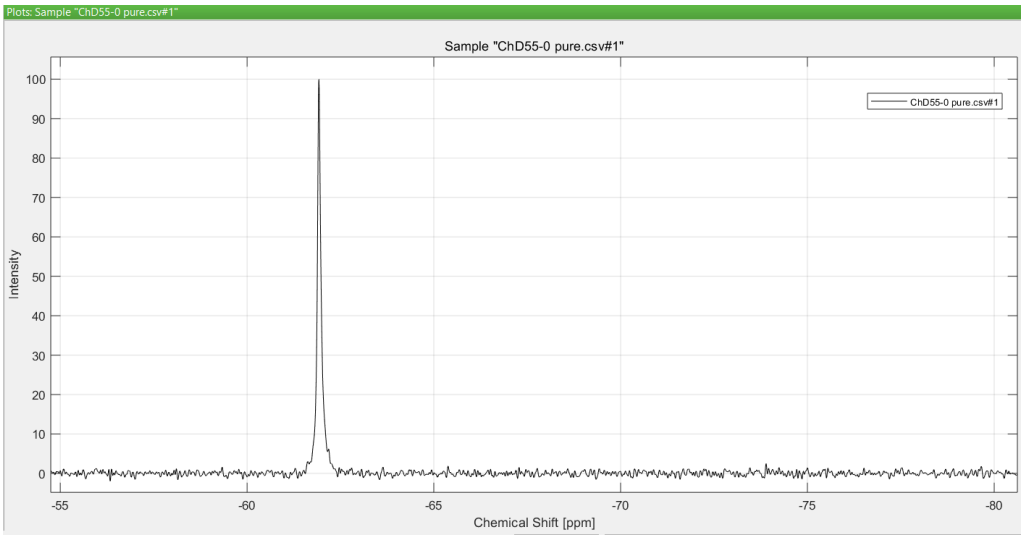

Figure 53: Recording ^{19}F-NMR (56.98 MHz, offline) spectrum of purified 3-CF_3-biphenyl (~0.2 M in MeCN) in reference to trichlorofluoromethane δ_F=0 ppm and spectrum processing.

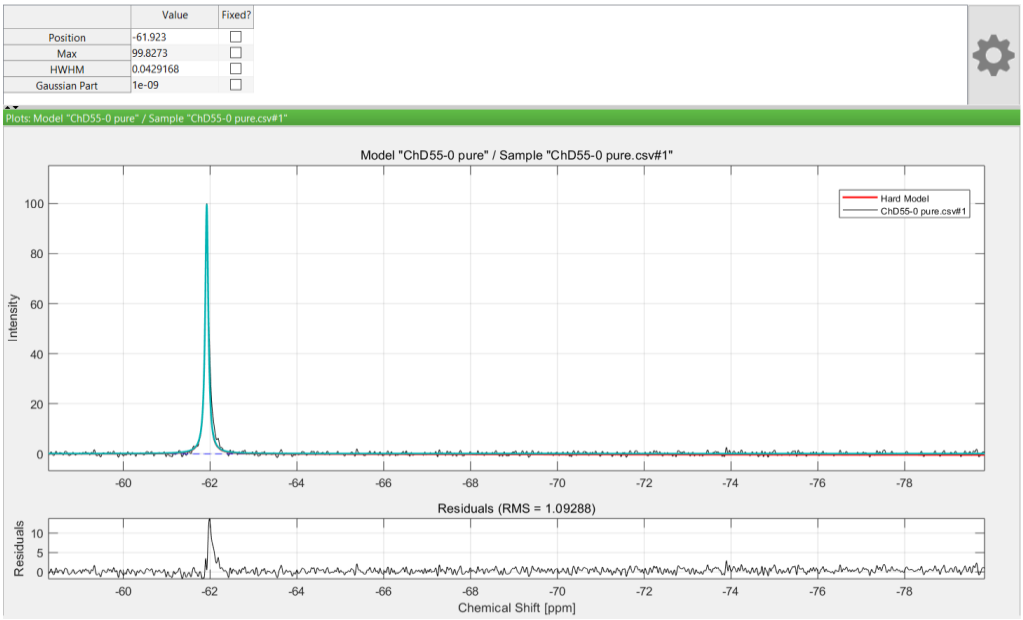

Figure 54: Creating a pure component model for purified 3-CF_3-biphenyl with PEAXACT 5.3; *turquoise* peak shape of hard model consisting of a single peak; top: peak parameters representing 3-CF_3-biphenyl ^{19}F- NMR.

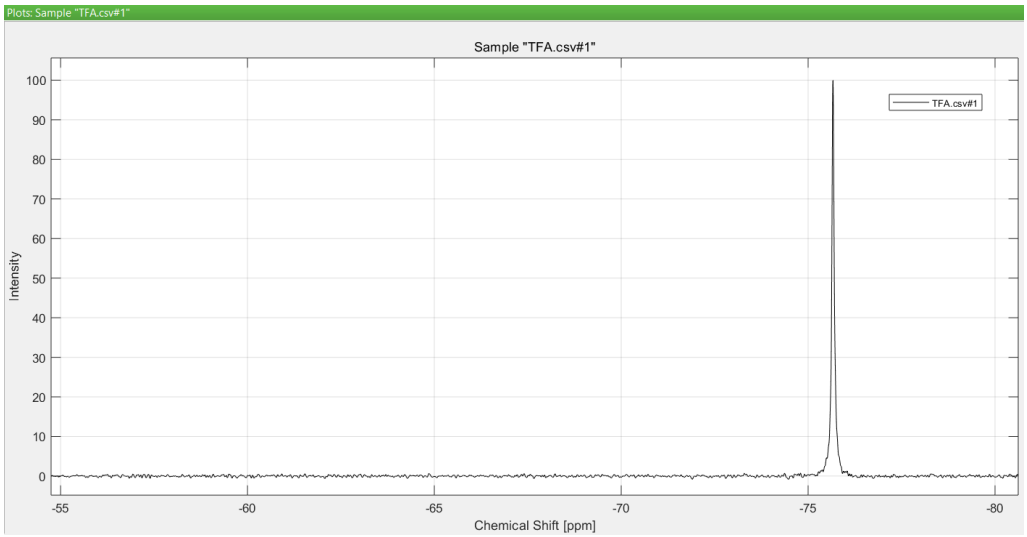

Figure 55: Recording ^{19}F-NMR (56.98 MHz, offline) spectrum of trifluoroacetic acid (0.4 M in MeCN) in reference to trichlorofluoromethane δ_F=0 ppm and spectrum processing.

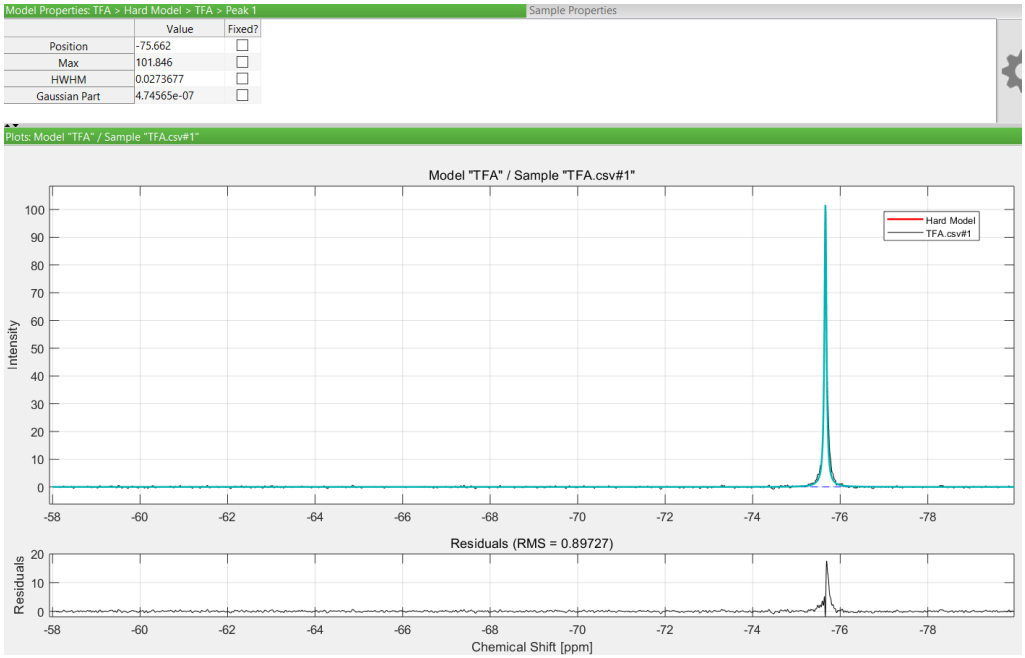

Figure 56: Creating a pure component model for trifluoroacetic acid with PEAXACT 5.3; *turquoise* peak shape of hard model consisting of a single peak; top: peak parameters representing trifluoroacetic acid ^{19}F- NMR.

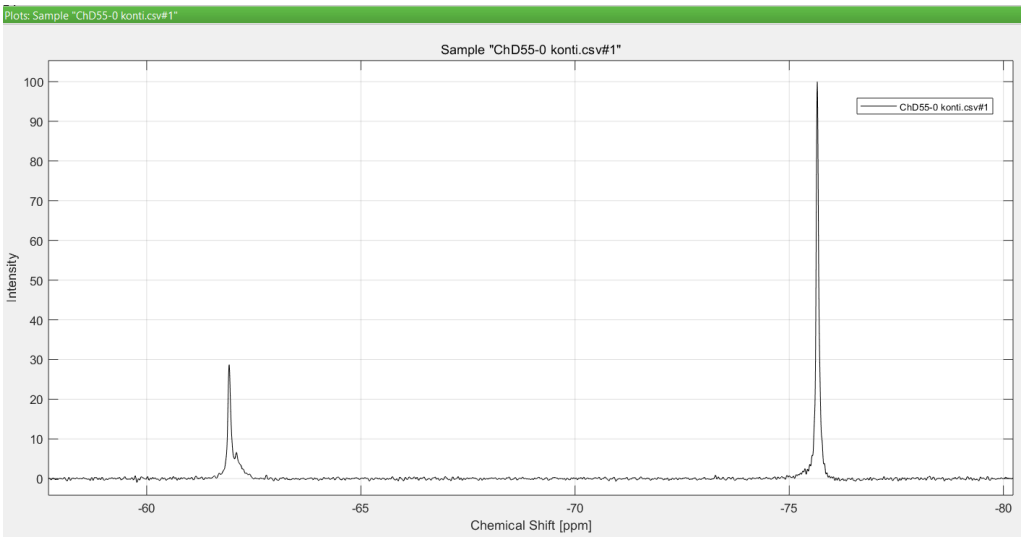

Figure 57: Recording online ^{19}F-NMR (56.98 MHz, PEEK flow cell) spectrum of continuous 3-CF_3-biphenyl synthesis in a FEP capillary photoreactor and spectrum processing; General reaction conditions: 200 mM 3-CF_3-aniline, 1.2 equiv. *t*-BuONO, 2 equiv. TFA in MeCN, MeCN/benzene V/V=1/1, 365 nm 50 W_{el}, 20 °C, 17 $bar_{exs;}$, 1.25 h residence time.

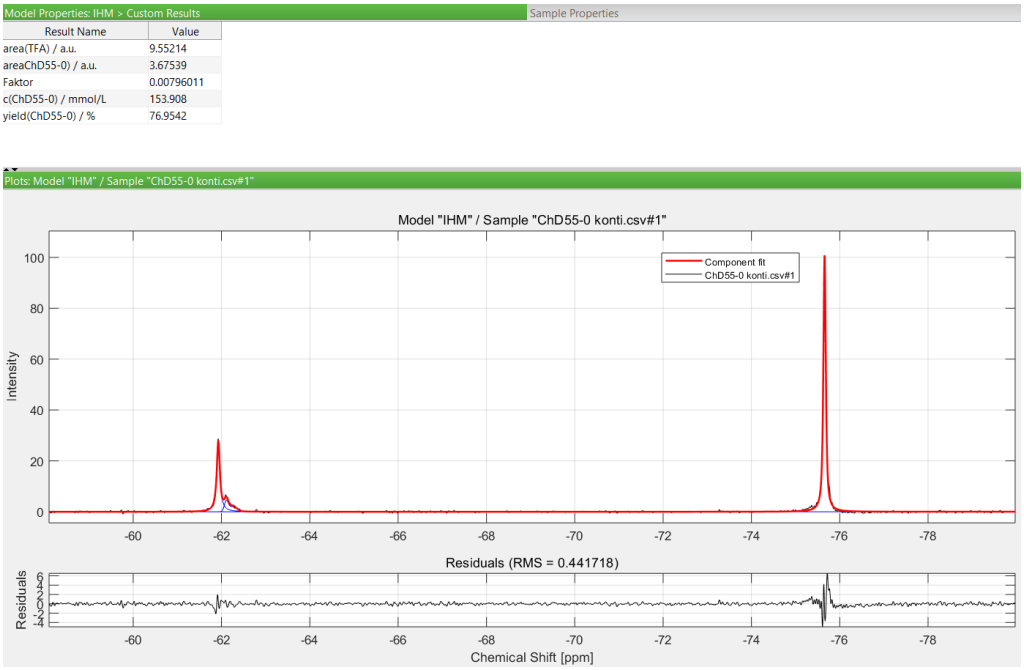

Figure 58: Peak fitting of an online ^{19}F-NMR spectrum (56.98 MHz, PEEK flow cell) with PEAXACT 5.3 of continuous 3-CF_3-biphenyl synthesis in a 1/16" FEP capillary photoreactor; *blue* peak shape of each pure component fits (and unknown substances), *red* component fit as result of a weighted sum of pure components; IHM model properties: Only variation of weights, baseline and peak position allowed (see Figure 232); top: Results of component fitting including yield of continuous 3-CF_3-biphenyl synthesis.

The IHM technique of PEAXACT 5.3 for quantitative evaluation of online ^{19}F-NMR spectra of continuous 3-CF_3-biphenyl synthesis results in 77±9% yield (Figure 58). This result is consistent to GC/MS analysis, whereas a high reliability is guaranteed due to peak modeling and fitting in comparison to standard integration.

The same Indirect Hard Model is now used for a continuous synthesis of the benchmark product with variating light intensity (Figure 59 and Figure 233 to Figure 236 in the appendix). Offline GC/MS analysis of those experiments shows a linear dependency. As expected, online ^{19}F-NMR spectroscopy (benchtop spectrometer equipped with a pressurized PEEK flow cell) gives same yield via Indirect Hard Modelling as expected.

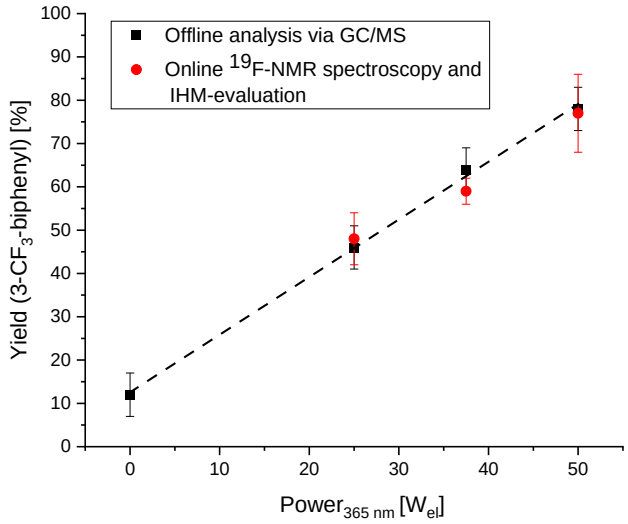

Figure 59: Continuous synthesis of 3-CF_3-biphenyl in a 1/16" FEP capillary photoreactor using different power for irradiation: ■ data points acquired with offline GC/MS, - - - data-trend; ● data points acquired via online ^{19}F-NMR spectroscopy (56.98 MHz, PEEK flow cell) and IHM in PEAXACT 5.3; General reaction conditions: 200 mM 3-CF_3-aniline, 1.2 equiv. *t*-BuONO, 2 equiv. TFA in MeCN, MeCN/benzene V/V=1/1, 365 nm, 20 °C, 17 bar_{exs}, 1.25 h residence time.

3.1.5 Scope evaluation of photochemical arylation using arene diazonium trifluoroacetates

The versatility of developed continuous synthesis route using the catalyst-free photoarylation via diazonium trifluoroacetates is tested with numerous benzene-like arenes (and furan). Herein, the diazonium compounds **25c** or 4-fluorophenyldiazonium trifluoroacetate **31a** (derived from 4-fluoroaniline **31**) are generated *in-situ* in all experiments within 10 minutes at 20 °C. After formation of the reactive intermediate, the corresponding neat arene **23a-m** is added and the mixture passes the 1/16" FEP capillary photoreactor (V=15 mL, 365 nm 50 W_{el}) at 17 bar_{exs}. Same conditions are applied for every reaction without further optimization.

Every sample (**25a-m**, **31b**) is monitored by online ^{19}F-NMR spectroscopy (via IHM, see Figure 237 to Figure 272 in the appendix) and the result is compared with the isolated yield and offline GC/MS evaluation (Table 15). Anilines, containing a fluorine-group, have to be used as a probe for the ^{19}F-NMR spectrometer.
Arenes like aryl halides, alkyl benzene, anisole, ethyl benzoate or phenylboronic acid pinacol ester are successfully photoarylated giving satisfactory yields in each sample. Most arenes give a mixture of *ortho*-, *meta*-, *para*-isomers after arylation. The isomer ratio is generally influenced by the coordinating effect (± I- or ± M-effect) of the functional-groups. With normal phase column chromatography, those isomers cannot be separated in most cases. High-field ^{19}F-NMR spectroscopy gives the same isomer ratio as GC/MS analysis. In all cases, the used benchtop NMR-spectrometer is not able to deliver separated fluorine-signals for the isomers. Only one signal is visible or the peaks overlap with each other. Therefore, online NMR quantification with the benchtop spectrometer is only feasible for determination of the overall yield.

Synthesis of 4-fluorobiphenyl **31b** (Table 15 entry #11) via the corresponding 4-fluorophenyldiazonium trifluoroacetate **31a** is feasible as well. Unfortunately, online ^{19}F-NMR analysis with a 56.98 MHz benchtop spectrometer cannot be applied for process quantification of **31b**. The low amount of fluorine per molecule, as well as a very bad SNR in combination with a signal splitting (loss of signal information in the noise) are main reasons (see Figure 266 in the appendix).

Table 15: Scope evaluation of continuous charge-transfer arylation using diazonium trifluoroacetates and online ^{19}F-NMR spectroscopy using IHM.[a]

#	product	yield-isolated	yield-GC/MS (*o*:*m*:*p*-ratio)	yield-online benchtop NMR spectroscopy
1	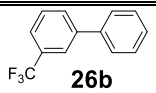 **26b**	65%	78±5% (-)	77±9%
2	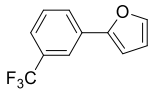 **26a**	40%	80±5% (-)	77±4%
3	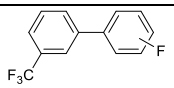 **26c**	45%	58±5% (55%:16%:29%)	64±7%
4	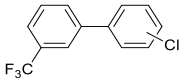 **26d**	37%	54±5% (59%:18%:23%)	63±9%
5	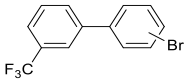 **26e**	30%	60±5% (57%:20%:23%)	57±24%
6	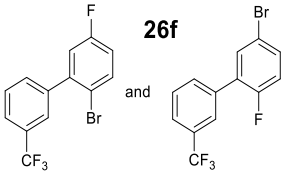 **26f** and	28%	36±5% (54%:46%)[b]	38±13%
7	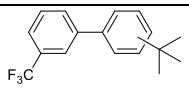 **26g**	29%	40±5% (20%:31%:49%)	43±11%
8	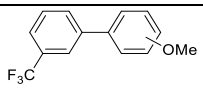 **26h**	40%	80±5% (78%:8%:14%)	82±3%
9	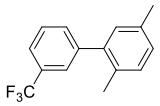 **26i**	42%	42±5% (-)	35±11%
10	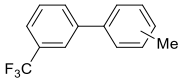 **26k**	50%	36±5% (60%:16%:24%)	65±4%
11	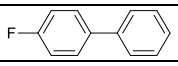 **31b**	80%	70±5% (-)	17±56%
12	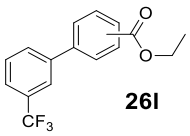 **26l**	26%	44±5% (22%:55%:23%)	39±2%
13	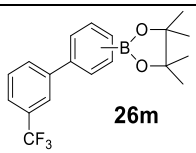 **26m**	22%	74±5% (25%:28%:47%)	82±3%

a: General reaction conditions: 200 mM aniline, 1.2 equiv. *t*-BuONO, 2 equiv. TFA in MeCN, 365 nm 50 W_{el}, 20 °C, 17 bar_{exs}, 1.25 h residence time, addition of neat arene or 4.5 M phenylboronic acid pinacol ester, respectively; **b:** 2-bromo-5-fluoro-3´-CF_3-biphenyl/5-bromo-2-fluoro-3´-CF_3-biphenyl (54%:46%)

3.1.5.1 Long-term continuous synthesis and quantification of selected examples

Long-term processing of two biphenyl samples is performed via the elaborated catalyst-free photoarylation route including online process monitoring via ^{19}F-NMR spectroscopy. When producing **26b** and **26m**, respectively, focus is especially put on the stability, sustainability and reliability of NMR-spectrometer.

Offline GC/MS analysis and quantitative NMR analysis (via IHM) leads to comparable results and 3-CF_3-biphenyl is synthesized with a specific productivity of ~0.125 mol×(L×h)$^{-1}$ (determined via GC/MS). Having an optimal workup procedure without any substance loss would give ~2.8 g of isolated product after ~6.75 h process time.

A long-term run **26m** has a specific productivity of ~0.118 mol×L^{-1}×h^{-1} (determined via GC/MS), using only 11 equivalents of the pinacol ester. In this case, optimal workup of the reaction mixture would yield ~4.9 g of the isolated isomers after ~8 h process time.

As the reactive pinacol ester is a promising starting material, **26m** can be used for subsequent sp^2-sp^3 bond formation via a Petasis borono-Mannich- or Suzuki–Miyaura reaction.[27,178]

As already mentioned, data of both analysis methods are comparable, whereas NMR-results for synthesis of **26m** seem to have a positive offset (see Figure 60 and Figure 61). Major advantage of online NMR-analysis is the shorter measuring time in contrast to offline GC/MS analysis. This allows a more detailed process monitoring at shorter intervals. With the chosen NMR-spectroscopy parameters, the process performance can be monitored every 3 minutes.

The reliability of online NMR-analysis is mainly influenced by the stability and uniformity of the spectrometer hardware, which changes slightly over time in the conducted long-term experiments (constant ambient temperature). This instability seems to have variable impact on different NMR-signals. In some cases TFA reference signal loses its Lorentzian line shape while product peak area is constant (refer Figure 273 and Figure 283). In some cases, the pure component model of trifluoroacetic acid has to be represented by two peaks for a better fit.

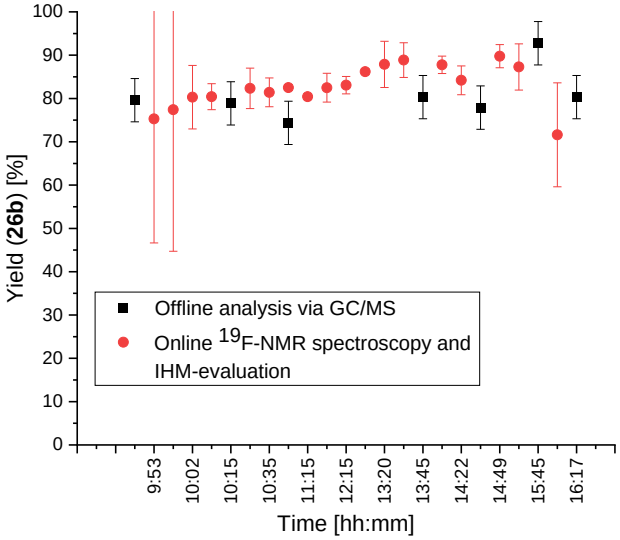

Figure 60: Long-term continuous synthesis of 3-CF_3-biphenyl **26b** in a 1/16" FEP capillary photoreactor: ■ data acquired with GC/MS; ● data acquired via online ^{19}F-NMR (56.98 MHz, PEEK flow cell) spectroscopy and IHM in PEAXACT 5.3; General reaction conditions: 200 mM 3-CF_3-aniline, 1.2 equiv. *t*-BuONO, 2 equiv. TFA in MeCN, MeCN/benzene V/V=1/1, 365 nm 50 W_{el}, 20 °C, 17 bar_{exs}, 0.2 mL×min^{-1}.

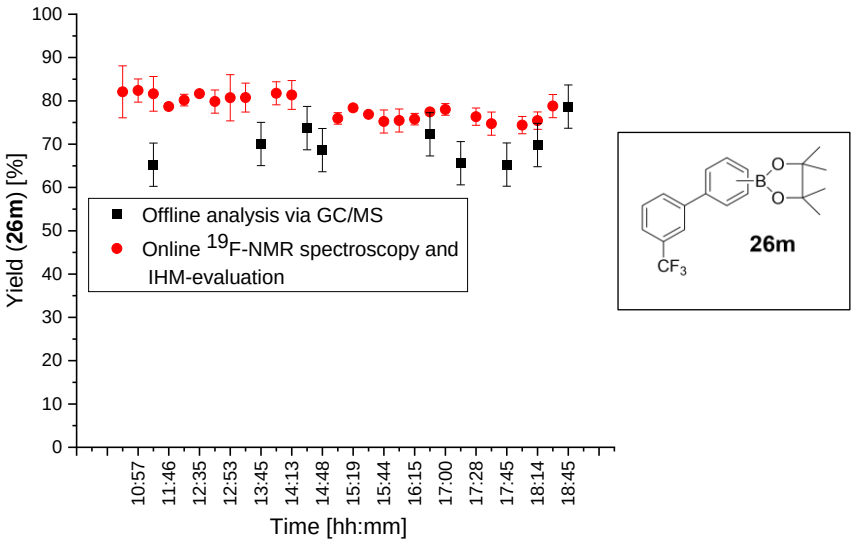

Figure 61: Long-term continuous synthesis of **26m** in a 1/16" FEP capillary photoreactor: ■ data acquired with GC/MS; ● data acquired via online ^{19}F-NMR (56.98 MHz, PEEK flow cell) spectroscopy and IHM in PEAXACT 5.3; General reaction conditions: 200 mM 3-CF_3-aniline, 1.2 equiv. *t*-BuONO, 2 equiv. TFA in MeCN; 2.25 M phenylboronic acid pinacol ester in MeCN, 365 nm, 50 W_{el}, 20 °C, 17 bar_{exs}, 0.2 mL×min^{-1}.

3.1.6 Studies on the mechanism of photochemical arylation using arene diazonium trifluoroacetates

3.1.6.1 Synthesis and stability of 3-CF_3-phenyldiazonium trifluoroacetate

Isolated 3-CF_3-phenyldiazonium trifluoroacetate **25c** is synthesized via an adapted procedure of Colas *et al.* [163] Due to its high solubility in polar and apolar solvents (acetone, diethyl ether, acetonitrile, benzene, dichloromethane), isolation of the pure solid is only possible in dichloromethane at -78 °C. The purified compound is stable for several days, when stored in the freezer. No significant decomposition is observed in the range of 1 h at 0-5 °C in the absence of light (see Figure 62 and Figure 292 in the appendix). As expected, NMR- spectroscopy of the isolated diazonium salt shows identical signals in comparison to the same *in-situ* generated species. Even if the substance is completely dissolved and fully dissociated, diazonium trifluoroacetate **25c** appears to be a double salt (see Figure 293 to Figure 296 in the appendix).

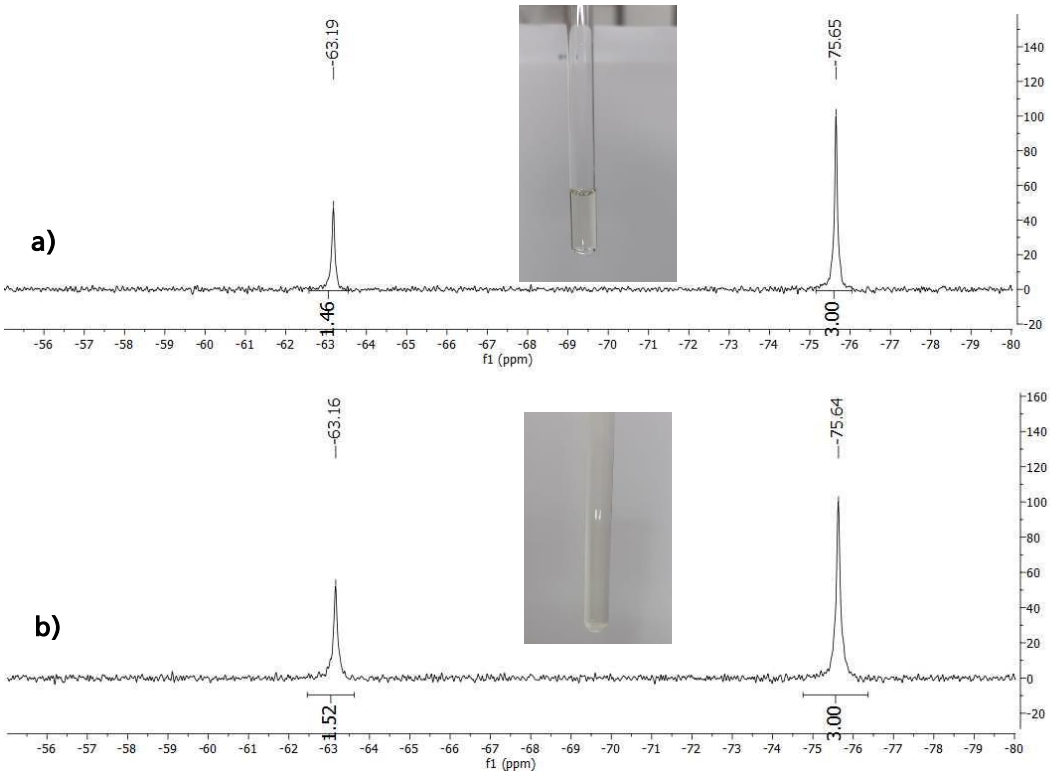

Figure 62: Monitoring stability of 0.1 M 3-CF_3-phenyldiazonium trifluoroacetate in MeCN with 19F-NMR spectroscopy (56.98 MHz, offline) at 0-5 °C and protected from light in reference to TFA δ_F= -75.65 ppm; after **a)** 8 minutes and **b)** 60 minutes.

3.1.6.2 Charge-transfer photoarylation with arene diazonium trifluoroacetates

Two major mechanistic pathways exist for direct C-H photoarylation of arenes with diazonium salts.

Slegt *et al.* describe direct formation of a phenyl cation from benzenediazonium tetrafluoroborate or 4-nitrophenyldiazonium tetrafluoroborate by direct excitation of the diazonium group with 254, 300 and 350 nm. In presence of a tetrafluoroborate anion in acetonitrile, they can observe fluorination (Schiemann product) and formation of the corresponding acetanilide (Ritter product) as well.[179]

A cationic mechanism is excluded when irradiating an *in-situ* generated 3-CF_3-phenyldiazonium trifluoroacetate at 365 nm in the presence of benzene, for the following reasons: Traces of corresponding acetanilide are found when using four equivalents of trifluoroacetic acid. A reduction to two equivalents TFA eliminates this traces nearly completely. It is stated, that acetanilide formation, starting from a diazonium salt, does not depend on the TFA amount either in a photochemical or thermic reaction, but traces of water should play a key role. Therefore, 10% of acetonitrile is replaced by water when using two equivalents of TFA. After 17 h irradiation in batch, no difference in amount of Ritter product is found in comparison to a ´water-free´ synthesis and the side-reaction is assigned to be induced thermally.

Another well discussed mechanism for C-H arylation with diazonium salts is the formation of charge-transfer/EDA complexes between the diazonium compound and the arene.[29,135] Formation of charge-transfer bands is observed with UV/VIS-spectroscopy (Figure 65). Even a small amount of diazonium trifluoroacetate **25c** in a mixture of acetonitrile and benzene (V=1/1) is needed to form this charge-transfer band. Electron-rich arenes (in comparison to benzene), like toluene, p-xylene or anisole eventually result in formation of a distinct local maximum at 363 nm (Figure 65 c).

In contrast to publications of Kosynkin and Fürst *et al.*, no radical chain transfer for C-H arylation is observed, since a linear dependency between yield and irradiation power is observed in Figure 59. This chain transfer would promote arylation after initial radical formation, even with a lack of any initiators or light.[29,135,180]

In continuous synthesis of 3-CF_3-phenyldiazonium trifluoroacetate **25c** a signal at δ_F=-62.25 ppm (3-CF_3-aniline) is observed (Figure 63 — graph). Offline UV/Vis-spectroscopy images formation of an additional charge-transfer complex between the diazonium salt and the starting material even in high dilution (see Figure 65 b). This explains colorization in Figure 43 e, despite using a high amount of trifluoroacetic acid.

As kinetic studies show, this charge-transfer complex has no additional electron donating effect on photochemical C-H arylation via diazonium trifluoroacetates. An identical kinetic behavior is observed in the continuous synthesis of 3-CF_3-biphenyl, when using either *in-situ* or separately generated diazonium trifluoroacetate at 365 nm irradiation (Figure 64).

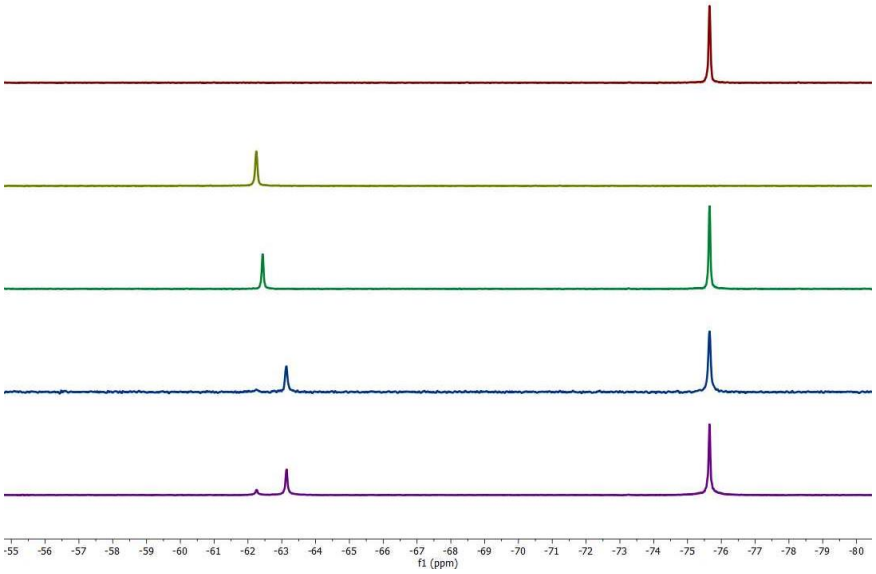

Figure 63: ^{19}F-NMR spectra (56.98 MHz, PEEK flow cell) at 0.1 mL×min^{-1} in MeCN in reference to $CFCl_3$ δ_F= 0 ppm: — TFA; — 3-CF_3-aniline; — 3-CF_3-aniline + TFA (1:2 molar ratio); — continuous synthesis of ~0.1 M 3-CF_3-phenyldiazonium trifluoroacetate after 10 minutes; — continuous synthesis of ~0.4 M 3-CF_3-phenyldiazonium trifluoroacetate after 10 minutes.

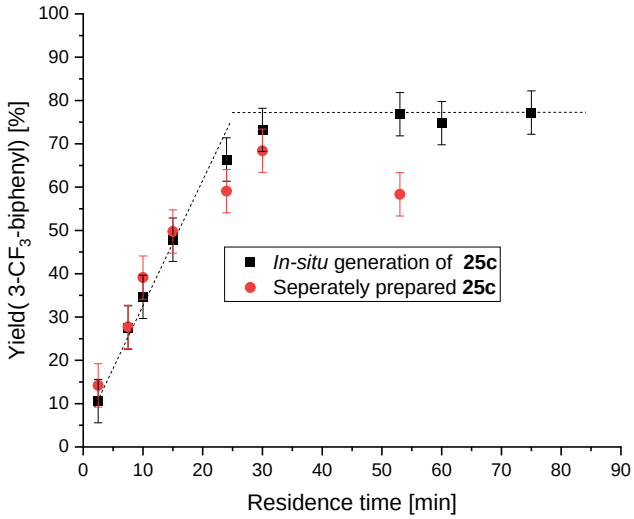

Figure 64: Continuous synthesis of 3-CF_3-biphenyl in a 1/16" FEP capillary photoreactor; General reaction conditions: 365 nm 50 W_{el}, 4 bar_{exs}, MeCN/benzene (V/V =1/1); ■ *in-situ* generation of ~0.1 M diazonium trifluoroacetate starting with 0.2 M 3-CF_3-aniline, ● 50 mM separately prepared 3-CF_3-phenyldiazonium trifluoroacetate; Determined by GC/MS.

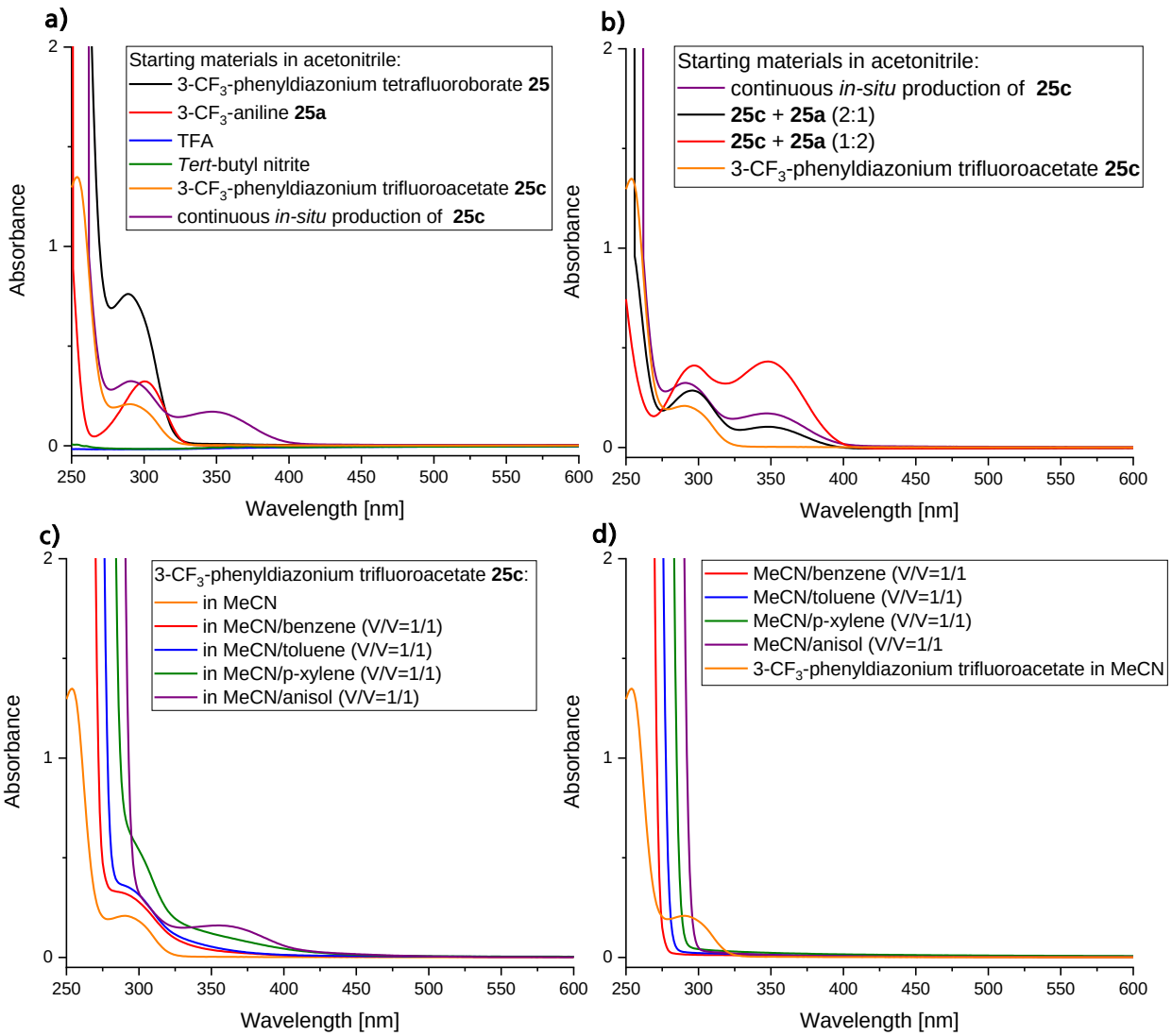

Figure 65: UV/Vis spectroscopy on catalyst-free C-H photoarylation using diazonium trifluoroacetates; **a)** in MeCN: — 5.0 mM 3-CF_3-phenyldiazonium tetrafluoroborate, — 1.25 mM 3-CF_3-aniline, — 1.5 mM *t*-BuONO, — 1.25 mM TFA, — 1.25 mM 3-CF_3-phenyldiazonium trifluoroacetate, — 1.25 mM 3-CF_3-phenyldiazonium trifluoroacetate continuous *in-situ* production; **b)** in MeCN: — 1.25 mM 3-CF_3-phenyldiazonium trifluoroacetate, — 1.25 mM 3-CF_3-phenyldiazonium trifluoroacetate continuous *in-situ* production, — ∑ 1.25 mM 3-CF_3-phenyldiazonium trifluoroacetate + 3-CF_3-aniline (2:1), — ∑ 1.25 mM 3-CF_3-phenyldiazonium trifluoroacetate + 3-CF_3-aniline (1:2); **c)** — 1.25 mM 3-CF_3-phenyldiazonium trifluoroacetate in MeCN, — 1.25 mM 3-CF_3-phenyldiazonium trifluoroacetate in MeCN/benzene V/V=1/1; — 1.25 mM 3-CF_3-phenyldiazonium trifluoroacetate in MeCN/toluene V/V=1/1; — 1.25 mM 3-CF_3-phenyldiazonium trifluoroacetate in MeCN/*p*-xylene V/V=1/1; — 1.25 mM 3-CF_3-phenyldiazonium trifluoroacetate in MeCN/anisole V/V=1/1; **d)** — 1.25 mM 3-CF_3-phenyldiazonium trifluoroacetate in MeCN, — MeCN/benzene V/V=1/1, — MeCN/toluene V/V=1/1, — MeCN/ *p*-xylene V/V=1/1, — MeCN/anisole V/V=1/1.

Investigations of Bockman *et al.* show a cofacial π-π stacking in this complex between arene as electron donor and diazonium compound as acceptor.[181] Subsequent excitation with an appropriate wavelength overcomes the rate limiting single electron-transfer, giving an aryl radical and aryl radial cation. Both can recombine to form the favored biphenyl. However, kinetic investigations show lower selectivity in the coupling step when 10 equivalents of benzene are used (see Figure 46). C-H arylation of another arene-molecule by the generated aryl radical seems to be more likely (Scheme 23).

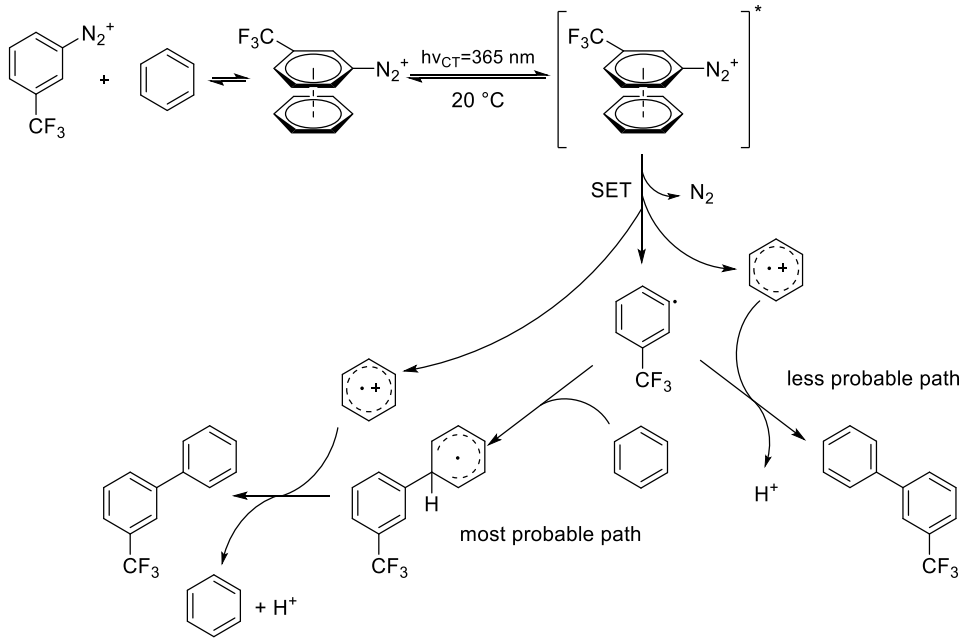

Scheme 23: Proposed mechanism of charge-transfer photoarylation using 3-CF_3-phenyldiazonium trifluoroacetate.

3.1.7 Conclusions and outlook

Different strategies, like heterogeneous photocatalysis or catalyst-free photoarylation for the synthesis of biphenyls via diazonium salts, are applied in the FFMR and the capillary photoreactor. In principle, the FFMR (anatase nanopowder immobilzed onto the reaction plate) is suitable to perform photoarylation under the given parameters (using one equivalent TFA to generate diazo intermediates *in-situ*).

The application of two equivalents TFA leads to a significant increase of conversion and selectivity, when 3-CF_3-phenyldiazonium trifluoroacetate containing an additional free acid per molecule unit is used as a precursor. UV/Vis-spectroscopy and kinetic studies reveal a direct C-H photoarylation of benzene-derivatives via a charge-transfer complex.

Even though the absorption maximum at 363 nm is weak, excitation of the arene diazonium salt/arene charge-transfer complex with UV-A light is possible. With optimized reaction conditions, 3-CF_3-biphenyl synthesis is started from convenient and safely handable substrates. Using adequate amounts of aniline, TFA, *tert*-butyl nitrite and arene, continuous flow photoarylation is conducted over a long period (several hours) at steady state conditions.

High conversion, yield and productivity of 13 samples is permanently monitored online by a LF-benchtop ^{19}F-NMR-spectrometer. The *m*-CF_3-group acts as a probe in every species. A reliable quantification using Indirect Hard Modeling of mixtures, with one or more products, is feasible and the results match with offline GC/MS analysis.

One can think about further process optimization steps: The amount of excess arene in the benchmark reaction and in all other samples is not adjusted yet. This would be necessary to enhance the atom efficiency for an even better sustainability. An increased productivity is certainly achievable by applying a higher concentration of the aniline substrate. Moreover, the catalyst-free procedure can be tested at the FFMR or FFMR-LARGE using an uncoated reaction plate.

3.2 Development of a (semi-)automated continuous lab-plant and the integration of online spectroscopy for a two-step synthesis of Z-stilbene

Preface:

This chapter is part of the project NMRplusX between the Canadian partners, Nanalysis Corp. (NAN) and Prof. Jason Hein from University of British Columbia (UBC), Vancouver, and the German partners Trout GmbH (TRT), as well as Fraunhofer Institute for Microengineering and Microsystems (Fraunhofer IMM). The NMRplusX consortium has expertise in the fields of NMR spectroscopy analysis, evaluation and spectrometer development (NAN), chemical reaction analysis regarding their catalytic mechanisms and reaction kinetics (UBC), software development for smart sensor technology and machine learning (TRT). Fraunhofer IMM provides expertise in reactor and plant development as well as integrated analysis tools for chemical reactions in continuously operated microreactors. Following persons contributed to this topic:

- Christoph Deckers: reactor layout; process and plant design; planning, coordination, processing and evaluation of all experiments; layout, evaluation, calibration and testing of NMR-spectroscopy, UV/Vis-spectroscopy, IR-spectroscopy, IR-sensor; layout and concept of control software; Software troubleshooting
- Thomas Rehm: Overall project coordinator
- Hans-Joachim Kost and mechanical workshop: Reactor and plant manufacturing
- Julian Höth: Hardware and software design, software programming and troubleshooting
- Ivette Krollmann: manufacturing of electronic components and hardware
- Juri Magomajew: Software troubleshooting
- Susanne Sigloch and Thomas Klotzbuecher: layout, design, construction of a nondispersive IR-sensor

Ongoing process development is one major topic in chemical industry, using digitalization as well as intelligent control- and analysis software or artificial intelligence, to make chemical production plants smarter every day (Industry 4.0).
Especially, when looking at process improvements, machine learning and artificial intelligence are able to overcome barriers in complex connections between input parameters and the consequential output. Together with the provision of data and intelligent hardware, machine learning is an optimal tool to predict and optimize chemical synthesis.[24,25]

Improvements in continuous synthesis (industry-, pilot- or lab-scale) often require huge costs and time to get one single data point. This effort usually consists of preliminary preparations, the start-up and an equilibration until reaching steady-state conditions. In plants without any online process monitoring, a sample has to be taken manually, analyzed and evaluated separately. Depending on the chosen or required parameters and techniques in a chemical reaction, such a cycle can last up to several hours. Beside optimization of process parameters for best conversion and selectivity of a reaction, management and handling of the process has to be reviewed as well. When considering both, an efficient and sustainable handling of chemicals, energy and working time are achieved.[46,182]

Digitalization, artificial intelligence and Flow Chemistry can overcome some of those hurdles or shorten idle time drastically.[183] It is necessary, that a synthesis plant is equipped with precise, computer assisted sensors to monitor e.g. temperature, flow rates, mass flow, pressure, pH-value or conversion/selectivity.
IR-,[184] Raman-,[185] UV/Vis-[186], NMR-spectroscopy[23,187] or mass spectrometry are established online process analysis tools, but only sparsely used in continuous (multi-step) synthesis.[188]

Moreover, a great desire of researchers, in the field of continuous flow synthesis, is a fully PC-based process control system, including data collection and evaluation. Additionally, convenient management of unknown reactions and kinetics is guaranteed, when DoE (design of experiments) optimization concepts[189] are automatically processed by a preliminary elaborated set of new process parameters.[190]

The development, initialization and testing of a (semi-)automated continuous flow plant in lab scale is described. Stable and reliable operating online analysis tools are mandatory, beside the implementation of the chemical reaction in the mechanized

plant. As a model reaction, the two-step synthesis of *Z*-stilbene is chosen to highlight opportunities and to mention all pitfalls in process development. Parts of this work are declared as a proof-of-concept, since there is no known application of online spectroscopy being used for this type of process.

As first step, a Wittig reaction gives a mixture of stilbene-isomers. NMR-spectroscopy and IR-spectroscopy are both used for online monitoring of conversion and selectivity. Nondispersive IR-spectroscopy (below mentioned as IR-sensor) is used in the subsequent *E*-*Z*-photoisomerization (second step) to harvest information on the selective generation of *Z*-stilbene.

3.2.1 Specification and design of a lab-plant considering physicochemical and technical challenges

3.2.1.1 Selection of components for a Wittig-olefination reaction

Double bond formation is an important procedure to build up organic molecules. Beside palladium catalyzed Heck cross coupling,[191] several of those reactions rely on the coupling of a carbonyl compound (aldehyde or ketone) and an olefination reagent.[192] The Wittig reaction, for example, uses α-CH-acid alkyl aryl phosphonium salts as precursor.

A reactive phosphorus ylide-ylene compound is formed by abstraction of a proton with a base in α-position. An oxaphosphetane is formed in a concerted reaction.[193,194] By elimination of phosphine oxide **36**, the corresponding alkene results. Investigations, using ^{31}P-NMR spectroscopy at low temperature, concluded the absence of a betaine intermediate in the mentioned mechanism.[195] Nevertheless, with lithium salts ("salt containing" conditions[130]) betaine formation can be promoted, while having a significant effect on stereochemistry resulting in *E*-alkenes (Schlosser modification).[193,196]

Information on diastereomerism of the alkene is already provided in the intermediate formation. Generally, a *Z*-alkene is produced as consequence of irreversible and quick addition by reactive components (kinetically favored product). A sterically hindered or slower reaction will give the thermodynamically controlled *E*-alkene. Non-stabilized triphenylphosphonium ylides (Ph_3PCHR) with R=alkyl give *Z*-isomers, semi-stabilized

ylides (R=aryl) show no clear tendency and *E*-alkene are formed with stabilized ylides (R= CO_2R' or CN). If phenyl groups of the phosphonium salt are replaced by alkyl groups, *E*-isomers will result.[197] In general, ylides with a benzylidene group (increased electron density at the α-carbon) will react quicker than those having an alkylidene group.[198]

The carbonyl compound influences reactivity as well. Aldehydes increase reactivity in comparison to ketones. If electron withdrawing groups are used at aryl aldehydes, kinetics can be increased even further.[199] Several studies deal with the influence of solvent polarity on Wittig reactions. For example, the reactivity of the stabilized carbomethoxymethylene(triphenyl)phosphorane and benzaldehyde is increased by a factor of ~925 when using methanol instead of benzene.[200]
Studies on olefination reactions of allylidene-(triphenyl)phosphorane and acetaldehyde in different solvents show no influence on *E*/*Z*-ratio of the products. Instead, significant impact on the reactivity/yield is observed when using different solvents. Lower yield is found in presence of apolar decalin or toluene, while polar THF gives higher yield. Polar protic solvents as *tert*-butyl alcohol are inappropriate, since they initiate quenching of the ylide.[201] In general, temperature has different influence on reactivity and selectivity. Non-stabilized ylides require cold temperatures to run smoothly, whereas stabilized and semi-stabilized ylides give increased yield when conducted at higher temperature.[200,201]

While planning/designing the model reaction, the hypothetical integration of an artificial intelligence, self-learning process development module should be feasible at all time. Therefore, reaction kinetics has to be slow enough, to provide significant changes when modifying process parameters, but fast enough for numerous variations in a reasonable time. Having mentioned theoretical information in mind, synthesis of stilbene **35** (1,2-diphenylethylene) is chosen as model reaction using benzyltriphenylphosphonium bromide (BTTP) **32** and benzaldehyde (BA) **34** as starting materials (Scheme 24).

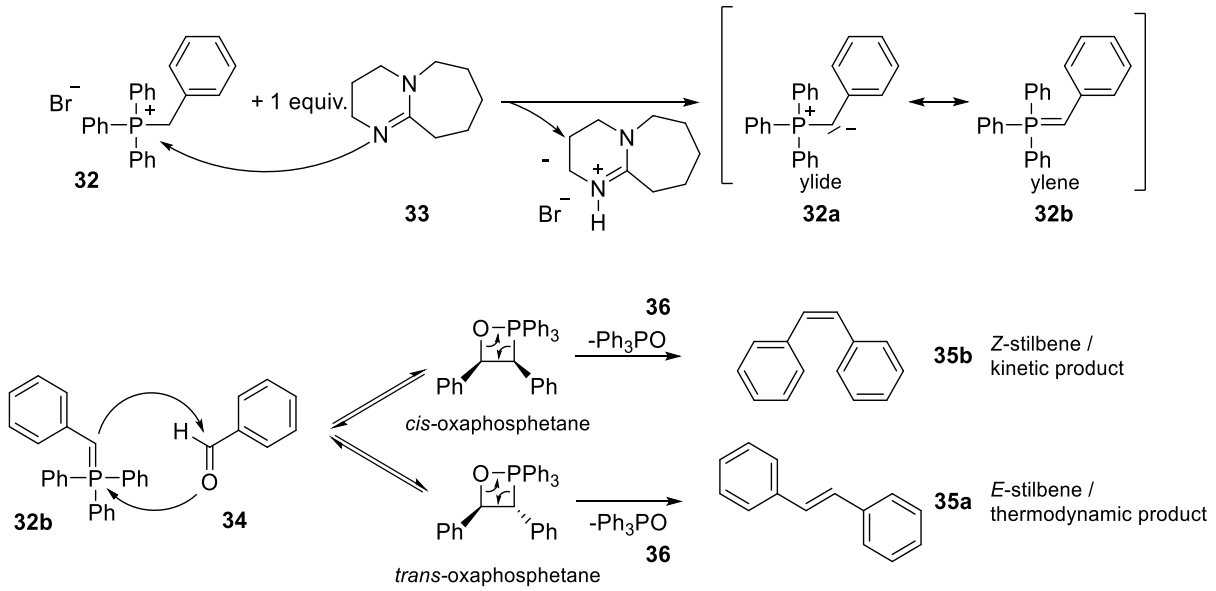

Scheme 24: Synthesis of stilbene **35**, using benzyltriphenylphosphonium bromide and DBU to generate the reactive intermediate. Subsequently, Wittig reaction via oxaphosphetanes follows and a double bond is formed.

Segmented (liquid-liquid) flow pattern with[202] or without[37] support of a phase transfer catalyst are often used, when conducting Wittig reaction in continuous flow. Usually, this flow pattern is chosen to overcome solubility issues of strong bases, which are required for deprotonation and ylide-generation (**32a**). Sodium hydroxide, potassium *tert*-butoxide are two common examples but contain inorganic counter ions[203], which prevents solvation in organic media.

The presented model reaction is performed in a homogeneous flow pattern for simple adaption of the flow rate (dependency of mixing efficiency is neglected[204]). The reaction is quenched by an acidic aqueous media in order to avoid further uncontrolled reaction. The quench media has to be removed via a continuously operating liquid-liquid phase separator (here: Zaiput Flow Technologies Sep-10[205]) for further processing and to keep volume small. This phase separation immediately yields in new requirements for the Wittig reaction. Water-miscible solvents, like THF or methanol, are inappropriate and a less polar, water immiscible matrix based on toluene has to be used.

An optimal mixture of toluene and methanol is elaborated to dissolve starting materials, intermediates and products. This is necessary to prevent clogging inside capillaries or sensitive spectrometer flow cells. In addition, a minimum amount of methanol should be used to keep volume loss, by quenching, extraction and phase separation, as low as possible.

Consequently, a soluble organic base deriving from guanidine (e.g. triazabicyclodecene TBD) or amidine (e.g. diazabicycloundecene DBU) is chosen to prevent clogging in the capillaries as well.[32,206]
Finally, 15vol% of methanol as solvent result in best stability and operability, when mixing the organic base DBU **33** (0.5 M; dissolved in toluene) with BTTP/BA (0.5 M each; dissolved in methanol/toluene) to initiate the reaction inside the thermal capillary reactor. An excess pressure of 3 bar is used to avoid any problems concerning the boiling point of the solvent.

Process monitoring of this continuous synthesis step is carried out with online NMR- and IR-spectroscopy. High concentrations have to be used to achieve a high SNR. Fortunately, a 0.25 M substrate concentration (in the capillary) shows best compromise between solubility and detectability.

3.2.1.2 E-Z-photoisomerization of stilbene

As IR-spectroscopy reveals (chapter 3.2.3.2), only triphenylphosphine oxide TPPO, *E*/*Z*-stilbene and benzaldehyde are present in the organic phase after quenching, extraction and phase separation.
Since *Z*-stilbene is not obtained selectively in the first step, a subsequent isomerization step is necessary.

UV-light could be used for proper excitation of the conjugated π-system of *E*-stilbene. A π-electron is excited into the π*-orbital and a diradical **35c** is formed. Isomerization continues via bond twisting to form *Z*-stilbene. Due to the application of light with a short wavelength, side-reactions or reverse isomerization can occur.[23,207]

A mild alternative is given by transition metal complexes, like $[Ru(bpy)_3]Cl_2$ **36** or $[Ir(ppy)_2(bpy)]PF_6$.[208] Different studies suggest a triplet-triplet energy transfer from the photosensitizer to *E*-stilbene.[62,209] Due to a small energy difference between the triplet states of *E*-stilbene (2.2 eV) and *Z*-stilbene (2.5 eV), the *E*-isomer is addressed only.[210] The appearing excited triplet state of **35a** finally initiates formation of the kinetic product (Scheme 25).

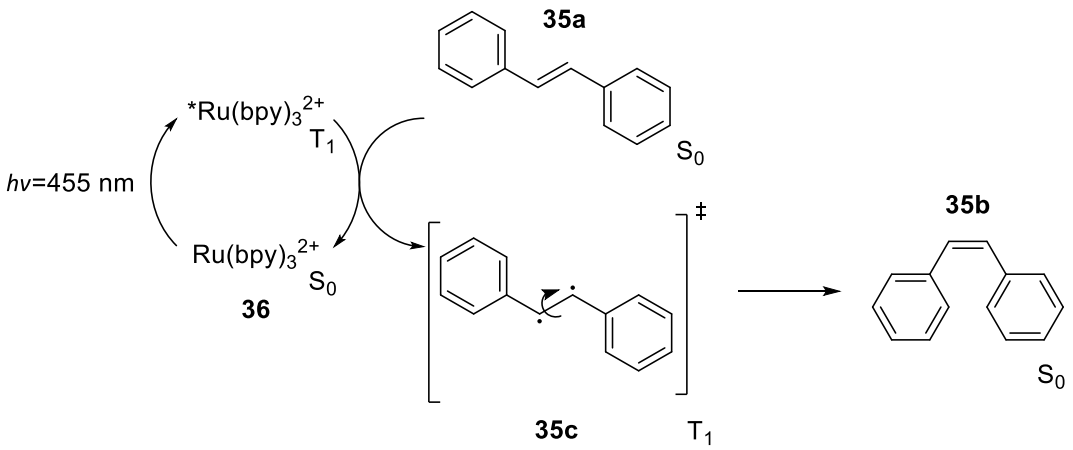

Scheme 25: *E-Z*-photoisomerization of stilbene using a photosensitizer to overcome the energy barrier.

Ronge *et al*. carry out photoisomerization of *E*-stilbene with the above-mentioned photosensitizers in acetonitrile. They achieve 78% conversion after 6 h in batch and 18 h are required for full conversion. Process intensification is realized with a continuous flow experiment and 92% *Z*-stilbene are obtained after ~30 min.[208]

A photoreactor (1/16" FEP capillary photoreactor V.0, 15 mL) will be used in the model reaction to conduct photoisomerization via $[Ru(bpy)_3]Cl_2$. Ten 455 nm LED-chips are equally placed in the center of the reactor to irradiate the capillary with a maximum power of ~11 W_{el}. A pulsed constant current power supply (2×350 mA) is used to dim and regulate the photon flux.

Since this photosensitizer is not soluble in toluene, reaction is performed in a mixture with methanol. The catalyst (2mol%) is added via a T-junction, which is directly connected to the outlet of first reaction step.

3.2.1.3 Lab plant design and construction

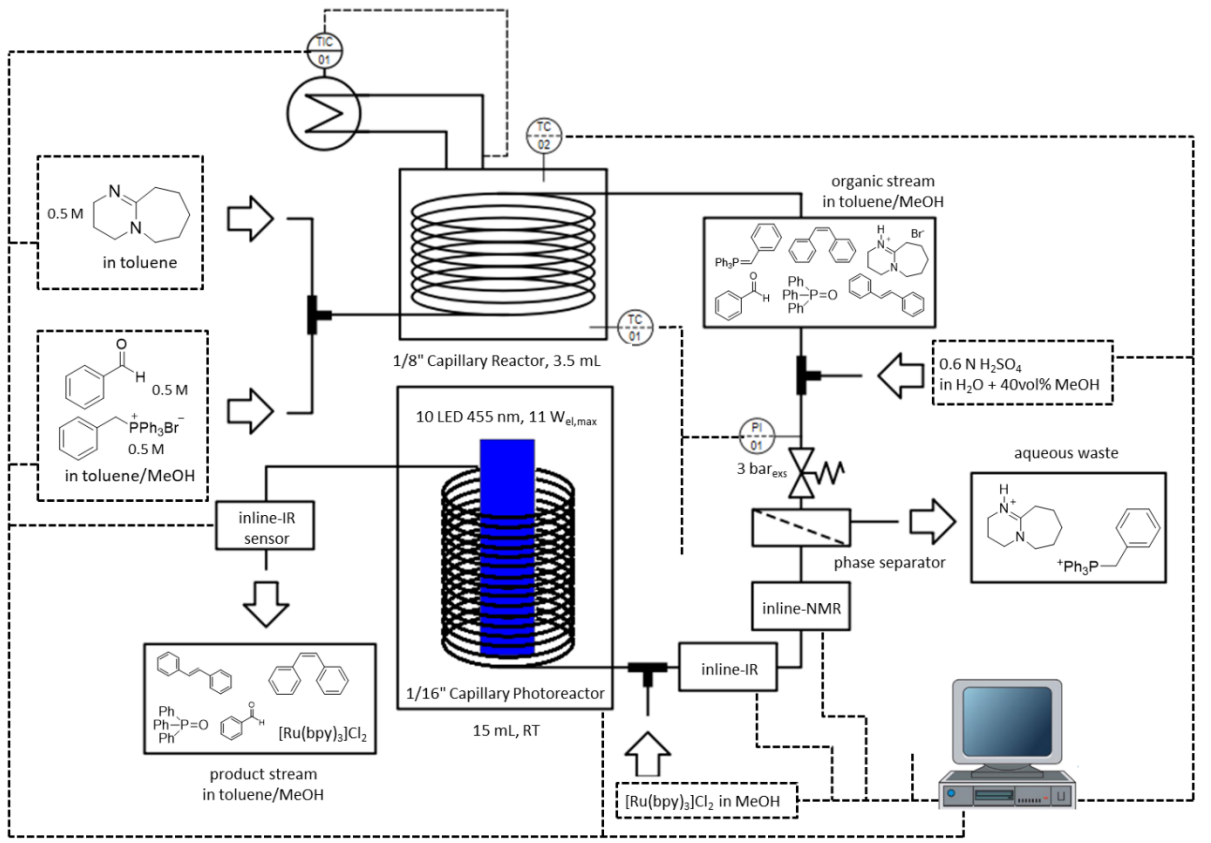

Figure 66: Lab plant design for the continuous two step synthesis of *Z*-stilbene including actuators as pumps, thermostat, photoreactor and sensors like thermocouples, pressure sensor and PAT tools; - - - connection between hardware and control unit (computer); not all connections are shown for better illustration; TIC-01=T_{ext}.

Based on the previously elaborated process conditions, the lab plant is designed (Figure ***66*** and Figure 67). Construction is assisted by CAD-software to fit all required hardware like containers, actuators, reactors, thermostats, spectrometers and sensors into a standard fume hood and to ensure accessibility to all components. All process parameters should be as variable as possible. Unfortunately, a high flexibility requires many actuators (pumps) and causes a complicated hardware and software setup.

Therefore, the two-step synthesis of *Z*-stilbene is minimalized to four material storage containers and four pumps. Two of them are used to provide Wittig component and base supply.

The aqueous quench-solution will be added via a third pump. Testing of a liquid-liquid phase separator shows best performance below an overall flow rate of 4 mL×min^{-1}, at identical flow rates of organic and aqueous media. This has to be considered when

dimensioning the thermal reactor (see Figure 297 in the appendix). After phase separation, inline NMR- and IR spectroscopy is conducted. A benchtop NMR-spectrometer (Nanalysis NMReady 60pro) with the ability to perform ^{1}H- or ^{31}P-experiments is equipped with a bottom-to-top PEEK flow cell (see Figure 229 in the appendix). An ATR-FTIR-spectrometer (Mettler Toledo ReactIR 15 equipped with flow cell probe and cell heating) is used for inline IR-analysis.

The photosensitizer is added via a fourth pump into the process stream and *E-Z*-photoisomerization is performed in the capillary photoreactor. Isomerization progress will be monitored with the nondispersive IR-sensor.

All hardware components and PAT spectrometers are monitored and controlled with via a software application (LabView 2018), which is elaborated and programmed especially for this purpose.

Figure 67: Complete lab plant including a reactors, online spectroscopy tools and control unit: *1* HPLC-pumps, *2* thermostat, *3* 1/8" thermal reactor, *4* 1/16" capillary photoreactor, *5* liquid-liquid separator-Zaiput Sep-10, *6* pressure sensor, *7* external thermocouple of thermostat T_{ext}, *8* back pressure regulator (spring loaded), *9* benchtop-NMR-spectrometer, *10* ATR-FTIR-spectrometer, *11* IR-sensor, *12* interphase, *13* control unit + software (computer).

3.2.2 Development of software and hardware components

All hardware components (pumps and spectrometers) are directly connected to the control unit. A hardware-interphase is designed to control and monitor all components (thermostat, pressure sensor, thermocouples, LED power source), which cannot be connected to the computer via Ethernet or USB. The thermostat receives a set-temperature from the control unit and an internal PID-controller (via external thermocouple Text; see Figure 67-*7*) will adjust the temperature of the reactor.

Process parameters and monitored data are defined (Table 16) preliminary to the software design. With those information, a structural plan for hardware and software communication is elaborated (Figure 68 to Figure 70), showing all necessities of the process. In addition, program flow charts for the (semi-)automated process are designed for characterization and realization of the software structure.

Table 16: Characterization and definition of set- and get-parameters for all used components.

hardware/software component	set parameter	get parameter	note	[unit]
cycle-number	i		cycle number of each experiment; start with i=1	a.u.
pump P-01	$\dot{V}_{P\text{-}01}$	$\dot{V}_{P\text{-}01}$	flow rate of P-01	µL×min^{-1}
		$p_{P\text{-}01}$	to monitor pump-faults P-01	bar
pump P-02	$\dot{V}_{P\text{-}02}$	$\dot{V}_{P\text{-}02}$	flow rate of P-02	µL×min^{-1}
		$p_{P\text{-}02}$	to monitor pump-faults P-02	bar
pump P-03	$\dot{V}_{P\text{-}03}$	$\dot{V}_{P\text{-}03}$	flow rate of P-03	µL×min^{-1}
		$p_{P\text{-}03}$	to monitor pump-faults P-03	bar
pump P-04	$\dot{V}_{P\text{-}04}$	$\dot{V}_{P\text{-}04}$	flow rate of P-04	µL×min^{-1}
		$p_{P\text{-}04}$	to monitor pump-faults P-04	bar
thermostat	T_{set}	T_{set}	reactor temperature	°C
		T_{int}	internal thermocouple of thermostat	°C
		T_{ext}	external thermocouple of thermostat	°C
thermocouples		T_{TC1}	TC1 for heating circuit inlet	°C
		T_{TC2}	TC1 for heating circuit outlet	°C
		T_{TC3}	TC3 for ambient temperature	°C
pressure		P_{01}	pressure in thermal reactor	bar
LED- power source	P_{LED}	P_{LED}	LED-power for the capillary photoreactor	%

hardware/software component	set parameter	get parameter	note	[unit]
NMR-spectrometer (Nanalysis NMReady 60pro)	connection status	connection status		
	experiment type		^{1}H or ^{31}P	
	number of scans			a.u.
	solvent		non-/deuterated solvents	
	spectral center			ppm
	spectral Width			ppm
	start experiment			
	save data	save data	as .dx &. jdx	
	monitor data	monitor data	in frequency domain	
IR-spectrometer	connection status	connection status		
	start experiment			
	stop experiment			
	trend BA	trend BA	get trend, while NMR Experiment is running	$mM \times L^{-1}$
	trend TPPO	trend TPPO	get trend, while NMR Experiment is running	$mM \times L^{-1}$
	trend(IR) *E*-stilbene	trend(IR) *E*-stilbene	get trend, while NMR Experiment is running	$mM \times L^{-1}$
	trend(IR) *Z*-stilbene	trend(IR) *Z*-stilbene	get trend, while NMR Experiment is running	$mM \times L^{-1}$
	save data	save data	as .txt	
IR-Sensor	connection status	connection status		
	start experiment			
	stop experiment			
	trend(IR-sensor) *E*-stilbene	trend(IR-sensor) *E*-stilbene	get trend any time	a.u.
	trend(IR-sensor) *Z*-stilbene	trend(IR-sensor) *Z*-stilbene	get trend any time	a.u.
	save data	save data	as .txt	

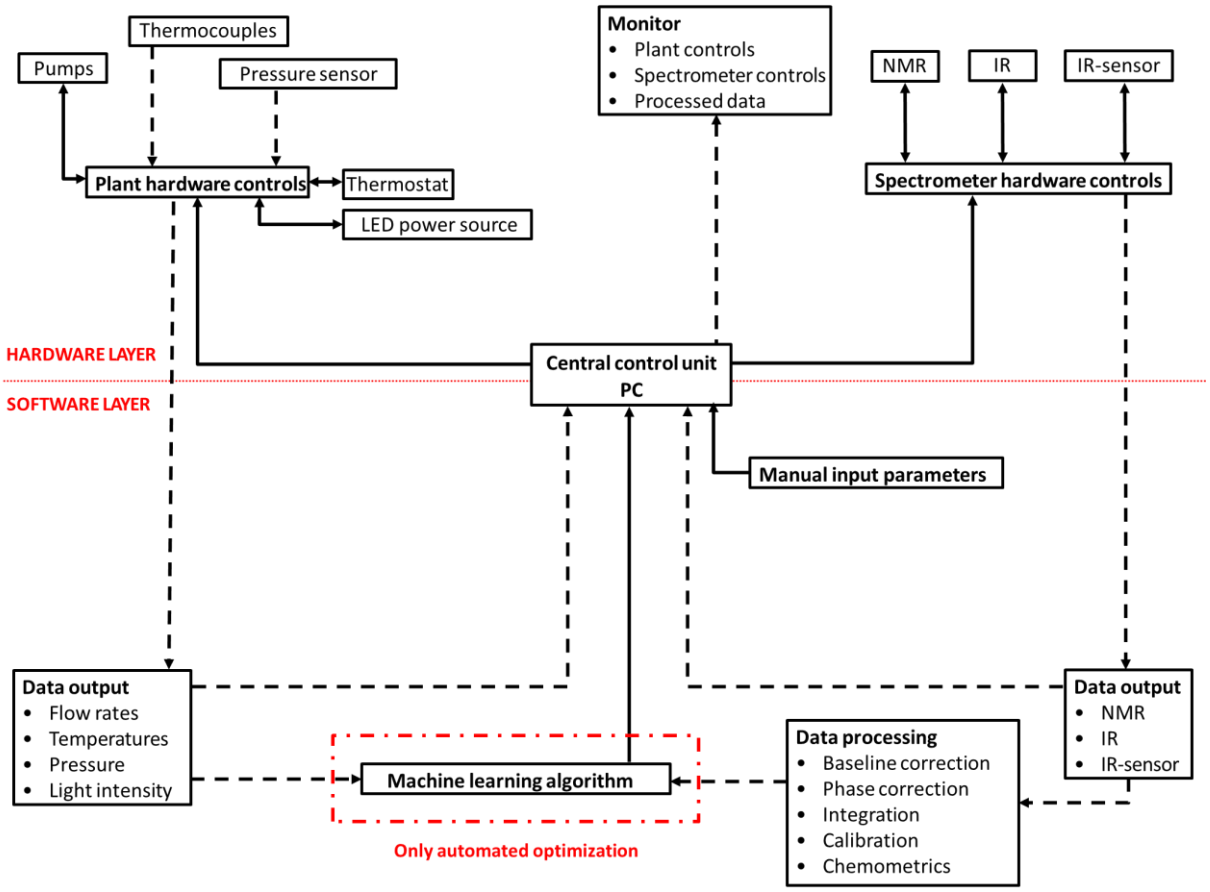

Figure 68: Structural plan for software design. The central control unit is responsible to manage all commands and settings on the hardware and software layer: — send command and parameters; - - - - send response and data; ↔ send and respond.

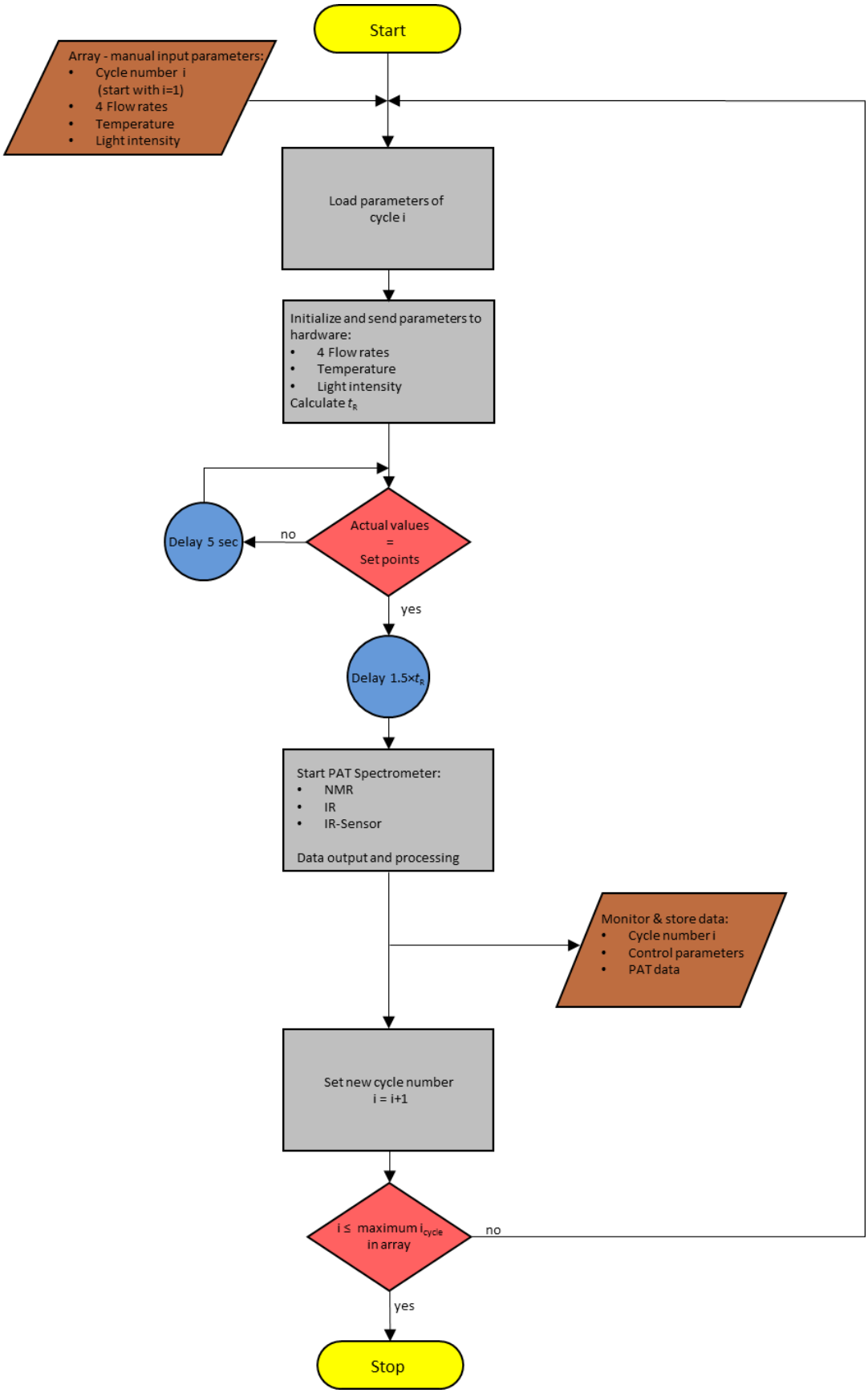

Figure 69: Flow chart for a semi-automated software program controlling a continuous synthesis setup (including online PAT).

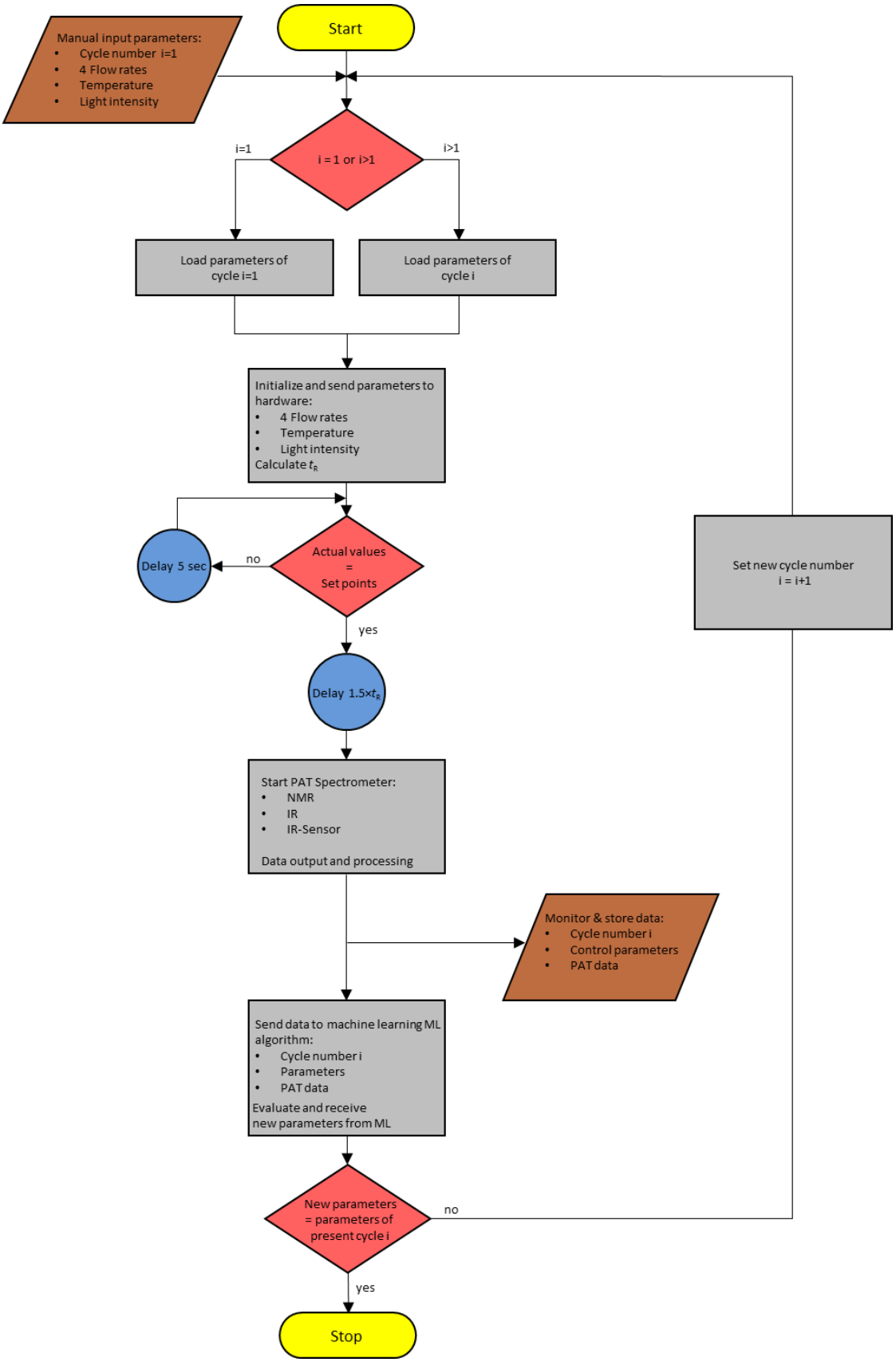

Figure 70: Flow chart for an automated, self-learning software program controlling a continuous synthesis setup (including online PAT).

During the software initialization process, connection to the PAT spectrometers is tested. The user is allowed to define parameters for the intended NMR-experiments (^{1}H or ^{31}P, number of scans, solvent, spectral width and spectral center). All other spectrometers are limited in parameter variation and settings have to be adjusted via their own software.

After initialization has finished, the user is able to predefine lab plant controls like flowrates, thermostat temperature and LED Power of the photoreactor into an array. Confirmation of these parameters will start the semi-automated process chart. First of all, IR-spectrometer and IR-sensor are triggered and their trends are recorded and monitored all time. Control parameters are send to all actuators. The hardware will adjust itself (*wait for set point*) until actual values confirm to set points. After that, software sends a delay of $1.5 \times t_R$ (*wait for dead time*) to reach a steady state in the continuous flow plant. t_R is calculated by the given flow rates and the overall internal volume including all components (reactors, capillaries, junctions/mixers, liquid-liquid separator, spectrometer flow cells). After reaching the end of delay, flow system has equilibrated, and process conditions are equal in the reactor and all PAT tools. NMR-Spectrometer will run an experiment as preliminary adjusted and save the spectrum in .dx and .jdx data type. Latest NMR-spectrum is visualized in the software. IR- and IR-sensor trends are collected and saved simultaneously. Data processing and calibration is implemented into the control unit and concentrations of the substances (in $mM \times L^{-1}$) are finally displayed with help of a calibration curve. Data processing includes phase- and baseline correction as well as peak integration. The same procedure is used for both other spectrometers.

A next row of parameters is loaded from the array and a new cycle is started. In the semi-automated process, the program will be executed unless no further entries are provided in the array anymore.

This program and laboratory setup is prepared for automated processing and integration of a machine learning ML algorithm. At least one set of parameters has to be provided by manual input via the array to start the self-learning optimization process.

The following paragraphs describe the different tabs of the software user interface.

KI Run:

This is the main screen (Figure 72) of the user interface. The user can monitor all hardware controls and set parameters (flowrates, temperature, LED power) in real time. The system displays the current state of a cycle (wait for set points, wait for dead time, measuring, send data to ML, read data from ML, set parameter for next cycle) and a time indicates remaining time until reaching the next step.

The (semi-)automated program sequence is activated via the start-button. A dialog window opens (Figure 71) after successful initialization of the hardware and hardware parameters can be set into the array by manual input. The system is put into safe conditions and switched off when pressing the stop button. All relevant physical process parameters are automatically saved in a file (IMM-data.txt) every 5 seconds.

Additional indicators show if all data will be sent to or received from Machine learning algorithm successfully.

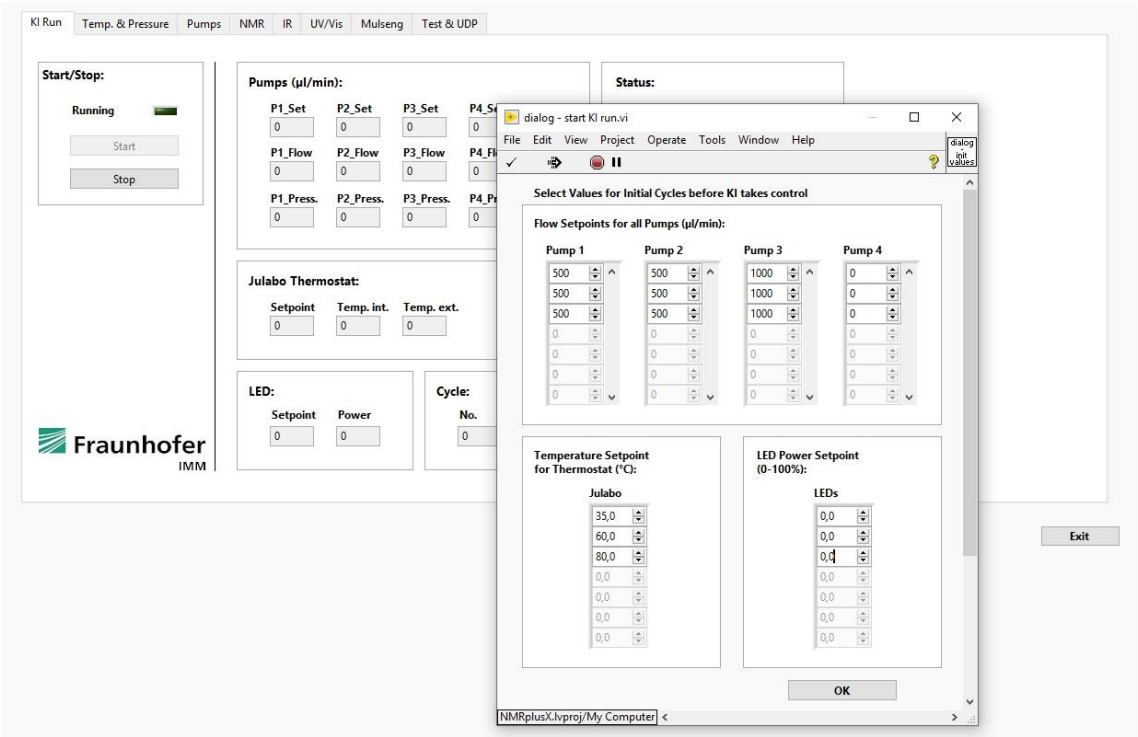

Figure 71: Dialog window after software initialization. Hardware parameters for different experiments are put in manually into the array.

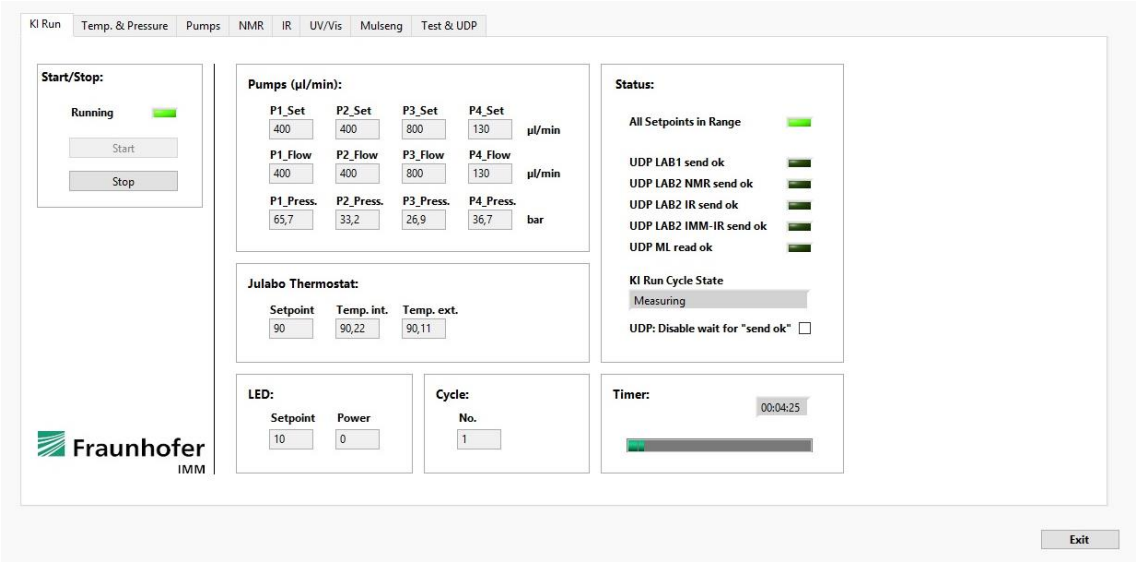

Figure 72: Tab "KI Run" as main graphical interface of the control software.

Temperature & Pressure:

All thermocouples of the lab plant are monitored in this tab (Figure 73). This includes the two sensors of the Julabo thermostat T_{int} and T_{ext}. The internal sensor measures the temperature of the reservoir, while the external sensor is used for adjustment and control. Two additional thermocouples (TC1 and TC2) are placed in the heat exchanger inlet and outlet of the thermal reactor. A third sensor (TC3) recorded ambient temperature in the fume hood/laboratory, while the pressure sensor is used to measure the overpressure in the capillary.

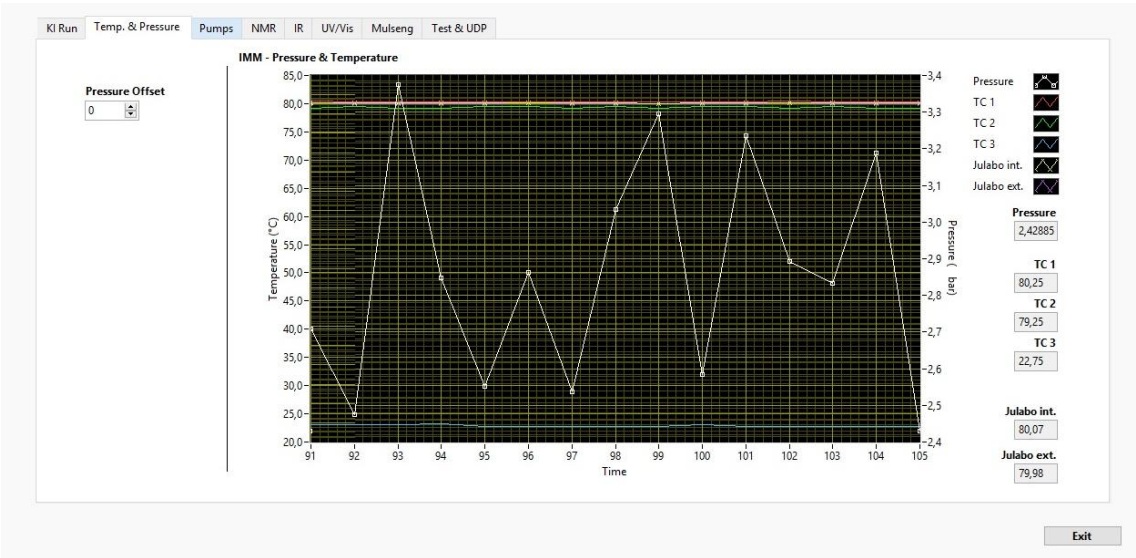

Figure 73: Tab "Temperature & Pressure" to monitor physical data of the thermocouples and pressure senor.

Pumps:

With this tab (Figure 74), the flow rates and backpressure of each HPLC-pumps is displayed. Large pressure fluctuation would indicate a fault and insufficient performance of the plant. New manual controls (start, stop, flowrate) can be initialized here for all pumps at any time.

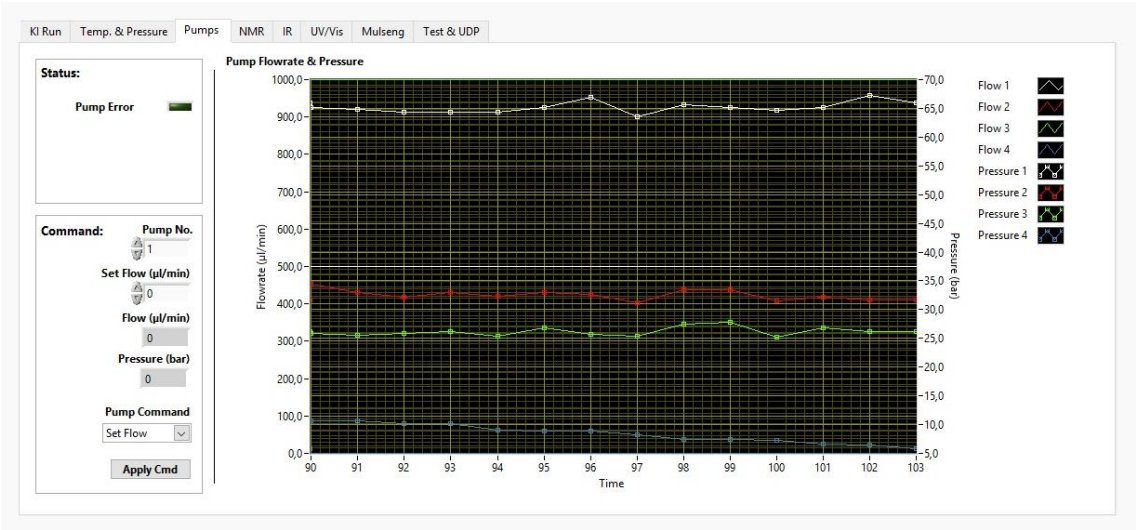

Figure 74: Tab "Pumps" for monitoring and control of all four HPLC-pumps. Flowrates as well as their individual back pressures are recorded.

NMR:

The latest NMR-spectrum is displayed here (Figure 75). In addition to the automated NMR-experiments, triggered by the software, a new experiment can be started manually at any time. ^{1}H or ^{31}P experiments can be selected.

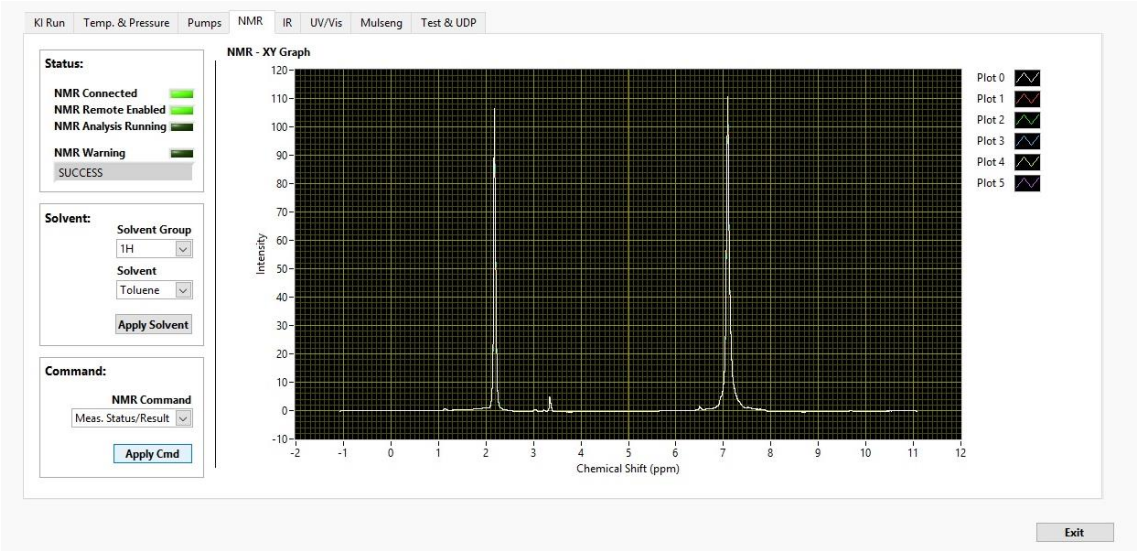

Figure 75: Tab "NMR" to control and select all necessary parameters of an NMR-experiment. The last spectrum is visualized.

IR:

Mettler Toledo ReactIR 15 requires its own *iC IR*-software, which has to run permanently while using the spectrometer. All data setting and processing is done in this software. Data trends of the different chemical compounds are recorded constantly. These trends are loaded via a client server into the *LabView* program and latest values are displayed here, while the NMR experiment is running (Figure 76).

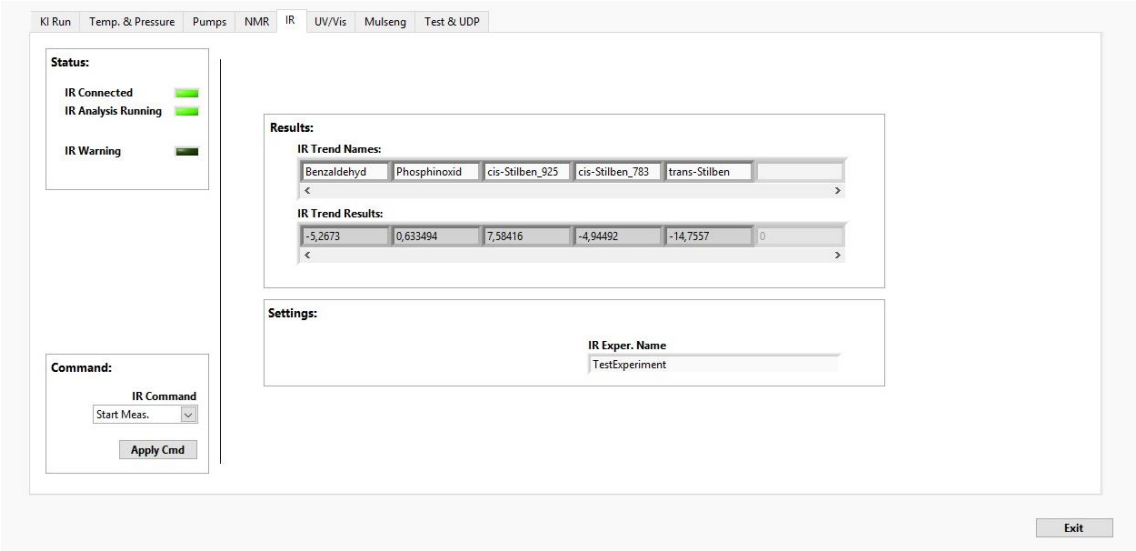

Figure 76: Tab "IR" to monitor the saved trend data of each experiment.

Mulseng:

The IR-sensor (nickname: Mulseng) can be manually controlled via this tab (Figure 77). Since measurement is triggered with the initial program start, the 10 latest data points are visualized here. This includes raw data of the sensor (transmission) as well as the processed data (via calibration). All data is achieved in the file "IMM-data.txt"

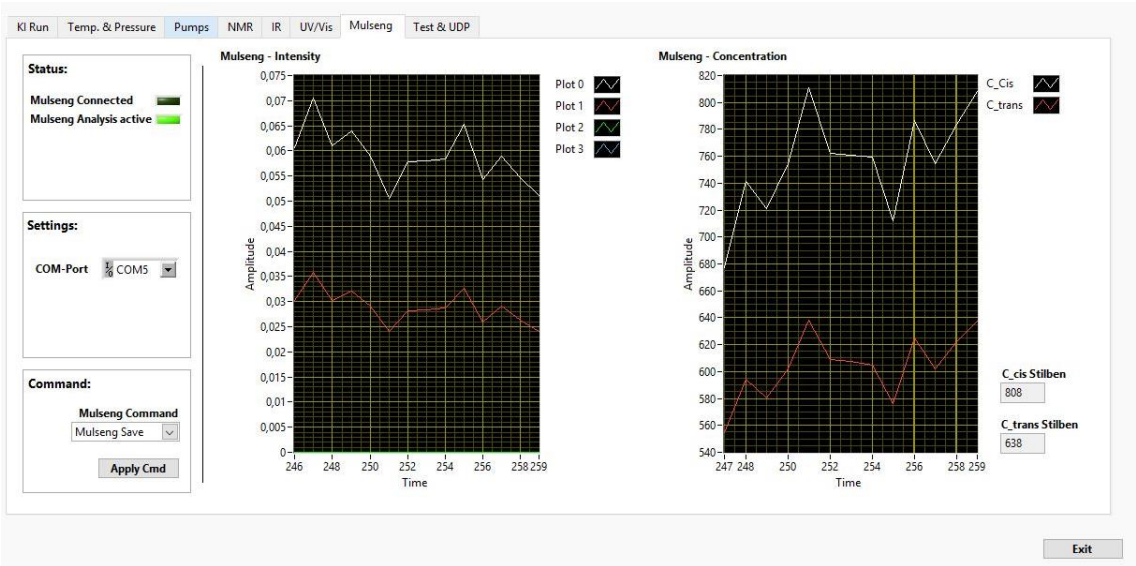

Figure 77: Tab "Mulseng" to monitor IR-sensor raw data as well as concentrations of *E*- and *Z*-stilbene after calibration.

Test & UDP:

Automated process control has to be used, if machine learning ML is applied. Connectivity and embedment into *LabView* software is realized by the User Datagram Protocol (UDP). Different messages containing text information and data-files can be send to or received from ML.

A text message (NMRplusX-LAB1) is sent every ~30 seconds to ML including following information: Cycle-number, current cycle state, temperatures (set point and actual values), ambient temperature, all flow rates of four pumps (set points and actual values), pump pressures, pressure inside the reactor, LED power. The data message type represents files with (processed) data of the NMR-, IR-spectrometer and the IR-sensor. This offers easy data distribution as small data packages are send. UDP is not configured to send NMR raw data, because data exceeds maximum size.[211]

If plant operation requires manual changes in thermostat temperature or light intensity, they can be set in this tab (Figure 78).

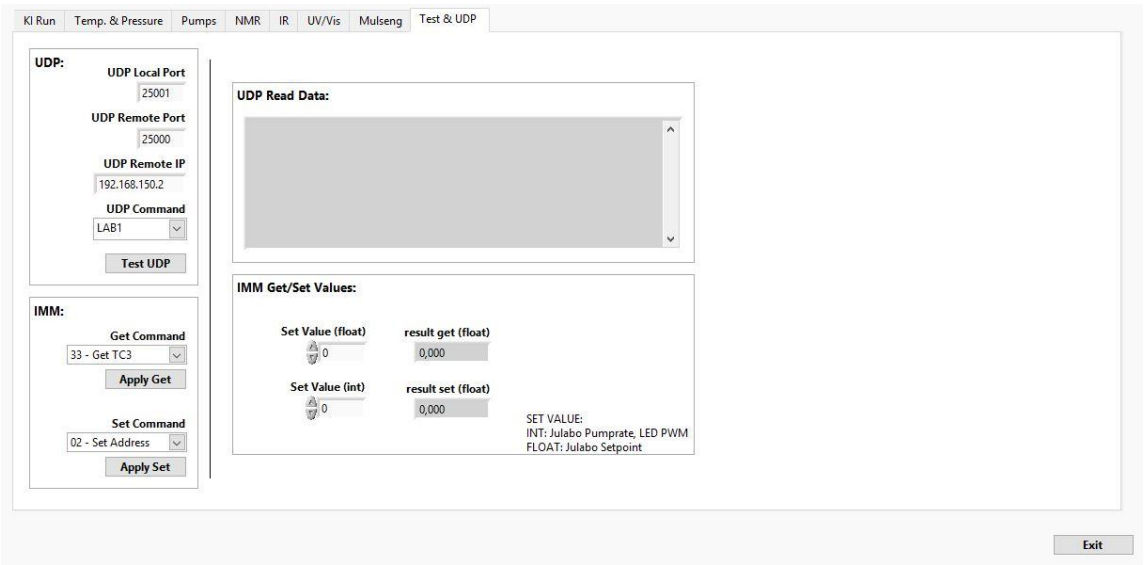

Figure 78: Tab "Test&UDP" to monitor and check UDP connection and set thermostat temperature or light intensity manually.

3.2.3 Implementation of calibration and chemometrics into the software

In preparation for calibration of the NMR-, IR-spectrometer, IR-sensor and UV/Vis-spectrometer, all relevant chemicals used in the Wittig reaction and photoisomerization are examined and the characteristic signals are determined. During the reaction, changes of signal intensity take place and conversion/selectivity can be monitored (Table 17). NMR signals are given as chemical shift δ [ppm] and in FTIR-spectroscopy characteristic bands are given in wavenumbers $1/\lambda$ [cm^{-1}], whereas UV/Vis bands are referenced to a wavelength [nm]. Characteristic signals stand out in the mentioned spectroscopic measurements, if they don´t show any overlap to signals of other chemical compounds. BTTP and triphenylphosphine oxide show identical characteristic IR-signals, leading to insufficient determination. Here, the beneficial effect of extraction and liquid-liquid phase separation can be used to overcome this issue.

Table 17: Characteristic chemical shifts and bands of used components in Wittig reaction and photoisomerization.

name - chemical structure	characteristic IR-bands [cm^{-1}]	characteristic ^{1}H-NMR signals (60 MHz, PEEK flow cell, stopped flow), δ [ppm]; reference toluene 2.18 ppm:	characteristic ^{31}P-NMR PEEK flow cell, stopped flow), δ [ppm]:	characteristic UV-bands [nm]	signal trend during reaction
benzaldehyde	1705.7	9.66 (singlet)	/	280-316	decreasing
BTTP 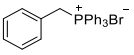	1029.7	5.04 doublet (J=15 Hz)	26.10 (singlet)	276-296	decreasing
ylide-ylene intermediate 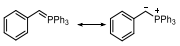	/	/	29.12(singlet)	/	decreasing
E-stilbene 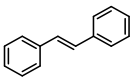	962.0 or 760.7	not detectable, due to overlap with aromatic signals	/	300-360	dynamic; unfavored product
Z-stilbene 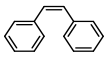	924.7 or 782.5	6.50 (singlet)	/	328-360	increasing; favored product

name - chemical structure	characteristic IR-bands [cm^{-1}]	characteristic ^{1}H-NMR signals (60 MHz, PEEK flow cell, stopped flow), δ [ppm]; reference toluene 2.18 ppm:	characteristic ^{31}P-NMR PEEK flow cell, stopped flow), δ [ppm]:	characteristic UV-bands [nm]	signal trend during reaction
TPPO 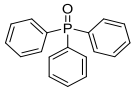	1029.7	/	27.53 (singlet)	280-296	increasing; by-product
Triphenyl phosphate 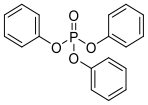	1022 or 963[212]	/	-14.42 (singlet)	/	internal standard for ^{31}P-NMR
tert-butylbenzene	/	1.25 (singlet)	/	/	internal standard for ^{1}H-NMR
TBD	/	3.74-3.32 (multiplet); 3.19-2.84 (multiplet); 2.84-2.51 (multiplet); 1.83-1.27 (multiplet)	/	/	not detected, due to extraction
DBU	/	3.57-3.26 (multiplet); 2.88-2.64 (multiplet); 1.75-1.20 (multiplet)	/	/	not detected, due to extraction
Photosensitizer $[Ru(bpy)_3]Cl_2 \cdot 6\ H_2O$	/	/	/	/	not detected, due to low concentration

Additional use of UV/Vis-spectroscopy preliminary to the phase separation is intended. High concentrations and the present substrate extinction coefficients lead to a complete absorption of light in commercial 1.5 and 10 mm inline flow cells. Even low concentrations (0.05 M, 20% of maximum concentration) lead to a complete saturation of the detector (absorbance >1, Figure 79). One could overcome this issue, when shortening the light pathway in the cell drastically. A reduction of the capillary dimensions would result in a higher back pressure in the plant and causing a

degradation of separation efficiency. A higher fraction of organic product phase in the aqueous phase is the consequence.

The large overlap of the characteristic bands results in large inaccuracy and UV/Vis-spectroscopy has to be neglected in the end.

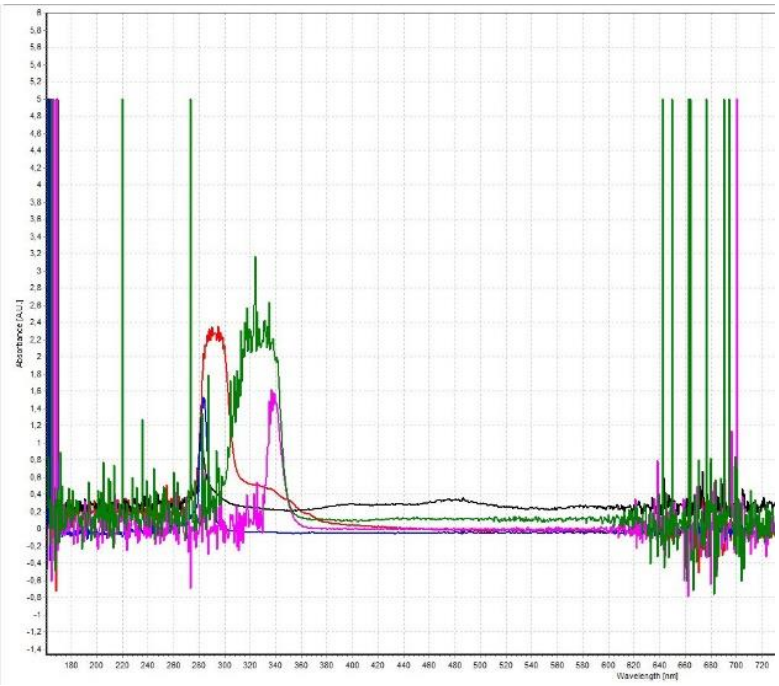

Figure 79: Overlap of characteristic bands in UV/Vis spectroscopy of the used chemical compounds (0.05 M in toluene/MeOH V/V=85/15); — benzaldehyde; — BTTP; — *E*-stilbene; — *Z*-stilbene; — TPPO; 1.5 mm flow cell; data processed with AvaSoft-basic.

3.2.3.1 Online NMR-spectroscopy

NMR-spectroscopy is conducted with a Nanalysis NMReady 60pro benchtop spectrometer. A bottom-to-top PEEK flow cell, presented in chapter 3.1, is mounted to run inline experiments.

External calibration, as well as calibration using an internal standard, are implemented in the control software. Both techniques come along with benefits and interferences, which are discussed in this chapter. In general, calibration referring to an internal standard can compensate peak intensity fluctuations better than essential external calibration. The latter relies and depends on spectrometer stability, especially when

long-term experiments are conducted. In this case, no interim shim can be performed while operating the plant, as dismantlement is required to insert the shim-standard.

In theory, ^{31}P-NMR spectroscopy is optimal for process monitoring of a Wittig reaction. Both, starting material BTTP and main by-product TPPO, contain a phosphorous nucleus and conversion can be measured directly. For this purpose, the NMR-spectrometer has to be located in front of the quench and extraction process in order to observe both species. Several experiments are conducted to test and verify quantitative online ^{31}P-NMR spectroscopy at 24.5 MHz, 80.62° pulse, 1.6 s acquisition time, 6.6 s repetition time, proton decoupling and 50 dB receiver gain. An experiment lasts ~3.5 minutes with 32 scans, which roughly equals the aspired reaction time. Different concentrations of BTTP and TPPO at different flow rates are pumped through the PEEK flow cell.

For example, 0.1 M BTTP in toluene/methanol (V/V=85/15) has only a SNR of 14 (see Figure 298 in the appendix) at 0 mL×min^{-1}. Unfortunately, a more serious issue is observed at high flow rates, where signal intensity is reduced. Increasing the flow rate from 0 to 1.5 mL×min^{-1} leads to an intensity loss of 20-25% (Figure 80). Main reasons are a reduced ^{31}P-nuclei sensitivity[213] accompanied by the intrinsic "inflow and outflow effect" of the flow cell.[117,121]

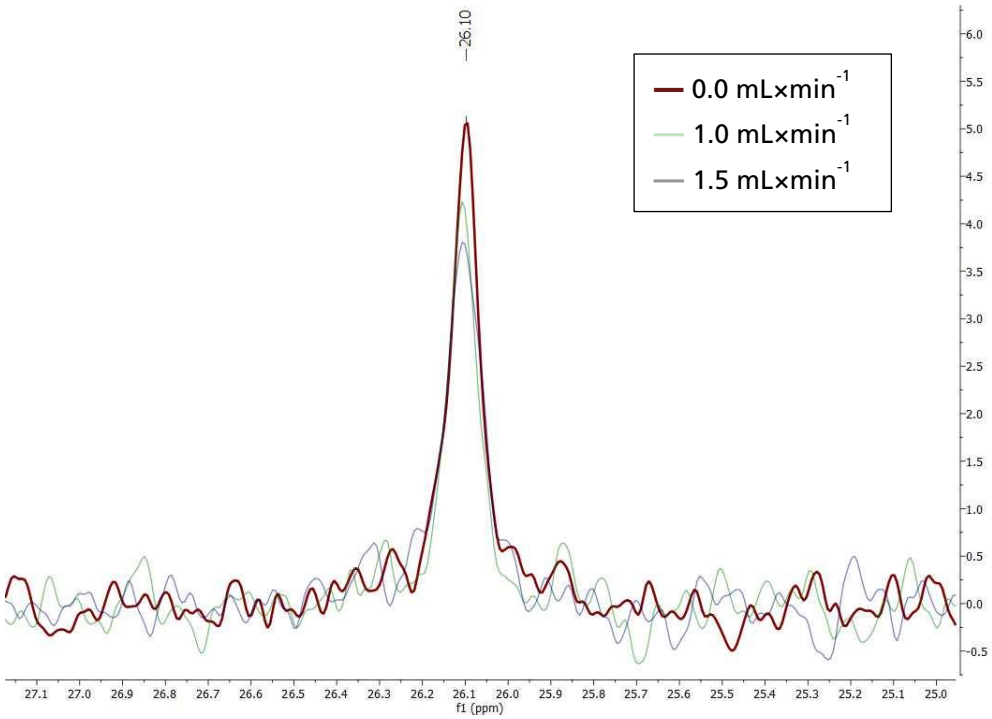

Figure 80: ^{31}P NMR-spectra (24.5 MHz, PEEK flow cell) of 0.1 M BTTP in toluene at different flowrates: — stopped flow, — 1.0 mL×min^{-1}, — 1.5 mL ×min^{-1}.

Since signal-to-noise ratio is proportional to the square root of scans, total acquisition time has to be increased dramatically.[214] This is in no relation to its possible benefit. Moreover, an "unrealistic" calibration depending on different flow rates is required.

Flow rate dependency can only be compensated by using an internal standard (e.g. triphenyl phosphate), but a high concentration (>0.1 M) of the internal standard is required to give satisfactory SNR. Unfortunately, this comes along with a significant impact on the solvent matrix. Moreover, triphenyl phosphate has overlapping IR-Bands with at TPPO and *Z*-stilbene. In order to keep the system as simple as possible, no internal ^{31}P-NMR standard is used and further testing is focused on ^{1}H-NMR spectroscopy.

With inline 1H-NMR spectroscopy, only benzaldehyde and *Z*-stilbene can be evaluated, due to several overlapping chemical shifts. It is accepted that *E*-stilbene and TTPO cannot be detected, since their characteristic bands appear at nearly the same chemical shift as the aromatic protons of toluene. The following settings are applied for ^{1}H-NMR spectroscopy: 60 MHz, 80.62° pulse, 2.7 s acquisition time, 2.9 s repetition time, gated decoupling and 14 dB receiver gain. One experiment lasts only ~47 seconds (16 scans), whereupon additional scans have no significant beneficial effect on the SNR.

The influence of different flow rates on the signal intensity is examined first. Hereby, signal fluctuation between changing flow rates (0 and 1.5 mL×min^{-1}) is smaller than variance at the same flow rate. The fourth diluted mixture (0.04 M *Z*- stilbene and 0.05 M benzaldehyde, Figure 81), used for external calibration, is pointed out exemplary. A SNR of 24 and 9% variance are achieved for benzaldehyde, whereas *Z*-stilbene results in a SNR of 45 and 11% variance (three measurements at 0 mL×min^{-1} and 1.5 mL×min^{-1}, respectively). These results are assigned to be sufficiently accurate as they improve for higher concentrations.

A direct quantification of concentrations via the proton equivalents of a standard (e.g. solvent signal or additional internal standard) is not possible in the considered cases. No internal standard was added in order to keep the number of components in the mixture as low as possible, leading to the determination of a response factor for each substance.

External calibration (Figure 82) is conducted with five different concentrations (solvent: toluene), where every sample is measured three times at 0 and 1.5 mL×min^{-1}. Mean areas of those measurements give linear fits for benzaldehyde and *Z*-stilbene (see Figure 84 and Figure 85). As no physicochemical interactions with the solvent are expected, chemical shift and signal intensity of the substances should be independent from the solvent matrix.

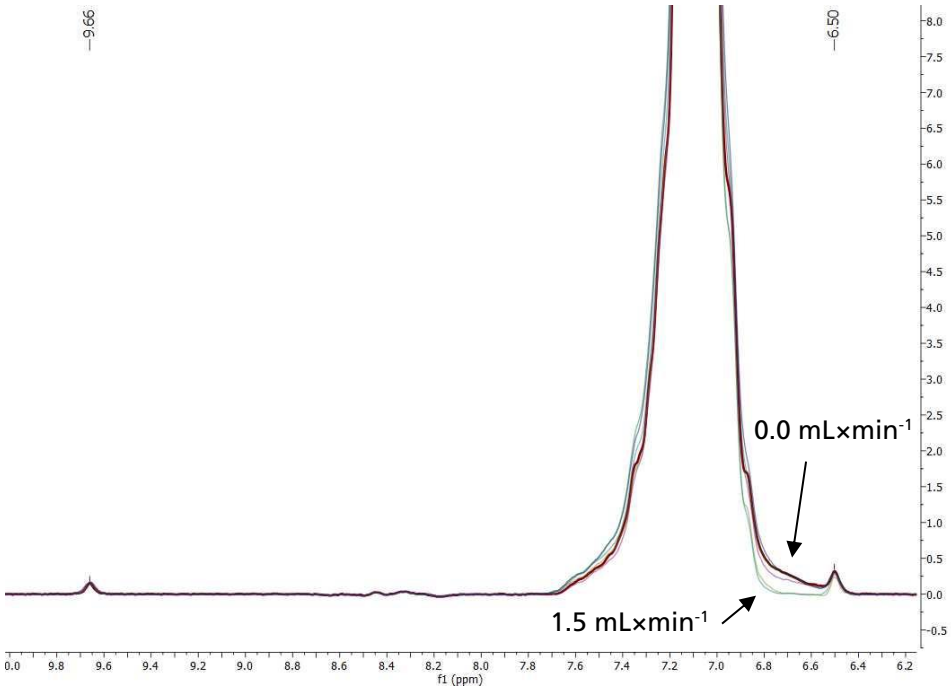

Figure 81: ^{1}H NMR-spectra (60 MHz, PEEK flow cell) of 0.04 M *Z*-stilbene (SNR 45, variance 10.7%) and 0.05 M benzaldehyde (SNR 24; variance 9%) in toluene at different flowrates: 0.0 and 1.5 mL×min^{-1}.

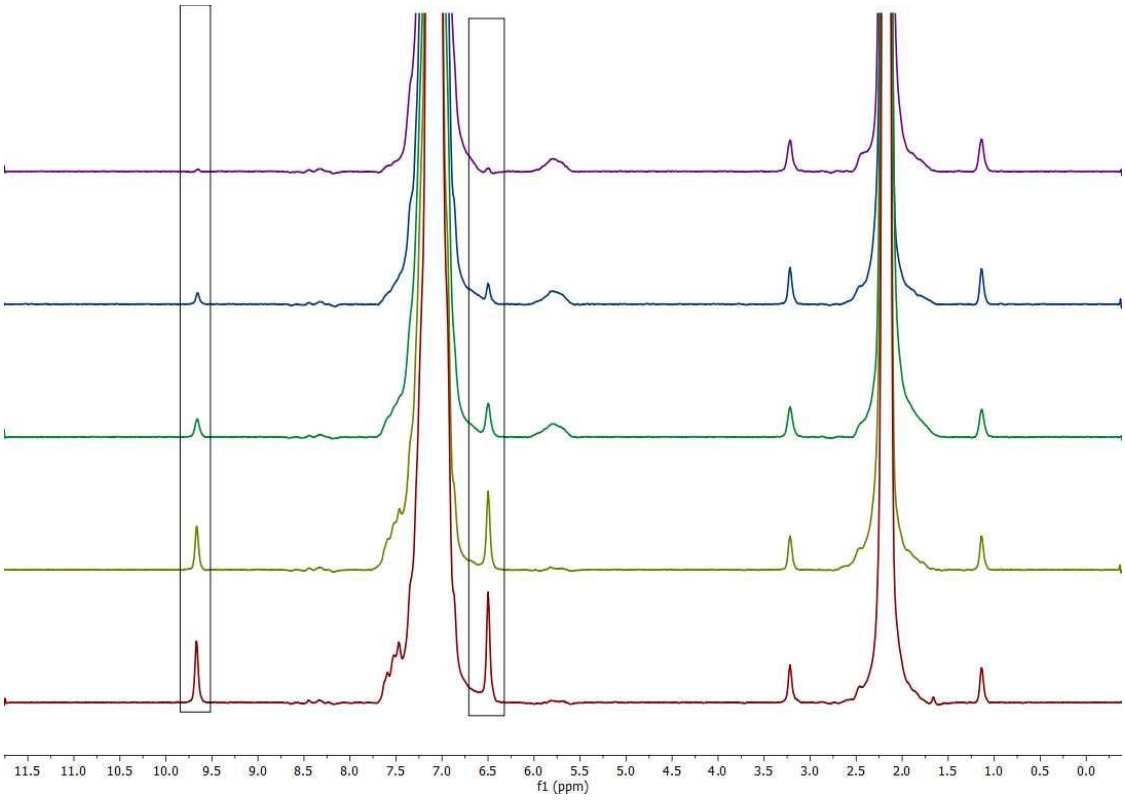

Figure 82: Exemplary ^{1}H NMR-spectra (60 MHz, PEEK flow cell) of *Z*-stilbene and benzaldehyde in toluene in five different concentrations used for spectrometer calibration; highest concentration ~250 mM (bottom), lowest concentration ~ 20 mM (top).

A Python script (programmed by NAN) is used for automated data processing during calibration and experiment. This script is embedded into control software and can be executed automatically via LabView (via a command, Figure 83). Concentrations are monitored and archived.

```
python -m twoplustwo -i "./NMRplusX_1D_1H_20211122_Mischung 4 16s PEEK1500.dx" -m integral -r 6.42 6.57 9.6 9.75 -o "./NMRplusX_1D_1H_20211122_Mischung 4 16s PEEK1500_integral.txt"
```

Figure 83: Exemplary command to trigger the Python script for NMR-spectrum processing and integral evaluation with the corresponding sectors for integration of the NMR-peaks.

Data processing procedure of the script is proceeded as followed: An NMR-spectrum (time domain) is loaded as .dx-file. In the "phase" mode, the spectrum is converted into the common frequency domain using Fourier transformation. This is followed by a phase- and baseline correction (Whittaker smoothing) and a processed spectrum is saved as .txt-file. In the "integral" mode, only integration of the Fourier-transformed data is performed according to the selected regions. In the "full" mode, both steps are combined, but giving integral values of the predefined regions only.

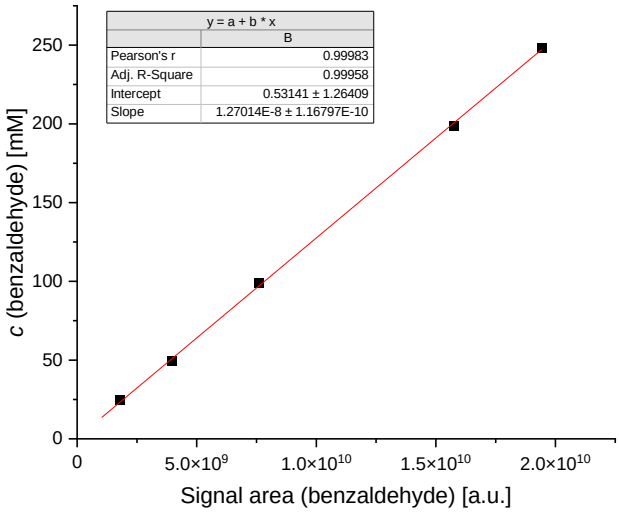

Figure 84: Fit parameters for an external calibration of benzaldehyde; acquired in a benchtop ^{1}H-NMR spectrometer (60 MHz, PEEK flow cell) with data evaluation via a Python script.

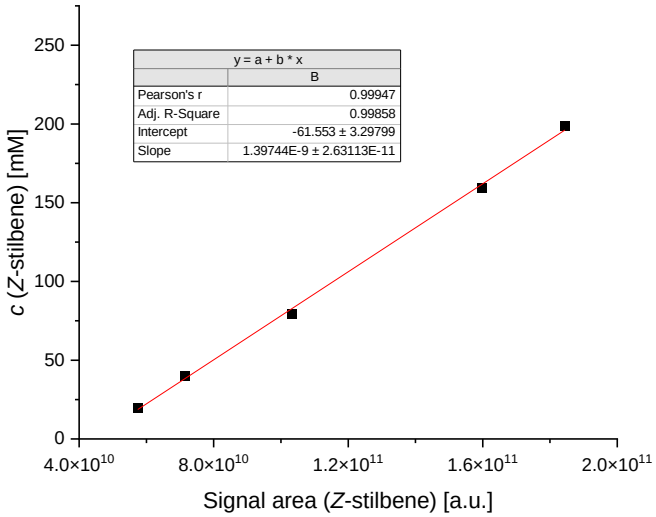

Figure 85: Fit parameters for an external calibration of *Z*-stilbene; acquired in a benchtop ^{1}H-NMR spectrometer (60 MHz, PEEK flow cell) with data evaluation via a Python script.

Subsequently, the calibration curves of benzaldehyde and *Z*-stilbene are verified (see Figure 86). Three samples (in toluene) containing randomly mixed samples are used for this purpose, which show an insufficient deviation to the gravimetric concentrations. Unfortunately, this deviation is caused by a miscalculation in the Python script (this aspect is not elaborated in detail).

Cross-checking of NMR raw-data with PEAXACT 5.3 gives satisfactory results (see Figure 299 and Figure 300 in the appendix, calibration via integration of signal areas). Generally, a 60 MHz benchtop ^{1}H-NMR spectrometer equipped with a flow cell, is an appropriate tool for Wittig reaction analysis, when carried out via the PEXACT chemometrics (Figure 86). This procedure is used in chapter 3.2.4 as well.

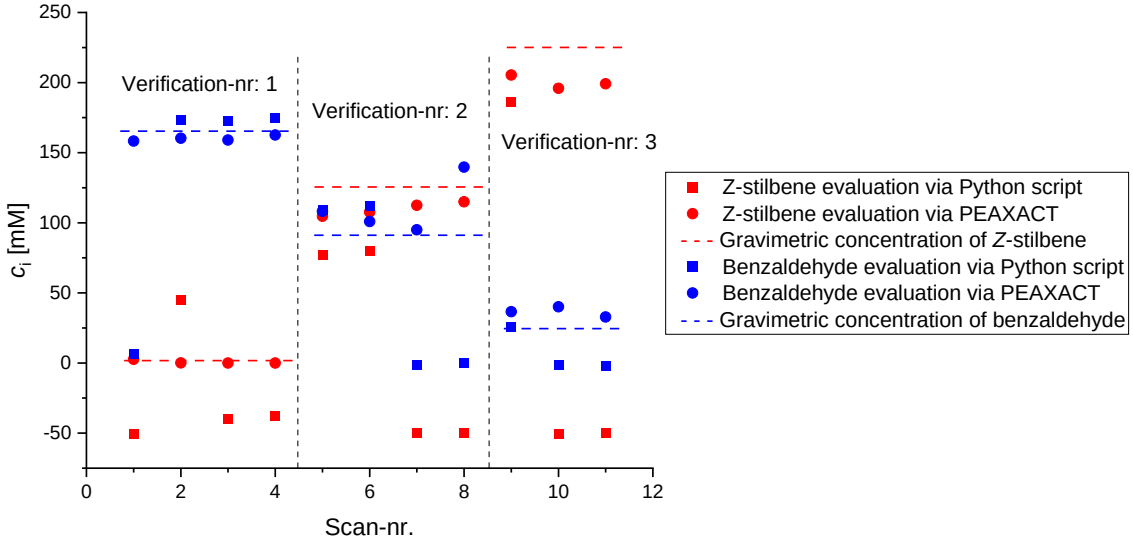

Figure 86: Validation of a ^{1}H benchtop NMR-spectrometer (60 MHz, PEEK flow cell) for benzaldehyde and *Z*-stilbene analysis; samples measured at stopped flow; ● benzaldehyde evaluation via PEAXACT; ■ benzaldehyde evaluation via Python script; - - - - gravimetric concentration of benzaldehyde; ● *Z*-stilbene evaluation via PEAXACT; ■ *Z*-stilbene evaluation via Python script; - - - - gravimetric concentration of *Z*-stilbene;.

3.2.3.2 Online ATR-FTIR-spectroscopy

A Mettler Toledo ReactIR 15 ATR-FTIR-spectrometer with a 50 µL bottom-to-top flow cell, heated to 30 °C, is used. Since online IR-process monitoring of the Wittig reaction will be done after liquid-liquid phase separation, several tests are conducted to elaborate the spectrometer performance at this position in the plant setup. Calibration and validation are conducted with ideal solutions, which represent the real process solution as best as possible. Therefore, all conditions have to be defined while initializing the spectrometer.

First, investigations are focused on the solvent spectrum of the Wittig reaction, especially in the regions where characteristic signals appear. Different spectra of toluene/methanol mixtures are recorded (Figure 87), whereby even small changes in the range of a few percent can be detected.

An aqueous quench (containing methanol) and phase extraction will be applied at the toluene/methanol solvent in the continuous Wittig reaction. Therefore, different inorganic acids, as hydrochloric acid and sulfuric acid, are tested. Both acids show similar extraction behavior, as IR-spectra show (Figure 88). Interestingly, identical spectra of an organic phase appear over and over, even if aqueous quench solutions are applied on

the organic matrix, while both phases contain changing amounts of methanol. Tests show that organic phase contains ~98% toluene and ~2% methanol after extraction every time.

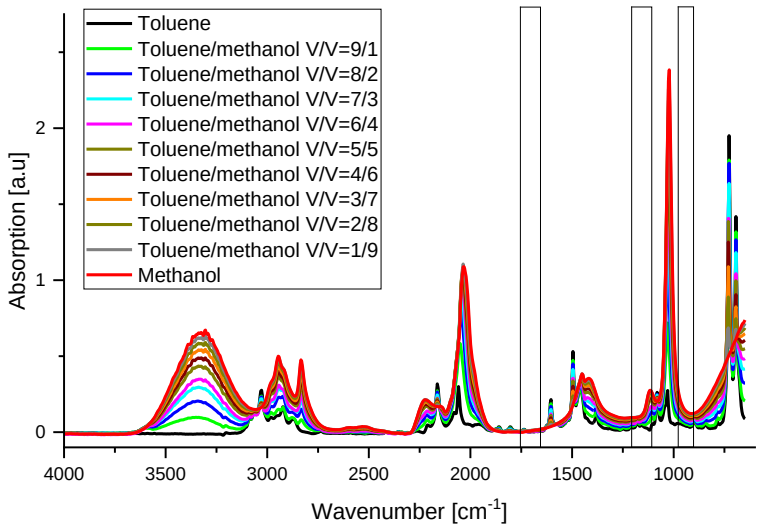

Figure 87: IR-Spectra of different mixtures of toluene and methanol. Spectra of neat chemicals as well as mixtures changing in 10%-steps are visualized: — neat toluene; — neat methanol; ▭ areas of high interest, as characteristic bands appear here.

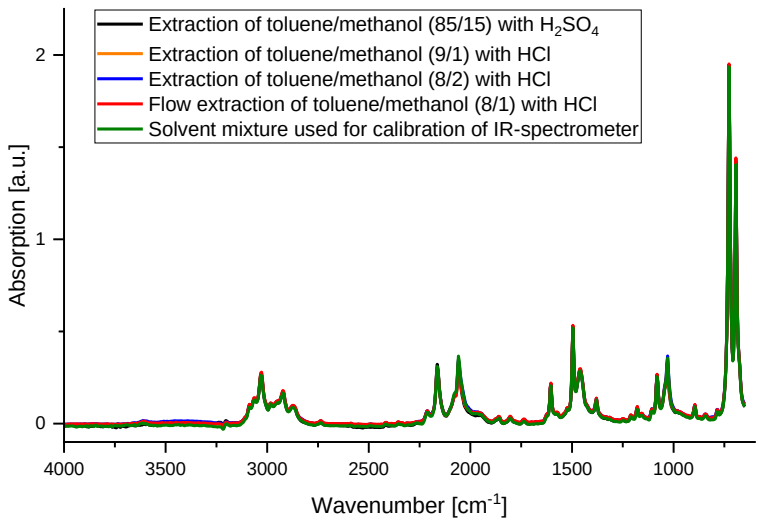

Figure 88: IR-spectra of organic media after different extraction tests; — extraction of toluene/methanol (V/V=9/1) with 1 N aqueous hydrochloric acid (diluted with 50vol% methanol), — extraction of toluene/methanol (V/V=8/2) with 1 N aqueous hydrochloric acid (diluted with 50vol% methanol), — continuous flow extraction (Zaiput Sep-10 and OB-900 membrane) of toluene/methanol (V/V=8/1) with 1 N aqueous hydrochloric acid (diluted with 50vol% methanol), — solvent mixture used for calibration of IR-spectrometer, — extraction of toluene/methanol (V/V=85/15) with 0.6 N aqueous sulfuric acid (diluted with 40vol% methanol).

Hydrophilic membranes are a better alternative, if organic media is emulsified in aqueous media. Due to presence of methanol, which is potentially soluble in both media, best membrane performance has to be figured out. A "re-entry" of methanol into the organic phase is observed with hydrophilic membranes. Fortunately, hydrophobic OB-900 membrane shows best long-term stability (see Figure 89). Long-term stability (see Figure 90) of the continuous liquid-liquid phase separator Zaiput Sep-10 is investigated at different potential membranes, since different types are available. If an aqueous phase is emulsified in the organic phase, separation performance is better when using a hydrophobic membrane.

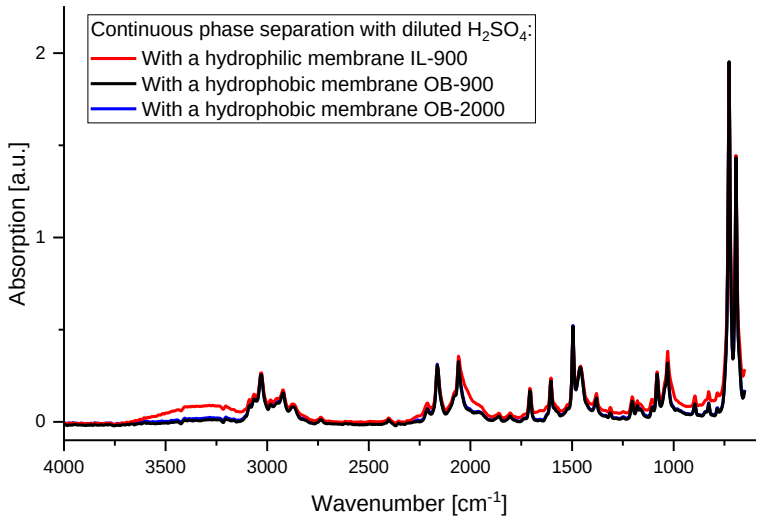

Figure 89: Exemplary IR-spectra of continuous liquid-liquid phase separation of toluene/methanol (V/V=85/15 + 0.25 M benzaldehyde) by 0.6 N aqueous sulfuric acid (diluted with 40vol% methanol) with a SEP-10 using different membranes: — hydrophobic membrane OB-900; — hydrophobic membrane OB-2000; — hydrophilic membrane IL-900.

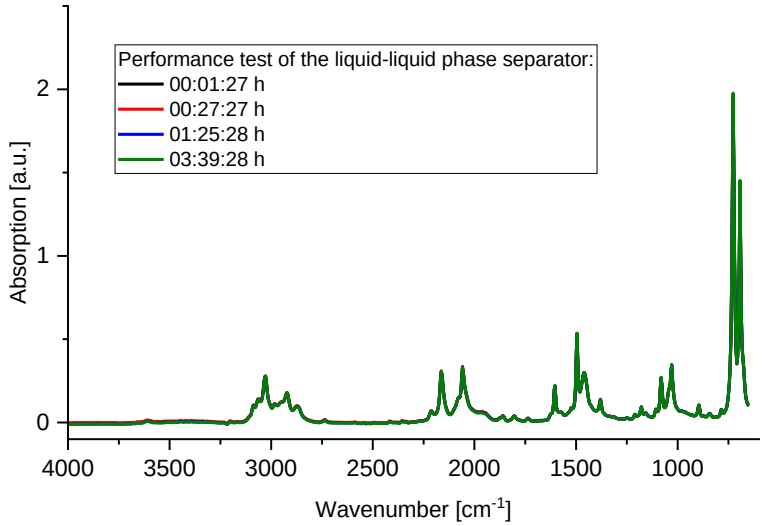

Figure 90: IR-spectroscopy in long-term stability and performance tests of liquid-liquid phase separator with hydrophobic membrane OB-900 after — 00:01:27 h; — 00:27:27 h; — 01:25:58 h and — 03:39:28 h. Continuous extraction of toluene/methanol (V/V=8/1) by 1 N aqueous hydrochloric acid (diluted with 50vol% methanol) is exemplarily shown.

The correct extraction and phase separation behavior of the different substances has to be investigated additionally. Benzaldehyde, *E*-/*Z*-stilbene and triphenylphosphine oxide remain in the organic phase completely, while BTPP and DBU migrate into the aqueous phase completely. This is successfully confirmed by IR-spectroscopy (Figure 91).

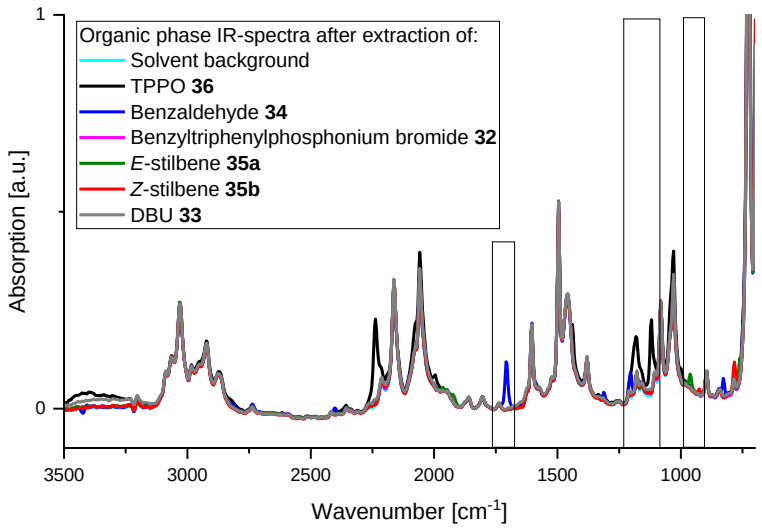

Figure 91: IR-spectra of different Wittig substances in the organic phase after manual extraction by 0.6 N aqueous sulfuric acid (diluted with 40vol% methanol); — solvent background; — triphenylphosphine oxide; — benzaldehyde; — *E*-stilbene; — *Z*-stilbene; — BTTP and — DBU are extracted into the aqueous media; ▭ areas of high interest, as characteristic bands appear here.

With these positive findings, the IR-spectrometer is now calibrated for benzaldehyde, *E*- and *Z*-stilbene and triphenylphosphine oxide, in order to determine conversion and selectivity of the Wittig reaction (Figure 92). Mettler Toledo software application offers integrated data processing, like solvent subtraction and signal integration. Therefore, univariate integration without any standard is performed in "IC Quant". LabView control software will one receive evaluated concentration trends.

The background signal is represented by an organic phase, which is preliminary obtained via extraction of toluene/methanol (V/V=85/15 + 0.25 M benzaldehyde) by 0.6 N aqueous sulfuric acid (diluted with 40vol% methanol). IR-Spectra of the four mentioned substances are recorded in stopped flow, as no difference to flow calibration is detected. Five different concentrations are used for calibration. Baseline correction at 1840 cm^{-1} and solvent subtraction is conducted in every spectrum (see Figure 92 left). Each characteristic signal is evaluated individually, since either signal height or signal area are used to get best results and regression line are finally obtained (Figure 93 and Table 18). Via creation of a template file (including all relevant method setting), the control software is able to trigger the IR-spectrometer and receive fully processed data.

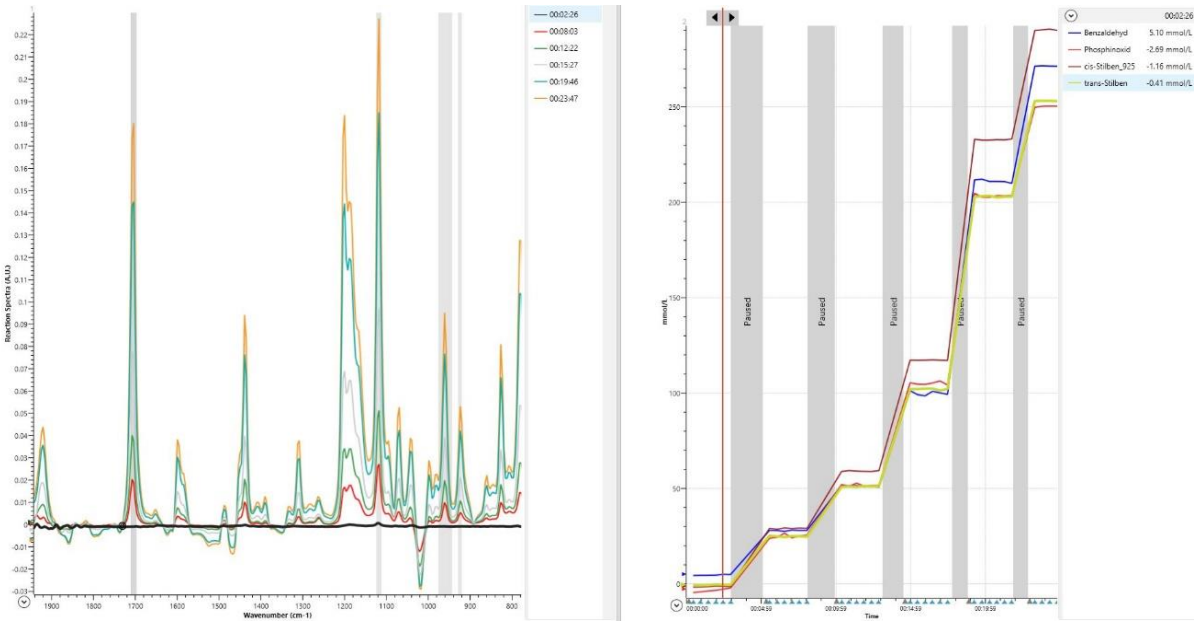

Figure 92: IR-spectra of the different substances and concentrations used in Wittig reaction after extraction; data processed with solvent subtraction and baseline correction; left: ■ characteristic bands appear here, — pure solvent; right: calibration trends after loading fit parameters for calibration of BA, TPPO, *E*-, *Z*-stilbene; samples measured at stopped flow; data processed with Mettler Toledo iC IR.

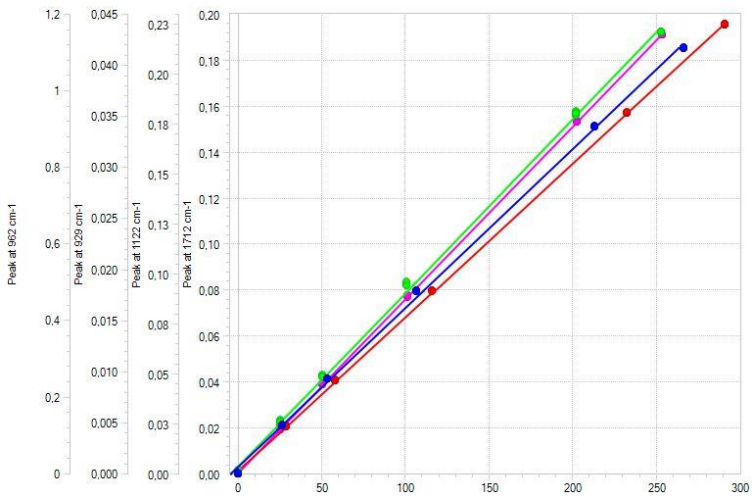

Figure 93: Linear fit of the four Wittig reaction components generated with Mettler Toledo IC Quant; — benzaldehyde; — triphenylphosphine oxide; — *Z*-stilbene, — *E*-stilbene.

Table 18: Fit parameters of four Wittig reaction components used for calibration generated with Mettler Toledo IC Quant.

substance	slope	intercept	R-square	characteristic band [cm^{-1}]	evaluation-type	region [cm^{-1}]	baseline reference[cm^{-1}]
benzaldehyde	0.0007	0.0029	0.9992	1705.7	height to single point baseline	1710 to 1698	1731
triphenyl-phosphine oxide	0.0009	0.0038	0.9992	1029.7	height to single point baseline	1124 to1112	1083
Z-stilbene	0.0002	0.0002	0.9999	924.7	height to single point baseline	928 to 920	943
E-stilbene	0.0045	0.0021	1.0	962.0	area to single point baseline	976 to 943	943

The IR-spectrometer calibration procedure is validated (Figure 94) with a set of four different samples. These mixtures consist of randomly mixed concentrations of benzaldehyde, triphenylphosphine oxide and *E*-/*Z*-stilbene. Deviation of the measured values to the gravimetric concentration of each component is around ~10-15 mM in each sample. This result is rated to be sufficient for continuous online process monitoring of the first reaction step.

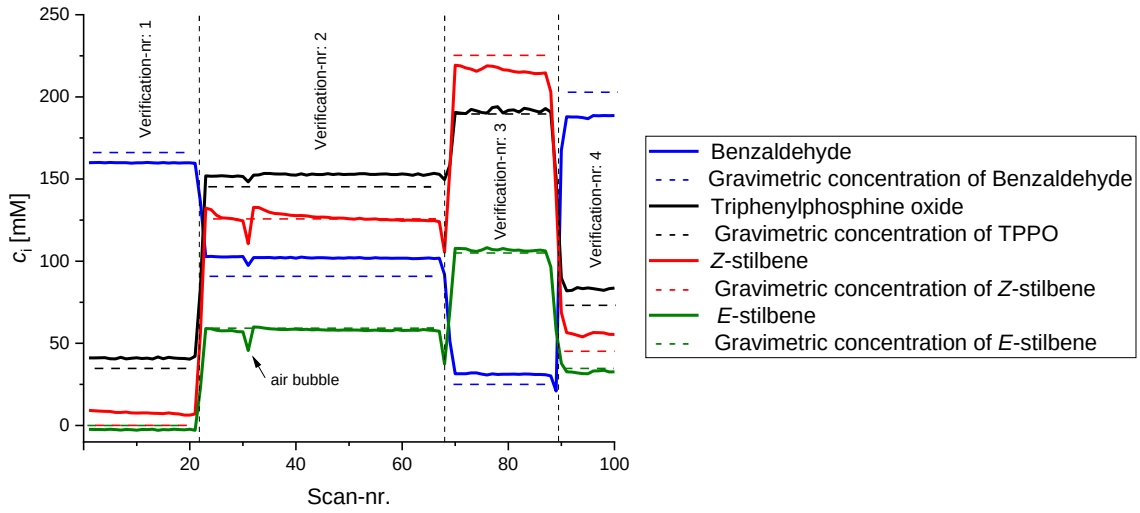

Figure 94: Validation of the IR-spectrometer (Mettler Toledo ReactIR15 equipped with a flow cell) for BA, triphenylphosphine oxide and *E*-/*Z*-stilbene analysis; samples measured at stopped flow; evaluated with IC IR: — benzaldehyde; - - - gravimetric concentration of benzaldehyde; — TPPO; - - - gravimetric concentration of TPPO; — *E*-stilbene; - - - gravimetric concentration of *E*-stilbene; — *Z*-stilbene; - - - gravimetric concentration of *Z*-stilbene; samples measured at stopped flow.

3.2.3.3 Online nondispersive IR-sensor

IR-spectroscopy is a common tool to monitor and evaluate a sample via molecular vibrations in case of quantitative analysis. In most cases, no complete IR-spectrum is required and a few bands are specifically selected.

As long as those bands are well defined, a less complex nondispersive IR-sensor can be suitable for quantification as well. Here, an IR-sensor (nickname "Mulseng") is used to quantify concentrations of *E*- and *Z*-stilbene. This sensor is technically based on an instrument (developed by Fraunhofer IMM), originally being used for the determination of the water content and the total base number (TBN) in oil of combustion engines (see Figure 301 in the appendix).[215,216]

In this setup (Figure 95) a hot plate is used to emit IR light. This non-dispersive and non-polarized spectrum is directed onto the sample compartment. Light passes a flow cell made by two ZnSe-crystals (100 µm distance between both windows). Only transmitted light (of all wavelengths) reaches the four-field thermopile detector. A voltage-signal is generated depending on the present light intensity. Four band pass filters (from Spectrogon Se) are selected, in order to monitor only the specific bands of the sample.

The whole device has to be operated at constant and equilibrated temperature as small changes will cause a signal drift.

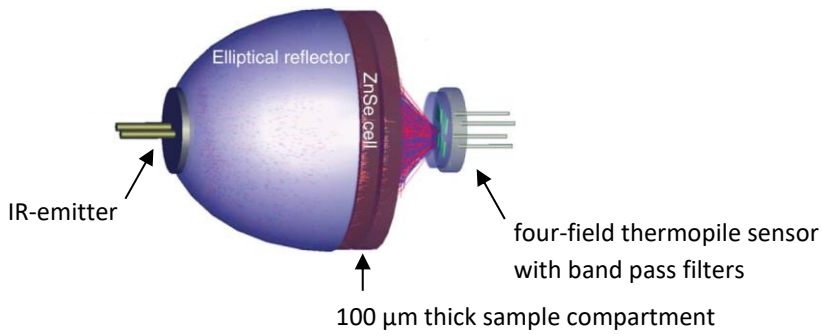

Figure 95: Schematic setup of the nondispersive IR-sensor used for online quantification of *E*- and *Z*-stilbene in continuous flow. Adapted with permission from Ref. [216] copyright 2010 SPIE.

The IR-sensor is tested on a continuous *E*-*Z*-photoisomerization of stilbene using 2mol% of $[Ru(bpy)_3]Cl_2$ as photosensitizer in acetonitrile, according to Ronge and co-workers.[208] For this purpose, the ZnSe flow cell is placed in a transmission-FTIR-spectrometer to create spectra of the solvent (background signal) and the stilbenes isomers. Characteristic bands are identified and the filters are selected (Figure 96 and Table 19 or Figure 302a in the appendix).

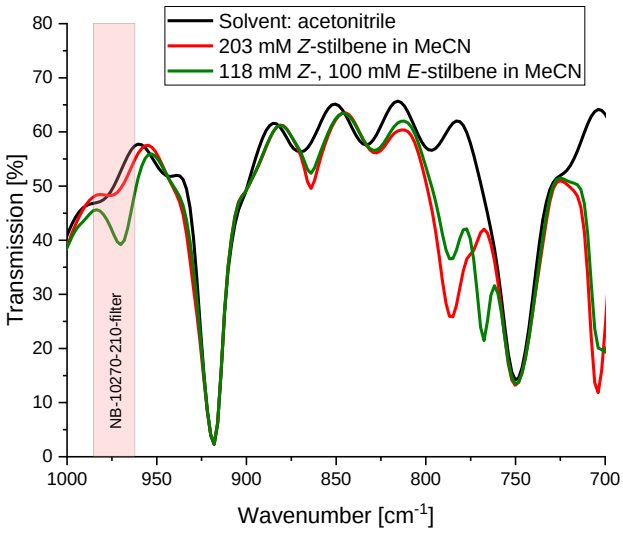

Figure 96: Transmission FTIR-spectra recorded with a ZnSe-flow cell (identical to IR-sensor) and chosen band pass filter for quantification of *E*-*Z*-photoisomerization in acetonitrile; — solvent, — 100 mM *E*-stilbene + 118 mM *Z*-stilbene ; — 203 mM *Z*-stilbene.

Table 19: Selected band pass filters for quantification of *E*-*Z*-photoisomerization in acetonitrile with an IR-sensor.

band pass filter CWL-HW [nm]	note
NB-2790-056	potential reference channel; only solvent signal
NB-5750-100	potential reference channel; only solvent signal
NB-10270-210	*E*-stilbene detection
NB-14180-284	*Z*-stilbene detection

Filter NB-14180-284 is used for the detection of *Z*-stilbene and filter NB-10270-210 is chosen for the *E*-isomer. Since the overlap of both isomers is large at 784 cm^{-1}, quantification is only provided by the filter being selective for the *E*-isomer. The sensor is calibrated (Figure 97) with eleven different mixtures (starting from 100 mM *E*-/ 0 mM *Z*-stilbene, 10% steps), while variance of each transmission data point is ± ~$7 \cdot 10^{-5}$.

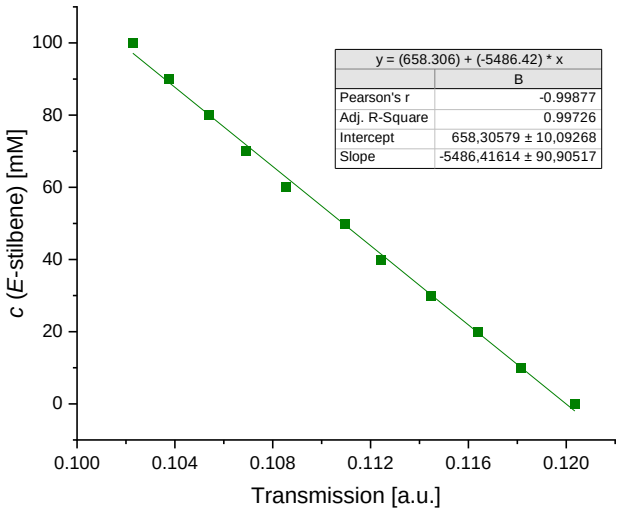

Figure 97: Fit parameters for the external calibration of *E*-stilbene in an IR-sensor; solvent MeCN; samples measured at stopped flow.

Around 95% conversion are achieved, when 100 mM *E*-stilbene (2mol% $[Ru(bpy)_3]Cl_2$ in acetonitrile) are irradiated by a 455 nm LED-array (6×6 LEDs, 6 W_{el}) in a 1/16" FEP capillary photoreactor (15 mL) at 0.5 mL×min^{-1}. This result is consistent to the observations made by Ronge *et al*.

The detector is able to identify highest concentration of *E*-stilbene correctly. Monitored conversion decreases to ~90% *Z*-stilbene, after several times switching on and off the

LED-array (Figure 98). This shift is stated to be an instrumental drift caused by small thermal changes over the long acquisition time, while the actual chemical conversion will stay constant.

This thermal drift can be corrected by monitoring the drift of the background signal. For example, a reference channel where no signal of the substances (only solvent) is observed can be used. Potential drift is recorded and can be used for correction of the relevant signals.

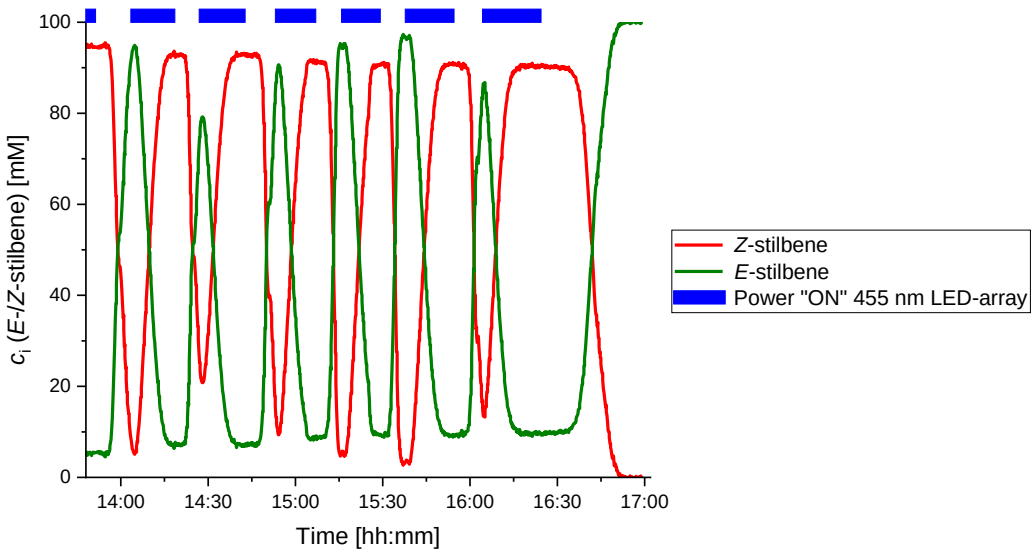

Figure 98: Concentrations of continuous flow (0.5 mL×min^{-1}) *E*-*Z*-photoisomerization in a 1/16" capillary photoreactor (800 µm ID, 15 mL, 455 nm 6x6 LED-array 6 W_{el}) using 2mol% $[Ru(bpy)_3]Cl_2$ as photosensitizer in MeCN quantified with an online IR-sensor; — *Z*-stilbene; — *E*-stilbene; ■ period with switched on LED-array.

In the next step, transmission FTIR-spectroscopy (Figure 99 or Figure 302 b in the appendix) is used to determine the characteristic signals of stilbenes in toluene/methanol (V/V=8/2) as solvent, as this mixture is estimated to be present in the second step of the model reaction. Two band pass filters are chosen and IR-sensor is calibrated individually on both stilbene isomers (Figure 100). In comparison to the studied mixtures in acetonitrile, a drastic change in slope of the linear fit occurs. This effects higher inaccuracy, as even small uncertainties in the background signal (for example) will have a large impact. Analysis of verification samples (Figure 101) confirms this suspicion, as deviation of ± 50 mM is observed for *E*-stilbene. Nevertheless, the applied setup is used to quantify continuous flow isomerization in the model reaction.

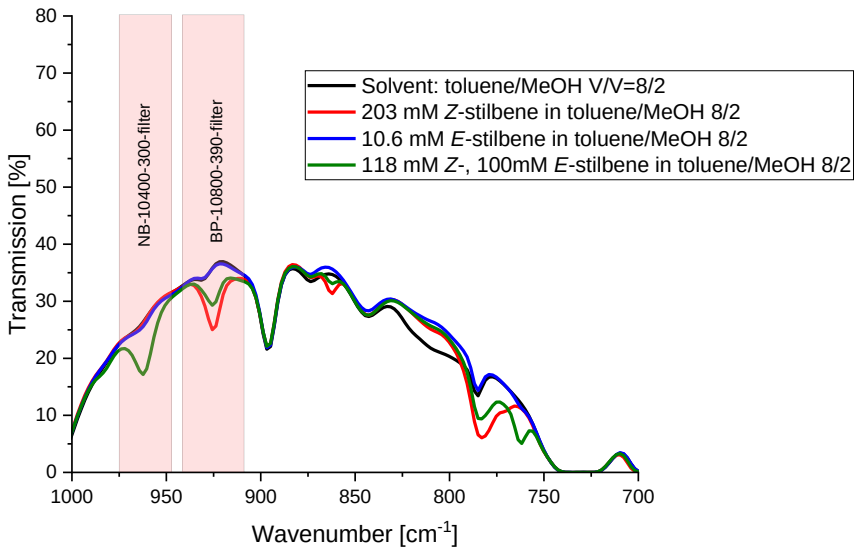

Figure 99: Transmission FTIR-spectra recorded with a ZnSe-flow cell (identical to IR-sensor) and chosen band pass filters for quantification of *E*-*Z*-photoisomerization in toluene/methanol; — toluene/methanol V/V=8/2; — 10.6 mM *E*-stilbene; — 100 mM *E*-stilbene + 118 mM *Z*-stilbene; — 203 mM *Z*-stilbene.

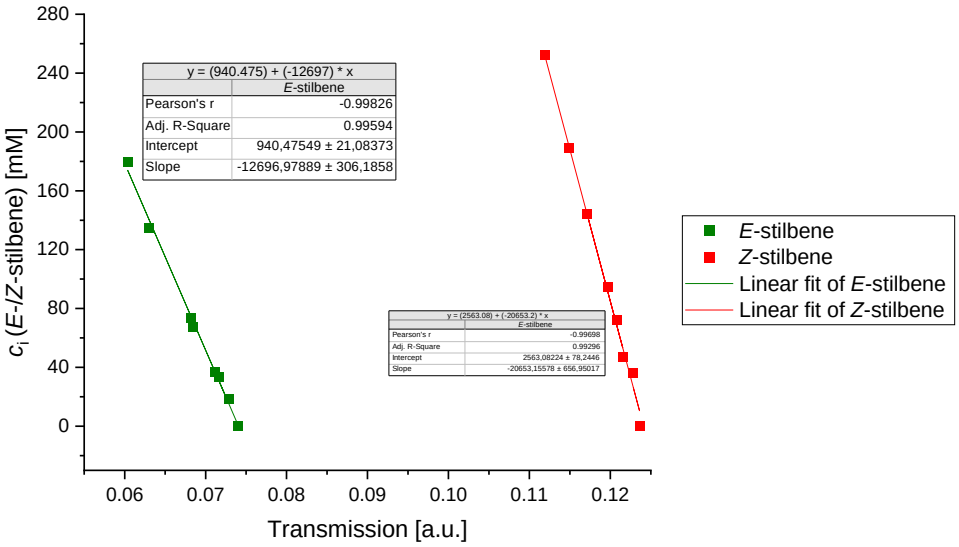

Figure 100: Fit parameters for external calibration of — *E*-stilbene and — *Z*-stilbene in an IR-sensor; solvent toluene/methanol V/V=8/2; samples measured at stopped flow.

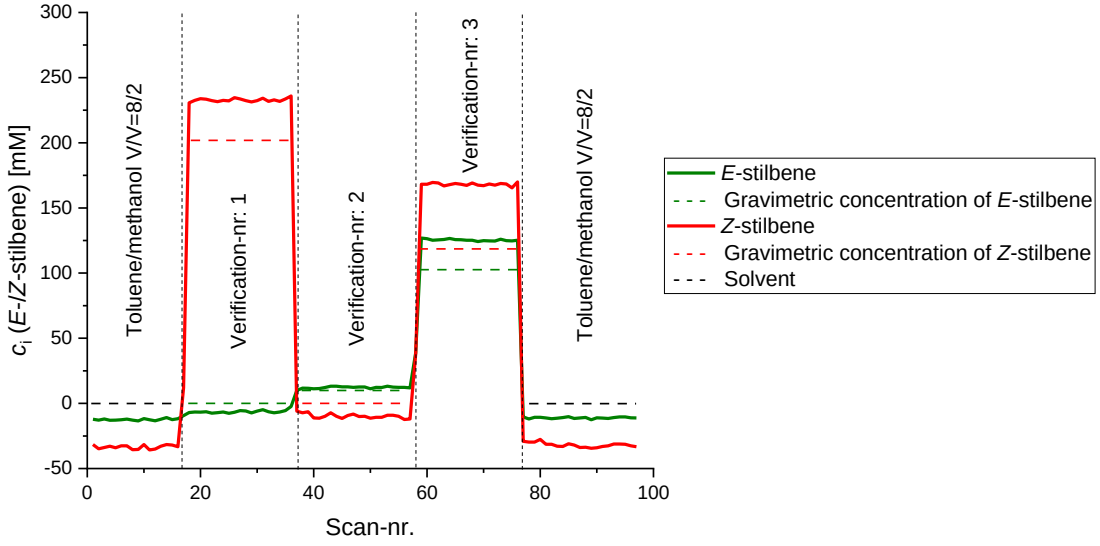

Figure 101: Validation of the IR-sensor *E*-/*Z*-stilbene quantification; samples measured at stopped flow in toluene/methanol V/V=8/2: — *E*-stilbene; - - - gravimetric concentration of *E*-stilbene; — *Z*-stilbene; - - - gravimetric concentration of *Z*-stilbene.

3.2.4 Verification of the developed process analysis tools at the continuous two-step synthesis of *Z*-stilbene

Process development of Wittig reaction is started with initial batch experiments to give information about kinetics of stilbene synthesis. The organic base DBU is used in temperature- and time-depended batch experiments (Figure 102). With that obtained information, the volume of the thermal reactor is adjusted with respect to manageable flow rates. The total reactor volume is initialized in the software, and the control unit is able to calculate the duration until the steady-state condition is present.

These experiments use the already discussed process conditions in order to represent the continuous flow setup as best as possible. Each reaction vial, originally containing 0.25 M benzaldehyde, 0.25 M BTPP and 0.25 M DBU in toluene (containing 15vol% methanol), is quenched individually with 0.6 N sulfuric acid (diluted by 40vol% methanol). After phase separation, each sample is analyzed with NMR- and IR-spectroscopy.

As expected, appropriate trends are found, when changing temperature and residence time. NMR- and IR-data show comparability for benzaldehyde, considering the evaluated error of each single spectrometer. Same behavior is observed for *Z*-stilbene (Table 20). In theory, the sum of the concentrations of *E*- and *Z*-stilbene should correlate

with the TPPO concentration. Deviation between those concentrations is observed, which is related to the inaccuracy of each single spectrometer again.

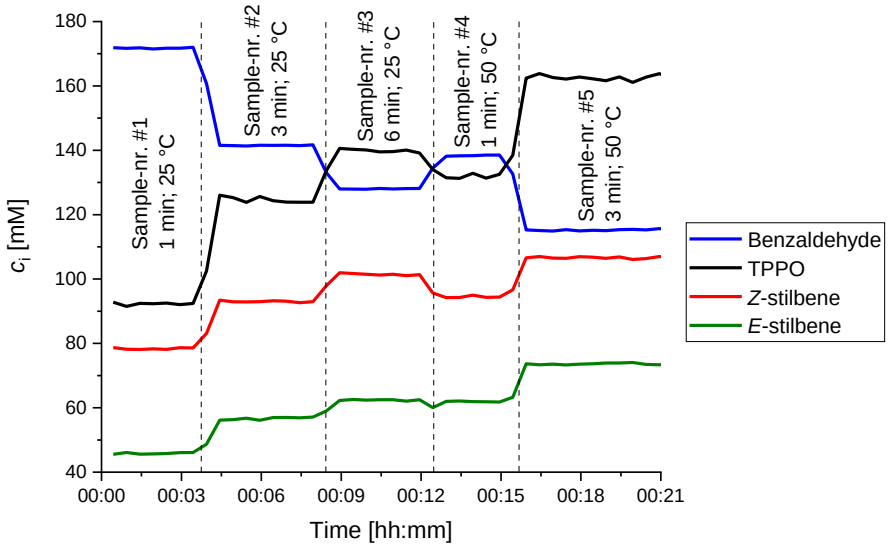

Figure 102: IR-spectra of stilbene Wittig reaction in batch: *#1* 1 min, 25 °C; *#2* 3 min, 25 °C; *#3* 6 min, 25 °C; *#4* 1 min, 50 °C; *#5* 3 min, 50 °C; — BA, — TPPO, — *Z*-stilbene, — *E*-stilbene; general reaction conditions: 0.25 M BA, 0.25 M BTPP, 0.25 M DBU in toluene (incl. 15vol% methanol) and quench with 0.6 N sulfuric acid diluted with 40vol% MeOH.

Table 20: Process monitoring of stilbene Wittig reaction in batch; NMR evaluation via PEAXACT; general reaction conditions: 0.25 M BA, 0.25 M BTPP and 0.25 M DBU in toluene (incl. 15vol% methanol) and quench with 0.6 N sulfuric acid diluted with 40vol% MeOH.

sample-nr.	reaction time [min]	temperature [°C]	*c*(BA) via NMR [mM]	*c*(*Z*-stilbene) via NMR [mM]	*c*(BA) via FTIR [mM]	*c*(TPPO) via FTIR [mM]	*c*(*E*-stilbene) via FTIR [mM]	*c*(*Z*-stilbene) via FTIR [mM]
#1	1	25	181	49	172	92	46	78
#2	3	25	130	60	142	125	56	92
#3	6	25	132	74	128	140	62	101
#4	1	50	115	55	138	132	61	94
#5	3	50	108	83	115	161	74	106

These batch experiments are now transferred into the continuous flow plant. Basic parameters as temperature, flow rate (residence time) and light intensity (photon flux) are adjusted and the effects are monitored with the different inline process analysis tools. Process parameters are only chosen exemplary and the final optimization process parameters is not focused.

3.2.4.1 Variation of temperature and flowrate as process parameters

The designed software and hardware run as expected. After the manual parameter input, all settings are initialized in the individual hardware components and temperature settings are attained quickly including the permanent data archiving. The pressure in the capillary is regulated by a proportional relief valve to ~3 bar_{exs}, which is monitored as well (Figure 103).

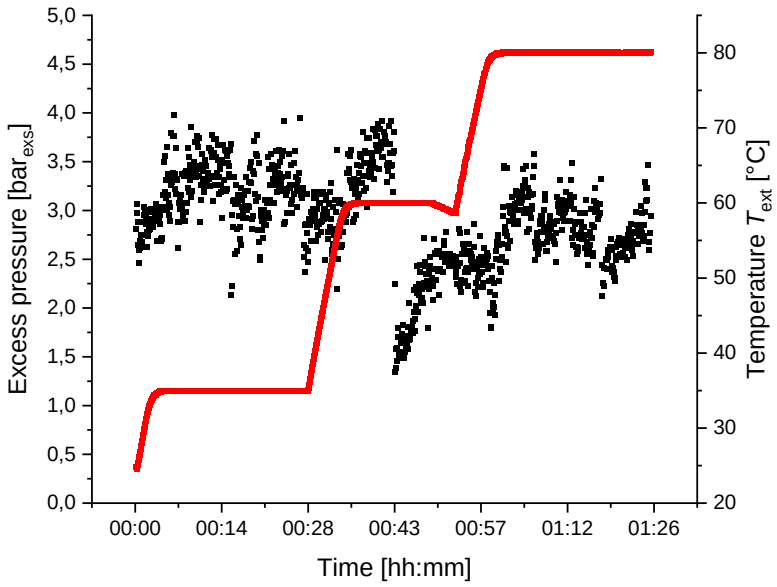

Figure 103: Pressure sensor and thermocouple T_{ext} monitoring while changing temperatures.

First investigations consider a temperature variation from 35 to 80 °C. As expected, product concentrations increase by a rising temperature, while benzaldehyde concentration decreases due to the ongoing Wittig reaction (Figure 104 and Table 21 sample #6 to #8). Unfortunately, this inversely proportional behavior is not found when changing the flow rates at a constant temperature (30 °C). In the presented sample, concentrations of all monitored substances (starting material and products) decrease, even when applying higher flow rates (Figure 105 and Table 21 sample #9 to #12). Therefore, benzaldehyde concentration should be high for short reaction time.

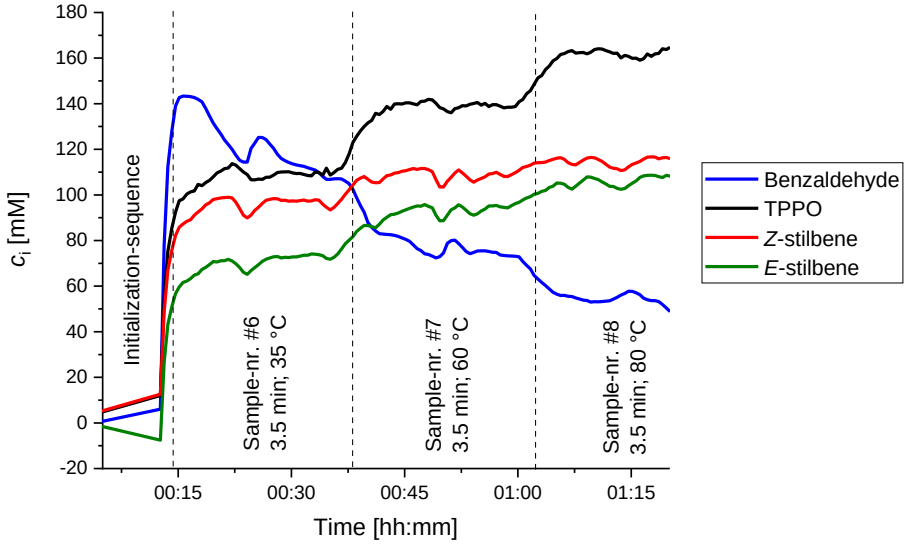

Figure 104: IR-spectra of continuous Wittig reaction with different temperatures at constant residence time: #*6* 35 °C; #*7* 60 °C; #*8* 80 °C; — BA, — TPPO, — *Z*-stilbene, — *E*-stilbene; general reaction conditions: 0.25 M BA, 0.25 M BTPP, 0.25 M DBU in toluene (incl. 15vol% methanol), 3.5 min residence time and quench with 0.6 N sulfuric acid diluted with 40vol% MeOH.

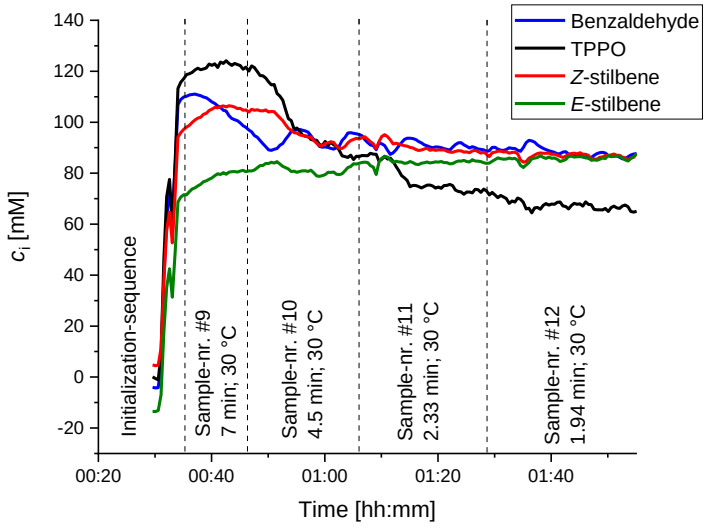

Figure 105: IR-spectra of continuous Wittig reaction with different residence time at constant temperature: #9 7 min; #10 3.5 min; #11 2.33 min; #12 1.94 min; — BA, — TPPO, — *Z*-stilbene, — *E*-stilbene; general reaction conditions: 0.25 M BA, 0.25 M BTPP, 0.25 M DBU in toluene (incl. 15vol% methanol), 30 °C and quench with 0.6 N sulfuric acid diluted with 40vol% MeOH.

Table 21: Online process monitoring of stilbene Wittig reaction in continuous flow; NMR evaluation via PEAXACT; general reaction conditions: 0.25 M BA, 0.25 M BTPP and 0.25 M DBU in toluene (incl. 15vol% methanol) and quench with 0.6 N sulfuric acid diluted with 40vol% MeOH.

sample-nr.	reaction time [min]	temperature [°C]	*c*(BA) via NMR [mM]	*c*(*Z*-stilbene) via NMR [mM]	*c*(BA) via FTIR [mM]	*c*(TPPO) via FTIR [mM]	*c*(*E*-stilbene) via FTIR [mM]	*c*(*Z*-stilbene) via FTIR [mM]
#6	3.5	35	132	68	121	106	67	91
#7	3.5	60	84	80	76	139	94	109
#8	3.5	80	47	74	53	161	108	116
#9	7	30	110	83	104	120	79	106
#10	3.5	30	83	43	90	91	79	91
#11	2.33	30	75	40	90	74	84	98
#12	1.94	30	75	38	92	65	85	86

The identical behavior is observed with both spectrometers, although they rely on totally different analyzation procedures. In theory, ^{1}H-NMR-spectroscopy should not be affected by changing flow rates and different temperature, as preliminary experiments have shown. A hypothetical change in solvent matrix could influence a shift of the characteristic peaks, while fixed integration ranges lead to a defective and insufficient spectra integration. This seems to be implausible, as no such behavior is recognized in other experiments. Another factor could be a (random) spectrometer uncertainty, which wasn´t observed prior to these experiments.

Detailed investigations of the recorded IR-spectra show the appearance of new and unclassified bands (Figure 106). Those cannot be reconstructed by the (ideal) test substances, as they are made by the real process matrix. A new IR-band appears at ~912 cm^{-1} and it is supposed that an overlap with the characteristic band of *Z*-stilbene occurs. This influences evaluation of *Z*-stilbene drastically, especially when a small band in the "finger-print" area is chosen. In consequence, even small changes in signal intensity and baseline (as reference) have a huge impact.

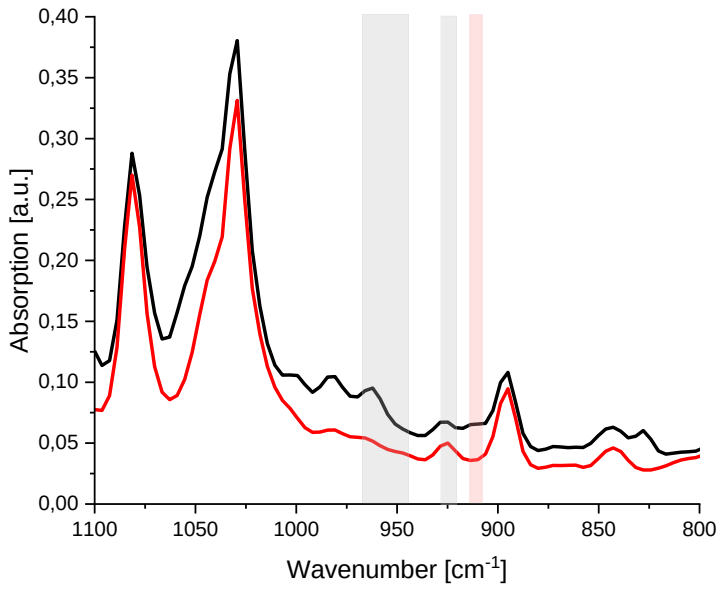

Figure 106: New unknown IR-band at 912 cm^{-1} (red area) in a — real spectrum of continuous synthesis; grey areas: characteristic bands of *E*- and *Z*-stilbene; — spectrum of *Z*-stilbene after quenching (ideal).

One could imagine a wrong or incomplete characterization of the liquid-liquid extraction process, as benzaldehyde or TPPO could partially migrate into the aqueous phase. This hypothesis is incorrect, as cross-checking with analytical HPLC shows. No benzaldehyde, TPPO or *E*-/*Z*-stilbene are found in the aqueous phase.

Additionally, offline analytic via HPLC shows correct behavior of the continuous Wittig reaction at changing flow rates (Table 22). The amount of TPPO as main by-product correlates to the sum of *E*- and *Z*-stilbene, when using HPLC.

Table 22: Process monitoring of stilbene Wittig reaction in continuous flow with offline HPLC analytics; general reaction conditions: 0.25 M BA, 0.25 M BTPP and 0.25 M DBU in toluene (incl. 15vol% methanol) and quench with 0.6 N sulfuric acid diluted with 40vol% MeOH.

sample-nr.	t_R [min]	*T* [°C]	*c*(BA) via offline HPLC [mM]	*c*(TPPO) via offline HPLC [mM]	*c*(*E*-stilbene) via offline HPLC [mM]	*c*(*Z*-stilbene) via offline HPLC [mM]
#9	7	30	198	148	60	113
#10	3.5	30	256	137	49	87
#11	2.33	30	265	92	33	63
#12	1.94	30	240	76	30	55

3.2.4.2 Variation of LED light intensity as process parameter

The outlet of the FTIR-spectrometer delivers a substance mixture of BA, TPPO and stilbene dissolved in ~98% toluene and ~2% methanol. To add the photosensitizer for the second step, $[Ru(bpy)_3]Cl_2$ has to be dissolved in the polar solvent methanol. Tests show, that ~19vol% of the solvent have to be methanol. Therefore, a solution, containing 1.87 g/100 mL of the ruthenium-catalyst, is provided to give a ~2mol% concentration in the reaction mixture. The substrate stream is then pumped into a 1/16" FEP capillary photoreactor V.0 (15 mL) and irradiated with the internal LED-array for ~20 min. Reaction conditions of the first step are set in a way to yield maximum amount of stilbene isomers and stay constant (see Figure 107) to characterize the influence of different light intensity in the second step.

The isomerization progress is observed with the nondispersive IR-sensor. As already mentioned, a constant process flow is required for such a sensor and solvent/ background signal should not change, as this leads to instable performance of the sensor.

Unfortunately, raw data of the IR-sensor show a constant trend (Figure 108) with no signal changes in both channels. In theory, the raw signal of *Z*-stilbene should decrease due to higher absorption and the *E*-stilbene signal has to increase since less light is absorbed. Additional offline HPLC-analysis (Table 23) of these experiments shows proceeding photo-isomerization of stilbene in toluene/methanol. Complete isomerization is observed after ~20 minutes at almost 40% of maximum LED power.

In consequence, the IR sensor with two separate band pass filters is not able to monitor concentration gradients between the two stilbene isomers in a real process environment. This is incongruent to the observations made in acetonitrile. Reasons could be overlapping bands or new additional bands, which appear during the reaction. To solve these problems, further detailed experimental studies are required.

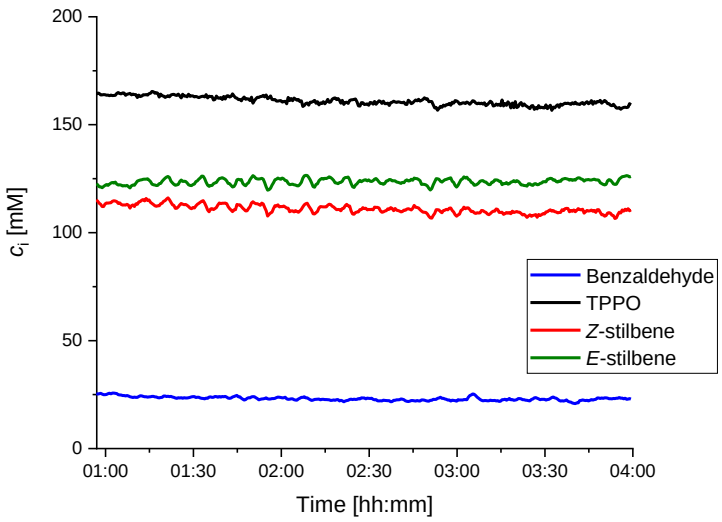

Figure 107: IR-spectra of continuous Wittig reaction at 90 °C and 4.37 min residence time; — BA, — TPPO, — *Z*-stilbene, — *E*-stilbene; general reaction conditions: 0.25 M BA, 0.25 M BTPP, 0.25 M DBU in toluene (incl. 15vol% methanol) and quench with 0.6 N sulfuric acid diluted with 40vol% MeOH.

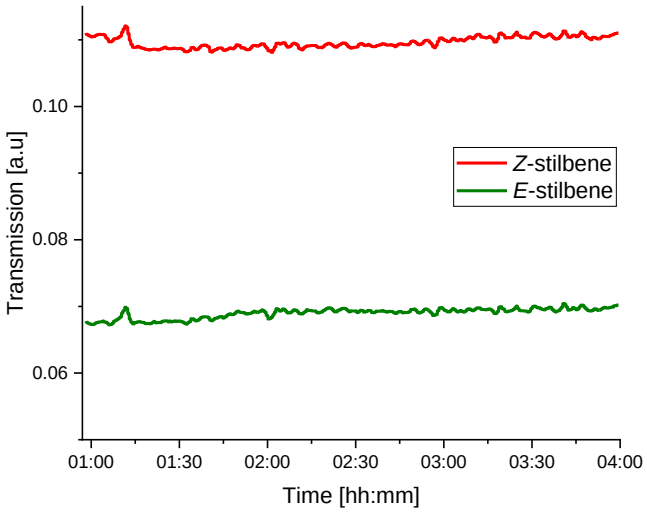

Figure 108: Raw data of the IR-sensor for online monitoring of *E*-*Z*-photoisomerization in toluene/methanol: — *Z*-stilbene, — *E*-stilbene.

Table 23: Process monitoring of *E*-*Z*-photoisomerization in continuous flow with offline HPLC analytics; general reaction conditions: 0.25 M BA, 0.25 M BTPP and 0.25 M DBU in toluene (incl. 15vol% methanol), 4.37 min, 90 °C and quench with 0.6 N sulfuric acid diluted with 40vol% MeOH; photoisomerization in a 16" capillary photoreactor (~20 min, 455 nm, maximum 11 W_{el}) using ~2mol% photosensitizer.

sample-nr	LED-power [%]	*c*(BA) via offline HPLC [mM]	*c*(TPPO) via offline HPLC [mM]	*c*(*E*-stilbene) via offline HPLC [mM]	*c*(*Z*-stilbene) via offline HPLC [mM]
#13	10	117	149	29	98
#14	20	133	159	13	109
#15	40	125	143	5	100
#16	60	115	149	4	88
#17	80	155	158	4	102

3.2.5 Conclusions and valuation of PAT in a continuous two-step synthesis of *Z*-stilbene

A (semi-)automated process plant including appropriate hard- and software is developed for a continuous two-step synthesis of *Z*-stilbene as a model system. Different hardware, like four pumps, one thermostat and three spectrometers for online process analysis, are controlled with a designed software. In the semi-automated mode, the open structure of the suited LabView-program provides the possibility to pre-define parameter sets. Once, all parameters for each cycles are selected, the control unit will automatically process every data set. Especially, this procedure is of high interest for DoE studies of unknown reactions performed in continuous flow.

^{1}H-NMR- and IR-spectroscopy are elaborated and used for online monitoring of a Wittig reaction, which produces a mixture of *E*- and *Z*-stilbene isomers. While both spectroscopy methods work perfectly with the ideal training solutions, process data evaluation is hindered by minor differences between the model and the real reaction mixture.

In NMR-spectroscopy it is assumed, that phase- and baseline correction of the spectrum leads to interference or overlap especially when the aromatic solvent signal is slightly shifted towards the characteristic signal of the product. In this special case, this inaccuracy is amplified by the SNR of the benchtop spectrometer.

Similar behavior leads to distortion in online IR-spectroscopy, as new bands appear in the real system, which can´t be simulated. These additional bands do not belong to any side-product, since they are excluded by HPLC analysis. Quenching of intermediates will therefore result in the starting material. Generally, spectroscopy, using any type of

absorption or transmission-mechanisms, relies on a well characterized background signal and its divergence can lead to false results.

Determination of conversion- and selectivity with the presented PAT tools is even more complicated, due to the applied model reaction. Extraction and phase separation leads to a change of volume and concentration, while the amount of substance keeps constant in the organic phase. In the presented concept, these shifts are significant and cannot be neglected. The volume change is larger than expected, as methanol is extracted into the aqueous phase. The unreacted starting material BTPP will migrate as well, depending on the conversion rate, as Table 24 shows. At low conversion, lots of BTPP is extracted into the aqueous phase and volume reduction is high. High conversion results in TPPO and stilbene, which will stay in the organic phase and therefore volume reduction is low. A volume reduction of 20-25% is observed in the continuous synthesis experiments and therefore being slightly higher as theoretical calculations.

Usage of the nondispersive IR-sensor has to be reevaluated, as chosen filters malfunction in the real system, with toluene and methanol as solvent. However, continuous *E*-*Z*-photoisomerization of stilbene in acetonitrile, using a photosensitizer and 455 nm, is successfully monitored with the online IR-sensor. This proves again that the background signal has to be determined accurately.

Table 24: Theoretical calculation of a volume reduction by extraction of 200 mL organic phase with 200 mL aqueous quench media depending on the conversion of Wittig reaction.

theoretical conversion	substance	weights [g] in organic phase by conversion	density [g/mL]	volume [mL] by conversion	volume of organic phase after quench and extraction
before quench	BTTP	21.66	1.4	15.48	100% (no extraction)
	BA	5.32	1.04	5.11	
	DBU	7.6119	1.02	7.46	
	toluene	127.48	0.867	147.03	
	methanol	20.4	0.79	25.83	
0%	BTTP	0	1.4	0	~ 77%
	BA	5.32	1.04	5.11	
	DBU	0	1.02	0	
	toluene	127.48	0.867	147.03	
	methanol	2.37	0.79	3	
50%	BTTP	10.83	1.4	7.74	~81%
	BA	5.32	1.04	5.11	
	DBU	0	1.02	0	
	toluene	127.48	0.867	147.03	
	methanol	2.37	0.79	3	
75%	BTTP	16.24	1.4	11.6	~83%
	BA	5.32	1.04	5.11	
	DBU	0	1.02	0	
	toluene	127.48	0.867	147.03	
	methanol	2.37	0.79	3	
100%	BTTP	21.66	1.4	15.48	~85%
	BA	5.32	1.04	5.11	
	DBU	0	1.02	0	
	toluene	127.48	0.867	147.03	
	methanol	2.37	0.79	3	

4 Experimental Section

4.1 General remarks

All chemicals are purchased from standard commercial vendors and are used as arrived unless otherwise noted. Photochemical/photocatalytic syntheses in batch scale are conducted in standard 30 mL clear glass screw neck vials ND24 from Th. Geyer GmbH & Co. KG.

The following hardware components are used for continuous flow synthesis:

Pumps in experiments regarding diazonium compounds:

P-01:
Supplier: Harvard Apparatus
Type: Pump 11 Elite

P-02:
Supplier: Chemyx Inc.
Type: Nexus 6000

P-03:
Supplier: KD Scientific Inc.
Type: KDS 100

P-04:
Supplier: Postnova Analytics GmbH
Type: PN1610

P-05/P-06:
Supplier: Knauer GmbH
Type: K-501

P-07:
Supplier: Knauer GmbH
Type: Smartline Pump 100

Pumps in experiments regarding stilbene synthesis:

P-01/P-03/P-04:
Supplier: Knauer GmbH
Type: Azura P 4.1S

P-02:
Supplier: Knauer GmbH
Type: Smartline Pump 100

Backpressure regulators for all Knauer HPLC-pumps (not mentioned in setup sketches)

Supplier: IDEX Health & Science LLC
Type: BPR Cartridge 750 psi incl. stainless steel cartridge holder

Capillary and tubing

Stainless steel capillary
Supplier: Swagelok Company
Type: 1/16" stainless steel tubing (570 µm ID)

FEP-capillary
Supplier: Bohlender GmbH
Type: 1/16" FEP-capillary (800 µm ID) and 1/8" FEP-capillary (1.6 mm ID)

Junctions and mixers

PEEK Y-junction
Supplier: IDEX Health & Science LLC
Type: IDEX H&S P-800

Stainless steel T-junction
Supplier: Swagelok Company
Type: 1/16" and 1/8" stainless steel T-junction

PCTFE T-junction
Supplier of 3D-design and construction: Fraunhofer IMM
Type: 1/16" and 1/8" junctions

3-Way valve

Stainless steel
Supplier: Swagelok Company
Type: SS-41GXS1

PTFE
Supplier: Bohlender GmbH
Type: F731-08; bore 1.6 mm

Various capillary and tubing connectors

Supplier: IDEX Health & Science LLC and Swagelok Company

Pressure detection used in experiments regarding diazo compounds:

Supplier: Greisinger electronic
Type: MSD 25 BAE with controller GMG 3155

Pressure detection in experiments regarding stilbene synthesis:

Supplier: WIKA Alexander Wiegand SE & Co. KG
Type: A-10, 40 bar, 4-20 mA

Rotameter for FFMR applications:

Supplier: Bailey-Fischer & Porter
Type: G10A6142, 660 $cm^3 \times min^{-1}$, 1 bar

Mass flow controller for SMBR applications:

Supplier: Bronkhorst Deutschland Nord GmbH
Type: F-200CV-005-AAD-11-V, 5 $cm^3 \times min^{-1}$, 2 bar

Proportional relief valve
Supplier: Swagelok Company
Type: SS-4R3A-KZ 1/4" Swagelok with a regulation range between 3.4 – 24.1 bar; 177-R3A-K1-A

Photoreactors and LED heat exchanger

Supplier of 3D-design and construction: Fraunhofer IMM

Type: - 2× 1/16" FEP capillary (15 mL volume each; 800 µm ID) with heat exchanger to carry hexagonal LED-arrays with 6×6 LEDs

- 2× 1/8" FEP capillary (30 mL volume each; 1.6 mm ID) with heat exchanger to carry hexagonal LED-arrays with 6×6 LEDs

- Version 0 1× 1/16" FEP capillary (15 mL volume; 800 µm ID) with heat exchanger to carry equally distributed with 5×2 LEDs

- Falling Film Micro Reactor with heat exchanger and inspection window to fit reaction plates with 78 mm length

Light emitting diodes LEDs (refer Table 41 and Figure 221 in the appendix)

Supplier: Nichia Corporation, Japan & Avonec, Germany

Type: royal blue for 4×1 LED-array: Nichia NCSC219BT-V1

royal blue for 5×2 LED-array: Nichia NCSC219BT-V1

royal blue for 6×6 LED-array: Avonec 3W High Power LED 455 - 460 nm

UV-A for 4×1 and 6×6 LED-array: Nichia NCSU276AT

green for 6×6 LED-array: Nichia NCSG219BT-V1

Power Supply for LEDs

Supplier: Conrad Electronic SE

Type: Voltcraft LSP-1403

Cryostat for LED- and heat exchangers

Supplier: Julabo GmbH

Type: F10 with HC E07 (control unit)

Thermostat

Supplier: Julabo GmbH

Type: HL-4

Low-frequency offline and online NMR-experiments are carried out with an NMReady-60PRO benchtop spectrometer (Nanalysis Corp.) with Larmor frequencies of 60.56 MHz for ^{1}H-NMR, 56.98 MHz for ^{19}F-NMR and 24.50 MHz for ^{31}P-NMR. In online analysis using the benchtop spectrometer, the sample holder is equipped with a PEEK bottom-to-top flow cell (3D-design, manufacturing, testing by Fraunhofer IMM). High-resolution ^{1}H, ^{13}C and ^{19}F spectra are recorded with an Avance III HD 300 NMR spectrometer or an Avance DSX 400 (both Bruker Corporation). Unless otherwise mentioned all spectra are processed with processed unless otherwise mentioned with MestReNova (Version 12.0.4-22023; Mestrelab Research S.L).

Analytical GC/MS is carried out with a Shimadzu GC-2010 Plus/QP2010 Ultra equipped with a Phenomex Zebron ZB-5 MSi column (30 m×0.25 mm×0.25 µm). Carrier gas is helium: 1.22 mL/min. GCMSsolution V2.72 by Shimadzu is used as software (refer Table **25**).

Table 25: Temperature settings for GC/MS-analysis.

injector temperature	250 °C	
column	start: 120°C	duration: 3 min
	heating: 20 °C min^{-1}	duration: 1.5 min
	constant 150 °C	duration: 2 min
	heating: 60 °C min^{-1}	duration: 2.5 min
	end: 300 °C	duration: 8 min
interface	235 °C	

Analytical HPLC is carried out with a Shimadzu SCL-10A equipped with a Phenomex Luna C18 column (150 mm×4.6 mm, 100 Å). Class-VP V6.14 by Shimadzu is used as software (refer Table 26).

Table 26: Gradient settings for analytical-HPLC analysis.

flowrate	0.8 mL×min^{-1}		
gradient	40% MeCN+0.1% TFA	60% H_2O+0.1% TFA	change: 3.75% ×min^{-1}
	100% MeCN+0.1% TFA	0% H_2O+0.1% TFA	Duration: 10 min
temperature	RT		

Preparative HPLC is carried out with a Büchi Sepacore® Flash X50 equipped with a Büchi FlashPure EcoFlex C18 220 g column (refer Table 27).

Table 27: Gradient settings for preparative HPLC-analysis.

flowrate	15 mL×min^{-1}		
gradient	30% MeCN	70% H_2O	change: 1.75% ×min^{-1}
	100% MeCN	0% H_2O	Duration: 35 min
temperature	RT		

UV/Vis spectra are recorded on a Perkin Elmer Lambda 1050 UV/VIS/NIS Spectrometer using software UV WinLab 6.0.3. Measurements are performed in 1 mm QS glass cuvettes from Hellma GmbH & Co. KG with acetonitrile as reference unless otherwise stated.

ATR-FTIR spectroscopy is conducted on a Mettler Toledo ReactIR 15 equipped with a DS Micro Flow Cell. Spectra are recorded from 4000 to 650 cm^{-1} with a resolution of 8 cm^{-1}. 128 scans are recorded per Spectra. Mettler Toledo iC IR 7.1.84.0 is used to control the spectrometer.

Transmission-FTIR spectroscopy is conducted on a Nicolet Instruments Magna-IR 750 spectrometer. Nicolet OMNIC 5.2 is used to control the spectrometer.

4.2 Continuous synthesis of biphenyls with a photochemical arylation of arenes via diazonium trifluoroacetates and its quantification with online ^{19}F-NMR spectroscopy

4.2.1 Biphenyl synthesis using heterogeneous photocatalysts in versatile reactor concepts

4.2.1.1 Synthesis of 3-CF_3-phenyldiazonium tetrafluoroborate 25

3-CF_3-phenyldiazonium tetrafluoroborate is synthesized from the corresponding aniline according to literature.[217] In a 100 mL round bottom flask 16 mL of distilled water are cooled to 0°C. 20 mmol 3-CF_3-aniline (3.2 g) are emulsified and 54 mmol of a 50% tetrafluoroboric acid (9 g) are added slowly. At 0 to 5 °C 22 mmol sodium nitrite (in 5.5 mL distilled water) are added over a period of 5 minutes. The mixture is stirred for 30 minutes at 0 to 5 °C and 1 h at RT. The precipitate is washed with 50 mL cold water and re-dissolved in 25 mL acetone. 3-CF_3-phenyldiazonium tetrafluoroborate is precipitated by dropping the solution into 75 mL of -20 °C cold diethyl ether to give 2.86 g of a white solid (11 mmol, 55% according to theory). The solid is stored in the fridge at 5 °C.

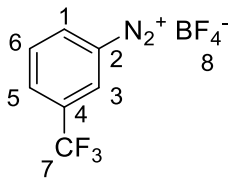

Figure 109: Structure of 3-CF_3-phenyldiazonium tetrafluoroborate **25** with numeric labels for NMR evaluation.

^{1}H-NMR (60.56 MHz; MeCN-d_3), δ[ppm]: 8.75-7.75 (m; 4H)

^{19}F-NMR (56.98MHz; MeCN-d_3), δ[ppm]: -62.92 (s; 3F; F^7), -149.92 (s, 4F; F^8)

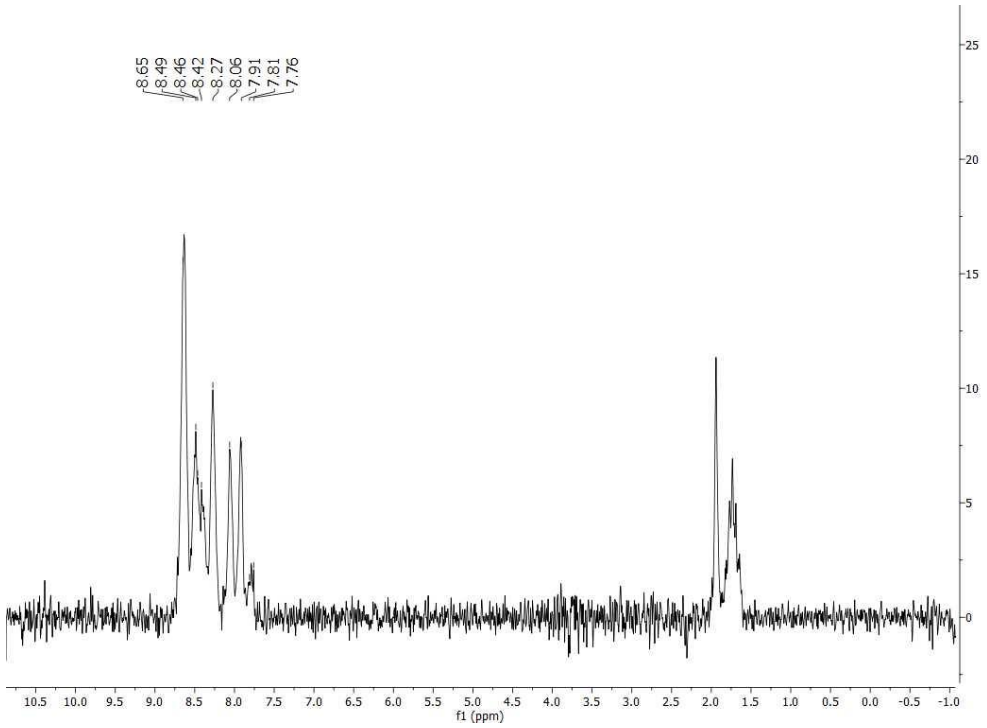

Figure 110: ^{1}H-NMR spectrum (60.56 MHz) of 3-CF_3-phenyldiazonium tetrafluoroborate in MeCN-d_3.

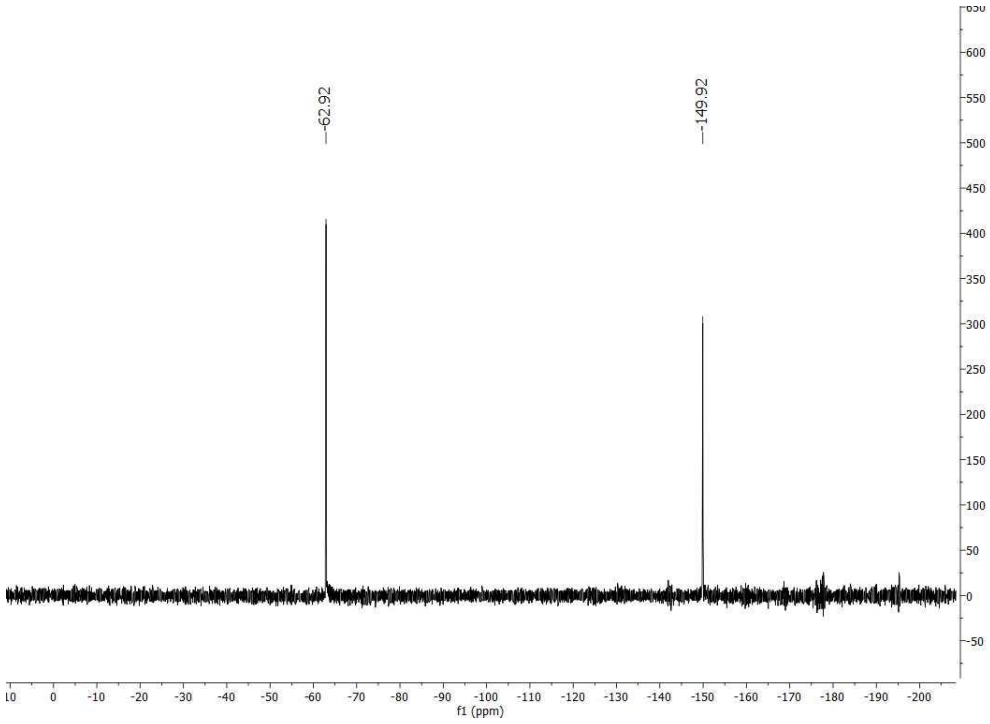

Figure 111: ^{19}F-NMR spectrum (56.98 MHz) of 3-CF_3-phenyldiazonium tetrafluoroborate in MeCN-d_3.

4.2.1.2 Synthesis of 4-chlorophenyldiazonium tetrafluoroborate 20

4-chlorophenyldiazonium tetrafluoroborate is synthesized from the corresponding aniline according to literature.[217] In a 250 mL round bottom flask 40 mL of distilled water are cooled to 0°C. 78 mmol 4-chloroaniline (10 g) are suspended and 203 mmol of a 50% tetrafluoroboric acid (35.7 g) are added slowly. At 0 to 5 °C 86 mmol sodium nitrite (in 16 mL distilled water) are added over a period of 10 minutes. The mixture is stirred for 30 minutes at 0 to 5 °C and 1 h at RT. The precipitate is washed with 50 mL cold water and re-dissolved in 50 mL acetone. 4-chlorophenyldiazonium tetrafluoroborate is precipitated by dropping the solution into 175 mL of -20 °C cold diethyl ether to give 9.51 g of a white solid (42 mmol, 54% according to theory). The solid is stored in the fridge at 5°C.

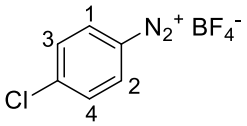

Figure 112: Structure of 4-chlorophenyldiazonium tetrafluoroborate **20** with numeric labels for NMR evaluation.

^{1}H-NMR (60.56 MHz; MeCN-d_3), δ[ppm]: 8.78-8.05 (m; 2H; H^{1+2}), 8.05-7.38(m; 2H; H^{3+4})

^{19}F-NMR (56.98MHz; MeCN-d_3), δ[ppm]: -149.73 (s, 4F)

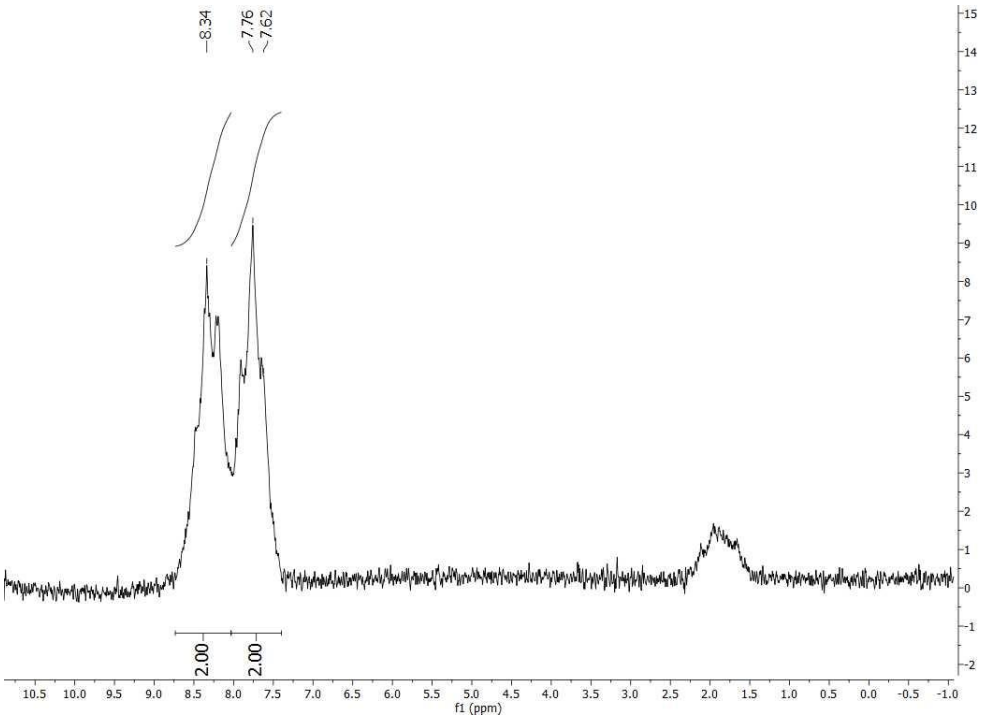

Figure 113: ^{1}H-NMR spectrum (60.56 MHz) of 4-chlorophenyldiazonium tetrafluoroborate in MeCN-d_3.

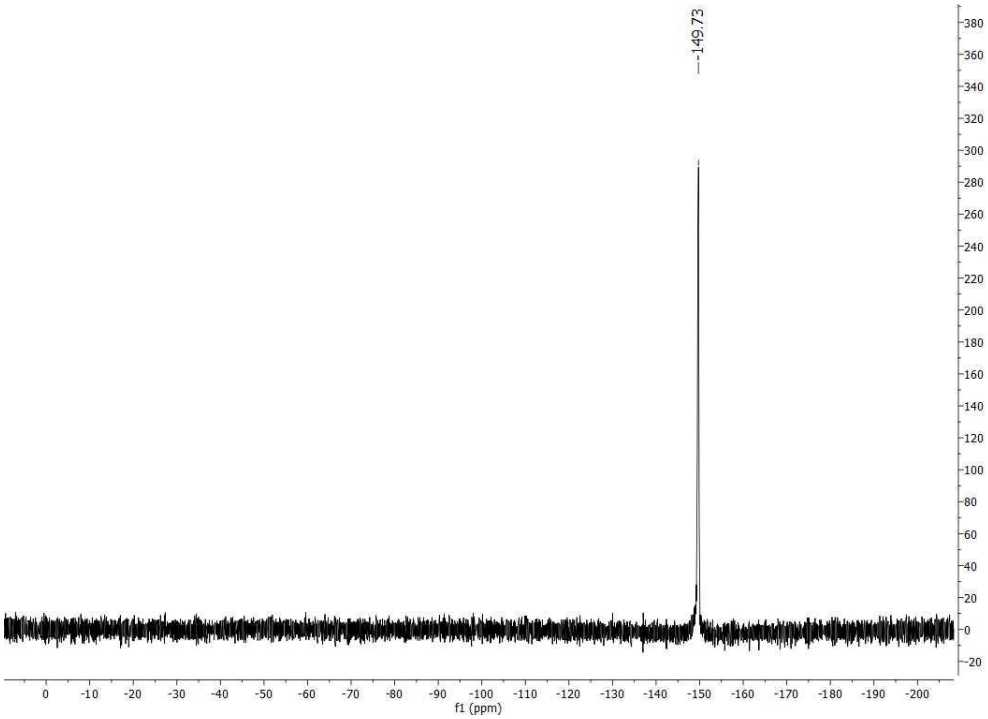

Figure 114: ^{19}F-NMR spectrum (56.98 MHz) of 4-chlorophenyldiazonium tetrafluoroborate in MeCN-d_3.

4.2.2.3 Catalyst investigation in batch for optimal synthesis of 26b

In a 30 mL clear glass vial containing 3-CF_3-phenyldiazonium tetrafluoroborate (130 mg, 0.05 M) in 5 mL benzene and 5 mL acetonitrile is added one equivalent of TiO_2 nanopowder (anatase or rutile modification), or $BaTiO_3$ and $SrTiO_3$, respectively. In one case, one equivalent trifluoroacetic acid is added beside one equivalent of anatase nanopowder. The vial is sealed with a cap, stirred by a magnetic stir plate and placed ~6 cm in front of a 6 W_{el} 4×1 455nm LED-array. By mounting the array on an aluminum heatsink for optimal heat dissipation, reaction temperature stays at RT and additional thermal effects are avoided. After 17 h an aliquot of 50 µL is diluted with 900 µL acetonitrile and 50 µL (50 mM) DL-menthol as external standard. Quantitative GC/MS-analysis is performed after filtration with a hydrophilic 0.45 µm syringe filter.

4.2.2.4 Explorative experiments with the falling film micro reactor

A vial is used to dissolve 3-CF_3-phenyldiazonium tetrafluoroborate (260 mg, 0.05 M) in 10 mL benzene and an appropriate solvent (10 mL ethanol or 10 mL ethanol/DMSO V/V=7/3). The solid is removed by filtration with a hydrophilic 0.45 µm syringe filter. The mixture is stirred to give Feed A, protected from light and pumped into the FFMR (P-07, 500 µL×min^{-1}). The FFMR is equipped with a reaction plate and cooled to 20 °C via a cryostat. The reaction plate has 32 microchannels with a channel architecture of 600 µm in width, 200 µm in depth and 78 mm length. Titanium(IV) oxide (anatase nanopowder) is immobilized on the reaction plate via a slurry wash coating and calcination according to literature procedures[31,91,218] resulting in 23 mg of immobilized anatase. A nitrogen gas flow of 15 mL×min^{-1} is set by a rotameter to support the outflow of the liquid stream. The liquid film is irradiated by a 4×1 455 nm LED-array 6 W_{el} with an aluminum heatsink for optimal heat dissipation. This array is placed in front of the optical window of the FFMR. An aliquot of 50 µL is diluted with 900 µL acetonitrile and 50 µL (50 mM) DL-menthol as external standard and analyzed by GC/MS. 1/16" capillaries are used to connect all components.

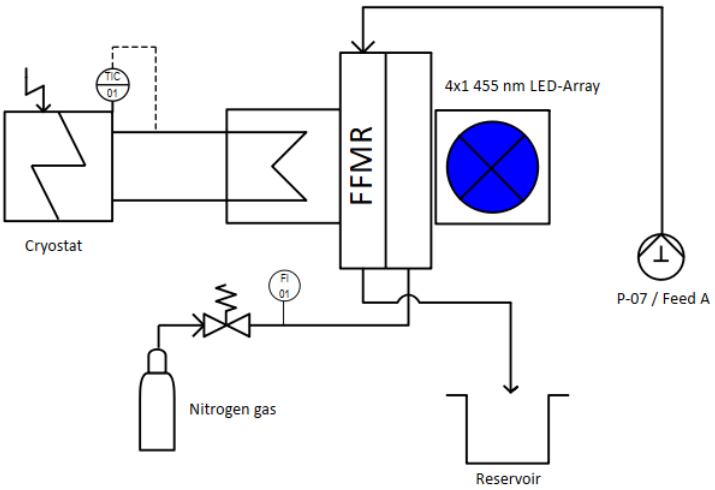

Figure 115: Setup for explorative experiments with the falling film microreactor FFMR.

4.2.2.5 Optimization of 26b using heterogeneous photoarylation via different arene diazonium salts and wavelengths

In a 30 mL clear glass vial containing 3-CF_3-aniline (80.5 mg, 0.05 M), organic acid (1.0 equiv.), 1 equivalent titanium(IV) oxide (anatase nanopowder, 40 mg) in 5 mL benzene and 5 mL of an appropriate solvent is added 1.2 equivalents *tert*-butyl nitrite (62 mg, 1.2 equiv.). The vial is sealed with a cap, stirred by a magnetic stir plate and placed ~6 cm in front of a 4×1 LED-array 6 W_{el}. By mounting the array on an aluminum heatsink for optimal heat dissipation, reaction temperature stays at RT and additional thermal effects are avoided. An aliquot of 50 µL is diluted with 900 µL acetonitrile and 50 µL (50 mM) DL-menthol as external standard, after finishing the reaction. Quantitative GC/MS-analysis is performed after filtration with a hydrophilic 0.45 µm syringe filter. Additional information is listed in Table 28. Entry 1 is purified with column chromatography (eluent: n-heptane) to give 64 mg (58%) of isolated yield as a colorless oil.

Table 28: Optimization of **26b** using heterogeneous photoarylation via different arene diazonium salts and wavelengths.

#	solvent	organic acid	photocatalyst	λ [nm]	irradiation time [h]
1	MeCN	TFA	TiO_2 - anatase	455	17
2	MeCN	CH_3SO_3H	TiO_2 - anatase	455	17
3	MeCN	CF_3SO_3H	TiO_2 - anatase	455	17
4	MeCN/EtOH (V/V=7/3)	TFA	TiO_2 - anatase	455	17
5	EtOH	TFA	TiO_2 - anatase	455	1
6	MeCN	TFA	TiO_2 - anatase	455	1
7	MeCN	TFA	-	455	1
8	MeCN	TFA	TiO_2 - anatase	365	1
9	MeCN	TFA	-	365	1

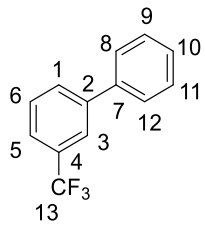

Figure 116: Structure of 3-CF_3-biphenyl **26b** with numeric labels for NMR evaluation.

R_f index (eluent: n-heptane) = 0.45

t_R(GC/MS) = 5.77 min

^{1}H-NMR (300 MHz; MeCN-d_3), δ[ppm]: 7.94 (s; 1H; H^3); 7.90 (d; 1 H; J=7.30 Hz; H^1); 7.72-7.61 (m; 4 H; $H^{5+6+8+12}$); 7.54-7.38 (m; 3 H; $H^{9+10+11}$); refer to [219]

^{13}C-NMR (75 MHz; MeCN-d_3), δ[ppm]: 141.88 (1C; C^2); 139.32 (1C; C^7); 130.82 (1C; C^4); 130.30 (1C; C^6); 129.74 (1C; C^1); 129.07 (2C; C^{9+11}); 128.20 (1C; C^{10}); 127.15 (2C; C^{8+12}); 124.4 (1C; $^1J_{C-F}$ = 270 Hz; C^{13}); 124.00 (1C; $^3J_{C-F}$ = 3.6 Hz; C^3); 123.55 (1C; $^3J_{C-F}$ = 3.6 Hz; C^5), refer to [219]

^{19}F-NMR (282 MHz; MeCN-d_3), δ[ppm]: -62.23 (s; 3F; F^{13})

MS(EI): found m/z = 152 (24%), 201 (18%), 222 ($[M]^+$, 100%); calc. for $C_{13}H_9F_3^+$ $[M]^+$: 222.0656; refer to [220]

IR (ATR)/[cm^{-1}]: 3067, 3039, 1484, 1458, 1426,1335, 1260, 1167, 1124, 900, 808, 761, 701; refer to [221]

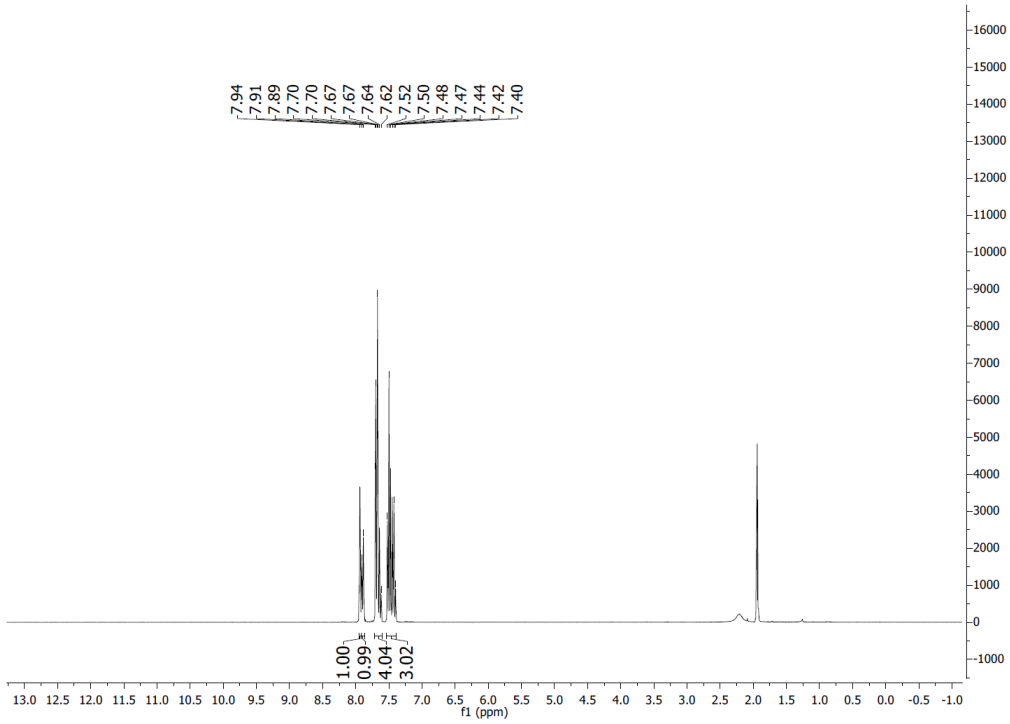

Figure 117: High-resolution ^{1}H-NMR spectrum of 3-CF_3-biphenyl in MeCN-d_3.

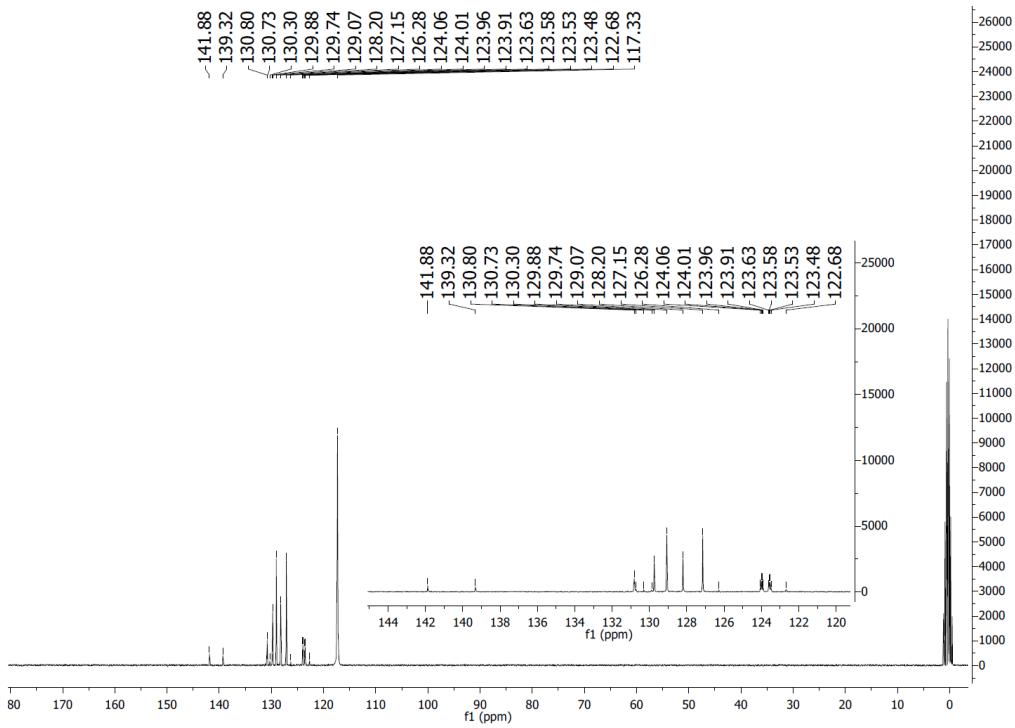

Figure 118: High-resolution ^{13}C-NMR spectrum of 3-CF_3-biphenyl in MeCN-d_3.

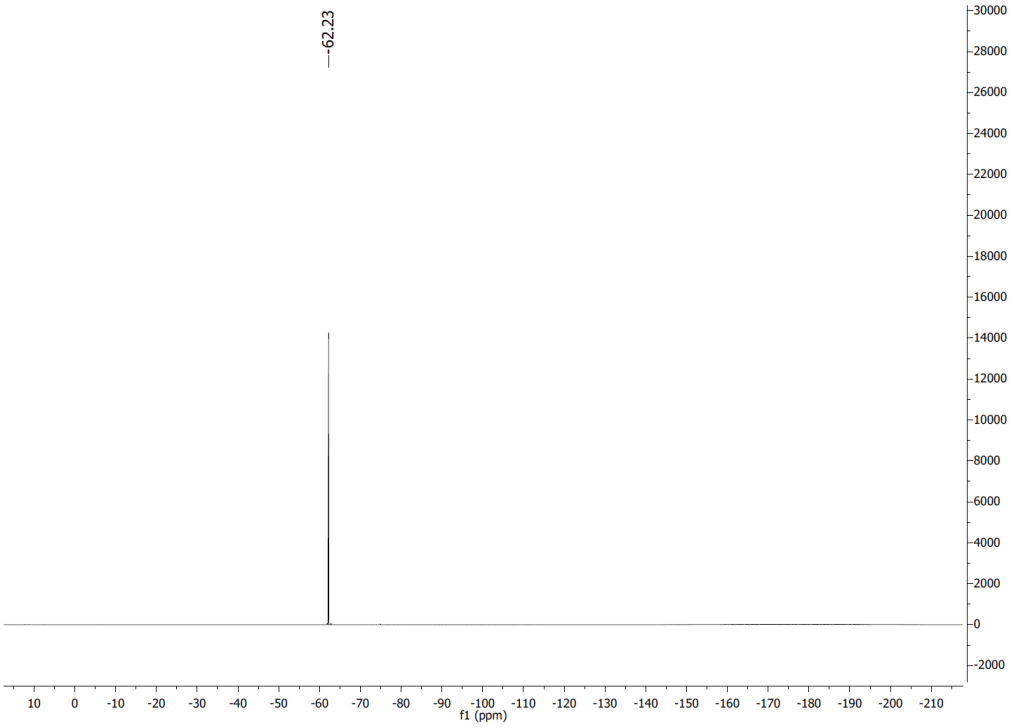

Figure 119: High-resolution ^{19}F-NMR spectrum of 3-CF_3-biphenyl in MeCN-d_3.

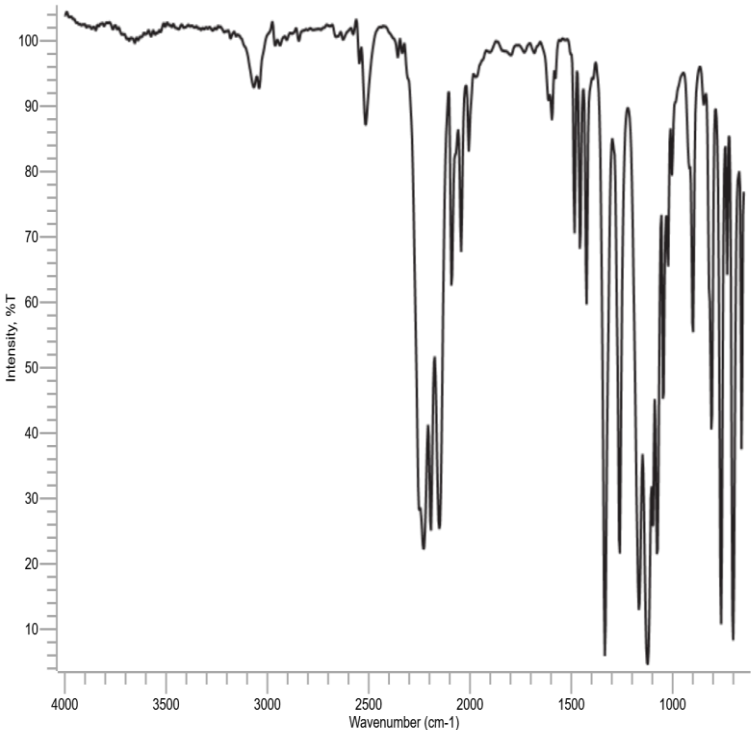

Figure 120: ATR-FTIR of 3-CF_3-biphenyl.

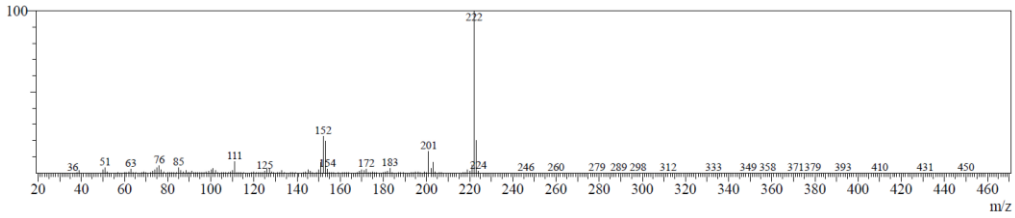

Figure 121: EI-MS spectrum of 3-CF_3-biphenyl.

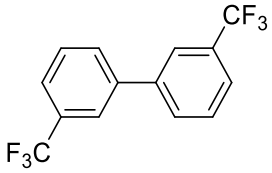

Figure 122: Structure of 3,3´-$(CF_3)_2$-biphenyl for evaluation.

R_f index (eluent: n-heptane) = 0.45

t_R(GC/MS) = 4.96 min

MS(EI): found m/z = 152 (8%), 201 (38%), 221 (10%), 290 ([M]$^+$, 100%); calc. for $C_{14}H_8F_6^+$ [M]$^+$: 290.05; refer [222]

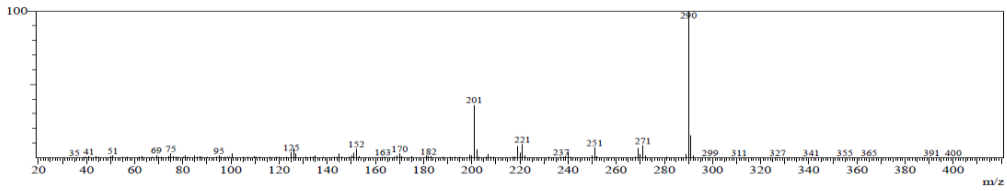

Figure 123: EI-MS spectrum of 3,3´-$(CF_3)_2$-biphenyl.

4.2.2.6 Influence of anatase and light on a batch synthesis of 26b via in-situ generated arene diazonium trifluoroacetate

In a 30 mL clear glass vial containing 3-CF_3-aniline (80.5 mg, 0.05 M), trifluoroacetic acid (57 mg, 1.0 equiv.), titanium(IV) oxide (anatase nanopowder, 40 mg) in 5 mL benzene and 5 mL acetonitrile is added dropwise *tert*-butyl nitrite (62 mg, 1.2 equiv.). The vial is sealed with a cap, stirred by a magnetic stir plate and placed ~6 cm in front of a 4×1 455 nm LED-array 6 W_{el}. By mounting the array on an aluminum heatsink for optimal heat dissipation, reaction temperature stays at RT and additional thermal effects are

avoided. After 0.5, 1, 1.5, 2, 3, 4, 5, 6, 7 and 17 h an aliquot of 50 µL is diluted with 900 µL acetonitrile and 50 µL (50 mM) DL-menthol as external standard. Quantitative GC/MS-analysis is performed after filtration with a hydrophilic 0.45 µm syringe filter. Abovementioned reaction is identically repeated by using only 455 nm irradiation as well as in abstinence of heterogeneous photocatalyst and light.

4.2.2.7 Iterative synthesis of 26b in a falling film micro reactor via a premixed reaction mixture

In a vial containing 3-CF_3-aniline (56.4 mg, 0.05 M), trifluoroacetic acid (40 mg, 1.0 equiv.), 3.5 mL benzene and 3.5 mL acetonitrile is added dropwise *tert*-butyl nitrite (43.2 mg, 1.2 equiv.) The mixture is stirred, transferred into a syringe to give Feed A, protected from light and pumped into the FFMR (P-02, 500 µL×min^{-1}). The FFMR is equipped with a reaction plate and cooled to 20 °C via a cryostat. The reaction plate has 32 microchannels with a channel architecture of 600 µm in width, 200 µm in depth and 78 mm length and carries 23 mg immobilized titanium(IV) oxide (anatase nanopowder). Titanium(IV) oxide is immobilized on the reaction plate via a slurry wash coating and calcination according to literature procedures.[31,91,218] A nitrogen gas flow of 15 mL×min^{-1} is set by a rotameter to support the outflow of the liquid stream. The liquid film is irradiated by a 4×1 455 nm LED-array 6 W_{el} with an aluminum heatsink for optimal heat dissipation. This array is placed in front of the optical window of the FFMR. The liquid phase is collected in a 100 mL flask and protected from light. After a full pass of Feed A, the liquid is transferred into the syringe via a capillary. An aliquot of 50 µL is diluted with 900 µL of acetonitrile and 50 µL (50 mM) DL-menthol as external standard and analyzed by GC/MS. This procedure is repeated twenty times. 1/16" capillaries are used to connect all components (refer to Figure 222 in the appendix).

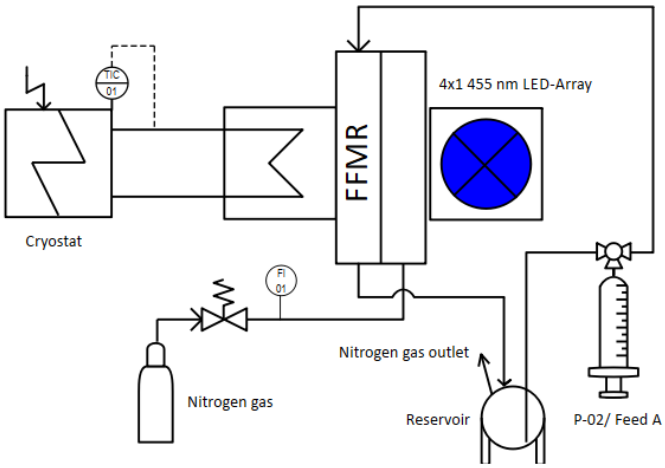

Figure 124: Setup for 3-CF_3-biphenyl synthesis in semi-batch using a falling film microreactor.

4.2.2.8 Synthesis of 26b in a semi-batch operated falling film micro reactor via an in-situ generated reaction mixture

20 mL of Feed A is prepared by dissolving 3-CF_3-aniline (644 mg, 0.2 M) and trifluoroacetic acid (456 mg, 1.0 equiv.) in acetonitrile. 20 mL of Feed B is prepared by dissolving *tert*-butyl nitrite (494 mg, 1.2 equiv.) in acetonitrile. Feed A and Feed B (P-05, P-06, 125 µL×min^{-1} each) are mixed by a T-junction and pass a residence time element (1/16" FEP capillary, 800 µm ID, 10 minutes, 20°C) before Feed C is added via a second T-junction. Feed C is neat benzene (P-07, 250 µL×min^{-1}). The mixture enters the FFMR loop via the infeed 3-way valve. The FFMR is equipped with a reaction plate and cooled to 20 °C via a cryostat. The reaction plate has 32 microchannels with a channel architecture of 600 µm in width, 200 µm in depth and 78 mm length and carries 23 mg immobilized titanium(IV) oxide (anatase nanopowder). Titanium(IV) oxide is immobilized on the reaction plate via a slurry wash coating and calcination according to literature procedures.[31,91,218] A nitrogen gas flow of 15 mL×min^{-1} is set by a rotameter to support the outflow of the liquid stream. The liquid film is irradiated by a 4×1 455 nm LED-array 6 W_{el} with an aluminum heatsink for optimal heat dissipation. The stream passes a vertically mounted glass pipette (sealed with a rubber cap and equipped with a syringe needle for nitrogen dissipation). The pipette tip is connected to the inlet of a continuously operating syringe pump P-04 (equipped with two 1 mL Hamilton glass syringes), which provides recirculation in the FFMR loop. The volume (dead volume 4 mL) of FFMR loop is exchanged at least 1.5 times via an outlet to gain a steady state. After this, infeed is closed and the solution is circulated for 2 hours. In the beginning

and the end an aliquot of 50 µL is diluted with 900 µL of acetonitrile and 50 µL (50 mM) DL-menthol as external standard and analyzed by GC/MS. 1/16" capillaries are used to connect all components.

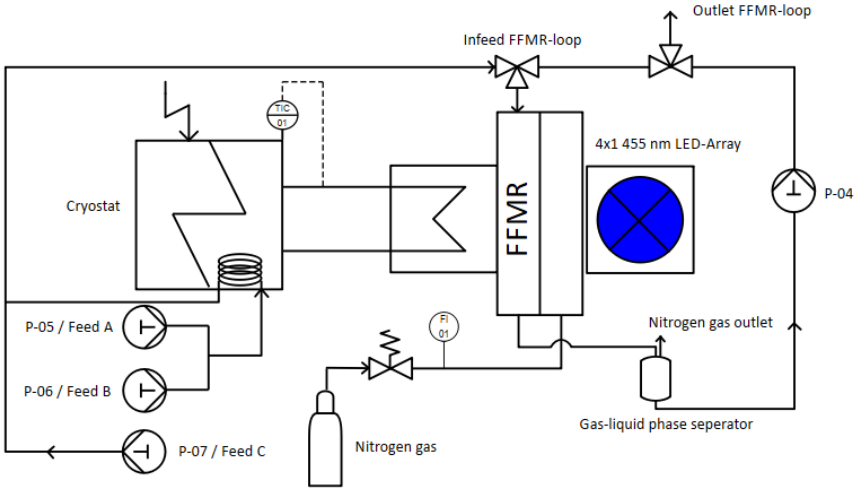

Figure 125: Setup for 3-CF_3-biphenyl synthesis in semi-batch using a falling film microreactor. The reaction mixture is generated *in-situ*. After the FFMR loop is filled, infeed is cut off for circulation.

4.2.2 Heterogeneous photocatalytic arylation in a capillary photoreactor

4.2.2.1 Batch screening reactions of 3-CF_3-biphenyl via diazo anhydrides

In a 30 mL clear glass vial containing 3-CF_3-aniline (80.5 mg, 0.05 M) in 5 mL acetonitrile and 5 mL benzene is added 1.2 equivalents *tert*-butyl nitrite (62 mg, 1.2 equiv.). The influence of a heterogeneous photocatalyst is studied by addition of 1 equivalent anatase nanopowder. Furthermore, the influence of 455 nm irradiation is tested, refer Table 29. Generally, the vials are sealed with a cap, stirred by a magnetic stir plate and placed ~6 cm in front of a 4×1 LED-array 6 W_{el} for 17 h. By mounting the array on an aluminum heatsink for optimal heat dissipation, reaction temperature stays at RT and additional thermal effects are avoided. An aliquot of 50 µL is diluted with 900 µL acetonitrile and 50 µL (50 mM) DL-menthol as external standard, after finishing the reaction. Quantitative GC/MS-analysis is performed after filtration with a hydrophilic 0.45 µm syringe filter.

Table 29: Parameters for batch screening reactions of **26b** using *in-situ* generated diazo anhydrides.

synthesis type	photo catalyst	λ [nm]	irradiation time [h]
batch	-	-	17
batch	anatase (1 equiv.)	455	17

4.2.2.2 General procedure for preparation of a catalyst slurry

The plunger of a 20 mL Braun Omnifix Luer Lock Solo syringe is removed. Anatase nanopowder and cylindrical stir bar 15×4.5 mm are added. After this, the plunger is remounted carefully and an appropriate solvent-(mixture) is soaked in. A Luer Lock cap is mounted and the syringe is placed in a vertically orientated Chemyx Nexus 6000 syringe pump (P-02). A spinning bar magnet mixes the catalyst slurry permanently (see Figure 224 to Figure 226 in the appendix).

4.2.2.3 Experiments with a gas-liquid(-solid) SMBR concept via diazo anhydrides

A HPLC pump P-07 is used to feed a liquid phase (Feed A, 0.2 mL×min^{-1}). Via a PEEK Y-junction (bore 1.6 mm) a slug flow is implemented, while nitrogen flow (0.2 mL×min^{-1}) is controlled with a mass flow controller. Via a first 3-way valve a second liquid (Feed B, P-03, 0.05 mL×min^{-1}) is added. A second 3-way valve (bore 1.6 mm) incorporates the catalyst slurry Feed C (0.05 mL×min^{-1}) into the capillary. 1/8" FEP capillaries as well as a 1/8" FEP capillary photoreactor (1.6 mm ID, 30 mL) are used in this setup. The SMBR flow passes the capillary photoreactor at 20°C. A hexagonal shaped 6×6 455 nm LED-array is placed in the center of the reactor and cooled to 20°C via a cooling finger to provide stable performance of the LEDs. When reaching steady state (>1.5×residence time), an aliquot of 50 µL is diluted with 900 µL acetonitrile and 50 µL (50 mM) DL-menthol as external standard, after finishing the reaction. Quantitative GC/MS-analysis is performed after filtration with a hydrophilic 0.45 µm syringe filter.

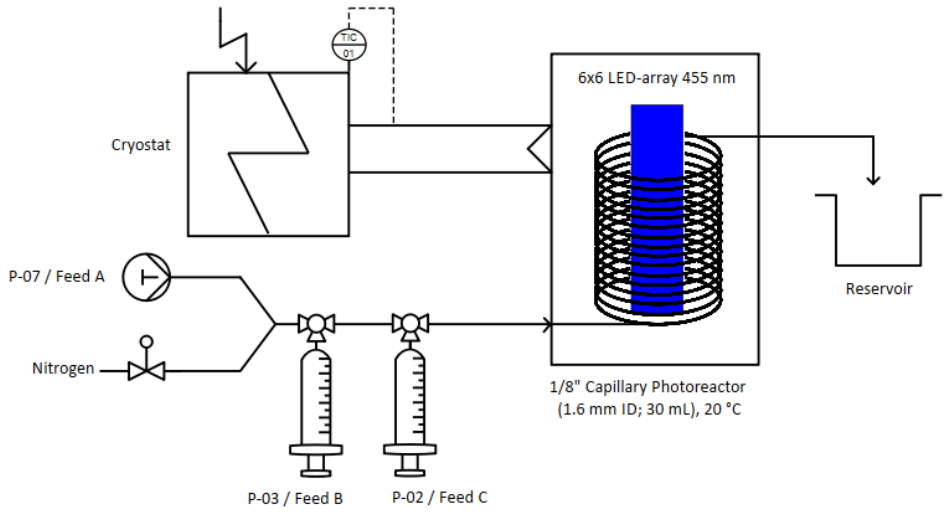

Figure 126: Setup for continuous photocatalysis using the gas-liquid(-solid) SMBR concept in a 1/8" FEP capillary photoreactor via *in-situ* generated diazo anhydride; All FEP capillaries have the dimension 1/8" (1.6 mm ID). The Y-junction as well as the two 3-way valves have a 1.6 mm bore. Nitrogen flow (0.2 mL×min^{-1}) is controlled via a mass flow controller, Liquid Feed A is pumped with P-07 (0.2 mL×min^{-1}). This generates a gas-liquid slug flow and a second Feed B (0.05 mL×min^{-1}) is added into liquid phase. The catalyst slurry Feed C (0.05 mL×min^{-1}) is constantly mixed with an attached mixing unit. After passing the photoreactor, the SMBR flow is collected and analyzed.

Table 30: Additional specifications to generate a gas-liquid(-solid) SMBR setup using *in-situ* generated diazo anhydride.

#	Feed A	Feed B	Feed C	irradiation time [h]^{a}	$P_{el,455}$ [W_{el}]
1	**b**	**c**	MeCN	1	-
2	**b**	**c**	MeCN	1	50
3	**b**	**c**	**d**	1	50

a: irradiation time calculated by flowrate; b: 75 mM 3-CF_3-aniline + 8.4 M benzene in MeCN; **c:** 360 mM *t*-BuONO in MeCN; **d:** anatase 480 mg in 5 mL ACN + 1 mL triglyme.

4.2.2.4 Experiments with a (gas-)liquid-liquid-solid SMBR concept via diazonium trifluoroacetate in a premixed catalyst slurry

Syringe pump P-01 is used to pump Fluorinert™ FC-40. Via a 3-way valve (bore 1.6 mm) the catalyst slurry Feed B is incorporated into the capillary photoreactor, giving a liquid-liquid-solid SMBR flow in the beginning. With proceeding time a fourth gaseous phase randomly elaborates. 1/16" FEP capillaries as well as a 1/16" FEP capillary photoreactor in a horizontal orientation (800 µm ID, 15 mL) are used in this setup. The SMBR flow will pass the capillary photoreactor at 20°C. A hexagonal shaped 6×6 455 nm LED-array is

placed in the center of the reactor and cooled to 20°C via a cooling finger to provide stable performance of the LEDs. When reaching steady state (>1.5×residence time), an aliquot of 50 µL is diluted with 900 µL acetonitrile and 50 µL (50 mM) DL-menthol as external standard, after finishing the reaction. Quantitative GC/MS-analysis is performed after filtration with a hydrophilic 0.45 µm syringe filter.

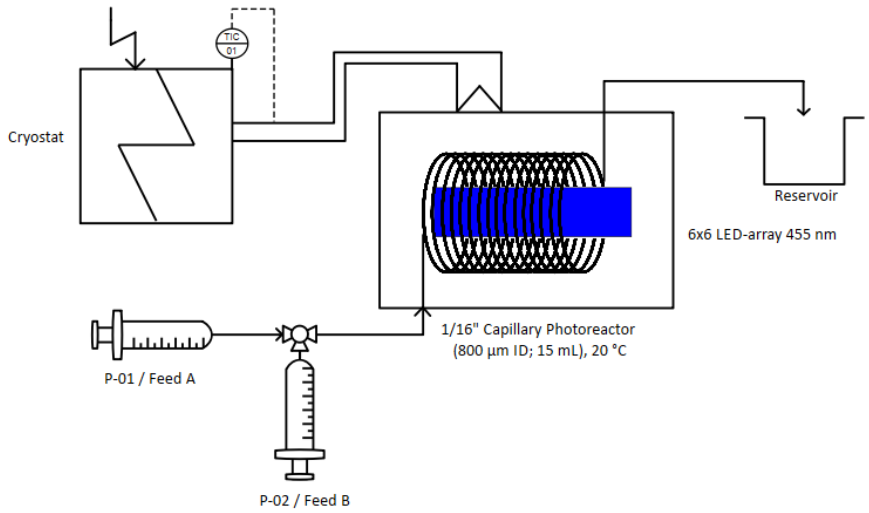

Figure 127: Setup for continuous photocatalysis with a (gas-)liquid-liquid-solid SMBR concept via diazonium trifluoroacetate in a premixed catalyst slurry; All FEP capillaries have the dimension 1/16" (800 µm ID). The 3-way valve has a 1.6 mm bore. First a liquid-liquid-solid plug flow is generated which is irradiated in a horizontally oriented 1/16" capillary photoreactor (800 µm ID, 15 mL). The catalyst slurry Feed C is constantly mixed with an attached mixing unit and contains all required components.

Table 31: Additional specifications to generate a (gas-)liquid-liquid-solid SMBR setup using diazonium trifluoroacetate in a premixed catalyst slurry.

#	Feed A	Feed B	flow rate Feed A [µL/min]	flow rate Feed A [µL/min]	irradiation time [h][a]	$P_{el,455}$ [W_{el}]
1	**b**	**c**	125.0	125.0	1	-
2	**b**	**d**	125.0	125.0	1	6
3	**b**	**d**	62.5	62.5	2	6
4	**b**	**d**	43.0	40.0	3	6

a: irradiation time calculated by flowrate; **b:** Fluorinert™ FC-40; **c:** MeCN/benzene V/V=1/1, 20 mL + 80 mg anatase; **d:** 50 mM 3-CF_3-aniline + 1.2 equiv. *t*-BuONO + 1 equiv. TFA in MeCN/benzene V/V=1/1, 20 mL + 80 mg anatase.

4.2.2.5 Experiments with a (gas-)liquid-liquid-solid SMBR concept via in-situ generated diazonium trifluoroacetate

Feed C and Feed D are mixed with two HPLC pumps and transported into a residence time element (10 min, 20 °C, 800 µm ID) to generate *in-situ* 3-CF_3-phenyldiazonium trifluoroacetate. This flow is combined via a Swagelok 1/16" T-junction with Fluorinert™ FC-40 (Feed A) to give a liquid-liquid plug flow. The catalyst slurry (Feed B) is added via a 3-way-valve (bore 1.6 mm) to give a liquid-liquid-solid SMBR flow. With proceeding time, a fourth gaseous phase randomly elaborates. 1/16" FEP capillaries as well as a 1/16" FEP capillary photoreactor (800 µm ID, 15 mL, horizontal orientation) are used in this setup. The SMBR flow will pass the capillary photoreactor at 20°C. A hexagonal shaped 6×6 LED-array is placed in the center of the reactor and cooled to 20°C via a cooling finger to provide stable performance of the LEDs. When reaching steady state (>1.5×residence time), an aliquot of 50 µL is diluted with 900 µL acetonitrile and 50 µL (50 mM) DL-menthol as external standard, after finishing the reaction. Quantitative GC/MS-analysis is performed after filtration with a hydrophilic 0.45 µm syringe filter.

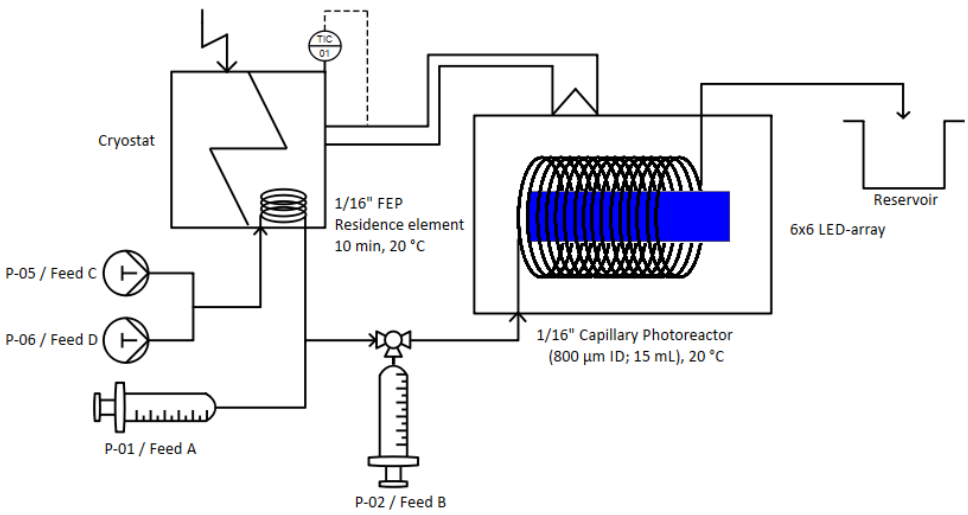

Figure 128: Setup for continuous photocatalysis with a (gas-)liquid-liquid-solid SMBR concept via *in-situ* generated diazonium trifluoroacetate; All FEP capillaries have the dimension 1/16" (800 µm ID). The 3-way valve has a 1.6 mm bore. First a liquid-liquid-solid plug flow is generated which is irradiated in a horizontally oriented 1/16" capillary photoreactor (800 µm ID, 15 mL). The catalyst slurry Feed C is constantly mixed with an attached mixing unit.

Table 32: Additional specifications to generate a (gas-)liquid-liquid-solid SMBR setup using *in-situ* generated diazonium trifluoroacetate.

#	Feed A	Feed B	Feed C	Feed D	flow rate Feed A [µL/min]	flow rate Feed B [µL/min]	flow rate Feed C + Feed D, each [µL/min]	t_R photoreactor [h][a]	wave-length [nm]	P_{el} [W_{el}]
1	-	**b**	**c**	**d**	0	500	250	0.25	-	-
2	-	**b**	**c**	**d**	0	250	125	0.5	-	-
3	-	**b**	**c**	**d**	0	62.5	31.25	2	-	-
4	-	**b**	**c**	**d**	0	500	250	0.25	455	6
5	-	**b**	**c**	**d**	0	250	125	0.5	455	6
6	-	**b**	**c**	**d**	0	62.5	31.25	2	455	6
7	-	**b**	**c**	**d**	0	500	250	0.25	455	50
8	-	**b**	**c**	**d**	0	62.5	31.25	2	455	50
9	-	**b**	**c**	**d**	0	500	250	0.25	365	50
10	-	**b**	**c**	**d**	0	250	125	0.5	365	50
11	-	**b**	**c**	**d**	0	125	62.5	1	365	50
12	-	**b**	**c**	**d**	0	63	31.25	2	365	50
13	-	**b**	**c**	**d**	0	42	20.8	3	365	50
14	**e**	**b**	**c**	**d**	400	300	150	0.25	365	50
15	**e**	**b**	**c**	**d**	25	50	25	2	365	50
16	**e**	**f**	**g**	**h**	50	132	34	1	365	50
17	**e**	**f**	**g**	**h**	100	264	64	0.5	455	6
18	**e**	**f**	**g**	**h**	50	132	34	1	455	6
18	**e**	**f**	**g**	**h**	25	66	17	2	455	6
19	**e**	**f**	**g**	**h**	25	66	17	2	455	50

a: irradiation time calculated by flow rate; **b:** neat benzene; **c:** 0.2 M 3-CF_3-aniline + 0.2 M TFA in MeCN; **d:** 0.24 M *t*-BuONO in MeCN; **e:** Fluorinert™ FC-40; **f:** 60 mg anatase in 10 mL benzene + 5 mL MeCN; **g:** 0.3 M 3-CF_3-aniline + 0.3 M TFA in MeCN; **h:** 0.36 M *t*-BuONO in MeCN.

4.2.3 Catalyst-free photochemical direct C-H arylation in a capillary photoreactor using arene diazonium trifluoroacetates and its process optimization

4.2.3.1 Standard working procedure for catalyst-free continuous synthesis of bi-(hetero-)arenes

This procedure describes all process development including temperature-sensitive investigations or experiments in dependency of trifluoroacetic acid. Moreover, experiments applying an excess pressure to the reactor are mentioned. Required feed solutions are prepared according to Table 33 using appropriate solvents. Feed A and B are mixed via a T-junction and transported with syringe pumps. Feed C is transported using a HPLC pump. If diazonium trifluoroacetates are generated, solution will pass a residence element (1/16" FEP (800 µm ID, 10 min), which is protected from light and cooled to 20 °C. This residence element is placed in the cryostat reservoir, unless

temperature-depended experiments are conducted. In those cases, the element is cooled to 20°C in a beaker. Via a second T-junction Feed-C (neat benzene) is added before entering the 1/16" FEP capillary photoreactor. Reaction mixture is directly collected in a reservoir when leaving the reactor outlet in setup #1 (Figure 129). If an excess pressure has to be applied onto the reactor system, a proportional relief valve and a manometer is added, giving setup #2 (Figure 130). Here, it is necessary to replace the syringe pumps by HPLC pumps to maintain pressure stability.

In some cases, diazonium tetrafluoroborates are used as starting material. For this reason, Feed C and the residence element can be dispensed. Feed A and B enter the photoreactor directly after mixing.

A hexagonal shaped 6×6 LED-array is placed in the center of the reactor and cooled to 20°C via a cooling finger to provide stable performance of the LEDs. When reaching steady state (>1.5×residence time), an aliquot of 50 µL is diluted with 900 µL acetonitrile and 50 µL (50 mM) DL-menthol as external standard. Quantitative analysis is performed via GC/MS. Experiments at higher concentrations (0.2 M) concentrations are diluted by a factor of four, before 50 µL of this aliquot are prepared for GC/MS analysis. All additional parameters are listed in Table 33.

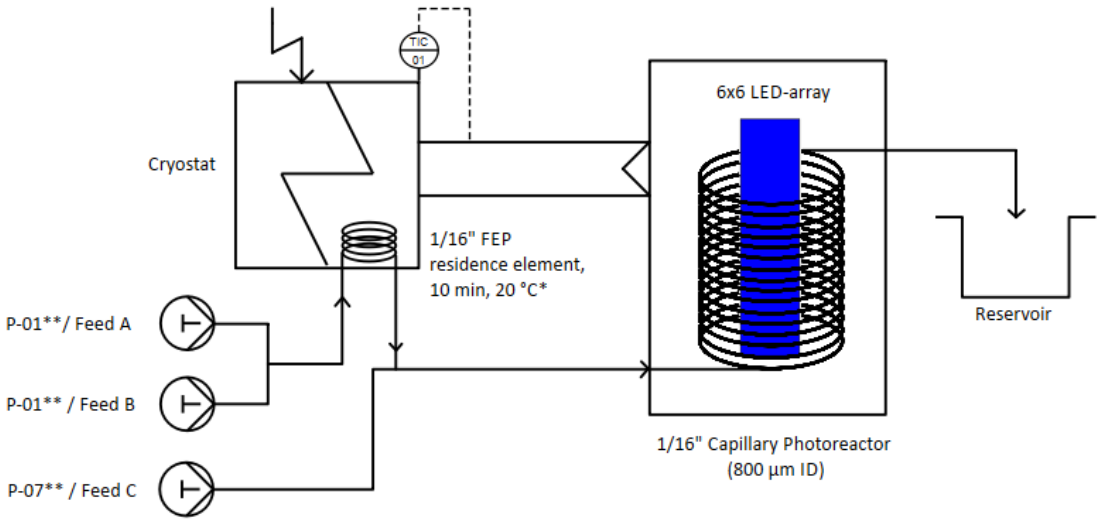

Figure 129: Setup #1 for continuous catalyst-free synthesis of 3-CF_3-biphenyl with a 1/16" FEP capillary photoreactor under standard atmosphere; * Residence element is cooled to 20 °C in a separate water bath and protected from light in case of temperature-sensitive experiments; ** Setup is used for homogeneous photocatalysis including 1mol% eosin Y as well: Feed A and B are pumped with P-05 and P-06 mixed with a T-junction and enter the photoreactor directly; Feed C not in use.

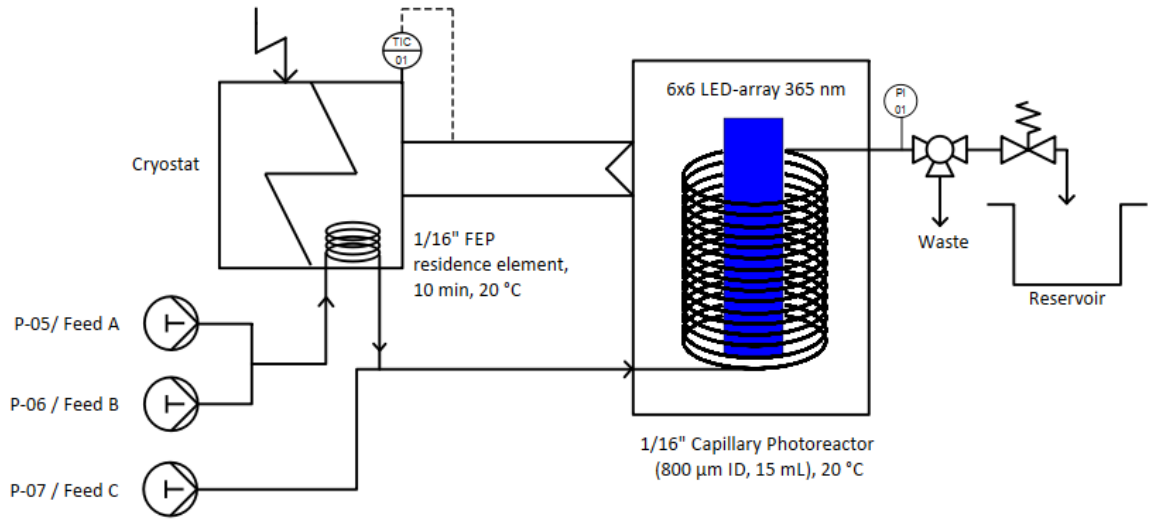

Figure 130: Setup #2 for continuous catalyst-free synthesis of 3-CF_3-biphenyl with a 1/16" FEP capillary photoreactor using excess pressure for precise control of residence and irradiation time.

Table 33: Parameters and additional information for continuous catalyst-free synthesis of **26b** in a 1/16" FEP capillary photoreactor.

#	setup	Feed A	Feed B	Feed C	flow rate Feed A, Feed B [µL×min^{-1}]	flow rate Feed C, [µL×min^{-1}]	$V_{reactor}$ [mL]	λ [nm]	P [W_{el}]	T [°C]	t_R [h][a]	p_{exs} [bar]
1	#1[b]	**c**	**d**	**e**	62.5	125	15	-	-	20	1.00	-
2	#1[b]	**c**	**d**	**e**	62.5	125	15	-	-	30	1.00	-
3	#1[b]	**c**	**d**	**e**	62.5	125	15	-	-	40	1.00	-
4	#1	**c**	**d**	**e**	250	500	15	365	7	20	0.25	-
5	#1	**c**	**d**	**e**	125	250	15	365	7	20	0.50	-
6	#1	**c**	**d**	**e**	62.5	125	15	365	7	20	1.00	-
7	#1	**c**	**d**	**e**	31.25	62.5	15	365	7	20	2.00	-
8	#1	**f**	**d**	**e**	62.5	125	15	365	50	20	1.00	-
9	#1	**g**	**d**	**e**	62.5	125	15	365	50	20	1.00	-
10	#1	**h**	**d**	**e**	62.5	125	15	365	50	20	1.00	-
11	#1	**k**	**d**	**e**	62.5	125	15	365	50	20	1.00	-
12	#1	**l**	**d**	**e**	62.5	125	15	365	50	20	1.00	-
13	#1	**m**	**d**	**e**	62.5	125	15	365	50	20	1.00	-
14	#1	**k**	**d**	**e**	250	500	15	365	50	20	0.25	-
15	#1	**k**	**d**	**e**	125	250	15	365	50	20	0.50	-
16	#1	**k**	**d**	**e**	62.5	125	15	365	50	20	2.00	-
17	#2	**k**	**d**	**e**	1500	3000	15	365	50	20	0.04	4
18	#2	**k**	**d**	**e**	500	1000	15	365	50	20	0.13	4
19	#2	**k**	**d**	**e**	370	740	15	365	50	20	0.17	4
20	#2	**k**	**d**	**e**	250	500	15	365	50	20	0.25	4
21	#2	**k**	**d**	**e**	160	320	15	365	50	20	0.40	4
22	#2	**k**	**d**	**e**	125	250	15	365	50	20	0.50	4
23	#2	**k**	**d**	**e**	71	142	15	365	50	20	0.88	4
24	#2	**k**	**d**	**e**	62.5	125	15	365	50	20	1.00	4
25	#2	**k**	**d**	**e**	62.5	125	15	365	50	20	1.00	0.28
26	#2	**k**	**d**	**e**	62.5	125	15	-	-	20	1.00	4

#	setup	Feed A	Feed B	Feed C	flow rate Feed A, Feed B [µL×min^{-1}]	flow rate Feed C, [µL×min^{-1}]	$V_{reactor}$ [mL]	λ [nm]	P [W_{el}]	T [°C]	t_R [h][a]	p_{exs} [bar]
27	#2	**k**	**d**	**e**	50	100	15	365	50	20	1.25	4
28	#2	**n**	**o**	**e**	62.5	125	15	365	50	20	1.00	6.4
29	#2	**n**	**o**	**e**	62.5	125	15	365	50	20	1.00	15.7
30	#2	**n**	**o**	**e**	62.5	125	15	365	50	20	1.00	17
31	#2	**n**	**o**	**e**	42	83	15	365	50	20	1.50	17
32	#2	**n**	**o**	**e**	50	100	15	365	50	20	1.25	17
33	#2	**n**	**o**	**e**	71	142	15	365	50	20	0.88	17
34	#2	**n**	**o**	**e**	142	284	15	365	50	20	0.44	17
35	#2	**n**	**o**	**e**	50	100	15	365	37.5	20	1.25	17
36	#2	**n**	**o**	**e**	50	100	15	365	25	20	1.25	17
37	#2	**n**	**o**	**e**	50	100	15	-	-	20	1.25	17
38	#2	**n**	**o**	**p**	42	83	15	365	50	20	1.50	17
39	#2	**n**	**o**	**p**	50	100	15	365	50	20	1.25	17
40	#2	**n**	**o**	**p**	71	142	15	365	50	20	0.88	17
41	#2	**n**	**o**	**p**	142	284	15	365	50	20	0.44	17
42	#1	**q**	**r**	-	100	-	15	365	50	20	1.25	-
43	#1	**s**	**r**	-	100	-	15	365	50	20	1.25	-
44	#1[t]	**u**	**v**	-	400	-	30	520	32	20	0.62	-
45	#1[t]	**u**	**w**	-	400	-	30	520	32	20	0.62	-

a: residence time calculated by flowrate; **b:** residence element for *in-situ* generation of diazo compound cooled to 20°C in a beaker; **c:** 0.2 M 3-CF_3-aniline + 0.2 M TFA in MeCN; **d:** 0.24 M *t*-BuONO in MeCN; **e:** benzene; **f:** 0.2 M 3-CF_3-aniline in MeCN; **g:** 0.2 M 3-CF_3-aniline + 0.1 M TFA in MeCN; **h:** 0.2 M 3-CF_3-aniline + 0.3 M TFA in MeCN; **k:** 0.2 M 3-CF_3-aniline + 0.4 M TFA in MeCN; **l:** 0.2 M 3-CF_3-aniline + 0.6 M TFA in MeCN; **m:** 0.2 M 3-CF_3-aniline + 0.8 M TFA in MeCN; **n:** 0.8 M 3-CF_3-aniline + 1.6 M TFA in MeCN; **o:** 0.96 M *t*-BuONO in MeCN; **p:** 8.0 M benzene in MeCN; **q:** 0.4 M 3-CF_3-aniline + 4.0 M benzene in MeCN; **r:** 0.48 M *t*-BuONO in MeCN; **s:** 0.4 M 4-chloroaniline + 4.0 M furan in MeCN; **t:** HPLC- instead of syringe-pumps; **u:** 0.4 M 3-CF_3-phenyldiazonium tetrafluoroborate **25** in DMSO; **v:** 4.0 M furan + 1mol% eosin Y in DMSO; **w:** 4.0 M benzene + 1mol% eosin Y in DMSO.

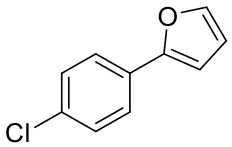

Figure 131: Structure of 2-(4-chlorophenyl)furan **24a** for evaluation.

R_f index (eluent: CH:EA 95:5) = 0.34

t_R(GC/MS) = 6.8 min

MS(EI): found m/z = 89 (12%), 115 (73%), 149 (39%), 178 ([M]$^+$, 100%); calc. for $C_{14}H_8F_6^+$ [M]$^+$: 178.02; refer to [223]

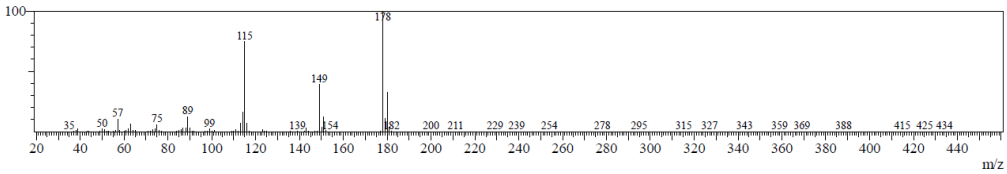

Figure 132: EI-MS spectrum of 2-(4-chlorophenyl)furan.

2-(3-CF_3-phenyl)furan **26a**, entry #44, is purified via the following procedure: 10 mL of the dark yellow reaction solution is collected in one vessel and stirred into cold water (100 mL). The resulting suspension is extracted with ethyl acetate (3 x 40 mL). The organic phases are combined, washed with water (2x 25 mL) and dried with sodium sulfate. Product is purified with column chromatography (eluent: CH) to give 16% of **26a** as a colorless liquid.

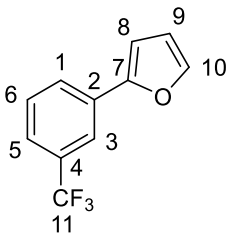

Figure 133: Structure of 2-(3-CF_3-phenyl)furan with numeric labels for NMR evaluation.

R_f index (eluent: CH) = 0.42

Purification: column chromatography (eluent: CH)

t_R(GC/MS) = 4.19 min

MS(EI): found m/z = 115 (60%), 183 (50%), 212 ([M]$^+$, 100%); calc. for $C_{11}H_7F_3O^+$ [M]$^+$: 212.04; refer to [224]

IR (ATR)/[cm^{-1}]: 3067, 1735, 1334, 1173, 1130, 1074, 810, 699; refer to [224]

^{1}H-NMR (300 MHz; $CDCl_3$), δ[ppm]: 7.92 (s; 1H; H^{11}); 7.83 (ddd; 1 H; J=5.56, 4.28, 1.83 Hz; H^3); 7.50 (dt; 3 H; J=4.97, 0.98 Hz; H^{1+5+6}); 6.74 (dd; 1 H; J=3.40, 0.78 Hz; H^8); 6.51 (dd; 1 H; J=3.40, 1.82 Hz; H^9); refer to [31]

^{13}C-NMR (75 MHz; $CDCl_3$), δ[ppm]: 152.62 (1C; C^7); 142.95 (1C; C^{10}); 131.67 (1C; C^2); 131.11 (1C; C^4); 129.32 (1C; C^6); 126.92 (1C; C^1); 126.00 (1C; $^1J_{C-F}$ = 279.75 Hz; C^{11}); 123.92 (1C; $^3J_{C-F}$ = 4.26 Hz; C^3); 120.66 (1C; $^3J_{C-F}$ = 4.26 Hz; C^5); 112.04 (1C; C^9); 106.45 (1C; C^8); refer to [31]

^{19}F-NMR (282 MHz; $CDCl_3$), δ[ppm]: -62.90 (s; 3F; F^{11}); refer to [31]

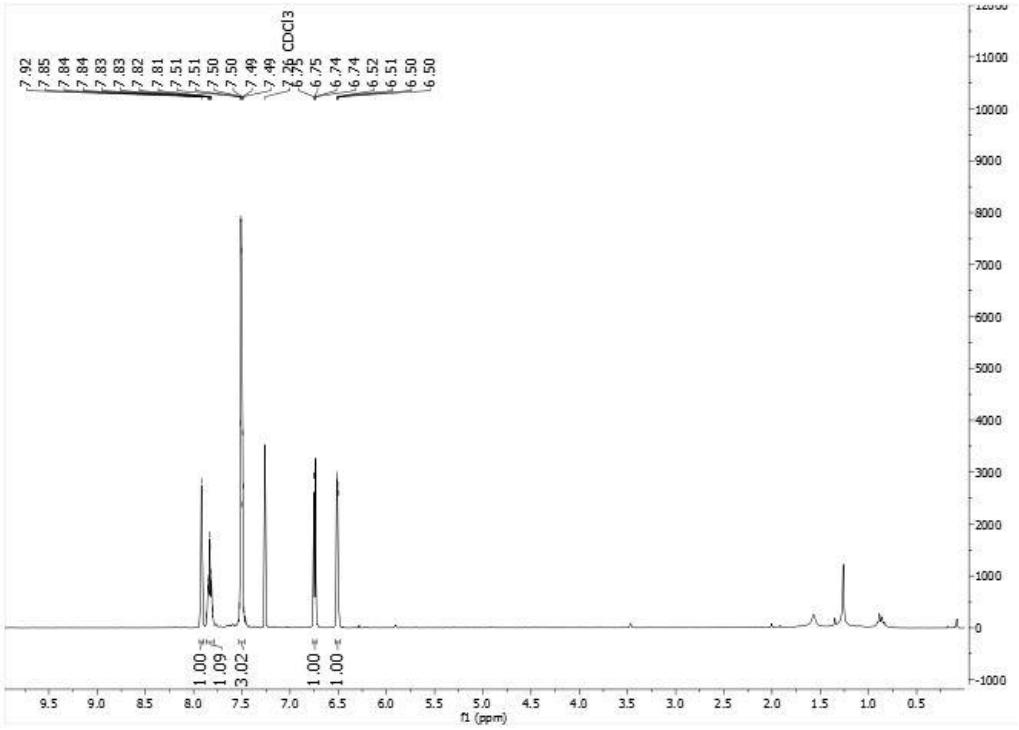

Figure 134: High-resolution ^{1}H-NMR spectrum of 2-(3-CF_3-phenyl)furan in $CDCl_3$.

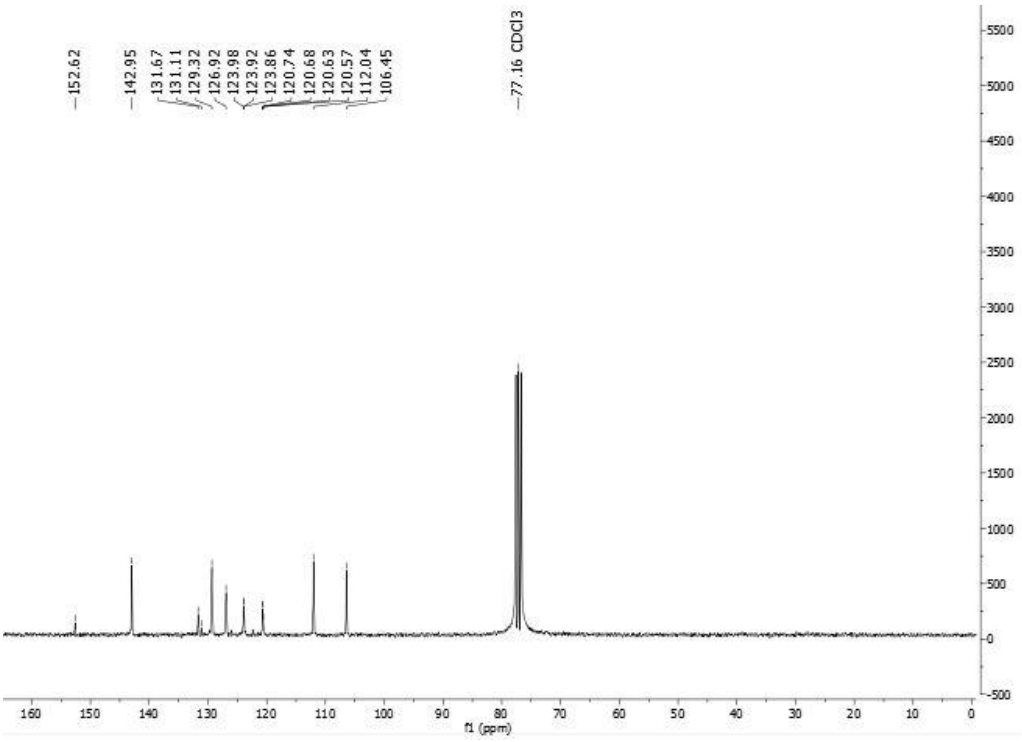

Figure 135: High-resolution ^{13}C-NMR spectrum of 2-(3-CF_3-phenyl)furan in $CDCl_3$.

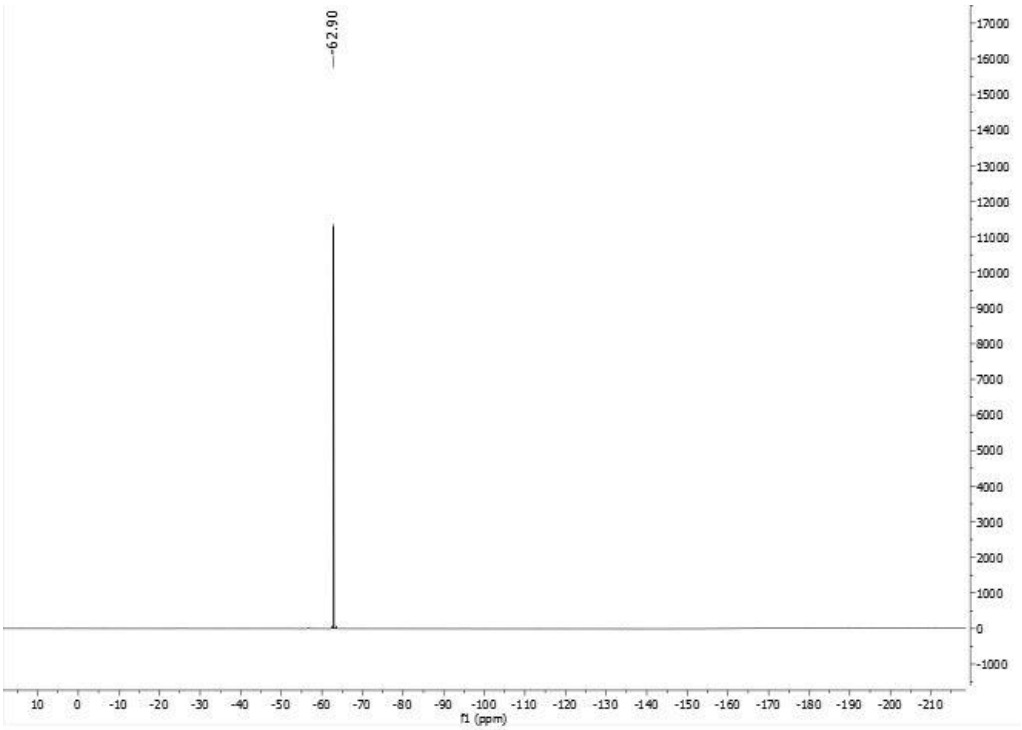

Figure 136: High-resolution ^{19}F-NMR spectrum of 2-(3-CF_3-phenyl)furan in $CDCl_3$.

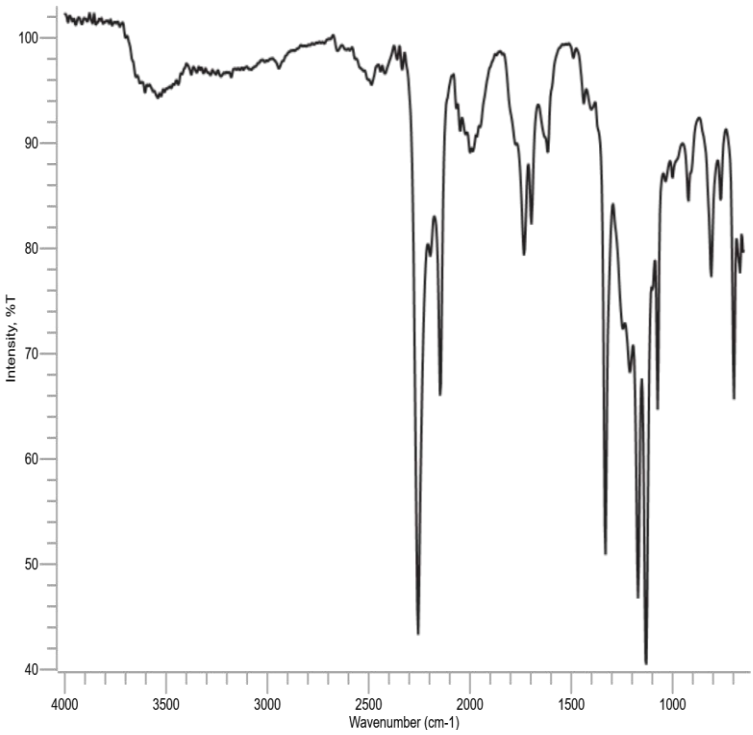

Figure 137: ATR-FTIR of 2-(3-CF_3-phenyl)furan.

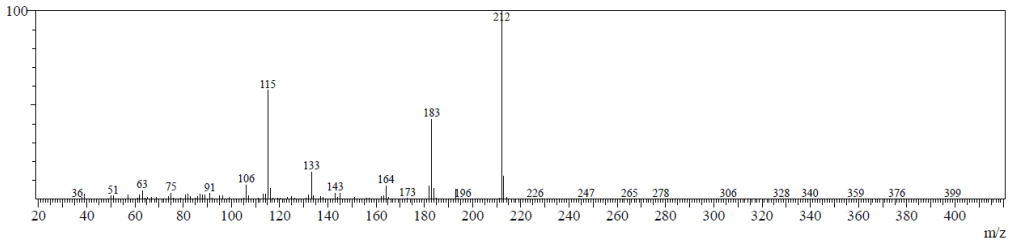

Figure 138: EI-MS spectrum of 2-(3-CF_3-phenyl)furan.

4.2.3.2 Colorization experiments of in-situ diazo compound generation

Seven different solutions (1 mL) of 200 mM 3-CF_3-aniline in acetonitrile containing 0, 0.5, 1, 1.5, 2, 3 and 4 equivalents of trifluoroacetic acid are prepared. Each solution is mixed with 1 mL 240 mM *tert*-butyl nitrite. Preparation of those seven mixtures is proceeded quickly for simultaneous visual observation. Mixtures are stirred with a magnetic stirrer and the reaction is monitored after 1, 3 and 20 minutes.

4.2.3.3 Batch-synthesis of 26b via optimized parameters

In a 30 mL clear glass vial containing 3-CF_3-aniline (322 mg, 0.2 M), trifluoroacetic acid (456 mg, 2.0 equiv.) in 5 mL benzene and 5 mL acetonitrile is added 1.2 equivalents *tert*-butyl nitrite (247 mg, 1.2 equiv.). The vial is sealed with a cap, stirred by a magnetic stir plate and placed ~6 cm in front of a 4×1 365 nm LED-array 6 W_{el}. By mounting the array on an aluminum heatsink for optimal heat dissipation, reaction temperature stays at RT and additional thermal effects are avoided. An aliquot of 200 µL is diluted with 600 µL acetonitrile. 50 µL of this sample are diluted with 900 µL acetonitrile and 50 µL (50 mM) DL-menthol as external standard. Quantitative GC/MS-analysis is performed after 0.25, 0.5, 1.0, 2.0, 3.0 h and 17 h.

4.2.3.4 Batch-synthesis of 26b using trimethylsilyl trifluoroacetate for diazotation

In a 30 mL clear glass vial containing 3-CF_3-aniline (161 mg, 0.2 M), trimethylsilyl trifluoroacetate (2.0 equiv.; 372 mg) in 2.5 mL benzene and 2.5 mL acetonitrile is added 1.2 equivalents *tert*-butyl nitrite (1.2 equiv.; 123 mg). The vial is sealed with a cap, stirred by a magnetic stir plate and placed ~6 cm in front of a 4×1 365 nm LED-array

6 W_{el}. By mounting the array on an aluminum heatsink for optimal heat dissipation, reaction temperature stays at RT and additional thermal effects are avoided. An aliquot of 200 µL is diluted with 600 µL acetonitrile. 50 µL of this sample are diluted with 900 µL acetonitrile and 50 µL (50 mM) DL-menthol as external standard. Quantitative GC/MS-analysis is performed after 17 h.

4.2.3.5 Standard procedure for experiments considering ^{19}F-NMR spectroscopy and scope evaluation

Required feed solutions are prepared according to Table 34 using acetonitrile as solvent solvents. Feed A and B are mixed via a T-junction and transported by HPLC pumps. Diazonium trifluoroacetate is generated *in-situ* when passing a residence element (1/16" FEP, 800 µm ID, 10 min), which is protected from light and cooled to 20 °C. This residence element is placed in the cryostat reservoir. Via a second T-junction Feed-C (arene) is added before entering the 1/16" FEP capillary photoreactor (800 µm ID, 15 mL, 20 °C).

The reactor outlet is connected to the PEEK flow cell of the benchtop Nanalysis NMReady60 pro for ^{19}F-NMR spectroscopy. Following settings are applied at the spectrometer: 64 scans, 80.49° pulse, 1.9 s acquisition time and 2.9 s repetition time, recently shimmed. The whole setup is pressurized to 17 bar_{exs} with a proportional relief valve. A manometer is used to monitor the pressure.

A hexagonal shaped 6×6 LED-array 365 nm is placed in the center of the reactor and cooled to 20°C via a cooling finger to provide stable performance of the LEDs. When reaching steady state (>1.5×residence time), an aliquot of 200 µL is diluted with 600 µL acetonitrile. 50 µL of this sample are diluted with 900 µL acetonitrile and 50 µL (50 mM) DL-menthol as external standard. Quantitative analysis is performed via GC/MS and inline ^{19}F NMR-spectroscopy. 5 mL of the raw product mixture are collected for further purification and characterization. The solvent and the excess amount of arene is removed under reduced pressure. The remaining substance is purified with column chromatography as mentioned in the substance characterizations below.

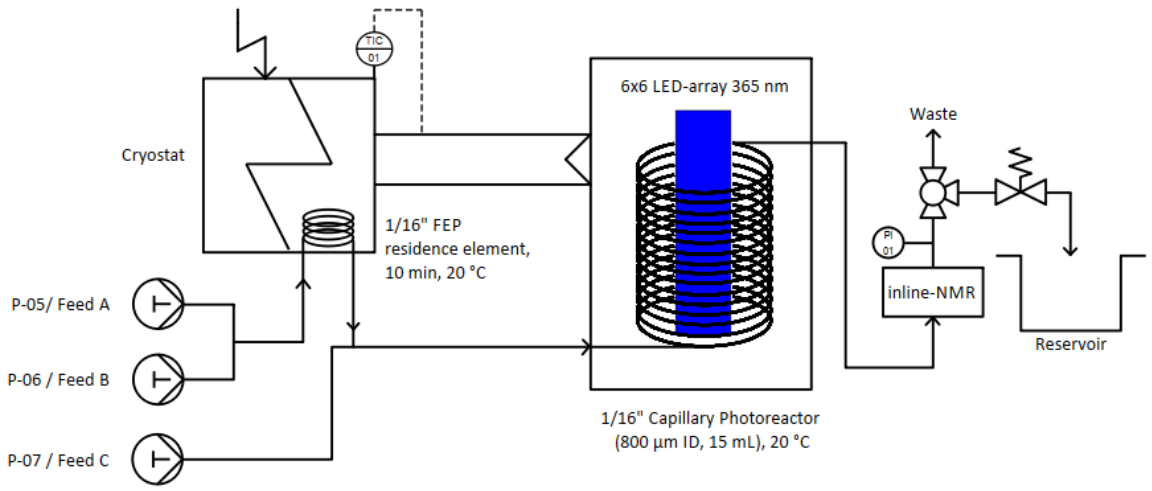

Figure 139: Setup for continuous catalyst-free biphenyl synthesis and online ^{19}F-NMR spectroscopy.

Table 34: Parameters and additional information for continuous catalyst-free biphenyl synthesis and online ^{19}F-NMR spectroscopy.

#	setup	Feed A	Feed B	Feed C	flow rate Feed A, Feed B [µL×min^{-1}]	flow rate Feed C, [µL×min^{-1}]	*P* [W_{el}]	*T* [°C]	t_R [h]^a
1	**b**	**c**	**d**	50	100	15	25	20	1.25
2	**b**	**c**	**d**	50	100	15	37.5	20	1.25
3	**b**	**c**	**d**	50	100	15	50	20	1.25
4	**b**	**c**	**e**	50	100	15	50	20	1.25
5	**b**	**c**	**f**	50	100	15	50	20	1.25
6	**b**	**c**	**g**	50	100	15	50	20	1.25
7	**b**	**c**	**h**	50	100	15	50	20	1.25
8	**b**	**c**	**i**	50	100	15	50	20	1.25
9	**b**	**c**	**k**	50	100	15	50	20	1.25
10	**b**	**c**	**l**	50	100	15	50	20	1.25
11	**b**	**c**	**m**	50	100	15	50	20	1.25
12	**b**	**c**	**n**	50	100	15	50	20	1.25
13	**o**	**c**	**d**	50	100	15	50	20	1.25
14	**b**	**c**	**p**	50	100	15	50	20	1.25
15	**b**	**c**	**q**	50	100	15	50	20	1.25

a: residence time calculated by flowrate; **b:** 0.8 M 3-CF_3-aniline + 1.6 M TFA in MeCN; **c:** 0.96 M *t*-BuONO in MeCN; **d:** neat benzene; **e:** neat furan; **f:** neat fluorobenzene; **g:** neat chlorobenzene; **h:** neat bromobenzene; **i:** neat 1-bromo-4-fluoro-benzene; **k:** neat *tert*-butylbenzene; **l:** neat anisole; **m:** neat *p*-xylene; **n:** neat toluene; **o:** 0.8 M 4-fluoro-aniline **31** + 1.6 M TFA in MeCN; **p:** neat ethyl benzoate; **q:** 4.5 M phenylboronic acid pinacol ester in MeCN.

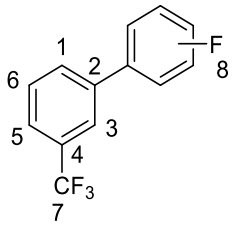

Figure 140: Structure of *o*,*m*,*p*-fluoro-3´-CF_3-biphenyl **26c** (55%:16%:29%) with numeric labels for NMR evaluation.

Experimental data of all isomers:

R_f index (eluent: CH) = 0.45

Purification: column chromatography (eluent: CH)

MS(EI): found m/z = 170 (15%), 219 (10%), 240 ($[M]^+$, 100%); calc. for $C_{13}H_8F_4^+$ $[M]^+$: 240.06

IR (ATR)/[cm^{-1}]: 3069, 1613, 1588, 1487, 1461, 1428, 1335, 1164, 1126, 1070, 904, 844, 807, 790, 762, 701

Experimental data of 2-fluoro-3´-CF_3-biphenyl:

t_R(GC/MS) = 5.64 min

^{19}F-NMR (282 MHz; $CDCl_3$), δ[ppm]: -62.17 (s; 3F; F^7); -117.63 (m; F; F^8)

Experimental data of 3-fluoro-3´-CF_3-biphenyl:

t_R(GC/MS) = 5.88 min

^{19}F-NMR (282 MHz; $CDCl_3$), δ[ppm]: -63.82 (s; 3F; F^7); -113.98 (m; F; F^8)

Experimental data of 4-fluoro-3´-CF_3-biphenyl:

t_R(GC/MS) = 5.79 min

^{19}F-NMR (282 MHz; $CDCl_3$), δ[ppm]: -63.84 (s; 3F; F^7); -112.06 (m; F; F^8)

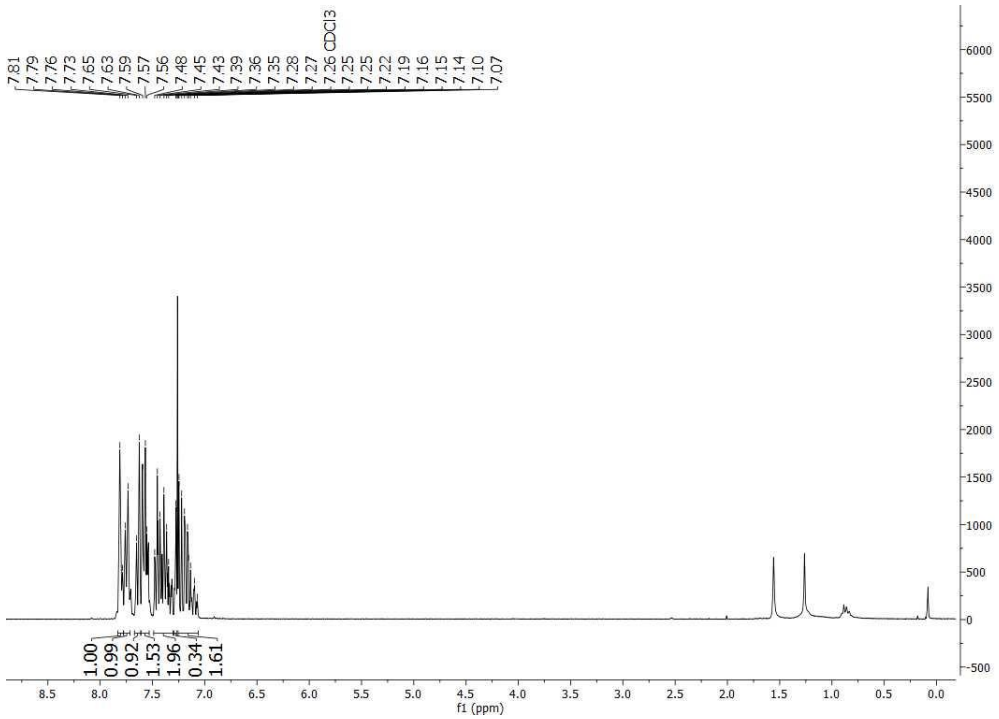

Figure 141: High-resolution ^{1}H-NMR spectrum of *o*,*m*,*p*-fluoro-3´-CF_3-biphenyl (mixture of isomers) in $CDCl_3$.

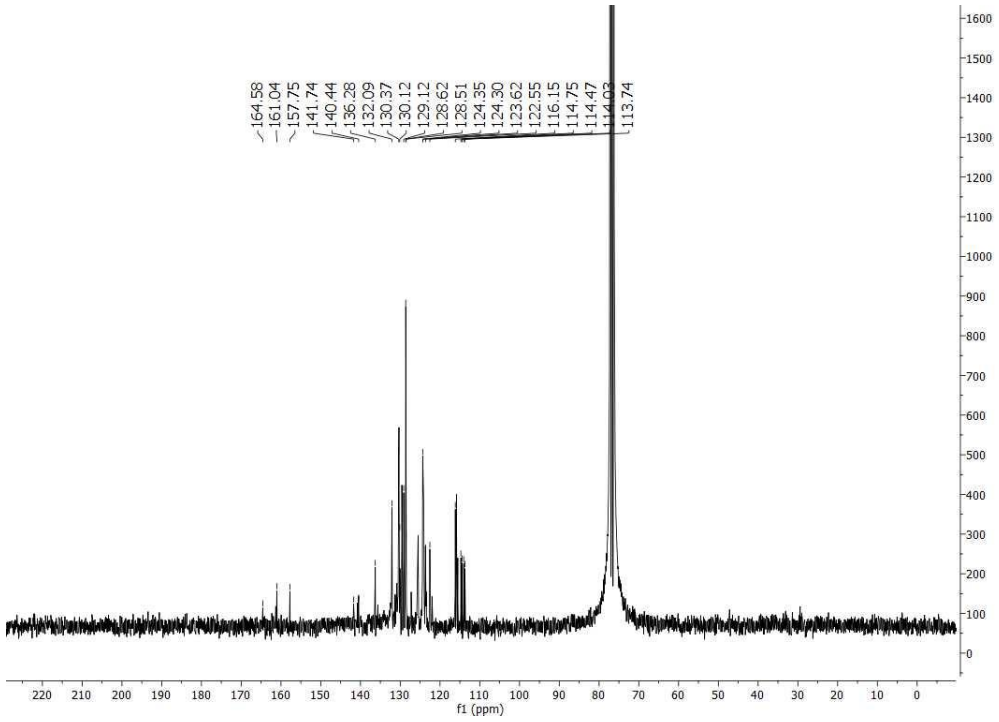

Figure 142: High-resolution ^{13}C-NMR spectrum of *o*,*m*,*p*-fluoro-3´-CF_3-biphenyl (mixture of isomers) in $CDCl_3$.

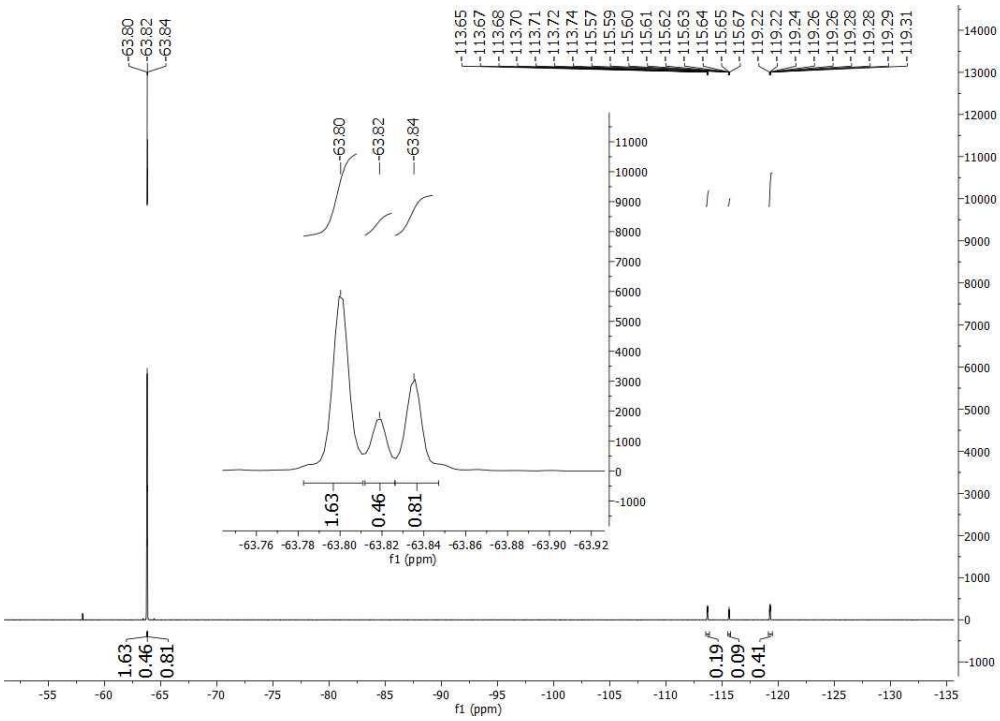

Figure 143: High-resolution ^{19}F-NMR spectrum of *o*,*m*,*p*-fluoro-3´-CF_3-biphenyl (mixture of isomers) in $CDCl_3$.

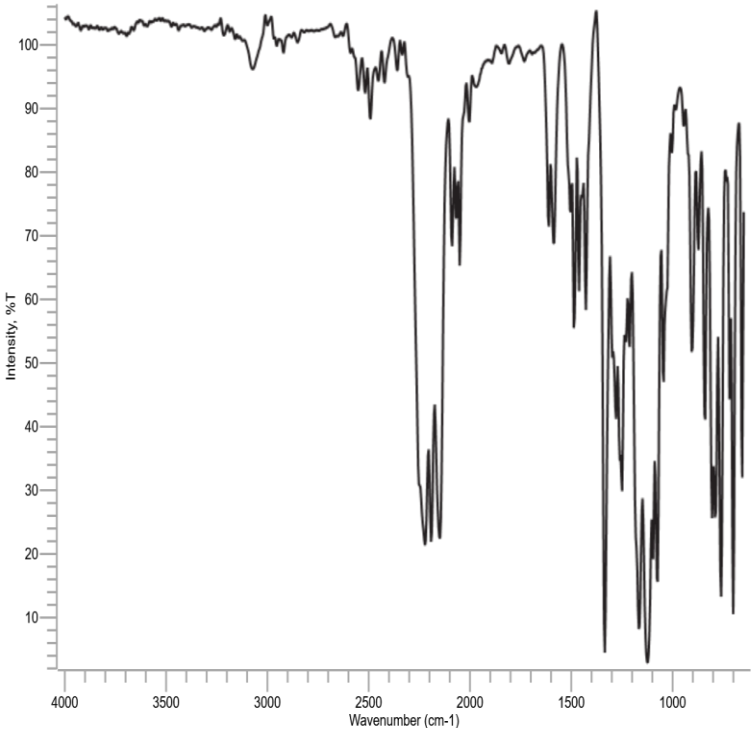

Figure 144: ATR-FTIR of *o*,*m*,*p*-fluoro-3´-CF_3-biphenyl (mixture of isomers).

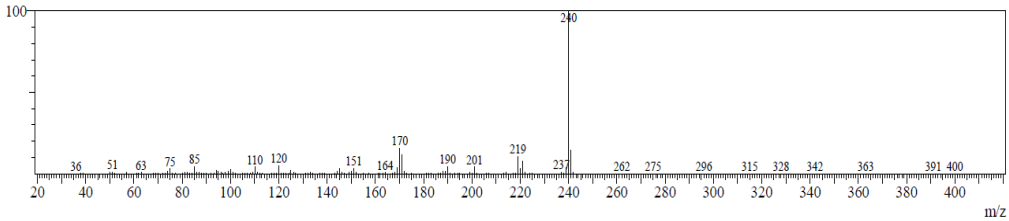

Figure 145: EI-MS spectrum of *o,m,p*-fluoro-3´-CF_3-biphenyl.

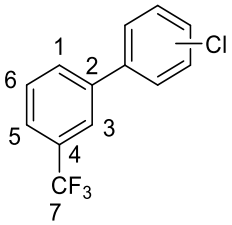

Figure 146: Structure of *o,m,p*-chloro-3´-CF_3-biphenyl **26d** (59%:18%:23%) with numeric labels for NMR evaluation.

Experimental data of all isomers:

R_f index (eluent: CH) = 0.45

Purification: column chromatography (eluent: CH)

MS(EI): found m/z = 152 (25%), 201 (21%), 256 ([M]$^+$, 100%); calc. for $C_{13}H_8ClF_3^+$ [M]$^+$: 256.03

IR (ATR)/[cm^{-1}]: 3069, 1741, 1475, 1441, 1332, 1261, 1167, 1126, 1074, 906, 806, 770, 701

Experimental data of 2-chloro-3´-CF_3-biphenyl:

t_R(GC/MS) = 7.25 min

^{19}F-NMR (282 MHz; $CDCl_3$), δ[ppm]: -62.60 (s; 3F; F^7)

Experimental data of 3-chloro-3´-CF_3-biphenyl:

t_R(GC/MS) = 7.76 min

^{19}F-NMR (282 MHz; $CDCl_3$), δ[ppm]: -62.68 (s; 3F; F^7)

Experimental data of 4-chloro-3´-CF_3-biphenyl:

t_R(GC/MS) = 7.69 min

^{19}F-NMR (282 MHz; $CDCl_3$), δ[ppm]: -62.68 (s; 3F; F^7)

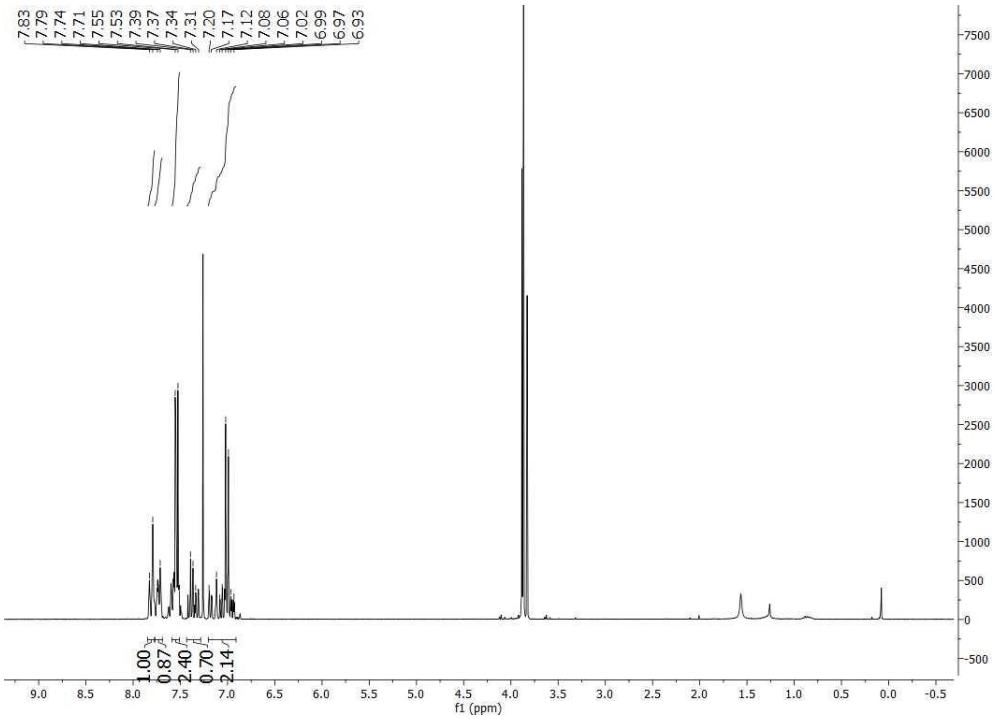

Figure 147: High-resolution ^{1}H-NMR spectrum of *o*,*m*,*p*-chloro-3´-CF_3-biphenyl (mixture of isomers) in $CDCl_3$.

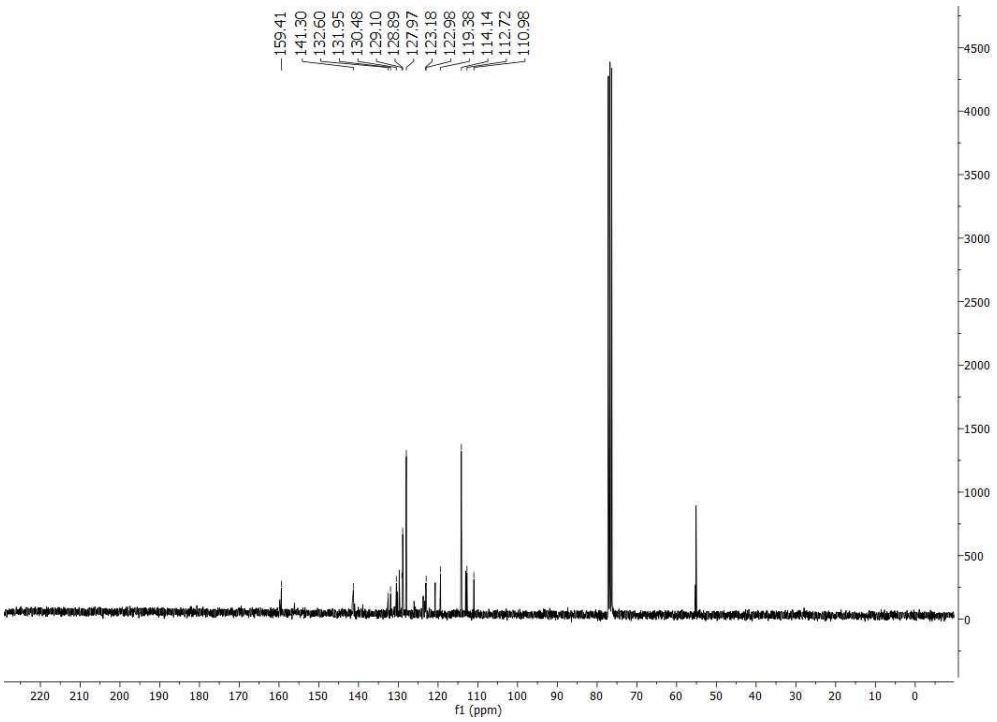

Figure 148: High-resolution ^{13}C-NMR spectrum of *o*,*m*,*p*-chloro-3´-CF_3-biphenyl (mixture of isomers) in $CDCl_3$.

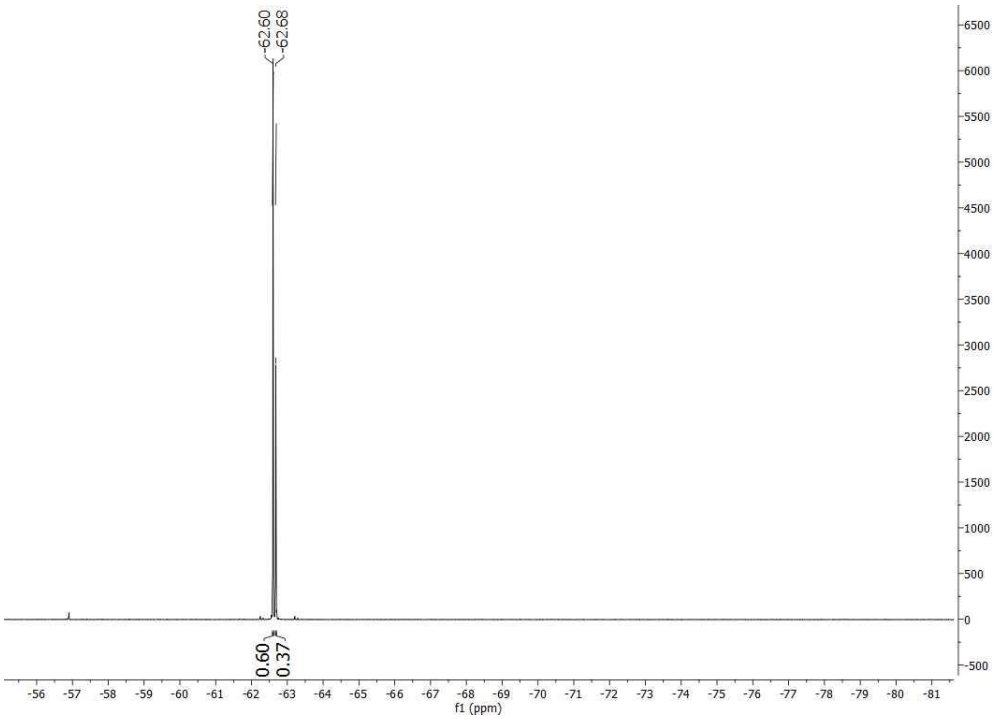

Figure 149: High-resolution ^{19}F-NMR spectrum of *o*,*m*,*p*-chloro-3´-CF_3-biphenyl (mixture of isomers) in $CDCl_3$.

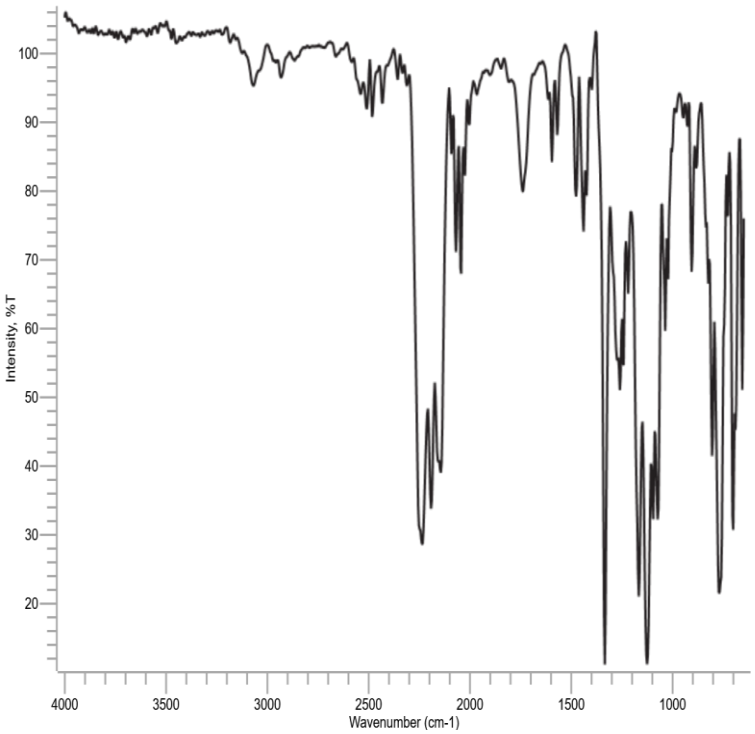

Figure 150: ATR-FTIR of *o*,*m*,*p*-chloro-3´-CF_3-biphenyl (mixture of isomers).

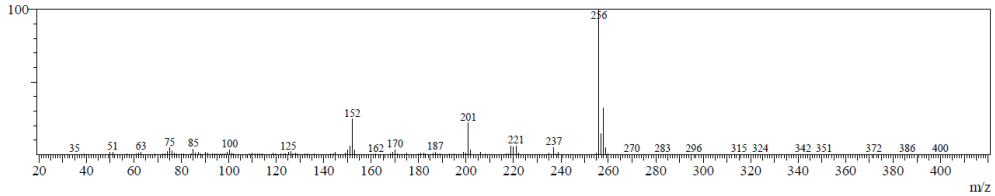

Figure 151: EI-MS spectrum of *o,m,p*-chloro-3´-CF_3-biphenyl.

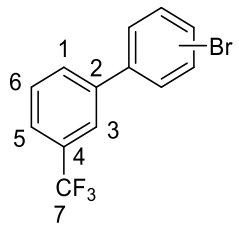

Figure 152: Structure of *o,m,p*-bromo-3´-CF_3-biphenyl **26e** (57%:20%:23%) with numeric labels for NMR evaluation.

Experimental data of all isomers:

R_f index (eluent: CH) = 0.45

Purification: column chromatography (eluent: CH)

MS(EI): found m/z = 152 (38%), 201 (75%), 300 ($[M]^+$, 100%); calc. for $C_{13}H_8BrF_3^+$ $[M]^+$: 299.98

IR (ATR)/[cm^{-1}]: 3065, 1596, 1439, 1336, 1265, 1169, 1130, 1078, 808, 763, 703

Experimental data of 2-bromo-3´-CF_3-biphenyl:

t_R(GC/MS) = 7.75 min

^{19}F-NMR (282 MHz; $CDCl_3$), δ[ppm]: -63.71 (s; 3F; F^7)

Experimental data of 3-bromo-3´-CF_3-biphenyl:

t_R(GC/MS) = 8.26 min

^{19}F-NMR (282 MHz; $CDCl_3$), δ[ppm]: -62.80 (s; 3F; F^7)

Experimental data of 4-bromo-3´-CF_3-biphenyl:

t_R(GC/MS) = 8.19 min

^{19}F-NMR (282 MHz; $CDCl_3$), δ[ppm]: -62.78 (s; 3F; F^7)

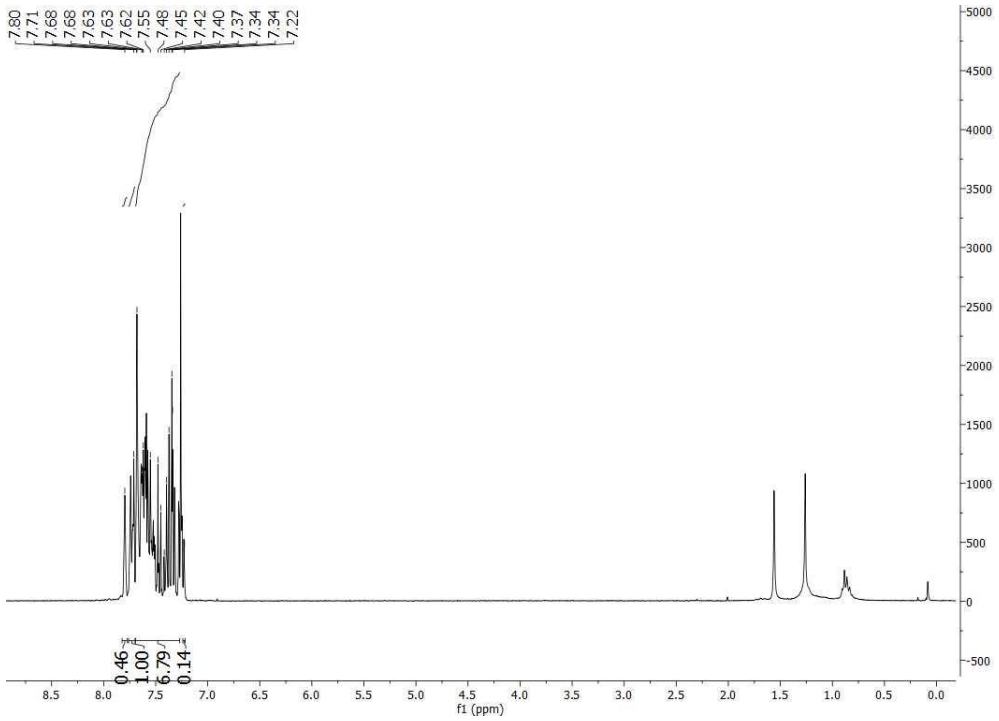

Figure 153: High-resolution ^{1}H-NMR spectrum of *o*,*m*,*p*-bromo-3´-CF_3-biphenyl (mixture of isomers) in $CDCl_3$.

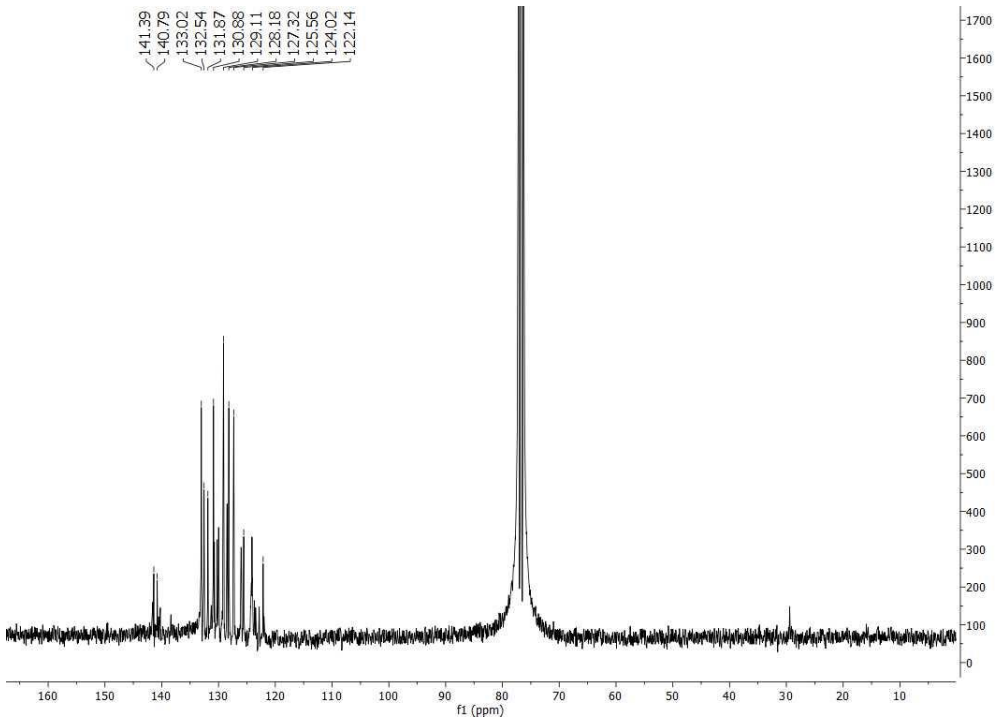

Figure 154: High-resolution ^{13}C-NMR spectrum of *o*,*m*,*p*-bromo-3´-CF_3-biphenyl (mixture of isomers) in $CDCl_3$.

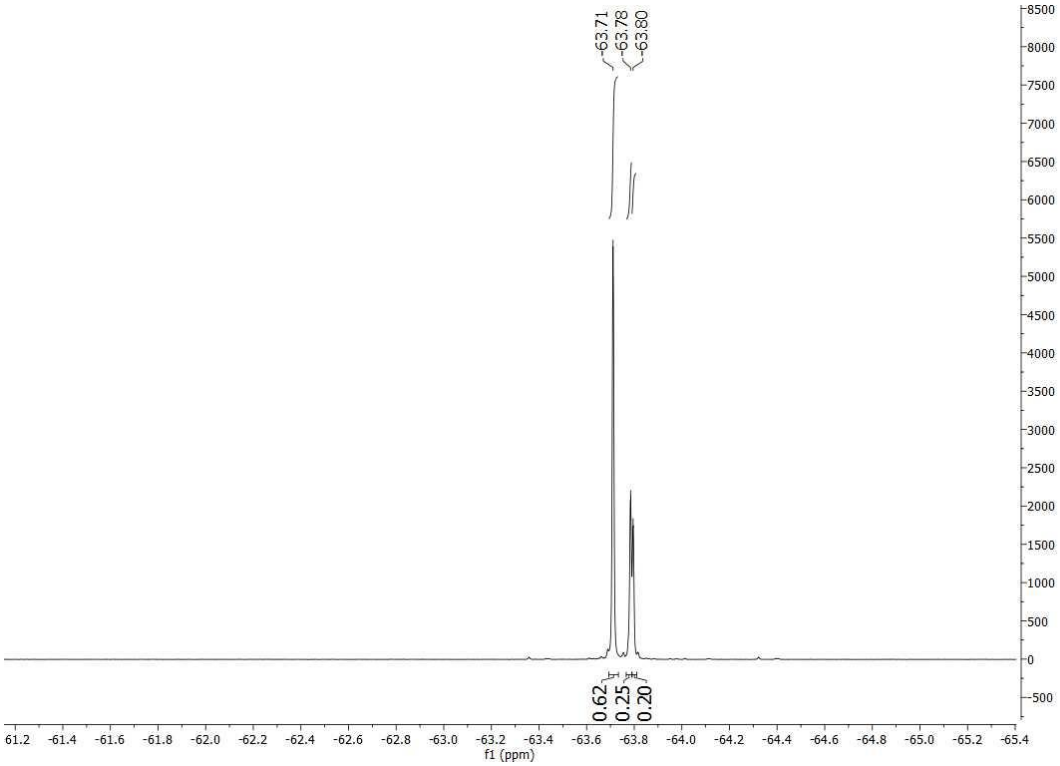

Figure 155: High-resolution ^{19}F-NMR spectrum of *o*,*m*,*p*-bromo-3´-CF_3-biphenyl (mixture of isomers) in $CDCl_3$.

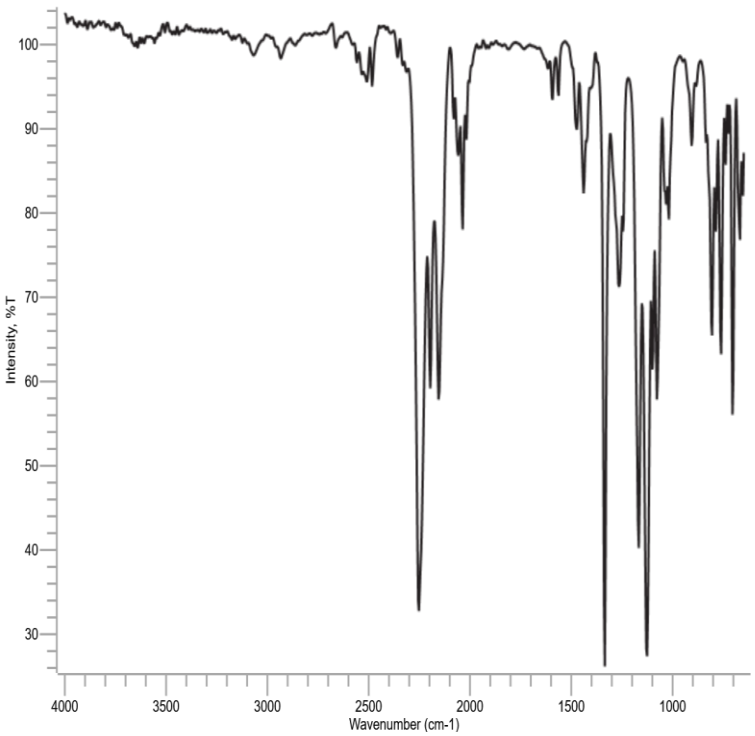

Figure 156: ATR-FTIR of *o*,*m*,*p*-bromo-3´-CF_3-biphenyl (mixture of isomers).

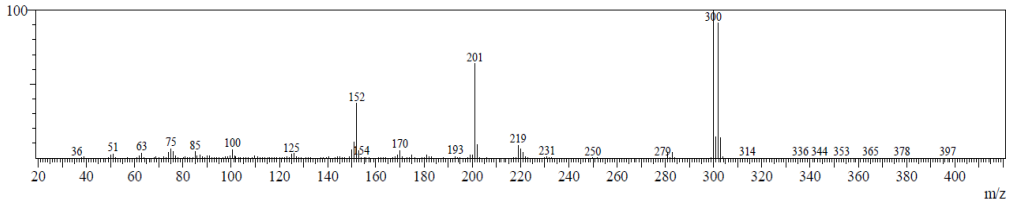

Figure 157: EI-MS spectrum of *o*,*m*,*p*-bromo-3´-CF_3-biphenyl.

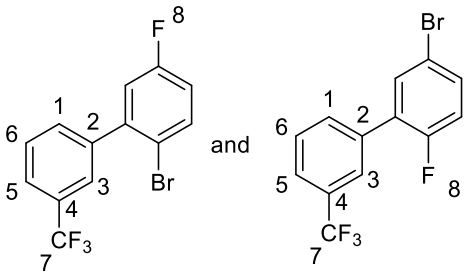

Figure 158: Structure of 2-bromo-5-fluoro-3´-CF_3-biphenyl/5-bromo-2-fluoro-3´-CF_3-biphenyl **26f** (54%:46%) with numeric labels for NMR evaluation.

Experimental data of all isomers:

R_f index (eluent: CH) = 0.45

Purification: column chromatography (eluent: CH)

MS(EI): found m/z = 170 (45%), 219 (60%), 300 ($[M]^+$, 100%); calc. for $C_{13}H_7BrF_4^+$ $[M]^+$: 317.97

IR (ATR)/[cm^{-1}]: 3071, 1576, 1469, 1432, 1332, 1252, 1167, 1126, 1077, 879, 811, 703

^{1}H-NMR (300 MHz; $CDCl_3$), δ[ppm]: 7.77 (s; 1H; H^3)

Experimental data of 2-bromo-5-fluoro-3´-CF_3-biphenyl:

t_R(GC/MS) = 7.56 min

^{19}F-NMR (282 MHz; $CDCl_3$), δ[ppm]: -63.77 (s; 3F; F^7); -115.69 (m; 1F; F^8)

Experimental data of 5-bromo-2-fluoro-3´-CF_3-biphenyl:

t_R(GC/MS) = 8.00 min

^{19}F-NMR (282 MHz; $CDCl_3$), δ[ppm]: -63.81 (s; 3F; F^7); -121.29 (m; 1F; F^8)

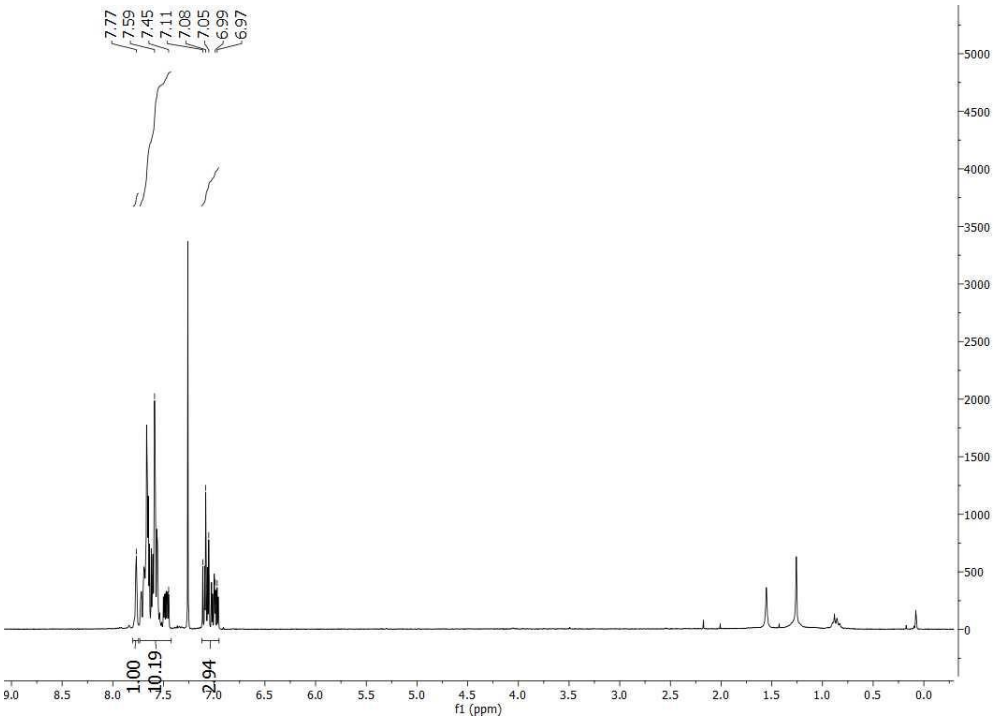

Figure 159: High-resolution ^{1}H-NMR spectrum of 2-bromo-5-fluoro-3´-CF_3-biphenyl/5-bromo-2-fluoro-3´-CF_3-biphenyl (mixture of isomers) in $CDCl_3$.

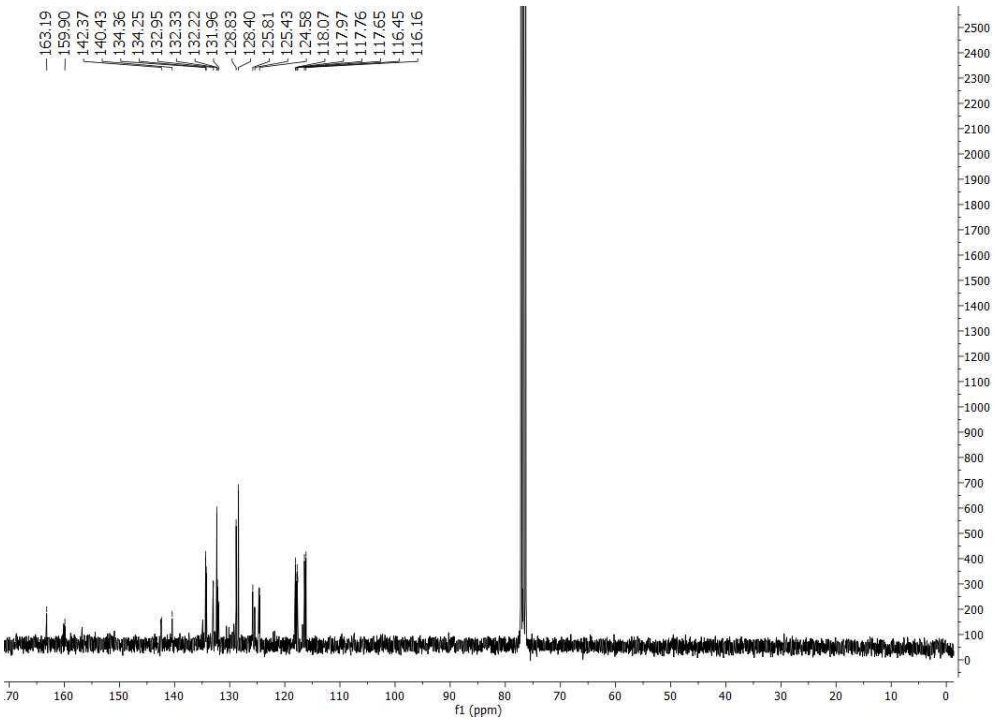

Figure 160: High-resolution ^{13}C-NMR spectrum of 2-bromo-5-fluoro-3´-CF_3-biphenyl/5-bromo-2-fluoro-3´-CF_3-biphenyl (mixture of isomers) in $CDCl_3$.

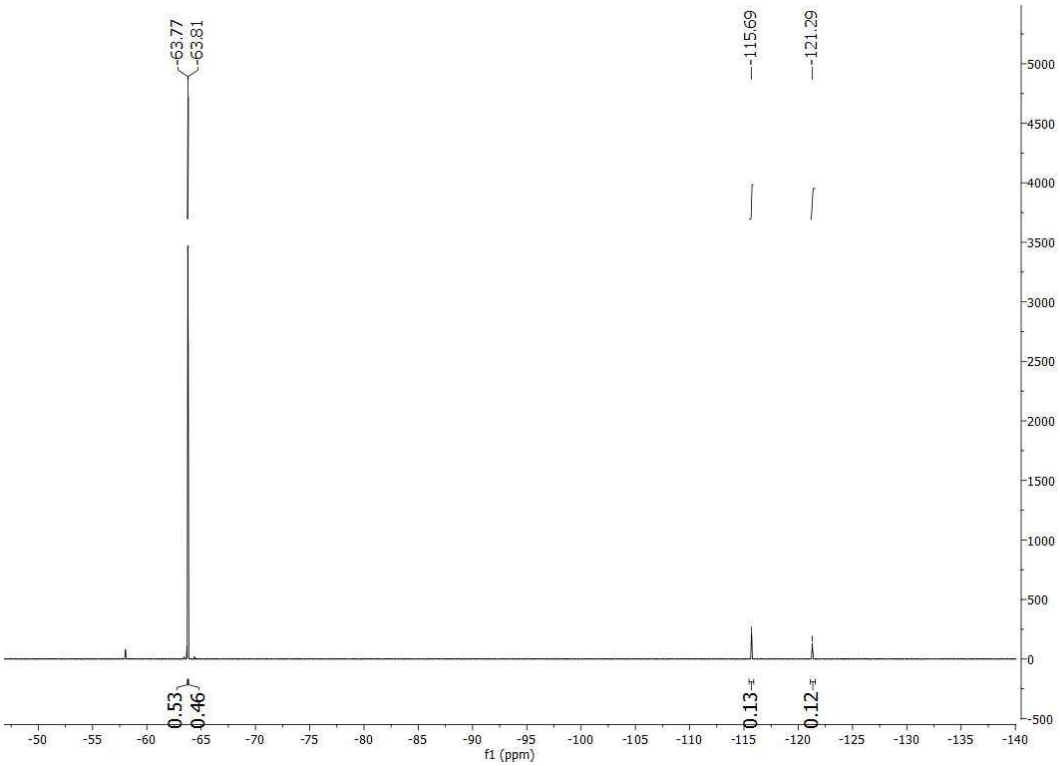

Figure 161: High-resolution ^{19}F-NMR spectrum of 2-bromo-5-fluoro-3´-CF_3-biphenyl/5-bromo-2-fluoro-3´-CF_3-biphenyl (mixture of isomers) in $CDCl_3$.

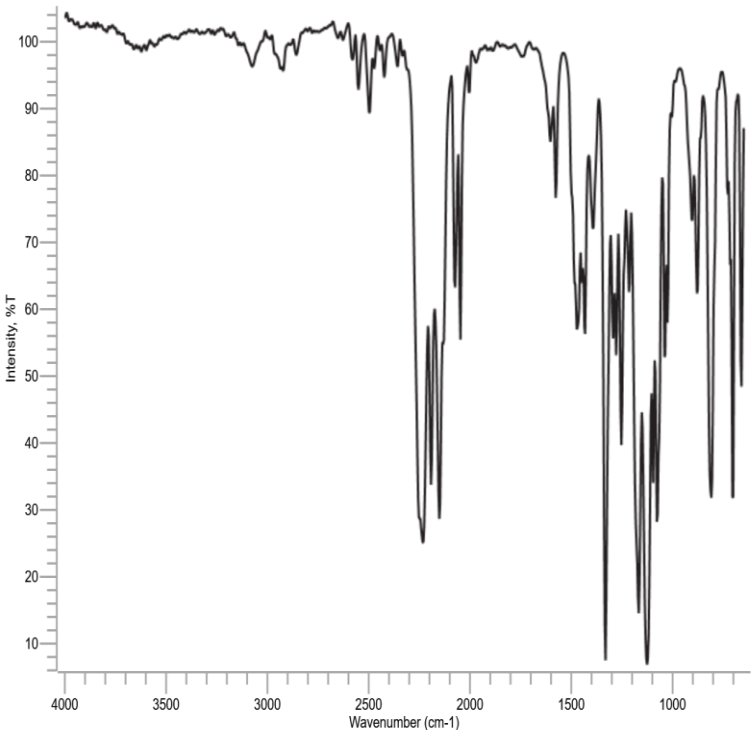

Figure 162: ATR-FTIR of 2-bromo-5-fluoro-3´-CF_3-biphenyl/5-bromo-2-fluoro-3´-CF_3-biphenyl (mixture of isomers).

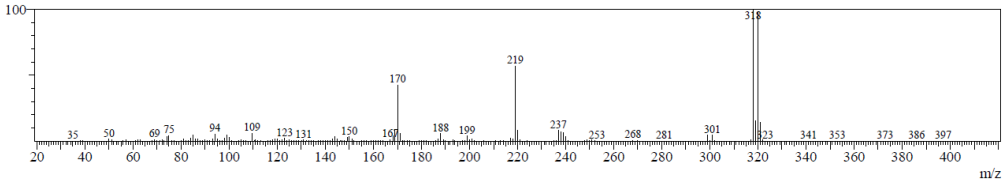

Figure 163: EI-MS spectrum of 2-bromo-5-fluoro-3´-CF_3-biphenyl and 5-bromo-2-fluoro-3´-CF_3-biphenyl.

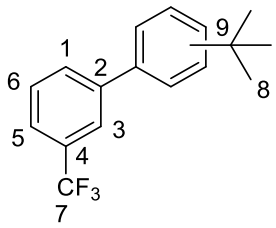

Figure 164: Structure of *o,m,p-tert*-butyl-3´-CF_3-biphenyl **26g** (20%:31%:49%) with numeric labels for NMR evaluation.

Experimental data of all isomers:

R_f index (eluent: CH) = 0.45

Purification: column chromatography (eluent: CH)

MS(EI): found m/z = 152 (5%), 179 (10%), 217 (15%), 235 (35%), 263 (100%), 278 ($[M]^+$, 28%); calc. for $C_{17}H_{17}F_3^+$ $[M]^+$: 278.13

IR (ATR)/[cm^{-1}]: 3065, 2966, 2872, 1482, 1334, 1263, 1167, 1126, 1074, 798, 708

Experimental data of 2-*tert*-butyl-3´-CF_3-biphenyl:

t_R(GC/MS) = 7.69 min

^{1}H-NMR (300 MHz; $CDCl_3$), δ[ppm]: 7.83 (s; 1H; H^3); 1.18 (s; 1 H; H^8)

^{13}C-NMR (75 MHz; $CDCl_3$), δ[ppm]: 37.08 (s; 3C, C^9); 33.20 (s; 3C, C^8)

^{19}F-NMR (282 MHz; $CDCl_3$), δ[ppm]: -63.72 (s; 3F; F^7)

Experimental data of 3-*tert*-butyl-3´-CF_3-biphenyl:

t_R(GC/MS) = 8.42 min

^{1}H-NMR (300 MHz; $CDCl_3$), δ[ppm]: 7.83 (s; 1H; H^3); 1.38 (s; 1 H; H^8)

^{13}C-NMR (75 MHz; $CDCl_3$), δ[ppm]: 35.18 (s; 3C, C^9); 31.89 (s; 3C, C^8)

^{19}F-NMR (282 MHz; $CDCl_3$), δ[ppm]: -63.76 (s; 3F; F^7)

Experimental data of 4-*tert*-butyl-3´-CF_3-biphenyl:

t_R(GC/MS) = 8.18 min

^{1}H-NMR (300 MHz; $CDCl_3$), δ[ppm]: 7.83 (s; 1H; H^3); 1.40 (s; 1 H; H^8)
^{13}C-NMR (75 MHz; $CDCl_3$), δ[ppm]: 35.43 (s; 3C, C^9); 31.96 (s; 3C, C^8)
^{19}F-NMR (282 MHz; $CDCl_3$), δ[ppm]: -63.70 (s; 3F; F^7)

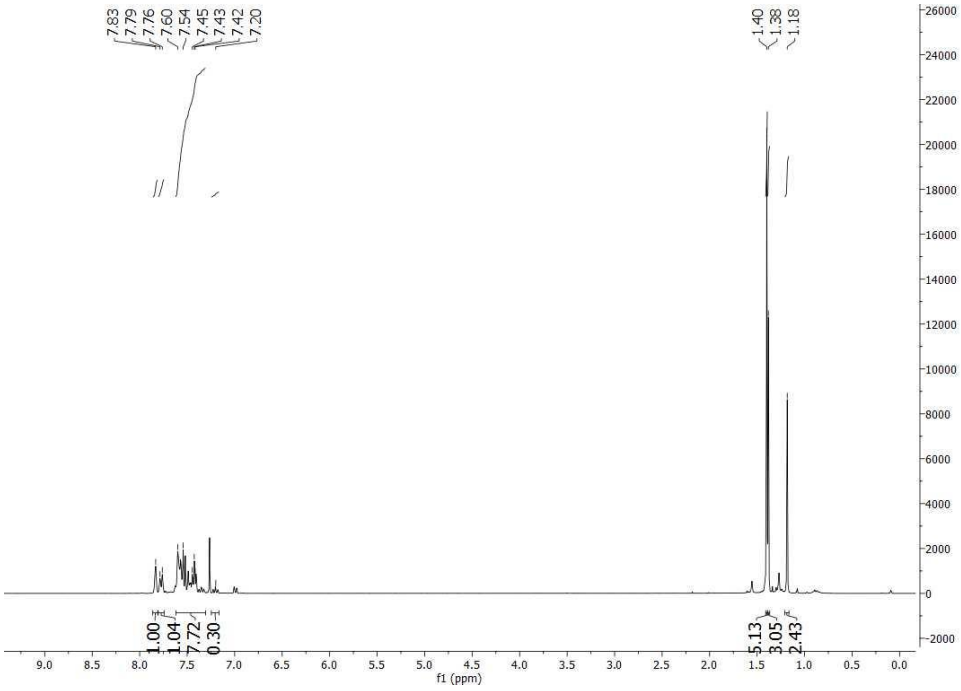

Figure 165: High-resolution ^{1}H-NMR spectrum of *o,m,p-tert*-butyl-3´-CF_3-biphenyl (mixture of isomers) in $CDCl_3$.

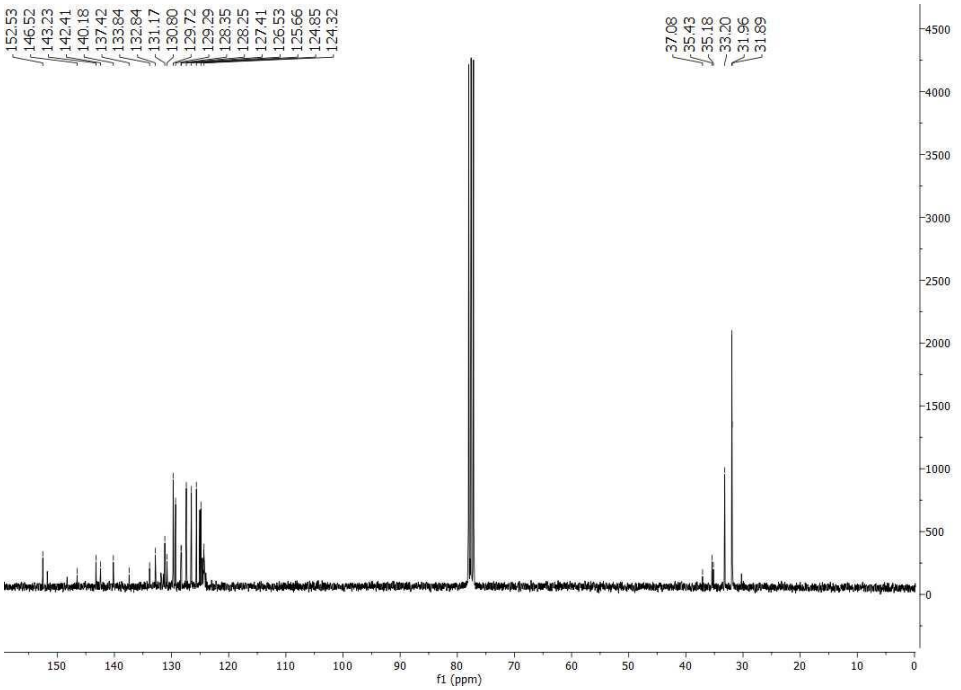

Figure 166: High-resolution ^{13}C-NMR spectrum of *o,m,p-tert*-butyl-3´-CF_3-biphenyl (mixture of isomers) in $CDCl_3$.

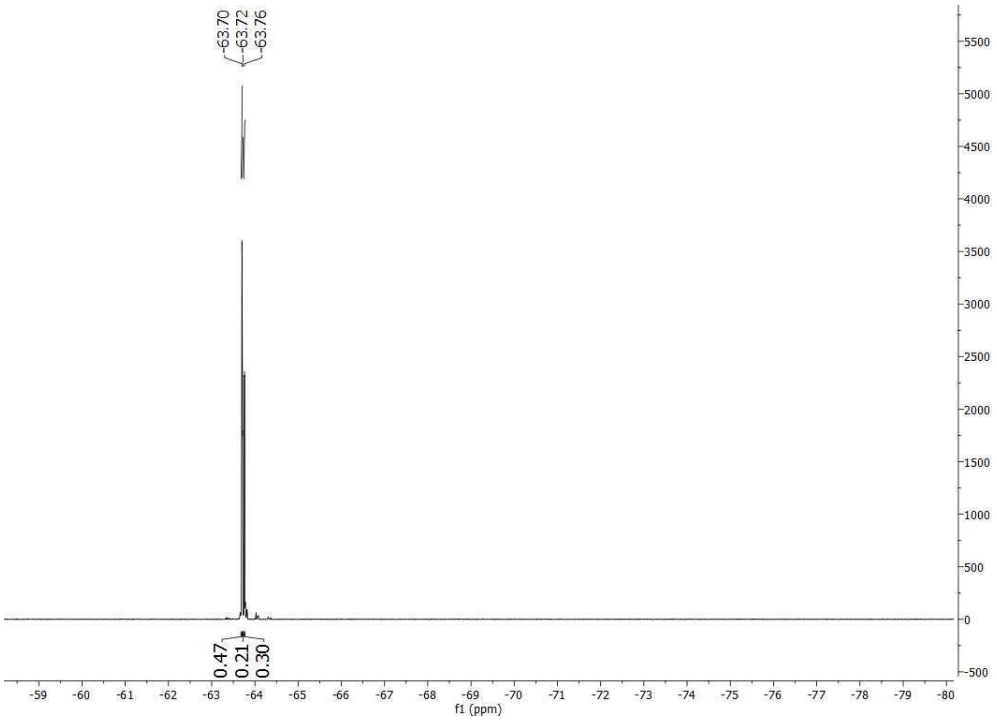

Figure 167: High-resolution ^{19}F-NMR spectrum of *o,m,p-tert*-butyl-3´-CF_3-biphenyl (mixture of isomers) in $CDCl_3$.

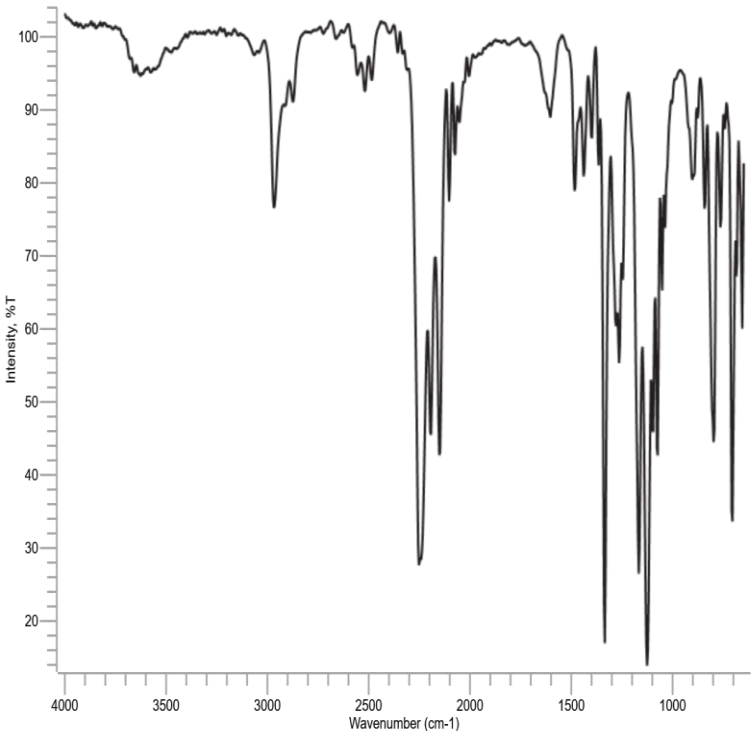

Figure 168: ATR-FTIR of *o,m,p-tert*-butyl-3´-CF_3-biphenyl (mixture of isomers).

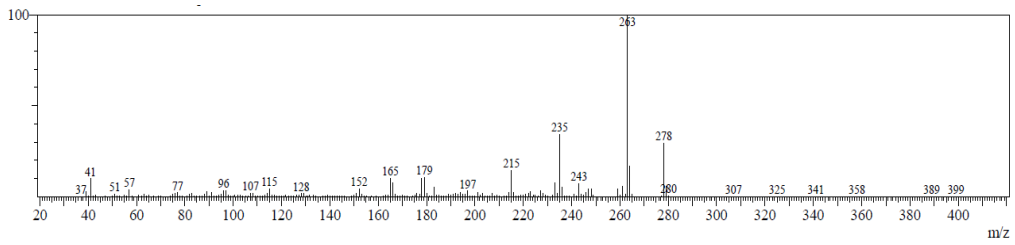

Figure 169: EI-MS spectrum of *o,m,p-tert*-butyl-3´-CF_3-biphenyl.

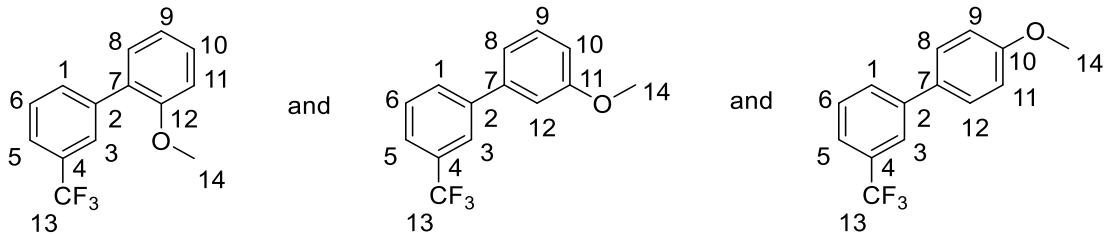

Figure 170: Structure of *o,m,p*-methoxy-3´-CF_3-biphenyl **26h** (78%:8%:14%) with numeric labels for NMR evaluation.

Experimental data of all isomers:

R_f index (eluent: n-heptane) = 0.24

Purification: column chromatography (eluent: n-heptane)

IR (ATR)/[cm^{-1}]: 3078, 2958, 2842, 1602, 1467, 1336, 1255, 1167, 1122, 1027, 905, 804, 755, 701, 656

Experimental data of 2-methoxy-3´-CF_3-biphenyl:

t_R(GC/MS) =7.76 min

MS(EI): found m/z = 168 (29%), 217 (43%), 252 ($[M]^+$, 100%); calc. for $C_{14}H_{11}F_3O^+$ $[M]^+$: 252.08

^{1}H-NMR (300 MHz; $CDCl_3$), δ[ppm]: 7.81 (s; 1H; H^3); 7.73 (s; 1H; J=7.46 Hz; H^8); 7.59 (d; 1H; J=7.82 Hz; H^5); 7.57-7.49 (m; 1 H; H^{10}); 7.41-7.30 (m; 2 H; H^{1+6}); 7.10-6.98 (m; 2 H; H^{9+11}); 3.83 (s; 3H; H^{14}); refer to [225]

^{13}C-NMR (75 MHz; $CDCl_3$), δ[ppm]: 156.50 (1C; C^{12}); 139.38 (1C; C^2); 133.02 (1C; C^7); 130.91 (1C; C^4); 130.27 (1C; C^1); 129.53 (1C; C^8); 129.26 (1C; C^6); 128.48 (1C; C^{10}); 126.46 (1C; $^3J_{C\text{-}F}$ = 3.75 Hz; C^3); 124.45 (1C; $^1J_{C\text{-}F}$ = 236 Hz; C^{13}); 123.76 (1C; $^3J_{C\text{-}F}$ = 3.75 Hz; C^5); 121.12 (1C; C^9); 111.41 (1C;C^{11}) 55.68 (1C; C^{14}); refer to [225]

^{19}F-NMR (282 MHz; $CDCl_3$), δ[ppm]: -63.35 (s; 3F); refer to [225]

Experimental data of 3-methoxy-3´-CF_3-biphenyl:

t_R(GC/MS) = 8.36min

MS(EI): found m/z = 209 (45%), 237 (39%), 252 ($[M]^+$, 100%); calc. for $C_{14}H_{11}F_3O^+$ $[M]^+$: 252.08

^{1}H-NMR (300 MHz; $CDCl_3$), δ[ppm]: 3.88 (s; 3H; H^{14}); refer to [226]

^{13}C-NMR (75 MHz; $CDCl_3$), δ[ppm]: 160.23 (1C; C^{11}); 55.69 (1C; C^{14}); refer to [226]

^{19}F-NMR (282 MHz; $CDCl_3$), δ[ppm]: -63.35 (s; 3F); refer to [226]

Experimental data of 4-methoxy-3´-CF_3-biphenyl:

t_R(GC/MS) = 8.19 min

MS(EI): found m/z = 183 (10%), 209 (19%), 222 (29%), 252 ($[M]^+$, 100%); calc. for $C_{14}H_{11}F_3O^+$ $[M]^+$: 252.08

^{1}H-NMR (300 MHz; $CDCl_3$), δ[ppm]: 3.87 (s; 3H; H^{14}); refer to [31]

^{13}C-NMR (75 MHz; $CDCl_3$), δ[ppm]: 159.83 (1C; C^{10}); 55.53 (1C; C^{14}); refer to [31]

^{19}F-NMR (282 MHz; $CDCl_3$), δ[ppm]: -63.35 (s; 3F); refer to [31]

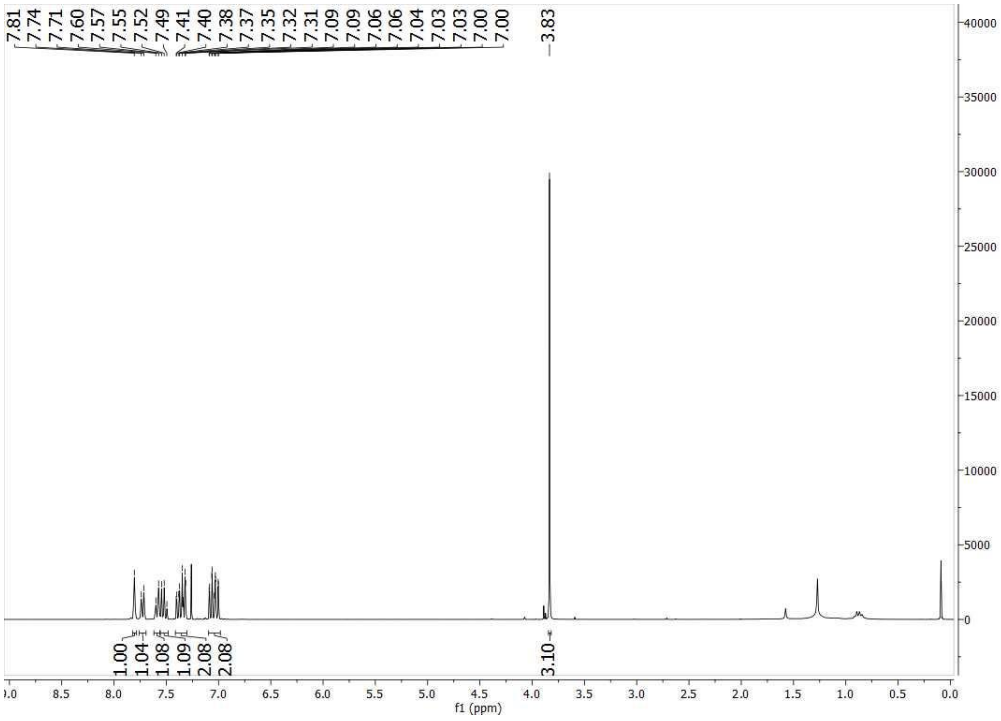

Figure 171: High-resolution ^{1}H-NMR spectrum of 2-methoxy-3´-CF_3-biphenyl in $CDCl_3$.

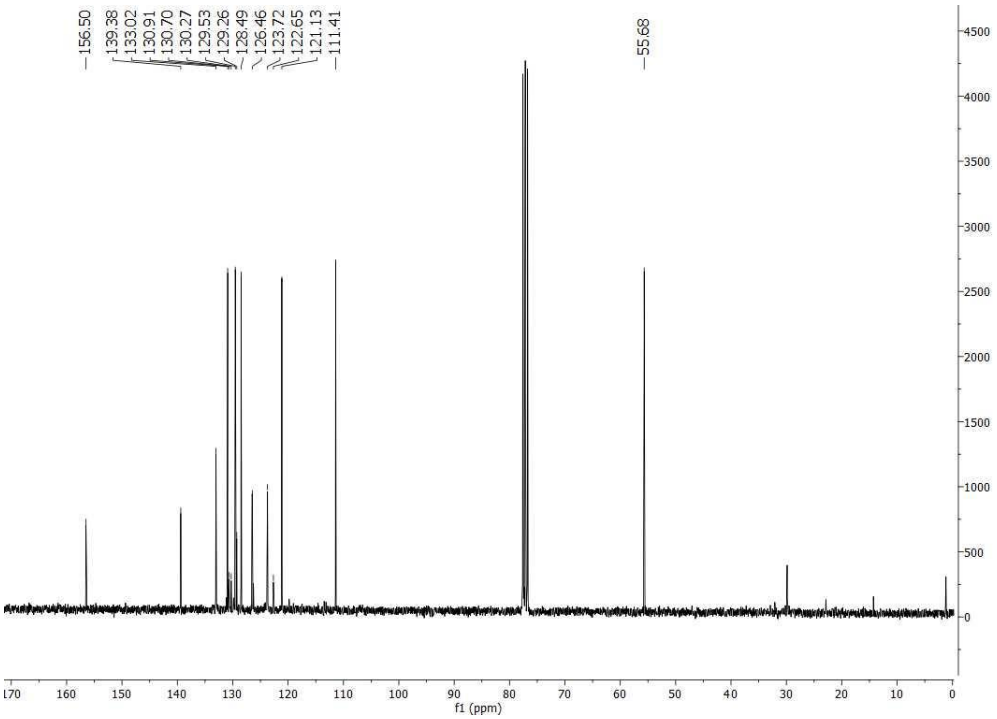

Figure 172: High-resolution ^{13}C-NMR spectrum of 2-methoxy-3´-CF_3-biphenyl in $CDCl_3$.

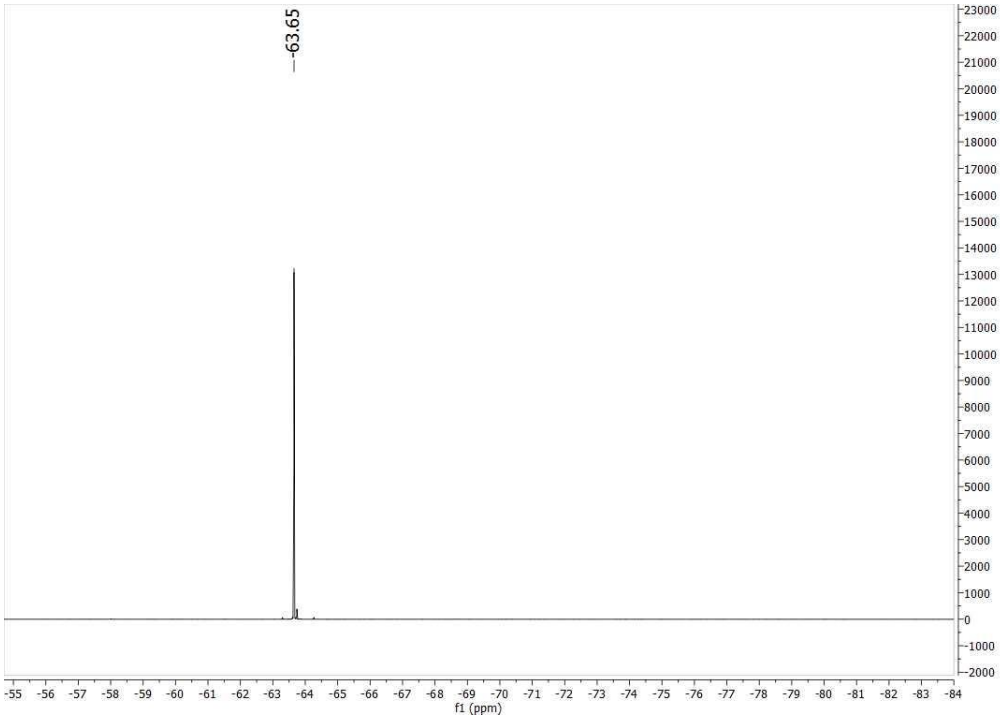

Figure 173: High-resolution ^{19}F-NMR spectrum of 2-methoxy-3´-CF_3-biphenyl in $CDCl_3$.

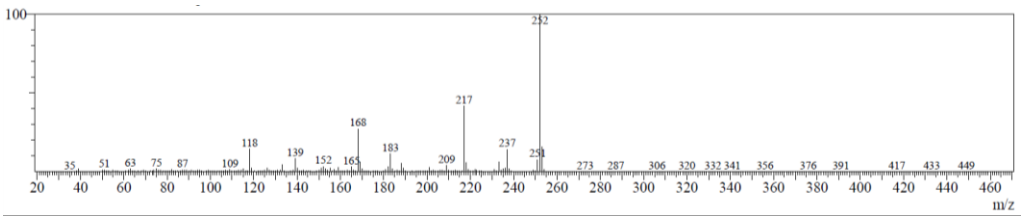

Figure 174: EI-MS spectrum of 2-methoxy-3´-CF_3-biphenyl.

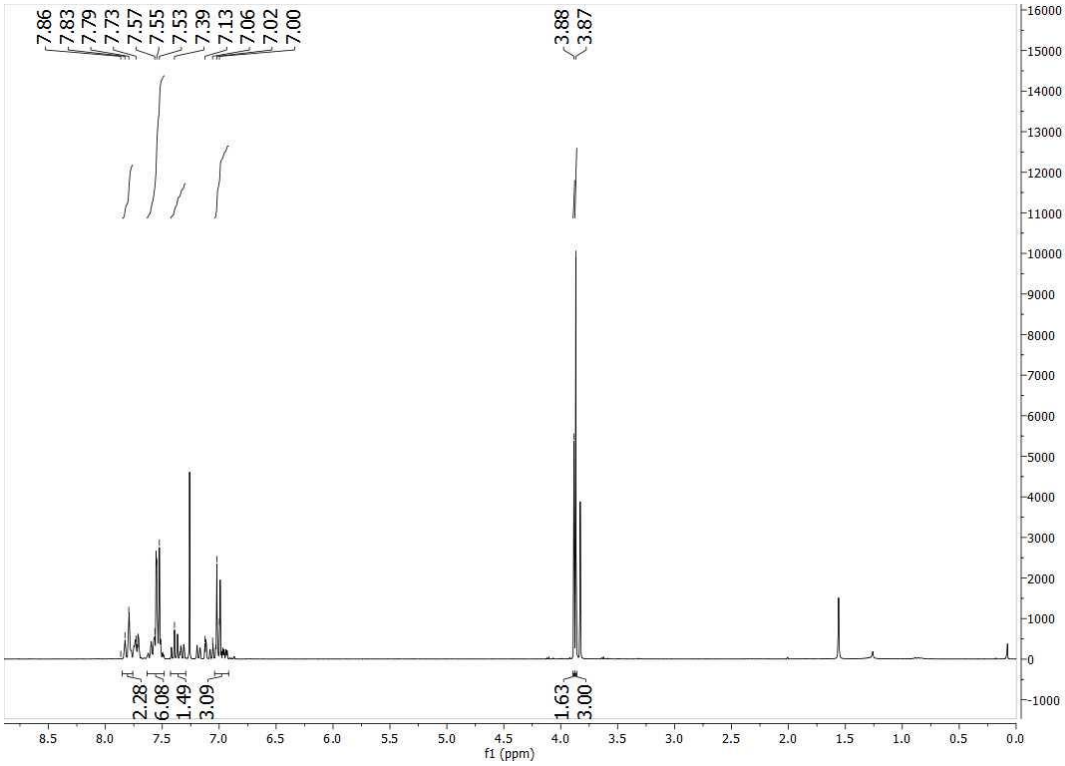

Figure 175: High-resolution ^{1}H-NMR spectrum of *m,p*-methoxy-3´-CF_3-biphenyl (mixture of isomers) in $CDCl_3$.

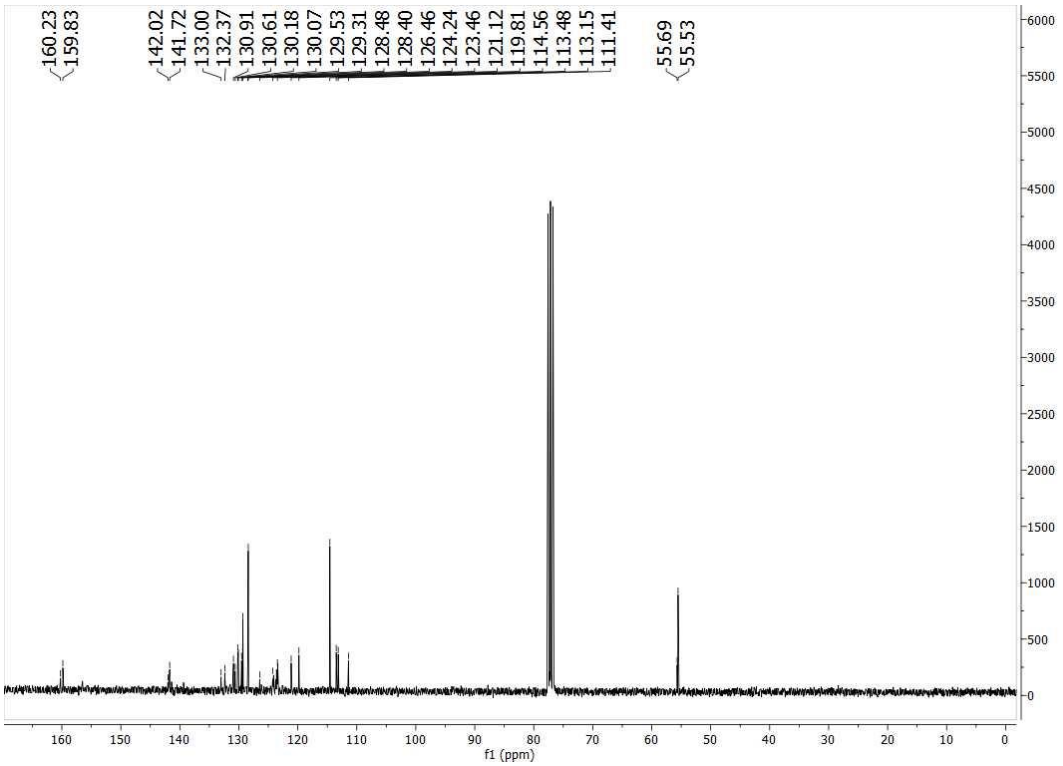

Figure 176: High-resolution ^{13}C-NMR spectrum of *m*,*p*-methoxy-3´-CF_3-biphenyl (mixture of isomers) in $CDCl_3$.

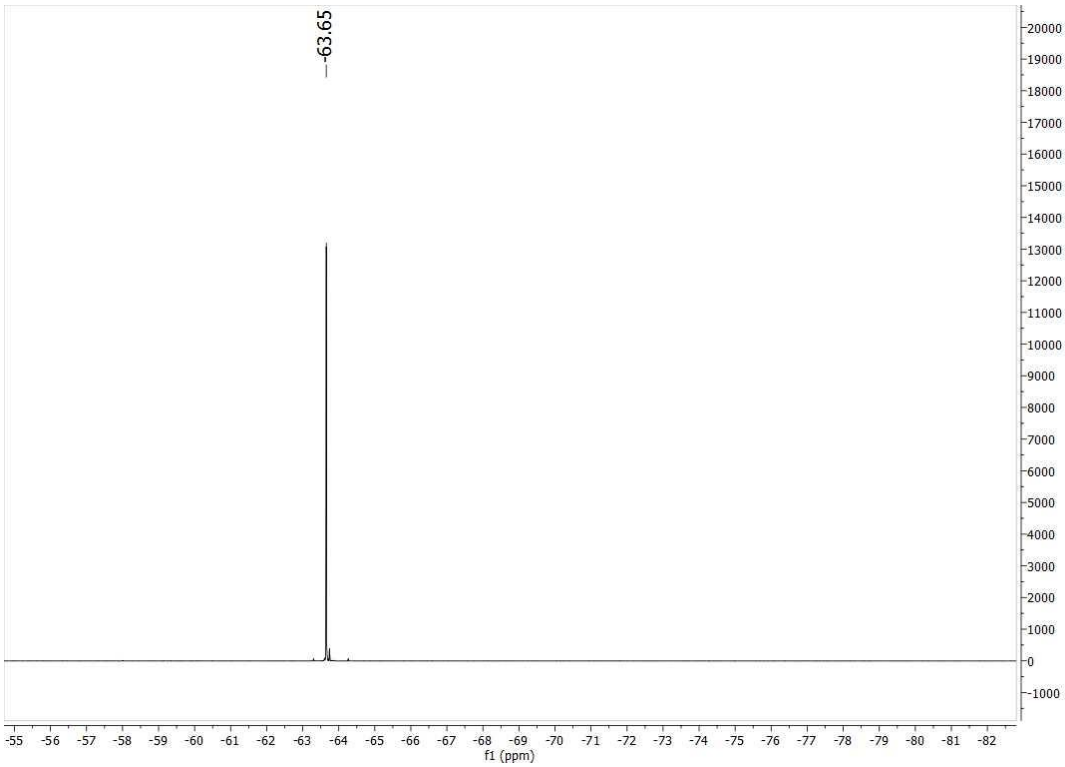

Figure 177: High-resolution ^{19}F-NMR spectrum of *m*,*p*-methoxy-3´-CF_3-biphenyl (mixture of isomers) in $CDCl_3$.

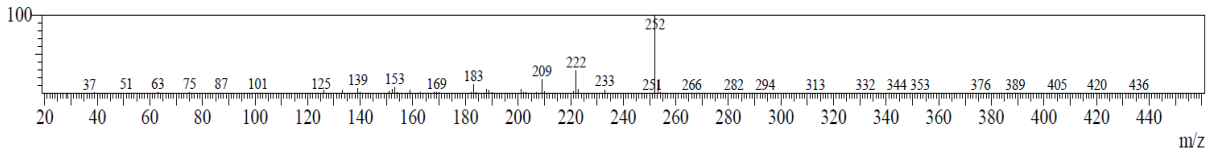

Figure 178: EI-MS spectrum of 3-methoxy-3´-CF_3-biphenyl.

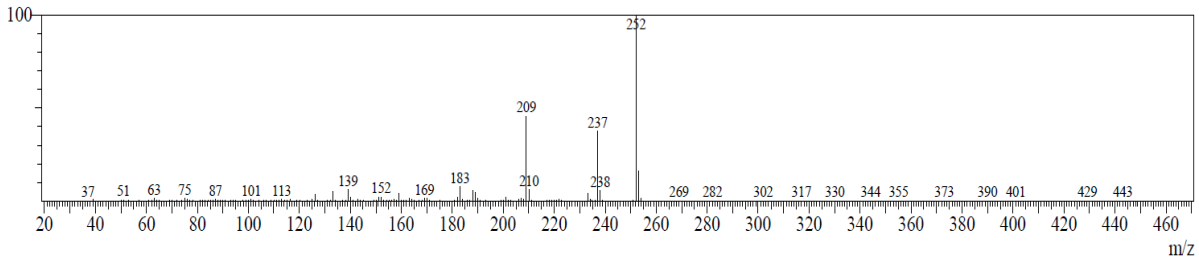

Figure 179: EI-MS spectrum of 4-methoxy-3´-CF_3-biphenyl.

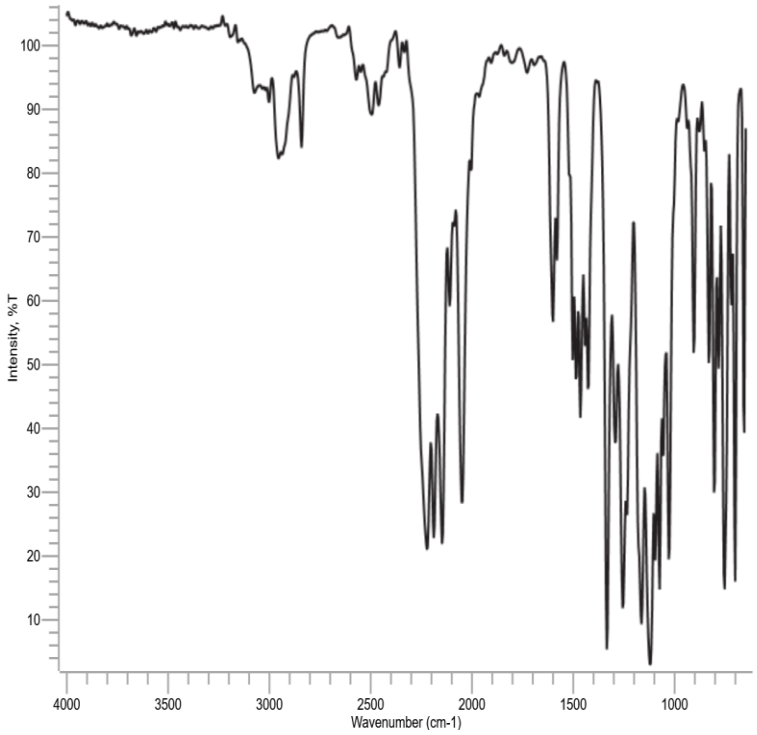

Figure 180: ATR-FTIR of *o,m,p*-methoxy-3´-CF_3-biphenyl (mixture of isomers).

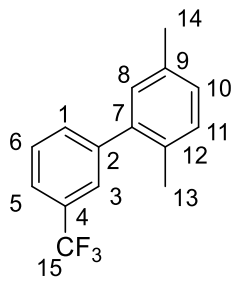

Figure 181: Structure of 2,5-dimethyl-3´-CF_3-biphenyl **26i** with numeric labels for NMR evaluation.

t_R(GC/MS) = 7.22 min

R_f index (eluent: CH) = 0.44

Purification: column chromatography (eluent: CH)

MS(EI): found m/z = 165 (33%), 181 (46%), 235 (46%) 250 ($[M]^+$, 100%); calc. for $C_{15}H_{13}F_3^+$ $[M]^+$: 250.10

IR (ATR)/[cm^{-1}]: 3020, 2925, 2870, 1488, 1433, 1334, 1295, 1261, 1164, 1123, 1074, 892, 806, 702

^{1}H-NMR (300 MHz; $CDCl_3$), δ[ppm]: 7.63-7.57 (m; 2H; H^{3+5}); 7.55-7.49 (m; 2H; H^{1+6}); 7.19 (d; 1H; J=8.0 Hz; H^{11}); 7.12 (d; 1H; J=8.0 Hz; H^{10}); 7.06 (s; 1H; H^8); 2.37 (s; 3H; H^{13}); 2.23 (s; 3H; H^{14})

^{13}C-NMR (75 MHz; $CDCl_3$), δ[ppm]: 142.94 (1C; C^2); 140.36 (1C; C^7); 135.64 (1C; C^9); 132.66 (1C; C^{12}); 132.21 (1C; C^{11}); 130.61 (1C; C^4); 130.60 (1C; C^1); 130.52 (1C; C^8); 128.74 (1C; C^6); 128.63 (1C; C^{10}); 126.07 (1C; $^3J_{C\text{-}F}$ = 3.90 Hz; C^3); 124.69 (1C; $^1J_{C\text{-}F}$ = 272 Hz; C^{15}); 123.65 (1C; $^3J_{C\text{-}F}$ = 4.0 Hz; C^5); 121.12 (1C; C^9); 21.02 (1C; C^{14}); 19.96 (1C; C^{13})

^{19}F-NMR (282 MHz; $CDCl_3$), δ[ppm]: -63.68 (s; 3F; F^{15})

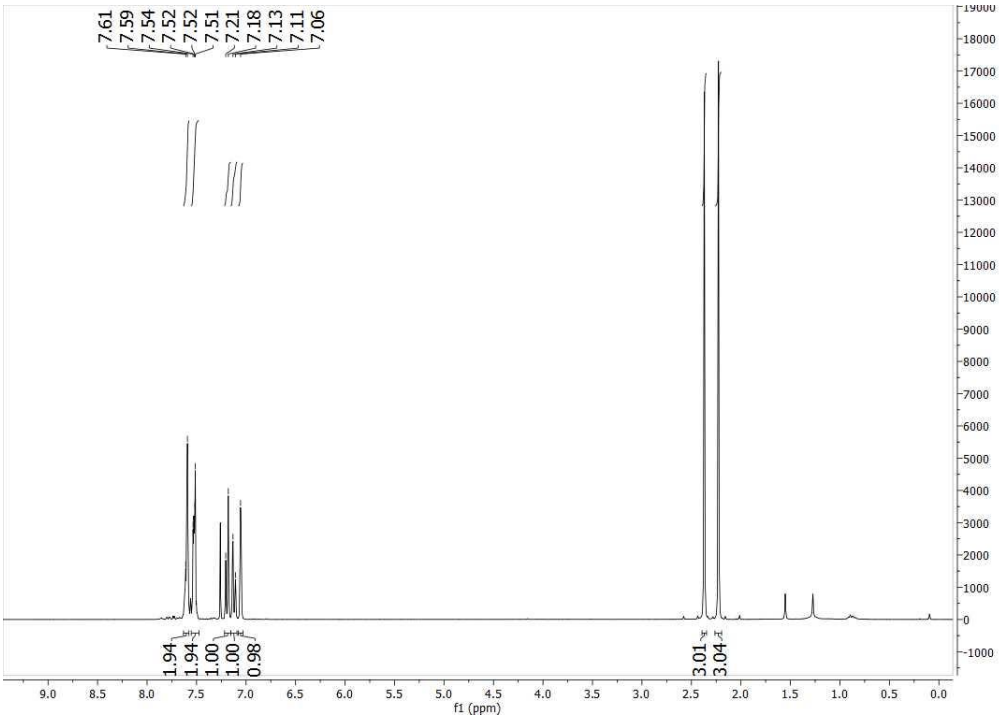

Figure 182: High-resolution ^{1}H-NMR spectrum of 2,5-dimethyl-3´-CF_3-biphenyl in $CDCl_3$.

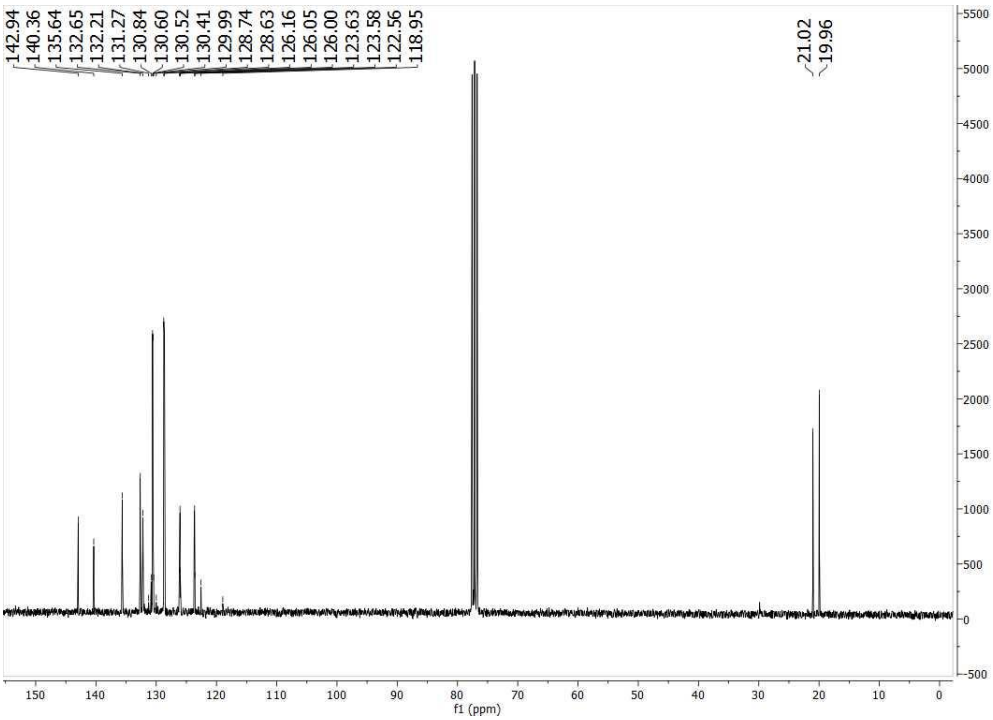

Figure 183: High-resolution ^{13}C-NMR spectrum of 2,5-dimethyl-3´-CF_3-biphenyl in $CDCl_3$.

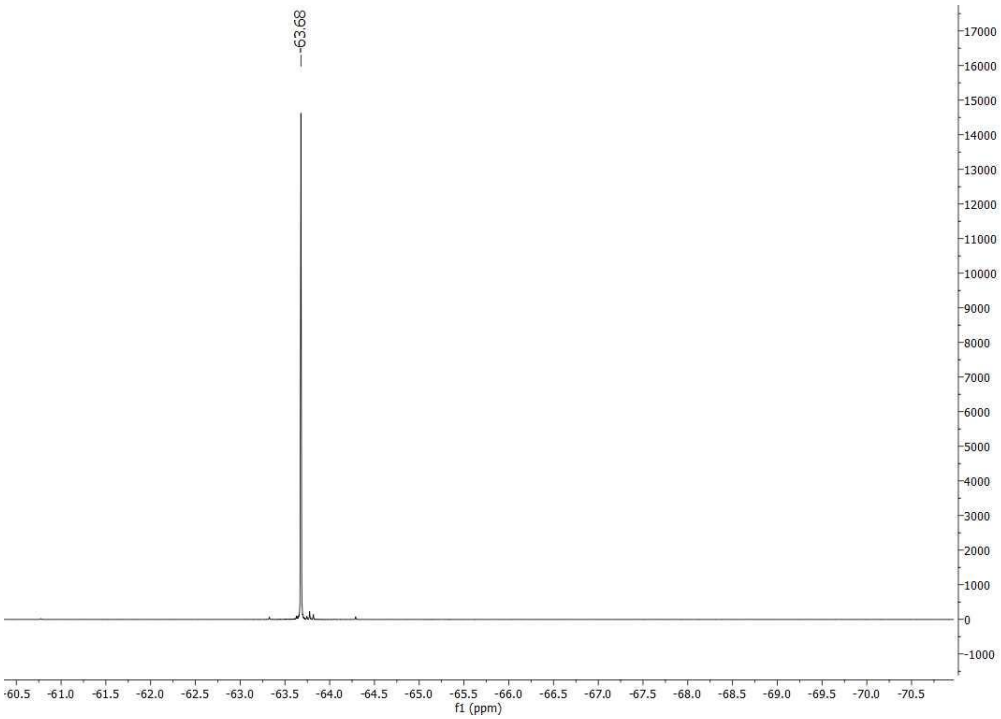

Figure 184: High-resolution ^{19}F-NMR spectrum of 2,5-dimethyl-3´-CF_3-biphenyl in $CDCl_3$.

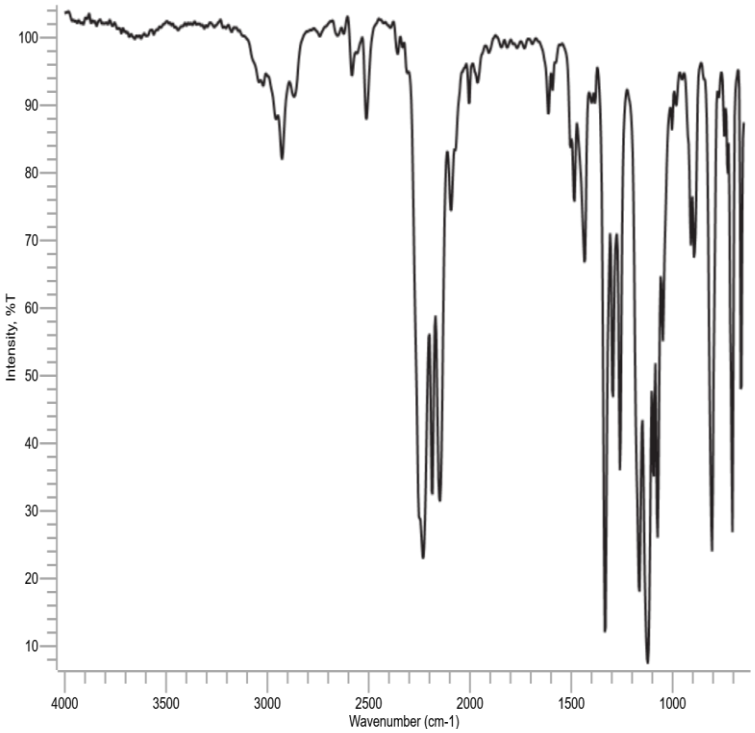

Figure 185: ATR-FTIR of 2,5-dimethyl-3´-CF_3-biphenyl.

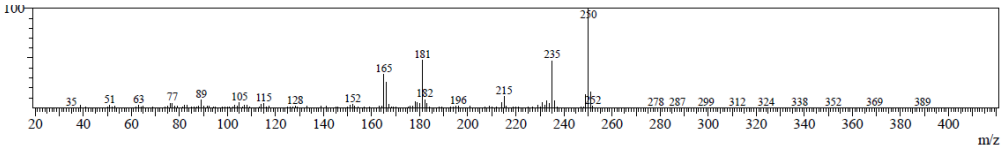

Figure 186: EI-MS spectrum of 2,5-dimethyl-3´-CF_3-biphenyl.

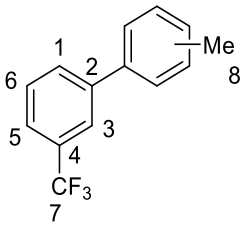

Figure 187: Structure of *o,m,p*-methyl-3´-CF_3-biphenyl **26k** (60%:16%:24%) with numeric labels for NMR evaluation.

Experimental data of all isomers:

R_f index (eluent: CH) = 0.45

Purification: column chromatography (eluent: CH)

MS(EI): found m/z = 152 (18%), 165 (43%), 167 (100%), 236 ($[M]^+$, 100%); calc. for $C_{14}H_{11}F_3^+$ $[M]^+$: 236.08

IR (ATR)/[cm^{-1}]: 3067, 2932, 1484, 1433, 1334, 1255, 1164, 1126, 1074, 905, 808, 761, 703.

Experimental data of 2-methyl-3´-CF_3-biphenyl:

t_R(GC/MS) = 6.10 min

^{1}H-NMR (300 MHz; $CDCl_3$), δ[ppm]: 2.27 (s; 1H; H^8)

^{13}C-NMR (75 MHz; $CDCl_3$), δ[ppm]: 20.48 (1C, C^8)

^{19}F-NMR (282 MHz; $CDCl_3$), δ[ppm]: -63.69 (s; 3F; F^7)

Experimental data of 3-methyl-3´-CF_3-biphenyl:

t_R(GC/MS) = 7.24 min

^{1}H-NMR (300 MHz; $CDCl_3$), δ[ppm]: 2.42 (s; 1H; H^8)

^{13}C-NMR (75 MHz; $CDCl_3$), δ[ppm]: 21.28 (1C, C^8)

^{19}F-NMR (282 MHz; $CDCl_3$), δ[ppm]: -63.75 (s; 3F; F^7)

Experimental data of 4-methyl-3´-CF_3-biphenyl:

t_R(GC/MS) = 7.13 min

^{1}H-NMR (300 MHz; $CDCl_3$), δ[ppm]: 2.44 (s; 1H; H^8); refer to [227]

^{13}C-NMR (75 MHz; $CDCl_3$), δ[ppm]: 21.66 (1C, C^8); refer to [227]
^{19}F-NMR (282 MHz; $CDCl_3$), δ[ppm]: -63.74 (s; 3F; F^7)

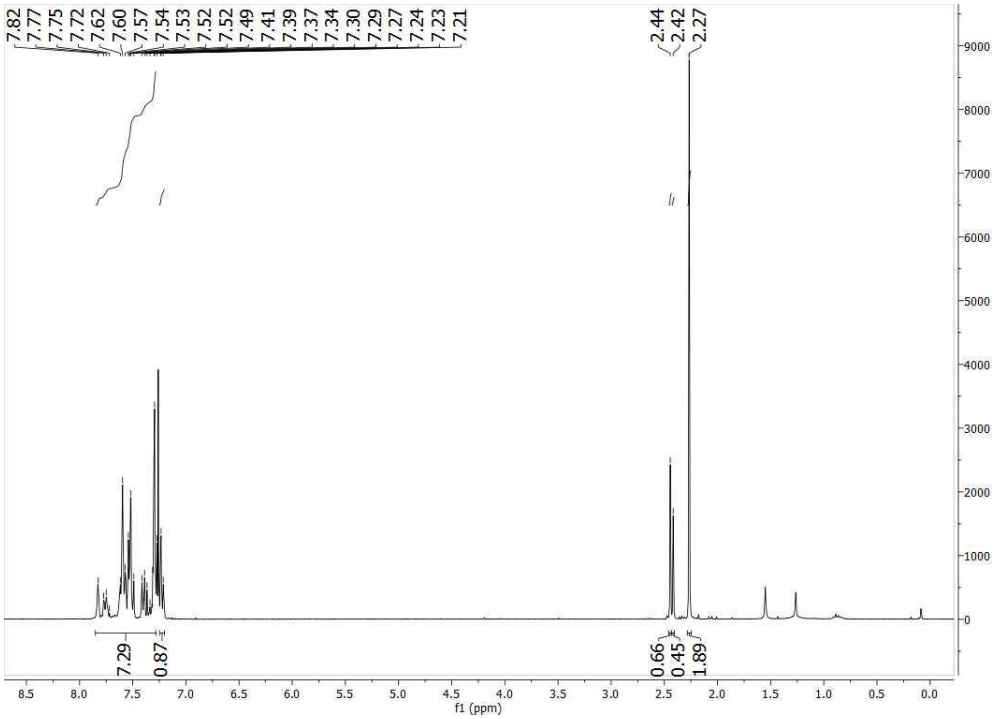

Figure 188: High-resolution ^{1}H-NMR spectrum of *o*,*m*,*p*-methyl-3´-CF_3-biphenyl (mixture of isomers) in $CDCl_3$.

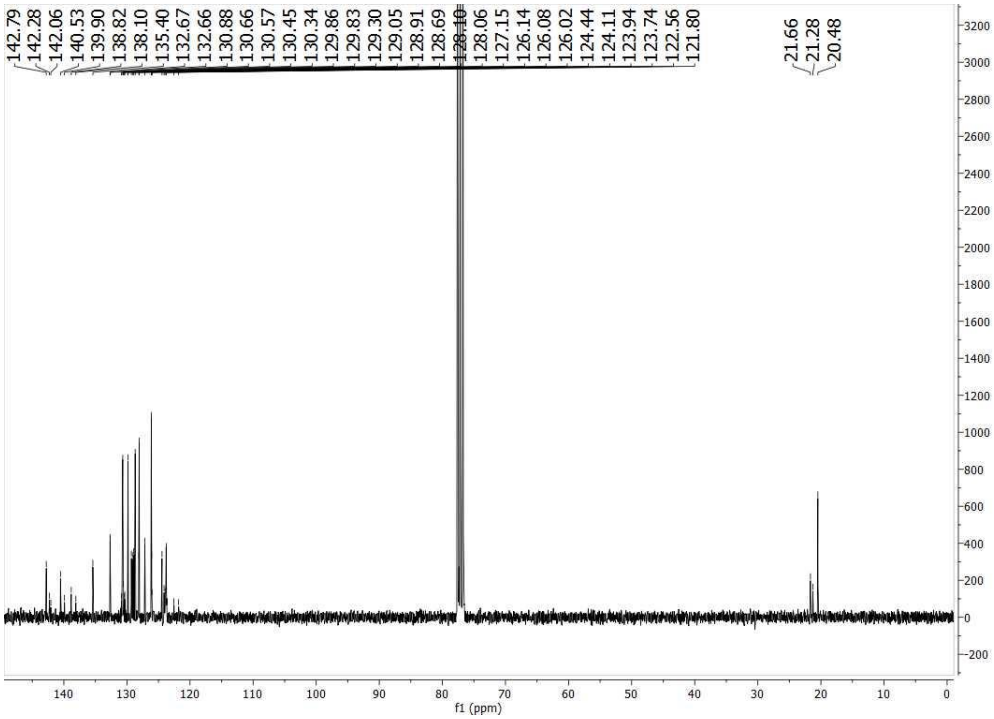

Figure 189: High-resolution ^{13}C-NMR spectrum of *o*,*m*,*p*-methyl-3´-CF_3-biphenyl (mixture of isomers) in $CDCl_3$.

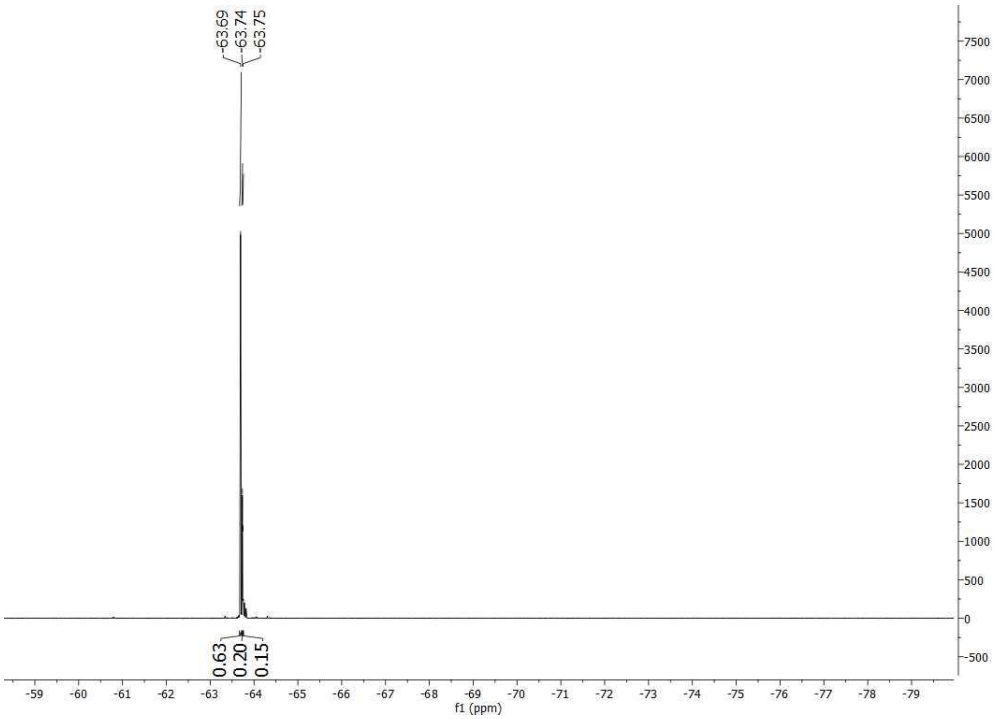

Figure 190: High-resolution ^{19}F-NMR spectrum of *o,m,p*-methyl-3´-CF_3-biphenyl (mixture of isomers) in $CDCl_3$.

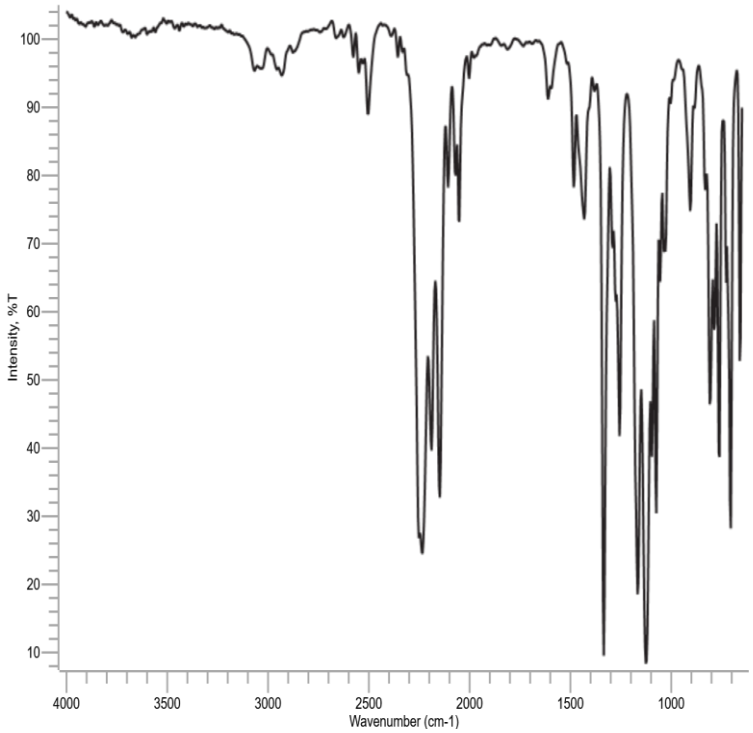

Figure 191: ATR-FTIR of *o,m,p*-methyl-3´-CF_3-biphenyl (mixture of isomers).

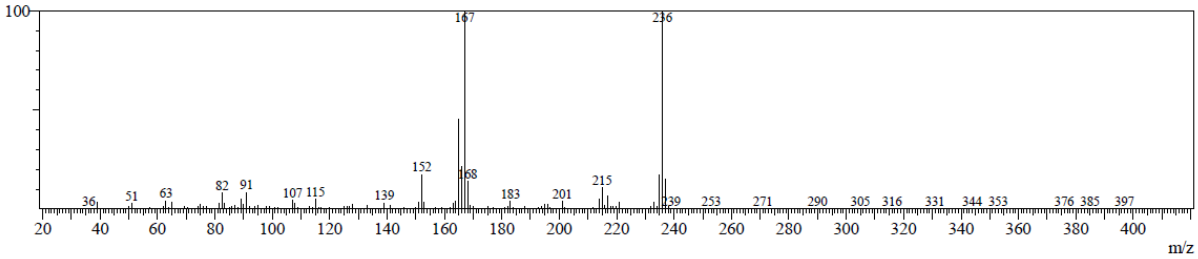

Figure 192: EI-MS spectrum of *o*,*m*,*p*-methyl-3´-CF_3-biphenyl.

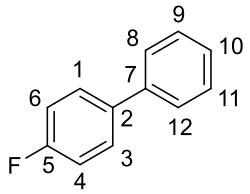

Figure 193: Structure of 4-fluoro-biphenyl **31b** with numeric labels for NMR evaluation.

t_R(GC/MS) = 6.01 min

R_f index (eluent: CH) = 0.60

Purification: column chromatography (eluent: CH)

MS(EI): found m/z = 85 (20%), 172 ([M]$^+$, 100%); calc. for $C_{12}H_9F^+$ [M]$^+$: 172.02; refer to [228]

IR (ATR)/[cm^{-1}]: 3065, 3031, 1608, 1518, 1486, 1225, 1160, 1008, 841, 763, 697

^{1}H-NMR (300 MHz; $CDCl_3$), δ[ppm]: 7.61-7.51 (m; 4H; $H^{1+3+8+12}$); 7.50-7.40 (m; 2H; H^{9+11}); 7.40-7.32 (m; 1H; H^{10}); 7.19-7.09 (m; 2H; H^{4+6}); refer to [229]

^{13}C-NMR (75 MHz; $CDCl_3$), δ[ppm]: 162.60 (1C; $^1J_{C-F}$ = 247 Hz; C^5); 140.39 (1C; C^7); 137.49 (1C; C^2); 128.96 (2C; C^{9+11}); 128.82 (2C; $^3J_{C-F}$ = 8.0 Hz C^{1+3}); 127.40 (1C; C^{10}); 127.16 (2C; C^{8+12}); 115.75 (2C; $^2J_{C-F}$ = 22.0 Hz; C^{4+6}); refer to [229]

^{19}F-NMR (282 MHz; $CDCl_3$), δ[ppm]: -117.01 (m; 3F; F^5); refer to [229]

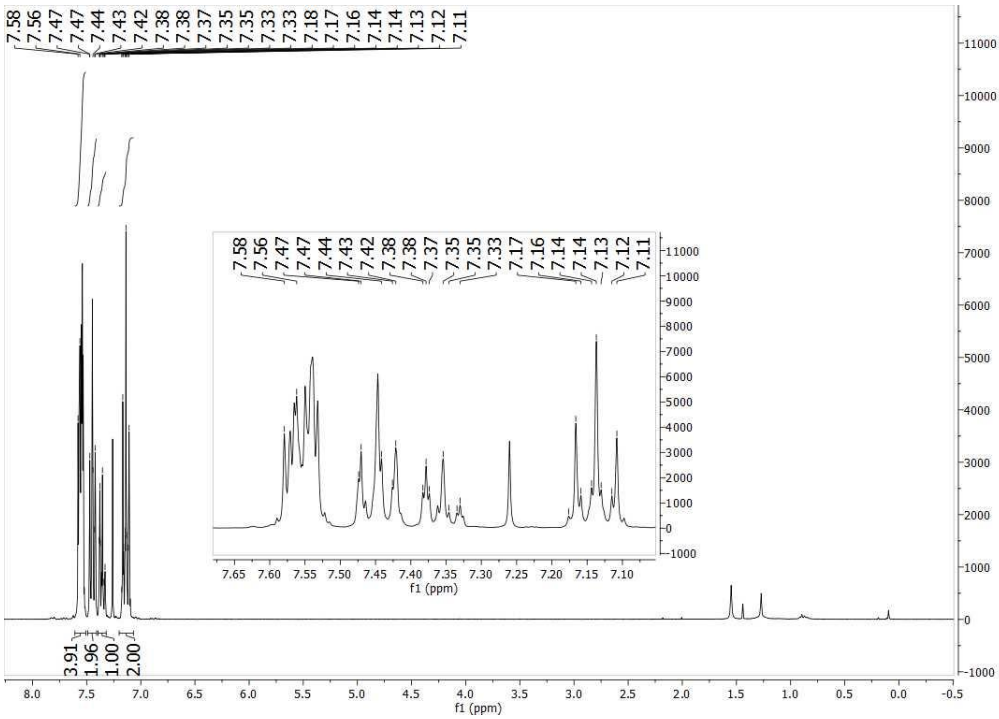

Figure 194: High-resolution ^{1}H-NMR spectrum of 4-fluorobiphenyl (mixture of isomers) in $CDCl_3$.

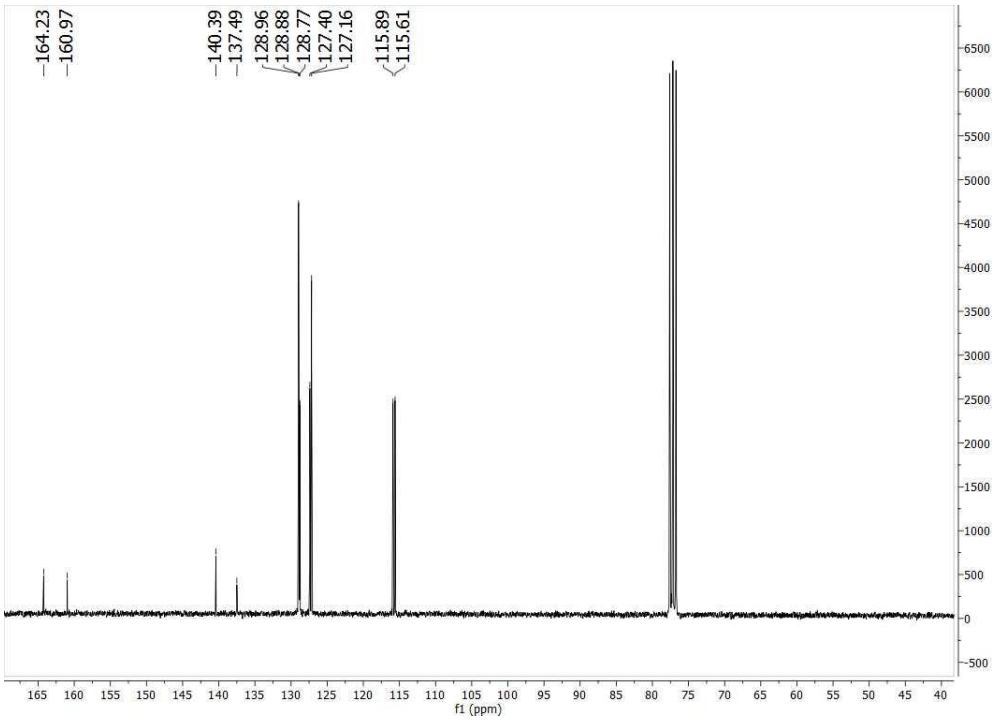

Figure 195: High-resolution ^{13}C-NMR spectrum of 4-fluorobiphenyl (mixture of isomers) in $CDCl_3$.

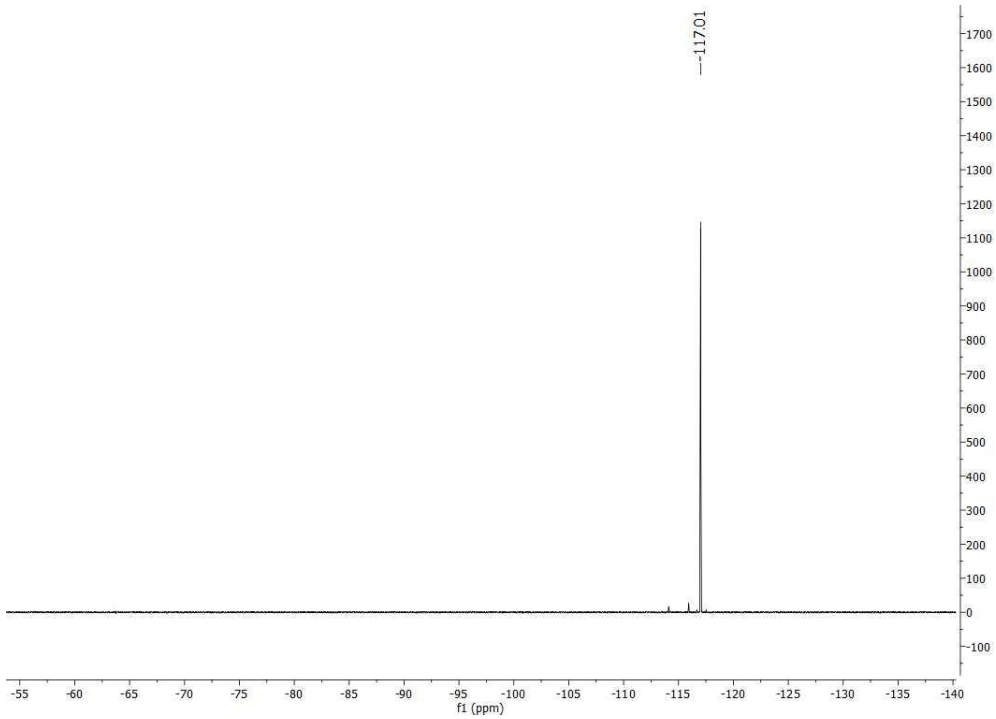

Figure 196: High-resolution ^{19}F-NMR spectrum of 4-fluorobiphenyl (mixture of isomers) in $CDCl_3$.

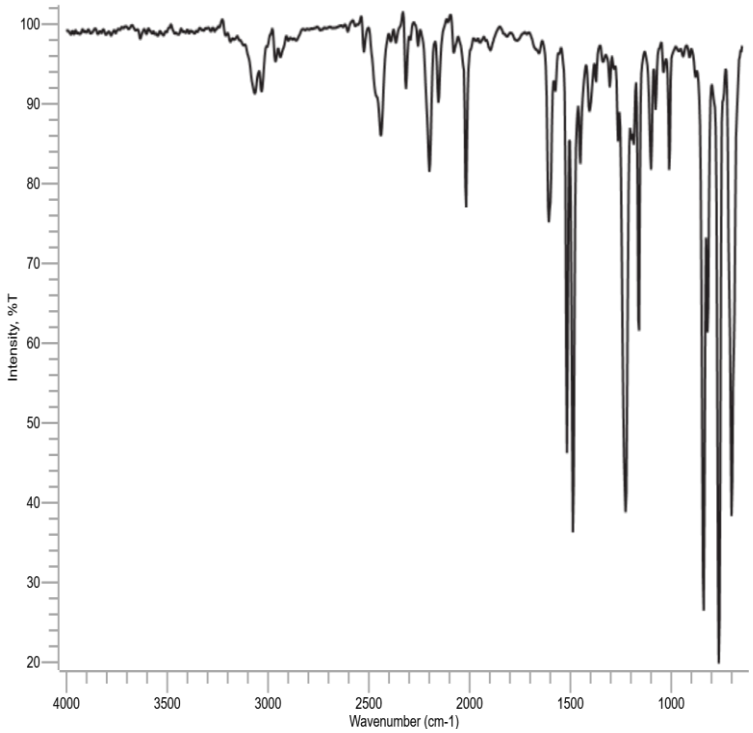

Figure 197: ATR-FTIR of 4-fluorobiphenyl.

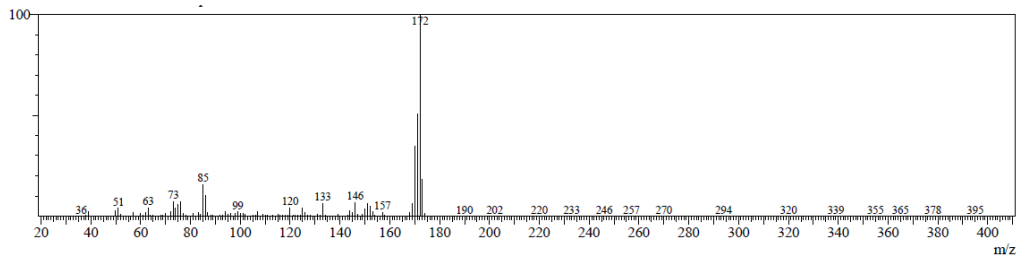

Figure 198: EI-MS spectrum of 4-fluorobiphenyl.

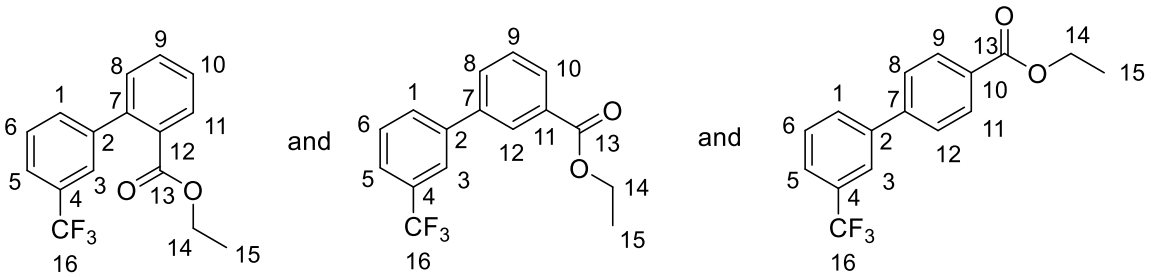

Figure 199: Structure of ethyl 3´-CF_3-biphenyl-*o*,*m*,*p*-carboxylate **26l** (22%:55%:23%) with numeric labels for NMR evaluation.

Experimental data of all isomers:

R_f index (eluent: CH:EA 19:1) = 0.34

Purification: preparative HPLC (eluent: MeCN/H_2O)

MS(EI): found m/z = 152 (21%), 201 (52%), 249 (100%), 266 (22%), 294 ($[M]^+$, 40%); calc. for $C_{16}H_{13}F_3O_2^+$ $[M]^+$: 294.09; refer to [230]

IR (ATR)/[cm^{-1}]: 3072, 2990, 1718, 1428, 1334, 1282, 1164, 1124, 1049, 905, 860, 808, 763, 701

Experimental data of ethyl 3´-CF_3-biphenyl-2-carboxylate:

t_R(GC/MS) = 8.83 min

^{1}H-NMR (300 MHz; MeCN-d_3), δ[ppm]: 8.31-8.26 (m; 1H; H^3); 8.14-7.57 (m; 7H; $H^{1+5+6+8-11}$); 4.37 (q; 2H; J=7.12 Hz; H^{14}); 1.38 (t; 1H; J=7.12 Hz; H^{15})

^{13}C-NMR (75 MHz; MeCN-d_3), δ[ppm]: 62.02 (1C; C^{14}); 14.51 (1C, C^{15})

^{19}F-NMR (282 MHz; MeCN-d_3), δ[ppm]: -63.06(s; 3F; F^{16})

Experimental data of ethyl 3´-CF_3-biphenyl-3-carboxylate:

t_R(GC/MS) = 8.32 min

^{1}H-NMR (300 MHz; MeCN-d_3), δ[ppm]: 7.85 (d; 2H; J=7.66 Hz; H^3); 7.72-7.67 (m, 1H, H^{12}); 7.66-7.48 (m; 5H; $H^{1+5+6+9+10}$); 7.43 (dd; 1H; J= 7.55 Hz + 1.04 Hz; H^8); 4.06 (q; 2H; J=7.15 Hz; H^{14}); 1.00 (t; 3H; J=7.12 Hz; H^{15})

^{13}C-NMR (75 MHz; MeCN-d_3), δ[ppm]: 168.75 (1C; C^{13}); 143.32 (1C; C^2); 141.47 (1C; C^7); 61.81 (1C; C^{14}); 13.92 (1C, C^{15})

^{19}F-NMR (282 MHz; MeCN-d_3), δ[ppm]: -63.01 (s; 3F; F^{16})

Experimental data of ethyl 3´-CF_3-biphenyl-4-carboxylate:

t_R(GC/MS) = 8.9 min

^{1}H-NMR (300 MHz; MeCN-d_3), δ[ppm]: 8.14-7.57 (m; 8H; $H^{1+3+5+6+8+9+11+12}$); 4.36 (q; 2H; J=7.12 Hz; H^{14}); 1.37 (t; 3H; J=7.12 Hz; H^{15})

^{13}C-NMR (75 MHz; MeCN-d_3), δ[ppm]: 61.91 (1C; C^{14}); 14.51 (1C, C^{15})

^{19}F-NMR (282 MHz; MeCN-d_3), δ[ppm]: -63.11(s; 3F; F^{16})

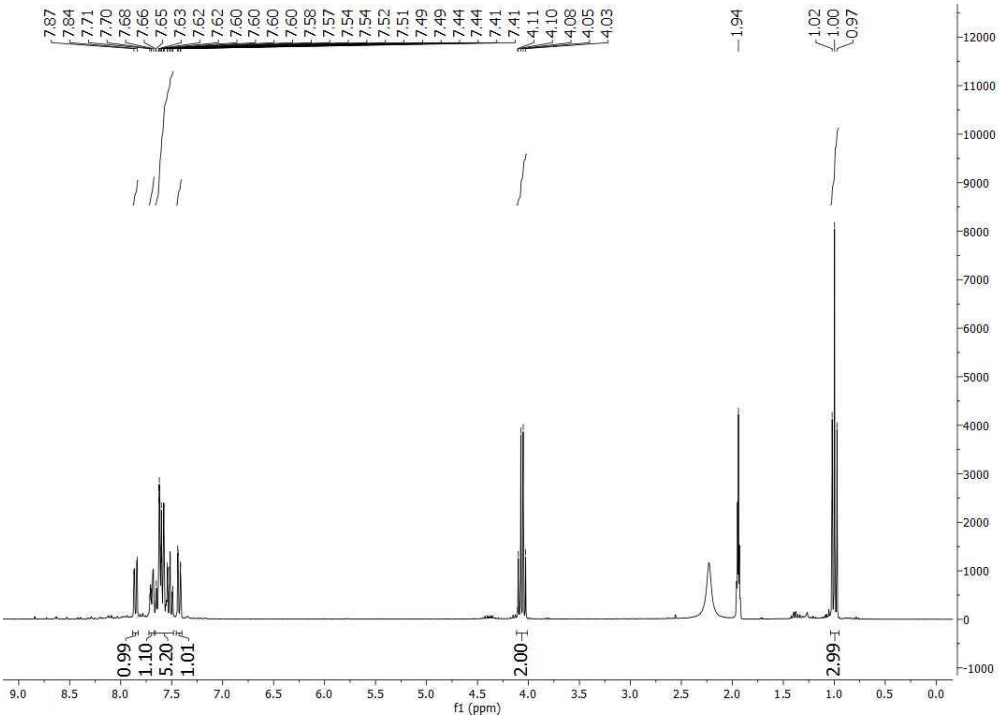

Figure 200: High-resolution ^{1}H-NMR spectrum of ethyl 3´-CF_3-biphenyl-3-carboxylate in MeCN-d_3.

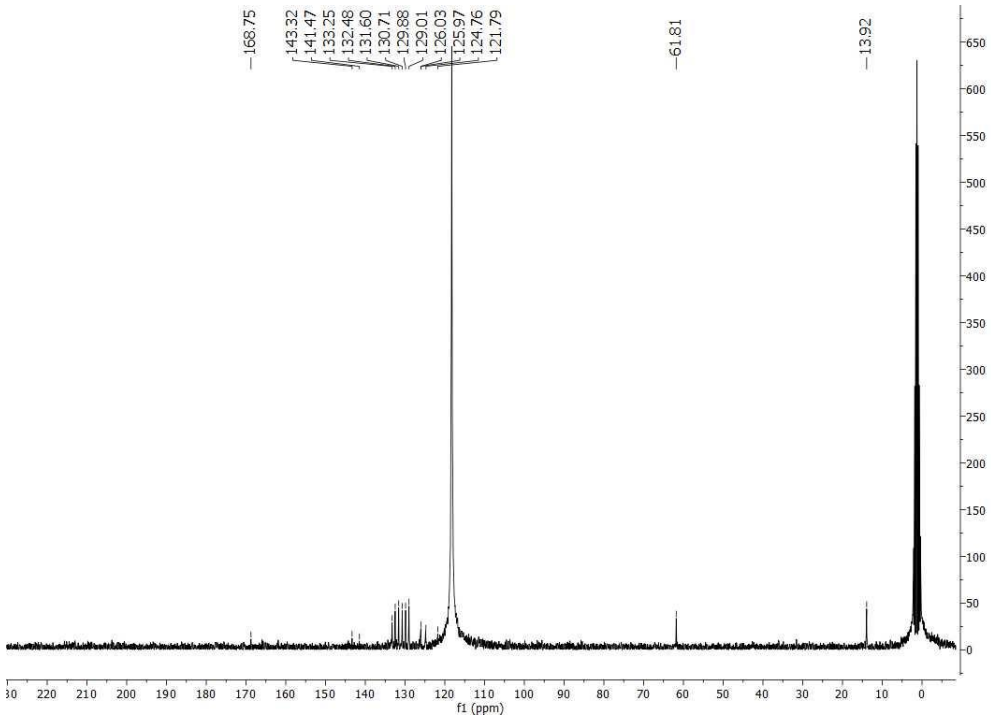

Figure 201: High-resolution ^{13}C-NMR spectrum of ethyl 3´-CF_3-biphenyl-3-carboxylate in MeCN-d_3.

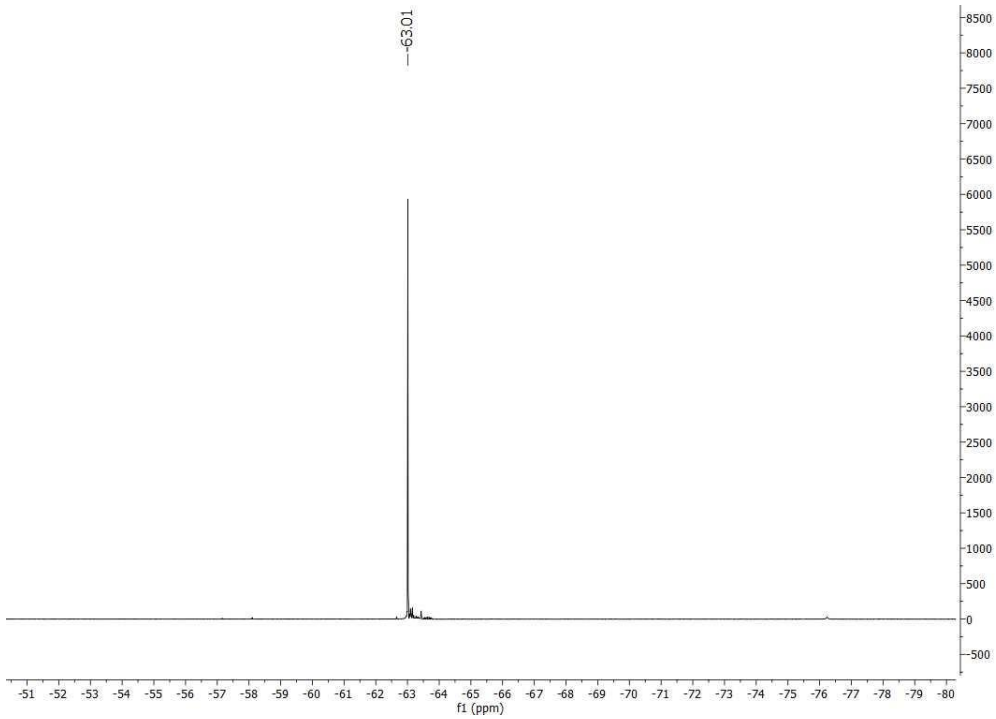

Figure 202: High-resolution ^{19}F-NMR spectrum of ethyl 3´-CF_3-biphenyl-3-carboxylate in MeCN-d_3.

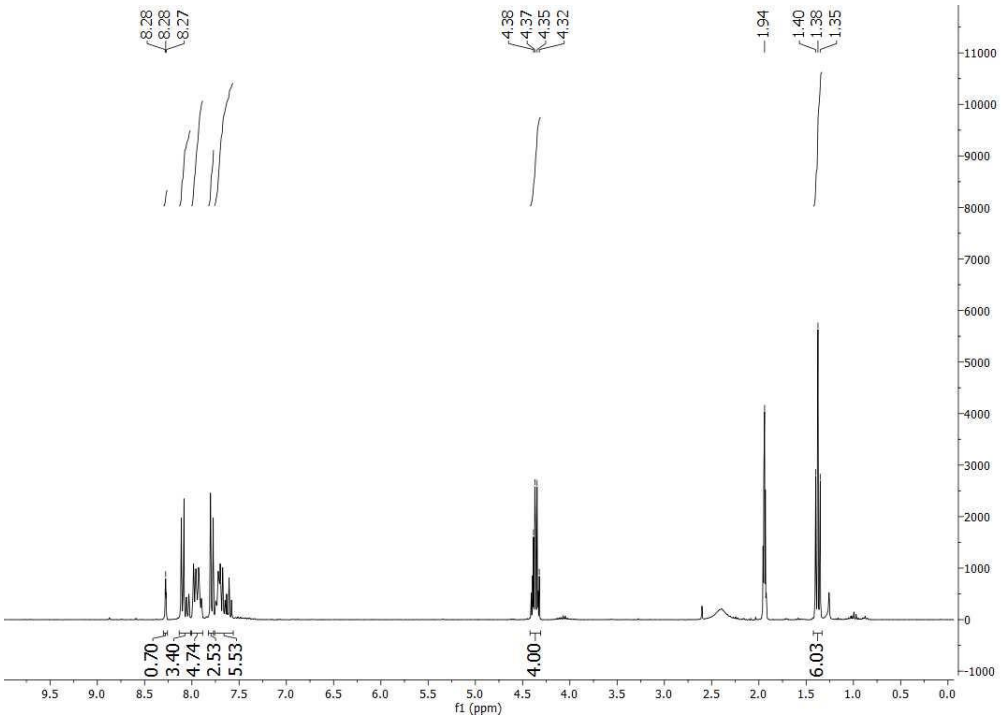

Figure 203: High-resolution ^{1}H-NMR spectrum of ethyl 3´-CF_3-biphenyl-*o*,*p*-carboxylate (mixture of isomers) in MeCN-d_3.

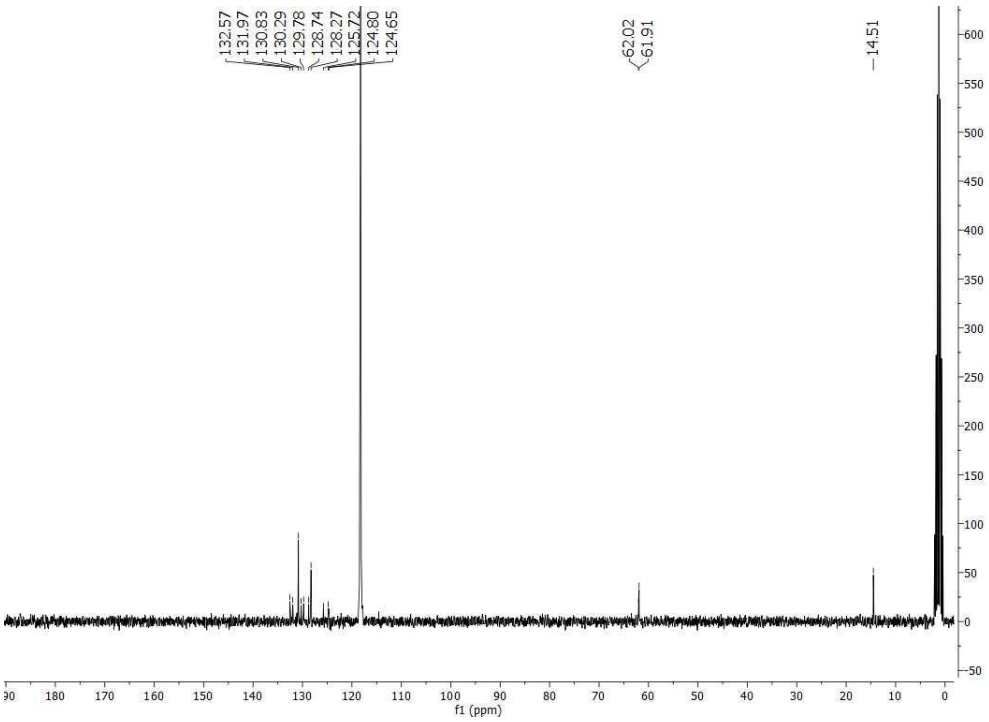

Figure 204: High-resolution ^{13}C-NMR spectrum of ethyl 3´-CF_3-biphenyl-*o*,*p*-carboxylate (mixture of isomers) in MeCN-d_3.

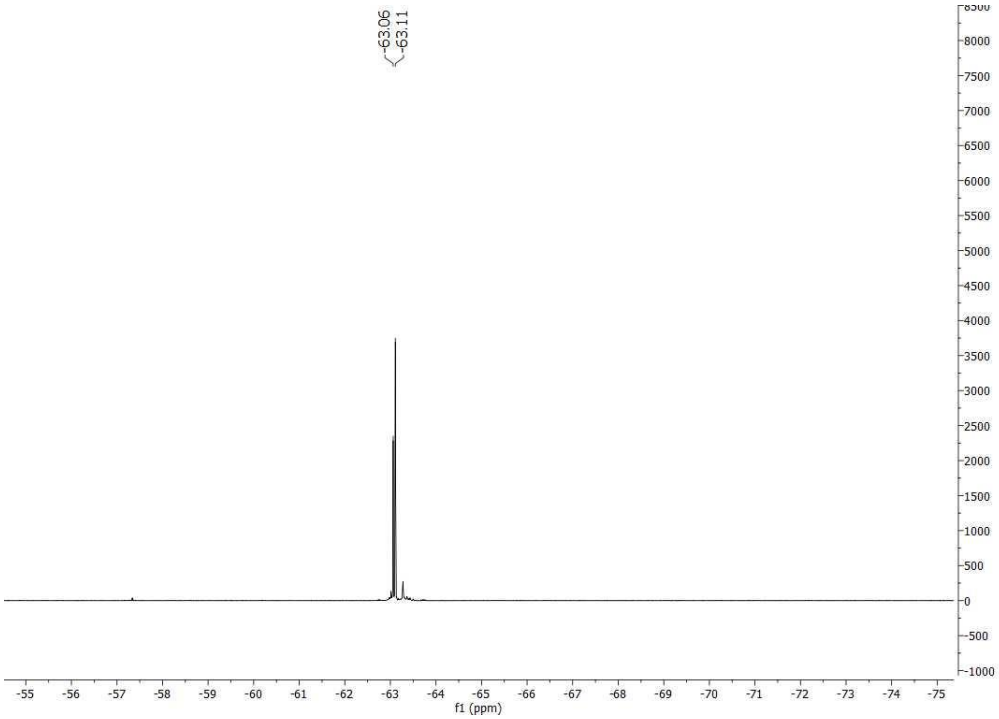

Figure 205: High-resolution ^{19}F-NMR spectrum of ethyl 3´-CF_3-biphenyl-*o*,*p*-carboxylate (mixture of isomers) in MeCN-d_3.

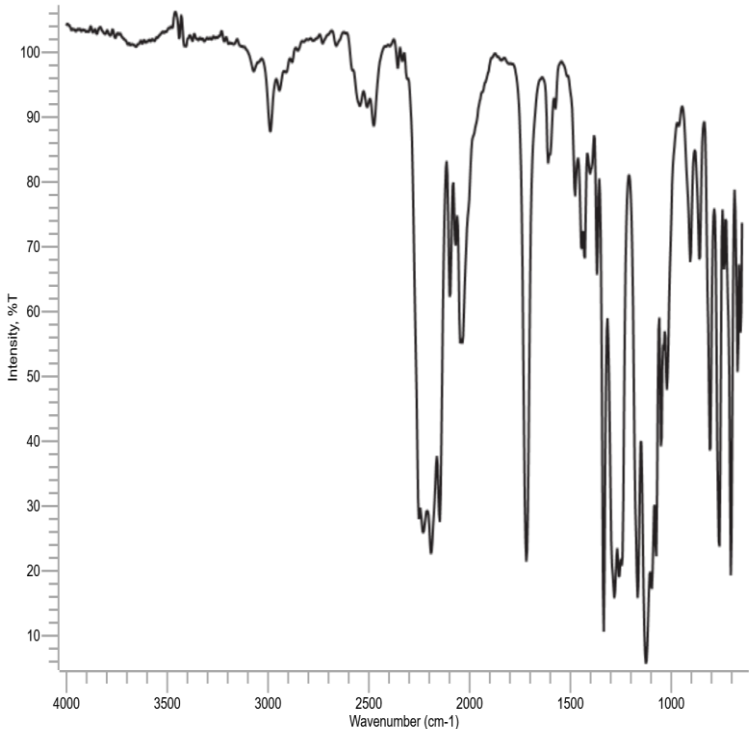

Figure 206: ATR-FTIR of ethyl 3´-CF_3-biphenyl-*o*,*m*,*p*-carboxylate (mixture of isomers).

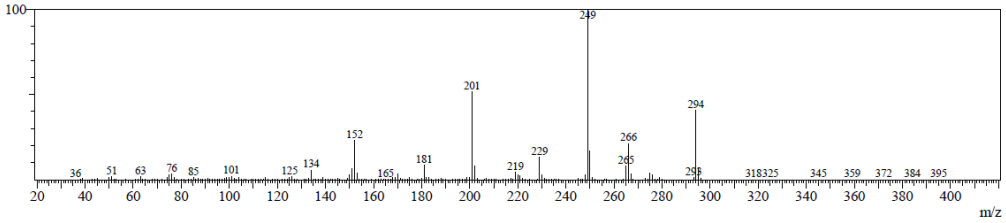

Figure 207: EI-MS spectrum of ethyl 3´-CF_3-biphenyl-*o*,*m*,*p*-carboxylate.

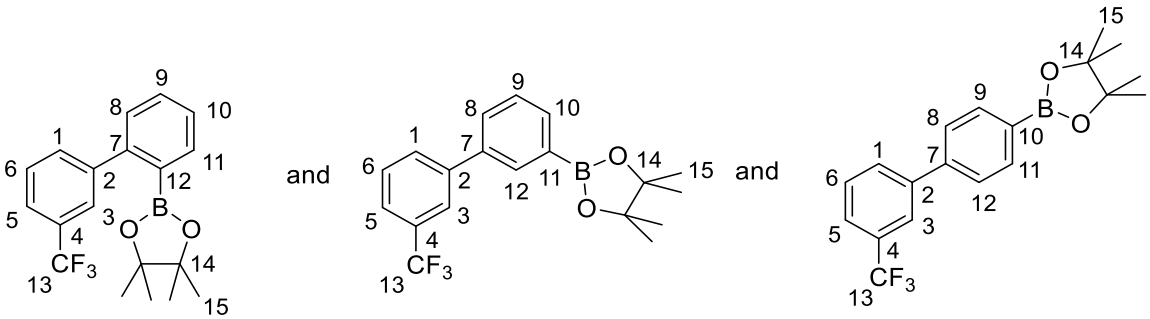

Figure 208: Structure of 4,4,5,5-tetramethyl-2-[3′-(trifluoromethyl)[1,1′-biphenyl]-*o*,*m*,*p*-yl]-1,3,2-dioxaborolane **26m** (25%:28%:47%) with numeric labels for NMR evaluation.

Experimental data of all isomers:

R_f index (eluent: CH:EA 19:1) = 0.4

Purification: preparative HPLC (eluent: MeCN/H_2O)

MS(EI): found m/z = 85 (24%), 163 (39%), 229 (100%), 247 (58%), 262 (68%), 333 (75%), 348 ($[M]^+$, 89%); calc. for $C_{19}H_{20}BF_3O_2^+$ $[M]^+$: 348.15

IR (ATR)/[cm^{-1}]: 3063, 2983, 2934, 1598, 1353, 1330, 1267, 1162, 1122, 1074, 1044, 963, 903, 857, 804, 766, 705

Experimental data of 4,4,5,5-tetramethyl-2-[3′-(trifluoromethyl)[1,1′-biphenyl]-2-yl]-1,3,2-dioxaborolane:

t_R(GC/MS) = 9.23 min

^{1}H-NMR (300 MHz; $CDCl_3$), δ[ppm]: 1.37 (s; 12H; H^{15})

^{13}C-NMR (75 MHz; $CDCl_3$), δ[ppm]: 84.18 (1C; C^{14}); 25.02 (1C, C^{15})

^{19}F-NMR (282 MHz; $CDCl_3$), δ[ppm]: -62.49 (s; 3F; F^{13})

Experimental data of 4,4,5,5-tetramethyl-2-[3′-(trifluoromethyl)[1,1′-biphenyl]-3-yl]-1,3,2-dioxaborolane:

t_R(GC/MS) = 9.37min

^{1}H-NMR (300 MHz; $CDCl_3$), δ[ppm]: 1.37 (s; 12H; H^{15})

^{13}C-NMR (75 MHz; $CDCl_3$), δ[ppm]: 84.11 (1C; C^{14}); 25.02 (1C, C^{15})

^{19}F-NMR (282 MHz; $CDCl_3$), δ[ppm]: -62.58 (s; 3F; F^{13})

Experimental data of 4,4,5,5-tetramethyl-2-[3′-(trifluoromethyl)[1,1′-biphenyl]-4-yl]-1,3,2-dioxaborolane:

t_R(GC/MS) = 8.81 min

^{1}H-NMR (300 MHz; $CDCl_3$), δ[ppm]: 7.81 (d; 1H; J=7.38 Hz; H^3); 7.65 (s; 1H; H^6); 7.62-7.54 (m; 2H; H^{9+11}); 7.52-7.45 (m; 2H; H^{8+12}); 7.43-7.37 (m; 1H; H^5); 7.37-7.31 (m; 1H; H^1); 1.19 (s; 12H; H^{15})

^{13}C-NMR (75 MHz; $CDCl_3$), δ[ppm]: 146.42 (1C; C^2); 143.89 (1C; C^7); 135.21 (2C; C^{9+11}); 132.34 (1C; C^{10}); 130.48 (1C; C^4); 129.20 (1C; C^1); 128.18 (1C; C^6); 126.96 (2C; C^{8+12}); 126.30 (1C; C^3); 124.94 (1C; C^{13}); 123.62 (1C; C^5); 83.84 (1C; C^{14}); 24.56 (1C, C^{15})

^{19}F-NMR (282 MHz; $CDCl_3$), δ[ppm]: -62.39 (s; 3F; F^{13})

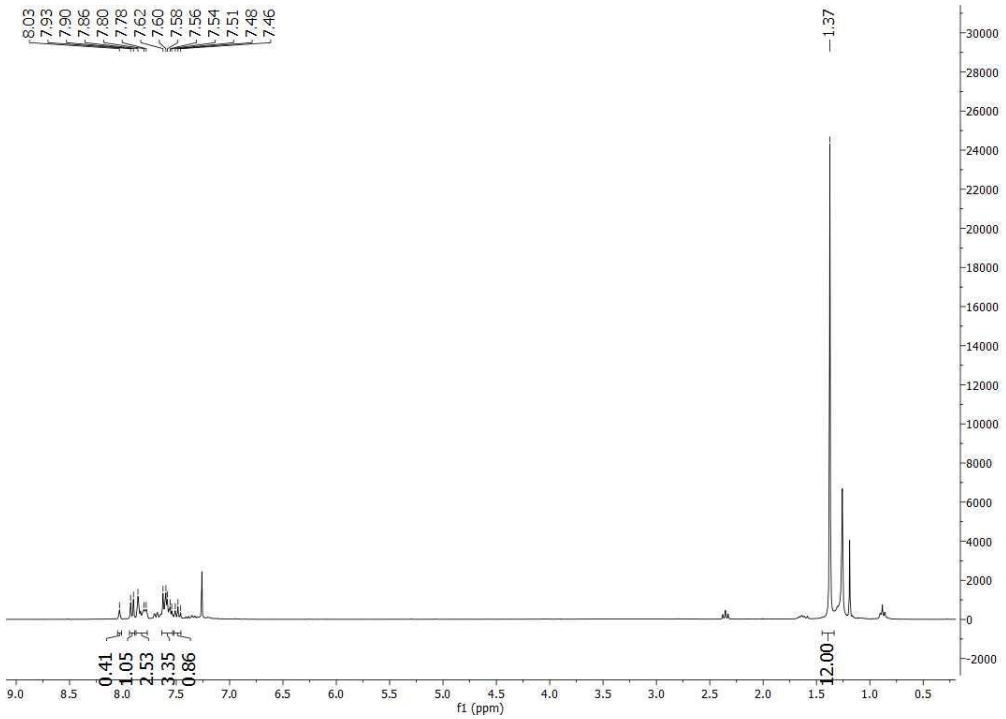

Figure 209: High-resolution ^{1}H-NMR spectrum of 4,4,5,5-tetramethyl-2-[3′-(trifluoromethyl)[1,1′-biphenyl]-*o*,*m*-yl]-1,3,2-dioxaborolane (mixture of isomers) in $CDCl_3$.

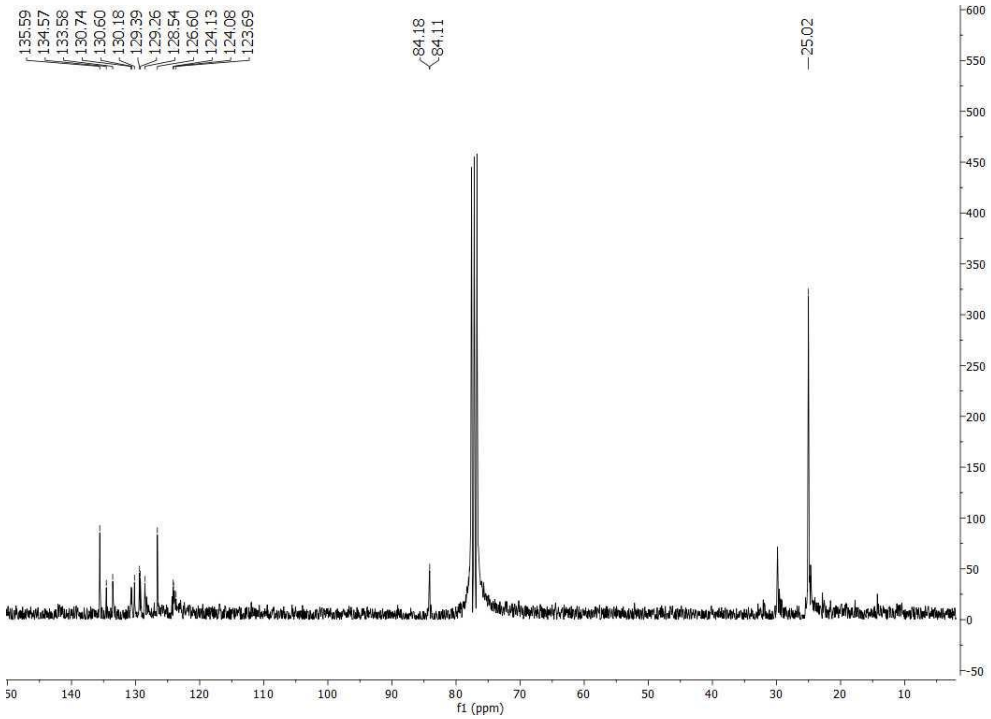

Figure 210: High-resolution ^{13}C-NMR spectrum of 4,4,5,5-tetramethyl-2-[3′-(trifluoromethyl)[1,1′-biphenyl]-*o*,*m*-yl]-1,3,2-dioxaborolane (mixture of isomers) in $CDCl_3$.

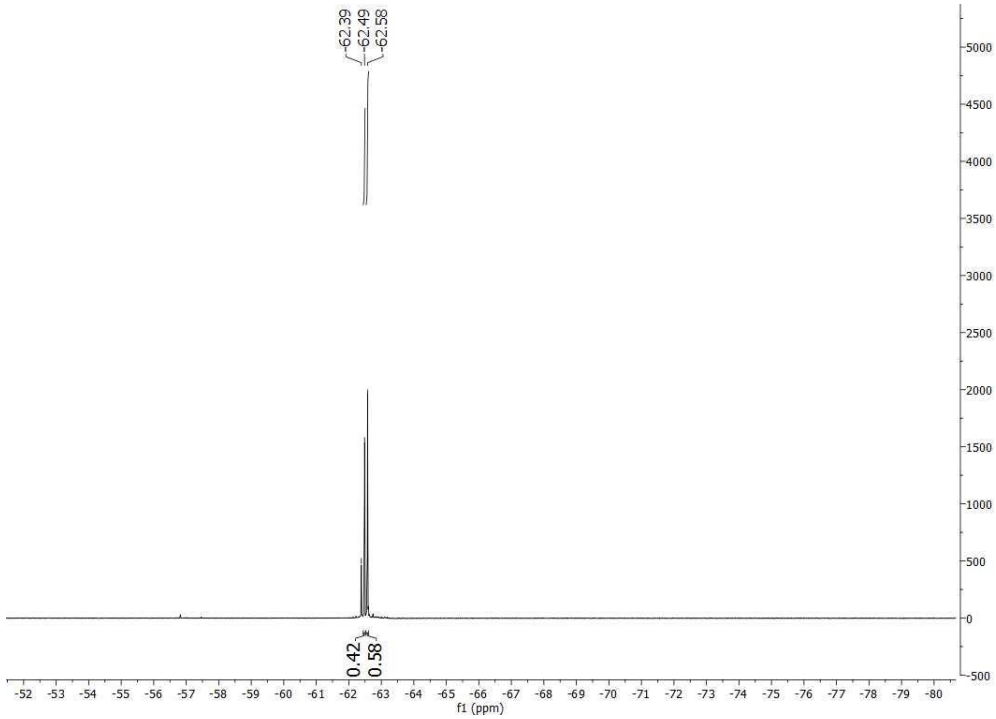

Figure 211: High-resolution ^{19}F-NMR spectrum of 4,4,5,5-tetramethyl-2-[3′-(trifluoromethyl)[1,1′-biphenyl]-*o*,*m*-yl]-1,3,2-dioxaborolane (mixture of isomers) in $CDCl_3$.

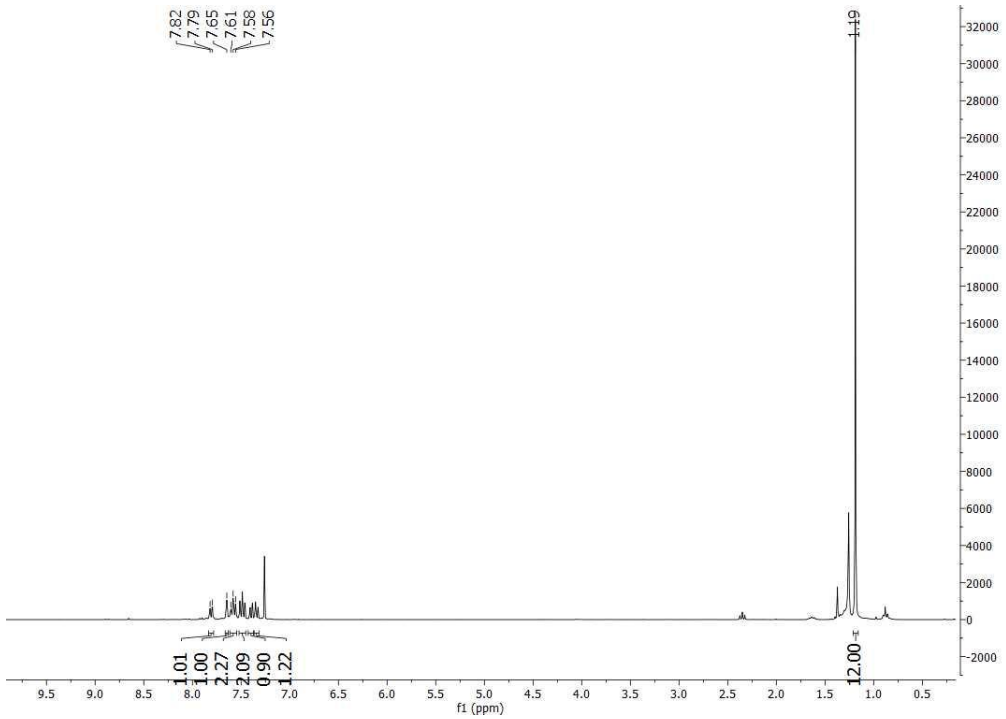

Figure 212: High-resolution ^{1}H-NMR spectrum of 4,4,5,5-tetramethyl-2-[3′-(trifluoromethyl)[1,1′-biphenyl]-4-yl]-1,3,2-dioxaborolane in $CDCl_3$.

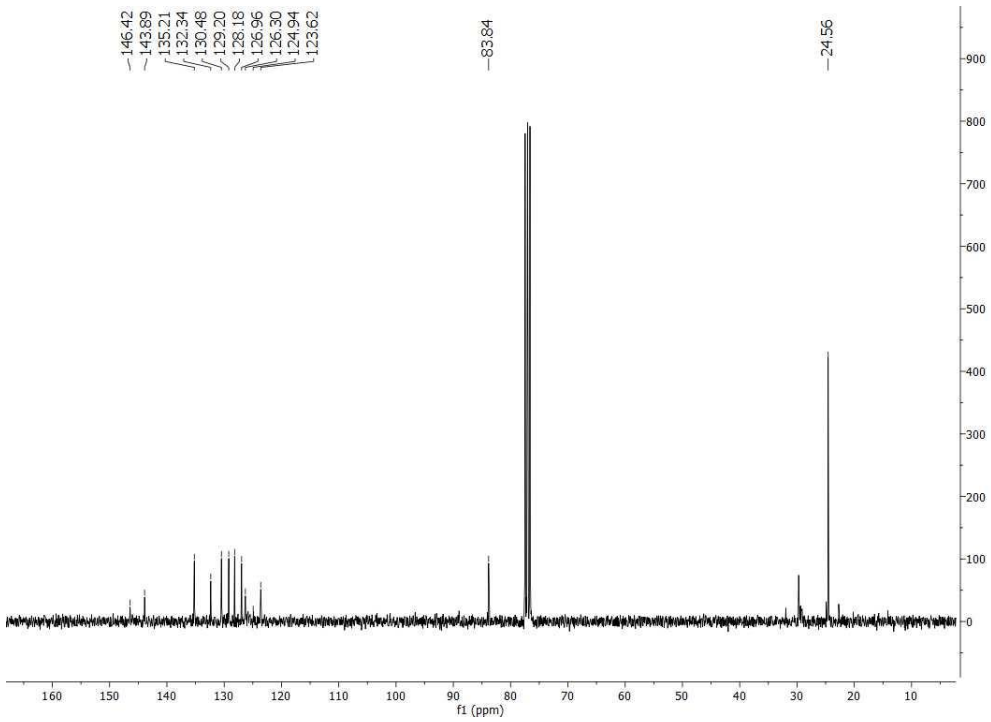

Figure 213: High-resolution ^{13}C-NMR spectrum of 4,4,5,5-tetramethyl-2-[3′-(trifluoromethyl)[1,1′-biphenyl]-4-yl]-1,3,2-dioxaborolane in $CDCl_3$.

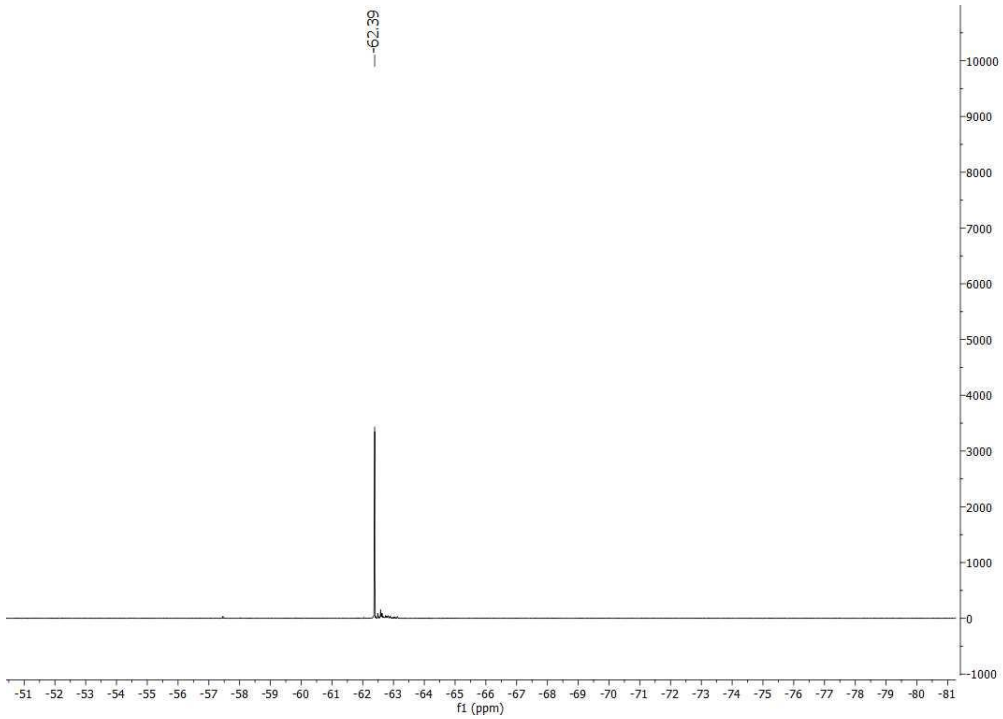

Figure 214: High-resolution ^{19}F-NMR spectrum of 4,4,5,5-tetramethyl-2-[3'-(trifluoromethyl)[1,1'-biphenyl]-4-yl]-1,3,2-dioxaborolane in $CDCl_3$.

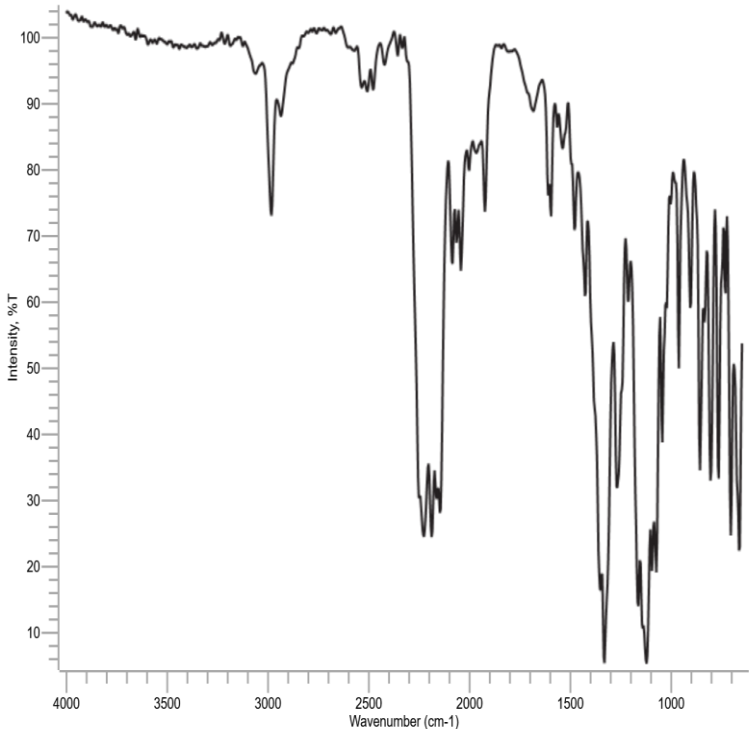

Figure 215: ATR-FTIR of 4,4,5,5-tetramethyl-2-[3´-(trifluoromethyl)[1,1´-biphenyl]-*o*,*m*,*p*-yl]-1,3,2-dioxaborolane (mixture of isomers).

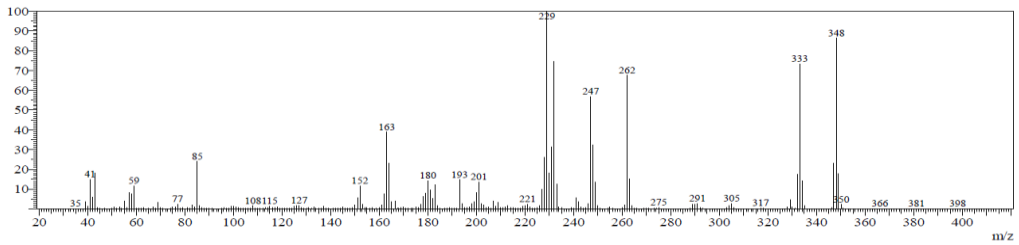

Figure 216: EI-MS spectrum of 4,4,5,5-tetramethyl-2-[3´-(trifluoromethyl)[1,1´-biphenyl]-*o*,*m*,*p*-yl]-1,3,2-dioxaborolane.

4.2.3.6 Long-term continuous synthesis and quantification of selected examples

Long-term continuous synthesis is conducted according to the Standard working procedure of chapter 4.2.3.5.

3-CF_3-biphenyl **26b** is synthesized at 1.25 h irradiation time using a 365 nm LED-array at 50 W_{el}. 0.8 M 3-CF_3-aniline + 1.6 M TFA in acetonitrile is used as Feed A (50 µL×min^{-1}). Feed B contains 0.96 M *tert*-butyl nitrite in acetonitrile (50 µL×min^{-1}) and Feed C transports benzene (100 µL×min^{-1}). After reaching the steady state (>1.5×residence time), ^{19}F-NMR experiments and GC/MS analysis is conducted according to the known procedures.

Table 35: Timestamps for online ^{19}F-NMR and offline GC/MS analysis in a long-term catalyst-free continuous photochemical synthesis of **26b**.

timestamp [hh:mm]	online ^{19}F-NMR analysis	offline GC/MS analysis		timestamp [hh:mm]	online ^{19}F-NMR analysis	offline GC/MS analysis
09:45		x		12:46	x	
09:53	x			13:20	x	
09:58	x			13:44	x	
10:02	x			13:45		x
10:07	x			13:48	x	
10:15		x		14:22	x	
10:25	x			14:45		x
10:35	x			14:49	x	
10:45	x	x		15:20	x	
11:15	x			15:45		x
11:41	x			16:00	x	
12:15	x			16:17		x

26m is synthesized at 1.25 h irradiation time using a 365 nm LED-array at 50 W_{el}. 0.8 M 3-CF_3-aniline + 1.6 M TFA in acetonitrile is used as Feed A (50 µL×min^{-1}). Feed B contains 0.96 M *tert*-butyl nitrite in acetonitrile (50 µL×min^{-1}) and Feed C transports 4.5 M phenylboronic acid pinacol ester (100 µL×min^{-1}). After reaching the steady state (>1.5×residence time), ^{19}F-NMR experiments and GC/MS analysis is conducted according to the known procedures.

Table 36: Timestamps for online ^{19}F-NMR and offline GC/MS analysis in a long-term catalyst-free continuous photochemical synthesis of **26m**.

timestamp [hh:mm]	online ^{19}F-NMR analysis	offline GC/MS analysis		timestamp [hh:mm]	online ^{19}F-NMR analysis	offline GC/MS analysis
10:53	x			15:19	x	
10:57	x			15:34	x	
11:18	x	x		15:44	x	
11:46	x			16:00	x	
11:55	x			16:15	x	
12:35	x			16:45	x	x
12:46	x			17:00	x	
12:53	x			17:15		x
13:17	x			17:28	x	
13:45		x		17:40	x	
13:46	x			17:45		x
14:13	x			18:04	x	
14:17		x		18:14	x	x
14:48		x		18:30	x	
14:49	x			18:45		x

4.2.3.7 Synthesis and isolation of 3-CF_3-phenyldiazonium trifluoroacetate

Synthesis of 3-CF_3-phenyldiazonium trifluoroacetate is adapted from Colas *et al.*[163] A 250 mL three-necked round bottom-flask is equipped with a stirrer and two septa. The flask is constantly purged and covered with nitrogen. 2.39 g trifluoroacetic acid (21 mmol, 2.1 equiv.) are added slowly to 13 mL dichloromethane and 1.60 g 3-CF_3-aniline (10 mmol). The mixture is constantly stirred and cooled to -12 °C. 1.24 g *tert*-butyl nitrite (12 mmol, 1.2 equiv.) are added via a syringe over a period of 10 minutes and stirred further for 20 minutes at -12 °C. The mixture is cooled to -78°C and diazonium salt will precipitate. The salt is separated and washed twice with 20 mL diethyl ether (-78 °C) to yield 2.75 g of a white solid (6.9 mmol, 69% according to theory). The solid is stored in the freezer at -20 °C.

Synthesis is repeated in an adapted 40 mmol scale to give 7.5 g of a white solid (18.4 mmol, 46% according to theory).

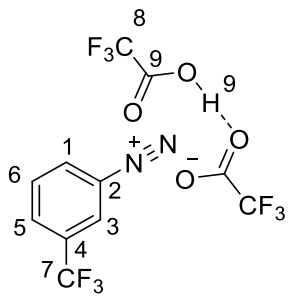

Figure 217: Structure of 3-CF_3-phenyldiazonium trifluoroacetate with numeric labels for NMR evaluation.

^{1}H-NMR (400 MHz; MeCN-d_3), δ[ppm]: 11.45 (s; 1H; H^9); 8.85 (s; 1H; H^3); 8.76 (d; 1H; J=8 Hz; H^5); 8.55 (d; 1 H; J=8 Hz; H^1); 8.16 (t; 1 H; J=8 Hz; H^6)

^{13}C-NMR (100 MHz; MeCN-d_3), δ[ppm]: 160.51 (2C; C^9); 139.45 (3C; C^{4+5+6}); 136.93 (1C; C^1); 134.22 (1C; C^3); 133.98 (2C; C^8); 130.73(1C; C^2); 119.97 (1C; $^1J_{C-F}$ = 270 Hz; C^7)

^{19}F-NMR (376 MHz; MeCN-d_3), δ[ppm]: -62.23 (s; 3F; F^7); -75.65 (s; 6F; F^8)

4.2.3.8 Studies on the mechanism of photochemical arylation using arene diazonium trifluoroacetates

Mechanistic studies are carried out according to the standard working procedure for continuous catalyst-free synthesis of 3-CF_3-biphenyl (4.2.3.1). Figure 218 is used as setup#1 and Figure 130 is used as setup #2. All feeds are transported by HPLC pumps.

In setup #2 diazonium trifluoroacetate is generated by mixing Feed A and B via a T-junction. Salt passes a residence element (1/16" FEP (800 µm ID, 10 min), which is protected from light and cooled to 20 °C. Via a second T-junction Feed-C (neat benzene) is added before entering the 1/16" FEP capillary photoreactor. Reactions using previously isolated diazonium trifluoroacetate are conducted in setup #1. Feed A consists of 0.1 M 3-CF_3-phenyldiazonium trifluoroacetate in acetonitrile. The solution is stored in a 100 mL round bottom flask and protected from light and air. The flask is cooled to 0-5 °C. Neat benzene represents Feed B.

an excess pressure of 4 bar_{exs} is applied in both setups and controlled via a proportional relief valve and a manometer.

A hexagonal shaped 6×6 LED-array 365 nm 50 W_{el} is placed in the center of the reactor and cooled to 20°C via a cooling finger to provide stable performance of the LEDs. When reaching steady state (>1.5×residence time), an aliquot of 50 µL is diluted with 900 µL acetonitrile and 50 µL (50 mM) DL-menthol as external standard. Quantitative analysis is performed via GC/MS. All further information and parameters are given in Table 37.

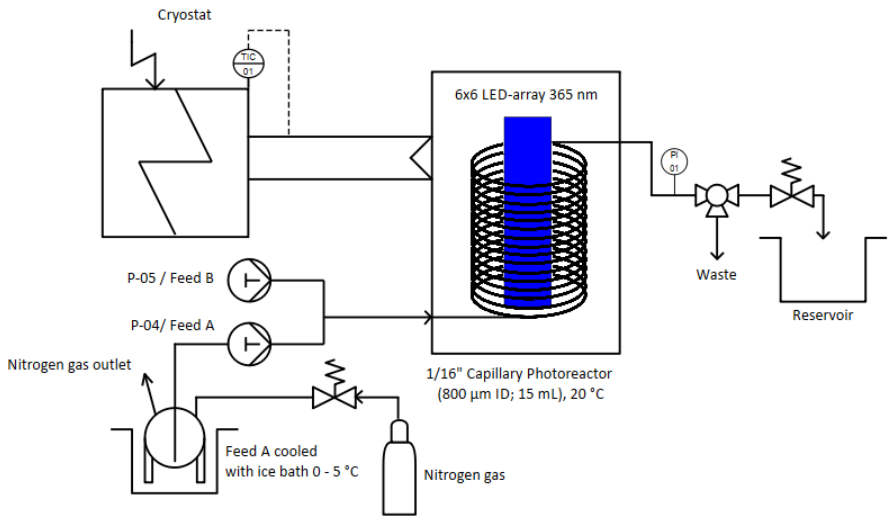

Figure 218: Setup #1 for studies on the mechanism of photochemical arylation using diazonium trifluoroacetates.

Table 37: Parameters and additional information for studies on the mechanism of photochemical arylation using diazonium trifluoroacetates.

#	setup	Feed A	Feed B	Feed C	flow rate Feed A, Feed B [µL×min^{-1}]	flow rate Feed C [µL×min^{-1}]	$V_{reactor}$ [mL]	λ [nm]	P [W_{el}]	T [°C]	t_R [h][a]
1	#1	**e**	**d**	-	70	140	15	365	50	20	53
2	#1	**e**	**d**	-	125	250	15	365	50	20	30
3	#1	**e**	**d**	-	156	312	15	365	50	20	24
4	#1	**e**	**d**	-	250	500	15	365	50	20	15
5	#1	**e**	**d**	-	375	750	15	365	50	20	10
6	#1	**e**	**d**	-	500	1000	15	365	50	20	7.5
7	#1	**e**	**d**	-	1500	3000	15	365	50	20	2.5
8	#2	**b**	**c**	**d**	50	100	15	365	50	20	75
9	#2	**b**	**c**	**d**	62.5	125	15	365	50	20	60
10	#2	**b**	**c**	**d**	70	140	15	365	50	20	53
11	#2	**b**	**c**	**d**	125	250	15	365	50	20	30
12	#2	**b**	**c**	**d**	156	312	15	365	50	20	24
13	#2	**b**	**c**	**d**	250	500	15	365	50	20	15
14	#2	**b**	**c**	**d**	375	750	15	365	50	20	10
15	#2	**b**	**c**	**d**	500	1000	15	365	50	20	7.5
16	#2	**b**	**c**	**d**	1500	3000	15	365	50	20	2.5

a: residence time calculated by flowrate; **b:** 0.2 M 3-CF_3-aniline + 0.4 M TFA in MeCN; **c:** 0.24 M *t*-BuONO in MeCN; **d:** neat benzene; **e:** 0.1 M 3-CF_3-phenyldiazonium trifluoroacetate in MeCN

4.2.3.9 Batch-synthesis of 3-CF_3-biphenyl to exclude a cationic mechanism

In a 30 mL clear glass vial containing 3-CF_3-aniline (81 mg, 0.05 M), trifluoroacetic acid (2.0 equiv.; 114 mg), in 5 mL benzene, 4.5 mL acetonitrile and 0.5 mL water is added 1.2 equivalents *tert*-butyl nitrite (1.2 equiv.; 62 mg). The vial is sealed with a cap, stirred by a magnetic stir plate and placed ~6 cm in front of a 4×1 365 nm LED-array 6 W_{el}. By mounting the array on an aluminum heatsink for optimal heat dissipation, reaction temperature stays at RT and additional thermal effects are avoided. An aliquot of 50 µL is diluted with 900 µL acetonitrile and 50 µL (50 mM) DL-menthol as external standard. Qualitative GC/MS-analysis is performed after 17 h.

4.2.3.10 Stability and decomposition test of 3-CF_3-phenyldiazonium trifluoroacetate

5 mL of a 0.1 M 3-CF_3-phenyldiazonium trifluoroacetate solution (in acetonitrile) are cooled to 0-5 °C and stored protected from light and air in a 100 mL round bottom flask. An aliquot of this solution is analyzed via ^{19}F-NMR spectroscopy via offline measurements in standard NMR-tubes. Following settings are applied: 64 scans, 80.49° pulse, 1.9 s acquisition time and 2.9 s repetition time. Samples are taken directly after preparation and after 8, 20 and 60 minutes.

4.3 Development of a (semi-)automatic continuous lab-plant and the integration of online spectroscopy for a two-step synthesis of *Z*-stilbene

4.3.1 Online UV/Vis-spectroscopy

UV/Vis-spectroscopy is tested with an Avantes fiber spectrometer (AvaSpec-ULS2048CL-EVO-RS including AvaLight-DH-S-BAL). A 1.5 mm micro flow cell from Avantes is used as a sample chamber. 0.05 M benzaldehyde, 0.05 M BTTP, 0.05 M TPPO, 0.05 M *E*-stilbene and 0.05 M *Z*-stilbene in toluene/MeOH V/V=85/15 are injected separately into the micro flow cell. Samples are acquired at an integration time of 90.000 ms and an average number of 10 scans.

4.3.2 Online ^{31}P-NMR spectroscopy

A Nanalysis NMReady60 pro is equipped with a PEEK flow cell. Following settings are used for ^{31}P-NMR experiments: 24.5 MHz, 80.62° pulse, 1.6 s acquisition time, 6.6 s repetition time, proton decoupling, 50 dB receiver gain and 32 scans. 0.1 M benzyltriphenylphosphonium bromide BTTP (in toluene) is analyzed at different flowrates: stopped flow, 1.0 mL×min^{-1} and blue 1.5 mL ×min^{-1}. 0.1 M TPPO and 0.1 M triphenyl phosphate (in toluene) are analyzed at stopped flow to determine the chemical shifts. 0.25 M BTTP and 0.25 M TBD are dissolved in toluene to determine the chemical shift of the ylide at stopped flow.

4.3.3 Online ^{1}H-NMR spectroscopy

A Nanalysis NMReady60 pro is equipped with a PEEK flow cell. Following settings are used for ^{1}H -NMR experiments: 60 MHz, 80.62° pulse, 2.7 s acquisition time, 2.9 s repetition time, gated decoupling, 14 dB receiver gain, 16 scans. Characteristic shifts are of benzaldehyde, BTTP, TPPO, *E*-, *Z*-stilbene, TBD, DBU, *tert*-butyl benzene are determined at 0.5 M concentration in toluene/methanol V/V=8/2.

4.3.3.1 Spectrometer calibration

248 mM Benzaldehyde and 199 mM *Z*-stilbene are dissolved in toluene for calibration purpose. This solution is diluted to 80%, 40%, 20% and 10% of the original concentration. Each solution is measured three times at 0 mL×min^{-1} and 1.5 mL×min^{-1}. The mean value of every concentration is used for calibration

The .dx-NMR spectra are evaluated with a Python script (with automated phase and baseline correction; provided by NAN) to give the peak areas. Integration range 6.42 - 6.57 ppm is used for *Z*-stilbene and 9.60 - 9.75 ppm is used for benzaldehyde.
NMR-spectra are evaluated with PEAXACT 5.3 (including phase and baseline correction; S-PACT GmbH) using the integration model. Integration range 6.44167 - 6.65567 ppm (baseline: linear fit) is used for *Z*-stilbene and 9.61919 - 9.80987 ppm (baseline: linear fit) is used for benzaldehyde (see Figure 299 in the appendix).

Validation of the ^{1}H-NMR spectrometer is performed with three samples (solvent: toluene), which are measured at stopped flow three times each. Sample 1 contains 166 mM benzaldehyde and 34 mM TPPO. Sample 2 contains 145 mM TPPO, 59 mM *E*-stilbene, 90 mM benzaldehyde and 125 mM *Z*-stilbene. Sample 3 contains 190 mM TPPO, 104 mM *E*-stilbene, 25 mM benzaldehyde and 226 mM *Z*-stilbene.

4.3.4 Online IR-spectroscopy and liquid-liquid phase separation

ATR-FTIR spectroscopy is conducted via a Mettler Toledo ReactIR 15 equipped with a DS Micro Flow Cell (50 µL sample volume). Spectra are recorded from 4000 to 650 cm^{-1} with a resolution of 8 cm^{-1}. 128 scans are recorded per spectrum.

4.3.4.1 IR-spectroscopy of toluene/methanol mixtures

Different solvent signals of toluene/methanol mixtures are recorded in stopped flow. Following mixtures are used: neat toluene, toluene/methanol V/V= 9/1, V/V= 8/2, V/V= 7/3, V/V= 6/4, V/V= 5/5, V/V= 4/6, V/V= 3/7, V/V= 2/8, V/V= 1/9, V/V= 85/15, V/V= 98/2, V/V= 99/1, neat methanol.

4.3.4.2 Solvent extraction and phase-separation performance test

The organic phase of a manual liquid-liquid solvent extraction after phase-separation is monitored with the IR-spectrometer:
- 5 mL toluene/methanol (V/V=9/1) is extracted with 5 mL 1 N aqueous hydrochloric acid (diluted with 50vol% methanol).
- 5 mL toluene/methanol (V/V=85/15) is extracted with 5 mL 0.6 N aqueous sulfuric acid (diluted with 40vol% methanol).
- 5 mL toluene/methanol (V/V=8/2) is extracted with 5 mL 1 N aqueous hydrochloric acid (diluted with 50vol% methanol).

Continuous liquid-liquid extraction is conducted in the lab plant setup (Figure 219). Feed A (toluene/methanol (V/V=8/1)) is extracted with Feed C (1 N aqueous hydrochloric acid (diluted with 50vol% methanol)). Both Feeds are pumped with a flow rate of 1 $mL \times min^{-1}$. A Zaiput Sep-10 liquid-liquid separator with a hydrophobic OB-900 membrane is used. Constant separation stability is monitored for 1.5 h at least.

Different membranes (OB-900, OB-2000, IL-900) are tested in continuous flow, using Feed A (toluene/methanol (V/V=85/15)+ 0.25 M benzaldehyde) and Feed C (0.6 N aqueous sulfuric acid (diluted with 40vol% methanol)). Both Feeds are pumped with a flow rate of 0.7 $mL \times min^{-1}$.

4.3.4.3 Substrate extraction and phase transfer experiments

Manual extraction experiments are conducted and each organic phase is monitored with the FTIR-spectrometer:

- 10 mL toluene/methanol V/V=9/1 are extracted with 10 mL 0.6 N aqueous sulfuric acid (diluted with 40vol% methanol)
- 10 mL 0.23 M TPPO in toluene/methanol V/V=9/1 are extracted with 10 mL 0.6 N aqueous sulfuric acid (diluted with 40vol% methanol)
- 10 mL 0.2 M BA in toluene/methanol V/V=9/1 are extracted with 10 mL 0.6 N aqueous sulfuric acid (diluted with 40vol% methanol)
- 10 mL 0.1 M BTTP in toluene/methanol V/V=9/1 are extracted with 10 mL 0.6 N aqueous sulfuric acid (diluted with 40vol% methanol)
- 10 mL 0.109 M *E*-stilbene in toluene/methanol V/V=9/1 are extracted with 10 mL 0.6 N aqueous sulfuric acid (diluted with 40vol% methanol)
- 10 mL 0.122 M *Z*-stilbene in toluene/methanol V/V=9/1 are extracted with 10 mL 0.6 N aqueous sulfuric acid (diluted with 40vol% methanol)
- 10 mL 0.10 M DBU in toluene/methanol V/V=9/1 are extracted with 10 mL 0.6 N aqueous sulfuric acid (diluted with 40vol% methanol)

4.3.4.4 IR-spectrometer calibration

The solvent for the background signal of IR-calibration is prepared as followed. 100 mL toluene/methanol (V/V=85/15) is extracted with 100 mL 0.6 N aqueous sulfuric acid (diluted with 40vol% methanol). Remaining organic phase is used for the further procedure. 253 mM TPPO, 253 mM *E*-stilbene, 266 mM benzaldehyde and 291 mM *Z*-stilbene are dissolved in the prepared solvent. This solution is diluted to 80%, 40%, 20% and 10% to give the other concentrations for calibration. Each sample is measured at least six times at stopped flow.

Linear regression with baseline correction at 1840 cm^{-1} and solvent subtraction is performed with Mettler Toledo IC Quant.

Validation of the IR-spectrometer is performed with four samples (solvent obtained via extraction), which are measured stopped flow. Sample 1 contains 166 mM benzaldehyde and 34 mM TPPO. Sample 2 contains 145 mM TPPO, 59 mM *E*-stilbene, 90 mM benzaldehyde and 125 mM *Z*-stilbene. Sample 3 contains 190 mM TPPO,

104 mM *E*-stilbene, 25 mM benzaldehyde and 226 mM *Z*-stilbene. Sample 4 contains 73 mM TPPO, 35 mM *E*-stilbene, 203 mM benzaldehyde and 46 mM *Z*-stilbene.

4.3.5 Online nondispersive IR-sensor

Transmission IR-spectroscopy is conducted with the original ZnSe flow cell setup. Two ZnSe windows are placed in a distance of 100 µm to give the sample chamber. Spectra of acetonitrile, 100 mM *E*-stilbene + 118 mM *Z*-stilbene in acetonitrile, 203 mM *Z*-stilbene in acetonitrile, toluene/methanol V/V=8/2, 10.6 mM *E*-stilbene in toluene/methanol V/V=8/2, 100 mM *E*-stilbene + 118 mM *Z*-stilbene in toluene/methanol V/V=8/2 and 203 mM *Z*-stilbene in toluene/methanol V/V=8/2 are recorded to elaborate the required band pass filters.

4.3.5.1 Sensor calibration in acetonitrile

Following samples are prepared for IR-sensor calibration. Each sample is measured at least ten times using band pass filter NB-10270-210 from Spectrogon Se:

- 100 mM *E*-stilbene + 0 mM *Z*-stilbene + 2mol% $[Ru(bpy)_3]Cl_2 \cdot 6\ H_2O$ in acetonitrile
- 90 mM *E*-stilbene + 10 mM *Z*-stilbene + 2mol% $[Ru(bpy)_3]Cl_2 \cdot 6\ H_2O$ in acetonitrile
- 80 mM *E*-stilbene + 20 mM *Z*-stilbene + 2mol% $[Ru(bpy)_3]Cl_2 \cdot 6\ H_2O$ in acetonitrile
- 70 mM *E*-stilbene + 30 mM *Z*-stilbene + 2mol% $[Ru(bpy)_3]Cl_2 \cdot 6\ H_2O$ in acetonitrile
- 60 mM *E*-stilbene + 40 mM *Z*-stilbene + 2mol% $[Ru(bpy)_3]Cl_2 \cdot 6\ H_2O$ in acetonitrile
- 50 mM *E*-stilbene + 50 mM *Z*-stilbene + 2mol% $[Ru(bpy)_3]Cl_2 \cdot 6\ H_2O$ in acetonitrile
- 40 mM *E*-stilbene + 60 mM *Z*-stilbene + 2mol% $[Ru(bpy)_3]Cl_2 \cdot 6\ H_2O$ in acetonitrile
- 30 mM *E*-stilbene + 70 mM *Z*-stilbene + 2mol% $[Ru(bpy)_3]Cl_2 \cdot 6\ H_2O$ in acetonitrile
- 20 mM *E*-stilbene + 80 mM *Z*-stilbene + 2mol% $[Ru(bpy)_3]Cl_2 \cdot 6\ H_2O$ in acetonitrile
- 10 mM *E*-stilbene + 90 mM *Z*-stilbene + 2mol% $[Ru(bpy)_3]Cl_2 \cdot 6\ H_2O$ in acetonitrile
- 0 mM *E*-stilbene + 100 mM *Z*-stilbene + 2mol% $[Ru(bpy)_3]Cl_2 \cdot 6\ H_2O$ in acetonitrile

4.3.5.2 Sensor calibration in toluene/methanol

Following samples are prepared for IR-sensor calibration. Each sample is measured at least ten times using band pass filters NB-10400-300 and BP-10800-390 from Spectrogon Se:

- toluene/methanol V/V=8/2
- 18.4 mM *E*-stilbene + 36.1 mM *Z*-stilbene in toluene/methanol V/V=8/2
- 33.6 mM *E*-stilbene + 47.3 mM *Z*-stilbene in toluene/methanol V/V=8/2
- 36.9 mM *E*-stilbene + 72.2 mM *Z*-stilbene in toluene/methanol V/V=8/2
- 67.3 mM *E*-stilbene + 94.6 mM *Z*-stilbene in toluene/methanol V/V=8/2
- 73.8 mM *E*-stilbene + 144.4 mM *Z*-stilbene in toluene/methanol V/V=8/2
- 134.7 mM *E*-stilbene + 189.2 mM *Z*-stilbene in toluene/methanol V/V=8/2
- 179.6 mM *E*-stilbene + 252.3 mM *Z*-stilbene in toluene/methanol V/V=8/2

Validation of the IR-sensor is performed with three samples, measured at stopped flow. Sample 1 contains 201 mM *E*-stilbene and 0 mM *Z*-stilbene in toluene/methanol V/V=8/2. Sample 2 contains 0 mM *E*-stilbene and 10 mM *Z*-stilbene in toluene/methanol V/V=8/2. Sample 3 contains 118 mM *E*-stilbene and 103 mM *Z*-stilbene in toluene/methanol V/V=8/2.

4.3.6 Continuous isomerization of E-stilbene and online analysis in MeCN

100 mL of 100 mM *E*-stilbene + 2mol% $[Ru(bpy)_3]Cl_2 \cdot 6\ H_2O$ in acetonitrile are prepared. This solution is pumped with a HPLC-pump (0.5 mL×min^{-1}) into a 1/16" FEP capillary photoreactor (15 mL, 800 µm ID, 20 °C). A hexagonal shaped 6×6 LED-array (455 nm 6 W_{el}) is placed in the center of the reactor and cooled to 20°C via a cooling finger to provide stable performance of the LEDs. The reaction is monitored online with the IR-sensor (filter: NB-10270-210). Sectors, in which irradiation takes place (LED-array switched on), are marked in Figure 98.

4.3.7 Stilbene synthesis in batch

In a 30 mL vial containing 2 mL 0.5 M benzaldehyde (106 mg) and 0.5 M BTTP (433 mg, 1 equiv.) in toluene/methanol (V/V=67/33) are added 2 mL 0.5 M DBU (152 mg, 1 equiv. in toluene). The mixture is stirred and heated in a water batch with the settings

mentioned in Table 38. 4 mL 0.6 N aqueous sulfuric acid (diluted with 40vol% methanol) is added to quench the reaction after reaching the proper reaction time. The two phases are separated and the organic phase is analyzed via offline ^{1}H-NMR and FTIR-spectroscopy at stopped flow. Both spectrometers are equipped with a flow cell.

Table 38: Process parameters for Wittig reactions in batch.

sample-nr.	reaction time [min]	temperature [°C]
#1	1	25
#2	3	25
#3	6	25
#4	1	50
#5	3	50

4.3.8 Continuous stilbene synthesis and variation process parameters

The setup, presented in Figure 219, is used for continuous Wittig synthesis including online NMR- and IR-spectroscopy. Feed A (0.5 M benzaldehyde and 0.5 M BTTP (1 equiv.) in toluene/methanol (V/V=54/26)) and Feed B (0.5 M DBU in toluene) are mixed via a T-junction. After passing the 1/8" FEP capillary reactor (3.5 mL, 1.6 mm ID) the reaction is quenched with Feed C (0.6 N aqueous sulfuric acid (diluted with 40vol% methanol)). Aqueous and organic feeds are mixed with a T-junction. A proportional relief valve generates a back pressure of 3 bar_{exs}. A FEP capillary (1/8", ~0.9 mL, 1.6 mm ID) is used to develop two separated phases, before the mixture enters a liquid-liquid phase separator (Zaiput Sep-10 with OB-900 membrane). The organic phase is analyzed via online ^{1}H-NMR- and IR-spectroscopy.

Table 39: Process parameters for Wittig reactions in the lab plant.

sample-nr.	reaction time [min]	temperature T_{Set} [°C]	flow rate Feed A [µL×min^{-1}]	flow rate Feed B [µL×min^{-1}]	flow rate Feed C [µL×min^{-1}]
#6	3.5	35	500	500	1000
#7	3.5	60	500	500	1000
#8	3.5	80	500	500	1000
#9	7	30	250	250	500
#10	3.5	30	500	500	1000
#11	2.33	30	750	750	1500
#12	1.94	30	900	900	1800

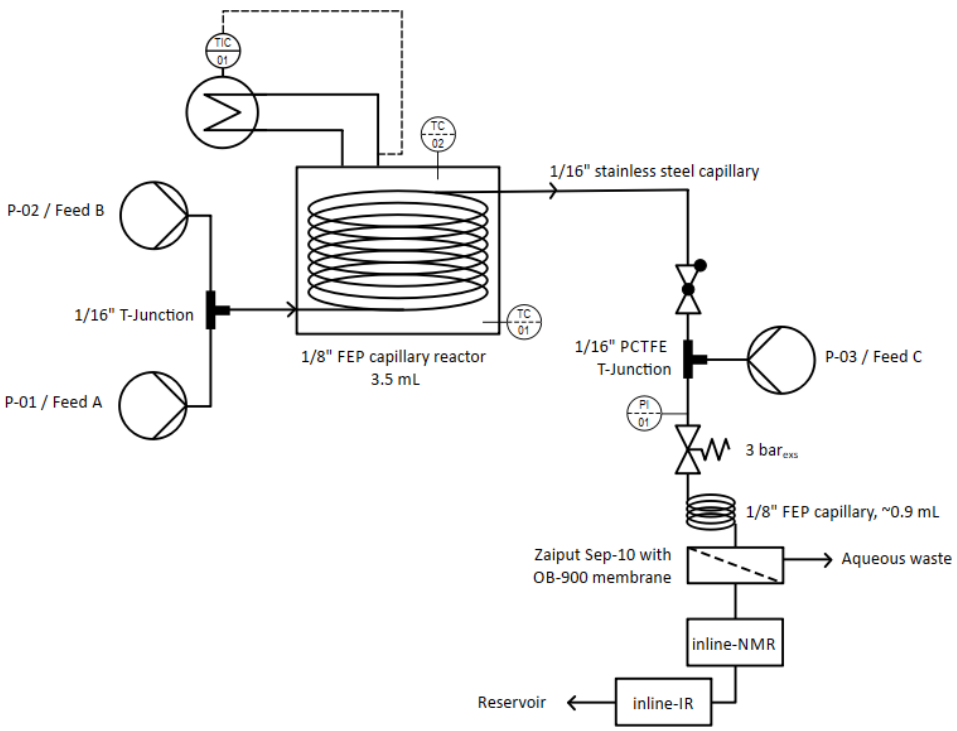

Figure 219: Lab plant design for a continuous Wittig reaction including PAT tools.

4.3.9 Continuous stilbene synthesis and variation of light intensity in the photoisomerization process

The lab plant setup of Figure 220 is extended by Feed D. Here, photosensitizer ($[Ru(bpy)_3]Cl_2$ 6 H_2O 1.87 g/100 mL in methanol) is added via a third T-Junction. The mixture enters the 1/16" FEP capillary photoreactor (15 mL, 800 µm ID, V.0) to undergo photoisomerization. The reactor is equipped with 5×2 equally distributed LEDs (455 nm, 11 $W_{el,max}$). The mixture is analyzed online via the nondispersive IR-sensor using band pass filters NB-10400-300 and BP-10800-390.

Table 40: Process parameters for the first and second reaction step in the lab plant.

sample-nr.	reaction time [min]	temperature T_{Set} [°C]	flow rate Feed A [µL×min^{-1}]	flow rate Feed B [µL×min^{-1}]	flow rate Feed C [µL×min^{-1}]	flow rate Feed D [µL×min^{-1}]	LED-power [%]
#13	4.37	90	400	400	800	130	10
#14	4.37	90	400	400	800	130	20
#15	4.37	90	400	400	800	130	40
#16	4.37	90	400	400	800	130	60
#17	4.37	90	400	400	800	130	80

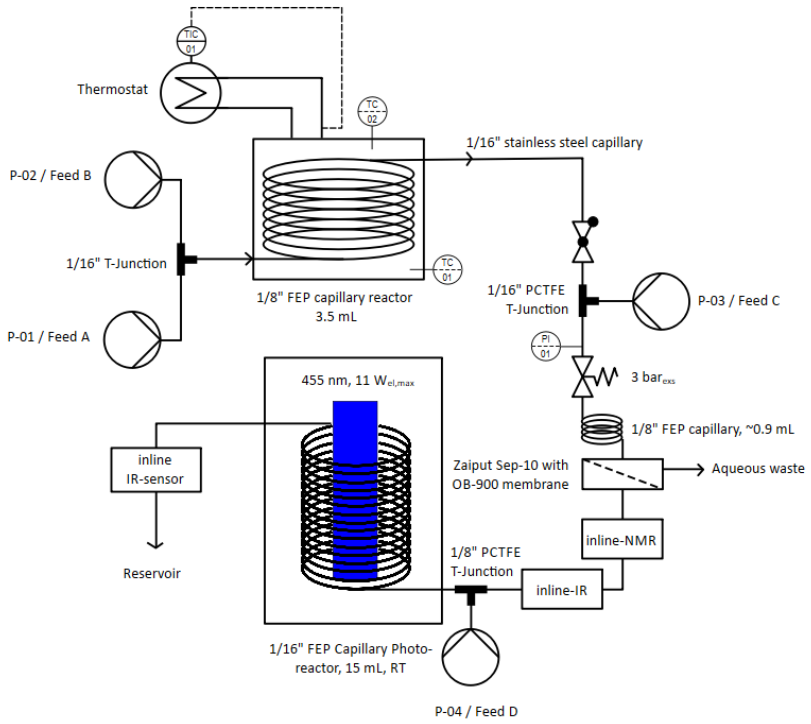

Figure 220: Lab plant design for a continuous two-step synthesis of Z-stilbene including PAT tools.

5 Appendix

Table 41: Electric settings of the used LED-arrays.

#	type of LED-array[a]	wavelength [nm]	voltage *U* [V]	current I [A]	el. Power of array $P_{el.}$ [$W_{el.}$]	radiant flux [W]	radiant efficiency [%]
1	6×6	520	17.68	1.800	32	8.8	28
2	4×1	455	12.74	0.438	6	5.3	88
3	4×1	365	14.41	0.414	6	2.5	42
4	6×6	455	16.26	0.367	6	3.7	62
5	6×6	455	19.43	2.100	50	30.6	61
6	6×6	365	20.07	0.350	7.0	3.2	46
7	6×6	365	21.56	1.162	25.0	10.9	44
8	6×6	365	22.30	1.681	37.5	15.7	42
9	6×6	365	23.80	2.100	50	19.6	39

a: first number indicates the LED connected in series; second number indicates the number of parallel connected LEDs.

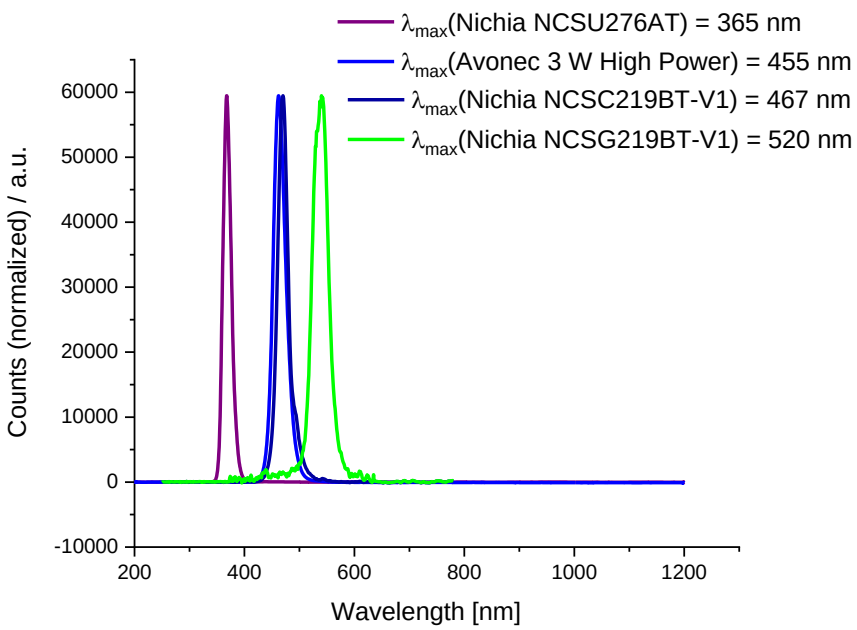

Figure 221: Normalized emission spectra of used light emitting diodes: l_{max}(Nichia NCSU276AT)= 367 nm; λ_{max}(Avonec 3 W High Power)= 459 nm; ⍰$_{max}$(Nichia NCSC219BT-V1)= 472 nm; λ_{max}(Nichia NCSC219BT-V1)= 472 nm; λ_{max}(Nichia NCSG219BT-V1)= 539 nm; Emission spectra are recorded with an AvaSpec-2048TEC-USB2 (Avantes BV) fibre-spectrometer; End of the optical fibre is focused in a 5-10 mm gap in front of one LED (6.6 mA); AvaSoft-basic is used with an integration range of ~10 ms.

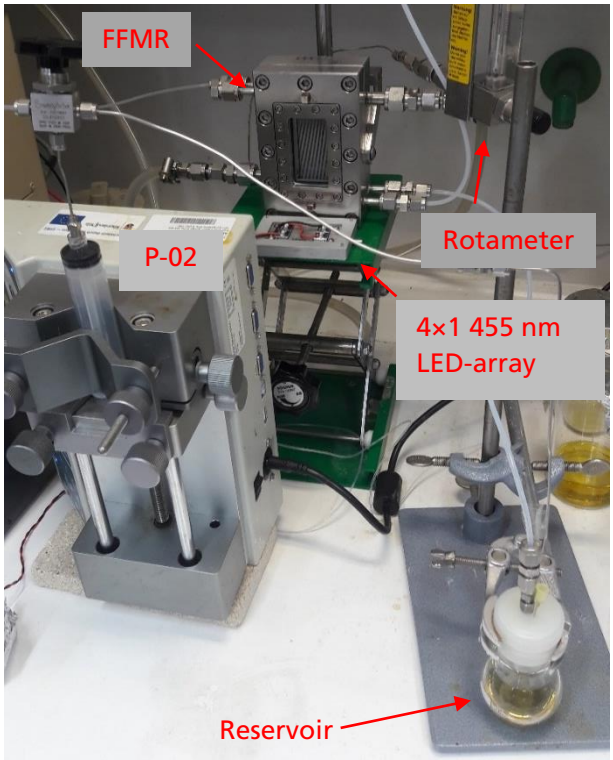

Figure 222: Setup for 3-CF_3-biphenyl synthesis in semi-batch using a falling film micro reactor; here: light protection of the reservoir is removed for illustration.

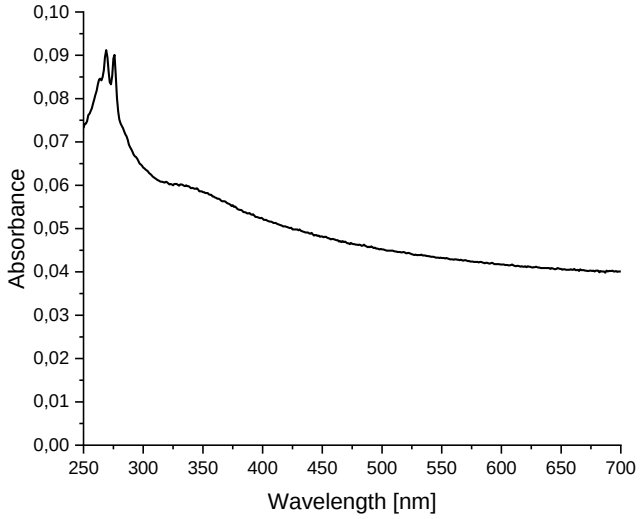

Figure 223: UV/Vis-spectrum of neat Fluorinert FC-40 (reference: air).

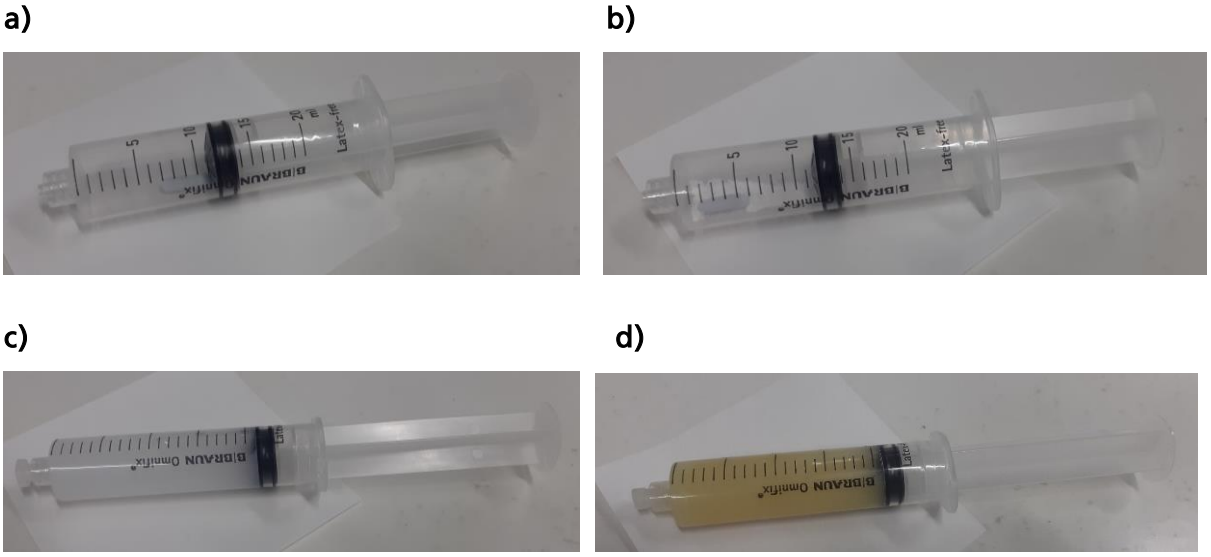

Figure 224: Preparation of a catalyst slurry for SMBR experiments; **a)** 20 mL syringe equipped with stir bar; **b)** 20 mL syringe equipped with stir bar and solid anatase particles (80 mg); **c)** 20 mL syringe equipped with stir bar and filled with a suspension of anatase (80 mg) in MeCN/benzene V/V=1/1 - freshly prepared; **d)** 20 mL syringe equipped with stir bar and filled with a suspension of anatase (80 mg) in 50 mM 3-CF_3-aniline, 1.2 equiv. *t*-BuONO, 1 equiv. TFA in MeCN/benzene V/V=1/1 - freshly prepared.

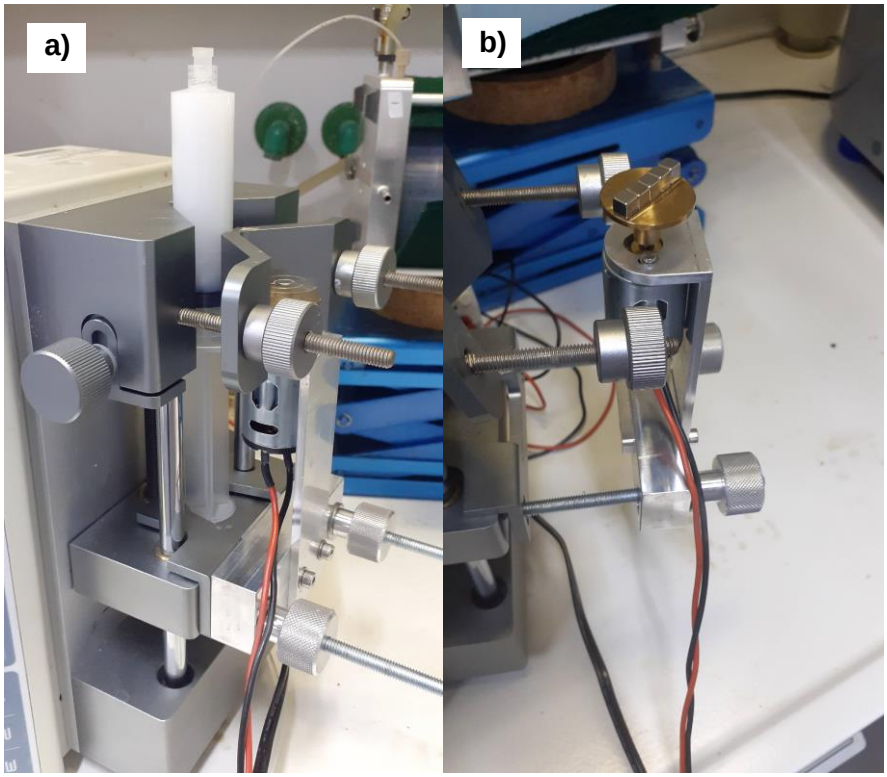

Figure 225: a) Catalyst slurry in a syringe (equipped with a stir bar) is permanently mixed with a spinning bar magnet; **b)** Setup of the spinning bar magnet (serious of 4 neodymium magnet driven by a 3V electromotor). A retainer is mounted at the piston driver of the syringe pump Chemyx Nexus 6000 to maintain constant spinning force.

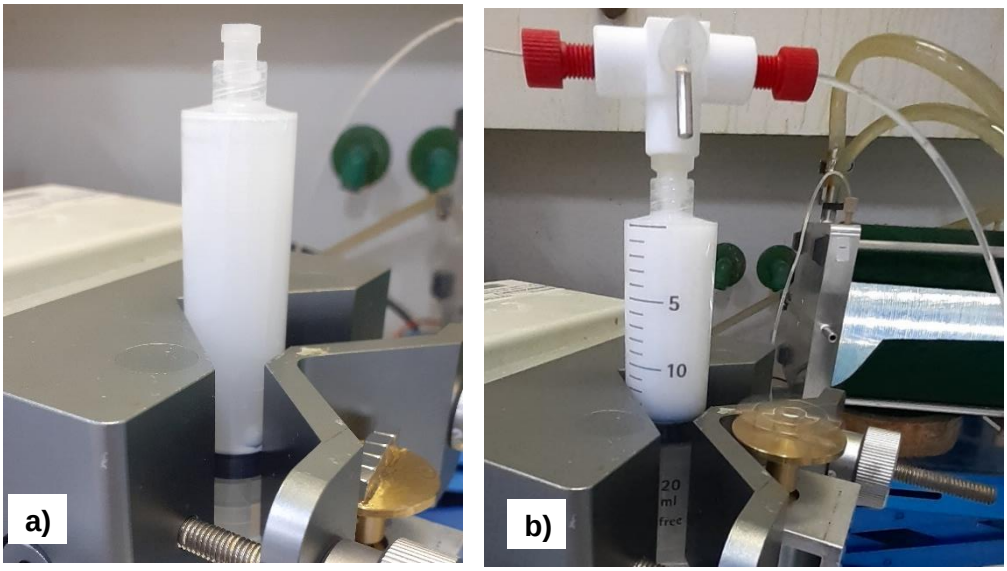

Figure 226: a) Catalyst slurry in a syringe (equipped with a stir bar) without mixing after 6 minutes; Most large particles have settled at the plunger; **b)** Stir bar drive keeps constant distance during emptying process.

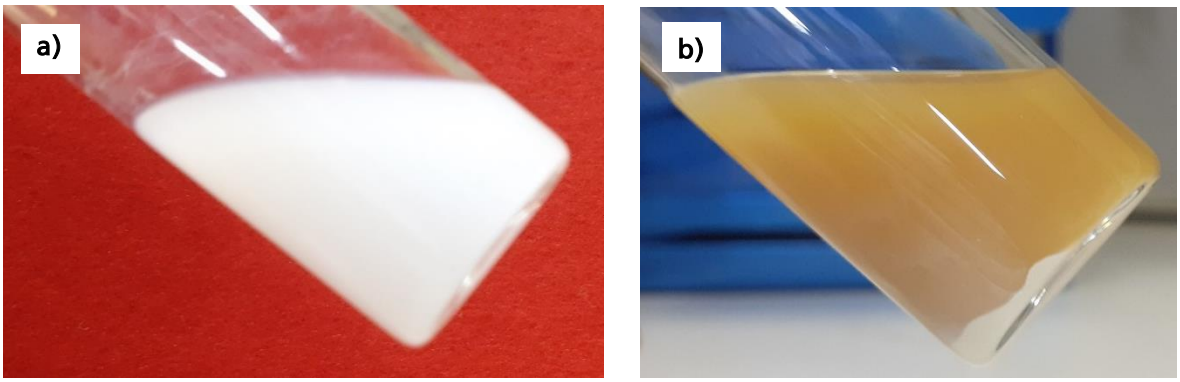

Figure 227: The high-density Fluorinert™ FC-40 does not migrate into vertically mounted the syringe (filled with catalyst slurry); **a)** Unstirred catalyst slurry consisting of anatase and MeCN/benzene V/V=1/1; **b)** Unstirred catalyst slurry consisting of anatase in 50 mM 3-CF_3-aniline, 1.2 equiv. *t*-BuONO, 1 equiv. TFA in MeCN/benzene V/V=1/1.

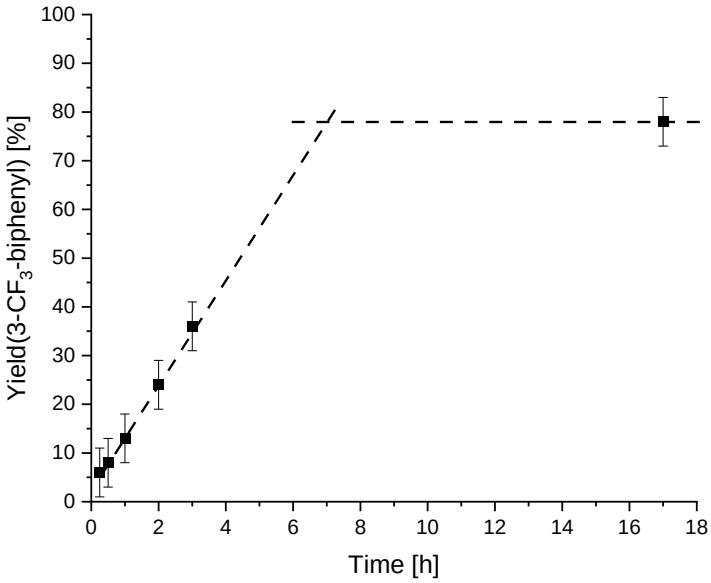

Figure 228: Batch synthesis of 3-CF_3-biphenyl via *in-situ* generated diazonium trifluoroacetate in glass vial; General reaction conditions: 200 mM 3-CF_3-aniline, 1.2 equiv. *t*-BuONO, 2 equiv. TFA and acetonitrile/benzene (V/V =1/1), RT, 365 nm 6 W_{el}; Determined by GC/MS.

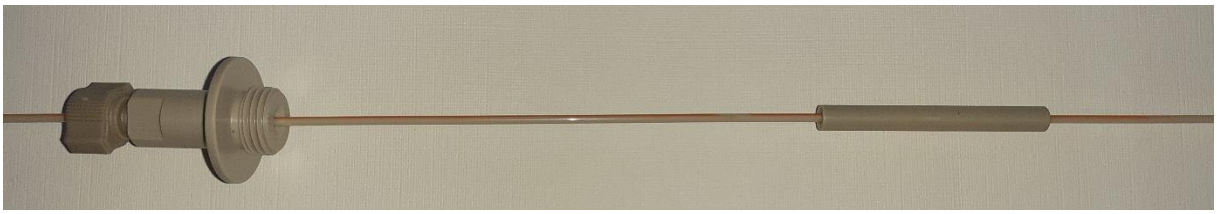

Figure 229: PEEK bottom-to-top flow cell for a Nanalysis NMReady60-PRO NMR spectrometer.

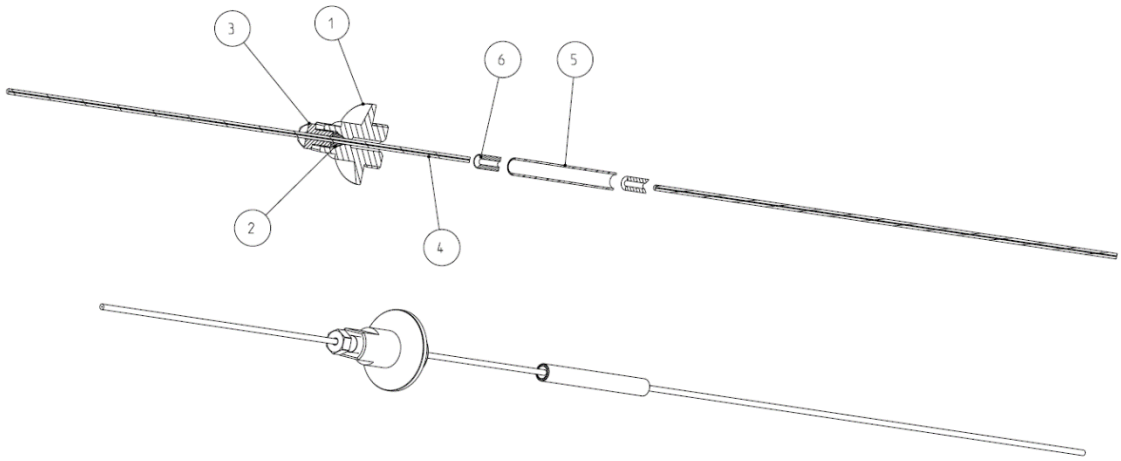

Figure 230: Drawing of the PEEK NMR flow cell; 1: adapter screw for correct flow cell positioning; 2: Ferrule 1/16"; 3: Internal nut 1/16"; 4: 1/16" PEEK capillary, 500 µm ID for inlet and outlet; 5: PEEK measuring cell, 44.0 mm length, 4.8 mm OD, 4.0 mm ID, ~330 µL internal volume; 6: PEEK bracket joining part 4 and 5; 25 bar_{exs} loading capacity.

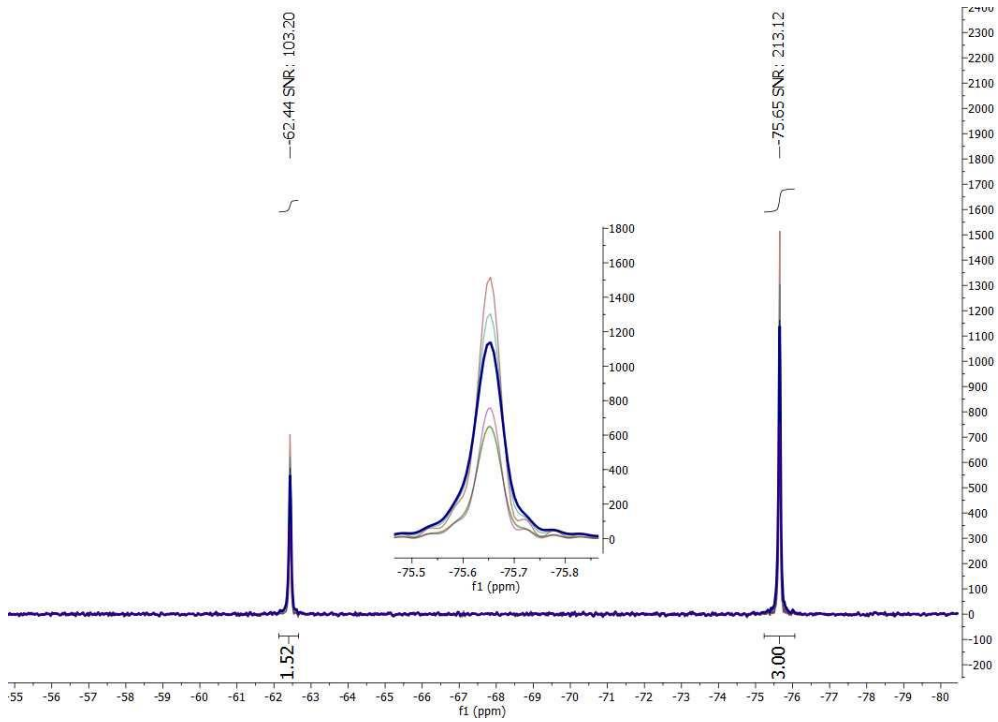

Figure 231: ^{19}F-NMR spectra (56.98 MHz, PEEK flow cell, stopped flow) of 0.2 M 3-CF_3-aniline and 0.4 M TFA in MeCN; height 1500 at δ_F=-75.65 ppm: original spectra + 32k zero filling; height 1300 at δ_F=-75.65 ppm: 0.5 Hz exponential apodization + 32k zero filling; height 1125 at δ_F=-75.65 ppm: 1.0 Hz apodization + 32k zero filling; height 750 at δ_F=-75.65 ppm: 64k zero filling; height 648 at δ_F=-75.65 ppm: 0.5 Hz exponential apodization + 64k zero filling; height 646 at δ_F=-75.65 ppm: 0.5 Hz exponential apodization + 64k zero filling + linear prediction.

Model Properties: IHM > Component Fit	
Peak Fitting	
Default Peak Type	Pseudo-Voigt
Auto-Fit Mode	Fast (Simultaneous)
Weighted Auto-Fit	No
Absolute Parameter Constraints	
HWHM	0.0001 0.1
Gaussian Part	0 1
Component Fitting	
Fitting Mode	Medium Interaction (W/B, Peak Positions)
Component Shift	No
No. of Considered Peaks	10
Component Weight Threshold	0.001
Relative Parameter Constraints	
Position	± 0.05
Max	± 50 %
HWHM	± 50 %
Gaussian Part	± 1
Constant Peak Intensity	Yes
Optimization (Expert Options)	
Linear Fitting	
Max. Iterations	200
Objective Function Tolerance	1e-14
Nonlinear Fitting	
Max. Iterations	300
Objective Function Tolerance	1e-06
Parameter Tolerance	1e-06
Constraint Fitting Algorithm	Active-set
Constraint Violation Tolerance	0.01

Figure 232: IHM model properties in PEAXACT 5.3 used for component fitting to evaluate online ^{19}F-NMR spectra.

Model Properties: IHM > Custom Results | Sample Properties

Result Name	Value
area(TFA) / a.u.	18.1515
area(ChD55-0) / a.u.	4.36718
Faktor	0.0151263
c(ChD55-0) / mmol/L	96.2383
yield(ChD55-0) / %	48.1192

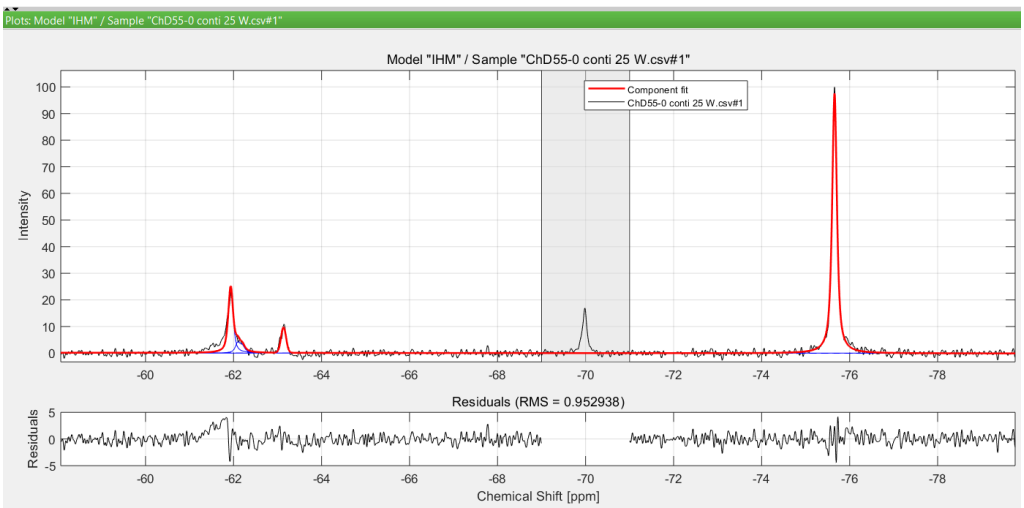

Figure 233: Evaluation of an online ^{19}F-NMR spectrum (56.98 MHz, PEEK flow cell) with PEAXACT 5.3 (component fit via IHM) of continuous 3-CF_3-biphenyl synthesis in a 1/16" FEP capillary photoreactor; General reaction conditions: 200 mM 3-CF_3-aniline, 1.2 equiv. *t*-BuONO, 2 equiv. TFA in MeCN, MeCN/benzene V/V=1/1, 365 nm 25 W_{el}, 20 °C, 17 bar_{exs}, t_R=1.25 h; Peak at -70 ppm is an artifact; *blue* peak shape of each pure component fits (and unknown substances), *red* component fit as result of a weighted sum of pure components; top: Results of component fitting including yield of continuous 3-CF_3-biphenyl synthesis.

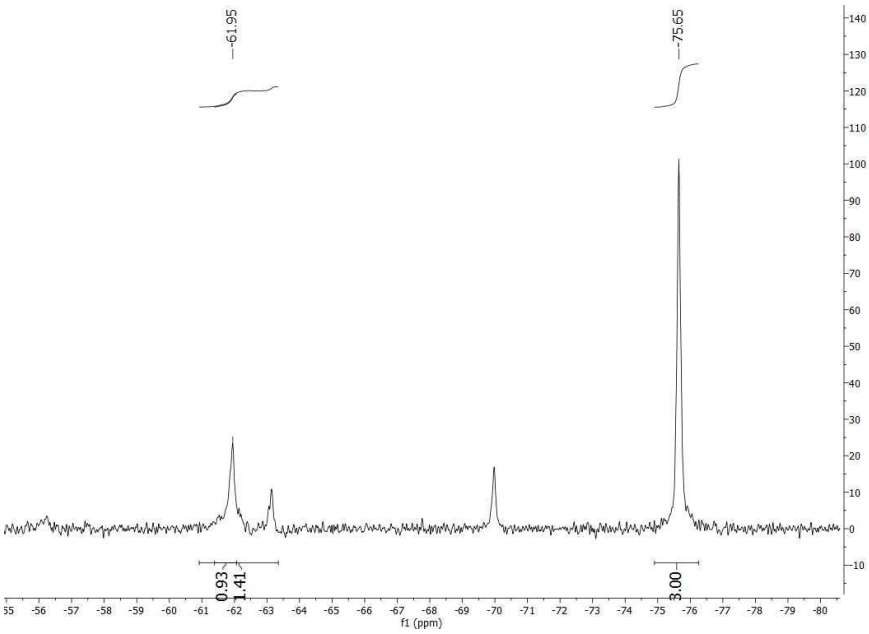

Figure 234: Evaluation of an online ^{19}F-NMR spectrum (56.98 MHz, PEEK flow cell) with MestReNova 12 (manual peak integration) of continuous 3-CF_3-biphenyl synthesis in a 1/16" FEP capillary photoreactor; General reaction conditions: 200 mM 3-CF_3-aniline, 1.2 equiv. *t*-BuONO, 2 equiv. TFA in MeCN, MeCN/benzene V/V=1/1, 365 nm 25 W_{el}, 20 °C, 17 bar_{exs}, t_R=1.25 h; Peak at -70 ppm is an artifact.

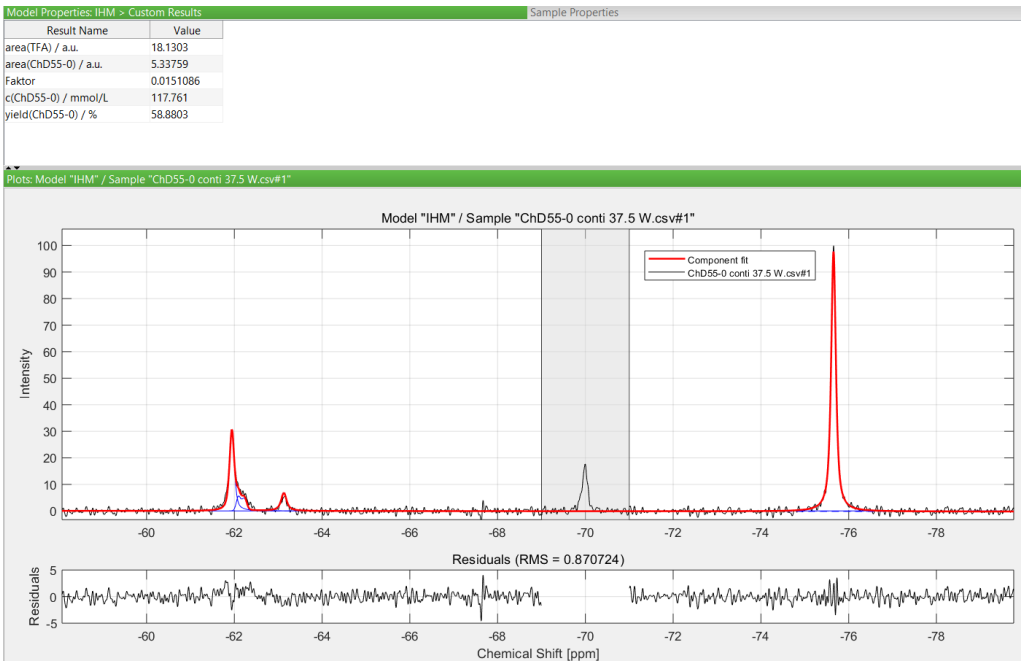

Figure 235: Evaluation of an online ^{19}F-NMR spectrum (56.98 MHz, PEEK flow cell) with PEAXACT 5.3 (component fit via IHM) of continuous 3-CF_3-biphenyl synthesis in a 1/16" FEP capillary photoreactor; General reaction conditions: 200 mM 3-CF_3-aniline, 1.2 equiv. *t*-BuONO, 2 equiv. TFA in MeCN, MeCN/benzene V/V=1/1, 365 nm 37.5 W_{el}, 20 °C, 17 bar_{exs}, t_R=1.25 h; Peak at -70 ppm is an artifact; *blue* peak shape of each pure component fits (and unknown substances), *red* component fit as result of a weighted sum of pure components; top: Results of component fitting including yield of continuous 3-CF_3-biphenyl synthesis.

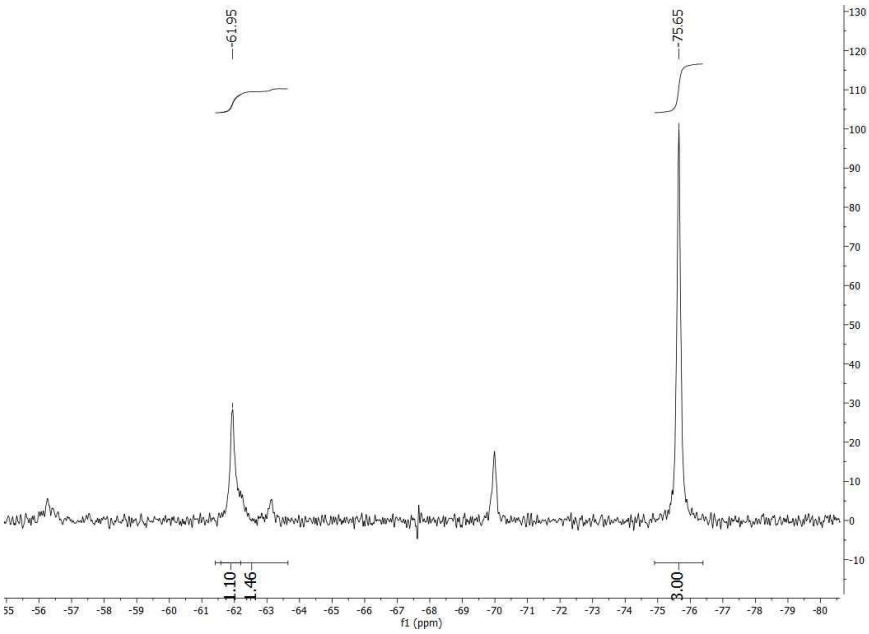

Figure 236: Evaluation of an online ^{19}F-NMR spectrum (56.98 MHz, PEEK flow cell) with MestReNova 12 (manual peak integration) of continuous 3-CF_3-biphenyl synthesis in a 1/16" FEP capillary photoreactor; General reaction conditions: 200 mM 3-CF_3-aniline, 1.2 equiv. *t*-BuONO, 2 equiv. TFA in MeCN, MeCN/benzene V/V=1/1, 365 nm 37.5 W_{el}, 20 °C, 17 bar_{exs}, t_R=1.25 h; Peak at -70 ppm is an artifact.

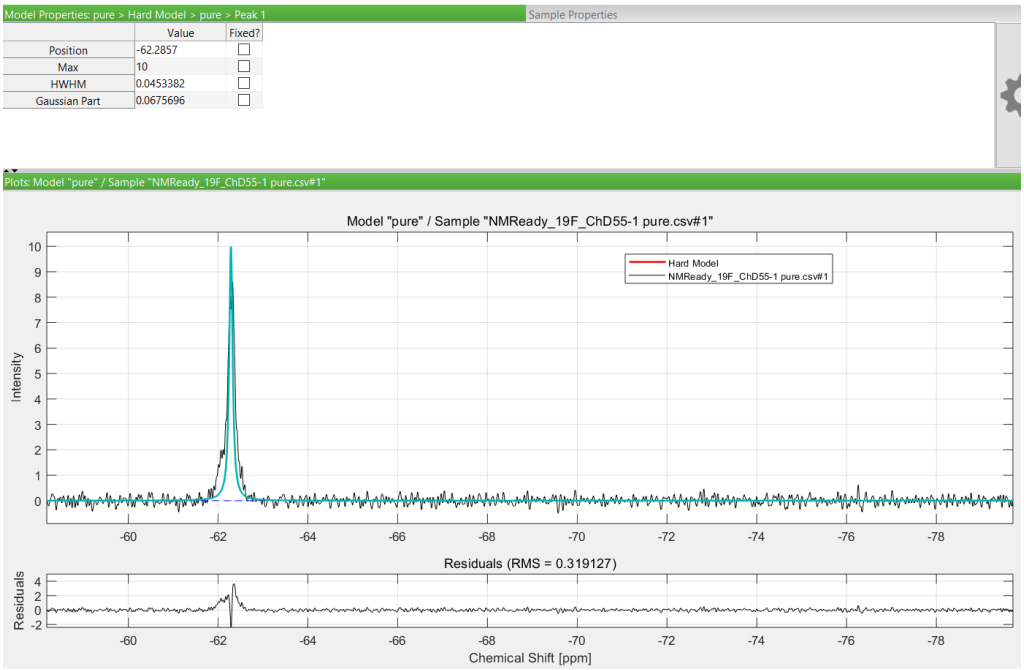

Figure 237: Pure component model for purified **26a** with PEAXACT 5.3; *turquoise* peak shape of hard model consisting of a single peak; top: peak parameters representing **26a** ^{19}F-NMR.

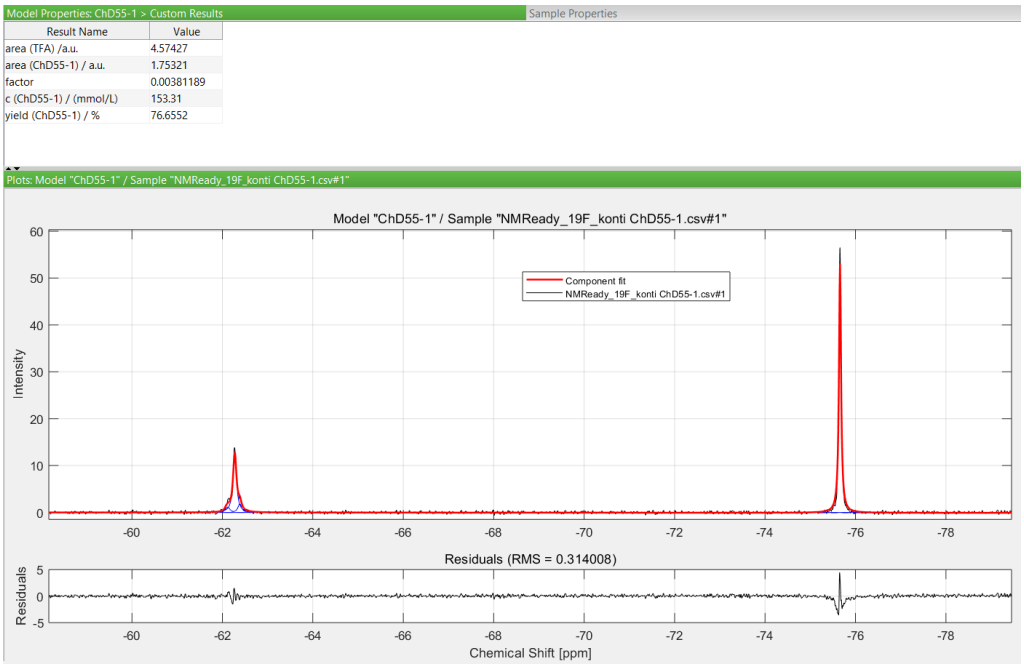

Figure 238: Evaluation of an online ^{19}F-NMR spectrum (56.98 MHz, PEEK flow cell) with PEAXACT 5.3 (component fit via IHM) of continuous **26a** synthesis in a 1/16" FEP capillary photoreactor; General reaction conditions: 200 mM 3-CF_3-aniline, 1.2 equiv. *t*-BuONO, 2 equiv. TFA in MeCN, MeCN/furan V/V=1/1, 365 nm 50 W_{el}, 20 °C, 17 bar_{exs}, t_R=1.25 h; *blue* peak shape of each pure component fits (and unknown substances), *red* component fit as result of a weighted sum of pure components; top: Results of component fitting including yield of continuous **26a** synthesis.

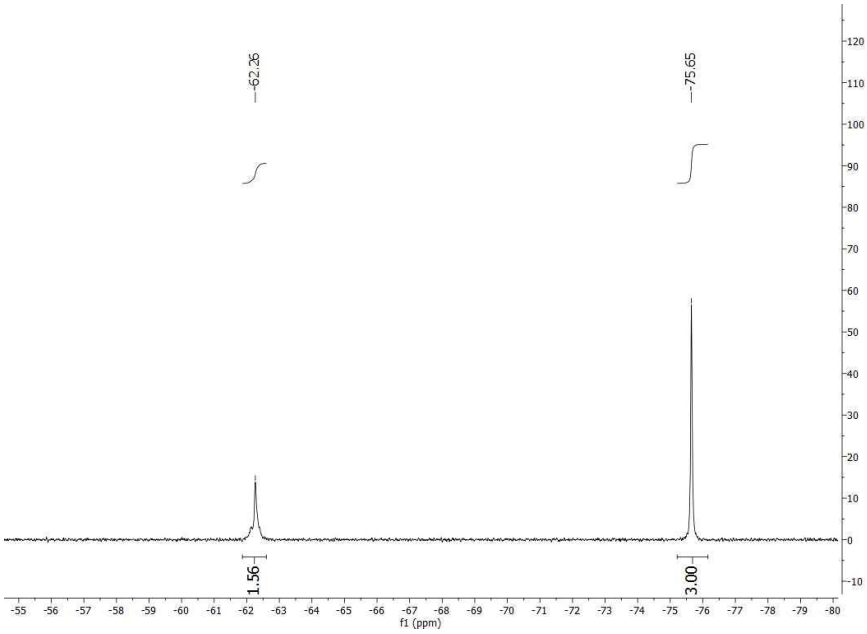

Figure 239: Variance evaluation at an online ^{19}F-NMR spectrum (56.98 MHz, PEEK flow cell) with MestReNova 12 (manual peak integration) of continuous **26a** synthesis in a 1/16" FEP capillary photoreactor; General reaction conditions: 200 mM 3-CF_3-aniline, 1.2 equiv. *t*-BuONO, 2 equiv. TFA in MeCN, MeCN/furan V/V=1/1, 365 nm 50 W_{el}, 20 °C, 17 bar_{exs}, t_R=1.25 h.

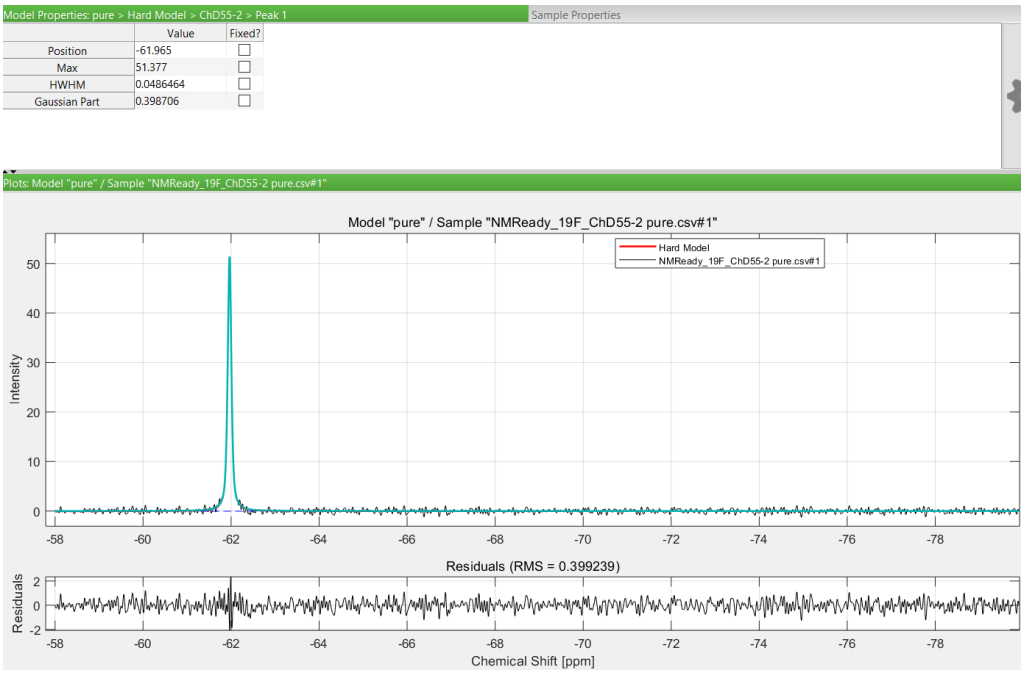

Figure 240: Pure component model for purified **26c** (mixture of isomers) with PEAXACT 5.3; *turquoise* peak shape of hard model consisting of a single peak; top: peak parameters representing **26c** ^{19}F-NMR.

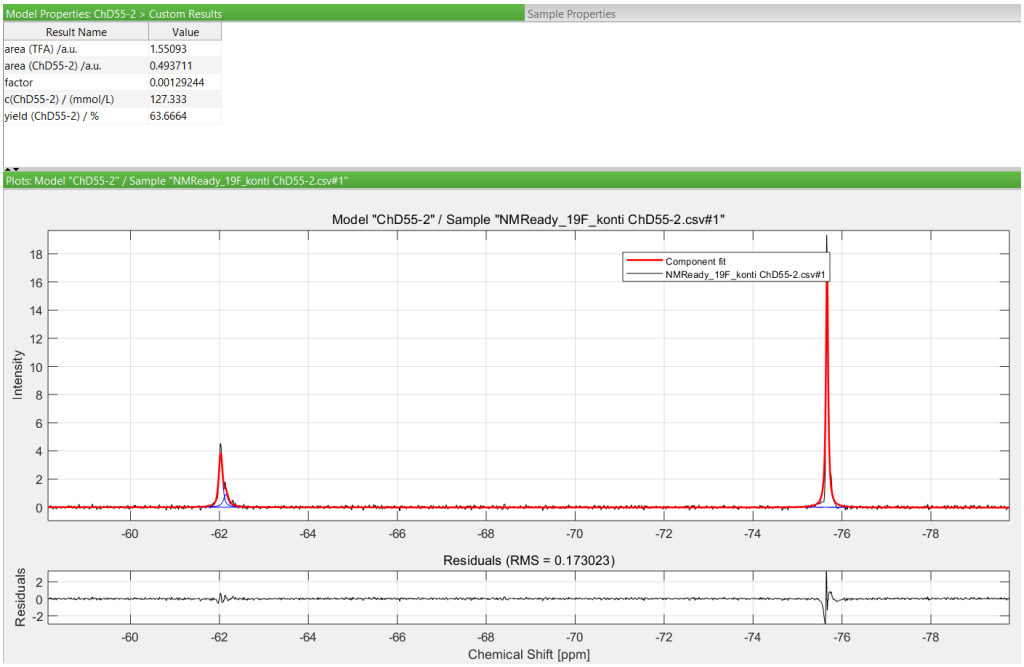

Figure 241: Evaluation of an online ^{19}F-NMR spectrum (56.98 MHz, PEEK flow cell) with PEAXACT 5.3 (component fit via IHM) of continuous **26c** synthesis in a 1/16" FEP capillary photoreactor; General reaction conditions: 200 mM 3-CF_3-aniline, 1.2 equiv. *t*-BuONO, 2 equiv. TFA in MeCN, MeCN/fluorobenzene V/V=1/1, 365 nm 50 W_{el}, 20 °C, 17 bar_{exs}, t_R=1.25 h; *blue* peak shape of each pure component fits (and unknown substances), *red* component fit as result of a weighted sum of pure components; top: Results of component fitting including yield of continuous **26c** (mixture of isomers) synthesis.

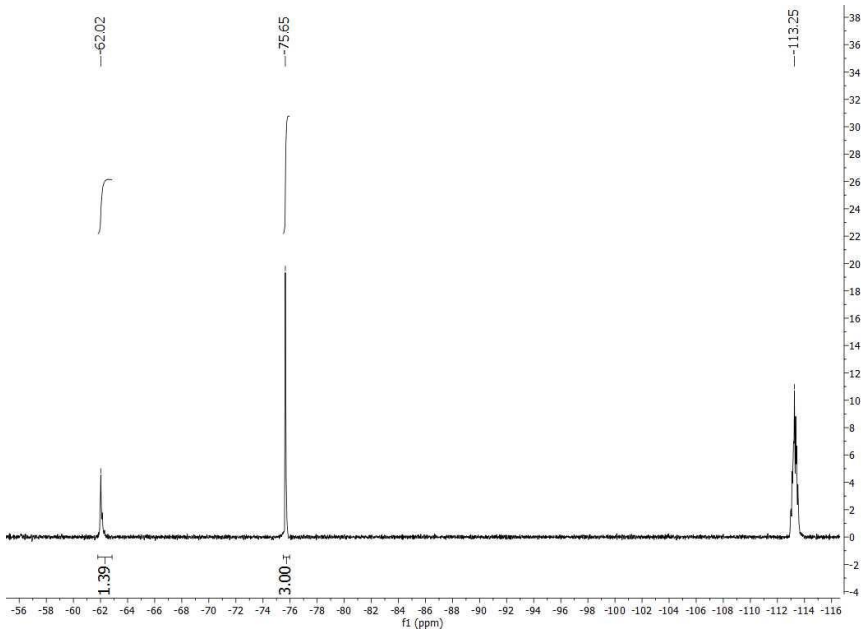

Figure 242: Variance evaluation at an online ^{19}F-NMR spectrum (56.98 MHz, PEEK flow cell) with MestReNova 12 (manual peak integration) of continuous **26c** (mixture of isomers) synthesis in a 1/16" FEP capillary photoreactor; General reaction conditions: 200 mM 3-CF_3-aniline, 1.2 equiv. *t*-BuONO, 2 equiv. TFA in MeCN, MeCN/fluorobenzene V/V=1/1, 365 nm 50 W_{el}, 20 °C, 17 bar_{exs}, t_R=1.25 h.

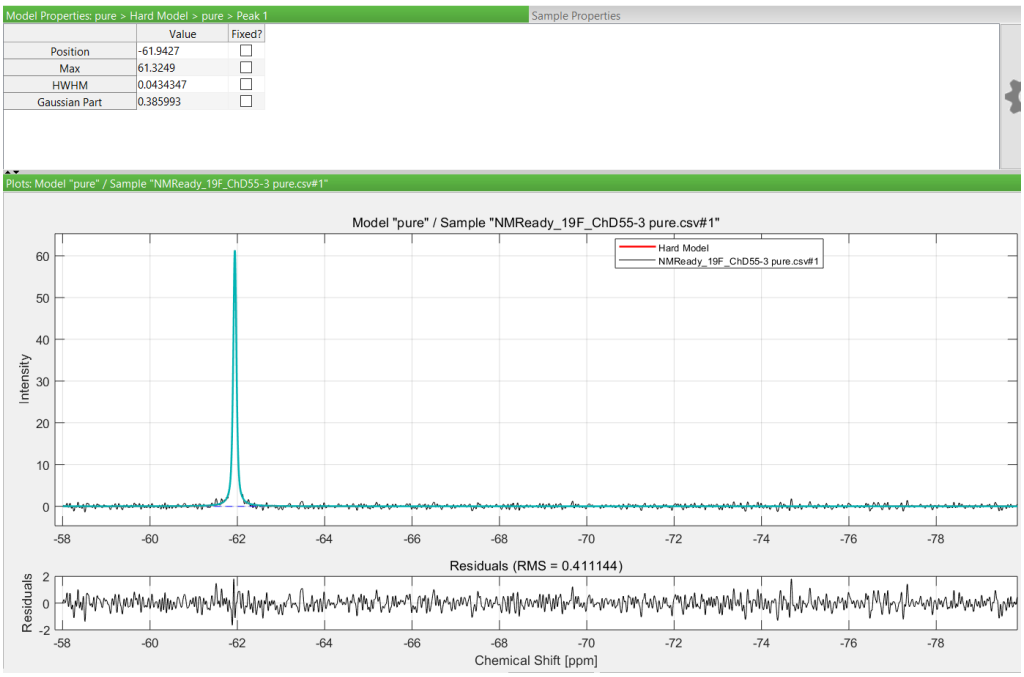

Figure 243: Pure component model for purified **26d** (mixture of isomers) with PEAXACT 5.3; *turquoise* peak shape of hard model consisting of a single peak; top: peak parameters representing **26d** ^{19}F-NMR.

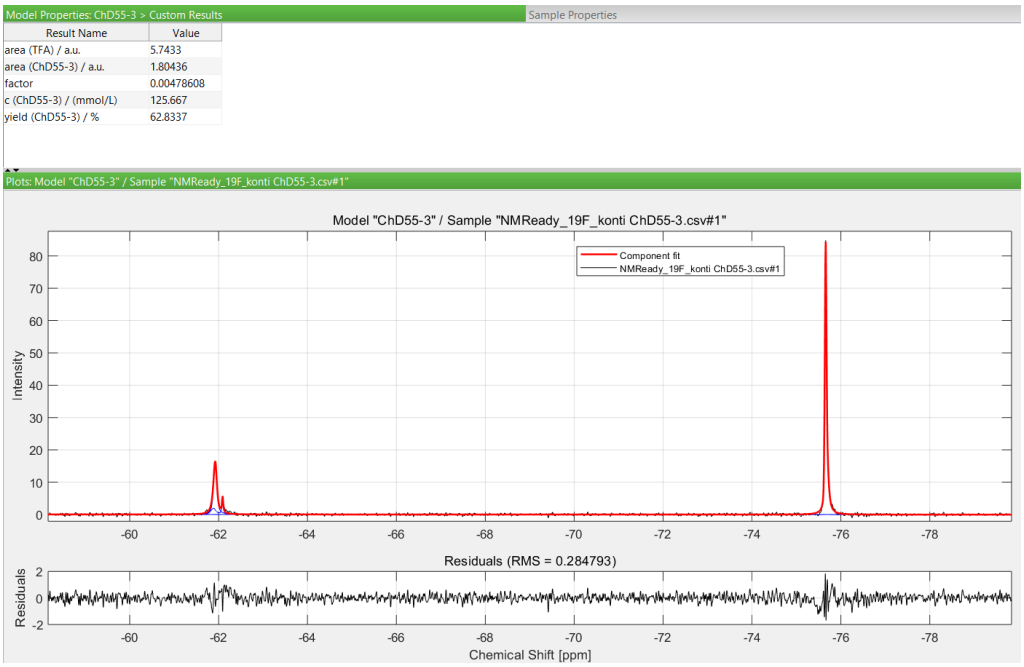

Figure 244: Evaluation of an online ^{19}F-NMR spectrum (56.98 MHz, PEEK flow cell) with PEAXACT 5.3 (component fit via IHM) of continuous **26d** synthesis in a 1/16" FEP capillary photoreactor; General reaction conditions: 200 mM 3-CF_3-aniline, 1.2 equiv. *t*-BuONO, 2 equiv. TFA in MeCN, MeCN/chlorobenzene V/V=1/1, 365 nm 50 W_{el}, 20 °C, 17 bar_{exs}, t_R=1.25 h; *blue* peak shape of each pure component fits (and unknown substances), *red* component fit as result of a weighted sum of pure components; top: Results of component fitting including yield of continuous **26d** (mixture of isomers) synthesis.

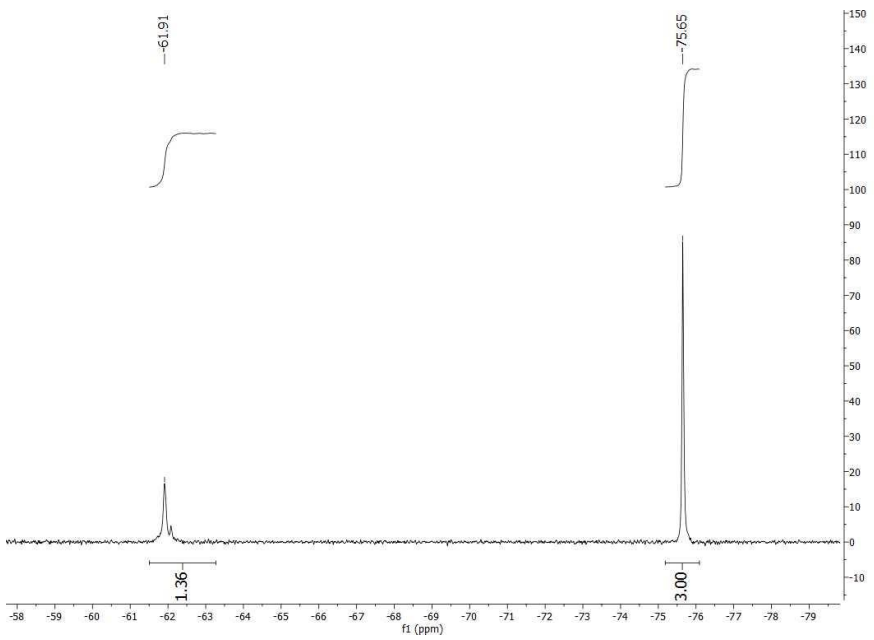

Figure 245: Variance evaluation at an online ^{19}F-NMR spectrum (56.98 MHz, PEEK flow cell) with MestReNova 12 (manual peak integration) of continuous **26d** (mixture of isomers) synthesis in a 1/16" FEP capillary photoreactor; General reaction conditions: 200 mM 3-CF_3-aniline, 1.2 equiv. *t*-BuONO, 2 equiv. TFA in MeCN, MeCN/chlorobenzene V/V=1/1, 365 nm 50 W_{el}, 20 °C, 17 bar_{exs}, t_R=1.25 h.

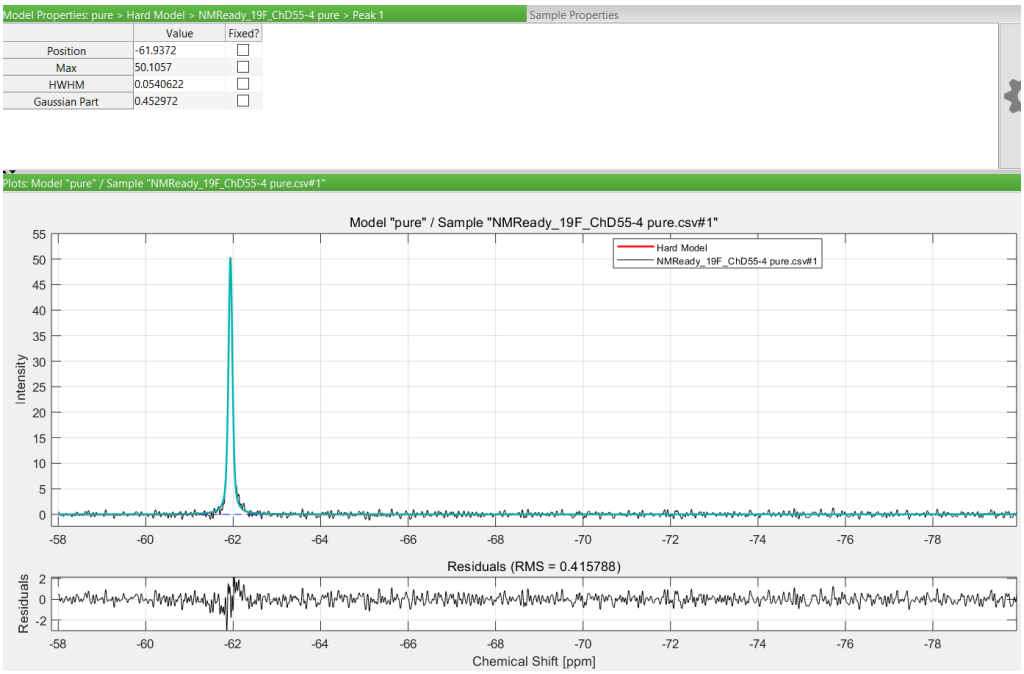

Figure 246: Pure component model for purified **26e** (mixture of isomers) with PEAXACT 5.3; *turquoise* peak shape of hard model consisting of a single peak; top: peak parameters representing **26e** ^{19}F-NMR.

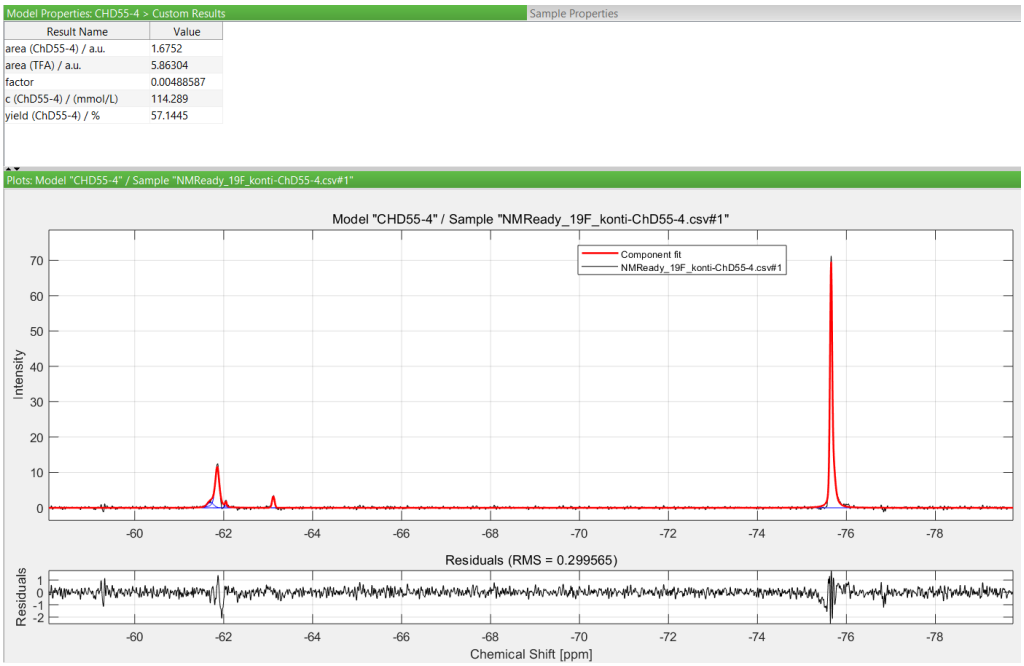

Figure 247: Evaluation of an online ^{19}F-NMR spectrum (56.98 MHz, PEEK flow cell) with PEAXACT 5.3 (component fit via IHM) of continuous **26e** synthesis in a 1/16" FEP capillary photoreactor; General reaction conditions: 200 mM 3-CF_3-aniline, 1.2 equiv. *t*-BuONO, 2 equiv. TFA in MeCN, MeCN/bromobenzene V/V=1/1, 365 nm 50 W_{el}, 20 °C, 17 bar_{exs}, t_R=1.25 h; *blue* peak shape of each pure component fits (and unknown substances), *red* component fit as result of a weighted sum of pure components; top: Results of component fitting including yield of continuous **26e** (mixture of isomers) synthesis.

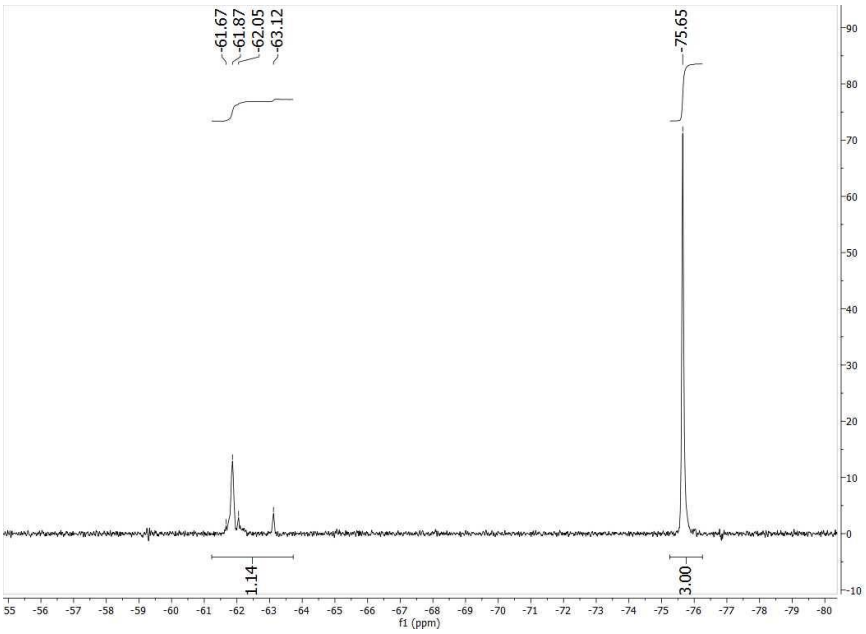

Figure 248: Variance evaluation at an online ^{19}F-NMR spectrum (56.98 MHz, PEEK flow cell) with MestReNova 12 (manual peak integration) of continuous **26e** (mixture of isomers) synthesis in a 1/16" FEP capillary photoreactor; General reaction conditions: 200 mM 3-CF_3-aniline, 1.2 equiv. *t*-BuONO, 2 equiv. TFA in MeCN, MeCN/bromobenzene V/V=1/1, 365 nm 50 W_{el}, 20 °C, 17 bar_{exs}, t_R=1.25 h.

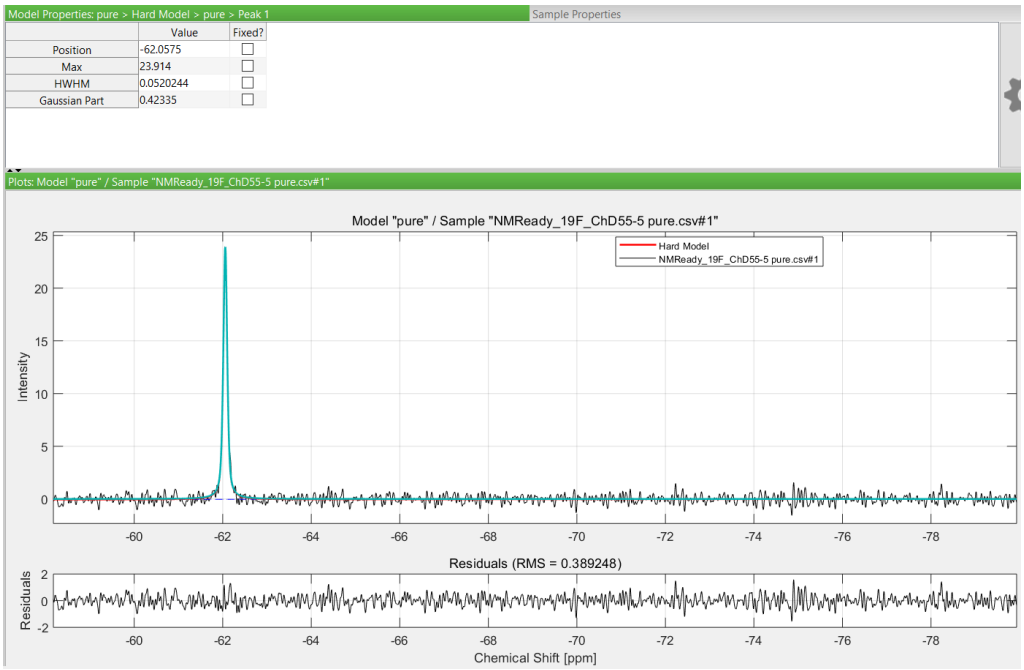

Figure 249: Pure component model for purified **26f** (mixture of isomers) with PEAXACT 5.3; *turquoise* peak shape of hard model consisting of a single peak; top: peak parameters representing **26f** ^{19}F-NMR.

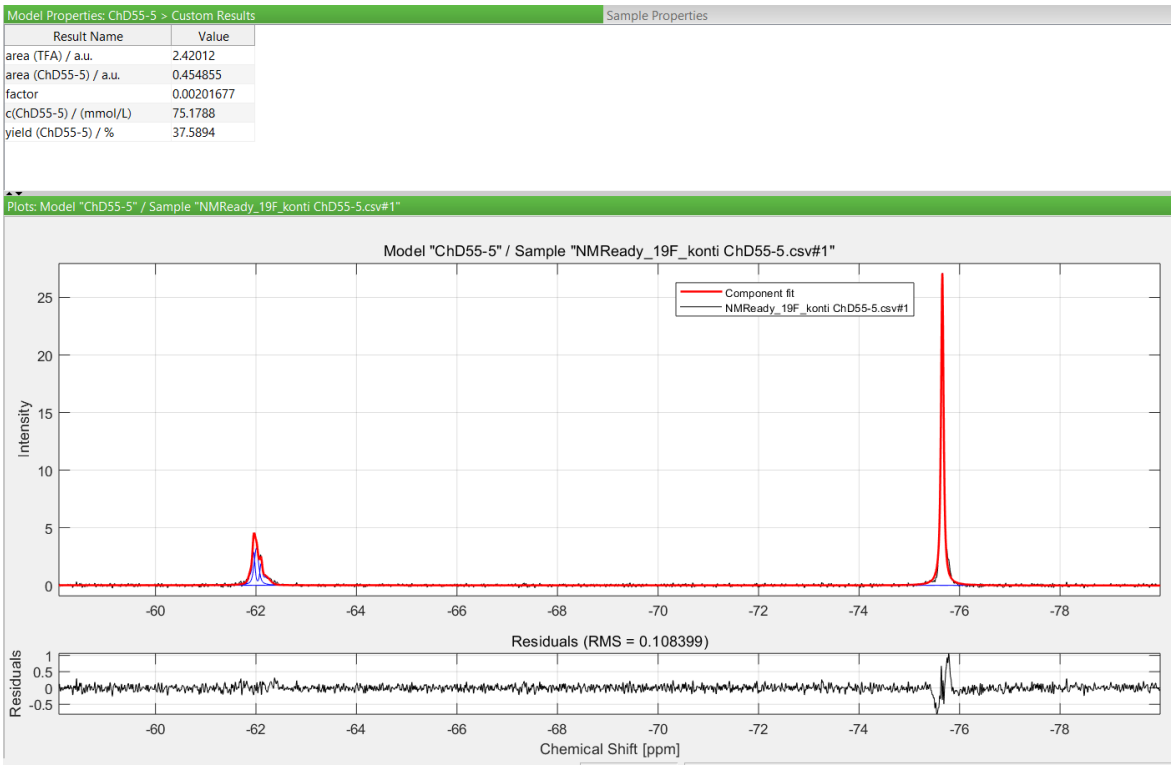

Figure 250: Evaluation of an online ^{19}F-NMR spectrum (56.98 MHz, PEEK flow cell) with PEAXACT 5.3 (component fit via IHM) of **26f** synthesis in a 1/16" FEP capillary photoreactor; General reaction conditions: 200 mM 3-CF_3-aniline, 1.2 equiv. *t*-BuONO, 2 equiv. TFA in MeCN, MeCN/4-fluorobromobenzene V/V=1/1, 365 nm 50 W_{el}, 20 °C, 17 bar_{exs}, t_R=1.25 h; *blue* peak shape of each pure component fits (and unknown substances), *red* component fit as result of a weighted sum of pure components; top: Results of component fitting including yield of continuous **26f** (mixture of isomers) synthesis.

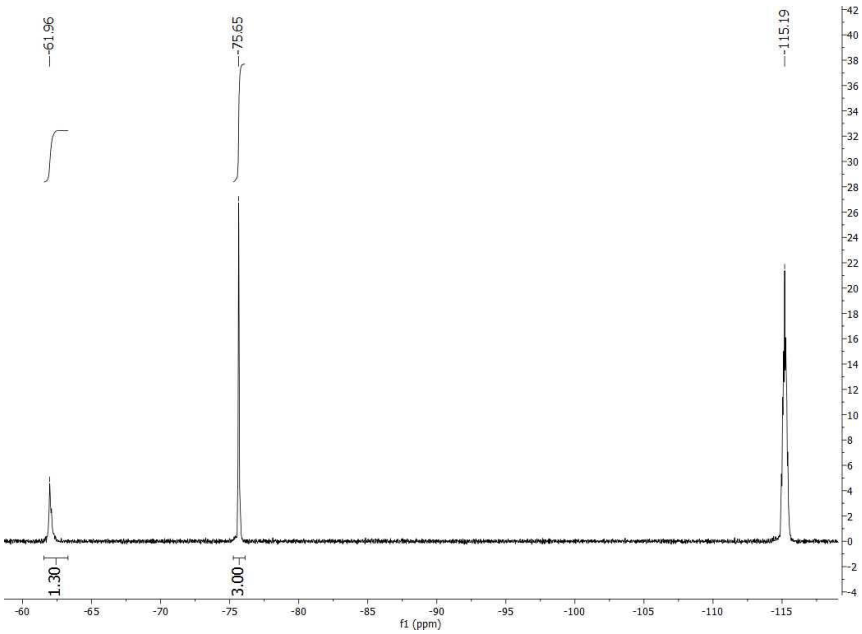

Figure 251: Variance evaluation at an online ^{19}F-NMR spectrum (56.98 MHz, PEEK flow cell) with MestReNova 12 (manual peak integration) of continuous **26f** (mixture of isomers) synthesis in a 1/16" FEP capillary photoreactor; General reaction conditions: 200 mM 3-CF_3-aniline, 1.2 equiv. *t*-BuONO, 2 equiv. TFA in MeCN, MeCN/4-fluorobromobenzene V/V=1/1, 365 nm 50 W_{el}, 20 °C, 17 bar_{exs}, t_R=1.25 h.

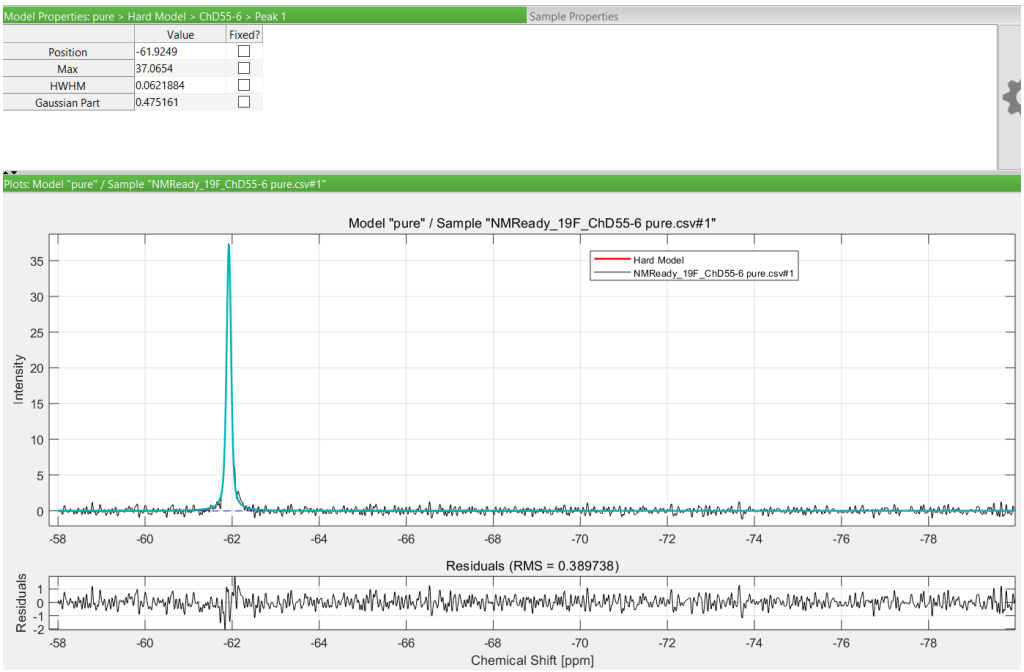

Figure 252: Pure component model for purified **26g** (mixture of isomers) with PEAXACT 5.3; *turquoise* peak shape of hard model consisting of a single peak; top: peak parameters representing **26g** ^{19}F-NMR.

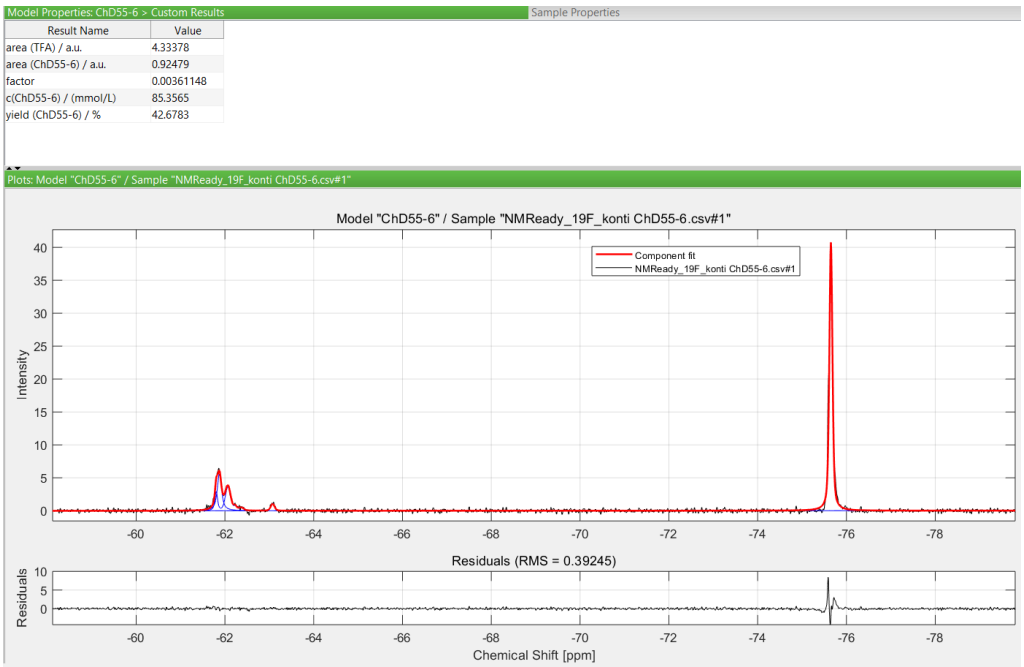

Figure 253: Evaluation of an online ^{19}F-NMR spectrum (56.98 MHz, PEEK flow cell) with PEAXACT 5.3 (component fit via IHM) of continuous **26g** synthesis in a 1/16" FEP capillary photoreactor; General reaction conditions: 200 mM 3-CF_3-aniline, 1.2 equiv. *t*-BuONO, 2 equiv. TFA in MeCN, MeCN/*tert*-butylbenzene V/V=1/1, 365 nm 50 W_{el}, 20 °C, 17 bar_{exs}, t_R=1.25 h; blue peak shape of each pure component fits (and unknown substances), red component fit as result of a weighted sum of pure components; top: Results of component fitting including yield of continuous **26g** (mixture of isomers) synthesis.

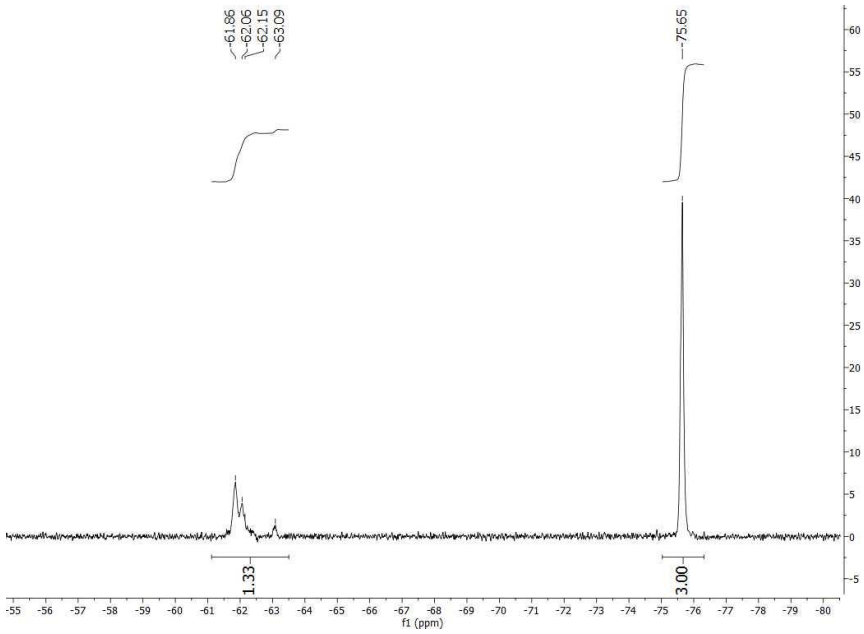

Figure 254: Variance evaluation at an online ^{19}F-NMR spectrum (56.98 MHz, PEEK flow cell) with MestReNova 12 (manual peak integration) of continuous **26g** (mixture of isomers) synthesis in a 1/16" FEP capillary photoreactor; General reaction conditions: 200 mM 3-CF_3-aniline, 1.2 equiv. *t*-BuONO, 2 equiv. TFA in MeCN, MeCN/*tert*-butylbenzene V/V=1/1, 365 nm 50 W_{el}, 20 °C, 17 bar_{exs}, t_R=1.25 h.

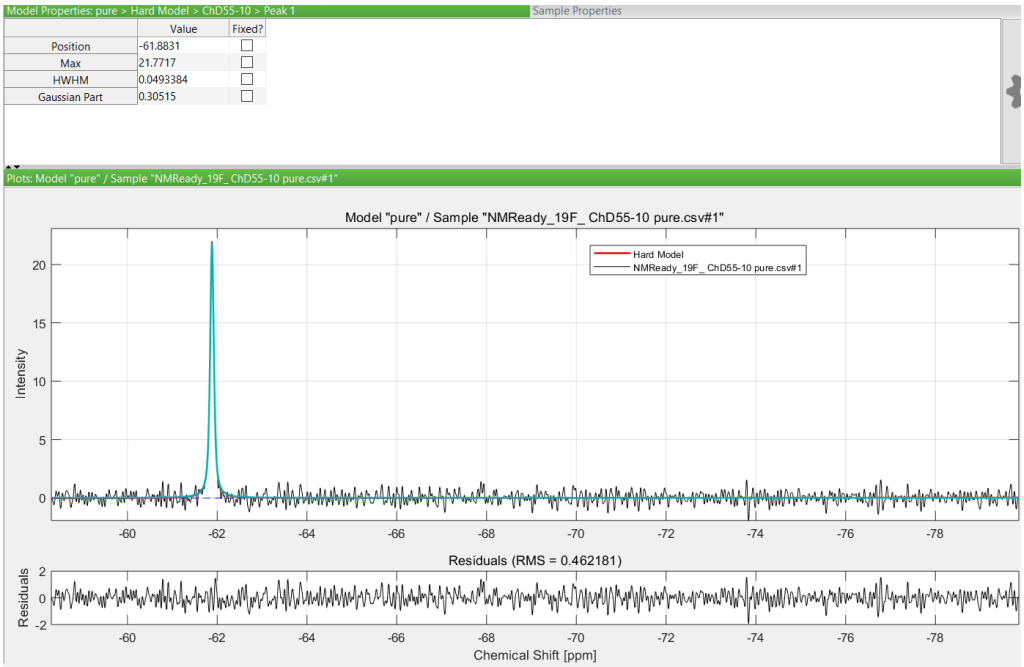

Figure 255: Pure component model for purified **26h** (mixture of isomers) with PEAXACT 5.3; *turquoise* peak shape of hard model consisting of a single peak; top: peak parameters representing **26h** ^{19}F-NMR.

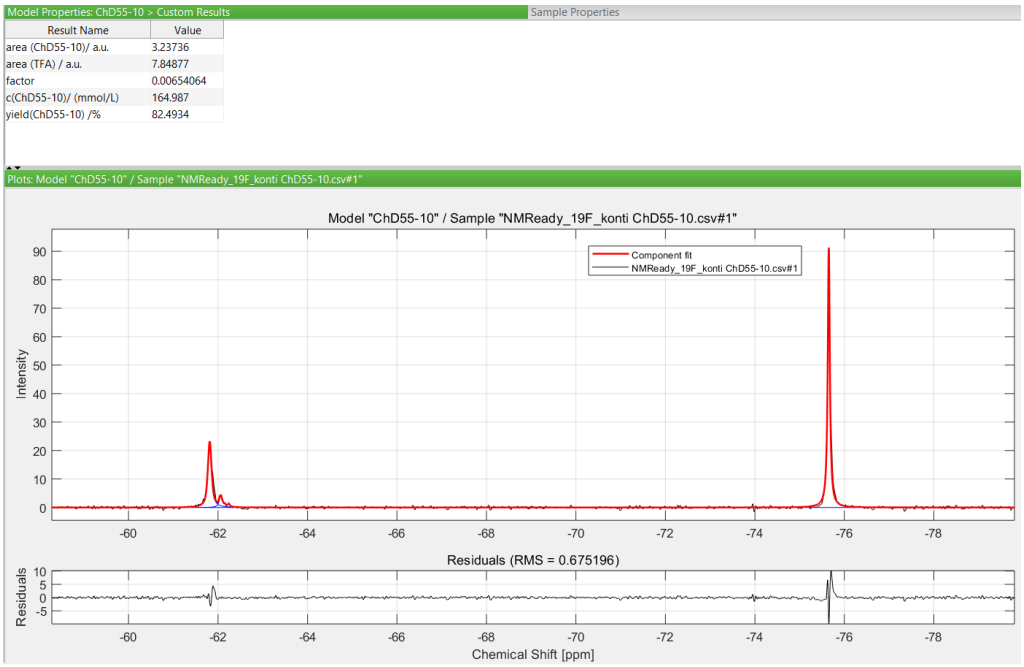

Figure 256: Evaluation of an online ^{19}F-NMR spectrum (56.98 MHz, PEEK flow cell) with PEAXACT 5.3 (component fit via IHM) of continuous **26h** synthesis in a 1/16" FEP capillary photoreactor; General reaction conditions: 200 mM 3-CF_3-aniline, 1.2 equiv. *t*-BuONO, 2 equiv. TFA in MeCN, MeCN/anisole V/V=1/1, 365 nm 50 W_{el}, 20 °C, 17 bar_{exs}, t_R=1.25 h; blue peak shape of each pure component fits (and unknown substances), red component fit as result of a weighted sum of pure components; top: Results of component fitting including yield of continuous **26h** (mixture of isomers) synthesis.

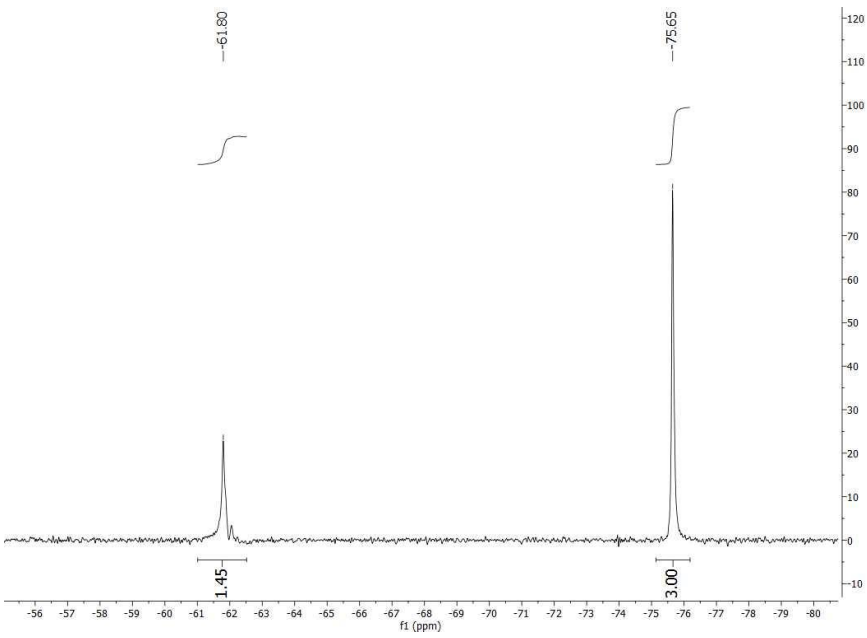

Figure 257: Variance evaluation at an online ^{19}F-NMR spectrum (56.98 MHz, PEEK flow cell) with MestReNova 12 (manual peak integration) of continuous **26h** (mixture of isomers) synthesis in a 1/16" FEP capillary photoreactor; General reaction conditions: 200 mM 3-CF_3-aniline, 1.2 equiv. *t*-BuONO, 2 equiv. TFA in MeCN, MeCN/anisole V/V=1/1, 365 nm 50 W_{el}, 20 °C, 17 bar_{exs}, t_R=1.25 h.

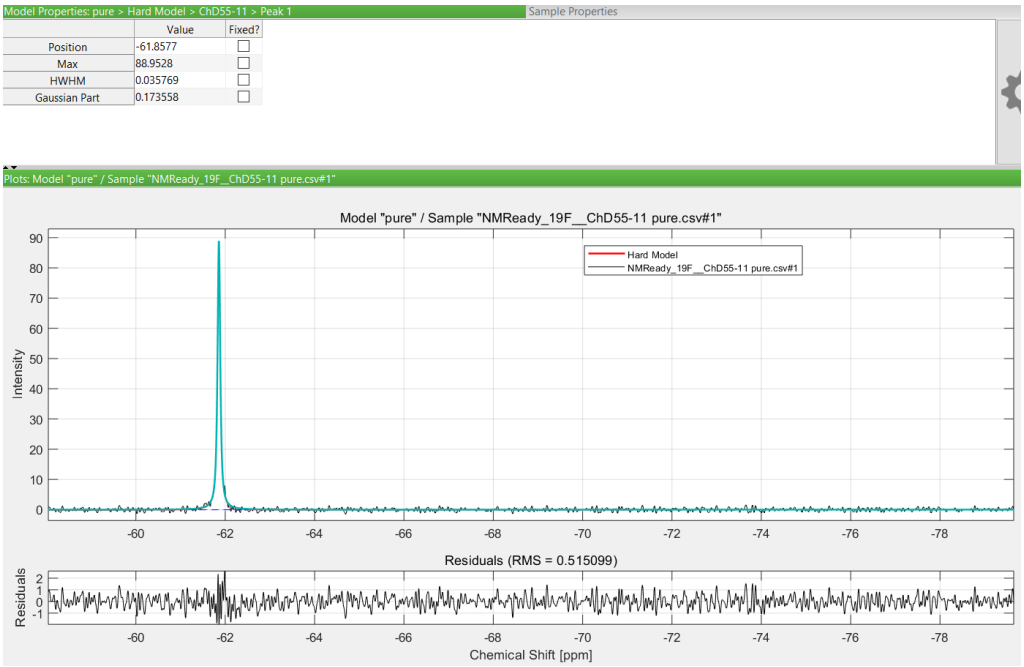

Figure 258: Pure component model for purified **26i** with PEAXACT 5.3; *turquoise* peak shape of hard model consisting of a single peak; top: peak parameters representing **26i** ^{19}F-NMR.

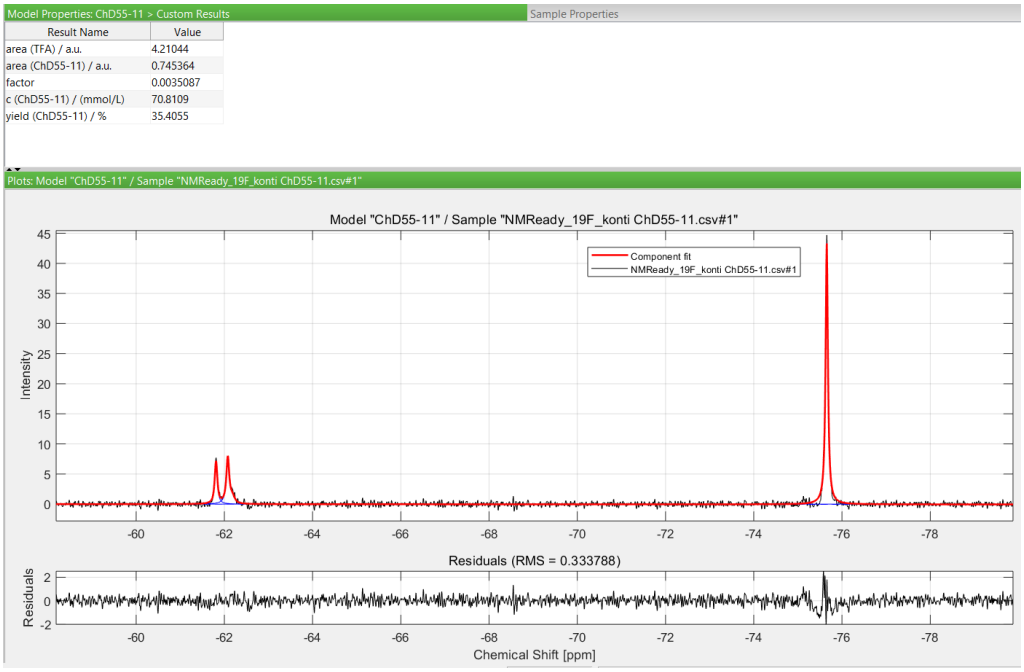

Figure 259: Evaluation of an online ^{19}F-NMR spectrum (56.98 MHz, PEEK flow cell) with PEAXACT 5.3 (component fit via IHM) of continuous **26i** synthesis in a 1/16" FEP capillary photoreactor; General reaction conditions: 200 mM 3-CF_3-aniline, 1.2 equiv. *t*-BuONO, 2 equiv. TFA in MeCN, MeCN/*p*-xylene V/V=1/1, 365 nm 50 W_{el}, 20 °C, 17 bar_{exs}, t_R=1.25 h ; blue peak shape of each pure component fits (and unknown substances), red component fit as result of a weighted sum of pure components; top: Results of component fitting including yield of continuous **26i** synthesis.

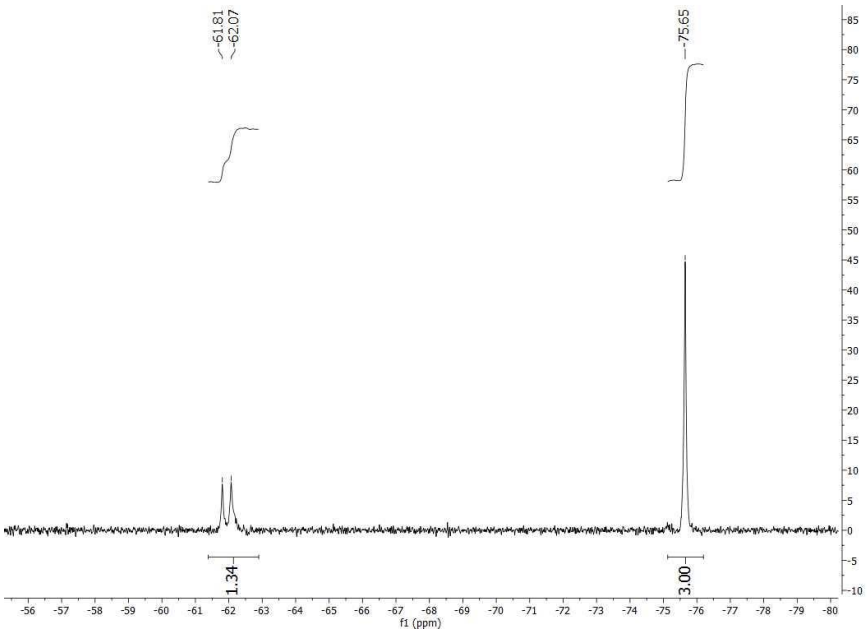

Figure 260: Variance evaluation at an online ^{19}F-NMR spectrum (56.98 MHz, PEEK flow cell) with MestReNova 12 (manual peak integration) of continuous **26i** synthesis in a 1/16" FEP capillary photoreactor; General reaction conditions: 200 mM 3-CF_3-aniline, 1.2 equiv. *t*-BuONO, 2 equiv. TFA in MeCN, MeCN/ *p*-xylene V/V=1/1, 365 nm 50 W_{el}, 20 °C, 17 bar_{exs}, t_R=1.25 h.

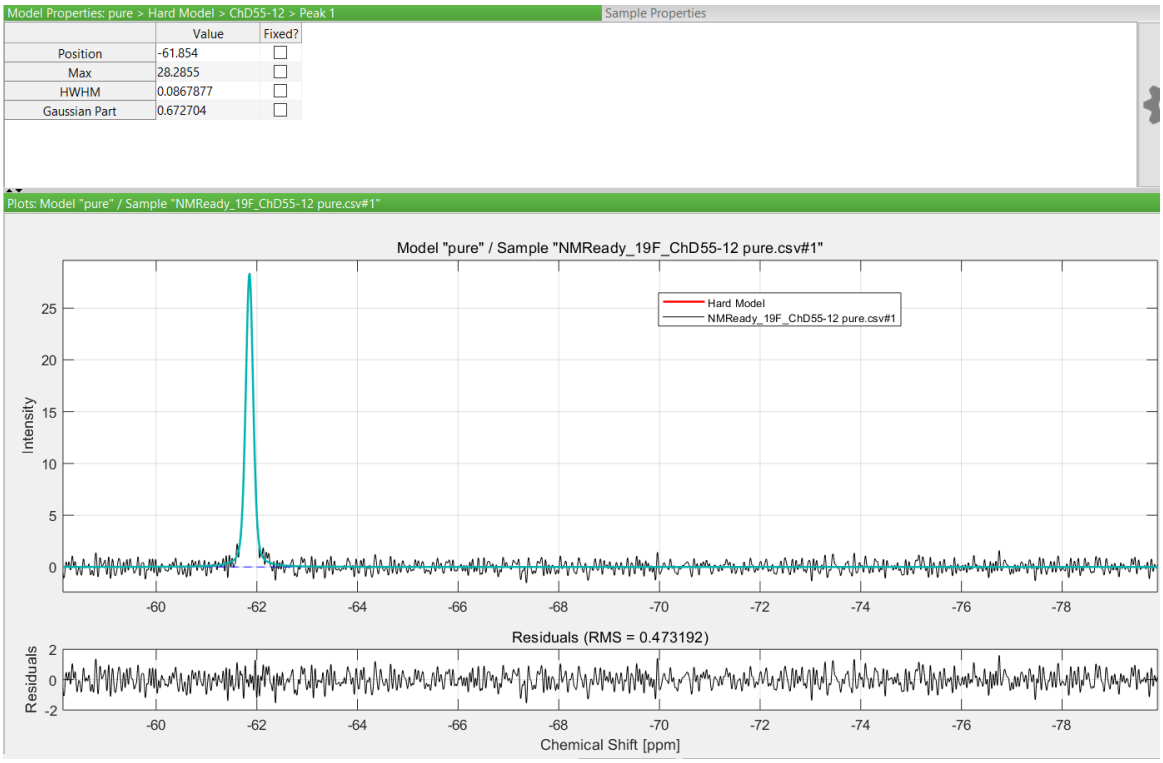

Figure 261: Pure component model for purified **26k** (mixture of isomers) with PEAXACT 5.3; *turquoise* peak shape of hard model consisting of a single peak; top: peak parameters representing **26k** ^{19}F-NMR.

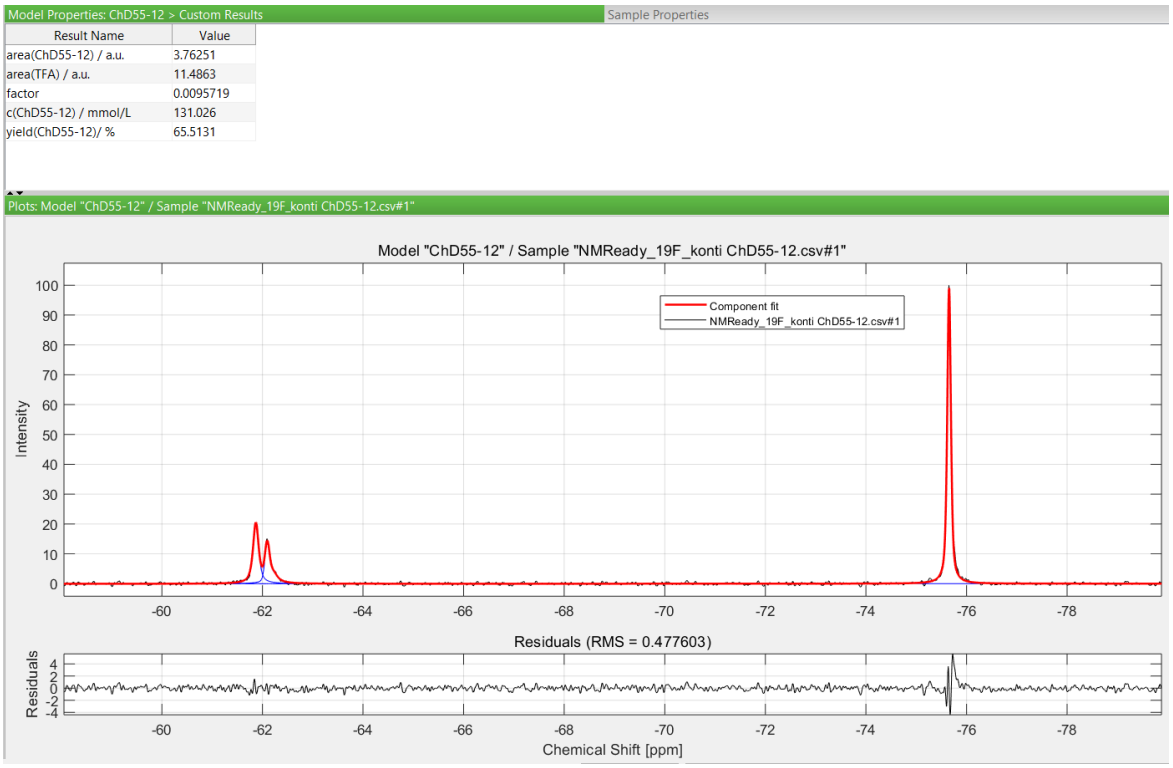

Figure 262: Evaluation of an online ^{19}F-NMR spectrum (56.98 MHz, PEEK flow cell) with Peaxact 5.3 (component fit via IHM) of continuous **26k** synthesis in a 1/16" FEP capillary photoreactor; General reaction conditions: 200 mM 3-CF_3-aniline, 1.2 equiv. *t*-BuONO, 2 equiv. TFA in MeCN, MeCN/toluene V/V=1/1, 365 nm 50 W_{el}, 20 °C, 17 bar_{exs}, t_R=1.25 h; blue peak shape of each pure component fits (and unknown substances), red component fit as result of a weighted sum of pure components; top: Results of component fitting including yield of continuous **26k** (mixture of isomers) synthesis.

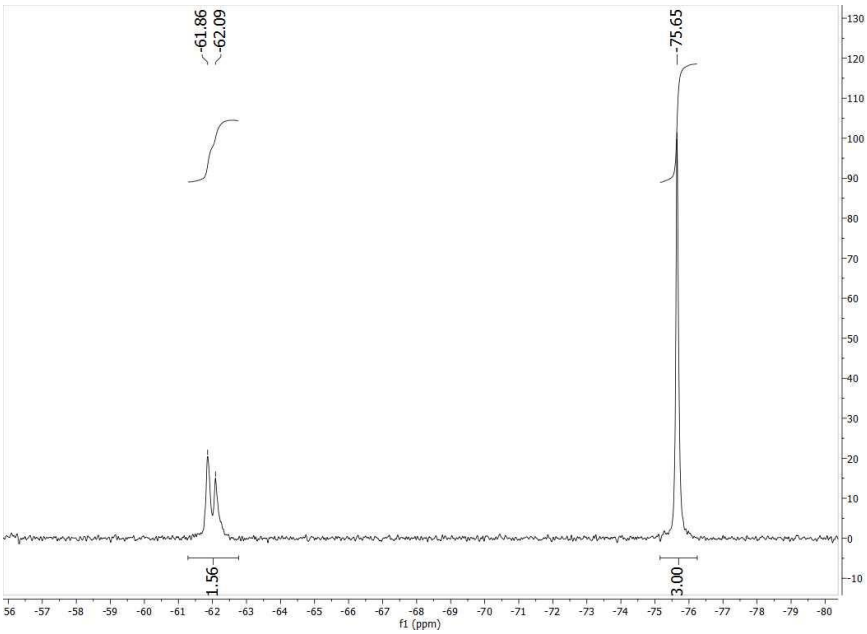

Figure 263: Variance evaluation at an online ^{19}F-NMR spectrum (56.98 MHz, PEEK flow cell) with MestReNova 12 (manual peak integration) of continuous **26k** (mixture of isomers) synthesis in a 1/16" FEP capillary photoreactor; General reaction conditions: 200 mM 3-CF_3-aniline, 1.2 equiv. *t*-BuONO, 2 equiv. TFA in MeCN, MeCN/toluene V/V=1/1, 365 nm 50 W_{el}, 20 °C, 17 bar_{exs}, t_R=1.25 h.

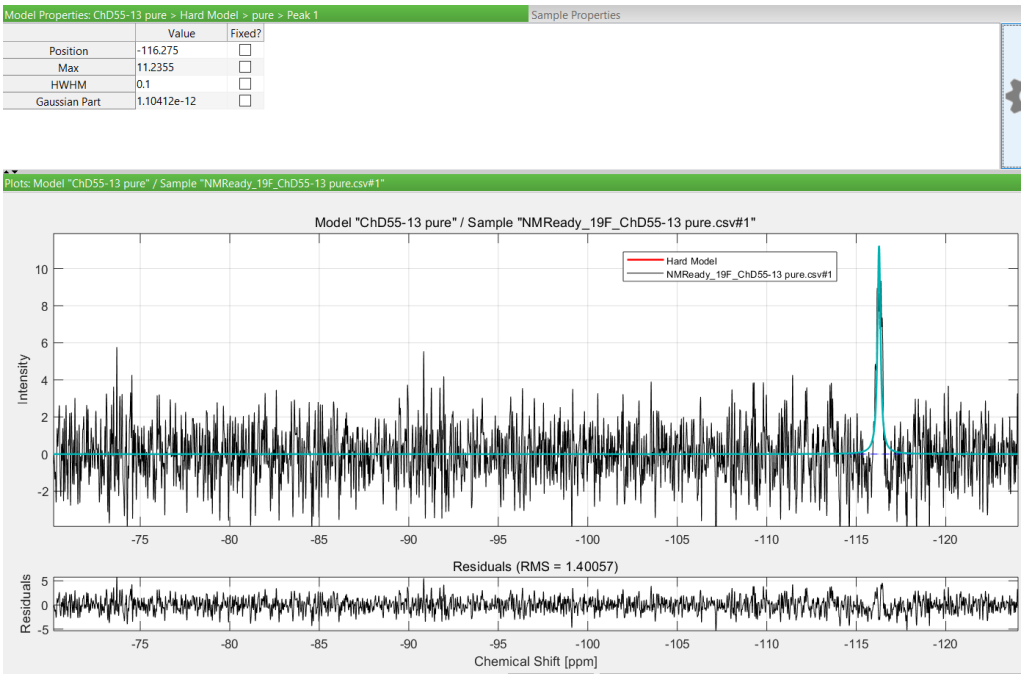

Figure 264: Pure component model for purified **31b** with PEAXACT 5.3; *turquoise* peak shape of hard model consisting of a single peak; top: peak parameters representing 4-fluorobiphenyl ^{19}F-NMR.

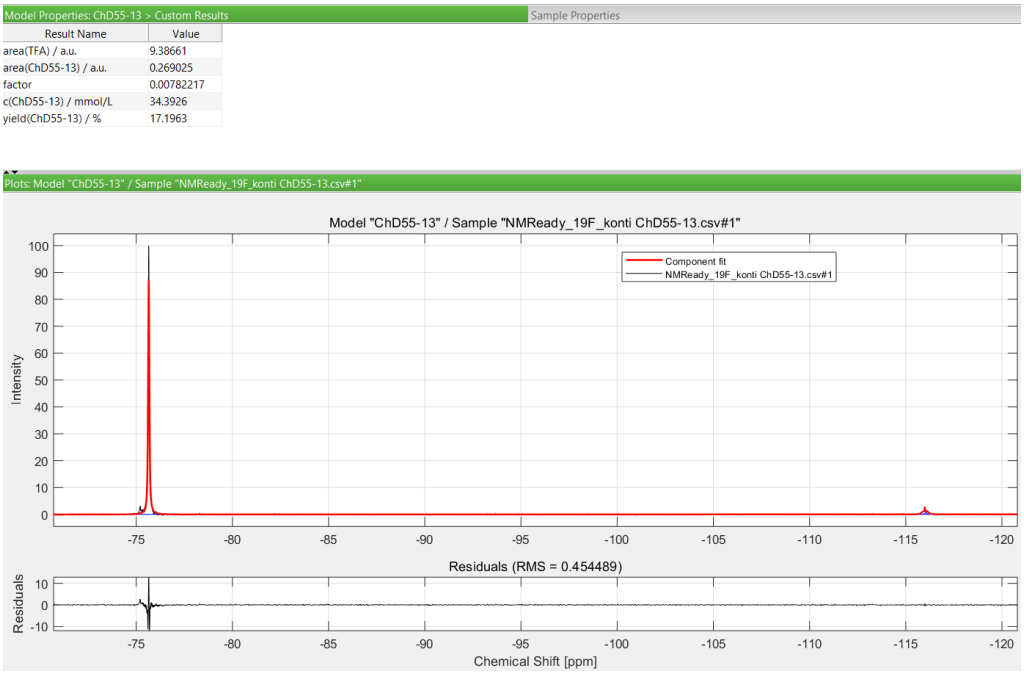

Figure 265: Evaluation of an online ^{19}F-NMR spectrum (56.98 MHz, PEEK flow cell) with PEAXACT 5.3 (component fit via IHM) of continuous **31b** synthesis in a 1/16" FEP capillary photoreactor; General reaction conditions: 200 mM 4-fluoroaniline, 1.2 equiv. *t*-BuONO, 2 equiv. TFA in MeCN, MeCN/benzene V/V=1/1, 365 nm 50 W_{el}, 20 °C, 17 bar_{exs}, t_R=1.25 h; blue peak shape of each pure component fits (and unknown substances), red component fit as result of a weighted sum of pure components; top: Results of component fitting including yield of continuous **31b** synthesis.

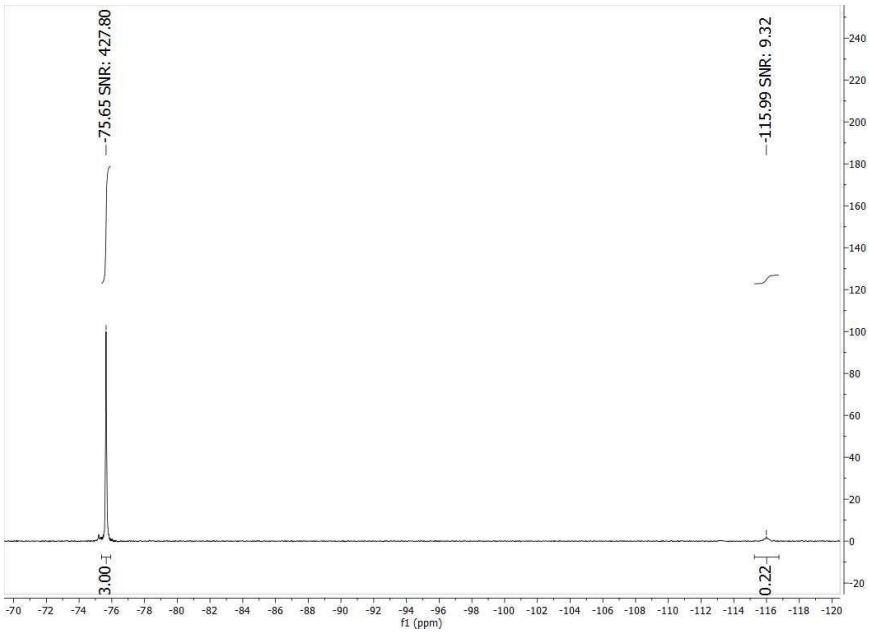

Figure 266: Variance evaluation at an online ^{19}F-NMR spectrum (56.98 MHz, PEEK flow cell) with MestReNova 12 (manual peak integration) of continuous **31b** synthesis in a 1/16" FEP capillary photoreactor; General reaction conditions: 200 mM 4-fluoroaniline, 1.2 equiv. *t*-BuONO, 2 equiv. TFA in MeCN, MeCN/benzene V/V=1/1, 365 nm 50 W_{el}, 20 °C, 17 bar_{exs}, t_R=1.25 h.

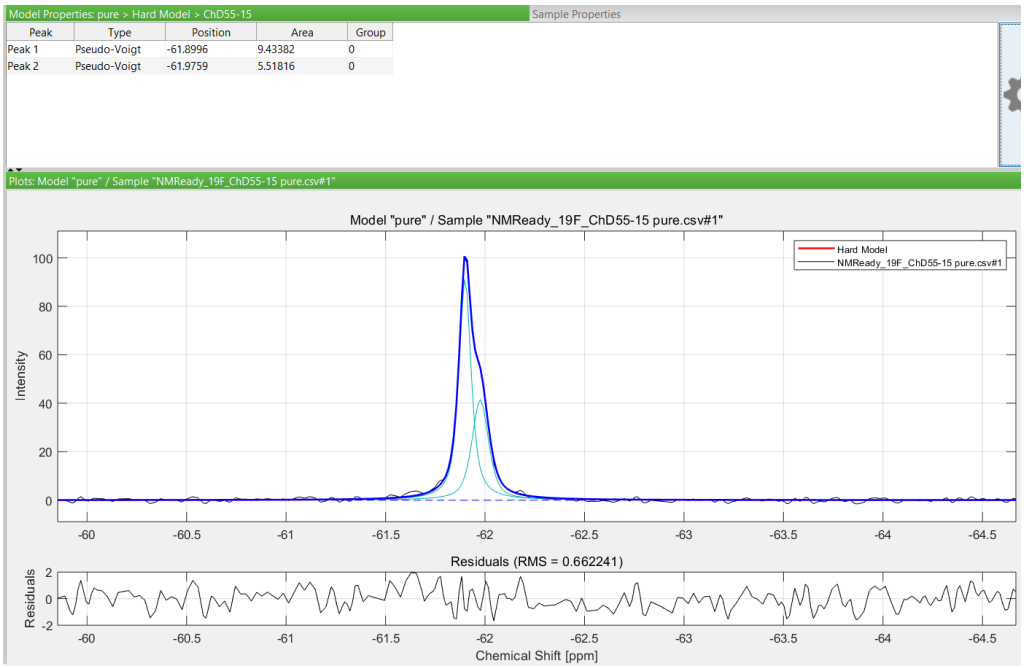

Figure 267: Pure component model (*blue*) for purified **26l** (mixture of isomers) with PEAXACT 5.3; *turquoise* peak shape of hard model consisting of a single peak; top: peak parameters representing purified **26l** ^{19}F-NMR.

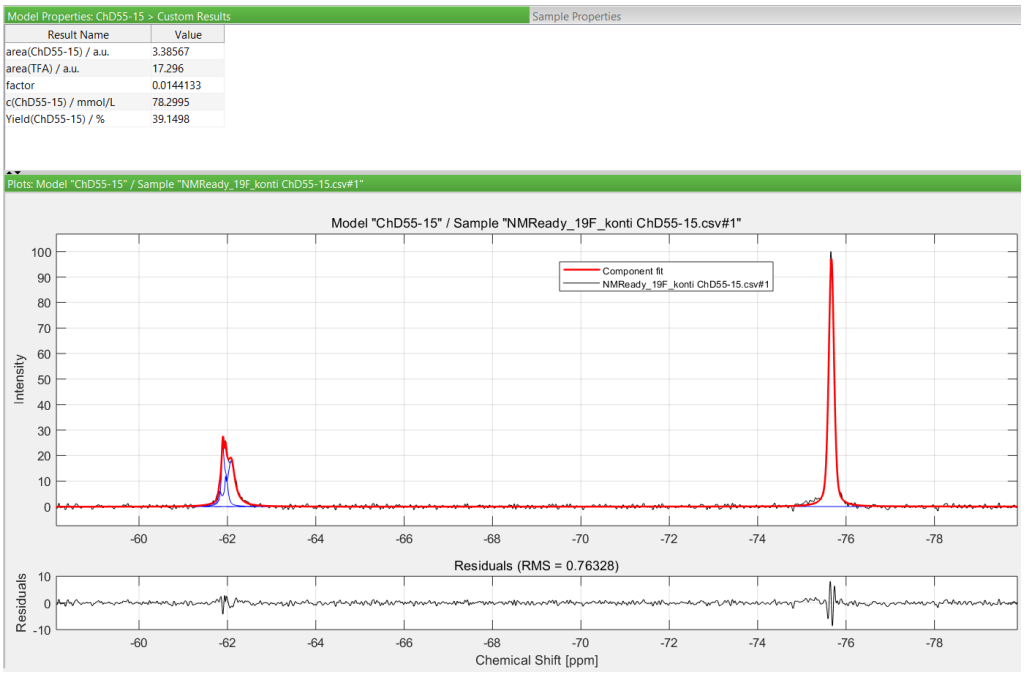

Figure 268: Evaluation of an online ^{19}F-NMR spectrum (56.98 MHz, PEEK flow cell) with PEAXACT 5.3 (component fit via IHM) of continuous **26l** synthesis in a 1/16" FEP capillary photoreactor; General reaction conditions: 200 mM 4-fluoroaniline, 1.2 equiv. *t*-BuONO, 2 equiv. TFA in MeCN, MeCN/ethyl benzoate V/V=1/1, 365 nm 50 W_{el}, 20 °C, 17 bar_{exs}, t_R=1.25 h; blue peak shape of each pure component fits (and unknown substances), red component fit as result of a weighted sum of pure components; top: Results of component fitting including yield of continuous **26l** (mixture of isomers) synthesis.

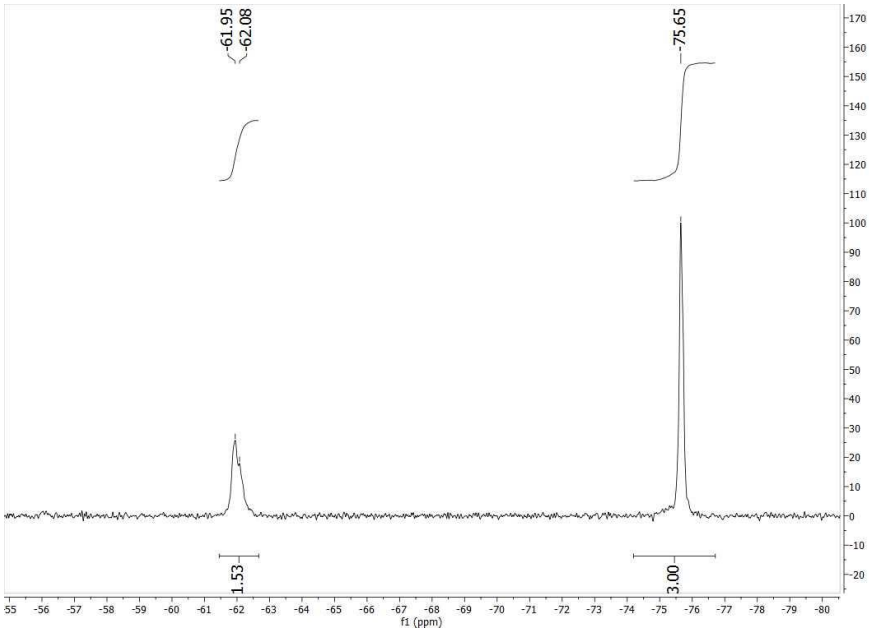

Figure 269: Variance evaluation at an online ^{19}F-NMR spectrum (56.98 MHz, PEEK flow cell) with MestReNova 12 (manual peak integration) of continuous **26l** (mixture of isomers) synthesis in a 1/16" FEP capillary photoreactor; General reaction conditions: 200 mM 3-CF_3-aniline, 1.2 equiv. *t*-BuONO, 2 equiv. TFA in MeCN, MeCN/ethyl benzoate V/V=1/1, 365 nm 50 W_{el}, 20 °C, 17 bar_{exs}, t_R=1.25 h.

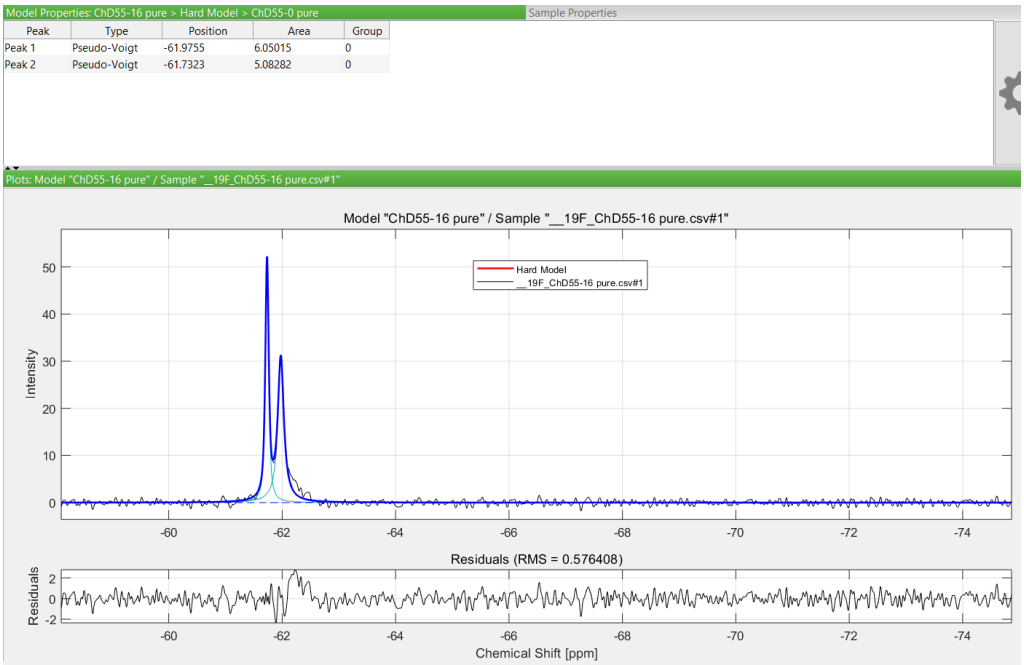

Figure 270: Pure component model (*blue*) for purified **26m** (mixture of isomers) with PEAXACT 5.3; *turquoise* peak shape of hard model consisting of a single peak; top: peak parameters representing **26m** ^{19}F-NMR.

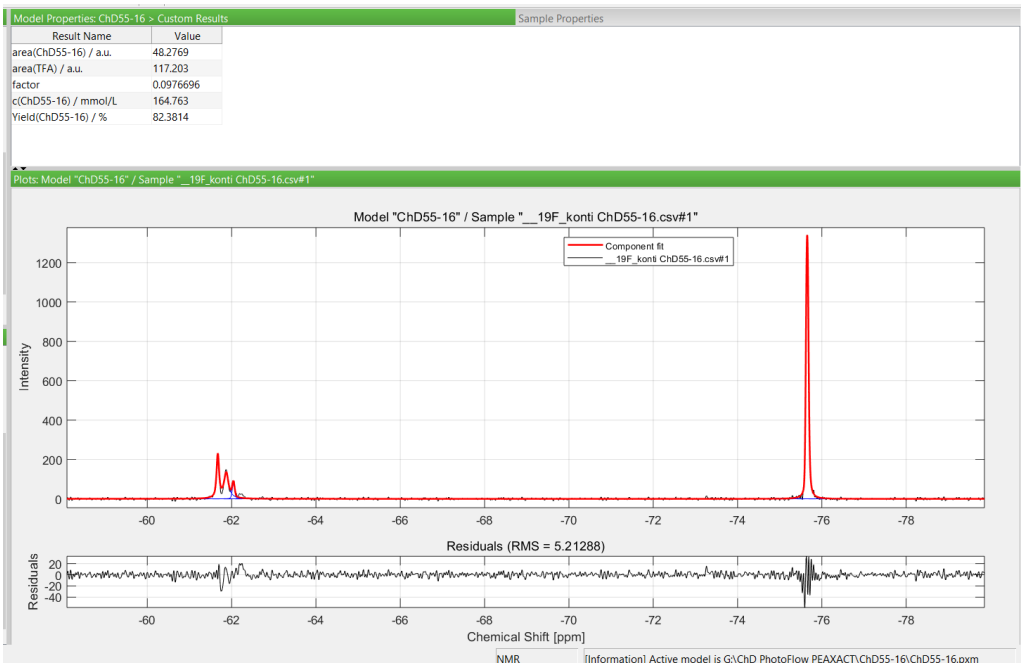

Figure 271: Evaluation of an online ^{19}F-NMR spectrum (56.98 MHz, PEEK flow cell) with PEAXACT 5.3 (component fit via IHM) of continuous **26m** synthesis in a 1/16" FEP capillary photoreactor; General reaction conditions: 200 mM 3-CF_3-aniline, 1.2 equiv. *t*-BuONO, 2 equiv. TFA in MeCN; 2.25 M phenylboronic acid pinacol ester in MeCN, 365 nm 50 W_{el}, 20 °C, 17 bar_{exs}, t_R=1.25 h; blue peak shape of each pure component fits (and unknown substances), red component fit as result of a weighted sum of pure components; top: Results of component fitting including yield of **26m** (mixture of isomers) synthesis.

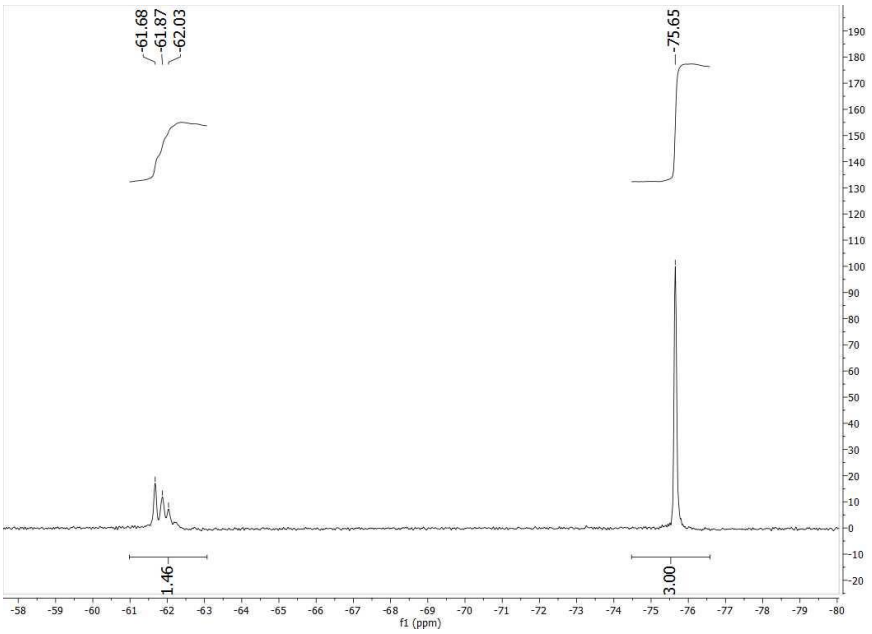

Figure 272: Variance evaluation at an online ^{19}F-NMR spectrum (56.98 MHz, PEEK flow cell) with MestReNova 12 (manual peak integration) of continuous **26m** (mixture of isomers) synthesis in a 1/16" FEP capillary photoreactor; General reaction conditions: 200 mM 3-CF_3-aniline, 1.2 equiv. *t*-BuONO, 2 equiv. TFA in MeCN, 2.25 M phenylboronic acid pinacol ester in MeCN, 365 nm 50 W_{el}, 20 °C, 17 bar_{exs}, t_R=1.25 h.

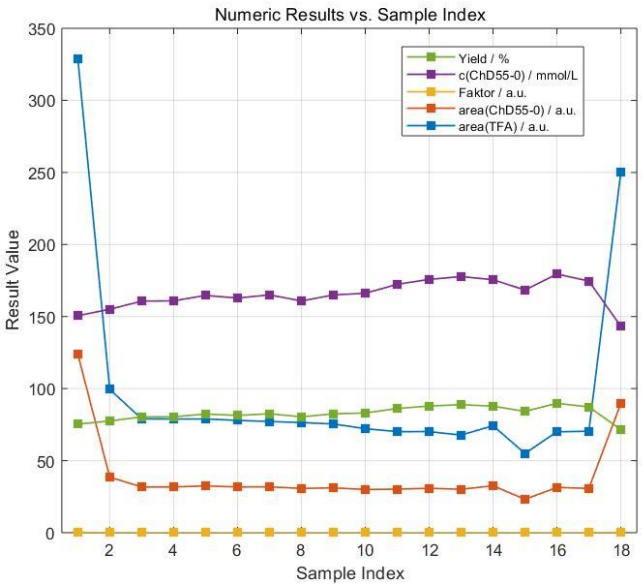

Figure 273: IHM evaluation data (via PEAXACT 5.3) of online ^{19}F-NMR spectroscopy in continuous (long-term) synthesis of **26b** in a 1/16" FEP capillary photoreactor.

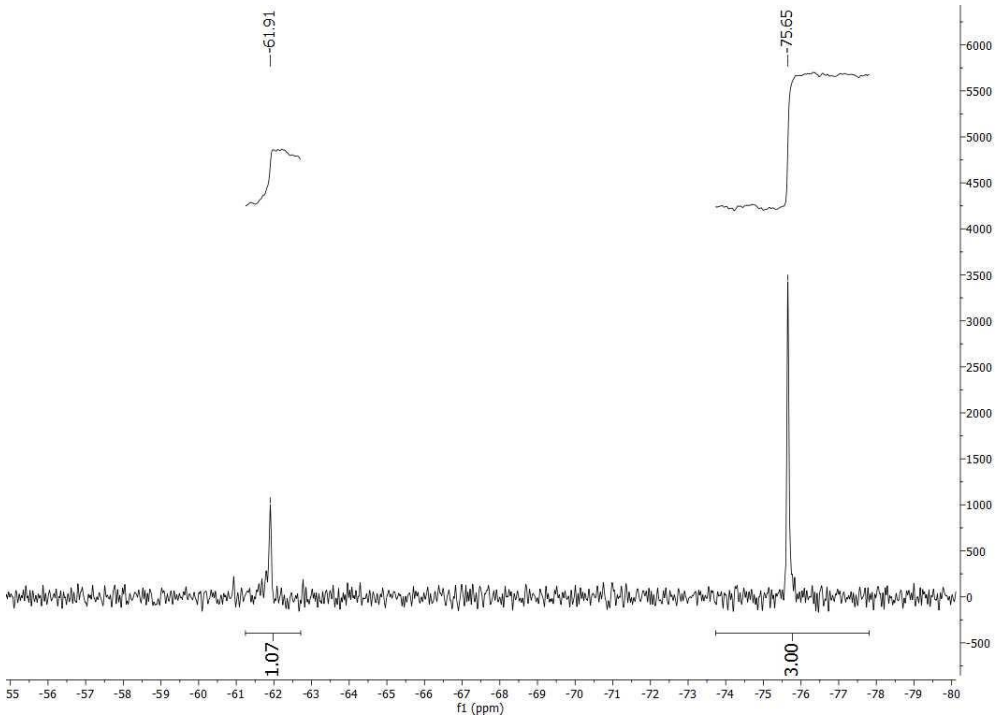

Figure 274: Variance evaluation at an online ^{19}F-NMR spectrum (56.98 MHz, PEEK flow cell) with MestReNova 12 (manual peak integration); Continuous (long-term) synthesis of **26b**; time stamp: 09:53.

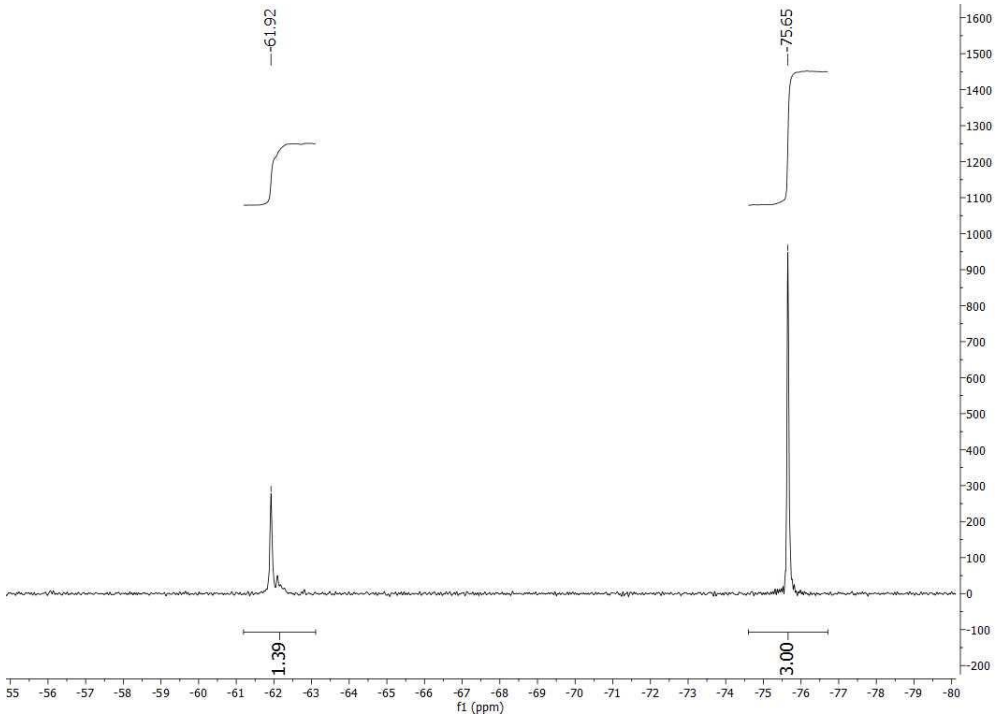

Figure 275: Variance evaluation at an online ^{19}F-NMR spectrum (56.98 MHz, PEEK flow cell) with MestReNova 12 (manual peak integration); Continuous (long-term) synthesis of **26b**; time stamp: 10:02.

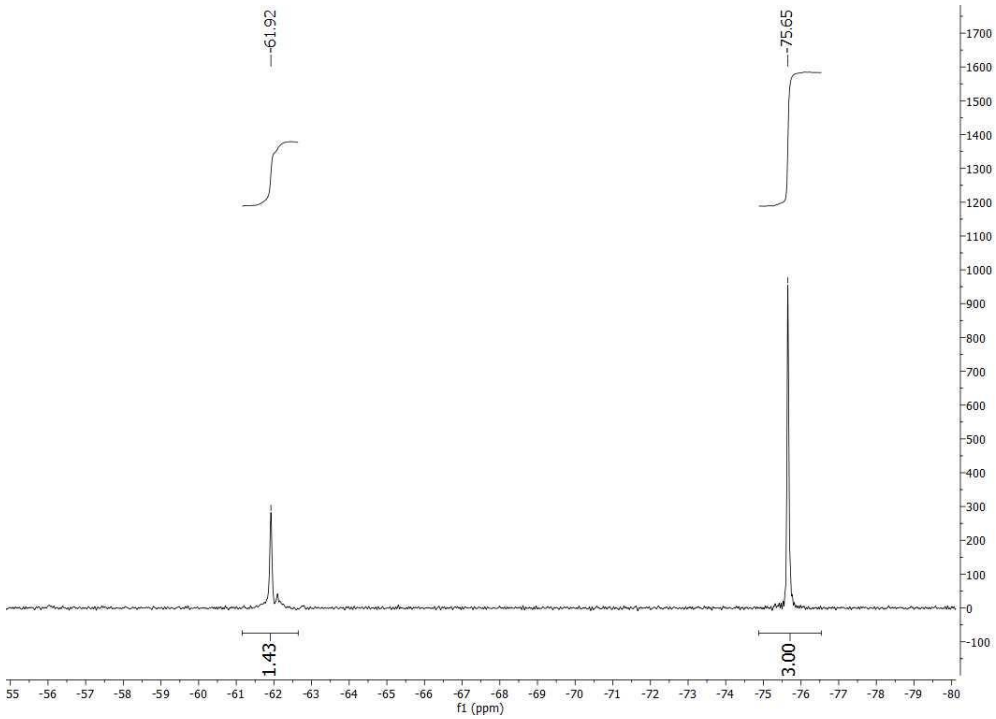

Figure 276: Variance evaluation at an online ^{19}F-NMR spectrum (56.98 MHz, PEEK flow cell) with MestReNova 12 (manual peak integration); Continuous (long-term) synthesis of **26b**; time stamp: 10:25.

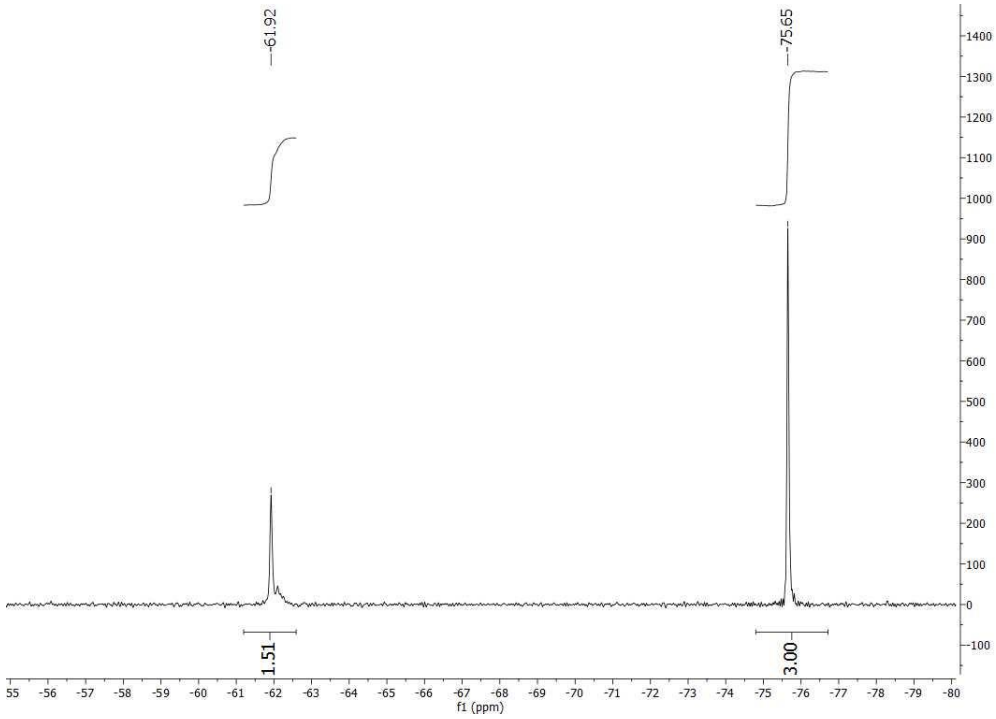

Figure 277: Variance evaluation at an online ^{19}F-NMR spectrum (56.98 MHz, PEEK flow cell) with MestReNova 12 (manual peak integration); Continuous (long-term) synthesis of **26b**; time stamp: 10:45.

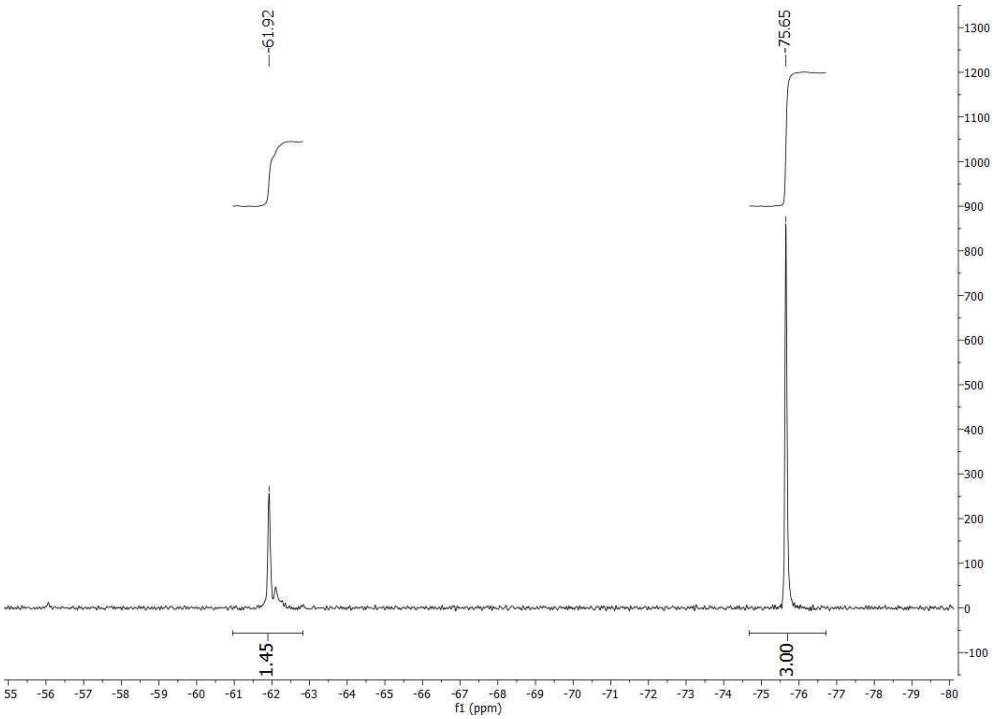

Figure 278: Variance evaluation at an online ^{19}F-NMR spectrum (56.98 MHz, PEEK flow cell) with MestReNova 12 (manual peak integration); Continuous (long-term) synthesis of **26b**; time stamp: 11:41.

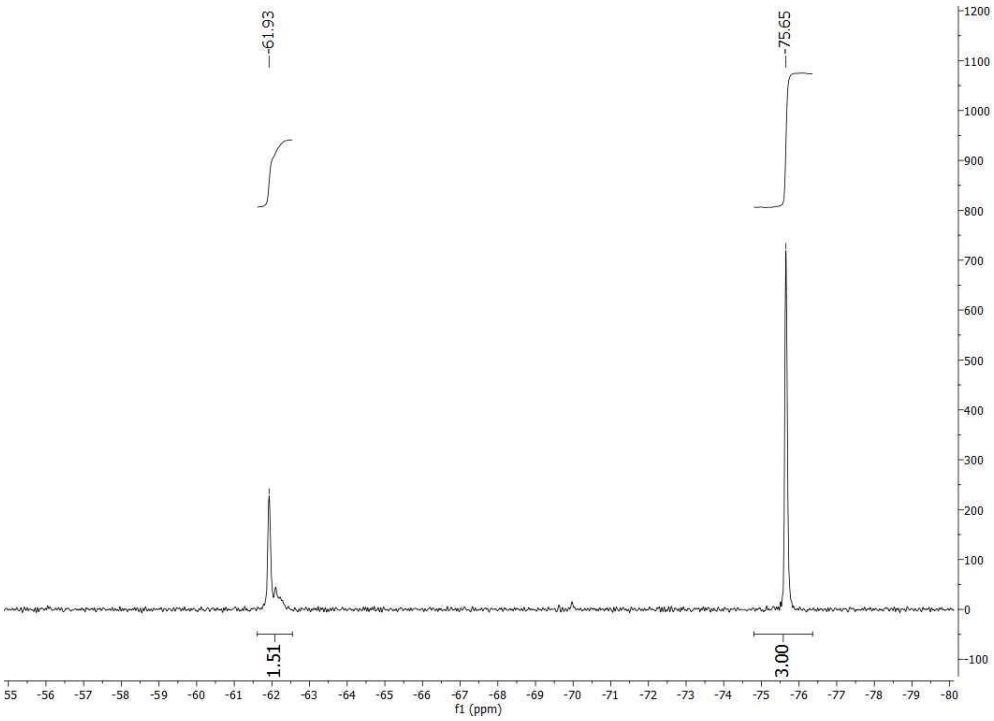

Figure 279: Variance evaluation at an online ^{19}F-NMR spectrum (56.98 MHz, PEEK flow cell) with MestReNova 12 (manual peak integration); Continuous (long-term) synthesis of **26b**; time stamp: 12:46.

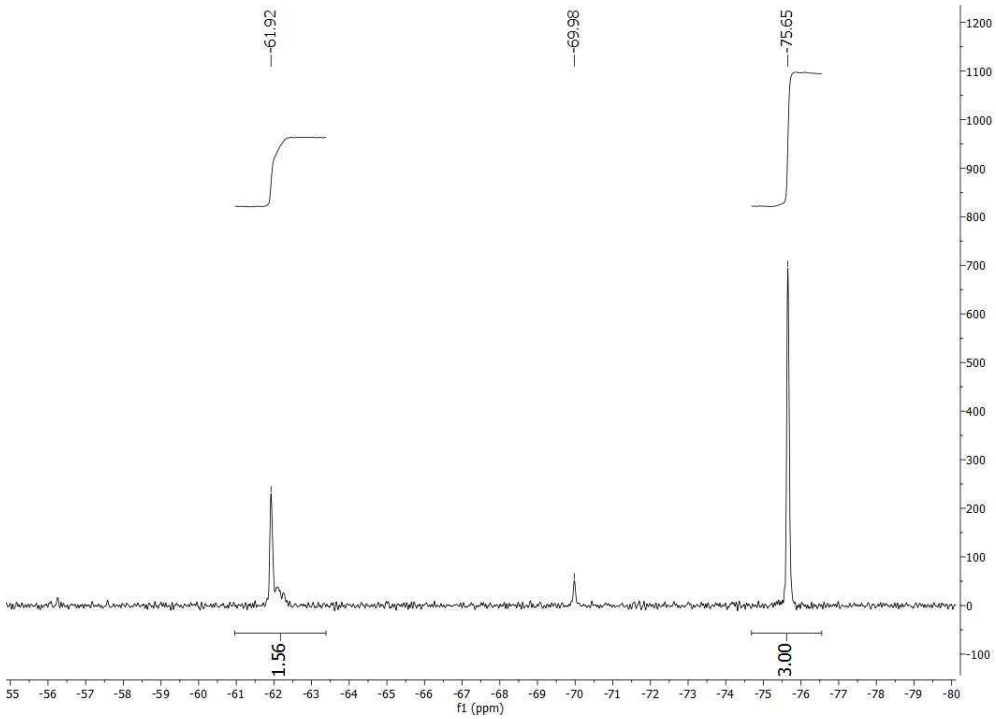

Figure 280: Variance evaluation at an online ^{19}F-NMR spectrum (56.98 MHz, PEEK flow cell) with MestReNova 12 (manual peak integration); Continuous (long-term) synthesis of **26b**; time stamp: 13:44.

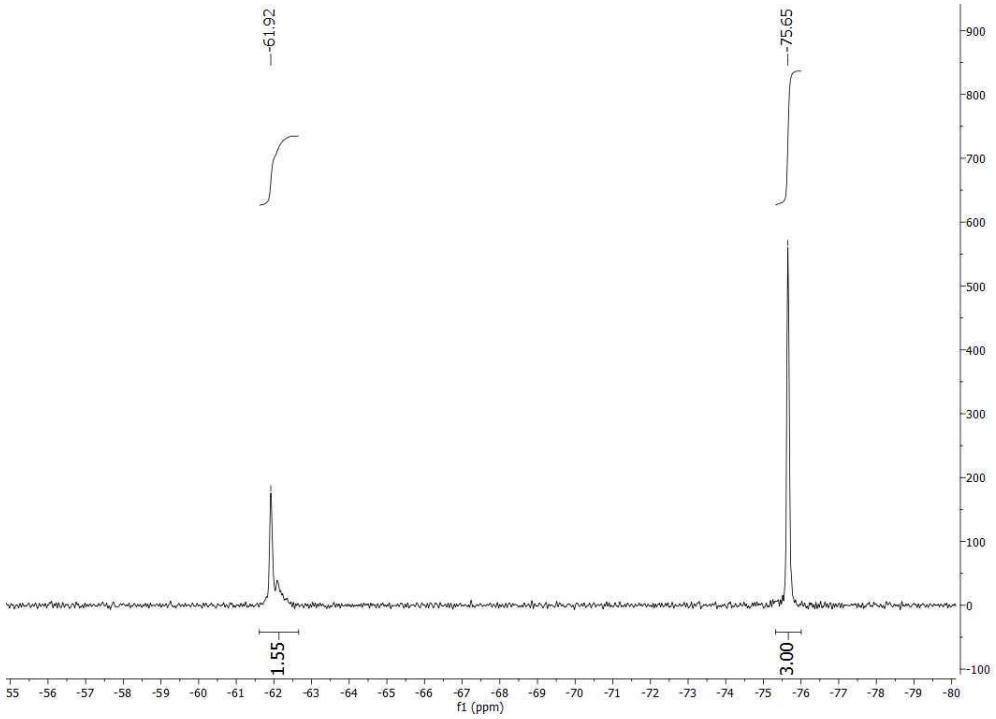

Figure 281: Variance evaluation at an online ^{19}F-NMR spectrum (56.98 MHz, PEEK flow cell) with MestReNova 12 (manual peak integration); Continuous (long-term) synthesis of **26b**; time stamp: 14:22.

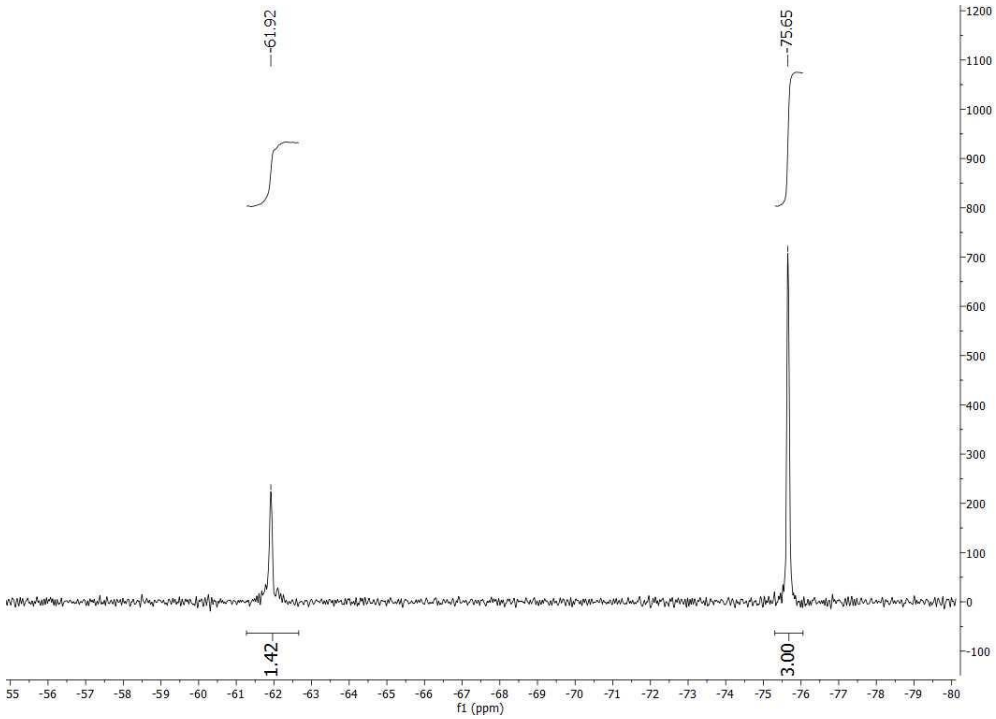

Figure 282: Variance evaluation at an online ^{19}F-NMR spectrum (56.98 MHz, PEEK flow cell) with MestReNova 12 (manual peak integration); Continuous (long-term) synthesis of **26b**; time stamp: 15:20.

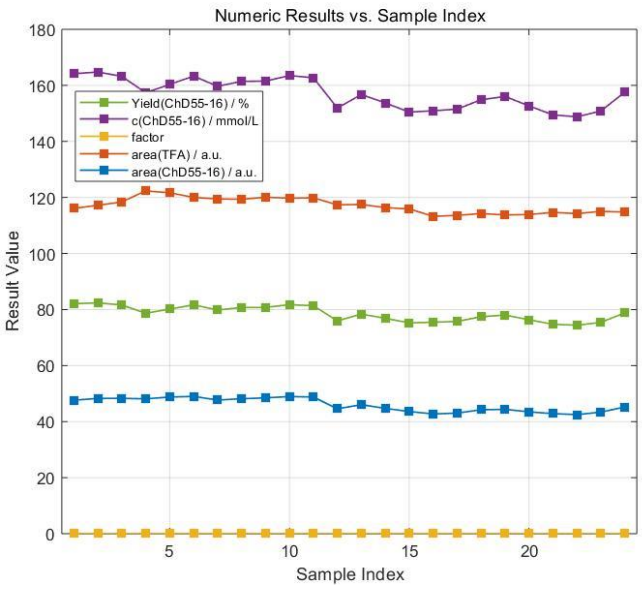

Figure 283: IHM evaluation data (via PEAXACT 5.3) of online ^{19}F-NMR spectroscopy in continuous (long-term) synthesis of **26m** in a 1/16" FEP capillary photoreactor.

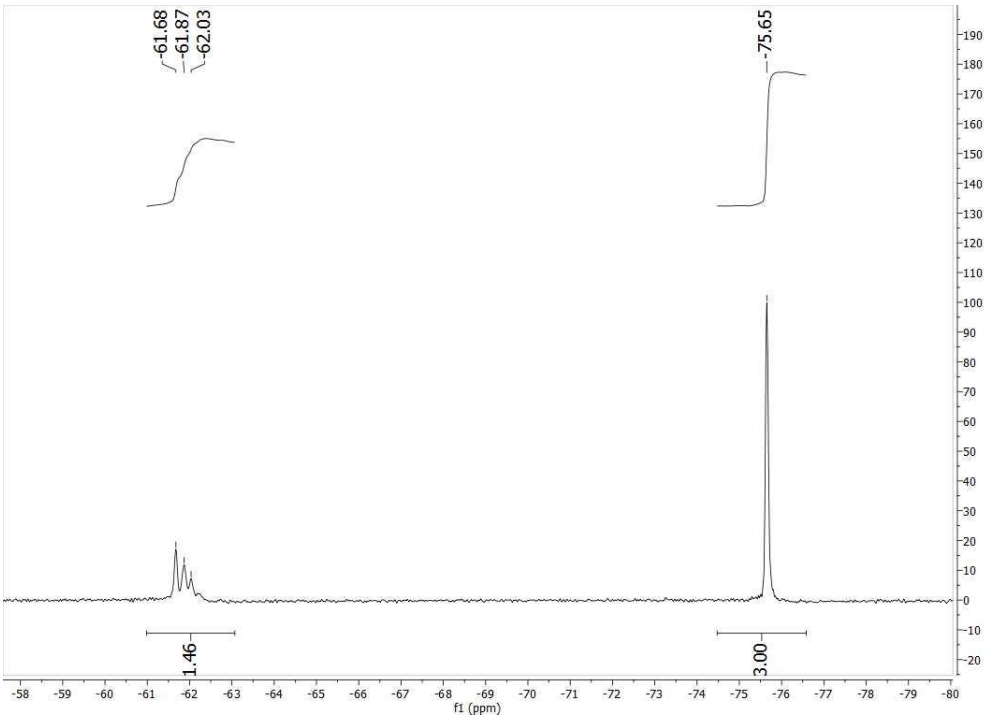

Figure 284: Variance evaluation at an online ^{19}F-NMR spectrum (56.98 MHz, PEEK flow cell) with MestReNova 12 (manual peak integration); Continuous (long-term) synthesis of **26m**; time stamp: 10:57.

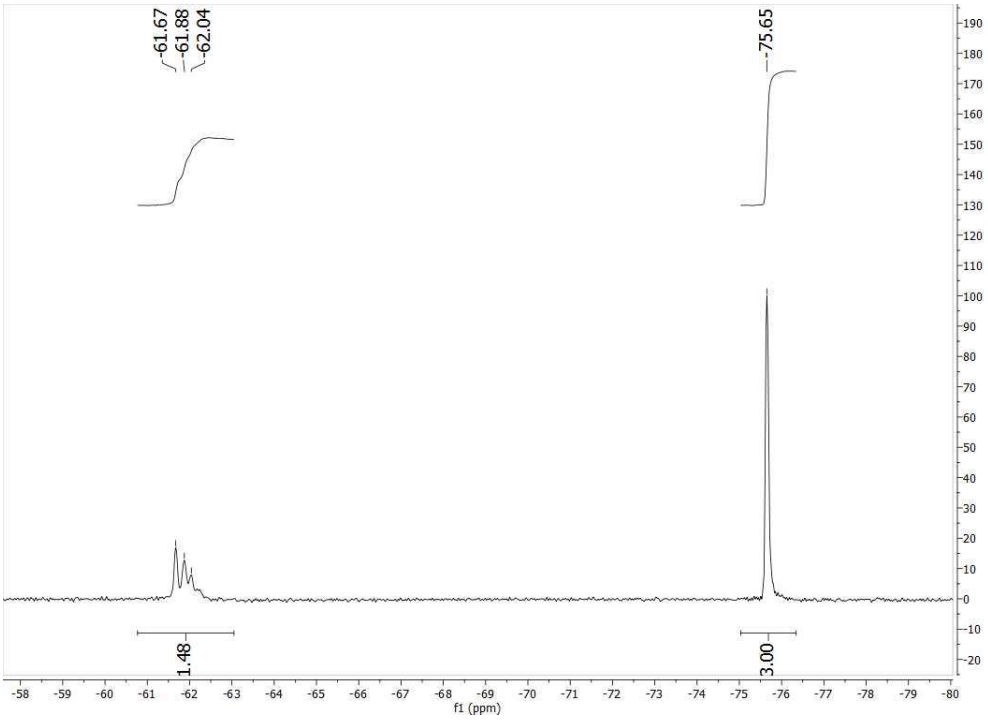

Figure 285: Variance evaluation at an online ^{19}F-NMR spectrum (56.98 MHz, PEEK flow cell) with MestReNova 12 (manual peak integration); Continuous (long-term) synthesis of **26m**; time stamp: 11:55.

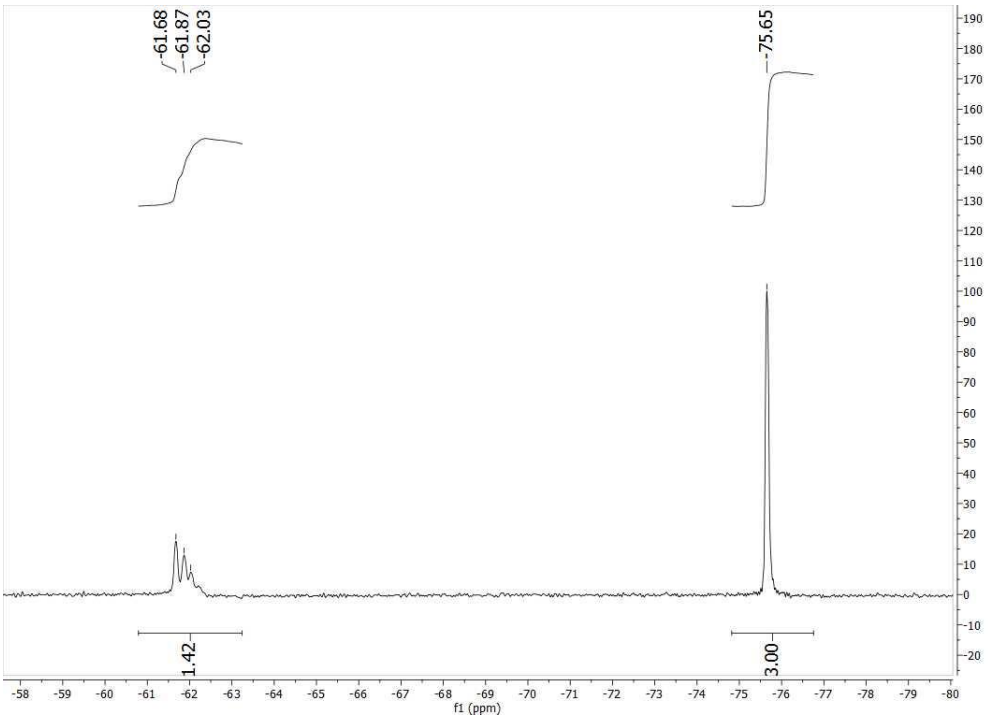

Figure 286: Variance evaluation at an online ^{19}F-NMR spectrum (56.98 MHz, PEEK flow cell) with MestReNova 12 (manual peak integration); Continuous (long-term) synthesis of **26m**; time stamp: 12:53.

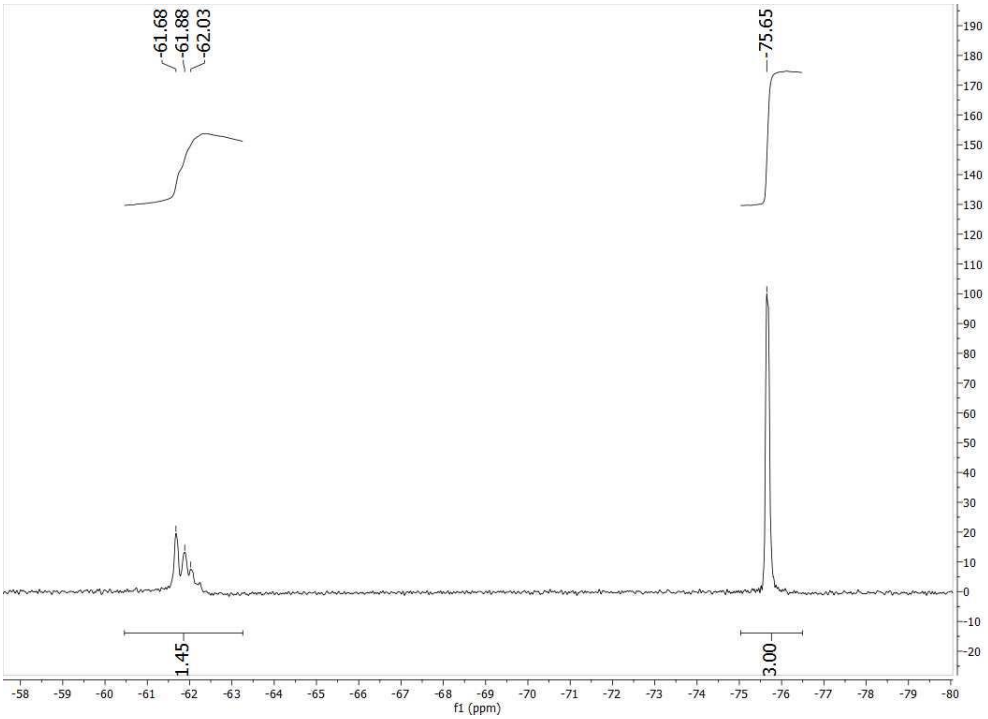

Figure 287: Variance evaluation at an online ^{19}F-NMR spectrum (56.98 MHz, PEEK flow cell) with MestReNova 12 (manual peak integration); Continuous (long-term) synthesis of **26m**; time stamp: 14:13.

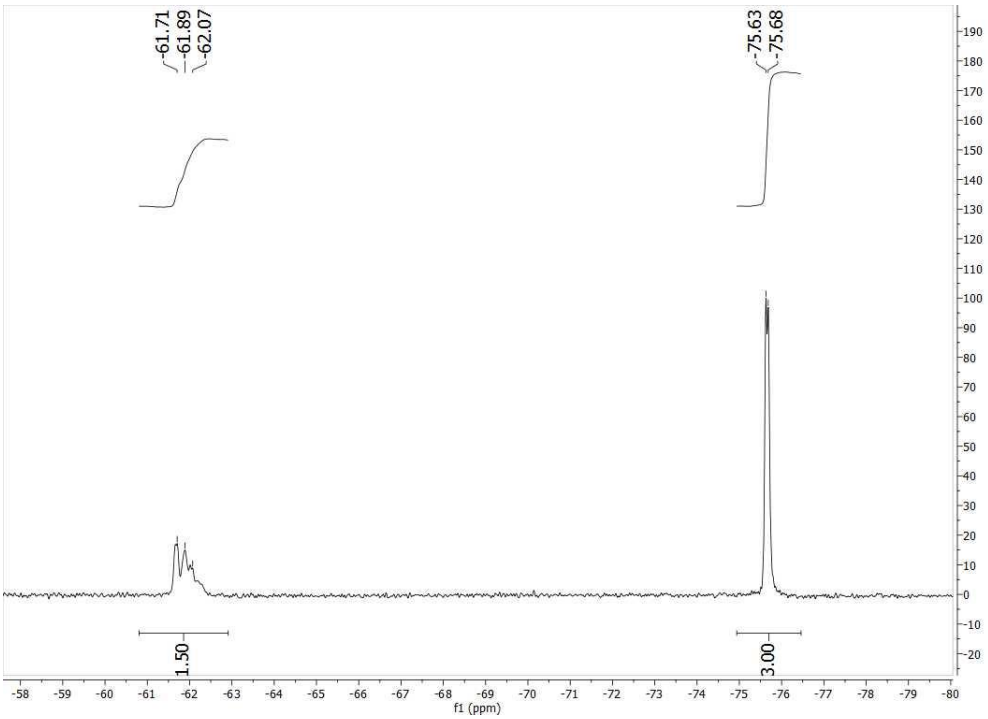

Figure 288: Variance evaluation at an online ^{19}F-NMR spectrum (56.98 MHz, PEEK flow cell) with MestReNova 12 (manual peak integration); Continuous (long-term) synthesis of **26m**; time stamp: 15:34.

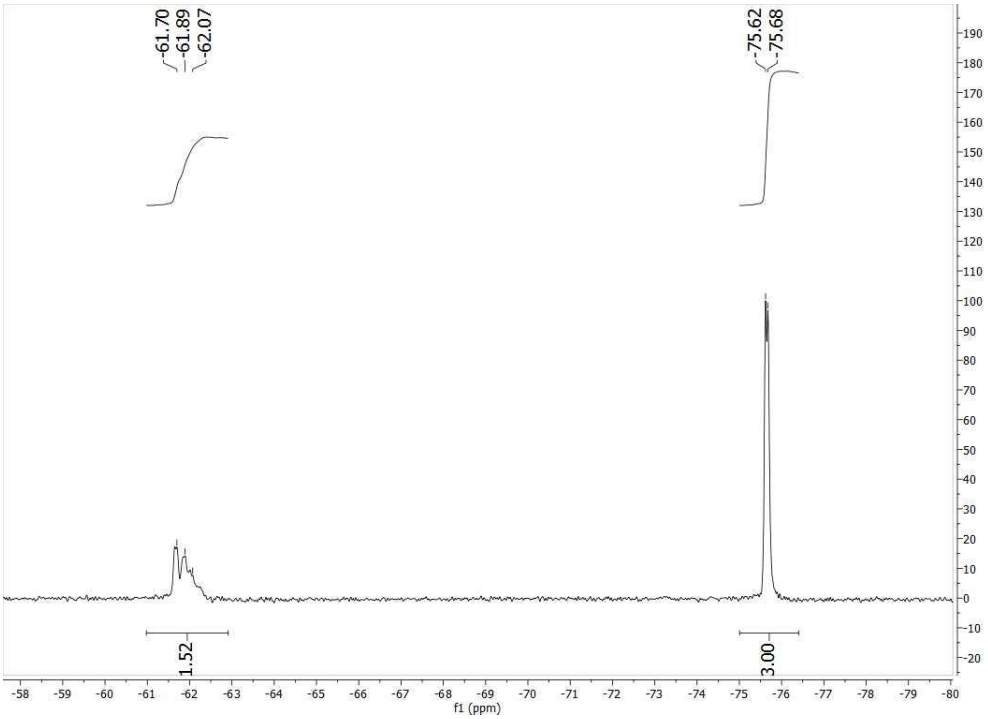

Figure 289: Variance evaluation at an online ^{19}F-NMR spectrum (56.98 MHz, PEEK flow cell) with MestReNova 12 (manual peak integration); Continuous (long-term) synthesis of **26m**; time stamp: 16:15.

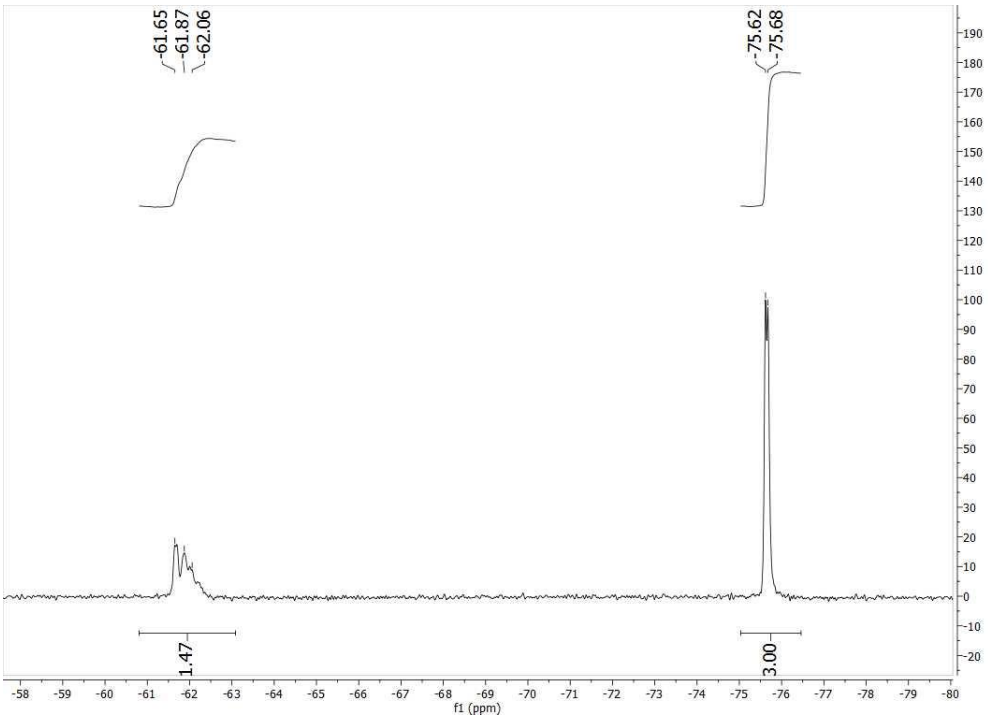

Figure 290: Variance evaluation at an online ^{19}F-NMR spectrum (56.98 MHz, PEEK flow cell) with MestReNova 12 (manual peak integration); Continuous (long-term) synthesis of **26m**; time stamp: 17:28.

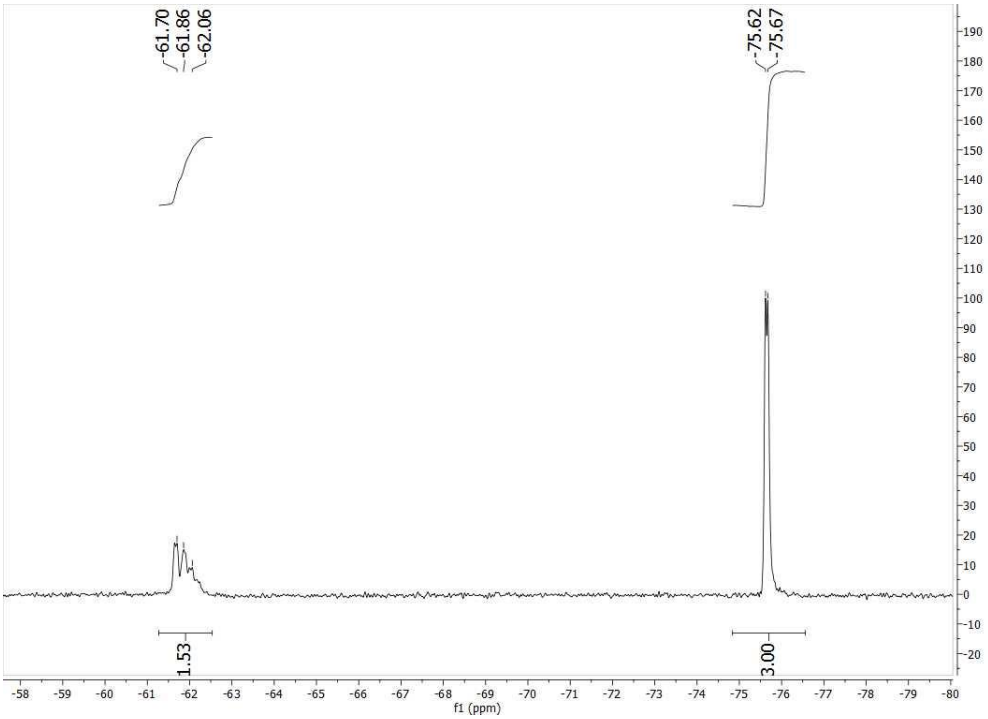

Figure 291: Variance evaluation at an online ^{19}F-NMR spectrum (56.98 MHz, PEEK flow cell) with MestReNova 12 (manual peak integration); Continuous (long-term) synthesis of **26m**; time stamp: 18:14.

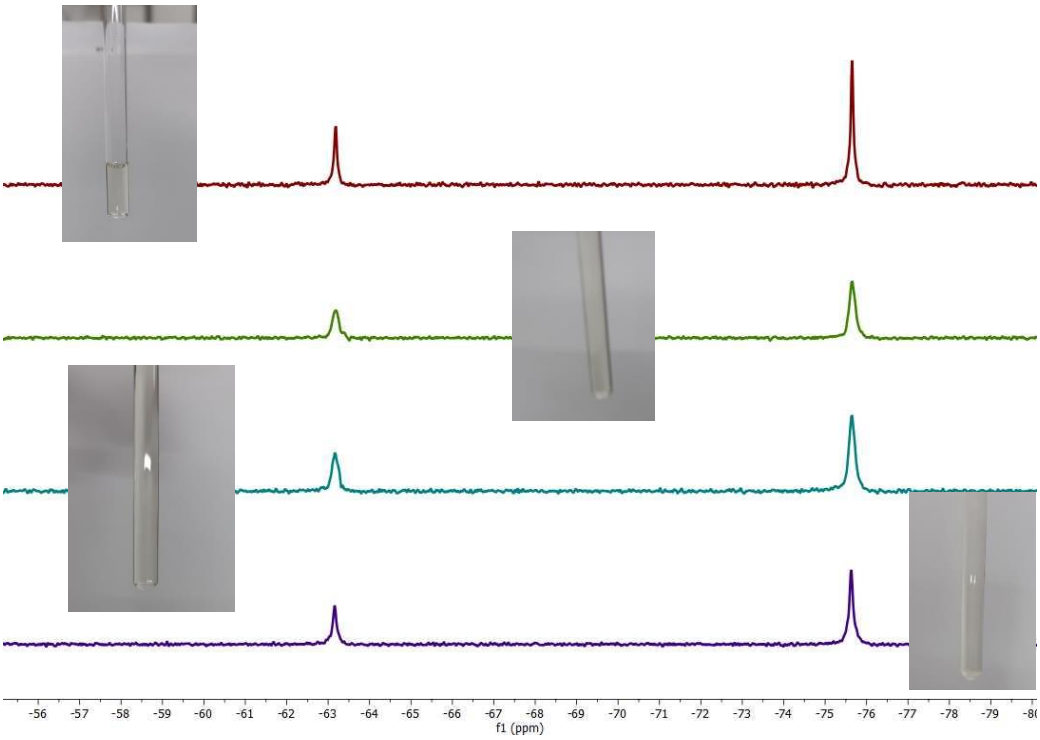

Figure 292: Monitoring stability of 0.1 M 3-CF_3-phenyldiazonium trifluoroacetate in MeCN with ^{19}F-NMR spectroscopy (56.98 MHz) at 0-5 °C and protected from light in reference to TFA δ_F= -75.65 ppm; Integrals left and right: — 1.46 and 3 of a freshly prepared solution, — 1.49 and 3 after 8 min, — 1.49 and 3 after 20 min, — 1.52 and 3 after 60 min.

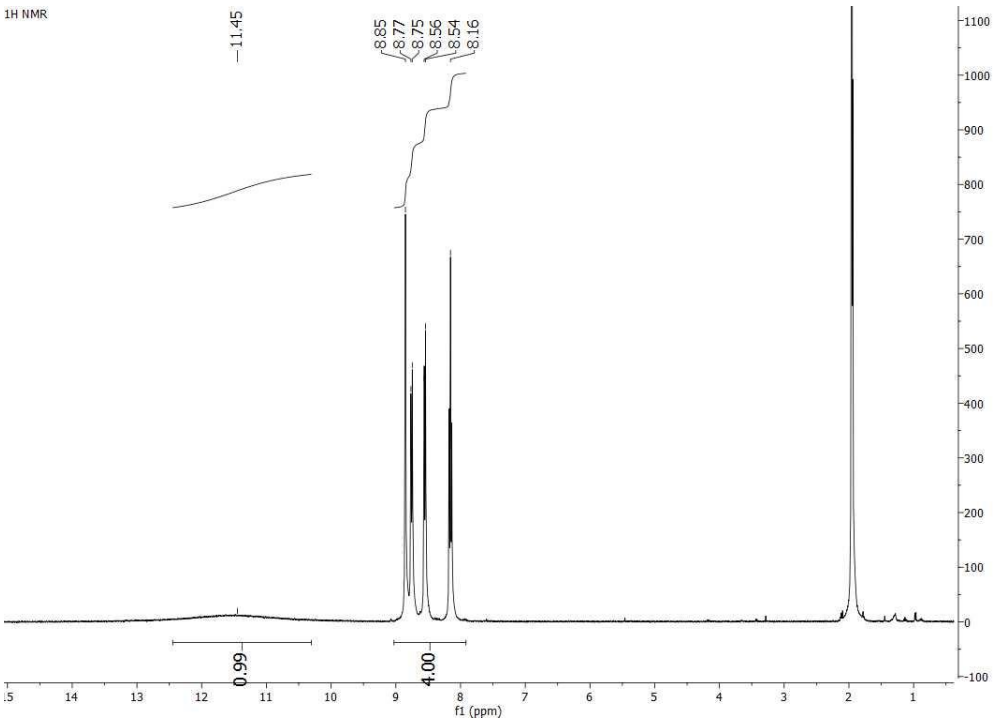

Figure 293: High-resolution ^{1}H-NMR of 3-CF_3-phenyldiazonium trifluoroacetate in MeCN-d_3.

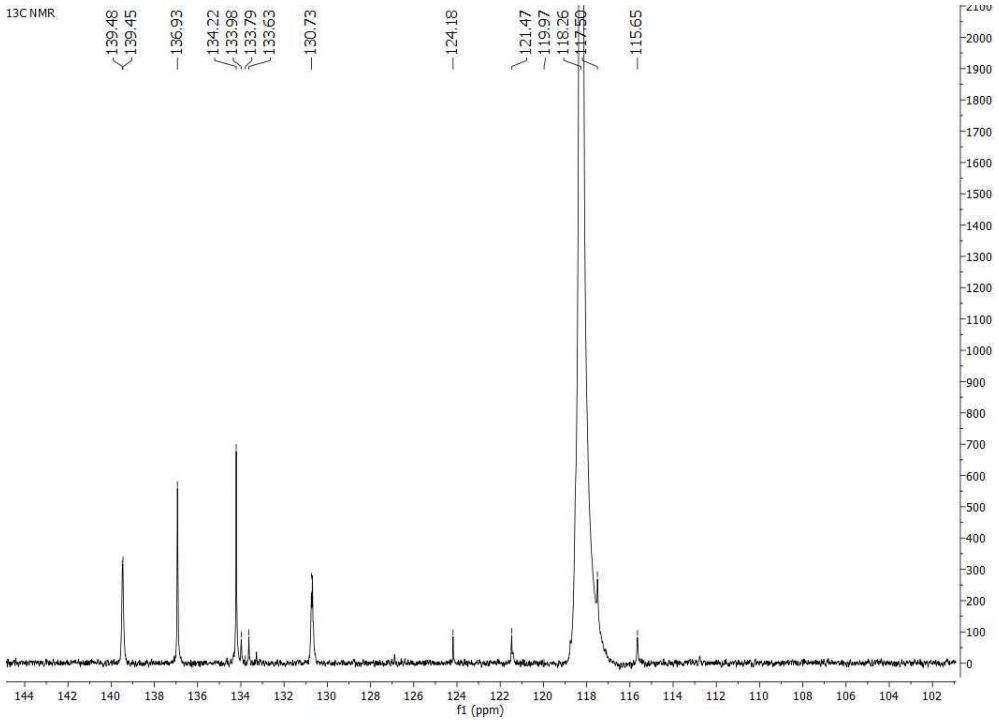

Figure 294: High-resolution ^{13}C-NMR of 3-CF_3-phenyldiazonium trifluoroacetate in MeCN-d_3.

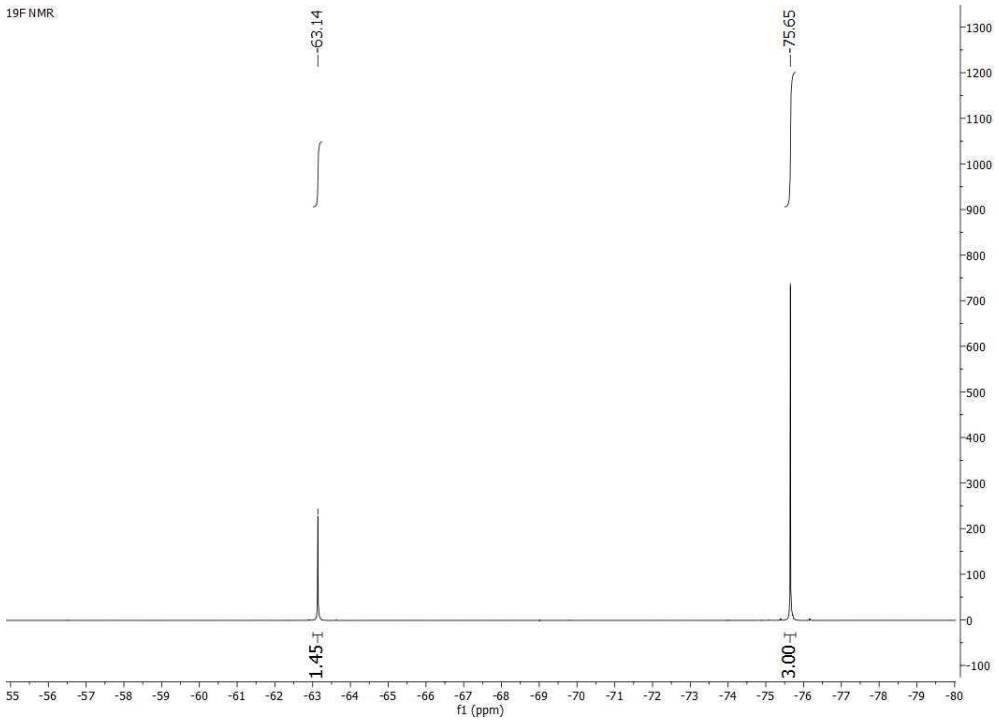

Figure 295: High-resolution ^{19}F-NMR of 3-CF_3-phenyldiazonium trifluoroacetate in MeCN-d_3.

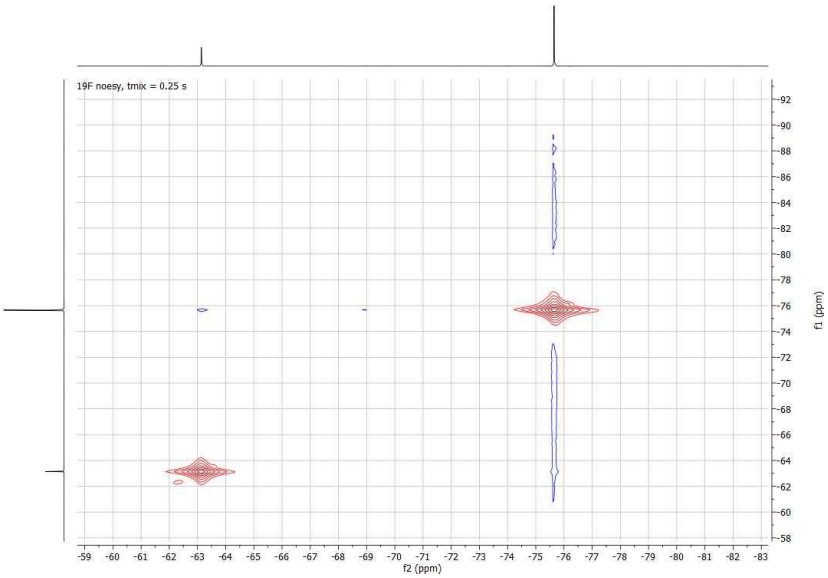

Figure 296: High-resolution ^{19}F-NOESY-NMR of 3-CF_3-phenyldiazonium trifluoroacetate in MeCN-d_3.

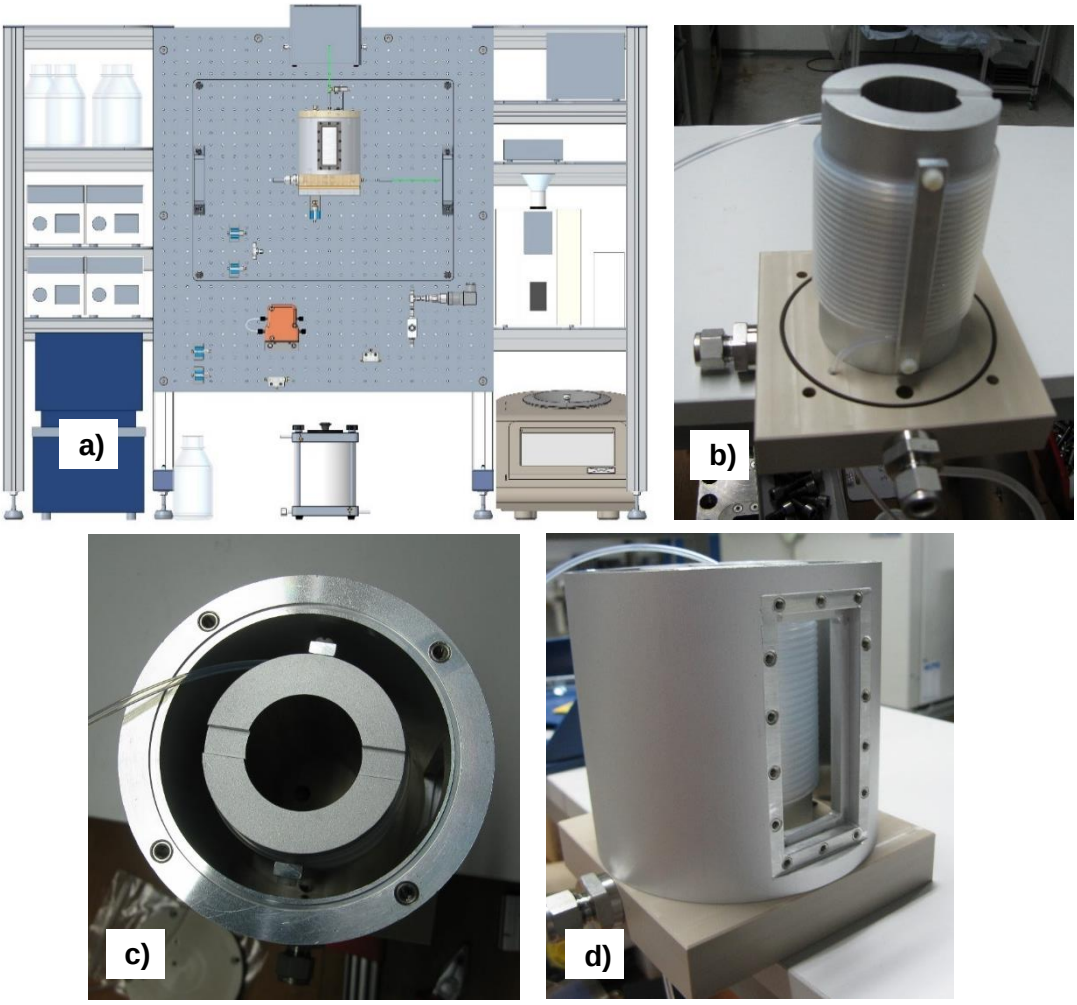

Figure 297: a) CAD of laboratory setup to fit all devices in one fume hood; b) Inside of the thermal reactor (here: 10 mL 1/8" FEP capillary); c) Top view and d) side view during assembly (© Fraunhofer IMM).

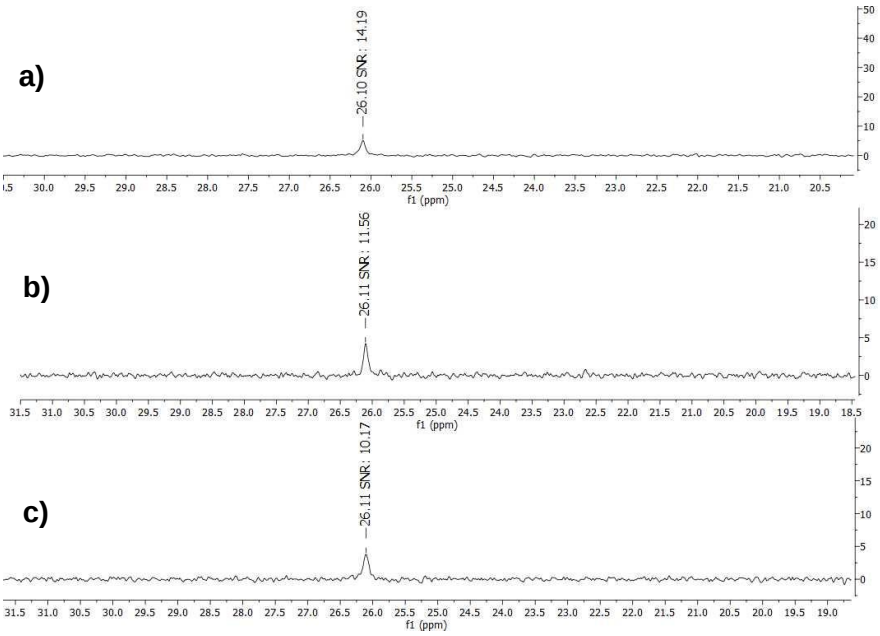

Figure 298: SNR values of 0.1 M BTTP in toluene; ^{31}P NMR-spectra (24.5 MHz, PEEK flow cell) recorded at different flowrates: **a)** stopped flow, **b)** 1.0 mL×min^{-1}, **c)** 1.5 mL ×min^{-1}.

Model Properties: NMRplusX PEAXCT > Integration Model > cis-stilbene

Peak	Lower Limit	Upper Limit	Baseline	BL Region 1 ...	BL Region 1 ...	BL Region 2 ...	BL Region 2 ...	Area
Peak 1	6.44167	6.65567	Linear Fit	N/A	N/A	N/A	N/A	73.7201

Model Properties: NMRplusX PEAXCT > Integration Model > benzaldehyde

Peak	Lower Limit	Upper Limit	Baseline	BL Region 1 ...	BL Region 1 ...	BL Region 2 ...	BL Region 2 ...	Area
Peak 1	9.61919	9.80987	Linear Fit	N/A	N/A	N/A	N/A	41.5473

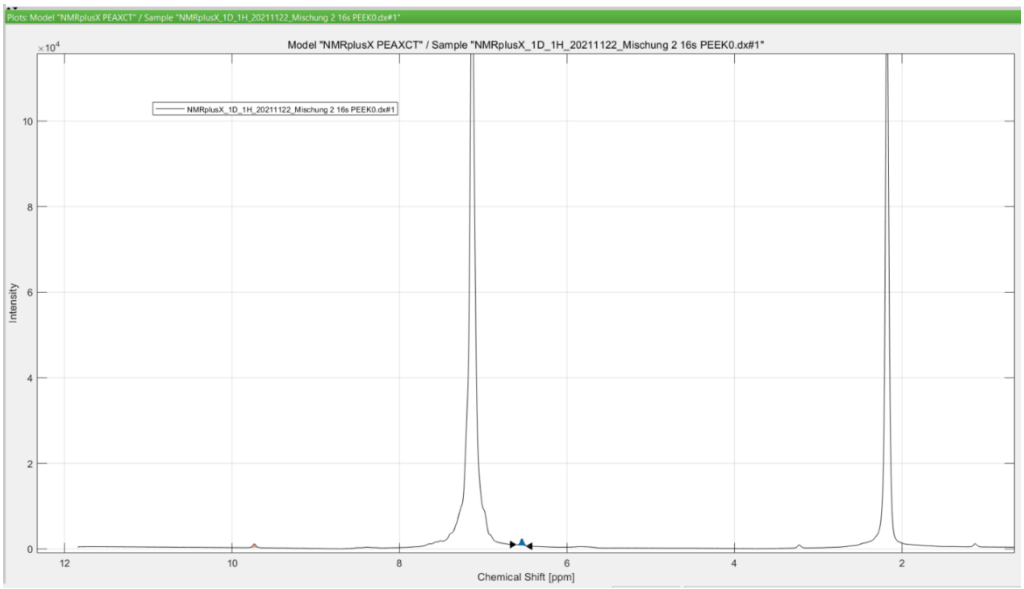

Figure 299: Integration method (PEAXACT 5.3) used for online ^{1}H-NMR spectra evaluation.

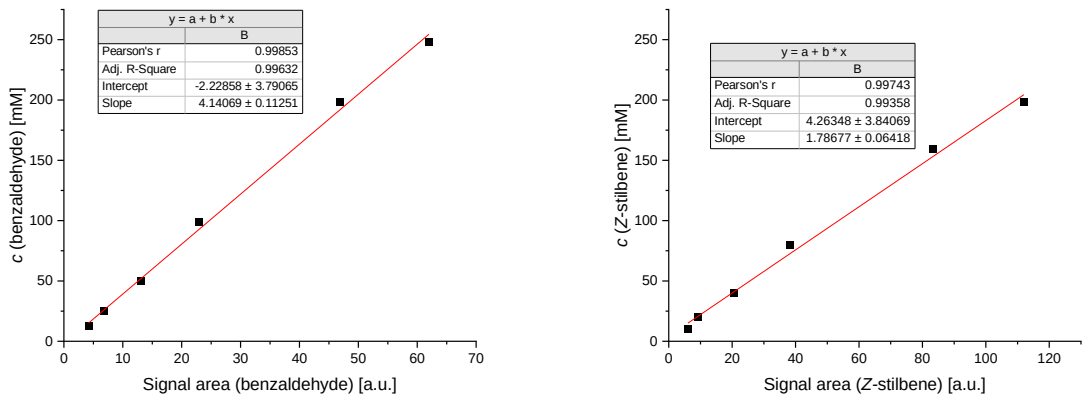

Figure 300: Fit parameters for an external calibration curve of **a)** benzaldehyde and **b)** *Z*-stilbene; acquired in a benchtop ^{1}H-NMR spectrometer (60 MHz, PEEK flow cell) with data evaluation via an integration method (PEAXCT 5.3).

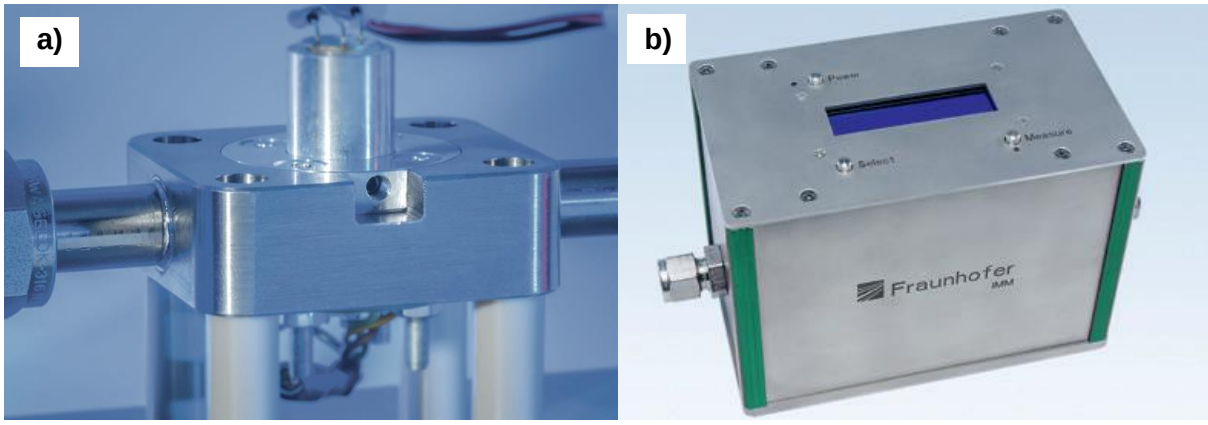

Figure 301: a) IR-sensor cell for online monitoring of *E*- and *Z*-stilbene; **b)** the IR-sensor can be operated as stand-alone device (©Fraunhofer IMM, similar to illustration).

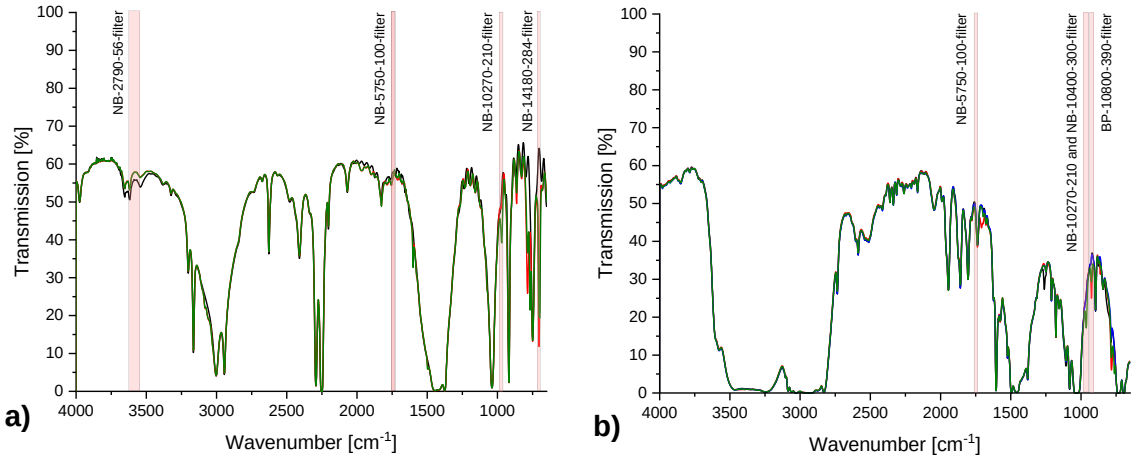

Figure 302: Transmission FTIR-spectra recorded with a ZnSe-flow cell (identical to IR-sensor) and chosen band pass filter for quantification of *E*-*Z*-photoisomerization in **a)** acetonitrile and **b)** toluene/methanol V/V=8/2; — solvent; — 100 mM *E*-stilbene + 118 mM *Z*-stilbene; — 203 mM *Z*-stilbene; — 10.6 mM *E*-stilbene in toluene/methanol.

6 Literature

[1] M. Panizza in *Electrochemical Water and Wastewater Treatment* (Eds.: C. A. Martínez-Huitle, M. A. Rodrigo, O. Scialdone), Elsevier, Oxford, **2018**, pp. 335–364.

[2] MDMadmin - News, "What are fine chemicals?", can be found under https://www.syntor.co.uk/syntor-fine-chemicals-fine-chemicals, **2019**.

[3] P. Pollak (Ed.) *Fine chemicals*. *The industry and the business*, J. Wiley & Sons, Hoboken, **2011**.

[4] IMARC Group, "Top Companies in the Global Active Pharmaceutical Ingredients Market", can be found under https://www.imarcgroup.com/top-players-global-active-pharmaceutical-ingredients-market, **2019**.

[5] Pro Generika e.V., *Where do our active pharmaceutical ingredients come from? - A world map of API production*, **2020**.

[6] B. P. Mason, K. E. Price, J. L. Steinbacher, A. R. Bogdan, D. T. McQuade, *Chem. Rev.* **2007**, *107*, 2300.

[7] R. L. Hartman, J. P. McMullen, K. F. Jensen, *Angew. Chem. Int. Ed.* **2011**, *50*, 7502.

[8] a) F. Darvas, V. Hessel, G. Dorman, *Flow Chemistry*. *Volume 1: Fundamentals*, De Gruyter, Berlin, **2014**; b) F. Darvas, V. Hessel, G. Dorman, *Flow Chemistry*. *Volume 2: Applications*, De Gruyter, Berlin, **2014**.

[9] M. B. Plutschack, B. Pieber, K. Gilmore, P. H. Seeberger, *Chem. Rev.* **2017**, *117*, 11796.

[10] N. Kockmann, M. Gottsponer, D. M. Roberge, *Chem. Eng. J.* **2011**, *167*, 718.

[11] a) M. Gomberg, W. E. Bachmann, *J. Am. Chem. Soc.* **1924**, *46*, 2339; b) C. Xie, Y. Yuan, B. Wang, L. Du, *Thermochim. Acta* **2022**, *709*, 179156.

[12] C. Schotten, A. H. Aldmairi, Y. Sagatov, M. Shepherd, D. L. Browne, *J. Flow Chem.* **2016**, *6*, 218.

[13] C. Schotten, S. K. Leprevost, L. M. Yong, C. E. Hughes, K. D. M. Harris, D. L. Browne, *Org. Process Res. Dev.* **2020**, *24*, 2336.

[14] D. C.-H. Lin, J. Zhang, R. Zhuang, F. Li, K. Nguyen, M. Chen, T. Tran, E. Lopez, J. Y. L. Lu, X. N. Li et al., *PloS one* **2011**, *6*, e27270.

[15] a) J. B. Houze, L. Zhu, Y. Sun, M. Akerman, W. Qiu, A. J. Zhang, R. Sharma, M. Schmitt, Y. Wang, J. Liu et al., *Bioorg. Med. Chem. Lett.* **2012**, *22*, 1267; b) Y. Fukui, T. Uruno, M. Kanai, K. Oisaki, R. Tsutsumi, EP3888651 (A1), **2019**.

[16] S. D. Walker, C. J. Borths, E. DiVirgilio, L. Huang, P. Liu, H. Morrison, K. Sugi, M. Tanaka, J. C. S. Woo, M. M. Faul, *Org. Process Res. Dev.* **2011**, *15*, 570.

[17] a) M. Inoue, Y. Sumii, N. Shibata, *ACS omega* **2020**, *5*, 10633; b) E. P. Gillis, K. J. Eastman, M. D. Hill, D. J. Donnelly, N. A. Meanwell, *J. Med. Chem.* **2015**, *58*, 8315.

[18] R. A. Tromp, S. van Ameijde, C. Pütz, C. Sundermann, B. Sundermann, J. K. von Frijtag Drabbe Künzel, A. P. IJzerman, *J. Med. Chem.* **2004**, *47*, 5441.

[19] E. Giacomini, S. Rupiani, L. Guidotti, M. Recanatini, M. Roberti, *Curr. Med. Chem.* **2016**, *23*, 2439.

[20] M. Cushman, D. Nagarathnam, D. Gopal, A. K. Chakraborti, C. M. Lin, E. Hamel, *J. Med. Chem.* **1991**, *34*, 2579.

[21] T. Neveselý, M. Wienhold, J. J. Molloy, R. Gilmour, *Chem. Rev.* **2022**, *122*, 2650.

[22] a) S. Kern, L. Wander, K. Meyer, S. Guhl, A. R. G. Mukkula, M. Holtkamp, M. Salge, C. Fleischer, N. Weber, R. King et al., *Anal. Bioanal. Chem.* **2019**, *411*, 3037; b) R. Galaverna, R. L. Ribessi, J. J. R. Rohwedder, J. C. Pastre, *Org. Process Res. Dev.* **2018**, *22*, 780; c) D. E. Fitzpatrick, C. Battilocchio, S. V. Ley, *ACS central science* **2016**, *2*, 131; d) K. Grabow, U. Bentrup, *ACS Catal.* **2014**, *4*, 2153; e) P. M. Tolstoy, B. Koeppe, G. S. Denisov, H.-H. Limbach, *Angew. Chem. Int. Ed.* **2009**, *48*, 5745; f) D. E. Fitzpatrick, C. Battilocchio, S. V. Ley, *Org. Process Res. Dev.* **2016**, *20*, 386; g) B. Musio, E. Gala, S. V. Ley, *ACS Sustainable Chem. Eng.* **2018**, *6*, 1489; h) D. C. Fabry, E. Sugiono, M. Rueping, *Isr. J. Chem.* **2014**, *54*, 341; i) R. J. Ingham, C. Battilocchio, D. E. Fitzpatrick, E. Sliwinski, J. M. Hawkins, S. V. Ley, *Angew. Chem. Int. Ed.* **2015**, *54*, 144; j) S. V. Ley, D. E. Fitzpatrick, R. J. Ingham, R. M. Myers, *Angew. Chem. Int. Ed.* **2015**, *54*, 3449.

[23] T. Maschmeyer, P. L. Prieto, S. Grunert, J. E. Hein, *Magn. Reson. Chem.* **2020**, *58*, 1234.

[24] C. W. Coley, R. Barzilay, T. S. Jaakkola, W. H. Green, K. F. Jensen, *ACS Cent. Sci.* **2017**, *3*, 434.

[25] C. W. Coley, W. H. Green, K. F. Jensen, *Acc. Chem. Res.* **2018**, *51*, 1281.

[26] a) D. Zhang, X. Gao, T. Cheng, G. Liu, *Sci. Rep.* **2014**, *4*, 5091; b) J.-P. Corbet, G. Mignani, *Chem. Rev.* **2006**, *106*, 2651; c) G. Ren, X. Cui, Y. Wu, *Eur. J. Org. Chem.* **2010**, *2010*, 2372.

[27] S.-P. Jiang, X.-Y. Dong, Q.-S. Gu, L. Ye, Z.-L. Li, X.-Y. Liu, *J. Am. Chem. Soc.* **2020**, *142*, 19652.

[28] D. Cantillo, C. Mateos, J. A. Rincon, O. de Frutos, C. O. Kappe, *Chem. Eur. J.* **2015**, *21*, 12894.

[29] M. C. D. Fürst, E. Gans, M. J. Böck, M. R. Heinrich, *Chem. Eur. J.* **2017**, *23*, 15312.

[30] A. d. A. Bartolomeu, R. C. Silva, T. J. Brocksom, T. Noël, K. T. de Oliveira, *J. Org. Chem.* **2019**, *84*, 10459.

[31] D. C. Fabry, Y. A. Ho, R. Zapf, W. Tremel, M. Panthöfer, M. Rueping, T. H. Rehm, *Green Chem.* **2017**, *19*, 1911.

[32] K. Okuma, O. Sakai, K. Shioji, *ChemInform* **2003**, *34*, 1675.

[33] K. Jähnisch, V. Hessel, H. Löwe, M. Baerns, *Angew. Chem. Int. Ed.* **2004**, *43*, 406.

[34] Y. Su, N. J. W. Straathof, V. Hessel, T. Noël, *Chem. Eur. J.* **2014**, *20*, 10562.

[35] S. Taghavi-Moghadam, A. Kleemann, G. Golbig, *Org. Process Res. Dev.* **2001**, *5*, 652.

[36] a) J.-i. Yoshida, *Flash Chemistry*, J. Wiley & Sons, Chichester, **2008**; b) L. T. Scott, Sumpter Chris A., *Org. Synth.* **1990**, *69*, 180.

[37] D. Karl, *PhD thesis*, Johannes Gutenberg-Universität Mainz, Mainz, **2017**.

[38] E. Shahbazali, *PhD thesis*, Eindhoven University of Technology, Eindhoven, **2018**.

[39] H. P. L. Gemoets, Y. Su, M. Shang, V. Hessel, R. Luque, T. Noël, *Chem. Soc. Rev.* **2016**, *45*, 83.

[40] P. R. Ogilby, *Chem. Soc. Rev.* **2010**, *39*, 3181.

[41] V. Misuk, *PhD thesis*, Johannes Gutenberg-Universität Mainz, Mainz, **2014**.

[42] H. Song, J. D. Tice, R. F. Ismagilov, *Angew. Chem. Int. Ed.* **2003**, *42*, 768.

[43] B. Pieber, M. Shalom, M. Antonietti, P. H. Seeberger, K. Gilmore, *Angew. Chem. Int. Ed.* **2018**, *57*, 9976.

[44] T. H. Rehm, *ChemPhotoChem* **2020**, *4*, 235.

[45] K. S. Elvira, X. C. i Solvas, R. C. R. Wootton, A. J. deMello, *Nat. Chem.* **2013**, *5*, 905.

[46] S.-i. In, M. G. Nielsen, P. C. K. Vesborg, Y. Hou, B. L. Abrams, T. R. Henriksen, O. Hansen, I. Chorkendorff, *Chem. Commun.* **2011**, *47*, 2613.

[47] D. Cambié, C. Bottecchia, N. J. W. Straathof, V. Hessel, T. Noël, *Chem. Rev.* **2016**, *116*, 10276.

[48] K. Wu, S. Kuhn, *Chim. Oggi* **2014**, *32*, 62.

[49] G. J. Verhoeven, *AARGnews* **2017**, *55*, 13.

[50] a) M. Planck, *Ann. Phys.* **1900**, *306*, 69; b) A. Einstein, *Ann. Phys.* **1905**, *322*, 132.

[51] M. Sender, D. Ziegenbalg, *Chem. Ing. Tech.* **2017**, *89*, 1159.

[52] G. O. Schenck, *Präparative Organische Photochemie*, Springer Berlin / Heidelberg, Berlin, Heidelberg, **1958**.

[53] a) S. Sajedi, H. Sabet, H. S. Choi, *Nanophotonics* **2019**, *8*, 99; b) A. Jablonski, *Nature* **1933**, *131*, 839.

[54] M. Klessinger, J. Michl, *Excited states and photochemistry of organic molecules*, VCH, New York, **1995**.

[55] E. A. Owens, M. Henary, G. El Fakhri, H. S. Choi, *Acc. Chem. Res.* **2016**, *49*, 1731.

[56] M. Hesse, H. Meier, B. Zeeh, *Spektroskopische Methoden in der organischen Chemie*, Thieme, Stuttgart, **1979**.

[57] C. van Wolfen, *PhD thesis*, Duisburg, **2002**.

[58] R. Graßl, C. Jandl, T. Bach, *J. Org. Chem.* **2020**, *85*, 11426.

[59] G. Book, J. Eggert, *Ber. dtsch. Chem. Ges. A/B* **1926**, *59*, 1192.

[60] A. Steiner, P. M. C. Roth, F. J. Strauss, G. Gauron, G. Tekautz, M. Winter, J. D. Williams, C. O. Kappe, *Org. Process Res. Dev.* **2020**, *24*, 2208.

[61] T. P. Yoon, M. A. Ischay, J. Du, *Nat. Chem.* **2010**, *2*, 527.

[62] C. K. Prier, D. A. Rankic, D. W. C. MacMillan, *Chem. Rev.* **2013**, *113*, 5322.

[63] Q.-Q. Zhou, Y.-Q. Zou, L.-Q. Lu, W.-J. Xiao, *Angew. Chem. Int. Ed.* **2019**, *58*, 1586.

[64] M. H. Shaw, J. Twilton, D. W. C. MacMillan, *J. Org. Chem.* **2016**, *81*, 6898.

[65] N. A. Romero, D. A. Nicewicz, *Chem. Rev.* **2016**, *116*, 10075.

[66] H. Kisch, *Angew. Chem. Int. Ed.* **2013**, *52*, 812.

[67] J. Zoller, D. C. Fabry, M. Rueping, *ACS Catal.* **2015**, *5*, 3900.

[68] M. Janczarek, E. Kowalska, *Catalysts* **2017**, *7*, 317.

[69] A. E. Cassano, C. A. Martin, R. J. Brandi, O. M. Alfano, *Ind. Eng. Chem. Res.* **1995**, *34*, 2155.

[70] N. Serpone, A. Salinaro, *Pure & Appl. Chem.* **1999**, *71*, 303.

[71] P. W. Atkins, J. de Paula, M. Bär, *Physikalische Chemie*, Wiley-VCH, Weinheim, **2013**.

[72] T. G. Mayerhöfer, H. Mutschke, J. Popp, *ChemPhysChem* **2016**, *17*, 1948.

[73] a) E. Shahbazali, T. Noël, V. Hessel, *J. Flow Chem.* **2016**, *6*, 252; b) M. Escribà-Gelonch, E. Shahbazali, M. Honing, V. Hessel, *Tetrahedron* **2018**, *74*, 3143; c) K. G. Maskill, J. P. Knowles, L. D. Elliott, R. W. Alder, K. I. Booker-Milburn, *Angew. Chem.* **2013**, *125*, 1539; d) A. Sugimoto, T. Fukuyama, Y. Sumino, M. Takagi, I. Ryu, *Tetrahedron* **2009**, *65*, 1593.

[74] a) J.-B. Xia, C. Zhu, C. Chen, *Chem. Commun.* **2014**, *50*, 11701; b) D. Cantillo, O. de Frutos, J. A. Rincon, C. Mateos, C. O. Kappe, *J. Org. Chem.* **2014**, *79*, 223.

[75] C. P. Haas, T. Roider, R. W. Hoffmann, U. Tallarek, *React. Chem. Eng.* **2019**, *4*, 1912.

[76] Nichia Corporation, "Product search. NCSU434A", can be found under https://led-ld.nichia.co.jp/en/product/led_search.html, **2022**.

[77] Peschl Ultraviolet GmbH, *Webinar - Successful Development of Photon Initiated Processes*, **2022**.

[78] Hellma GmbH & Co. KG, "Glasmaterialien-Materialcode", can be found under https://www.hellma.com/laborbedarf/kuevetten/materialien-und-technische-informationen/, **2022**.

[79] Röhm GmbH, "PLEXIGLAS GS, UV transmitting", can be found under https://www.plexiglas.de/files/plexiglas-content/pdf/technische-informationen/222-6-PLEXIGLAS-GS-UV-transmitting_Clear_2458_and_SC_EN.pdf, **2022**.

[80] A.M.S. Galante, O. L. Galante, L. L. Campos, *Nuclear Instruments and Methods in Physics Research Section A: Accelerators, Spectrometers, Detectors and Associated Equipment* **2010**, *619*, 177.

[81] T. Horie, M. Sumino, T. Tanaka, Y. Matsushita, T. Ichimura, J.-i. Yoshida, *Org. Process Res. Dev.* **2010**, *14*, 405.

[82] L. D. Elliott, M. Berry, B. Harji, D. Klauber, J. Leonard, K. I. Booker-Milburn, *Org. Process Res. Dev.* **2016**, *20*, 1806.

[83] Boldender GmbH, "Schläuche - Bola", can be found under https://www.bola.de/produkte/schlaeuche-folien-platten/schlaeuche/579/schlaeuche-bola, **2022**.

[84] a) M. Renner, A. Griesbeck, *J. Chem. Educ.* **2020**, *97*, 3683; b) E. J. Rastelli, D. Yue, C. Millard, P. Wipf, *Tetrahedron* **2021**, *79*, 131875; c) A. J. Capel, S. Edmondson, S. D. R. Christie, R. D. Goodridge, R. J. Bibb, M. Thurstans, *Lab Chip* **2013**, *13*, 4583; d) T. Noël, *J. Flow Chem.* **2020**, *10*, 585.

[85] P. Löb, H. Löwe, V. Hessel, *J. Fluorine Chem.* **2004**, *125*, 1677.

[86] IMM Institut für Mikrotechnik GmbH, *The Catalogue*. *chemical micro process technology made by imm*, **2009**.

[87] V. Hessel, S. Hardt, H. Löwe, *Chemical Micro Process Engineering*. *Fundamentals, Modelling and Reactions*, Wiley-VCH, Weinheim, **2006**.

[88] H. Ehrich, D. Linke, K. Morgenschweis, M. Baerns, K. Jähnisch, *Chimia* **2002**, *56*, 647.

[89] K. Jähnisch, U. Dingerdissen, *Chem. Eng. Technol.* **2005**, *28*, 426.

[90] O. Shvydkiv, C. Limburg, K. Nolan, M. Oelgemöller, *J. Flow Chem.* **2012**, *2*, 52.

[91] R. Zapf, G. Kolb, H. Pennemann, V. Hessel, *Chem. Eng. Technol.* **2006**, *29*, 1509.

[92] T. H. Rehm, C. Berguerand, S. Ek, R. Zapf, P. Löb, L. Nikoshvili, L. Kiwi-Minsker, *Chem. Eng. J.* **2016**, *293*, 345.

[93] a) N. Steinfeldt, R. Abdallah, U. Dingerdissen, K. Jähnisch, *Org. Process Res. Dev.* **2007**, *11*, 1025; b) M.H.H. van Dam, J.-P. Corriou, N. Midoux, A.-S. Lamine, C. Roizard, *Chem. Eng. Sci.* **1999**, *54*, 5311.

[94] a) B. D. A. Hook, W. Dohle, P. R. Hirst, M. Pickworth, M. B. Berry, K. I. Booker-Milburn, *J. Org. Chem.* **2005**, *70*, 7558; b) O. Shvydkiv, A. Yavorskyy, S. B. Tan, K. Nolan, N. Hoffmann, A. Youssef, M. Oelgemöller, *Photochem. Photobiol. Sci.* **2011**, *10*, 1399.

[95] S. Durieux, *Master thesis*, Ecole Polytechnique Federale De Lausanne, Lausanne, **2017**.

[96] Präzisions Glas & Optik GmbH, "BOROFLOAT® 33", can be found under https://www.pgo-online.com/de/borofloat.html, **2022**.

[97] D. Bertagna Silva, G. Buttiglieri, S. Babić, *Environ. Sci. Pollut. Res.* **2021**, *28*, 103.

[98] T. H. Rehm, C. Hofmann, D. Reinhard, H.-J. Kost, P. Löb, M. Besold, K. Welzel, J. Barten, A. Didenko, D. V. Sevenard et al., *React. Chem. Eng.* **2017**, *2*, 315.

[99] J. Haupt, *Master thesis*, Johannes Gutenberg-Universität Mainz, Mainz, **2016**.

[100] M. A. Morin, W. P. Zhang, D. Mallik, M. G. Organ, *Angew. Chem. Int. Ed.* **2021**, *60*, 20606.

[101] P. W. Fedick, R. L. Schrader, S. T. Ayrton, C. J. Pulliam, R. G. Cooks, *J. Chem. Educ.* **2019**, *96*, 124.

[102] U. Holzgrabe, *Prog. Nucl. Magn. Reson. Spectrosc.* **2010**, *57*, 229.

[103] D'Ans, Lax in *Taschenbuch für Chemiker und Physiker*. *Band 3: Elemente, anorganische Verbindungen und Materialien, Minerale* (Ed.: R. Blachnik), Springer Berlin / Heidelberg, Berlin, Heidelberg, **1998**, pp. 10–1010.

[104] R. Deubner, *Dissertation*, Bayerische Julius-Maximilians-Universität Würzburg, Würzburg, **2004**.

[105] Q Magnetics, "QM-125", can be found under www.qmagnetics.com, **2022**.

[106] T. Maschmeyer, L. P. E. Yunker, J. E. Hein, *React. Chem. Eng.* **2022**, *7*, 1061.

[107] Bruker, "Fourier 80", can be found under www.bruker.com/en/products-and-solutions/mr/nmr/fourier80.html, **2022**.

[108] Bruker, "InsightMR", can be found under www.bruker.com/en/products-and-solutions/mr/nmr-pharma-solutions/InsightMR.html, **2022**.

[109] Magritek, "Spinsolve-60", can be found under www.magritek.com/products/benchtop-nmr-spectrometer-spinsolve/spinsolve-60, **2022**.

[110] Magritek, "Spinsolve 80", can be found under www.magritek.com/products/benchtop-nmr-spectrometer-spinsolve/spinsolve-80/, **2022**.

[111] Magritek, "Spinsolve 90", can be found under www.magritek.com/products/benchtop-nmr-spectrometer-spinsolve/spinsolve-90-mhz/, **2022**.

[112] Nanalysis, "NMReady-60e", can be found under www.nanalysis.com/nmready-60e, **2022**.

[113] Nanalysis, "NMReady-600PRO", can be found under www.nanalysis.com/nmready-60pro, **2022**.

[114] Nanalysis, "100PRO", can be found under https://static1.squarespace.com/static/5707ede0d210b8708e037a1e/t/5d8395ed959dbe10bfc1cd47/1568904688390/NANA_100PRO_Brochure-Q-Web-R1-sm.pdf, **2022**.

[115] Oxford Instruments, "X-Pulse", can be found under www.nmr.oxinst.com/x-pulse, **2022**.

[116] Thermo Scientific, "picoSpin Series II", can be found under https://assets.thermofisher.com/TFS-Assets/CAD/Specification-Sheets/NMR-SII-SpecSheet-416.pdf, **2022**.

[117] F. Dalitz, M. Cudaj, M. Maiwald, G. Guthausen, *Prog. Nucl. Magn. Reson. Spectrosc.* **2012**, *60*, 52.

[118] K. Meyer, S. Kern, N. Zientek, G. Guthausen, M. Maiwald, *TrAC, Trends Anal. Chem.* **2016**, *83*, 39.

[119] S. Wold, M. Sjöström, L. Eriksson, *Chemom. Intell. Lab. Syst.* **2001**, *58*, 109.

[120] S. Kern, K. Meyer, S. Guhl, P. Gräßer, A. Paul, R. King, M. Maiwald, *Anal. Bioanal. Chem.* **2018**, *410*, 3349.

[121] B. Gouilleux, B. Charrier, S. Akoka, P. Giraudeau, *Magn. Reson. Chem.* **2017**, *55*, 91.

[122] a) Y. Y. Pan, J. Huang, Z. M. Wang, D. W. Yu, B. Yang, Y. G. Ma, *RSC Adv.* **2017**, *7*, 26697; b) G. Koleva, B. Galabov, J. I. Wu, H. F. Schaefer, P. v. R. Schleyer, *J. Am. Chem. Soc.* **2009**, *131*, 14722.

[123] H. Zollinger, *Acc. Chem. Res.* **1973**, *6*, 335.

[124] A. Khazaei, M. Kazem-Rostami, A. Zare, A. R. Moosavi-Zare, M. Sadeghpour, A. Afkhami, *J. Appl. Polym. Sci.* **2013**, *129*, 3439.

[125] T. Sandmeyer, *Ber. Dtsch. Chem. Ges.* **1884**, *17*, 1633.

[126] G. Balz, G. Schiemann, *Ber. dtsch. Chem. Ges. A/B* **1927**, *60*, 1186.

[127] R. Brückner, *Reaktionsmechanismen*. *Organische Reaktionen, Stereochemie, moderne Synthesemethoden*, Spektrum Akad. Verl., Heidelberg, **2011**.

[128] I. Ghosh, L. Marzo, A. Das, R. Shaikh, B. König, *Acc. Chem. Res.* **2016**, *49*, 1566.

[129] C. Wittwer, H. Zollinger, *HCA* **1954**, *37*, 1954.

[130] H. G. O. Becker, W. Berger, *Organikum*. *Organisch-chemisches Grundpraktikum*, Wiley-VCH, Weinheim, **2015**.

[131] P. Müller, H. Müller-Dolezal, H.-G. Padeken, R. Stoltz, H. Söll, *Houben-Weyl Methods of Organic Chemistry Vol. X/3, 4th Edition*. *Diazonium Salts; Azo-, Azoxy-Compounds II; Diazenes II; Azides; Nitrile Oxides*, Thieme, Stuttgart, **2014**.

[132] T. Kauffmann, H. O. Friestad, H. Henkler, *Justus Liebigs Ann. Chem.* **1960**, *634*, 64.

[133] L. Wolff, R. Krüche, *Eur. J. Org. Chem.* **1912**, *394*, 23.

[134] B. L. Kaul, H. Zollinger, *HCA* **1968**, *51*, 2132.

[135] D. Kosynkin, T. M. Bockman, J. K. Kochi, *J. Am. Chem. Soc.* **1997**, *119*, 4846.

[136] a) H. Wieland, L. Gattermann (Eds.) *Die Praxis des organischen Chemikers*, De Gruyter, Berlin, New York, **1982**; b) M. L. Crossley, R. H. Kienle, C. H. Benbrook, *J. Am. Chem. Soc.* **1940**, *62*, 1400.

[137] T. Hu, I. R. Baxendale, M. Baumann, *Molecules* **2016**, *21*, 918.

[138] D. P. Hari, P. Schroll, B. König, *J. Am. Chem. Soc.* **2012**, *134*, 2958.

[139] P. Schroll, D. P. Hari, B. König, *ChemistryOpen* **2012**, *1*, 130.

[140] a) M. R. Heinrich, *Chem. Eur. J.* **2009**, *15*, 820; b) F. P. Crisóstomo, T. Martín, R. Carrillo, *Angew. Chem. Int. Ed.* **2014**, *53*, 2181.

[141] T. B. Patrick, R. P. Willaredt, D. J. DeGonia, *J. Org. Chem.* **1985**, *50*, 2232.

[142] S. Crespi, S. Protti, M. Fagnoni, *J. Org. Chem.* **2016**, *81*, 9612.

[143] M. Teci, M. Tilley, M. A. McGuire, M. G. Organ, *Chem. Eur. J.* **2016**, *22*, 17407.

[144] D. B. Kimball, M. M. Haley, *Angew. Chem. Int. Ed.* **2002**, *41*, 3338.

[145] D. M. Monzón, T. Santos, F. Pinacho-Crisóstomo, V. S. Martín, R. Carrillo, *Chem. Asian J.* **2018**, *13*, 325.

[146] M. R. Pettit, M. Stacey, J. C. Tatlow, *J. Chem. Soc.* **1953**, 3081.

[147] M. R. Pettit, J. C. Tatlow, *J. Chem. Soc.* **1954**, 1941.

[148] J. C. Yu, W. Ho, J. Yu, S. K. Hark, K. Iu, *Langmuir* **2003**, *19*, 3889.

[149] a) I. A. Mohammed, A. Mustapha, *Molecules* **2010**, *15*, 7498; b) H. Dürr, H. Bouas-Laurent (Eds.) *Photochromism*. *Molecules and systems*, Elsevier, Amsterdam, **2003**; c) M. H. Plumlee, M. Reinhard, *Environ. Sci. Technol.* **2007**, *41*, 6170; d) J. C. Beard, T. M. Swager, *J. Org. Chem.* **2021**, *86*, 2037; e) M. Piskorz, T. Urbanski, *Bulletin de l'Académie polonaise des sciences. Série des sciences chimiques.* **1963**, *11*, 607.

[150] a) J. Xu, L. Li, Y. Yan, H. Wang, X. Wang, X. Fu, G. Li, *J. Colloid Interface Sci.* **2008**, *318*, 29; b) N. Nakayama, T. Hayashi, *Colloids Surf., A* **2008**, *317*, 543; c) M. M. Jalili,

K. Davoudi, E. Zafarmand Sedigh, S. Farrokhpay, *Adv. Powder Technol.* **2016**, *27*, 2168.

[151] J. C. Colmenares, V. Nair, E. Kuna, D. Łomot, *Ultrason. Sonochem.* **2018**, *41*, 297.

[152] F. Scheiff, D. W. Agar in *Biological and medical physics, biomedical engineering* (Eds.: M. Köhler, B. P. Cahill), Springer-Verlag, Berlin, Heidelberg, **2014**, pp. 103–148.

[153] a) A. Ufer, D. Sudhoff, A. Mescher, D. W. Agar, *Chem. Eng. J.* **2011**, *167*, 468; b) K. Olivon, F. Sarrazin, *Chem. Eng. J.* **2013**, *227*, 97.

[154] a) P. Jankowski, D. Ogończyk, W. Lisowski, P. Garstecki, *Lab Chip* **2012**, *12*, 2580; b) C. Deckers, M. Linden, H. Löwe, *Chem. Eng. Technol.* **2019**, *42*, 2044; c) D. Karl, P. Börner, V. Misuk, H. Löwe, *Chem. Eng. Technol.* **2017**, *40*, 1124; d) D. Karl, H. Löwe, *J. Flow Chem.* **2017**, *7*, 9.

[155] a) K. Mayer, B. O. Kolbesen, WO2008003450 (A1), **2007**; b) S. M. Igumnov, V. I. Sokolov, V. K. Men'shikov, O. A. Mel'nik, V. E. Boiko, V. I. Dyachenko, L. N. Nikitin, E. V. Khaidukov, G. Y. Yurkov, V. M. Buznik, *Dokl. Chem.* **2012**, *446*, 183; c) H. J. Behrens, W. Ebert, T. Foellinger, W. Alewelt, H. D. Brandt, DE10054935 (A1), **2000**.

[156] a) P. Riente, T. Noël, *Catal. Sci. Technol.* **2019**, *9*, 5186; b) Z. Wen, T. Wan, A. Vijeta, C. Casadevall, L. Buglioni, E. Reisner, T. Noël, *ChemSusChem* **2021**, *14*, 5265; c) M. Woźnica, N. Chaoui, S. Taabache, S. Blechert, *Chem. Eur. J.* **2014**, *20*, 14624.

[157] W. A. Redmond, *PhD thesis*, University of Windsor, Windsor (ON), **1964**.

[158] J. Clayden, N. Greeves, S. G. Warren, *Organische Chemie*, Springer Spektrum, Berlin, **2017**.

[159] a) R. D. Beaty, W. K. R. Musgrave, *J. Chem. Soc.* **1952**, 875; b) P. H. Cheek, R. H. Wiley, A. Roe, *J. Am. Chem. Soc.* **1949**, *71*, 1863; c) W. Lange, E. Müller, *Ber. dtsch. Chem. Ges. A/B* **1930**, *63*, 1058.

[160] a) H. Hill, University of London, London, **1983**; b) H. Meerwein, P. Laasch, R. Mersch, J. Spille, *Chem. Ber.* **1956**, *89*, 209; c) R. C. Petterson, J. T. Bennett, D. C. Lankin, G. W. Lin, J. P. Mykytka, T. G. Troendle, *J. Org. Chem.* **1974**, *39*, 1841.

[161] E. Müller, H. Haiss, *Chem. Ber.* **1962**, *95*, 1255.

[162] E. Bamberger, *Ber. Dtsch. Chem. Ges.* **1896**, *29*, 446.

[163] C. Colas, M. Goeldner, *Eur. J. Org. Chem.* **1999**, *1999*, 1357.

[164] a) A. Jabłoniec, S. Horstmann, J. Gmehling, *Ind. Eng. Chem. Res.* **2007**, *46*, 4654; b) K. Fischer, M. Wilken, *J. Chem. Thermodyn.* **2001**, *33*, 1285; c) R. P. Kennan, G. L. Pollack, *J. Chem. Phys.* **1990**, *93*, 2724.

[165] a) B.-T. Guan, Y. Wang, B.-J. Li, D.-G. Yu, Z.-J. Shi, *J. Am. Chem. Soc.* **2008**, *130*, 14468; b) X. Zhang, Y. Mei, Y. Li, J. Hu, D. Huang, Y. Bi, *Asian J. Org. Chem.* **2021**, *10*, 453; c) I. Chakrabarty, M. O. Akram, S. Biswas, N. T. Patil, *Chem. Commun.*

2018, *54*, 7223; d) S. Witzel, K. Sekine, M. Rudolph, A. S. K. Hashmi, *Chem. Commun.* **2018**, *54*, 13802; e) T. H. Rehm, *Chem. Eur. J.* **2020**, *26*, 16952; f) F.-X. Felpin, S. Sengupta, *Chem. Soc. Rev.* **2019**, *48*, 1150; g) M. Christakakou, M. Schön, M. Schnürch, M. Mihovilovic, *Synlett* **2013**, *24*, 2411; h) M. Krumb, L. M. Kammer, S. O. Badir, M. J. Cabrera-Afonso, V. E. Wu, M. Huang, A. Csakai, L. A. Marcaurelle, G. A. Molander, *Chem. Sci.* **2022**, *13*, 1023.

[166] Y.-F. Liang, R. Steinbock, L. Yang, L. Ackermann, *Angew. Chem. Int. Ed.* **2018**, *57*, 10625.

[167] a) Y.-F. Liang, L. Massignan, L. Ackermann, *ChemCatChem* **2018**, *10*, 2768; b) Y. Hu, B. Zhou, C. Wang, *Acc. Chem. Res.* **2018**, *51*, 816.

[168] a) K. F. Eidman, P. J. Nichols in *Encyclopedia of reagents for organic synthesis* (Ed.: L. A. Paquette), Wiley, Chichester, **1995**; b) G. K. Friestad, B. P. Branchaud in *Encyclopedia of reagents for organic synthesis* (Ed.: L. A. Paquette), Wiley, Chichester, **1995**.

[169] M. Chakraborty, A. K. Panda, *Spectrochim. Acta, Part A* **2011**, *81*, 458.

[170] J. M. Karlsson, M. Gazin, S. Laakso, T. Haraldsson, S. Malhotra-Kumar, M. Mäki, H. Goossens, W. van der Wijngaart, *Lab Chip* **2013**, *13*, 4366.

[171] D. D. Meng, J. Kim, C.-J. Kim, *J. Micromech. Microeng.* **2006**, *16*, 419.

[172] A. M. Skelley, J. Voldman, *Lab Chip* **2008**, *8*, 1733.

[173] C. Lochovsky, S. Yasotharan, A. Günther, *Lab Chip* **2012**, *12*, 595.

[174] a) T. P. Petersen, A. Polyzos, M. O'Brien, T. Ulven, I. R. Baxendale, S. V. Ley, *ChemSusChem* **2012**, *5*, 274; b) P. B. Cranwell, M. O'Brien, D. L. Browne, P. Koos, A. Polyzos, M. Peña-López, S. V. Ley, *Org. Biomol. Chem.* **2012**, *10*, 5774; c) M. A. Eddings, B. K. Gale, *J. Micromech. Microeng.* **2006**, *16*, 2396; d) J. Xu, R. Vaillant, D. Attinger, *Microfluid. Nanofluid.* **2010**, *9*, 765; e) Y. Okamoto, H.-C. Chiang, M. Fang, M. Galizia, T. Merkel, M. Yavari, H. Nguyen, H. Lin, *Membranes* **2020**, *10*.

[175] S-Pact GmbH, *User Manual*, **2020**.

[176] E. Kriesten, F. Alsmeyer, A. Bardow, W. Marquardt, *Chemom. Intell. Lab. Syst.* **2008**, *91*, 181.

[177] a) P. Beumers, D. Engel, T. Brands, H.-J. Koß, A. Bardow, *Chemom. Intell. Lab. Syst.* **2018**, *172*, 1; b) E. Kriesten, D. Mayer, F. Alsmeyer, C. B. Minnich, L. Greiner, W. Marquardt, *Chemom. Intell. Lab. Syst.* **2008**, *93*, 108; c) A. Michalik-Onichimowska, S. Kern, J. Riedel, U. Panne, R. King, M. Maiwald, *J. Magn. Reson.* **2017**, *277*, 154; d) A. Dondoni, P. P. Giovannini, A. Massi, *Org. Lett.* **2004**, *6*, 2929.

[178] a) N. R. Candeias, F. Montalbano, P. M. S. D. Cal, P. M. P. Gois, *Chemical reviews* **2010**, *110*, 6169; b) M. Oliva, F. Martens, E. V. van der Eycken, U. K. Sharma, *STAR Protocols* **2022**, *3*, 101162; c) J. L. Farmer, H. N. Hunter, M. G. Organ, *Journal of the American Chemical Society* **2012**, *134*, 17470.

[179] a) J. J. Ritter, P. P. MINIERI, *J. Am. Chem. Soc.* **1948**, *70*, 4045; b) M. Slegt, H. S. Overkleeft, G. Lodder, *Eur. J. Org. Chem.* **2007**, *2007*, 5364; c) L. Yang, C.-P. Zhang, *ACS omega* **2021**, *6*, 21595; d) C. G. Swain, R. J. Rogers, *J. Am. Chem. Soc.* **1975**, *97*, 799; e) S. Milanesi, M. Fagnoni, A. Albini, *J. Org. Chem.* **2005**, *70*, 603.

[180] a) A. Wetzel, V. Ehrhardt, M. R. Heinrich, *Angew. Chem. Int. Ed.* **2008**, *47*, 9130; b) A. Wetzel, G. Pratsch, R. Kolb, M. R. Heinrich, *Chem. - Eur. J.* **2010**, *16*, 2547; c) R. Bolton, G. H. Williams, *Chem. Soc. Rev.* **1986**, *15*, 261; d) R. A. Rossi, A. B. Pierini, A. B. Peñéñory, *Chem. Rev.* **2003**, *103*, 71.

[181] T. M. Bockman, D. Kosynkin, J. K. Kochi, *J. Org. Chem.* **1997**, *62*, 5811.

[182] C.-J. Li, B. M. Trost, *PNAS* **2008**, *105*, 13197.

[183] P. P. Plehiers, C. W. Coley, H. Gao, F. H. Vermeire, M. R. Dobbelaere, C. V. Stevens, K. M. van Geem, W. H. Green, *Front. Chem. Eng.* **2020**, *2*, 420.

[184] a) C. F. Carter, H. Lange, S. V. Ley, I. R. Baxendale, B. Wittkamp, J. G. Goode, N. L. Gaunt, *Org. Process Res. Dev.* **2010**, *14*, 393; b) K. L. A. Chan, S. Gulati, J. B. Edel, A. J. de Mello, S. G. Kazarian, *Lab Chip* **2009**, *9*, 2909.

[185] a) M. Lee, J.-P. Lee, H. Rhee, J. Choo, Y. Gyu Chai, E. Kyu Lee, *J. Raman Spectrosc.* **2003**, *34*, 737; b) S. Mozharov, A. Nordon, D. Littlejohn, C. Wiles, P. Watts, P. Dallin, J. M. Girkin, *J. Am. Chem. Soc.* **2011**, *133*, 3601.

[186] a) F. Lauterbach, V. Abetz, *Macromol. Rapid Commun.* **2020**, *41*, e2000029; b) H. Lu, M. A. Schmidt, K. F. Jensen, *Lab Chip* **2001**, *1*, 22.

[187] S. T. Knox, S. Parkinson, R. Stone, N. J. Warren, *Polym. Chem.* **2019**, *10*, 4774.

[188] a) P. Sagmeister, R. Lebl, I. Castillo, J. Rehrl, J. Kruisz, M. Sipek, M. Horn, S. Sacher, D. Cantillo, J. D. Williams et al., *Angew. Chem. Int. Ed.* **2021**, *60*, 8139; b) D. Ghislieri, K. Gilmore, P. H. Seeberger, *Angew. Chem.* **2015**, *127*, 688; c) J. Britton, C. L. Raston, *Chem. Soc. Rev.* **2017**, *46*, 1250; d) V. Sans, L. Cronin, *Chem. Soc. Rev.* **2016**, *45*, 2032.

[189] a) G. E. P. Box, J. S. Hunter, W. G. Hunter, *Statistics for experimenters*. *Design, innovation, and discovery*, Wiley-Interscience, Hoboken, **2005**; b) H. Bandemer, A. Bellmann, *Statistische Versuchsplanung*, Teubner, Stuttgart, Leipzig, **1994**; c) A. Gioiello, V. Mancino, P. Filipponi, S. Mostarda, B. Cerra, *J. Flow Chem.* **2016**, *6*, 167; d) C. J. Taylor, A. Baker, M. R. Chapman, W. R. Reynolds, K. E. Jolley, G. Clemens, G. E. Smith, A. J. Blacker, T. W. Chamberlain, S. D. R. Christie et al., *J. Flow Chem.* **2021**, *11*, 75.

[190] P. Sagmeister, J. D. Williams, C. A. Hone, C. O. Kappe, *React. Chem. Eng.* **2019**, *4*, 1571.

[191] R. F. Heck, J. P. Nolley, *J. Org. Chem.* **1972**, *37*, 2320.

[192] a) M. Julia, J.-M. Paris, *Tetrahedron Letters* **1973**, *14*, 4833; b) D. J. Peterson, *J. Org. Chem.* **1968**, *33*, 780.

[193] E. Vedejs, M. J. Peterson in *Topics in Stereochemistry* (Eds.: E. L. Eliel, S. H. Wilen), John Wiley & Sons, Hoboken, **1994**, pp. 1–157.

[194] E. L. Eliel, S. H. Wilen (Eds.) *Topics in Stereochemistry*, John Wiley & Sons, Hoboken, **1994**.

[195] a) E. Vedejs, K. A. J. Snoble, *J. Am. Chem. Soc.* **1973**, *95*, 5778; b) P. A. Byrne, D. G. Gilheany, *Chem. Soc. Rev.* **2013**, *42*, 6670; c) B. E. Maryanoff, A. B. Reitz, *Chem. Rev.* **1989**, *89*, 863.

[196] M. Schlosser, K. F. Christmann, *Angew. Chem.* **1966**, *78*, 115.

[197] R. Robiette, J. Richardson, V. K. Aggarwal, J. N. Harvey, *J. Am. Chem. Soc.* **2006**, *128*, 2394.

[198] Y. Le Bigot, M. Delmas, A. Gaset, *Synthetic Communications* **1982**, *12*, 107.

[199] S. Frattini, M. Quai, E. Cereda, *Tetrahedron Letters* **2001**, *42*, 6827.

[200] A. J. Speziale, D. E. Bissing, *J. Am. Chem. Soc.* **1963**, *85*, 3878.

[201] Jerome Thomas Kresse, *PhD thesis*, University of Florida, **1965**.

[202] a) D. Cheng, F.-E. Chen, *Ind. Eng. Chem. Res.* **2020**, *59*, 4397; b) E. Šinkovec, M. Krajnc, *Org. Process Res. Dev.* **2011**, *15*, 817.

[203] a) M. Grabarnick, S. Zamir, *Org. Process Res. Dev.* **2003**, *7*, 237; b) A. E. Siegrist, *HCA* **1967**, *50*, 906.

[204] W. Ehrfeld, K. Golbig, V. Hessel, H. Löwe, T. Richter, *Ind. Eng. Chem. Res.* **1999**, *38*, 1075.

[205] a) E. Chow, B. Raguse, E. Della Gaspera, S. J. Barrow, J. Hong, L. J. Hubble, R. Chai, J. S. Cooper, A. Sosa Pintos, *React. Chem. Eng.* **2020**, *5*, 356; b) H. P. L. Gemoets, G. Laudadio, K. Verstraete, V. Hessel, T. Noël, *Angew. Chem. Int. Ed.* **2017**, *56*, 7161.

[206] D. Simoni, M. Rossi, R. Rondanin, A. Mazzali, R. Baruchello, C. Malagutti, M. Roberti, F. P. Invidiata, *Org. Lett.* **2000**, *2*, 3765.

[207] a) D. H. Waldeck, *Chem. Rev.* **1991**, *91*, 415; b) R. A. Caldwell, L. Zhou, *J. Am. Chem. Soc.* **1994**, *116*, 2271; c) W. Fuß, C. Kosmidis, W. E. Schmid, S. A. Trushin, *Angew. Chem.* **2004**, *116*, 4273.

[208] D. C. Fabry, M. A. Ronge, M. Rueping, *Chem. - Eur. J.* **2015**, *21*, 5350.

[209] a) M. Wrighton, J. Markham, *J. Phys. Chem.* **1973**, *77*, 3042; b) K. N. Swanick, S. Ladouceur, E. Zysman-Colman, Z. Ding, *RSC Adv.* **2013**, *3*, 19961; c) H. Meier, *Angew. Chem. Int. Ed.* **1992**, *31*, 1399; d) M. Osawa, M. Hoshino, Y. Wakatsuki, *Angew. Chem. Int. Ed.* **2001**, *40*, 3472; e) K. Singh, S. J. Staig, J. D. Weaver, *J. Am. Chem. Soc.* **2014**, *136*, 5275.

[210] W. G. Herkstroeter, D. S. McClure, *J. Am. Chem. Soc.* **1968**, *90*, 4522.

[211] L. Eggert, Fairhurst G., "Unicast UDP Usage Guidelines for Application Designers", can be found under https://www.ietf.org/rfc/rfc5405.txt, **2008**.

[212] C.-C. Zhang, F.-S. Zhang, *Chem. Eng. J.* **2014**, *240*, 10.

[213] H. Friebolin, *Ein- und zweidimensionale NMR-Spektroskopie*. *Eine Einführung*, Wiley-VCH, Weinheim, **2013**.

[214] S. G. Hyberts, S. A. Robson, G. Wagner, *J. Biomol. NMR* **2013**, *55*, 167.

[215] F. Gindele, M. Holzki, U. Schwab, J. Bellew, A. Aranzabe, A. Arnaiz, *Infrared Sensor System for On-Line Oil Analysis*, Preston, UK, **2006**.

[216] L. Ben Mohammadi, F. Kullmann, M. Holzki, S. Sigloch, T. Klotzbuecher, J. Spiesen, T. Tommingas, P. Weismann, G. Kimber in *SPIE Proceedings* (Eds.: F. Berghmans, A. G. Mignani, C. A. van Hoof), SPIE, **2010**, 77260M.

[217] P. Hanson, J. R. Jones, A. B. Taylor, P. H. Walton, A. W. Timms, *J. Chem. Soc., Perkin Trans. 2* **2002**, 1135.

[218] R. Zapf, C. Becker-Willinger, K. Berresheim, H. Bolz, H. Gnaser, V. Hessel, G. Kolb, P. Löb, A.-K. Pannwitt, A. Ziogas, *Chem. Eng. Res. Des.* **2003**, *81*, 721.

[219] S. L. Buchwald, J. R. Naber, B. P. Fors, X. Wu, J. T. Gunn, *HETEROCYCLES* **2010**, *80*, 1215.

[220] B. Schmidt, R. Berger, *Adv. Synth. Catal.* **2013**, *106*, 463.

[221] J. Li, Y. Huang, M. Cai, *J. Chem. Res.* **2006**, *2006*, 658.

[222] F. Singh, H. Stefani, *Synlett* **2008**, *2008*, 3221.

[223] A. S. K. Hashmi, T. L. Ruppert, T. Knöfel, J. W. Bats, *J. Org. Chem.* **1997**, *62*, 7295.

[224] S. Shaaban, A. Jolit, D. Petkova, N. Maulide, *Chem. Commun.* **2015**, *51*, 13902.

[225] L. M. Castelló, V. Hornillos, C. Vila, M. Giannerini, M. Fañanás-Mastral, B. L. Feringa, *Org. Lett.* **2015**, *17*, 62.

[226] H. Min, H. Miyamura, S. Kobayashi, *Chem. Lett.* **2016**, *45*, 837.

[227] J. Albaneze-Walker, R. Raju, J. A. Vance, A. J. Goodman, M. R. Reeder, J. Liao, M. T. Maust, P. A. Irish, P. Espino, D. R. Andrews, *Org. Lett.* **2009**, *11*, 1463.

[228] J. Masllorens, I. González, A. Roglans, *Eur. J. Org. Chem.* **2007**, *2007*, 158.

[229] T. Furuya, H. M. Kaiser, T. Ritter, *Angew. Chem. Int. Ed.* **2008**, *47*, 5993.

[230] F. M. Piller, A. Metzger, M. A. Schade, B. A. Haag, A. Gavryushin, P. Knochel, *Chem. - Eur. J.* **2009**, *15*, 7192.